STRUCTURAL AND BIOPHYSICAL STUDIES OF INTERACTION OF ANTHRACYCLINES WITH G-QUADRUPLEX DNA

Ph.D. THESIS

by

ZIA TARIQ

DEPARTMENT OF BIOTECHNOLOGY
INDIAN INSTITUTE OF TECHNOLOGY ROORKEE
ROORKEE-247667, INDIA
MAY, 2019

STRUCTURAL AND BIOPHYSICAL STUDIES OF INTERACTION OF ANTHRACYCLINES WITH G-QUADRUPLEX DNA

A THESIS

Submitted in partial fulfilment of the requirements for the award of the degree

of

DOCTOR OF PHILOSOPHY

in

BIOTECHNOLOGY

by

ZIA TARIQ

DEPARTMENT OF BIOTECHNOLOGY
INDIAN INSTITUTE OF TECHNOLOGY ROORKEE
ROORKEE-247667, INDIA
MAY, 2019

INDIAN INSTITUTE OF TECHNOLOGY ROORKEE
ROORKEE

CANDIDATE'S DECLARATION

I hereby certify that the work which is being presented in the thesis entitled "**STRUCTURAL AND BIOPHYSICAL STUDIES OF INTERACTION OF ANTHRACYCLINES WITH G-QUADRUPLEX DNA**", in partial fulfilment of the requirements for the award of the degree of Doctor of Philosophy and submitted in the Department of Biotechnology of the Indian Institute of Technology Roorkee, Roorkee is an authentic record of my own work carried out during a period from July, 2013 to May, 2019 under the supervision of Dr. Ritu Barthwal, Professor, Department of Biotechnology, and Dr. Mala Nath, Professor, Department of Chemistry, Indian Institute of Technology Roorkee, Roorkee.

The matter presented in the thesis has not been submitted by me for the award of any other degree of this or any other institute.

(**ZIA TARIQ**)

This is to certify that the above statement made by the candidate is correct to the best of our knowledge.

(RITU BARTHWAL)
Supervisor

(MALA NATH)
Supervisor

Dated:

Table of Contents

ABSTRACT

Guanine rich sequences form non-canonical four stranded G-quadruplex DNA structures, which are self assembled array of guanine tetrads formed through Hoogsteen base pairing stabilized by the presence of central monovalent cationic tract. Telomerase, a ribonucleoprotein enzyme, elongates linear DNA at the end of chromosome which forms a dynamic nucleoprotein assembly called telomere. Telomeric regions in humans and other organisms comprise guanine-rich repeats of few hundred base pairs in 3´-end overhangs which can fold into G-quadruplex DNA (G4) structure under *in vivo* conditions. Absence of telomerase activity leads to end to end fusion of linear chromosomal DNA ends and subsequent cell senescence through apoptosis signaling due to chromosomal instability. Tumor cells become immortalized through activation of telomerase enzyme that stabilizes the length of telomeres. Telomerase levels have been found to correlate with cancer progression and metastatic state and the enzyme is not expressed in normal human tissue but is present in at least 85% of tumor cells. The RNA template of telomerase as well as capping function require extended single stranded DNA primer for effective hybridization and folding of telomeric repeats into higher order DNA structures (e.g. G-quadruplex) would hinder these processes. The general consensus is that G-quadruplex binders, which stabilize G4 structure, interfere with DNA damage response activation, oncogene expression and genomic stability and hence possess potential to act as regulatory elements of different processes. Consequently G-quadruplex binding agents can serve as a viable therapeutic strategy, also due to their selectivity since they would not show cytotoxic effect outside tumor. This paved the way for discovery of novel anticancer agents by focusing much research activity on design approaches based on molecular interactions of ligands specific with G4 DNA sequences. A large number of compounds e.g. alkaloids, flavonoids, porphyrins, anthraquinones, anthracyclines, porphyrin derivatives, metalloporphyrins, etc. are being evaluated for their affinity and specificity for G4 DNA.

Anthracyclines have been used in past as anticancer drugs. Daunomycin isolated from *Streptomyces peucetius* is found to be active against acute lymphoblastic or myeloblastic leukemias, while its 14-hydroxy derivative, adriamycin (doxorubicin) is active against specific solid tumors. It is well established that these drugs interact with duplex DNA through classical mode of intercalation between base pairs by uncoiling DNA, block DNA/RNA synthesis and act as topoisomerase-II poison. Recent findings point towards the role of daunomycin/adriamycin in maintenance of telomeres and induced telomere dysfunction by suppressing telomerase association with telomeres. Competition dialysis and spectroscopy techniques have revealed that the anthracyclines bind to different forms of DNA and exert their

influence by following multiple strategies involving complex mechanisms, which are not well understood.

In the present thesis, a comprehensive study of interaction of three anthracycline based ligands namely, daunomycin, 4'-epiadriamycin and adriamycin, with 7-mer tetramolecular parallel stranded [d-(TTGGGGT)]$_4$ and 22-mer unimolecular d-[GGGG(TTGGGG)$_3$] G4 DNA, containing telomeric DNA sequence TTGGGG from protozoan *Tetrahymena thermophilia*, has been undertaken by absorption, steady state & life time fluorescence, Circular Dichroism (CD) and Nuclear Magnetic Resonance (NMR) spectroscopy. We have also determined real time binding affinity using Surface Plasmon Resonance (SPR). The melting profiles of DNA and its complexes with these ligands have been obtained by absorption, CD and Differential Scanning Calorimetry (DSC). These investigations have been supplemented by molecular docking studies to understand mode of interaction. The thesis has been divided into eight chapters.

Chapter 1 comprises general introduction on various forms of DNA, telomere, telomerase and structure of G-quadruplex DNA. A detailed literature survey on various ligands, particularly anthracyclines, interacting with G-quadruplex; study of ligand-quadruplex DNA interactions by various biophysical techniques; structure of their complexes determined by NMR techniques; the implications of telomerase inhibition as a strategy for development of anticancer therapeutics; and biological evidence of telomerase dysfunction by anthracyclines are discussed. The specific objectives of the present research work have been spelled out.

Chapter 2 comprises materials and methods used for carrying out the structural and biophysical studies on interaction of the three ligands with the two selected G-quadruplex DNA sequences. The mathematical models and equations used to obtain binding parameters like binding constant, quenching constant, stoichiometry of ligand-DNA complexes, etc. using biophysical studies such as - UV-visible absorption, steady state and time-resolved Fluorescence and Circular Dichroism (CD) spectra are stated. Techniques of determining binding affinity by Surface Plasmon Resonance (SPR) and thermal denaturation by Differential Scanning Calorimetry (DSC) are discussed. The detailed experimental parameters used in 1D ^{1}H, ^{31}P and 2D Nuclear Magnetic Resonance (NMR) experiments namely, ^{1}H-^{1}H NOESY at different mixing times, ^{1}H-^{13}C HSQC, ^{1}H-^{31}P HMBC and their pulse programs are given. The methodology used for building NMR based model of ligand-DNA complex following restrained Molecular Dynamics (rMD) and molecular docking are also stated.

Chapter 3 presents studies of daunomycin binding to 7-mer [d-(TTGGGGT)]$_4$ G4 DNA by absorption, fluorescence, and CD spectroscopy. Also molecular docking and thermal denaturation by absorption/CD spectroscopy are given. Absorbance, flourescence and CD spectra show significant change on interaction with no change in wavelength maxima. The binding affinity is K_b ~10^5 M^{-1} for the 1:1 and 2:1 stoichoimetric drug-DNA complexes. CD spectra show minor changes in DNA conformation suggesting end stacking and groove binding of daunomycin monomer. The daunomycin dimers present in free state in solution, are disrupted on binding. Thermal stabilization of G4 DNA by 10-15 °C upon daunomycin binding is obtained from absorbance and CD measurements. The molecular docking studies establish well defined binding of daunomycin at two different sites of G4 DNA.

Chapter 4 comprises results of binding studies of daunomycin complexation to 7-mer [d-(TTGGGGT)]$_4$ G4 DNA, primarily by NMR techniques, SPR and Diffusion Ordered SpectroscopY (DOSY). Proton and phosphorus-31 NMR spectra show chemical shift changes, line broadening and sequence specific interaction with a clear proof of absence of intercalation of daunomycin chromophore between base quartets or stacking between G-quadruplexes. Several Nuclear Overhauser Enhancement (NOE) correlations between daunomycin and G4 DNA are found. Restrained Molecular Dynamics (rMD) simulations using short inter proton distance contacts depict interaction at molecular level. The interactions involving ring A and daunosamine protons, stacking of aromatic ring of daunomycin with terminal G6 quartet by displacing T7 base and external groove binding close to T1-T2 bases lead to thermal stabilization of 15 °C, determined by DSC experiments.

Chapter 5 presents results on interaction of daunomycin with 22-mer d-[GGGG(TTGGGG)$_3$] G4 DNA in K^+ rich aqueous solution. Using SPR, we demonstrate real time binding. Changes in absorption/CD spectra and efficient quenching of fluorescence accompanied by minor change in wavelength establish external binding of daunomycin with no scope of classical intercalation as observed on its binding to duplex DNA. Multiple stoichiometric complexes coexist in solution. Proton NMR spectra show significant shifts in aromatic protons of ring B/D, daunosamine sugar protons and 14 short inter molecular contacts, exhibiting specificity of interaction. Large downfield shifts in phosphorus-31 NMR spectra are absent. Molecular docking confirms external binding by formation of complex with negative binding energy. DSC experiments show binding profiles with melting temperature T_m increasing with incremental addition of daunomycin to DNA and total thermal stabilization, ΔT_m = 10 °C.

Chapter 6 comprises absorption, fluorescence and CD studies on binding of 4'epiadriamycin and adriamycin with 7-mer [d-(TTGGGGT)]$_4$ G4 DNA. Absorbance measurements show 56% hyposchromism while 95% quenching of fluorescence of ligands is observed with no change in wavelength maxima. The binding affinity is K_b ~10^5-10^6 M^{-1}. Fluorescence lifetime remains unaffected on complexation. CD spectra show significant changes and ligands are found to bind in monomeric form. Thermal stabilization of G4 DNA by 13-16 °C is determined by absorbance and CD measurements. The molecular docking studies show binding of ligands at two different sites of G4 DNA.

Chapter 7 comprises extensive analysis of binding of 4'epiadriamycin and adriamycin with 7 mer [d-(TTGGGGT)]$_4$ G4 DNA by NMR techniques. SPR and Diffusion Ordered SpectroscopY (DOSY) experiments are also carried out. Proton and phosphorus-31 NMR spectra show chemical shift changes, line broadening and sequence specific interaction with a clear proof of absence of intercalation of daunomycin chromophore between base quartets or stacking between two G4 DNA structures. Significant difference in phophrus-31 NMR and inter proton ligand-DNA distances are observed in the complexes formed by 4'epiadriamycin and adriamycin with G4 DNA. Restrained molecular dynamics simulations have been performed to get optimised conformation of complexes. The interactions at molecular level lead to thermal stabilization up to 23 °C, determined by DSC experiments.

Chapter 8 comprises absorption, fluorescence and CD studies on binding of 4'epiadriamycin and adriamycin with 22-mer d-[GGGG(TTGGGG)$_3$] G4 DNA in K^+ rich aqueous solution. SPR results demonstrate real time binding. Changes in absorption/CD spectra and efficient quenching of fluorescence are accompanied by minor change in wavelength. Isobestic or iso-emissive points are not observed. Job plot shows that 1:1 and 2:1 ligand-G4 DNA stoichiometric complexes coexist in solution. Molecular docking confirms external binding by formation of daunomycin-DNA complex with negative binding energy -6.0 to -7.7 kcal/mole. DSC experiments show binding profiles with melting temperature T_m increasing with daunomycin to DNA ratio and total thermal stabilization, ΔT_m = 5 °C.

The findings have implication in design of analogues that could produce de novo anthracycline that acts as a potent telomerase inhibitor with enhanced selectivity towards G-quadruplex and hence reduced cellular toxicity.

Acknowledgments

I would like to thank almighty for bestowing blessings on me to pursue this course with intellect, patience, strength, and determination. Saying thanks would be least I could do to *Papa, Ammi, Bade-Abbu, Badi-Ammi, Gudia Appi, Nuri Appi, Gazala Appi, Rufeeda, Nida, Zeba, Faiz, Ayan, Areeba, Rayyan,* all my *niece, cousins* and *relatives* for making my life comfortable and ongoing through their immense love, support and encouragement all these years.

My life and work would have been incomplete without the enjoyable moments, care, affection and support of all my friends especially *Dr. Meenakshi, Dr. Arun, Nidhi, Anita, Nupur, Shahbaz, Vasi, Fahad, Nilesh, Wasif, Faraz, Ankit, Prabhjot, Sachin, Mohit, Dr. Varun, Kartika, Dr. Intekhab, Dr. Ejaz, Mohsin, Pradeep Soni, Dr. Madhusudan, Dr. Rajat, Dr. Shailendra, Dr. Tamoghna, Dr. Nitin, Rakesh Sir, Pranav Sir, Khursheed Sir, Dinesh Sir* and all my seniors, juniors, colleagues and well-wishers whom I forgot to mention here unintentionally. I thank you all for making my life colorful, dynamic, glorious and wonderful.

I would express my sincere gratitude to my supervisor *Prof. Ritu Barthwal* for guiding and teaching me the various aspects of research, academics, as well as other necessary administrative skills required to pursue a career in the related field. I am thankful to my supervisor from Department of Chemistry, *Prof. Mala Nath,* and the Head of Department, *Prof. A.K. Sharma,* and my SRC committee members: *Prof. R.P. Singh, Prof. R.K. Peddinti, Prof. Debabrata Sircar,* and faculty members of Department of Biotechnology for their continuous support and help during this course. I am grateful to *Prof. Kaushik Ghosh* for providing me access to utilize Central NMR Facility during the final year of my thesis work. I am thankful to *Mr. Charan Singh* in the Central NMR Facility for his unconditional support.

I warmly thank past lab members: *Dr. Pradeep T.P., Dr. Sweta Tripathi, Dr. Padmapriya Kumar,* current lab mates: *Dr. Anuradha, Dr. Kumud, Shailja, Arpita, Jyoti, Anjana,* all B.Tech. and M.Sc. project students for their support, fruitful discussions, *'Chapos'* and birthday celebrations.

I thank all the staff members of Department of Biotechnology, Administrative Block, Azad Bhawan, Student's Club, Multi-Activity Centre and Cultural club for providing their service and support for my smooth and effortless stay in the campus.

Finally, I would like to acknowledge the Ministry of Human Resource and Development, Government of India, for providing me the financial assistance.

List of publications

Zia Tariq and Ritu Barthwal, (2019) Affinity of anticancer drug daunomycin toward *Tetrahymena* telomeric G-quadruplex DNA d-[GGGG(TTGGGG)$_3$], ACS Omega, 4, 6347−6359.

Zia Tariq and Ritu Barthwal, (2018) Binding of anticancer drug daunomycin to parallel G-quadruplex DNA [d-(TTGGGGT)]$_4$ leads to thermal stabilization: A multispectroscopic investigation, International Journal of Biological Macromolecules, 120B, 1965-1974.

Ritu Barthwal and **Zia Tariq**, (2018) Molecular recognition of parallel G-quadruplex [d-(TTGGGGT)]$_4$ containing *Tetrahymena* telomeric DNA sequence by anticancer drug daunomycin: NMR-based structure and thermal stability, Molecules, 23, 2266-2292.

Zia Tariq and Ritu Barthwal, (2019) Solution structure of 4'-epiadriamycin and adriamycin complexed with intermolecular G-quadruplex DNA [d-(TTGGGGT)]$_4$, (manuscript under preparation).

Zia Tariq and Ritu Barthwal, (2019) Multispectroscopic investigation of binding of 4'-epiadriamycin and adriamycin with intermolecular parallel G-quadruplex DNA [d-(TTGGGGT)]$_4$, (manuscript under preparation).

Zia Tariq and Ritu Barthwal, (2019) Multispectroscopic investigation of binding of 4'-epiadriamycin and adriamycin with intramolecular 22-mer G-quadruplex DNA from telomeric sequence of *Tetrahymena* thermophilia, (manuscript under preparation).

List of presentations in conferences

Zia Tariq, Ritu Barthwal "Solution structure and thermal stabilization of G quadruplex DNA [d-(TTGGGGT)]$_4$ bound to anticancer drug Adriamycin" accepted in Conference on Magnetic Resonance in Medicine & 25th National Magnetic Resonance Society Meeting, February 13-16, 2019, Indian National Science Academy (INSA), New Delhi, India.

Zia Tariq, Ritu Barthwal "Multispectroscopic investigation of anticancer drug Epiadriamycin bound to parallel G-quadruplex sequence d-TTGGGGT" accepted in 24th conference of Nuclear Magnetic Resonance Society February 16-19, 2018 Department of Physics, IISER Mohali, Punjab, India.

Zia Tariq, Ritu Barthwal "Interaction of anticancer drug Epiadriamycin with parallel G-quadruplex sequence d-TTGGGGT" **Oral Presentation** in National Conference on Biotechnology and Environment (NCOBE-2017) April 10-11, 2017, Department of Biotechnology, Jamia Millia Islamia, New Delhi, India.

Zia Tariq, Ritu Barthwal "Mutlispectroscopic studies of anticancer drug Daunomycin with G-quadruplex sequence d-TTGGGGT" presented in Annual Symposium of Indian Biophysical Society, March 22-25, 2017, IISER Mohali, India.

Zia Tariq, Ritu Barthwal "Interaction of anthracycline Daunomycin bound to *Tetrahymena* G quadruplex sequence d-TTGGGGT" presented in 7th Asia Pacific NMR Symposium and the 23rd Annual Meeting of the National Magnetic Resonance Society, India February 16-19, **2017**, Indian Institute of Science, Bangalore, India**.**

Zia Tariq, Ritu Barthwal "Structure of Daunomycin bound to *Tetrahymena* G quadruplex sequence d-(TTGGGGT)$_4$" presented in Recent Advances in Biomedical Research Strategies and Innovation SYSCON 2016, May 26-27, 2016, AIIMS, New Delhi, India.

Zia Tariq, Rudrarapu Rajgopal and Ritu Barthwal "Structure of Doxorubicin bound to *Tetrahymena* G quadruplex sequence d-(TTGGGGT)$_4$" presented in RASBDD (Recent Advances in Structural Biology & Drug Discovery), Oct 9-11, 2014, IIT Roorkee, India.

Discovery of “nuclein" (later termed as a nucleic acid) by Friedrich Miescher in 1869 gave an indispensable lead to understand the composition of the nucleus within cells (Olby, 1969; Dahm, 2008). Numerous experiments were conducted to find out the function of nucleic acid. Afterwards, Hershey and Chase in 1952 confirmed the role of DNA as a genetic material which means genetic messages stored in these macromolecules are passed on from one generation to next (Hershey & Chase, 1952). In 1953, Watson and Crick established the double helical structure of DNA and proposed the replication mechanism of DNA by unwinding and duplication through complementary base pairing for transfer of genetic information (Watson & Crick, 1953). They also proposed the “central dogma” of molecular biology by stating that the information in DNA is translated into protein through RNA. The mystery of protein synthesis was still not solved until the genetic codes were explored by Robert W. Holley, Har Gobind Khorana, and Mashall W. Nirenberg for which they shared Noble Prize in 1968. The genetic code refers to the rules which reveal the information encrypted in the genetic material within living cells through transcription and translation. A set of three nucleotides (or triplet codons) specifies a single amino acid and a majority of genes encode through same canonical genetic codes. At this point, it was globally accepted that nucleic acid is a major constituent among all species including viruses and is rightly called as “molecule of hereditary”.

1.1 Composition and types of DNA

Nucleic acids (DNA/RNA) are polymers of nucleotide monomer unit which is composed of phosphoric acid esterified to sugar moiety of the nucleoside. A nucleoside consists of nitrogenous bases (purines/pyrimidines) and pentose sugar (deoxyribose/ribose) linked through β-glycosidic linkage. Pyrimidines (cytosine, thymine, and uracil) comprise six member heterocyclic ring composed of carbon and nitrogen. Thymine is different from uracil in having methyl group at the C5 position with a carbonyl group at C4 and C2 positions (Fig. 1.1 a). Purines (adenine and guanine) consist of six member pyrimidine ring fused with imidazole moiety (Fig. 1.1 b). Pentose sugar in RNA consists of 2’-hydroxyl group in contrast to DNA which contains hydrogen atom at the same position (Fig. 1.2). Non-planar pentose sugar in DNA adopts various conformations known as sugar puckering. This puckering could be either in twisted or envelope forms. The pentose sugar in DNA adopts either C2’/C3’-*endo* (corresponding carbon atom above plane) or C2’/C3’-*exo* (corresponding carbon atom below the plane) confirmation.

a

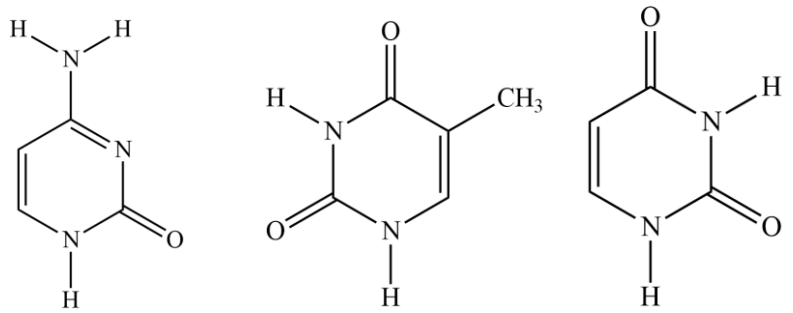

b

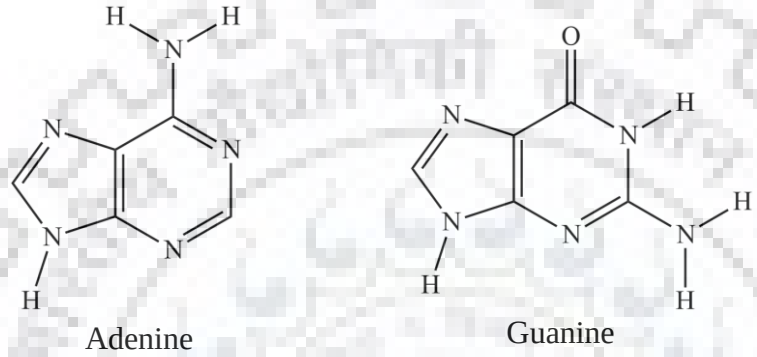

Figure 1.1 Chemical structures of a) pyrimidines and b) purines

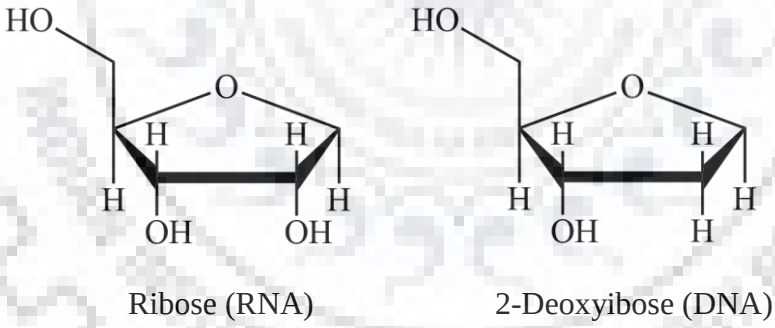

Figure 1.2 Chemical structures of pentose sugar rings of nucleic acids.

The sugar puckering is determined by Pseudo rotation phase angle (P) and the amplitude of puckering (τ_m) from the sugar endocyclic torsional angles (ν_0- ν_4) as shown by pseudorotation wheel (Altona & Sundaralingam, 1972) (Fig. 1.3). The conformation of DNA backbone is determined by the torsion angles, namely α, β, γ, δ, ε and ζ adopting a stable structure with minimum repulsion from negatively charged phosphates. C1' of pentose sugar is linked to N1 and N9 of pyrimidines and purines, respectively through glycosidic bond having torsion angle (χ) around the sequence of atoms O4'-C1'-N9-C4 for purine and O4'-C1'-N1-C2 for pyrimidine derivatives. Bases can adopt either *anti* or *syn* conformation relative to their orientation around sugar moiety. The *anti* form exists with bases oriented away from sugar moiety whereas *syn*

form exists with bases aligned above the sugar moiety. The endocyclic torsional angles, DNA backbone angles, and glycosidic bond rotation angle are shown in Fig. 1.4.

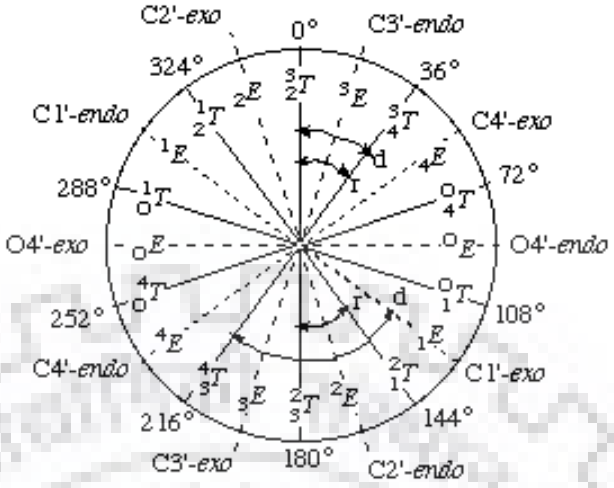

Figure 1.3 Pseudo rotation wheel showing various conformations of pentose sugar ring (Altona & Sundaralingam, 1972).

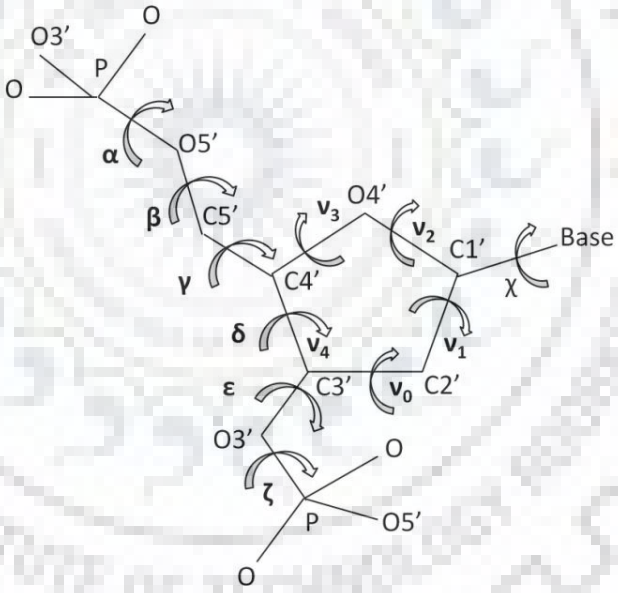

Figure 1.4 Representation of endocyclic torsional angles, DNA backbone angles, and glycosidic bond rotation angles.

Secondary structure of duplex DNA is formed when two strands of DNA are held together by Watson-Crick base pairing between complementary base pairs. The Watson-Crick base pairing between adenine and thymine or guanines and cytosine occurs through the formation of the hydrogen bond between electron donors (NH, NH_2) and electron acceptors (N, C=O). Different types of base pairing exist in nucleic acids and most common and canonical is Watson-Crick

base pairing. Other types of the base pairing also referred to as non-canonical base pairing include reverse Watson-Crick base, Hoogsteen, reverse Hoogsteen and Wobble (Fig. 1.5).

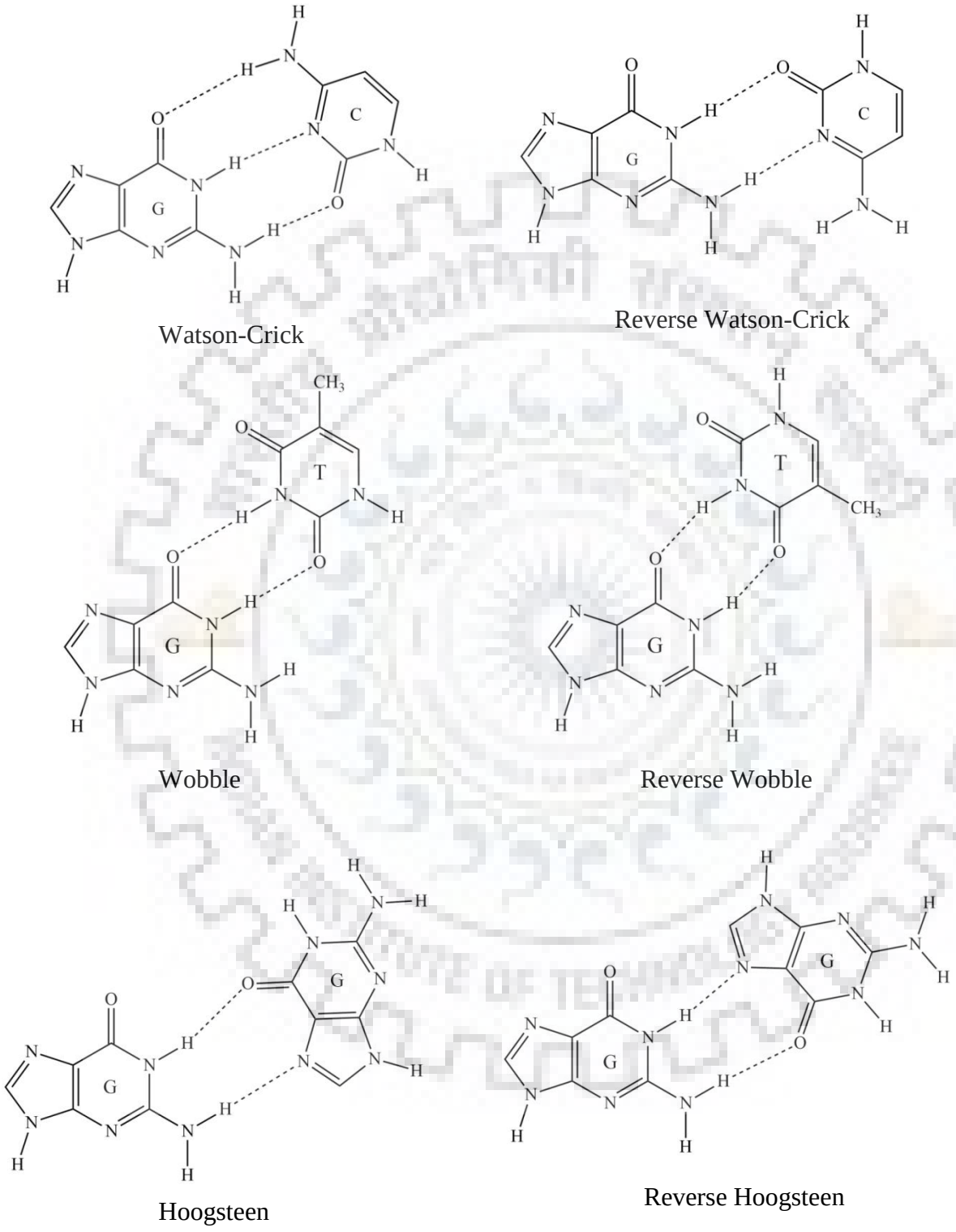

Figure 1.5 Representation of various types of base pairing in DNA. R represents deoxyribose sugar moiety.

1.1.1 Duplex DNA

DNA exhibits polymorphism depending on the conditions such as salt concentration, base sequence, hydrations, etc. It is found in basically three different forms, namely A, B, and Z DNA. B DNA is the most common form of DNA found in aqueous conditions whereas A DNA and Z DNA are formed under anhydrous and high salt concentration conditions, respectively. Many other differences in the structure of A, B, and Z DNA are summed up in Table 1.1. Major groove of B DNA is wide and deep while the minor groove is narrow and deep. Similarly, major groove in A and Z DNA is narrow/deep and flat, respectively whereas minor groove in A and Z DNA is wide/shallow and narrow/deep, respectively. The grooves of DNA offer an important site for the interaction of proteins and various other molecules during cellular processes (Pristovsek et al., 2003; D. Wang, Ulyanov, & Zhurkin, 2010; Hamilton & Arya, 2012). Other forms of DNA structures, such as slipped loop structures and pseudo square knots, are also reported (Ulyanov et al., 1998).

Table 1.1 Different structural features of A, B, and Z DNA.

Features	A DNA	B DNA	Z DNA
Helix sense	Right-handed	Right-handed	Left-handed
Repeating unit	1 bp	1 bp	2 bp
Rotation/bp (Twist angle)	33.6°	35.9°	60°/2
Mean bp/turn	10.7	10.4	12.0
Rise/bp along axis	2.3 Å	3.32 Å	3.8 Å
Pitch/turn of helix	24.6 Å	33.2 Å	45.6 Å
Mean propeller twist	+18°	+16°	0°
Glycosyl angle	*anti*	*anti*	*anti* for cytosine, *syn* for guanine
Sugar pucker	C3'-*endo*	C2'-*endo*	C2'-*endo* for C,T,A C3'-*endo* for G
Diameter	26 Å	20 Å	18 Å
Major Groove	Narrow and deep	Wide and deep	Flat
Minor Groove	Wide and shallow	Narrow and deep	Narrow and deep

1.1.2 Triplex DNA

Triplex DNA is formed by the association of one polypurine or polypyrimidine strand to the polypurine strand of duplex DNA through Hoogsteen or reverse Hoogsteen base pairing. It is known to exist in parallel and antiparallel forms based on the binding orientation of third strand (or TFO- triplex forming oligonucleotide) to duplex DNA from 5'-3' or 3'-5' direction, respectively (Beal & Dervan, 1991). Intermolecular and intramolecular triplex DNA structures are formed depending on the association of triplex-forming oligonucleotide. Triple helix is also observed in the pyrimidine-rich RNA motif of telomerase in *Kluyveromyces lactis* (Cash et al., 2013).

1.1.3 Quadruplex DNA

As the name suggests quadruplex DNA is four-stranded structures formed by the association of nucleotides through Hoogsteen base pairing with bases stacked on top of each other. Four guanines are arranged in square planar shape forming G-quartet (or G-tetrad) through the formation of two hydrogen bonds between adjacent guanines along with the presence of central monovalent/divalent cations (Fig. 1.6). Quadruplex DNA are known to exist in guanine and cytosine-rich sequences (Gellert, Lipsett, & Davies, 1962; Gehring, Leroy, & Guéron, 1993) although formation of quartet is also reported in synthetic oligonucleotides rich in adenine (Prasanta K Patel, Koti, & Hosur, 1999; Gavathiotis, Heald, Stevens, & Searle, 2003) and thymine (P K Patel & Hosur, 1999). Gellert et al. in 1962 demonstrated the formation of tetrameric structures of guanylic acids through X-ray diffraction studies (Gellert et al., 1962). Formation of G quadruplex DNA in mammalian cells (Biffi, Tannahill, McCafferty, & Balasubramanian, 2013; Henderson et al., 2014) and its role in gene regulation makes it an attractive drug target. Hydrogen bond formation between N1H, N2H with C6=O, N7, respectively among four guanines from neighboring/adjacent strand makes G-tetrad. These G-tetrads are stacked over each other to form G-quadruplex DNA (Balasubramanian & Neidle, 2009). Also monovalent or divalent cations such as K^+, Na^+, Cs^+, Li^+, Ca^{2+}, Mg^{2+}, etc. are present in the central cavity of G-quartet forming coordination between C=O groups of guanines. Presence of these positively charged ions plays a very critical role in determining the topology and conformation of G-quadruplex DNA. G-quadruplex structures are stabilized by eight hydrogen bonds along with the presence of metal ions in the central core of G-quartet.

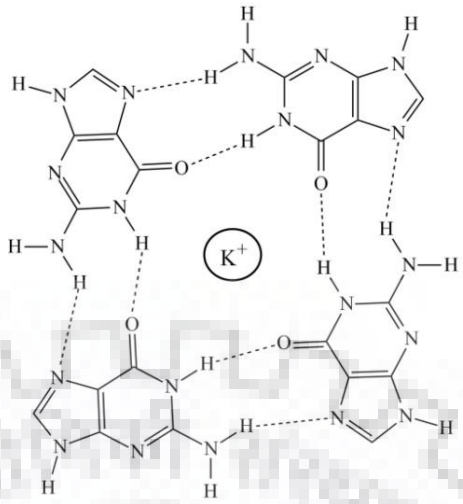

Figure 1.6 Structure of G-tetrad in the presence of K^+ ions

DNA sequences rich in cytosine, under low pH or neutral pH conditions, form quadruplex referred to as i-motifs (Gehring et al., 1993). Protonation of cytosine under acidic condition results in a mismatch in duplex DNA. Two duplex DNA containing these protonated cytosines when arranged in head to tail forms i-motifs. These i-motifs are known to be present in various regions of the human genome (e.g. telomeric DNA, c-myc promoter, etc.) and have significant role in gene regulation and cancer development (Leroy, Gueron, Mergny, & Helene, 1994; Y. Xu & Sugiyama, 2006; Dai, Hatzakis, Hurley, & Yang, 2010).

1.1.3.1 Types of G-quadruplex DNA

G-quadruplex DNA is broadly classified on the basis of number and directionality of the strands involved in the formation of G-quartets.

Unimolecular G-quadruplex DNA: They are formed by the folding of a single strand of G-rich DNA sequence to form a Hoogsteen base pairing among guanine repeats. Different types of loop arrangements are also present in these G-quadruplex structures in order to form G-tetrads from a single strand of DNA. Loops in these G-quadruplex DNA determines the directionality of strands in parallel, antiparallel or mixed/hybrid forms (Fig. 1.7) depending on the composition or length of sequence and identity of cations.

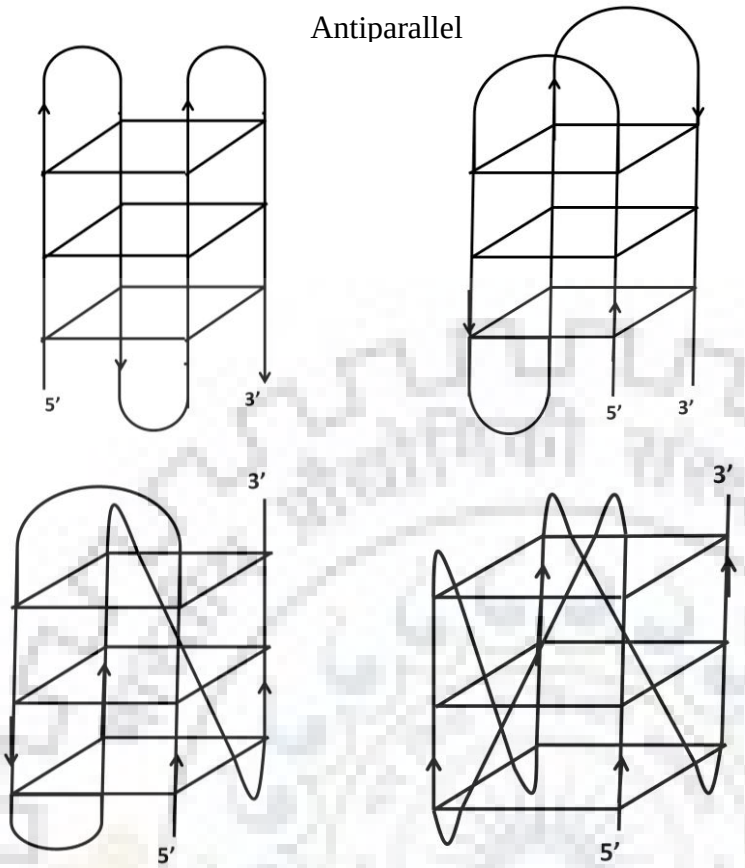

Figure 1.7 Schematic representations of various forms of unimolecular G-quadruplex DNA.

Bimolecular G-quadruplex DNA: Two individual G-rich DNA strands forms intramolecular hairpin fold and assemble to form G-quartets. On the basis of loop orientations (diagonal or lateral), different types of bimolecular G-quadruplex DNA conformations are possible (Fig. 1.8). The final dimeric structure of quadruplex DNA depends on the length and base composition of sequence (Keniry, Strahan, Owen, & Shafer, 1995).

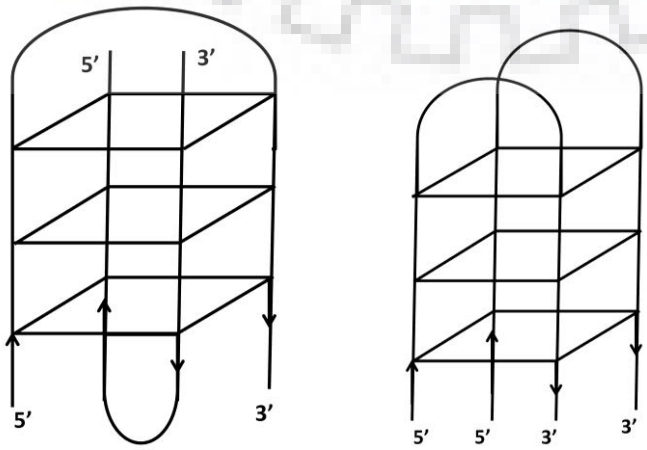

Figure 1.8 Schematic representation of bimolecular G-quadruplex DNA.

Tetramolecular G-quadruplex DNA: Four separate strands of G-rich DNA, having same base sequence, are associated with each other through Hoogsteen base pairing having all nucleotides in *anti* glycosidic bond conformation without any loops present in their structure (Y. Wang & Patel, 1993a; Prasanta K Patel et al., 1999; Gavathiotis et al., 2003) (Fig. 1.9).

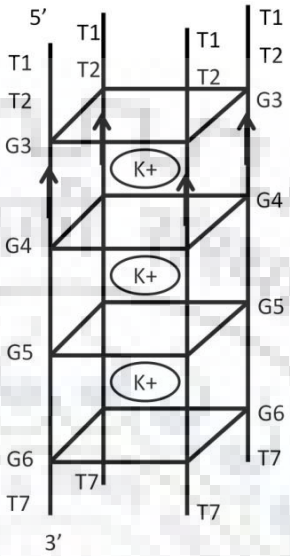

Figure 1.9 Schematic representation of tetramolecular parallel stranded G quadruplex DNA [d-(TTGGGGT)]$_4$.

G-quadruplex DNA, on the basis of orientation of different strands, can be divided into two types namely, parallel and antiparallel forms. In parallel conformation, all four strands are oriented in the same direction while in antiparallel conformation two strands are oriented in opposite directions. In some intramolecular G-quadruplex DNA, three stands are oriented in the same direction while the fourth strand orients itself in the opposite direction. This arrangement of strands in G-quadruplex DNA is called as 3+1 mixed or hybrid structure containing both *anti* and *syn* conformations of nucleotides. Human telomeric DNA is known to adopt hybrid or mixed (hybrid 1 or hybrid 2) conformation in physiologically relevant conditions containing K^+ ions where they exhibit polymorphism in G-quadruplex structures (Ambrus et al., 2006; Dai, Carver, Punchihewa, Jones, & Yang, 2007; Dai, Carver, & Yang, 2008; Phan, Luu, & Patel, 2006). Various types of loops present in unimolecular or bimolecular G-quadruplex DNA connect strands and dictate the orientation of strands in parallel or antiparallel fashion. For example, lateral or edgewise loops are extended above or below the G-quartets to connect two strands in antiparallel fashion. Diagonal loops span diagonally above or below the G-tetrad and connect two strands in antiparallel manner. A propeller or double chain reversal loops run along sides of G-quartet and connect two adjacent strands to align them in parallel orientation (Fig. 1.7).

1.2 Cancer, Telomerase and telomeric G-quadruplex DNA

Cancer is a dreadful disease causing millions of deaths worldwide every year. According to WHO cancer ranks second major cause of deaths globally. It is characterized by uncontrolled growth of normal cells in the body mainly due to mutations at several locations of the cellular genome. Mostly these abnormal cells have a tendency to invade from one organ to another through a process known as metastasis. Majority of deaths are caused due to the metastasis of cancer cells to a secondary site of the body. In normal cells, with every cell division, the ends of chromosome or telomere get shortened due to end replication problems. Signals for cell senescence are generated after a particular telomere length is reached (Hayflick's limit) and cell death occurs (Hayflick & Moorhead, 1961; Hayflick, 1965) (Fig. 1.10).

However, in the case of embryonic stem and cancer cells (80-85%), the length of the telomere is maintained through a reverse transcriptase enzyme known as telomerase, imparting immortality to these cells. Remaining 10-15% cancer cells adopt a distinct pathway for extension of telomere known as Alternative Lengthening of Telomere (ALT) pathway through various recombination processes (Bryan, Englezou, Dalla-Pozza, Dunham, & Reddel, 1997).

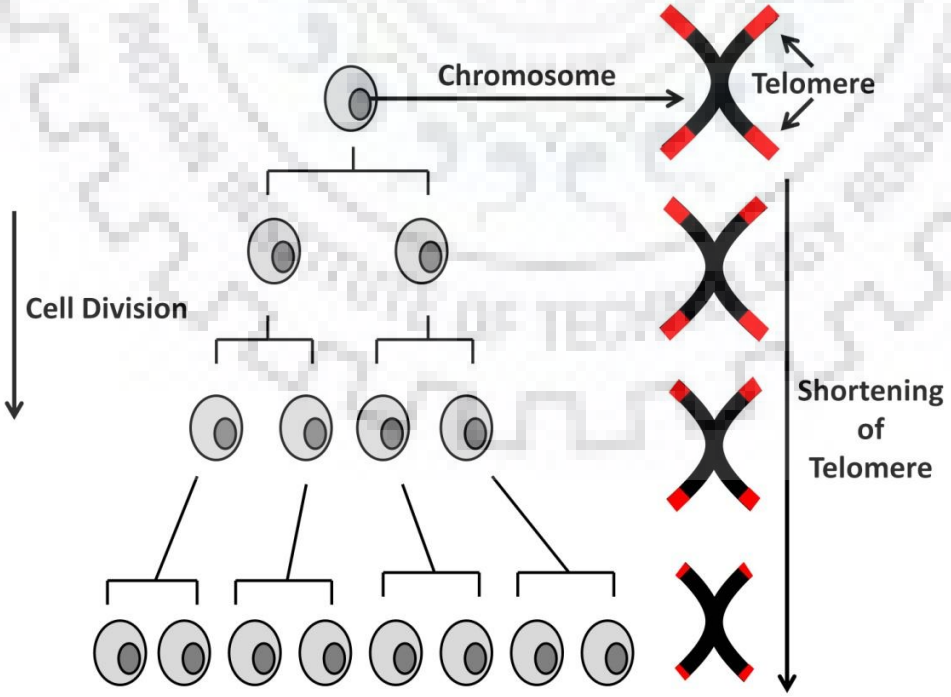

Figure 1.10 Diagrammatic representation of telomere shortening with every cell division.

Telomerase enzyme is a ribonucleoprotein complex composed of two subunits namely, TER and TERT which represent large RNA template and catalytic protein subunits, respectively (Sauerwald et al., 2013). Other proteins associated with the telomerase complex such as dyskerin, NHP2, NOP10, GAR, etc. are involved in the assembly, stability, and landing of telomerase onto telomeres (Townsley, Dumitriu, & Young, 2014) (Fig. 1.11). TERT is composed of several domains namely reverse transcriptase (RT), C-terminal (CTE), telomerase essential N-terminal (TEN) and RNA binding domain (RBD) (Podlevsky, Li, & Chen, 2016). TER contains RNA template which varies greatly among different species and posses two distinct motifs, that is, the template/pseudoknot (t/PK) domain and a stem-terminus element (STE) (Nelson & Shippen, 2015; Podlevsky, Bley, Omana, Qi, & Chen, 2008).

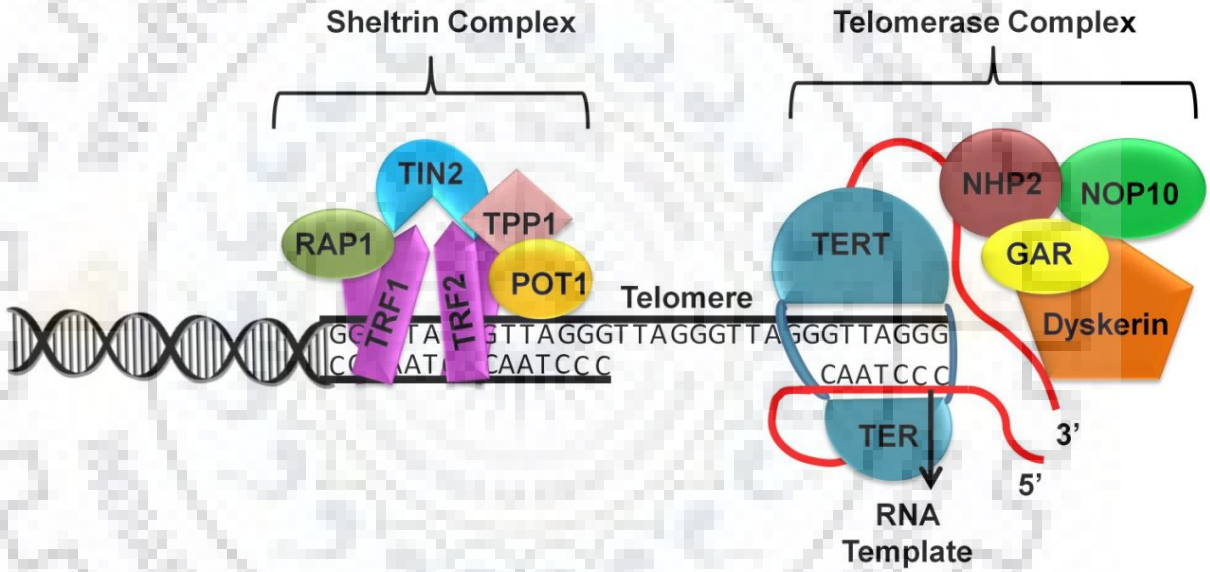

Figure 1.11 Figure of Telomerase enzyme with hTER and hTERT subunits

Recently, Jiang et al. reported the 4.8 Å resolution structure of telomerase enzyme complexed with DNA of *Tetrahymena* through cryo-electron microscopy giving insights of catalytic core (Jiang et al., 2018). The extension of telomeric single-stranded 3' overhangs occurs through the reverse transcription of the RNA template of the telomerase enzyme. Inhibition of telomerase activity results in the shortening of telomere length in cancer cells which ultimately cause cell death (Hahn et al., 1999; X. Zhang, Mar, Zhou, Harrington, & Robinson, 1999) (Fig. 1.12).

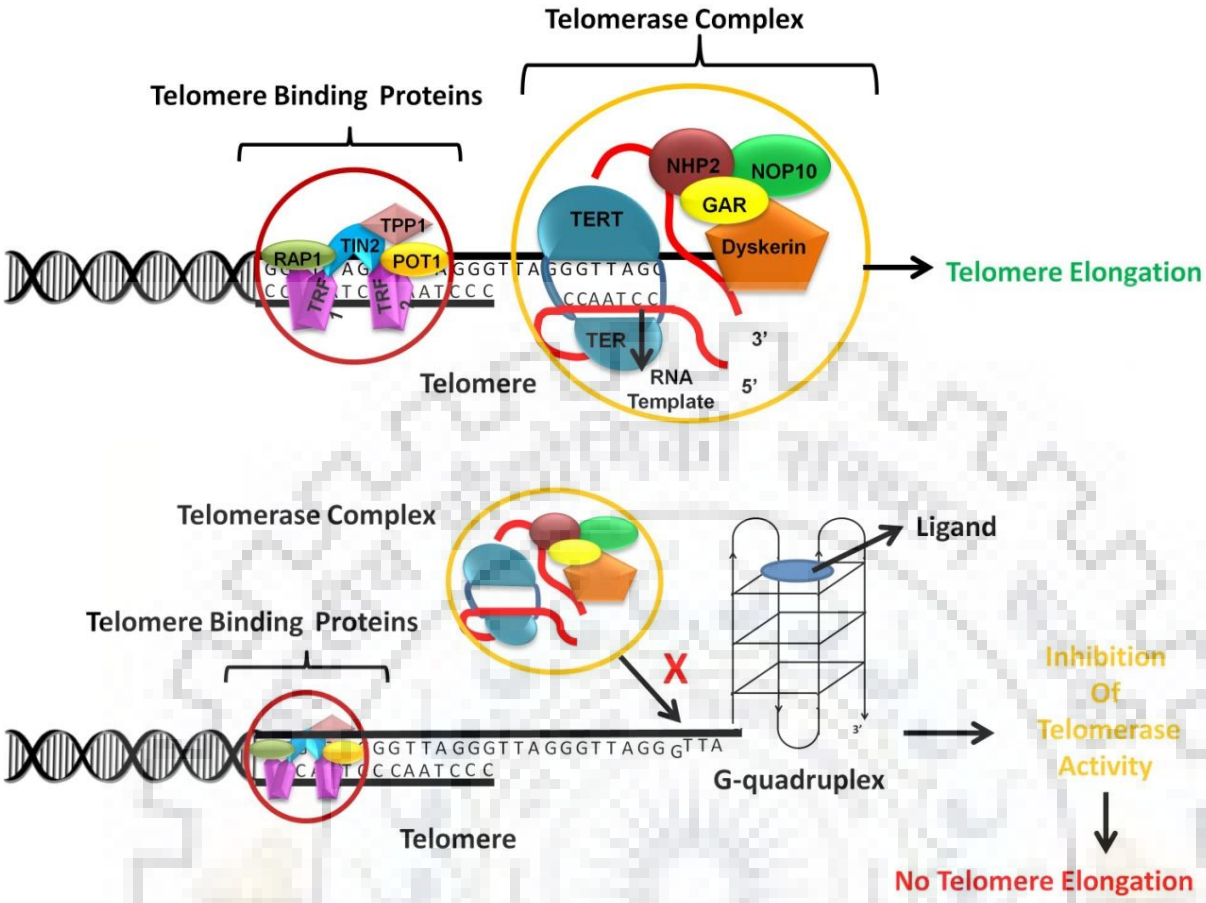

Figure 1.12 Inhibition of telomerase enzyme by the formation of G-quadruplex DNA

Telomeres are important for the maintenance of chromosomal stability by avoiding an end to end fusion and recombinational errors (E H Blackburn & Szostak, 1984; E H Blackburn, 1991). Telomeres are protected by a group of proteins known as "shelterin complex" which prevent degradation of telomeres from DNA damage responses. Shelterin complex comprises of three major proteins subunit namely TRF1, TRF2 and POT1 in association with additional subunits RAP1, TPP1, and TIN2 (Houghtaling, Cuttonaro, Chang, & Smith, 2004) (Fig. 1.11). Shelterin complexes are not present in other regions of chromosomes and have specific functions related to telomeres (Lange, 2005). Telomeric regions in chromosomes of different eukaryotic organisms, vary in lengths, sequence and posses conserved guanines residues (Podlevsky et al., 2008). The vertebrate telomere is composed of a long repetitive sequence of 5'-d-TTAGGG-3' and ciliate telomere contains repeats of the guanine-rich sequence of 5'-d-TTGGGG-3' maintained by various telomere binding proteins. Telomeric ends are mostly duplex DNA and their extreme 3' ends are single strand overhangs of ~200 bases. These guanine-rich non-coding regions of telomere fold over to form non-canonical DNA structures known as G-quadruplex (E H Blackburn, 1991). G-quadruplex DNAs are also known to be present at various other locations in the human genome such as oncogenic promoter regions (Siddiqui-

Jain, Grand, Bearss, & Hurley, 2002; Fernando et al., 2006), immunoglobin switch regions (Sen & Gilbert, 1990), etc. Eventually, the formation of G-quadruplex DNA at telomeric ends disrupts the binding of telomerase onto telomeres hence resulting in telomerase inhibition. Therefore, stabilization of G-quadruplex DNA by small molecules offers an attractive strategy against cancer (Wheelhouse, Sun, Han, Han, & Hurley, 1998; Han & Hurley, 2000; Buket, Clement, & Danzhou, 2014; Yang & Okamoto, 2010) (Fig. 1.12).

1.3 Literature review on G-quadruplex interacting ligands

Interaction of ligands with biomolecules can be studied using multiple techniques, example Absorption, Fluorescence, CD, Molecular Docking, NMR spectroscopy etc. (S. Kumar, Pandya, Pandav, Gupta, & Chopra, 2012; Lin et al., 2018; Bidisa Sengupta & Sengupta, 2002; Chaudhuri, Pahari, & Sengupta, 2009; Pahari, Chaudhuri, Chakraborty, & Sengupta, 2015; Agrawal, Kumar, Bal, Siddiqi, & Arora, 2007; Gurbani et al., 2012). Various classes of ligands such as anthraquinones, alkaloids, flavonoids, anthracyclines, etc. are known to interact with G-quadruplex DNA (Fig. 1.13).

2,6-diamido anthraquinone is the first known ligand which stabilizes human telomeric DNA sequence as determined by ^{1}H NMR and causes inhibition of telomerase activity with IC_{50} = 23 μM (D. Sun et al., 1997). Later on, numerous studies were carried out in this particular area of research for finding out the potential G-quadruplex binders. Anthraquinone derivatives such as, 2,6-disubstituted anthracene-9,10-diones, 2,7-disubstituted amidofluorenone (Perry, Reszka, et al., 1998; Perry, Gowan, et al., 1998; Perry et al., 1999), disubstituted amido anthraquinones (H. S. Huang et al., 2005; H.-S. Huang et al., 2007), and lysyl-peptidyl-anthraquinone conjugates (Zagotto et al., 2011) are reported to causes telomerase inhibition. Other derivative such as neomycin-anthraquinone conjugate (Ranjan, Davis, Xue, & Arya, 2013) and aryl ethyl anthraquinones (Percivalle et al., 2014) are demonstrated to bind to G-quadruplex DNA through various spectroscopic techniques. Riva B et al. in 2015 studied the interaction of naphthoquinone derivatives (1a-h) with several G quadruplex DNA through fluorescence assays, NMR spectroscopy, and modeling. These compounds were reported to selectively bind to G quadruplexes than duplex through thiazole orange dye (TO) displacement fluorescence experiments (Riva et al., 2015).

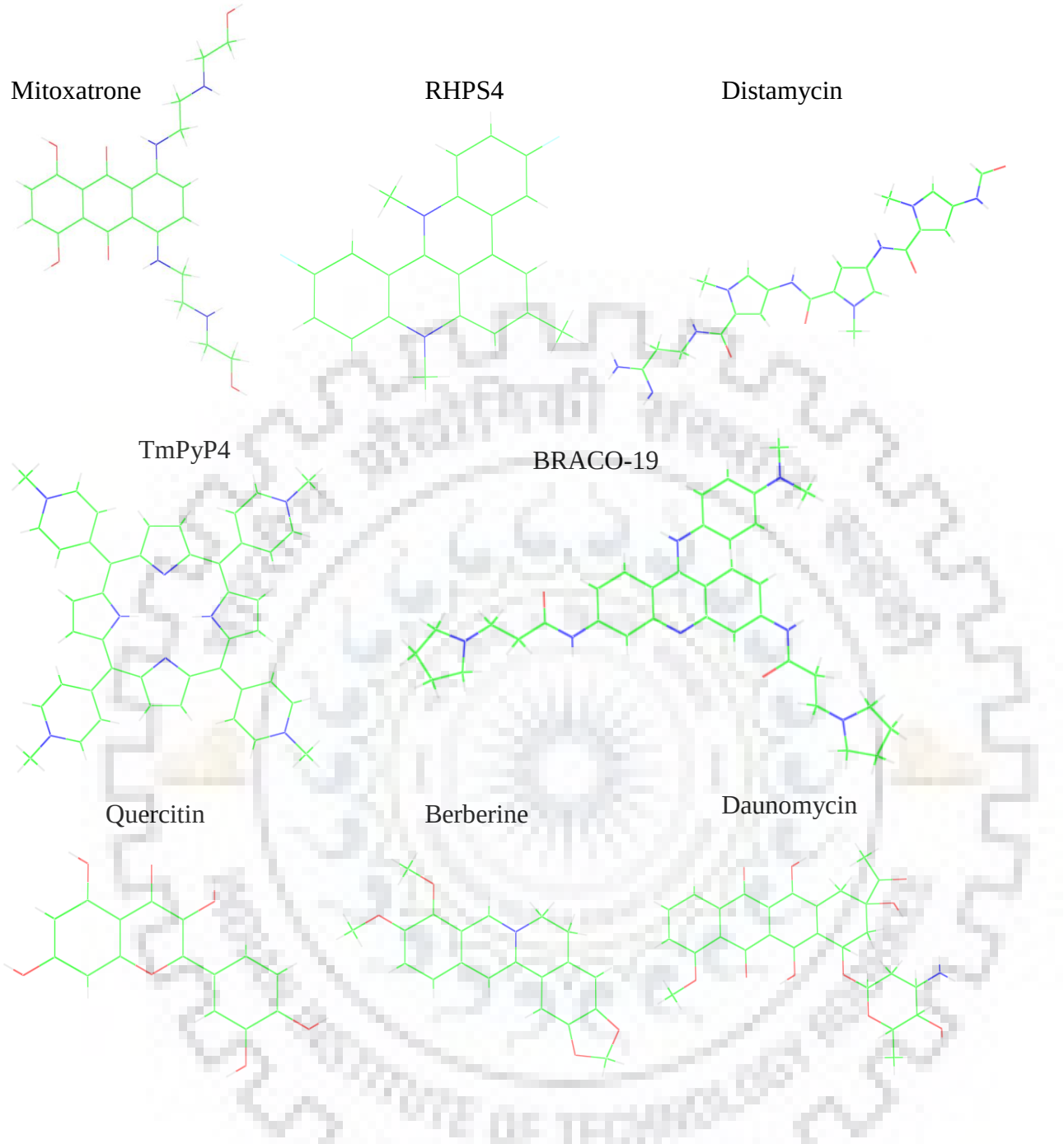

Figure 1.13 Schematic diagrams of few G-quadruplex interacting ligands

Similarly, TMpyP4 which is a cationic porphyrin with large surface area and planar structure stacks on to G-quartets, stabilizes G-quadruplex DNA resulting in telomerase inhibition (Wheelhouse et al., 1998). Also, cationic porphyrin H_2TMpyP4 is reported to bind G-quadruplex DNA with affinity two times greater than duplex DNA (Anantha, Azam, & Sheardy, 1998). Among porphyrin derivatives, CuTMpyP4 (Evans et al., 2007), metalloporphyrins such as NiII-TMPyP4 and NiII-TImidP4 (Rubio-Magnieto et al., 2015) are known to bind different G-quadruplex DNA. A macrocyclic compound, Telomestatin, posses an extended structure which binds over G-quadruplex surface, imparts stabilization leading to

inhibition of telomerase activity (Kim, Vankayalapati, Shin-ya, Wierzba, & Hurley, 2002). Acridines and their derivatives such as 9-amido acridine (Ruben Ferreira et al., 2013), RHPS4, BRACO, BRACO-19, BSU 6039, etc. are the planar compounds having anthracene heterocyclic ring which interacts with G-quadruplex DNA through stacking interactions. Also linked compounds such as acridine and quindoline oligomers linked through a 4-aminoproline binds and stabilizes G-quadruplex DNA (Rubén Ferreira et al., 2011). RHPS4 binds to intermolecular parallel G-quadruplex DNA through end stacking mode resulting in thermal stabilization of ~20 °C (Gavathiotis et al., 2003) and inhibits telomerase enzyme activity with an IC_{50} = 0.33 ± 0.13 μM (Gowan, Heald, Stevens, & Kelland, 2001). BRACO and its derivative BRACO-19 are also known to bind G-quadruplex DNA. Although, BRACO is a weak G-quadruplex binder, BRACO-19 exhibit greater binding to G-quadruplex DNA leading to telomerase inhibition (Incles et al., 2004). Campbell et al. in 2008 studied the interaction of BRACO-19 through X-ray crystallography which showed that the drug gets stacked between bimolecular G-quadruplex DNA formed by human telomere repeat sequence d(TAGGGTTAGGGT) making a sandwiched structure of the complex (Campbell, Parkinson, Reszka, & Neidle, 2008). A similar mode of binding and formation of the sandwiched complex was also observed in first ever NMR based quadruplex-ligand complex structure by Hurley research group in 1998 of PIPER (3,4,9,10 -perylenetetracarboxylic diimide) with human G-quadruplex DNA sequences (Fedoroff et al., 1998). Through chemical shift perturbations and NOE correlations, it was observed that PIPER binds to terminals of G-quartets by end stacking mode. However, few compounds such as distamycin, mitoxantrone, etc. are reported to bind as a dimer into grooves of parallel intermolecular G-quadruplex DNA of *Tetrahymena* telomeric repeat sequence (Martino et al., 2007; Pradeep & Barthwal, 2016). Distamycin and netropsin bind to duplex DNA in the minor groove with higher affinity as compared to G-quadruplex DNA (Randazzo, Galeone, Esposito, Varra, & Mayol, 2002). Martino et al. in 2007 determined through NMR titration and ITC experiments that two dimers of distamycin molecules simultaneously bind to two opposite grooves of G-quadruplex DNA. Structural and biophysical studies from our lab demonstrated the differential recognition of human and *Tetrahymena* G-quadruplex DNA by mitoxantrone (Pradeep & Barthwal, 2016; Tripathi & Barthwal, 2018). Mitoxantrone binds as a dimer to two opposite grooves of G-quadruplex DNA formed by *Tetrahymena* telomeric DNA sequence d-(TTGGGGT) (Tarikere Palakshan Pradeep & Barthwal, 2016) whereas it binds as a monomer to two different sites of G-quadruplex DNA formed by human telomeric DNA sequence d-(TTAGGGT) (Tripathi & Barthwal, 2018). Well known classical duplex DNA intercalator, Ethidium Bromide (EtBr), is also known to bind G-quadruplex DNA although with lesser affinity than duplex DNA (Ren & Chaires, 1999).

Flavonoids such as Quercitin, Rutin, Fisetin, Naringenin etc. are also known to recognize and bind G-quadruplex DNA through end stacking or groove binding mechanisms (H. Sun et al., 2006; H. Sun, Xiang, Tang, & Xu, 2007; Bidisha Sengupta, Pahari, Blackmon, & Sengupta, 2013; Bhattacharjee, Chakraborty, Sengupta, & Bhowmik, 2016). Sun et al. in 2006 determined that quercitin recognizes different binding sites of monomeric and dimeric G-quadruplex DNA through NMR and other spectroscopic techniques. It binds to the groove of dimeric G-quadruplex DNA whereas end stacking is reported for monomeric form (H. Sun et al., 2006). Rutin binds to different G-quadruplex sequences in a different fashion as shown by Sun et al. in 2007 through absorption, fluorescence and NMR spectroscopy. It was demonstrated that rutin intercalates between terminals of G-quartets in the blunt end extended G-quadruplex structures and promotes the formation of monomers while for interlocked end extended G-quadruplex structures the intercalation is inhibited by the phosphate groups. Binding of fisetin to the diagonal loops of G-quadruplex DNA facing the G-quartet was demonstrated for the first time by Sengupta et al. in 2013 through various spectroscopic and chromatographic techniques (Bidisha Sengupta et al., 2013). Bhattacharjee et al. in 2016 showed through spectroscopic and modeling techniques that fisetin binds strongly to G-quadruplex DNA as compared to duplex DNA whereas in case of naringenin binding for duplex DNA was stronger compared to G-quadruplex DNA (Bhattacharjee et al., 2016).

Interaction of alkaloids such as berberine, palmatine, coralyne, and sanguinarine with G-quadruplex DNA by calorimetric and spectroscopic studies shows affinity in order coralyne>sanguinarine>EtBr>berberine>palmatine (Bhadra & Kumar, 2011). Binding of coralyne and sanguinarine to G-quadruplex DNA is entropy driven opposite to the binding of palmatine and berberine which is enthalpy driven. Binding of berberine, palmatine, and coralyne to t-RNA^{phe} is also investigated through spectroscopic and molecular modeling studies (Islam, Pandya, Chowdhury, Kumar, & Kumar, 2008; Islam, Pandya, Kumar, & Kumar, 2009) apart from duplex and quadruplex DNA. Binding of these alkaloids to t-RNA^{phe} occurs in a cooperative manner through partial intercalation leading to thermal stabilization. Recent structural and biophysical studies from our lab demonstrated binding of coralyne and palmatine to G-quadruplex DNA forms 2:1 complex and leads to thermal stabilization (Padmapriya & Barthwal, 2017; P. Kumar & Barthwal, 2018). Recently, Lin et al. in 2018 reported the binding of epiberberine to human telomeric G-quadruplex DNA along with its capability to rearrange and convert other G4 DNA forms present in K^+ solution to hybrid-2 telomeric DNA (Lin et al., 2018).

Detailed literature review of anthracyclines binding to duplex and quadruplex DNA is discussed in further sections.

1.4 Literature review on the interaction of anthracyclines with duplex DNA and RNA

Binding of daunomycin to duplex DNA has been studied through equilibrium dialysis, absorption and fluorescence spectrometry (Chaires, Dattagupta, & Crothers, 1982). Interaction of daunomycin with duplex DNA results in strong quenching of fluorescence with significant redshift and hypochromism suggesting intercalation as a mode of binding. G+C rich DNAs are preferred by daunomycin for intercalation, at the binding site containing adjacent G.C base pairs flanked by A.T base pairs, over other DNAs (Chaires, Fox, Herrera, Britt, & Waring, 1987). Numerous structural studies have successfully established the intercalative mode of binding of anthracyclines to duplex DNA. NMR spectroscopy is a powerful technique to elucidate structures of macro and small molecules and to perform interactions studies (Ulyanov & James, 1995; Emwas et al., 2015; Khurana et al., 2005; Singh, Bharti, Agarwal, Roy, & Misra, 2014). In 1978, Patel et al. described the structural features of daunomycin-DNA complex using ^{1}H NMR spectroscopy (D. J. Patel & Canuel, 1978). Later in 1981, Patel et al. studied the intercalation of daunomycin and its analog 11-deoxydaunomycin with poly (dA-dT) through ^{1}H and ^{31}P NMR spectroscopy (D. J. Patel, Kozlowski, & Rice, 1981). Intercalation and stacking of daunomycin within G.C base pairs were investigated by 2D NMR (Barthwal, Mujeeb, & Govil, 1994). 2D ^{1}H-NMR and ^{31}P-NMR coupled with molecular dynamics techniques were used to investigate the intercalation of (2S)-2-methoxymorphlino doxorubicin and morpholino doxorubicin with hexanucleotide d$(CGATCG)_2$ and d$(CGTACG)_2$ (Mazzini, Mondelli, & Ragg, 1998). This study confirms the insertion of aglycone moiety of anthracylines leading deformation of DNA due to changes in backbone torsional angles at intercalation site.

Various X-ray crystallographic studies also reported the intercalation of anthracyclines into duplex DNA. Wang et al. in 1987 deduced the structure of daunomycin-d-$(CGTACG)_2$ complex (A. H.-J. Wang, Ughetto, Quigley, & Rich, 1987). It shows that the aglycone moiety of daunomycin intercalates between CpG sites at both ends of hexamer while daunosamine sugar moiety interacts with a minor groove through bridging water molecules. In another study, Frederick et al. in 1990 compared the structures of daunomycin-d-$(CGATCG)_2$, daunomycin-d-$(CGTACG)_2$ and adriamycin-d-$(CGATCG)_2$ complex (Frederick, Williams, Ughetto, Marel, et al., 1990). These structures also confirmed the intercalation of aglycone moiety at GC base

pairs of hexamers along with the binding of sugar moiety into the grooves of DNA. Also, there was no effect of change of DNA sequence or addition of hydroxyl group (adriamycin) on the interaction of aglycone moiety with DNA. A similar structure was observed for 4'-epiadriamycin- d(TGATCA)$_2$ complex in a study carried out by Langlois d' Estaintot et al., 1992 showing intercalation of aglycone moiety at GC base pairs (D'Estaintot, Gallois, Brown, & Hunter, 1992). Abhi Das et al. compared and confirmed the binding of anthracyclines, daunomycin and aristololactam-β-D-glucoside with poly(A) (Das, Bhadra, Achari, Chakraborty, & Kumar, 2011), tRNA^{phe} (Das, Bhadra, & Kumar, 2011) and ss RNA (Das & Kumar, 2013) through spectroscopic and calorimetric studies. These studies provided useful insight and energetics of binding mechanism of these drugs with different forms of nucleic acid structures.

1.5 Literature review on the interaction of anthracyclines with G-quadruplex DNA

Ren and Chaires in 1999 described the binding of 15 different types of ligands with 13 different types of the nucleic acid structure by competition dialysis experiments (Ren & Chaires, 1999). Among selected ligands were the classical intercalators (i.e. ethidium bromide, daunomycin and actinomycin D), groove binders (i.e. distamycin, netropsin and DAPI), putative triplex (BePI, coralyne, and berberine) and tetraplex [H_2TmPyP, 5,10,15,20-tetrakis[4-(trimethylammonio)phenyl]-21H,23H-porphine, and N-methyl mesoporphyrin IX] binding agents. These ligands were evaluated for their structural selectivity against single-stranded, duplex, triplex, quadruplex DNA, RNA, and DNA-RNA hybrids. Classical intercalators used in the study such as EtBr shows modest binding to almost all DNA forms except single-stranded DNA, triplex and quadruplex DNA. Daunomycin and actinomycin D, on the other hand, shows almost negligible binding to RNA and DNA-RNA hybrids and only apparent binding to Z DNA. Daunomycin also shows interaction with triplex and quadruplex DNA while actinomycin D shows interaction with only quadruplex DNA leaving behind triplex and duplex DNA containing only AT base pairs. Groove binders such as distamycin, netropsin, and DAPI bind strongly to right-handed duplex DNA with the preference of AT-rich sequence and almost no binding to RNA. Netropsin and DAPI show very slight binding to quadruplex DNA.

Clark et al. in 2003 determined the first crystal structure of parallel G-quadruplex DNA [d(TGGGGT)]$_4$-daunomycin complex (Clark, Pytel, Squire, & Neidle, 2003). Two layers of three coplanar daunomycin molecules are present between the two stacked end to end (5' to 5') quadruplex DNA. Three coplanar daunomycin molecules are held together in one layer by van

der Waals interactions. Each layer of three daunomycin molecules stacks with terminal guanines through weak π-π interactions. Daunosamine sugar moiety hangs in three out of four grooves with cationic amine substituent (N3*) forming H-bonds to the phosphate oxygen. H-bonds are also formed between the exocyclic OH groups to the phosphate oxygen. Binding of a daunosamine sugar moiety to groove does not alter the width of groove instead small movement occurs in phosphate groups. The crystal structure shows that the binding of daunomycin to G-quadruplex occurs through end stacking rather than intercalation between G-quadruplex layers.

Phan et al. in 2005 described a novel G-quadruplex fold from the element in *MYC* promoter region i.e. nuclease-hypersensitivity element III (NHE III), specifically the purine-rich strand (*Pu24*) of this element. Interaction of several ligands like Hoechst 33258, daunomycin, ethidium and TMPyP4 with *Pu24I* were studied through NMR (Phan, Kuryavyi, Gaw, & Patel, 2005). All these ligands were found to stack on top the G-quadruplex with different position, stability, and kinetics. In 1:1 ligand-DNA complexes imino protons of G4 andG13 residues of top tetrad were most perturbed (upfield shifted and broadened). In case of daunomycin, both G4 and G13 imino protons were broadened and upfield shifted showing stacking of three daunomycin molecules on top of G-quadruplex as mentioned by Clark et al. in 2003 in the crystal structure.

Karina C. Gornall et al. in 2007 determined the interaction of alkaloid berberine, its derivative SS14 and daunomycin (DNM) with duplex DNA (16 mer) and quadruplex DNA $[d(TTGGGGGT)]_4$ through ESI MS technique (Gornall, Samosorn, Talib, Bremner, & Beck, 2007). At 12 times higher DNM concentration in DNM-duplex mixture up to five DNM molecules were bound to duplex DNA with a majority of 2:1 (drug: DNA) complex. However, up to four DNM molecules were bound to quadruplex DNA $[d(TTGGGGGT)]_4$ with a majority of 1:1 complex. Similarly, at 12 fold higher berberine concentration in berberine-duplex DNA mixture shows several binding with a majority of 1:1 complex formation whereas in berberine-quadruplex DNA mixture equal abundance of 1:1 and 2:1 berberine: quadruplex DNA was obtained. Interestingly, in case of SS14-duplex DNA mixture, no complex was detected but up to three SS-14 molecules were bound to quadruplex DNA $[d(TTGGGGGT)]_4$ suggesting preference of binding over duplex DNA. Binding of DNM, berberine, and SS-14 was determined with a single-stranded sequence showing up to six DNM and six berberine molecule binding to ss DNA but no binding was observed for SS-14-ss DNA mixture. From this study, it was determined that daunomycin shows a slightly more binding preference for

duplex DNA over quadruplex which is vice versa in case of berberine and SS-14 molecules show modest binding only with quadruplex DNA.

Manet et al. in 2010 studied the interaction of two anthracylines i.e. Adriamycin (compound 1) and Sabarubicin (compound 2) with human telomeric sequence 5'-d[GGG(TTAGGG)$_3$]-3'(21-mer) forming quadruplex in the presence of K^+ through fluorescence, absorption, CD spectroscopy and isothermal titration calorimetry (ITC) experiments (Manet, Manoli, Zambelli, Andreano, Masi, Cellai, & Monti, 2011). Results from the experiments suggested binding stoichiometries of 1:1 and 2:1 of the drug: DNA coexists in solution. Efficient quenching of drug fluorescence suggested stacking of these drugs onto the top/bottom of G quadruplex structure with favorable orientation in close proximity of guanine residues for electron transfer. From ITC experiments, it was deduced that the first binding event in case of both the drugs leads to enthalpy gain suggesting hydrogen bond formations and non-covalent π-π stacking interactions. However second binding event shows $T\Delta S$ values similar to groove binders suggesting groove binding might exist due to multiple site availability. Thermal stabilization of DNA by 5 °C was observed upon complex formation as obtained by using CD spectroscopy.

Manet et al. in 2011 studied the interaction of anthracycline drugs adriamycin (compound 1) and sabarubicin (compound 2) with human telomeric sequence 5'-d[GGG(TTAGGG)$_3$]-3'(21-mer) forming basket G-quadruplex conformation in the presence of Na^+ using multiple techniques (Manet, Manoli, Zambelli, Andreano, Masi, Cellai, Ottani, et al., 2011). It was observed that stoichiometry of 1:1 and 2:1 of the drug: 21-mer DNA coexists in solution. Favorable enthalpy gain and loss of entropy indicated stacking interaction of drugs on top/bottom of G quadruplex. Data also suggested binding at more than two sites along with the possibility of groove binding. The self-association was not observed in the case of compound 2 whereas disruption of dimers results from titration of DNA in a solution containing compound 2. Melting studies through CD spectroscopy show the unaltered melting temperature of DNA upon complex formation in case of both the drugs i.e. 55 °C in case of both free DNA and the complexes.

Niusheng Xu et al. in 2012 determined the relative binding mode and relative binding affinities of six alkaloids with parallel intermolecular G-quadruplex [d(TGGGGT)]$_4$ and duplex DNA through Electrospray Ionization Mass Spectrometry (ESI-MS) technique. Well, known G-quadruplex binder i.e. daunomycin, netropsin, and ethidium bromide were used to compare the binding mode of alkaloids with quadruplex DNA (N. Xu et al., 2012). It was shown that

tetrandrine and fangchinoline follow the same dissociation pattern as that of daunomycin-quadruplex complex suggesting their binding through end stacking mode. Also, berberine, jatrorrhizine, and palmatine follow the same dissociation pattern as that of ethidium bromide-quadruplex complex showing that they follow intercalation mode of binding.

Clark et al. in 2012 determined the crystal structure of daunomycin-[d-(GGGG)]$_4$ complex showing four layers of daunomycin, with each layer containing four daunomycin molecules, stacked between 5' ends of two quadruplex DNA [d-(GGGG)]$_4$ (Clark, Pytel, & Squire, 2012). In each layer four daunomycin molecules are held together by van der Waals force while π-π stacking is present between daunomycin layers and G terad-daunomycin interface. In the case of [d-(TGGGGT)]$_4$ quadruplex all the grooves were of different depths and width whereas all grooves are equivalent in [d-(GGGG)]$_4$ quadruplex. Therefore, unlike crystal structure of daunomycin-[d-(TGGGGT)]$_4$ complex which shows groove interaction of daunosamine sugar moiety, no groove interaction was observed in daunomycin-[d-(GGGG)]$_4$ complex. It was inferred that the absence of thymine residues at the ends results in reduced interference and higher order stacking of daunomycin molecules in daunomycin-[d-(GGGG)]$_4$ complex.

Rivera et al. in 2012 studied the interaction of supramolecular G-quadruplexes (SGQs) with anticancerous drug doxorubicin through Förster Resonance Energy Transfer (FRET) technique (Rivera, Martín-Hidalgo, & Rivera-Ríos, 2012). Derivatives of 8-aryl-2′-deoxyguanosine (8ArG) self assemble in aqueous/organic medium to form SGQs. Coumarin labeled and unlabelled derivative of 8-(m-acetylphenyl)-2′-dG were coassembled to form hetero supramolecular quadruplexes (hSGQs). G tetrad thus formed provide the platform for interaction with ligand just like oligonucleotide-based G-quadruplexes (OGDs). The absorbance of doxorubicin acting as an acceptor (490 nm) matches very well with the emission of coumarin moiety acting as the donor (477 nm). Addition of doxorubicin results in efficient quenching of fluorescence of coumarin moiety showing the interaction of doxorubicin to hSGQs. Thermal stabilization of ΔT_m= 9 °C was observed by DSC upon addition of doxorubicin to hSGQs. Doxorubicin also induces the small amount of SGQs formation along with random aggregates as observed from NMR experiments. Addition of KCl further shifts the equilibrium towards the greater formation of SGQs.

Anand R et al. in 2012 determined the interaction of doxorubicin (DOX or adriamycin) with γ-cyclodextrin (γ-CyD) through CD, UV-vis absorption, fluorescence spectroscopy, laser flash photolysis and molecular dynamics simulation studies (Anand, Ottani, Manoli, Manet, &

Monti, 2012). Characteristic peaks for dimers, i.e. positive-negative splitting of peaks in the visible regions, were persistent showing that addition of γ-CyD is unable to disrupt dimers of DOX in solution. Stoichiometries of 1:2 and 2:2 γ-CyD: DOX coexist in solution. Triplet state properties of DOX dimers were determined by laser flash photolysis indicating that the environment of DOX, in DOX-γ-CyD complex, is ethanol like. Molecular dynamics and simulation studies showed the interaction of both aglycone and daunosamine sugar moieties with the primary rim of γ-CyD and/or inside the cavity of the γ-CyD macrocycle. However primary binding with γ-CyD macrocycle involved interaction with aglycone part and secondary binding occurs with the sugar moiety of doxorubicin.

Nawara K et al. in 2013 determined the role of methoxy and daunosamine sugar moieties in the stability of Fe^{3+}-anthracycline complexes (Nawara, Beeckman, Krysiński, & Blanchard, 2013). Structure of drug idarubicin is identical to daunorubicin but $4OCH_3$ is absent in idarubicin making it more lipophilic. The lifetime of idarubicin (1.55 ns) is more than daunorubicin (1.03 ns) which indicates that the methoxy group is involved in the non-radioactive decay of daunomycin. Idarubicin forms a faster and stronger complex with iron (III) than daunorubicin which results in faster hydrolysis of the complex. Methoxy group in daunomycin causes steric hindrance for iron (III) complexation while the pendant daunosamine moiety destabilizes that complexation with Fe^{3+}.

Scaglioni L et al. in 2016 studied the interaction of anticancer drug nemorubicin and doxorubicin with several G-quadruplex sequences and c-MYC promoter element Pu22 through NMR spectroscopy, ESI MS and molecular modeling (Scaglioni, Mondelli, Artali, Sirtori, & Mazzini, 2016). Significant broadening and upfield shift of A3H2, G4NH and G6NH resonances along with intermolecular NOEs shows binding at these sites of $[d(TAGGGTT)]_4$-nemorubicin complex. Stoichiometry of 1:1 and 2:1 of the drug: DNA complexes were obtained from ESI MS with the abundance of 2:1 complex as evident by NMR experiments as well. It was shown that nemorubicin binds to quadruplex $[d(TTGGGTT)]_4$ at G5pT6 site with T6 pushed away from G5 losing π-π stacking interactions. Similar results were obtained for titration of nemorubicin with quadruplex $[d(TTTGGGT)]_4$ showing binding at G6pT7 site. ESI MS studies also determine the stoichiometry of 1:1 of nemorubicin: $[d(TTGGGTT)]_4$ complex similar to NMR experiments. Interaction of doxorubicin with quadruplex $[d(TAGGGTT)]_4$ gave similar results as that of nemorubicin with a binding site at A3pG4. Titration of Pu22 with nemorubicin results in changes introduced by ligand showing binding event taking place at G22/G18NH and G7/G11/G18NH region of Pu22 quadruplex. One molecule of nemorubicin

binds to 5' end and other binds to 3' end of the tetrad of Pu22 quadruplex with π-π stacking interactions forming 2:1 of nemorubicin: Pu22 complex.

Changenet-Barret P et al. in 2016 studied the process of electron transfer in doxorubicin-quadruplex and doxorubicin-duplex complexes through femtosecond fluorescence spectroscopy (Changenet-Barret, Gustavsson, Markovitsi, & Manet, 2016). Absorption titration experiments of Tel-21 with doxorubicin (along with previous studies) indicate the existence of two independent binding sites on quadruplex i.e. BS1 and BS2. The first site (BS1) is expected to be at bottom of G-quadruplex favoring π-π stacking arrangement of the drug for efficient electron transfer whereas second site (BS2) might be near groove which is less favorable for electron transfer from guanines to the drug.

Das A et al. in 2017 determined the interaction of human telomeric G quadruplex DNA d[AGGG(TTAGGG)$_3$] called as H22 DNA (22 mer) in the presence of K^+ with aristololactam-β-D-glucoside (ADG) and daunomycin (DAN) through multi-spectroscopic and calorimetric techniques (Das, Chatterjee, & Suresh Kumar, 2017). Binding constants obtained for ADG and DAN interaction with H22 DNA from spectroscopic data were greater than the interaction of both the drugs with HT DNA indicating their higher binding affinity towards quadruplex DNA. Thiazole orange (TO) displacement assay also suggested binding of both the drugs on to the external surface of G-tetrad of H22 DNA. Also, absorbance titration experiments suggested the presence of π-π stacking interactions in drug-DNA complexes in accordance with CD experiments. Melting studies showed thermal stabilization of quadruplex H22 DNA and subsequent increase in melting temperature up to 7 °C and 11 °C by ADG and DAN, respectively. ITC experiments showed that DAN has a greater affinity towards H22 DNA than ADG and whole complexation process in both the cases is entropy driven with small favorable enthalpy contribution. Molecular docking studies showed binding preference of ADG and DAN over the surface of G-quartet through hydrophobic interaction and non-covalent hydrogen binding.

Shen et al. in 2017 determined the interaction of daunomycin with G-quadruplex [d(TGGGGT)]$_4$ through molecular dynamics and simulation studies which provide in-depth knowledge of energetics and dynamics of the binding process (Shen, Mulholland, Zheng, & Wu, 2017). Two binding modes of daunomycin to G-quadruplex DNA were observed i.e. groove binding (38%) and end stacking (45%). End stacking mode of daunomycin to quadruplex is similar to the X-ray crystal structure of DNM-[d(TGGGGT)]$_4$ complex with

anthraquinone ring stacked on top of tetrad and daunosamine sugar moiety interacting with the groove of the quadruplex. As the surface area of daunomycin (160 $Å^2$) is much smaller than G-quadruplex (390 $Å^2$) therefore three molecules of daunomycin can accommodate over the quadruplex surface as shown in the crystal structure of DNM-$[d(TGGGGT)]_4$ complex. However theoretical calculation shows almost equivalent binding energies for end stacking and groove binding modes i.e. -45.5 kcal/mol and -42.3 kcal/mol, respectively showing the existence of equal possibility for either binding modes.

1.6 Structure and biological activity of anthracyclines

Anthracyclines are extracted from *Streptomyces peucetius* which contains tetracyclic ring along with a sugar moiety attached through a glycosidic bond. The tetracyclic ring also called as aglycone is named as ring A, B, C and D with generally a methoxy substituent at C-4 in ring D (present in daunomycin, adriamycin, 4'-epiadriamycin), quinone-hydroquinone groups in ring B and C, sugar moiety attached to ring A at the C-7 position. Despite being known for almost 100 years after their discovery anthracyclines are still believed to be "evergreen drugs" with thousand of derivatives and still holding the chance for improvement of the therapeutic index (Minotti, Menna, Salvatorelli, Cairo, & Gianni, 2004). Anthracyclines are clinically used against the majority of cancers i.e. breast cancer, leukemia, sarcomas, etc. but their use is limited by dose dependant cardiotoxicity and congestive heart failure (CHF) problems (Jain et al., 1985; Ryberg et al., 1998; Weiss, 1992). In this regards only a few modified anthracylines are available for clinical use having low cardiotoxicity, namely 4'-epiadriamycin (EPI), idarubicin (IDA), pirarubicin, aclarubicin and mitoxantrone (MTX). 4'-epiadriamycin is an isomer of adriamycin with low cardiotoxic effects even at higher doses. Similarly, idarubicin, an analog of daunomycin with the absence of methoxy group, shows increased response in MDR (multi-drug resistant) phenotypes and greater cellular uptake and low cardiotoxicity (Toffoli, Simone, Gigante, & Boiocchi, 1994; Jonsson-Videsater, Anderson, Bergh, & Paul, 2003). Pirarubicin and aclarubicin were found to have only minor improvement over daunomycin and adriamycin. Reports on low cardiotoxicity of mitoxantrone as compared to anthracylines are conflicting and needs further confirmation. Anthracyclines are reported to have several mechanisms of action which includes topoisomerase II inhibition, intercalation into DNA, free radical generation leading to DNA damage, telomerase inhibition etc. (Binaschi et al., 2001; Perego et al., 2001; Zunino, Pratesi, & Perego, 2001; Gille & Nohl, 1997; Minotti, Cairo, & Monti, 1999).

Topoisomerase causes breaks in DNA which are resealed after a change in the twist of DNA but anthracylines stabilize the ternary complex (anthracylines-DNA-topoisomerase-II) and resist the resealing process. Intercalation into DNA takes place through ring B and C between the base pairs and the sugar moiety is located in the minor grooves. Anthracyclines are known to have increased the p53 protein level which might be involved in apoptosis hence responsible for the cytotoxicity of these drugs (Dunkern, Wedemeyer, Baumgärtner, Fritz, & Kaina, 2003). These drugs have a high affinity for proteosomes in the cytoplasm which is then transported to nucleus after binding and drug dissociates from drug-proteosomes complex and bind to DNA due to higher affinity for DNA than proteosomes (Kiyomiya, Satoh, et al., 2002; Kiyomiya, Kurebe, Nakagawa, & Matsuo, 2002). Another mode of action is through the generation of free radicals by gaining electron to quinone moiety of ring C then reducing oxygen to form reactive oxygen species (ROS) and causes oxidative damage in tumor cells (Gille & Nohl, 1997; Minotti et al., 1999). Anthracyclines are known to increase to malondialdehyde (MDA) which is mutagenic to cells and is responsible for cell cycle arrests (Plastaras, Dedon, & Marnett, 2002). The reaction of an anthracycline with formaldehyde (HCHO) results in conjugates having increased toxicity for anthracycline-resistant and sensitive cells (Taatjes, Fenick, & Koch, 1998). Cardiotoxicity is the major problem for the clinical usage of anthracyclines. It results due to many reasons major being; 1) low level of catalase in cardiomyocytes and inactivation of GSH-peroxidase-1 (GSH-Px1) after DOX exposure (Doroshow, Locker, & Myers, 1980; Siveski-Iliskovic, Hill, Chow, & Singal, 1995), 2) apoptosis of cardiomyocytes due activation of NF-κB (S. Wang et al., 2002), 3) formation and accumulation of anthracycline secondary alcohols, thus increasing cardiotoxicity (Stewart et al., 1993; Licata, Saponiero, Mordente, & Minotti, 2000). Liposome-encapsulated anthracycline (e.g. liposomal DNR or DaunoXome) shows enhancement over microsomes or nanoparticles and passively targets tumors cells with improved cardiotoxicity (Byrne et al., 2002). Several analogs have been developed for improving the therapeutic index of anthracylines but only a few reached for clinical trials e.g. PNU-159548, MEN 10755 or Sabarubicin and these were reported to show less cardiotoxic effects than adriamycin (ADM), 4'-epiadriamycin (EPI), or DNM (Sacco et al., 2003; Torre et al., 2001).

In 1973, Schwartz and Grindey proposed that the effectiveness of doxorubicin might be due to the immune defense mechanism of the host against tumors (Schwartz & Grindey, 1973). In 1986 Aringa et al. found an increased level of cytotoxic T-cell functions, interleukin (IL-2), immature monocyte count, and $CD8^+$ T-cell count in patients treated with doxorubicin (Arinaga, Akiyoshi, & Tsuji, 1986). Later, Ehrke et al. in 1984 and Maccubbin et al. in 1992

demonstrated that doxorubicin increases the tumoricidal action of macrophages and natural killer (NK) cells in mice through induction of specific immune function and cytokine expression (Ehrke, Ryoyama, & Cohen, 1984; Maccubbin et al., 1992). In 2003, Ujhazy et al. showed enhanced production of cytokines e.g. tumor necrosis factor, interleukin (IL-1), and interferon- γ (IFN γ) in mice treated with doxorubicin. They also demonstrated that doxorubicin induces an immune response which involves macrophage and NK cell activity (Ujhazy, Zaleskis, Mihich, Ehrke, & Berleth, 2003). Bhardwaj et al. in 2007 explained that the tumoricidal action of immune defense system is complex and can be mediated by cells of the innate immune system, (e.g. macrophages or NK cells) as well as by the adaptive immune system (e.g. B and T cells) (Bhardwaj, 2007). Ishigami et al. in 2000 explained that infiltration of malignant tumors with NK or T-cells results in better clinical outcomes, therefore, these effector cell targeting tumors acts as immune-based therapeutics strategies (Ishigami et al., 2000). However, S. Bien et al. in 2012 demonstrated that doxorubicin induces the secretion of IFN-γ and modulates several interferon responsive and immunomodulatory genes via IFN γ - JAK1-STAT1 signaling, which leads to apoptosis (Hussner et al., 2012).

Ogretmen B et al. in 2001 demonstrated that the exogenous or endogenous increase in the level of ceramide decreases the level of c-Myc transcription factor which in turn reduces the h-TERT mRNA expression level and hence the telomerase activity (Ogretmen et al., 2001). Endogenous increase in the level of ceramide was induced by treatment of A549 cells (lung adenocarcinoma cell line) with 1μM of daunomycin for 6 hours which resulted in the decrease of telomerase and c-Myc activities.

Elmore et al. in 2002 demonstrated in a well-characterized breast cancer model system (MCF-7) that both functional p53 and telomere dysfunction are required for the onset of senescence program in adriamycin-treated cells (Elmore et al., 2002). Degradation and functional loss of p53 by E6 protein of human papillomavirus type 16 (HPV-16) expressed in MCF-7 cells convert the senescent phenotype to apoptosis after adriamycin treatment. MCF-7-hTERT cells treated with adriamycin increased telomere dysfunction and induced many structural changes at chromosomal ends like an end to end fusion, end breaks, etc. causing lack of chromosome end protection which ultimately resulted in replicative senescence.

Nakajima et al. in 2003 demonstrated that the inhibition of telomerase activity resulting in telomere shortening induces apoptosis in HAL-01 cells (a human acute lymphoblastic leukemia cell line) expressing dominant negative (DN)-hTERT (Nakajima et al., 2003). HAL-01 cells

expressing DN-hTERT were treated with daunorubicin (DNR), etoposide (VP-16), vincristine (VCR), 6-mercaptopurine (6-MP), and methotrexate (MTX) to observe the effect on apoptosis. DNR showed a two-fold increase and early apoptosis in HAL-01 cells expressing DN-hTERT while no enhancement of apoptosis was observed in the case of VP-16, VCR, 6-MP, and MTX. Authors also confirmed *in vivo* inhibition of telomerase activity by DN-hTERT. Further, primary blast cells of acute leukemia from four patients with acute myeloid leukemia (AML-M2) were treated with telomestatin resulting in shortening of telomere length and eventually induced apoptosis. In this study telomere dysfunction in HAL-01 cells were not determined however it was shown that combination of inhibition of telomerase along with chemotherapeutic agents could be an effective approach in the treatment of acute leukemia.

Zhang et al. in 2012 demonstrated that anthracylines (doxorubicin and epirubicin) disrupt telomere maintenance, in a dose-dependent manner, through ubiquitination and proteasomal degradation of PINX1 protein which is responsible for landing of telomerase onto telomeres (B. Zhang et al., 2012). Unlike anthracyclines, other DNA damaging agents such as etoposide (Et) and camptothecin, do not show any damage at telomeric region or downregulation of PINX1 proteins. Doxorubicin and epirubicin do not affect telomerase expression or its activity but decreases PINX1 expression to induce telomere dysfunction only in telomerase positive cells. PINX1 mediated telomere dysfunction is a novel anticancer mechanism of anthracyclines which provides a new clue for the development of new anticancer drugs.

Wójcik K et al. in 2017 demonstrated the effects of daunomycin, at clinically relevant concentrations, on the linker or core histones and DNA in HeLa cells. Daunomycin causes dissociation of H1.1 linker histones from DNA without disrupting core histones of nucleosomes at lower concentrations (25 nM- 250 nM) resulting in loss of higher-order chromatin structures (Wójcik, Zarebski, Cossarizza, & Dobrucki, 2013). Binding of daunomycin to DNA causes changes in DNA structure not suitable for binding of H1.1 linker protein. Some of the detached H1.1 histones are degraded while remaining were found to be accumulated in the nucleolus of cells. However, at low concentrations (50 nM) of daunomycin, replication and transcription of cells do not stop but are slightly decreased. No immediate effect of daunomycin, at lower concentrations, is evident on cell replication, transcription or cell death. Application of lower concentrations of daunomycin (25 nM) on cells causes the morphological changes leading to apoptosis after 192 hours whereas these changes were evident only in 48 hours at concentrations ≥ 500 nM. Thus the application of daunomycin

interferes with the H1.1 linker histone binding to DNA resulting in loss of higher order chromatin structure and henceforth, effecting replication and transcription.

1.7 Scope of the thesis

The literature survey shows that the anticancer action by anthracyclines follows multiple strategies of action by targeting different forms of DNA and interferes with complex mechanisms involved in gene functioning. Ever since competition dialysis showed that daunomycin binds to G-quadruplex DNA (Ren & Chaires, 1999) besides GC rich duplex DNA, there has been a renewed interest to examine if it binds specifically to G-quadruplex DNA and determine its molecular basis of action using structural and other techniques. Apart from few studies by X-ray/NMR/ESI-MS and modeling, there are no corresponding investigations on interaction of anthracyclines with intermolecular parallel stranded G-quadruplexes on any DNA sequence containing three or four guanines, e.g. $[d\text{-}(TGGGGT)]_4$, $[d\text{-}(TTGGGGT)]_4$, $[d\text{-}(TTTGGGT)]_4$, $[d\text{-}(TTAGGGT)]_4$, etc. by optical spectroscopy methods. Several features of mode of interaction, such as end stacking, groove binding, intercalation, and external binding through electrostatic interactions as well as mechanistic insights of interaction can be evaluated by absorption, fluorescence, and CD spectroscopy. For instance, such studies could easily distinguish between the X-ray crystallographic structure of daunomycin layers stacked between two $[d\text{-}(TGGGGT)]_4$ quadruplexes (Clark et al., 2003) and that binding externally to $[d\text{-}(TGGGGT)]_4$ (Shen et al., 2017) as obtained by molecular dynamics simulations, which are totally at variance with each other. Further, corresponding thermal stabilization of intermolecular parallel G-quadruplexes has also not been reported in the literature which could substantiate if binding directly results in enhanced stability of DNA, which is a major therapeutic index for G-quadruplex based drugs. Also, the interaction of daunomycin, doxorubicin, and sabarubicin with 21/22-mer human telomeric sequence in K^+ and Na^+ rich solutions by optical spectroscopy methods were reported recently but there are no studies on G-quadruplex DNA having 4 guanines, e.g. d-TTGGGGT, the telomeric DNA sequence from *Tetrahymena thermophilia*, which forms more stable structures.

G-quadruplex structures formed by human or *Tetrahymena* telomeric DNA repeats, $(TTAGGG)_n$ and $(TGGGGT)_n$, respectively can form intermolecular (Y. Wang & Patel, 1992) or intramolecular (Y. Wang & Patel, 1993b) complexes depending upon sequence length, nature of cations, their concentration and flanking bases at 5'-/3'-end (Balagurumoorthy & Brahmachari, 1994; Smargiasso et al., 2008; Phan, Modi, & Patel, 2004; Phan & Patel, 2003; Parkinson, Lee,

& Neidle, 2002; Vorlíčková et al., 2012). Intermolecular quadruplexes are biologically relevant since they have been found to strongly interact with HIV gp120 protein acting as specific inhibitors for infection *in vitro* (Wyatt et al., 1994). The intracellular ionic environment where potassium is present in high concentrations favors tetra molecular parallel quadruplex structures over fold-back structures (Miura, Benevides, & Thomas, 1995; Sen & Gilbert, 1990; Crnugelj, Hud, & Plavec, 2002). The intermolecular types of structures have also been found to occur *in vivo* in recombination, telomere pairing, etc. (Wellinger, Wolf, & Zakian, 1993; Rhodes & Giraldo, 1995). Secondly, the conformation of the stem of these quadruplexes is very close to the central core of intramolecular parallel quadruplexes found for human telomeric repeats (Phan & Patel, 2003; Parkinson et al., 2002) or other motifs. In addition, long telomeric sequences usually exist in several folded forms with different topologies and intermolecular aggregates (Neidle, 2009; De Cian et al., 2008), which makes ligand-intramolecular G-quadruplex interactions difficult to interpret. For such cases, intermolecular quadruplexes may be visualized as simpler models of biologically relevant tetrads and several groups have used such motifs to obtain high resolution data on drug-DNA interactions (D. Sun et al., 1997; Gornall et al., 2007; N. Xu et al., 2012; Clark et al., 2003; Clark et al., 2012; Shen et al., 2017; Scaglioni et al., 2016; Y. Wang & Patel, 1992; Fedoroff et al., 1998; Cocco, Hanakahi, Huber, & Maizels, 2003; Gavathiotis et al., 2003; Gai et al., 2013). Intermolecular parallel G-quadruplexes, $[d\text{-}(TGGGGT)]_4$ and $[d\text{-}(TTGGGGT)]_4$, containing *Tetrahymena* telomeric DNA sequence have been used for interaction with various ligands e.g. PIPER (Fedoroff et al., 1998), distamycin (Cocco et al., 2003), RHPS4 (Gavathiotis et al., 2003), cyanine dye (Gai et al., 2013), mitoxantrone (Tarikere Palakshan Pradeep & Barthwal, 2016), coralyne (Padmapriya & Barthwal, 2017), palmatine (P. Kumar & Barthwal, 2018). We have selected $[d\text{-}(TTGGGGT)]_4$ since it is structurally well characterized (P. Kumar & Barthwal, 2018; Padmapriya & Barthwal, 2017; Pradeep & Barthwal, 2016). Thymine base has been added in the seventh position to avoid dimerization of TTGGGG by the end to end stacking (Y. Wang & Patel, 1992).

Daunomycin lacks selectivity of binding to DNA quadruplex over DNA duplex. While attempting to design G-quadruplex ligands as successful drugs, an understanding of the molecular basis of interactions in non-selective drugs which bind to both duplex as well as quadruplex is essential.

We have therefore undertaken a study of three anthracycline drugs, daunomycin, adriamycin, and 4' epi-adriamycin, to intermolecular parallel stranded 7-mer $[d\text{-}(TTGGGGT)]_4$ and intramolecular 22-mer $[d\text{-}GGGG(TTGGGG)_3]$ G-quadruplex DNA containing TTGGGG

telomeric DNA sequence from *Tetrahymena thermophilia* by absorption, steady state and lifetime fluorescence, CD, SPR, molecular modelling and NMR spectroscopy. Thermal denaturation of G4 DNA and its complexes with three drugs has been investigated by absorbance, CD, and DSC measurements.

The specific objectives are as follows:

- To determine the binding affinity of daunomycin, adriamycin and 4'epiadriamycin to 7-mer [d-(TTGGGGT)]$_4$ (Tet7) and 22-mer [d-GGGG(TTGGGG)$_3$] (Tet22) G4 DNA by absorption, fluorescence, CD spectroscopy and SPR techniques.
- To determine the NMR based structure of the complex of daunomycin, adriamycin, and 4'epiadriamycin with Tet7.
- To investigate binding interaction of daunomycin, adriamycin and 4'epiadriamycin 24-mer [d-(TTGGGG)$_4$] (Tet24) G4 DNA by molecular docking
- To investigate thermal stabilization of Tet7 and Tet22 on binding daunomycin, adriamycin, and 4'epiadriamycin.

This chapter deals with the description of chemicals, samples, instruments, and methodology used to perform experiments. Specific details of samples such as concentration range, D/N ratios, etc. are given within each chapter.

2.1 Chemicals and sample preparation

All chemicals i.e. desalted oligonucleotide sequences d-(TTGGGGT), d-(TTAGGGT), d-[GGGG(TTGGGG)$_3$], d-[AGGG(TTAGGG)$_3$] and 5' biotin-labeled oligos (d-(TTGGGGT) and d-[GGGG(TTGGGG)$_3$]), daunomycin, adriamycin, 4'-epiadriamycin, HEPES, KCl, K_2HPO_4, EDTA, Trimethyl Silyl Propionic acid (TSP), deuterated water (D_2O), etc. were purchased from Sigma Aldrich Co., U.S.A., Ltd. and/or from Merck chemicals and were used without any further purification. Oligonucleotide sequences were dissolved in 10 mM KBPES buffer containing 10 mM K_2HPO_4, 1 mM EDTA and 100 mM KCl (pH 7.0) and heated at 90 °C for 5 min and then allowed to cool gradually overnight for the proper quadruplex formation and stored at 4 °C. The concentration of [d-(TTGGGGT)]$_4$ (Tet7) and d-[GGGG(TTGGGG)$_3$] (Tet22) was calculated using molar absorption coefficient, ε = 65,900 and 213400 per single strand based on nearest neighbor method, respectively. A fresh stock solution of daunomycin, adriamycin and 4'-epiadriamycin was prepared every time before use. Concentration of drugs were calculated by using ε = 11,500 M^{-1} cm^{-1} at λ_{max} = 480 nm using absorption spectroscopy. List of λ_{max} with a molar absorption coefficient of DNA and ligand used in the study are given in Table 2.1.

Table 2.1 List of λ_{max} with a molar absorption coefficient of DNA and ligands

Samples	λ_{max} (nm)	Molar absorption coefficient ($M^{-1}cm^{-1}$)
d-(TTGGGGT)	260	65900
d-(TTAGGGT)	260	69800
d-[GGGG(TTGGGG)$_3$]	260	213400
d-[AGGG(TTAGGG)$_3$]	260	228500
Daunomycin	480	11500
Adriamycin	480	11500
4'-Epiadriamycin	480	11500

2.2 Surface Plasmon Resonance

Surface Plasmon Resonance experiments were done on a Biacore T200 instrument optical biosensor system (GE Healthcare). DNA samples were immobilized on to streptavidin-derivatized sensor chip (BIACORE SA) on flow cell 2 and 4. HEPES buffer (0.01 M of HEPES, 3 mM of EDTA, 0.005% P20 surfactant) containing 100 mM KCl (pH 7.4) was passed overflow cell 1 and 3 having no immobilized DNA and used as a reference. Drug solutions (1.87-960 µM) prepared in the same buffer were passed overflow cell 2 and 4 having immobilized quadruplex DNA with a flow rate 30 µl/min at 25 °C until a steady-state response was reached. The drug solutions were then replaced by regeneration buffer (1 mM NaCl and 50 µM NaOH) causing dissociation of the complex. Response from the reference cells i.e. flow cell 1 (or flow cell 3) was subtracted from corresponding flow cell 2 (or flow cell 4) to get a response from the bound ligand. Results were fitted and analyzed using Biacore T200 evaluation software available with the instrument to get binding constant (K_b).

2.3 Absorbance Measurements

Absorption studies were carried out by using CARY-100 Bio UV-visible spectrophotometer (Varian, USA) equipped with Peltier controlled thermostatic cell holder and quartz cuvette of 1 cm path length. For absorbance measurements, increasing amounts of G-quadruplex DNA (Tet7 or Tet22) were added to a fixed concentration of the drug (7 µM) to obtain drug (D) to DNA (N) molar ratios D/N = 0.16-4.6. Samples were incubated for 5 min at 25 °C before recording each spectrum at 200-800 nm. The equilibrium binding constant (K_b) was calculated according to the following equation:

$$[DNA] / (\varepsilon_a - \varepsilon_f) = [DNA] / (\varepsilon_b - \varepsilon_f) + 1 / K_b (\varepsilon_b - \varepsilon_f) \quad \ldots\ldots\ldots (1)$$

where [DNA] = [N] is the concentration of G-quadruplex DNA (Tet7 or Tet22), K_b is the equilibrium binding constant, ε_a is the apparent molar absorption coefficient (ratio of observed absorbance of drug-DNA complex to drug concentration i.e. $A_{obs}/[D]$), ε_f and ε_b refer to the molar absorption coefficient of the drug in its free and bound form, respectively.

1 µM of free quadruplex DNA [d-(TTGGGGT)]$_4$, corresponding to 4 µM single strand concentration of [d-(TTGGGGT)], was used to obtain a melting profile of free DNA by absorbance measurements. Appropriate amounts of drug were added to it to get samples of the

complex at D/N = 0.5, 1.0, 2.0, 3.0, and 4.0. Each sample was scanned from 20-90 °C with a scan rate of 1°C/min at 260 nm. Melting temperature (T_m) was obtained from the plot of the rate of change of absorbance (A) with respect to temperature (T), that is, dA/dT versus temperature for each sample.

2.4 Fluorescence Measurements

Fluorescence experiments were performed by using Fluorolog-3 spectrofluorimeter (Horiba Jobin Yvon, Japan). Drug molecules were excited at λ_{ex} = 480 nm and the emission spectra were recorded in the wavelength range of 520-650 nm at 25 °C. The fluorescence quenching constant (K_{sv}), binding constant (K_b) and stoichiometry of complex (n) were calculated by the following equations:

$$F_0 / F = 1 + K_{sv} [DNA] \quad \text{..... (2)}$$

$$\log [(F_0 - F) / F] = \log K_b + n \log [DNA] \quad \text{..... (3)}$$

where F_0 and F are the fluorescence intensities in the absence and presence of quadruplex DNA at 592 nm, [DNA] = [N] is the concentration of G-quadruplex DNA (Tet7 or Tet22), n is the stoichiometry of complex and K_{sv} is the Stern-Volmer quenching constant. The plot of log [(F_0 - F) / F] versus log [DNA] yielded K_b and n whereas the plot of F_0 / F versus [DNA] yielded K_{sv}. To obtain binding constants for binding of two molecules of the drug to DNA, we tried to fit the data in non-linear curve fitting regression analysis by giving user-defined equation written in OriginPro 2018 (Thordarson, 2011; Hargrove, Zhong, Sessler, & Anslyn, 2010). In case of 2:1 stoichiometry, where two drug (D) molecules bind to a single DNA (N) molecule, we get a cubic equation instead of a quadratic equation involving two binding constants K_{b1} and K_{b2} which is represented by the following equation:

$$F = k_0 * C_f + \left\{ \frac{k_1 K_{b_1} C_f + k_2 K_{b_1} K_{b_2} C_f^2}{1 + K_{b_1} C_f + K_{b_1} K_{b_2} C_f^2} \right\} C_{Nt} \quad \text{..... (4)}$$

where, F is the observed fluorescence intensity, k_0, k_1, k_2 are the proportionality constants, C_f is the concentration of the free drug, C_{Nt} is total DNA concentration. Newton's method of minimization was used to iteratively determine the free drug concentration at every data point.

Time-resolved fluorescence measurements were carried out in Fluoro-Cube-Fluorescence lifetime system, (Horiba Jobin Yvon, Japan) operating in a time-correlated single photon counting (TCSPC) mode equipped with Nano LED (λ_{ex} = 456 nm and λ_{em} = 590 nm) using a 10 mm path length quartz cuvette at 25 °C. All decay traces were measured using 2048 channel analyzer. The lifetime values were calculated for 7 μM of free drug and its complexes with G-quadruplex DNA (Tet7 or Tet22) at D/N = 0.3, 0.5, 1.0, 2.0, 3.0 and 4.0. Typical parameters for these experiments were: time resolution = 0.2 ns, accuracy = ±0.5 nm, speed = 150 nm/s, TAC range = 200 ns. The data were fitted using a re-convolution method provided with the DAS 6.3 software producing best chi-square values; the error was obtained from the standard deviation of fitted curves.

2.5 Job Plot using Fluorescence

Continuous variation analysis procedure i.e. Job plot was used to establish the binding stoichiometry of drug-DNA complex using fluorescence spectroscopy. The fluorescence emission was measured at λ_{em} = 592 nm using λ_{ex} = 480 nm at a constant temperature of 25 °C. The relative mole fractions of G-quadruplex DNA (Tet7 or Tet22) and drug were varied keeping the total concentration of DNA and drug constant at 4 μM (or 7 μM). The difference in fluorescence intensity of free (F_0) and bound (F) drug (i.e. $\Delta F = F_0$-F) was plotted as a function of mole fraction of drug. The inflection point indicates the change in slope which gives the stoichiometry of drug bound to G-quadruplex DNA according to the following equation:

$$\mathbf{n} = \frac{\boldsymbol{\chi}_{\mathbf{drug}}}{\mathbf{1} - \boldsymbol{\chi}_{\mathbf{drug}}} \qquad \text{..... (5)}$$

where $\boldsymbol{\chi}_{\mathbf{drug}}$ is mole fraction of drug at the point of inflection and n is stoichiometry of the complex.

2.6 Circular Dichroism (CD) Measurements

CD experiments were performed using model Chirascan (Applied Photophysics, UK) spectropolarimeter equipped with Quantum North West TC 125 Peltier unit-controlled sample compartment using quartz cuvette of 10 mm path length. Before igniting xenon lamp and throughout the course of experiments, the instrument was continuously purged with pure nitrogen gas using nitrogen generator (make SAS F-DGS, Every, France model HPNG10/1). The CD spectra were recorded at 25 °C using 10 mm quartz cuvette in the range of 200-600

nm, bandwidth = 1 nm, step size = 0.5 nm and time per point = 0.25 s. During titrations, the concentration of G-quadruplex DNA (Tet7 or Tet22) was kept constant as 15.0 μM (or 10.0 μM) and the drug was added progressively to it at D/N = 0.1-5.0. In another set of experiments, drug concentration was kept constant at 400 μM and DNA was added stepwise at D/N = 0.5-5.0 at 25 °C. The final spectra were averaged over two scans, baseline subtracted and smoothed by using the Savitzky-Golay algorithm provided by Chirascan software.

To obtain binding constants for 2:1 stoichiometry, we tried to fit the CD data in non-linear curve fitting regression analysis by giving user-defined equation written in OriginPro 2018 (Thordarson, 2011; Hargrove et al., 2010) using the equation:

$$CD = k_0 * C_f + \left\{\frac{k_1 K_{b_1} C_f + k_2 K_{b_1} K_{b_2} C_f^2}{1 + K_{b_1} C_f + K_{b_1} K_{b_2} C_f^2}\right\} C_{Nt} \quad \text{..... (6)}$$

where CD is the observed ellipticity (mdegree). Thermal melting studies of 10 μM of free quadruplex DNA [d-(TTGGGGT)]$_4$ its complex with drug at D/N = 0.5, 1.0, 2.0, 3.0 and 4.0 were performed in temperature range 25-90 °C at the rate of 1 °C/min at 265 nm in steps of 3 °C. Melting temperature (T_m) was obtained from the plot of derivative of CD (θ) with respect to temperature (T), that is, dθ/dT versus temperature.

2.7 Molecular Docking studies

Molecular docking experiment for drug binding with G-quadruplex DNA (Tet7 or Tet24) was performed using Autodock 4.2 software package to obtain the binding mode and insight into the crucial functional group interacting with the quadruplex sequence. Structure of tetramolecular quadruplex DNA [d-(TTGGGGT)]$_4$ and unimolecular quadruplex DNA d-[TTGGGG(TTGGGG)$_3$] were obtained from PDB ID: 139D and PDB ID: 186D, respectively. Three-dimensional (3D) conformer of daunomycin, adriamycin and 4'-epiadriamycin were obtained from PubChem CID: 30323, 31703 and 41867, respectively. Necessary files (i.e. PDBQT files) for both drug and quadruplex DNA were prepared by removing water and adding Gasteiger charges and polar hydrogens. The size of the grid was set up using AutoGrid program with grid points 0.375 Å apart and x, y and z dimensions of 60 Å x 60 Å x 60 Å to enclose DNA molecule. Docking calculations were done using the Lamarckian algorithm for 50 docking runs with 25,000,000 energy evaluations for each run. Best conformations having lowest binding energies were selected for analysis. The docked poses were analyzed in PyMol software.

2.8 Nuclear Magnetic Resonance

1.03-2.13 mM of G-quadruplex DNA (Tet7 or Tet22) was prepared by heating DNA sequence in 10 mM KBPES buffer (in 90% H_2O + 10% D_2O solvent or 100% D_2O solvent) containing 10 mM K_2HPO_4, 1 mM EDTA and 100 mM KCl (pH 7.0) at 90 °C for 5 min and kept overnight at room temperature. The stock solution of the drug was prepared in water and titration of the drug to DNA was done to obtain different D/N ratios. All NMR spectra were recorded in 500 MHz Bruker Avance NMR spectrometer equipped with TXI (triple inverse probe) probe, BBO (Broad Band Observed probe) probe and BVT (Variable Temperature Unit) at Central NMR Facility, IIT Roorkee, India. All the parameters and pulse programs used in the present study were obtained from Bruker pulse program catalog. ^{1}H and ^{31}P resonances were calibrated using 0.1 µl of 0.1 M Trimethyl Silyl Propionic acid (TSP) as standard internal reference and 85% phosphoric acid as an external reference, respectively.

2.8.1 One Dimensional NMR experiments

One dimensional (1D) ^{1}H spectra were recorded with zgpr pulse program from Bruker library parameters for achieving water suppression with data points (TD) = 64 K, number of scans (NS) = 64-128, pulse width (P1) = 11.49-14.9 µs, spectral width (SW) = 20 ppm, relaxation delay (D1) = 2.0 s at 25 °C, 30 °C and 35 °C. 1D ^{31}P spectra were recorded at different temperatures by pulse program zgpg30 with TD = 64 K, NS = 64-128, P1 = 13.60-14.9 µs, SW = 10 ppm, D1 = 2.0 s. Thermal melting studies were performed by acquiring 1D ^{1}H NMR spectra of free [d-(TTGGGGT)]$_4$ and drug-[d-(TTGGGGT)]$_4$ complexes at D/N ratio = 1.0-4.0 in the range of 25 °C to 80 °C. All samples were incubated for 10 min at respective temperatures before performing any experiment.

2.8.2 Two Dimensional (2D) NMR experiments

Details and experimental parameters for two dimensional NMR experiments are discussed below.

2.8.2.1 Two dimensional ^{1}H-^{1}H NOESY experiments

Nuclear Overhauser Effect SpectroscopY (NOESY) experiment is mostly used to obtain distances among protons in macromolecules like DNA, RNA and protein to determine their structure and conformation (Jeener, Meier, Bachmann, & Ernst, 1979) (A. Kumar, Wagner,

Ernst, & Wüthrich, 1981; Ulyanov & James, 1995). It based on the principle of Nuclear Overhauser Effect (NOE) which is a relaxation parameter of two spatially close nuclear dipole moments (up to 5 Å in a 500 MHz NMR spectrometer). The relaxation results from nuclear dipole-dipole interaction leading to NOE cross peaks (or correlation) and its intensity depends on the distance between two interacting nuclei. The NOESY pulse program used in our study contains three 90° pulses (Fig. 2.1).

First 90° pulse turns magnetization in the x-y plane. So after a time delay of t_1, different spins of nuclei (having different chemical shift values) have the different extent of magnetization in the x-y plane. Now another 90° pulse turns magnetization to the z-axis and during mixing time (τ_m) cross relaxation occurs for transfer of magnetization between neighboring protons. Mixing time is kept constant throughout the experiment. The third 90° pulse rotates the magnetization again into the x-y plane and it is recorded during acquisition time t_2 yielding 2D NOESY spectra after Fourier transformation with cross peaks corresponding to two different chemical shifts.

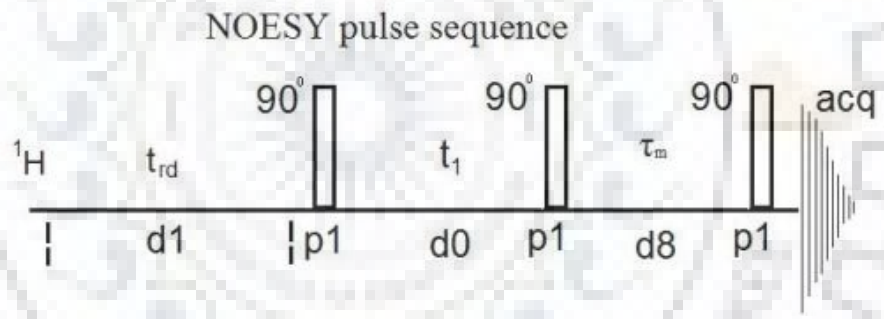

Figure 2.1 Pulse program of 2D NOESY Pulse program used for NOESY NMR experiments (adopted from Bruker training course manual, © Sep2005, Bruker AG, Switzerland).

2D ^{1}H-^{1}H NOESY experiments were done using pulse program noesyphpr with States-TPPI mode in TXI probe at 25 °C along with mixing time (τ_m) = 400 ms, 250 ms, 200 ms and 100 ms, NS = 64, data size = 256 (t_1) x 2048 (t_2), P1 = 11.49-14.9 µs, SW = 20 ppm on both F1 and F2 dimensions and D1= 1.9 s at D/N = 1.0, 2.0, 3.0 and 4.0. Interproton distances were calculated using isolated spin pair approximation (ISPA) method from 2D ^{1}H-^{1}H NOESY spectra of complex recorded at 25 °C using τ_m = 250 ms as it is within linear approximation range. Integration of well-separated cross peak volume was done using SPARKY software 3.114 and subsequently, distances were calculated using thymine H6-CH_3 as a reference distance (2.95 Å) assuming NOE cross peak intensity to be inversely proportional to the sixth power of distance. A range of ±0.5 Å was used as distance restraints to avoid errors during integration.

2.8.2.2 Two dimensional ^{1}H-^{1}H COSY experiments

COrrelation SpectroscopY (COSY) experiments give information about spin-spin coupling constants obtained from two bond (or germinal) and three bond (or vicinal) scalar coupling. The vicinal coupling constant (^{3}J) can be used to get dihedral angle applying Karplus equation (Schmidt, Blümel, Löhr, & Rüterjans, 1999; Lohr, Mayhew, & Rüterjans, 2000). COSY pulse program contains one 90° pulse which rotates magnetization to x-y plane followed by an evolution time (t_1) (Fig. 2.2). During t_1, nuclei with different chemical shift value differ in the extent of magnetization. Another 45° pulse causes the transfer of magnetization between coupled nuclei giving cross peaks both above and below diagonal. COSY spectra were obtained pulse program cosygpqf following acquisition parameters: NS=32, data size=256 (t_1) × 2048 (t_2) complex points, SW=20.0 ppm along both F1and F2 dimension, D1=1.2-1.5 s.

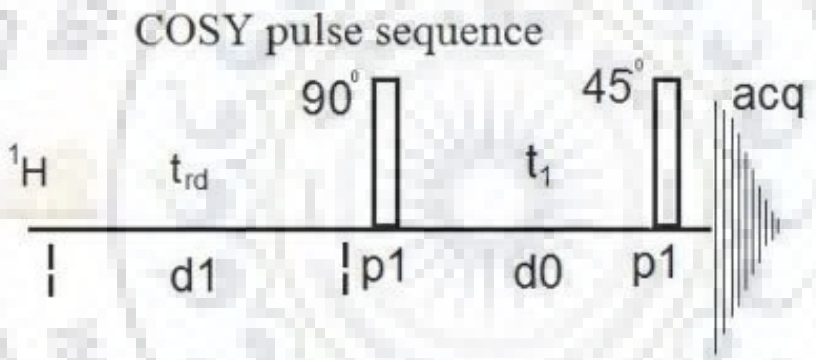

Figure 2.2 Pulse program used for COSY NMR experiments (adopted from Bruker training course manual, © Sep2005, Bruker AG, Switzerland).

2.8.2.3 Two dimensional ^{1}H-^{1}H ROESY experiments

Rotating-frame Overhauser Effect SpectroscopY (ROESY) experiment is used to obtain the NOE correlation of small molecules through dipolar coupling under spin-locked conditions. Pulse sequence consists of a 90° pulse which is followed by evolution time of t_1 and spinlock period which a mixing time after which acquisition of proton signals is done. It is similar to a NOESY experiment except that cross relaxation is observed from x-axis in spin-locked condition rather than initial magnetization in the z-axis (Fig. 2.3). ^{1}H-^{1}H ROESY spectra were acquired for drug molecules in States-TPPI mode and pulse program roesyphpr using the following acquisition parameters, spinlock duration (p15)=200 ms, NS=32, data size=256 (t_1) × 2048 (t_2) complex points, SW=20.0 ppm along both F1 and F2 dimension, D1=1.2 s.

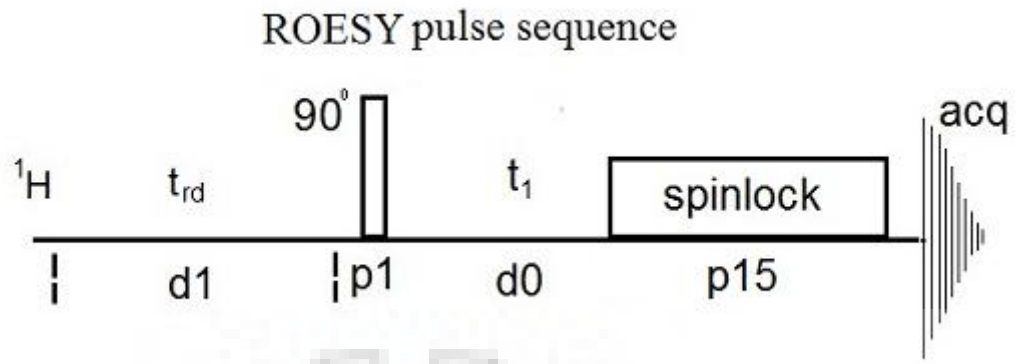

Figure 2.3 Pulse program used for ROESY NMR experiments (adopted from Bruker training course manual, © Sep2005, Bruker AG, Switzerland).

2.8.2.4 Two dimensional ^{13}C-^{1}H HSQC experiments

Hetero-nuclear Single Quantum Correlation (HSQC) experiments are used to find out correlation among directly bound nucleus through a single covalent bond (Bax & Subramanian, 1986). HSQC experiments are based on the transfer of magnetization from ^{1}H to X nuclei (usually ^{13}C or ^{15}N) using the Insensitive Nuclei Enhanced by Polarization Transfer (INEPT) sequence. A trim pulse is also used in hsqcetgpsi pulse program during a first INEPT sequence for suppression of long-range ^{13}C-^{1}H couplings. The first INEPT step is used to create proton antiphase magnetization which is then transferred to the directly attached X nuclei. The X nuclei magnetization evolves with its chemical shift during t_1 (evolution time). A gradient experiment is used to improve the quality of spectra and to obtain spectra in a shorter time since phase cycling is reduced (Fig. 2.4). 2D ^{13}C-^{1}H HSQC experiments were carried out in TXI probe to find out the proton and carbon correlation of free drug, free DNA and drug-[d-(TTGGGGT)]$_4$ complexes (i.e. D/N = 1.0, 2.0, 3.0 and 4.0) at 25 °C using pulse program hsqcetgpsi with NS = 64, data size = 256 (t_1) x 2048 (t_2), SW = 200 ppm in F1 dimension and 20 ppm in F2 dimensions and D1 = 1.9 s.

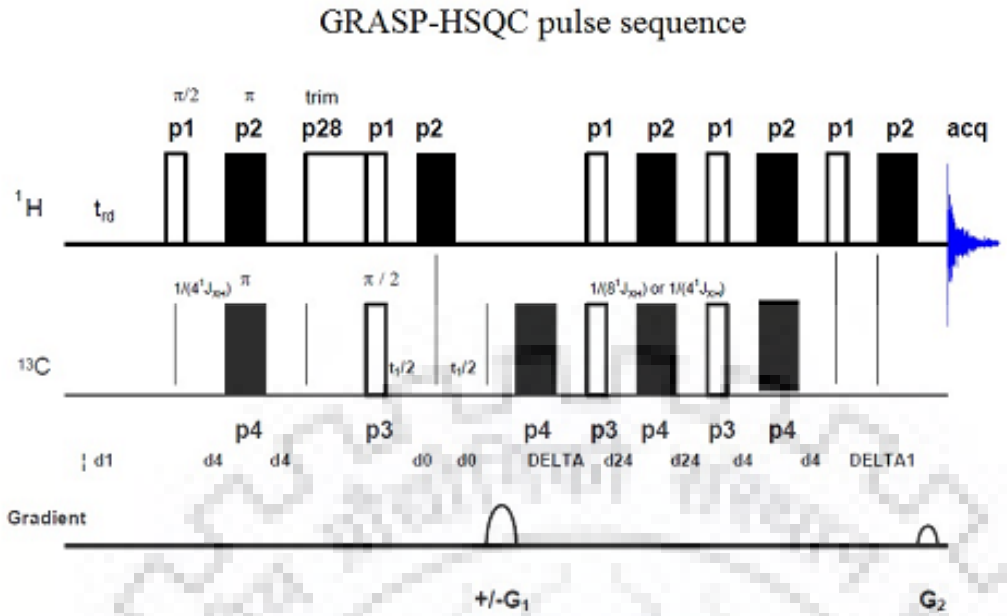

Figure 2.4 Pulse program used for HSQC NMR experiments (adopted from Bruker training course manual, © Sep2005, Bruker AG, Switzerland).

2.8.2.5 Two dimensional ^{1}H-^{31}P HMBC experiments

Heteronuclear Multiple Bond Correlation (HMBC) experiment is used to obtain a correlation between long-range coupled heteronuclei. present study ^{1}H-^{31}P HMBC experiments was done for assignment of ^{31}P in the backbone of DNA which gives correlation with H3′ and H5′/5″ deoxyribose sugar protons which are 2 and 3 bonds away though scalar coupling (Sklenár & Bax, 1987). Since the HMBC experiment gives long-range scalar couplings, a low pass J-filter is used to suppress single bond correlation (Fig. 2.5). The intensity of the respective resonance is directly proportional to the magnitude of coupling constant. 2D ^{1}H-^{31}P HMBC experiments were recorded in BBO probe using pulse program hmbcgpndqf (gradient) at 25 °C with NS = 64, data size = 256 (t_1) x 2048 (t_2), SW = 10 along F1 dimension and 20 ppm along F2 dimension and D1 = 1.9 s at D/N = 1.0, 2.0, 3.0 and 4.0.

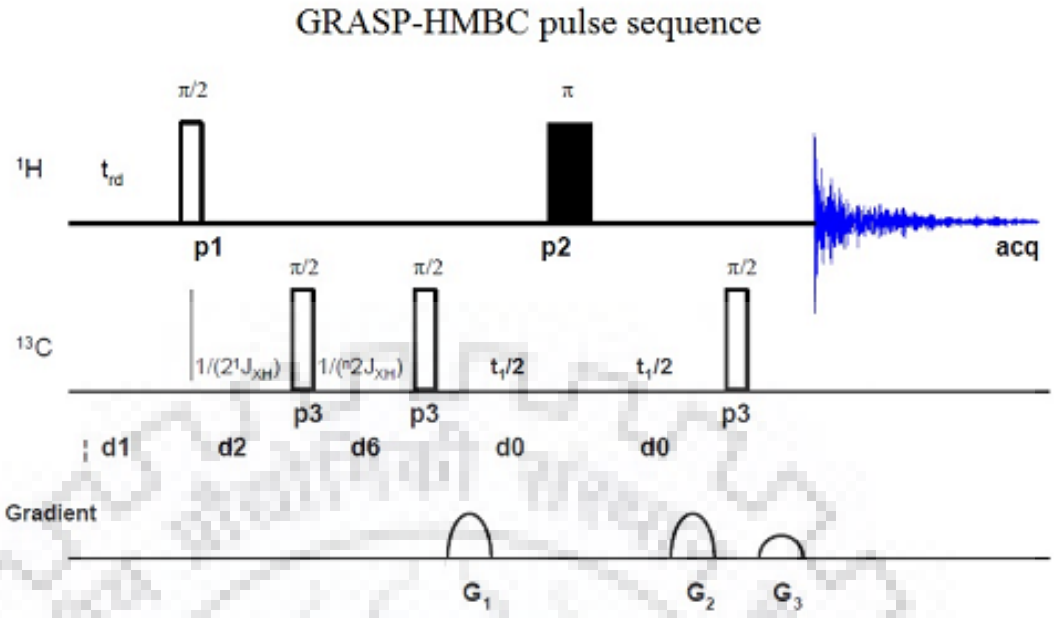

Figure 2.5 Pulse program used for HMBC NMR experiments (adopted from Bruker training course manual, © Sep2005, Bruker AG, Switzerland).

2.8.2.6 Diffusion Ordered SpectroscopY (DOSY) experiments

Diffusion Ordered SpectroscopY (DOSY) experiment is used to measure the diffusion coefficient of molecules in solution. Diffusion of any molecule is dependent on size and shape, temperature and viscosity of the medium. A pulse field gradient is used to spatially label the molecule position by a process called q -space imaging (Stejskal & Tanner, 1965**;** Wu, Chen, & Johnson, 1995; Johnson, 1999). The NMR signal is measured as an integral over the whole sample volume and the signal intensity is attenuated according to the diffusion time (Δ), diffusion gradient length (δ), the strength of the gradient (G_z) parameters used in the experiment.

DOSY spectra was acquired for free drug, free quadruplex DNA $[d(TTGGGGT)]_4$ and drug-$[d(TTGGGGT)]_4$ complex using the following acquisition parameters: pulse program = ledbpgppr2s, data points = 16 K, spectral width = 20.0 ppm in F2 direction and 16 free induction decays in F1 direction with number of scans (NS) = 8. During the experiment, diffusion time (Δ or D20) = 50 ms and diffusion gradient length (δ or P30) = 2.2 ms were kept constant while the gradient range was varied from 5 to 95 G/cm in 16 steps with a linear ramp at 25 °C. The gradient shape SMSQ 10 and 100 were used with eddy current D21 = 5 ms. The diffusion coefficients were measured from DOSY experiment using the relation between

translational self-diffusion and the measurable NMR parameters, as given by the following equation:

$$I/I_0 = - \exp [D_t\gamma_H^2\delta^2G_z^2 (\Delta-\delta/3)] \quad \text{……..... (7)}$$

where I is the measured peak intensity (or volume), I_0 is the maximum peak intensity, D_t is the translational diffusion constant (m^2/s), γ_H is the gyromagnetic ratio of a proton ($2.67x10^4$ G^{-1} s^{-1}), δ is the duration of the gradient, Δ is the time between gradients and G_z is the strength of the gradient (in G/cm). Data were plotted as –ln (I/I_0) versus $\gamma_H^2\delta^2G_z^2$ (Δ-δ/3) and D_t was calculated from the slope of the plot. The diffusion coefficient (D_t) is obtained from the slope of the linear graph of –ln (I/I_0) versus $\gamma_H^2\delta^2G_z^2$ (Δ-δ/3) using diffusion-decay curve fitting carried out with SimFit algorithm in Topspin 3.5.

To estimate the binding affinity of the drug NMR titration data of the drug-DNA complex was used. We tried to fit the data in non-linear curve fitting regression analysis by giving a user-defined equation in OriginPro 2018 (Hargrove et al., 2010).

$$\boldsymbol{\delta_b - \delta_f = \frac{k_0-k_1}{2}\left\{\left(C_t + C_{N_t} + \frac{1}{K_b}\right) - \sqrt{\left(C_t + C_{N_t} + \frac{1}{K_b}\right)^2 - 4C_tC_{N_t}}\right\}} \quad \text{…..... (8)}$$

where δ_f and δ_b are the chemical shift (ppm) values of free $[d(TTGGGGT)]_4$ and drug-$[d(TTGGGGT)]_4$ complex respectively, k_0 and k_1 are the proportionality constants, C_t and C_{Nt} are the total concentrations of drug and nucleotide respectively, K_b is the binding affinity.

2.9 Restrained Molecular Dynamics simulations

The restrained Molecular Dynamics (rMD) simulations were done on Silicon Graphics Fuel workstation enabled with INSIGHT II (version 2005) and DISCOVER software program. The initial structure of G-quadruplex DNA $[d-(TTGGGGT)]_4$ was obtained from PDB ID: 139D and was used further by replacing aromatic bases in biopolymer module of INSIGHT II (version 2005) for maintaining the potential setup. Initial structures of drugs were constructed using restraints obtained from NOE cross peaks builder module of INSIGHT II (version 2005). Distances were categorized as strong (s) = 2.0-3.0 Å, medium (m) = 3.0-4.0 Å and weak (w) = 4.0-5.0 Å. Upper and lower bounds of distances were set as 0.5 Å for intermolecular restraints. Force constant of 10.0 kcal mol^{-1} $Å^{-2}$ was used for each NOE contacts. Drug molecules were placed manually at the position and distance obtained from NOE cross peaks and minimized

using 1000 steps of steepest descent and conjugate gradient using a Constant Valence Force Field (CVFF) force field in DISCOVER software (version 2005). Simulated annealing restrained molecular dynamics protocol was used for conformational search. The molecule was heated to 800 K in steps of 100 K so that chances of the molecule being trapped in local minima is lost and reaches to global minima. Molecular dynamics simulations were carried out for 1000 iterations with a time step of 1 fs at 800 K. The molecule was annealed from 800 K to 300 K with 100 K steps (each step with 100 runs) using MD runs of 1000 iterations of 1 fs each thus a total of 600 ps. In the end, all structures were minimized 1000 steps Steepest Descent until a predefined convergence limit of root mean square derivative of <0.001 kcal mol^{-1} $Å^{-1}$ was reached. Total of 10 lowest structures was chosen for RMSD analysis out of 100 structures save at regular interval of 10 fs during the final step of molecular dynamics.

2.10 Differential Scanning Calorimetry

Excess heat capacity as a function of temperature was measured to obtain thermal transitions of free G-quadruplex DNA (Tet7 or Tet22) and its complexes with the drug at D/N ratio = 0.5-4.0 using MicroCal VP-DSC instrument (MicroCal, Northampton, MA). All samples were prepared in 10 mM KBPES buffer containing 10 mM K_2HPO_4, 1 mM EDTA and 100 mM KCl (pH 7.0). All samples were properly degassed before the experiment. Each sample was scanned from 25 to 120 °C with a scan rate of 60 °C/h at approximately constant pressure ~ 33 psi. Buffer was scanned repeatedly under similar conditions as that of the sample until the proper baseline was obtained. 50 µM of free G-quadruplex DNA (Tet7 or Tet22) was scanned to obtain the melting profile of free DNA. Each set of the complex with increasing drug concentrations and fixed G-quadruplex DNA (Tet7 or Tet22) concentration of 50 µM at D/N ratio = 0.5-4.0 were scanned to obtain the melting profile of bound forms. Each scan was subtracted from the buffer baseline. The thermograms were then deconvoluted and fitted in 2, 3 or 4-state model of unbound quadruplex DNA and its complexes using Origin 7.1 software provided with the instrument.

3.1 Introduction

Recent findings in literature point towards the role of daunomycin/adriamycin in disruption of telomere maintenance (Elmore et al., 2002; Ogretmen et al., 2001; Nakajima et al., 2003; Sabatino et al., 2010; Zhang et al., 2012; Hussner et al., 2012). These findings demonstrate that anthracyclines bind to different forms of DNA, involving mechanisms which are not well understood. Several features of mode of interaction, such as end stacking, groove binding, intercalation, and external binding through electrostatic interactions as well as mechanistic insights of interaction can be evaluated by absorption, fluorescence, and CD spectroscopy. For instance, such studies could easily distinguish between the X-ray crystallographic structure of daunomycin layers stacked between two [d-(TGGGGT)]$_4$ quadruplexes (Clark et al., 2003) and that binding externally to [d-(TGGGGT)]$_4$ (Shen et al., 2017), which are totally at variance with each other. Further, the corresponding thermal stabilization of intermolecular parallel G-quadruplexes has also not been reported in the literature. We have monitored titrations of daunomycin (Fig. 3.1) with [d-(TTGGGGT)]$_4$ (Tet7) (Fig. 1.9) by absorbance, steady state & lifetime fluorescence, and CD spectroscopy. We have also obtained melting profiles of daunomycin-DNA complexes at varying Daunomycin (D) to Nucleic acid (N) ratios (D/N). The findings have been supplemented by two-dimensional ^{1}H-^{1}H Nuclear Overhauser Enhancement SpectroscopY (NOESY) experiments which give short interproton distance contacts. The docking of daunomycin with Tet7 throws light on the mode of interaction.

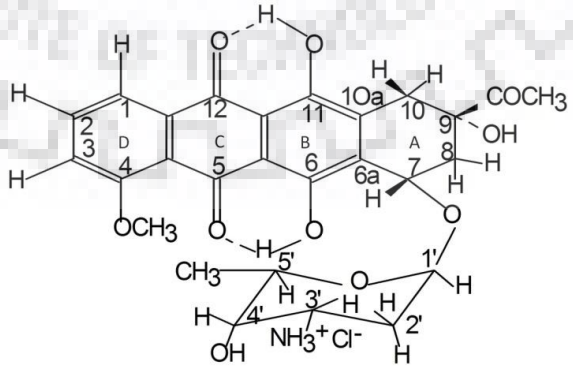

Figure 3.1 Chemical structure of daunomycin.

3.2 Materials and Methods

Details of Materials and Methods are given in Chapter 2. For absorbance measurements, increasing amounts of Tet7 were added to 7 μM daunomycin to obtain daunomycin (D) to DNA (N) molar ratios D/N = 0.16-4.6 in a set of 34 samples. 1 μM of free quadruplex DNA $[d\text{-}(TTGGGGT)]_4$, corresponding to 4 μM single strand concentration of [d-(TTGGGGT)], was used to obtain a melting profile of free DNA by measuring absorbance at 260 nm. Appropriate amounts of daunomycin were added to it to get samples of complex at D/N = 0.5, 1.0, 2.0, 3.0, and 4.0 and each sample was scanned from 20-90 °C with a scan rate of 1°C/min at λ = 260 nm to get absorbance as a function of temperature. Fluorescence measurements were performed on the same samples as that used in absorbance studies by exciting daunomycin at λ_{ex} = 480 nm and the emission spectra were recorded in the wavelength range of 520-650 nm at 25 °C. The lifetime values were calculated for 7 μM free daunomycin and its complexes at D/N = 0.3, 0.5, 1.0, 2.0, 3.0 and 4.0 using λ_{ex} = 456 nm and λ_{em} = 590 nm. For titrations monitored by CD spectroscopy, daunomycin was added progressively to 15.0 μM Tet7 at D/N = 0.1-5.0 in a set of 31 samples. In another set of experiments, DNA was added stepwise to 400 μM daunomycin at D/N = 0.5-4.9 in a set of 12 samples at 25 °C. Thermal melting studies of 10 μM of free quadruplex DNA Tet7 and its complex with daunomycin at D/N = 0.5, 1.0, 2.0, 3.0 and 4.0 were performed in temperature range 25-90 °C by heating at the rate of 1 °C/min in steps of 3 °C and measuring CD at 265 nm. For molecular docking studies, the structure of tetramolecular quadruplex DNA Tet7 was obtained from PDB ID: 139D. Three-dimensional (3D) conformer of a drug molecule was obtained from PubChem CID: 30323. 1.16 mM of G-quadruplex DNA Tet7 and its complex at D/N = 3.0 was used for NMR studies.

3.3 Results and Discussion

3.3.1 Absorption

Daunomycin shows absorption maxima at 290 and 481 nm which has been attributed to $^1A \rightarrow {}^1L_a$ and $^1A \rightarrow {}^1L_b$ π-π* transitions polarized along the short and long axis of the chromophore, respectively. The band at 481 nm in visible range strongly depends on self-aggregation but is insensitive to the protonation of the daunosamine moiety (Manet, Manoli, Zambelli, Andreano, Masi, Cellai, & Monti, 2011). A concentration of 7 μM was used to carry out titrations with G-quadruplex DNA sequence since daunomycin undergoes self-association at concentrations >10 μM (Chaires, Dattagupta, & Crothers, 1982; Agrawal, Barthwal, & Barthwal, 2009). Stepwise

addition of Tet7 up to D/N = 0.16 (selected data are shown in Fig. 3.2 a) results in hypochromism of ~55% at 481 nm (inset of Fig. 3.2 a) accompanied by redshift $\Delta\lambda_{max}$~3 nm. Classical intercalation of ligands in duplex DNA result in redshift $\Delta\lambda_{max}$ = 20-45 nm while partial stacking in quadruplex DNA show red shift $\Delta\lambda_{max}$ ~15 nm (Tarikere Palakashan Pradeep & Barthwal, 2016). The observed minor shift is indicative of the external binding of daunomycin to Tet7. The data does not show any isosbestic point in the entire region of D/N ratios indicating the presence of multiple daunomycin-DNA complexes. The plot of reciprocal of absorbance, 1/A versus D/N, shows inflection points at D/N = 1.0 and 2.0 due to change in slope (Fig. 3.2 b) so that stoichiometry of daunomycin-DNA complexes is likely to be 1:1 or 2:1. Using equation (1), we get intrinsic binding constant K_b = 1.6-6.8 x10^5 M^{-1} which may be considered as a rough estimate (Fig. 3.2 c). The Scatchard plots are nonlinear and do not fit into a combination of straight lines and therefore cannot be used to estimate affinity constant K_b with confidence. This may be due to the presence of two stoichiometries as well as multiple conformations so that the affinity constant may actually be considered as an average value (Manet, Manoli, Zambelli, Andreano, Masi, Cellai, & Monti, 2011). There are no such investigations on the binding of daunomycin to short DNA sequences having pure parallel stranded G-quadruplex conformations in literature.

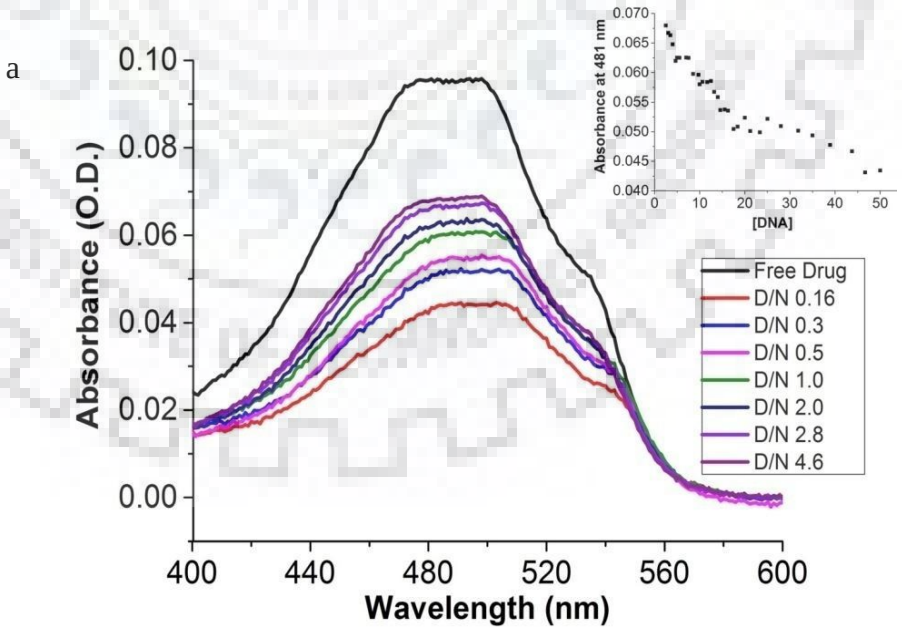

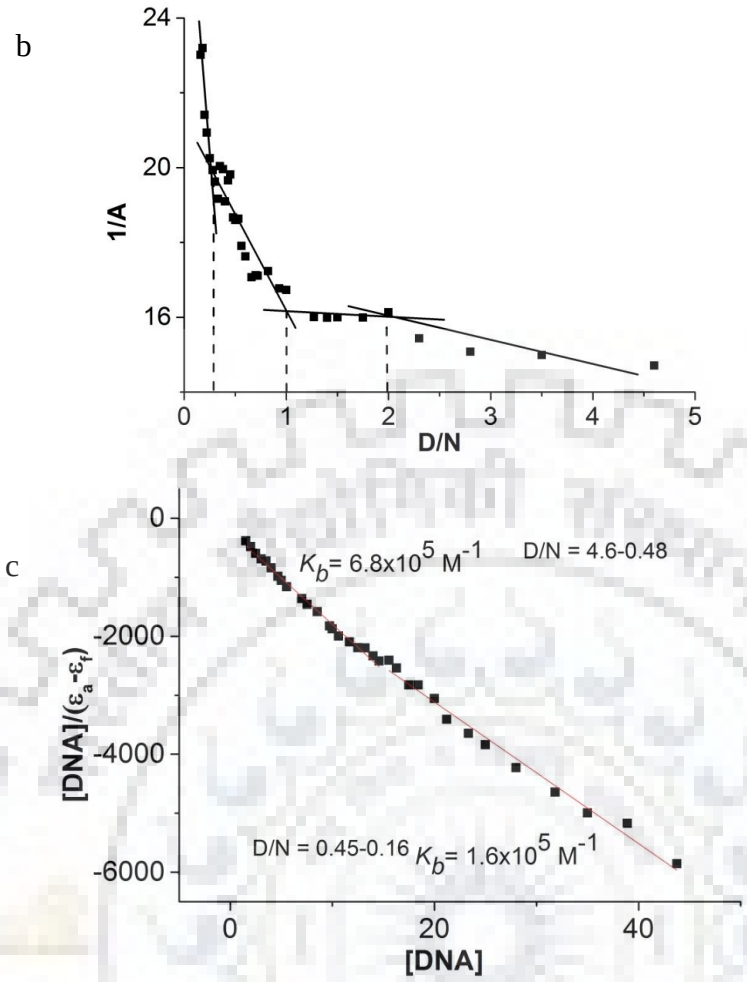

Figure 3.2 a) Titrations of 7 µM daunomycin with increasing concentration of Tet7 at D/N = 0.16-4.6 (data at some selected D/N ratios shown). The inset shows plot of absorbance at 481 nm as a function of DNA concentration [DNA] in µM; b) Plot of reciprocal of absorbance (1/A) as a function of D/N ratio at 481 nm; c) Plot of [DNA]/(ε_a-ε_f) as a function of concentration of DNA, [DNA], in µM at 481 nm for D/N = 0.48-4.6 and D/N = 0.16-0.46 yielding value of binding constants (K_b).

3.3.2 Fluorescence

Excitation of daunomycin at 480 nm results in intense emission having maxima at 557 and 592 nm which has been assigned to $^1A \rightarrow {}^1L_b$ transition (Manet, Manoli, Zambelli, Andreano, Masi, Cellai, & Monti, 2011). Addition of Tet7 results in quenching of fluorescence intensity up to 95% at D/N = 0.16 accompanied by a redshift $\Delta\lambda_{em}$ = 2-4 nm in both the emission maxima (selected data shown in Fig. 3.3 a) indicating strong interaction. A plot of 1/F versus D/N shows (Fig. 3.3 b) inflection at D/N = 0.5, 1.0 and 2.0. The Stern-Volmer plot showing F_0 / F versus concentration of DNA (Fig. 3.3 c) and plot of log [(F_0 - F) / F] versus log [DNA] (Fig. 3.3 d) using equations (2) and (3), respectively give K_{SV} and K_b in the range 1.6-6.9x10^5 M^{-1}.

The bimolecular quenching constant, Kq~4×10^{14} $M^{-1}s^{-1}$, obtained by using K_{sv} = 4.0x10^5 M^{-1} and fluorescence lifetime τ = 1.0 ns is much greater than collision constant for a biomolecule and small molecule as a ligand, i.e. 2×10^{10} $M^{-1}s^{-1}$, excluding the possibility of any dynamic quenching. Presence of static quenching owing to ground state interactions is also evident from the accompanying changes in absorbance and no change in fluorescence lifetime (discussed later). The fluorescence data gave very good fit in equation (4) for 2 independent binding sites (Thordarson, 2011; Hargrove, Zhong, Sessler, & Anslyn, 2010) having K_{b1} = 6.3x10^5 M^{-1} and K_{b2} = 1.3x10^5 M^{-1} (Fig. 3.3 e). Alternate models of exclusive 1:1 or 2:1 or higher stoichiometries yielded unsatisfactory fits.

The fluorescent decay of daunomycin was measured using time-correlated single photon counting using $\Delta\lambda_{ex}$ = 456 nm and $\Delta\lambda_{em}$ = 590 nm at 25 °C. The decay was monoexponential with lifetime τ = 1.03 ns (Fig. 3.3 f). The decay for several complexes at D/N = 0.3, 0.5, 1.0-4.0 remained monoexponential with lifetime τ = 0.97-1.00 ns (Fig. 3.3 f, Table 3.1). This may be due to similar values of a lifetime for free and bound daunomycin; alternately if both complexes are non-emissive (Manet, Manoli, Zambelli, Andreano, Masi, Cellai, & Monti, 2011), the observed lifetime is due to free daunomycin itself. Similar results have been reported on the binding of doxorubicin to the 21-mer human sequence in the literature (Manet, Manoli, Zambelli, Andreano, Masi, Cellai, Ottani, et al., 2011; Manet, Manoli, Zambelli, Andreano, Masi, Cellai, & Monti, 2011).

a

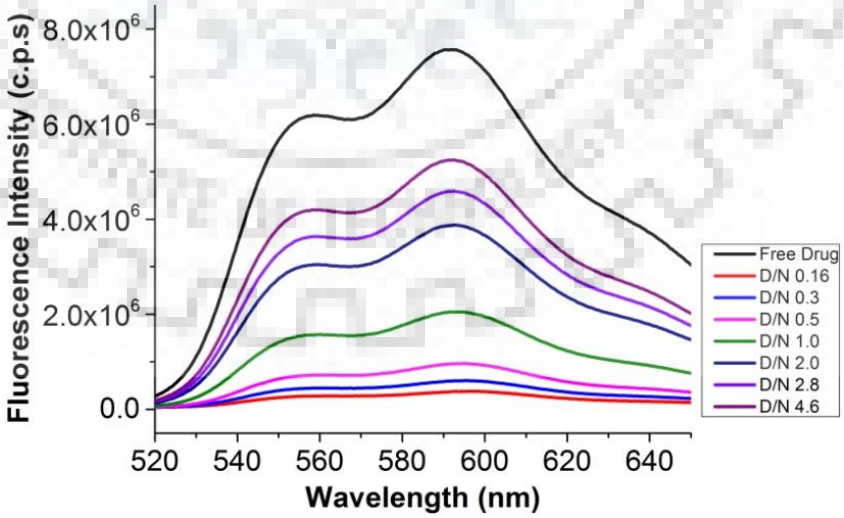

b

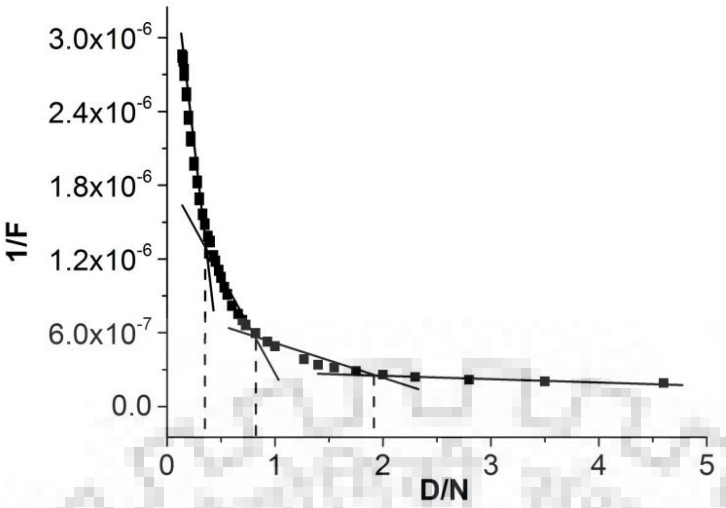
3.0x10-6
2.4x10-6
1.8x10-6
1.2x10-6
6.0x10-7
0.0
1/F
0
1
2
3
4
5
D/N

c

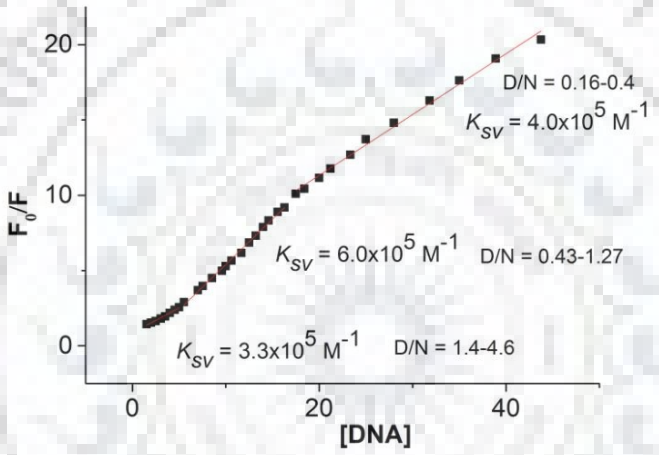
20
10
0
F0/F
D/N = 0.16-0.4
Ksv = 4.0x10^5 M^-1
Ksv = 6.0x10^5 M^-1
D/N = 0.43-1.27
Ksv = 3.3x10^5 M^-1
D/N = 1.4-4.6
0
20
40
[DNA]

d

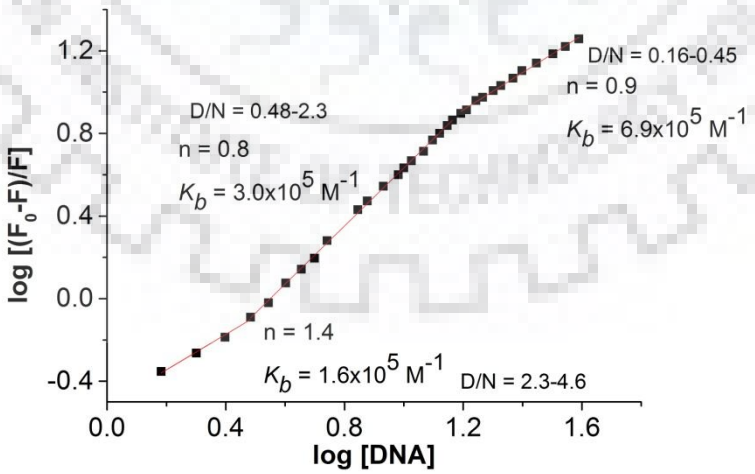
1.2
0.8
0.4
0.0
-0.4
log [(F0-F)/F]
D/N = 0.16-0.45
n = 0.9
Kb = 6.9x10^5 M^-1
D/N = 0.48-2.3
n = 0.8
Kb = 3.0x10^5 M^-1
n = 1.4
Kb = 1.6x10^5 M^-1
D/N = 2.3-4.6
0.0
0.4
0.8
1.2
1.6
log [DNA]

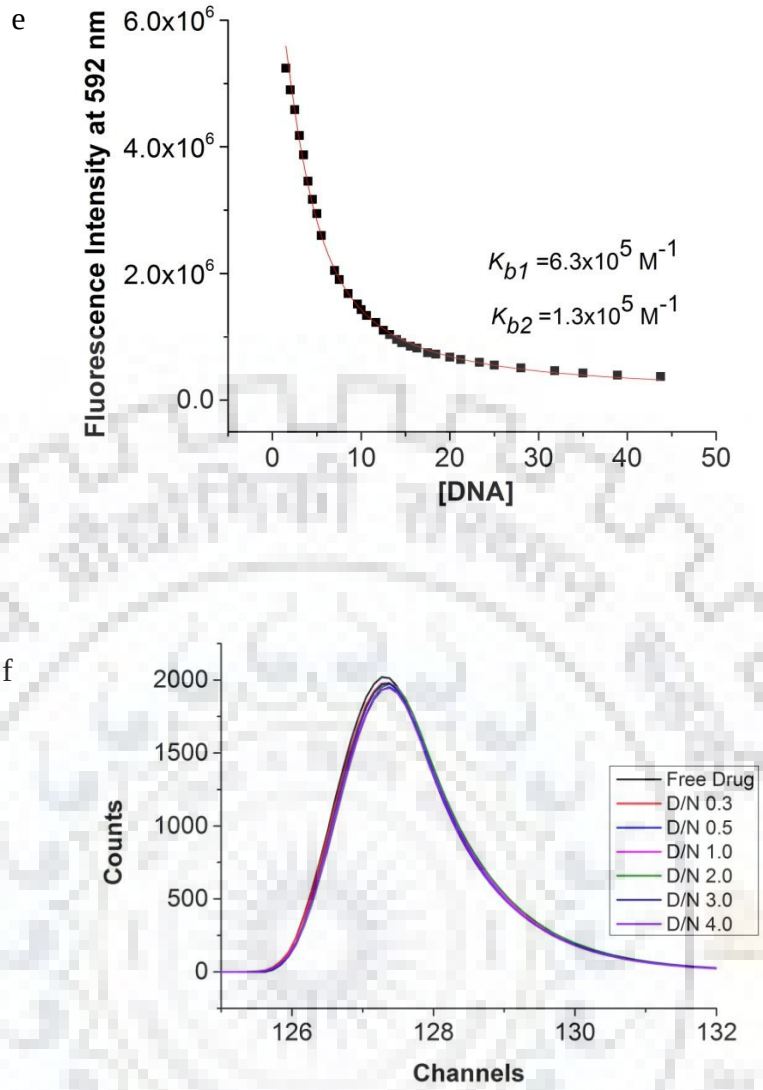

Figure 3.3 a) Fluorescence emission spectra of 7 µM daunomycin with increasing concentration of Tet7 (data at some selected D/N ratios shown); b) Plot of reciprocal of fluorescence intensity (1/F) at 592 nm as a function of D/N ratio; c) Plot of F_0/F versus DNA concentration (µM) at 592 nm giving Stern Volmer constant (K_{sv}); d) Plot of log (F_0-F/F) versus log [DNA] at 592 nm showing binding constants (K_b) and stoichiometry (n); e) Nonlinear fitted curve (red) for binding at two binding sites for observed fluorescence emission intensity at 592 nm as a function of DNA concentration (µM) showing two binding constants (K_{b1} and K_{b2}); f) Fluorescence decay profiles of free daunomycin and daunomycin-Tet7 complexes at varying D/N ratios.

Table 3.1 Lifetime (τ) of free daunomycin (7 µM) and daunomycin-Tet7 complex at D/N = 0.3, 0.5, 1.0, 2.0, 3.0 and 4.0 with λ_{ex} = 456 nm and λ_{em} = 590 nm at 25 °C.

Sample	τ(ns)	%	χ^2
Free Daunomycin	1.03	100	0.91
D/N 0.3	1.00	100	1.01
D/N 0.5	1.00	100	1.01
D/N 1.0	0.97	100	0.96
D/N 2.0	1.00	100	0.99
D/N 3.0	1.00	100	0.97
D/N 4.0	0.97	100	0.99

3.3.3 Circular Dichroism

The circular dichroism spectra of Tet7 (Fig. 3.4 a) shows a well-defined positive band at 264 nm indicating stacking arrangements of tetrads that is characteristic of parallel stranded G-quadruplex DNA with *anti* conformation of glycosidic bond rotation (Karsisiotis et al., 2011; Dapić et al., 2003; Esposito, Virgilio, Randazzo, Galeone, & Mayol, 2005; Petraccone et al., 2007; Masiero et al., 2010), along with a negative band at 242 nm representing right-handed helicity of DNA. We did not observe the CD band at 295 nm, which is characteristic of antiparallel orientation, confirming that all the four strands of intermolecular G-quadruplex are in parallel orientation (Dapić et al., 2003; Esposito et al., 2005; Petraccone et al., 2007; Masiero et al., 2010). Upon progressive addition of daunomycin to 15 µM Tet7 at D/N = 0.1-5.0 (selected data shown in Fig. 3.4 a), both positive and negative bands decrease in magnitude significantly by 54% (inset of Fig. 3.4 a) and 80%, respectively accompanied by a redshift Δλ = 1 nm in both CD bands. This shows a strong interaction between ligand and DNA molecules. No observed change in the overall shape of CD bands and minor shift in wavelength maxima are indicative of external binding of daunomycin to Tet7 (Tarikere Palakashan Pradeep & Barthwal, 2016; White et al., 2007). Plot of CD signal at 264 nm and 242 nm show inflection at D/N = 1.0 and 2.0 suggesting the stoichiometry of complex. Non-linear curve fitting of the plots of magnitude of CD at 264 and 242 nm as a function of daunomycin concentration (Fig. 3.4 b,c) using equation (5) yield affinity constant K_b = 7.9x10^5 and 2.8x10^4 M^{-1}, respectively. The data fitted well in a single binding site which is understandable if two K_b values are of same order and are not distinguishable in CD spectra. In order to examine the existence of induced CD bands of daunomycin on binding to DNA, we recorded CD spectra of 400 µM free daunomycin (Fig. 3.4 d). This showed bisignate CD bands characteristic of a dimer with

positive and negative peaks at ~460 and ~540 nm, respectively and cross over point at 500 nm (Gallois, Fiallo, & Garnier-Suillerot, 1998). On progressive addition of DNA at D/N = 0.5-4.9, the bisignate CD bands disappeared and small positive band at ~458-460 nm appeared (selected data are shown in Fig. 3.4 d), which continuously decreased and disappeared at last (inset of Fig. 3.4 d). These results show that there is practically no free daunomycin in solution and that most of it bind in monomeric form.

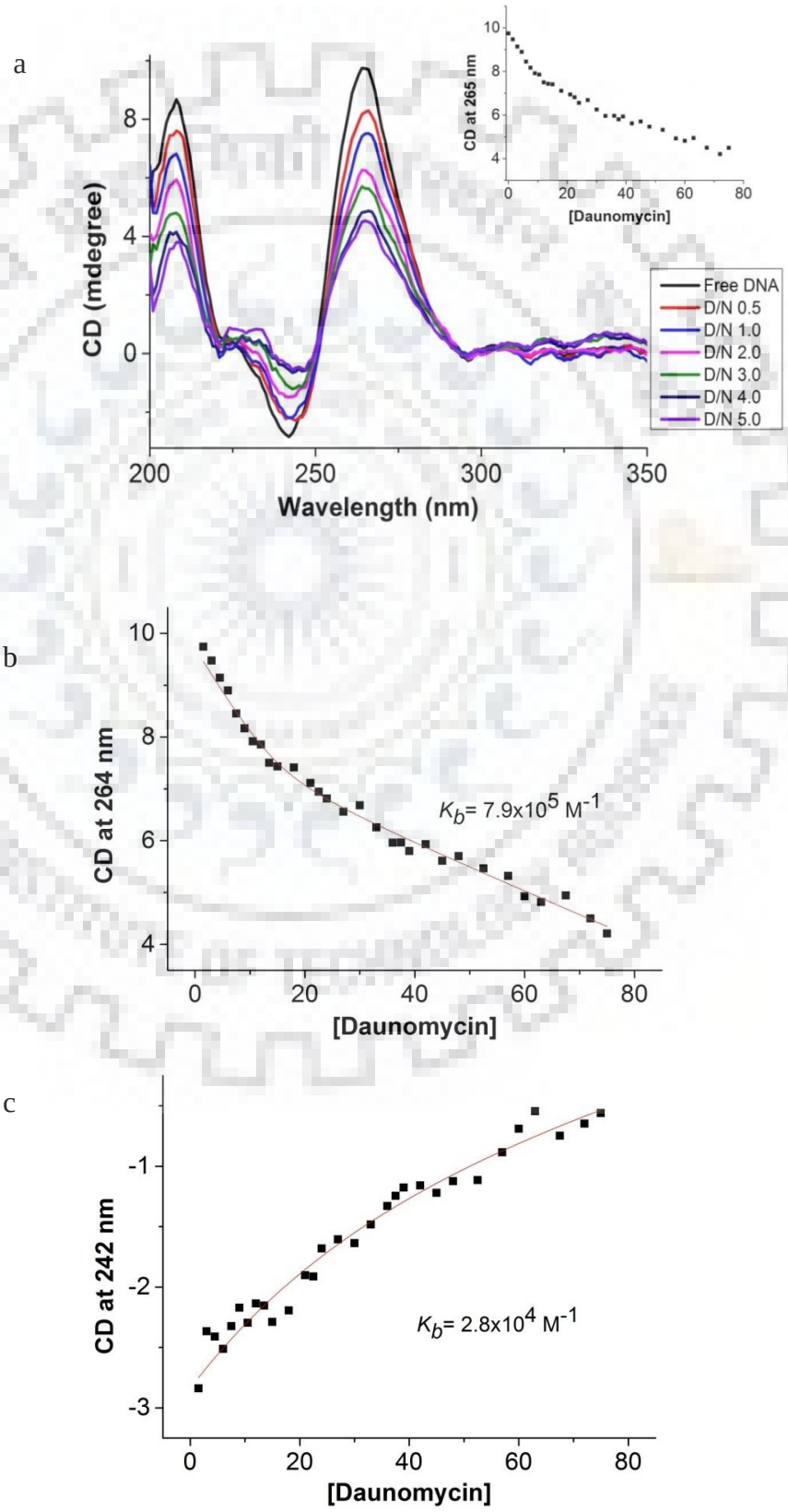

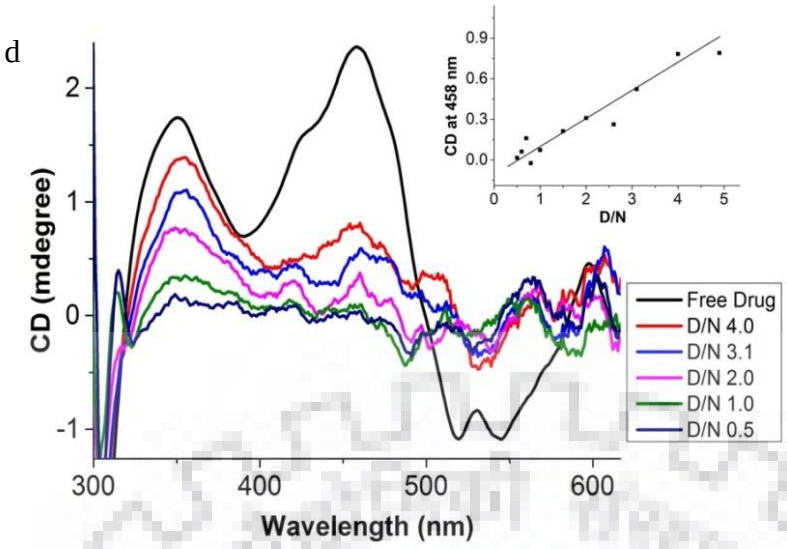

Figure 3.4 a) CD spectra of 15 µM free Tet7 and its complex on progressive addition of daunomycin at D/N ratio = 0.1-5.0 (data at some selected D/N shown). The inset shows a plot of CD (mdegree) at 265 nm as a function of daunomycin concentration (µM) at 25 °C; Nonlinear fitted curve (red) for simultaneous binding at two sites in daunomycin-Tet7 complexes for the observed CD (mdegree) at b) 264 nm and; c) 242 nm as a function of daunomycin concentration (µM) showing binding constants (K_b); d) CD spectra of 400 µM daunomycin in free form and its complex with increasing concentration of Tet7 at D/N = 0.5-4.9 (data at some selected D/N shown). The inset shows a plot of CD (mdegree) at 458 nm as a function of D/N ratio.

3.3.4 Thermal denaturation of DNA

The change in melting temperature (ΔT_m) of folded → unfolded free quadruplex DNA Tet7 and its complex with daunomycin at D/N = 0.5, 1.0, 2.0, 3.0 and 4.0 were obtained using absorbance at 260 nm (Fig. 3.5 a, Table 3.2) (E. Henderson, Hardin, Walk, Tinoco, & Blackburn, 1987; Hardin, Corregan, Lieberman, & Brown II, 1997). It has been shown by Mergny et al. 1998 (Mergny, Phan, & Lacroix, 1998) that reversible absorbance change at 295 nm allows precise monitoring of "intramolecular" G-quartet formation and dissociation as compared to that at 260 nm (which leads to uncertainty). However, the "intermolecular" quartets involving four independent strands e.g. $[d\text{-}(TGGGG)]_4$ are usually parallel stranded with all guanines in *anti* conformation and a notable absence of positive CD peak at 295 nm. In these DNA, the absorbance versus wavelength plot is dominated by 260 nm peak and the transitions at 295 nm were neither found to be reversible nor reliable at KCl concentration of 100 mM. The transitions at 260 nm have since been used to get an estimate of T_m (Henderson et

al., 1987; Hardin et al., 1997). Free DNA shows a melting transition at 55 ± 1 °C which gets stabilized on the binding of daunomycin. The T_m increases with D/N ratio (inset of Fig. 3.5 a) and is ~65 °C at D/N = 4.0 yielding total thermal stabilization, ΔT_m = 10 ± 2 °C.

Thermal transitions from folded → unfolded form of free Tet7 and its complexes were also measured independently through CD at 265 nm (Fig. 3.5 b, Table 3.3). In "intermolecular" G-quadruplex, CD measurements at ~260/263 nm are more reliable as CD has single positive band at ~260 nm with no contribution at 295 nm (Dapić et al., 2003; Esposito et al., 2005; Petraccone et al., 2007; Masiero et al., 2010). T_m measurements by recording CD at 263 nm have been reported earlier in literature, that is, for [d-(TGGGGT)]$_4$ (Esposito et al., 2005) and for [d-(TGGGT)]$_4$ (Petraccone et al., 2007). Free quadruplex DNA Tet7 of concentration 10 µM show a melting transition at 61 ± 3 °C. The melting temperature increases with D/N (inset of Fig. 3.5 b) and is 76 °C at D/N = 4.0 yielding total thermal stabilization, ΔT_m = 15 ± 3 °C.

It may be noted that we were unable to perform FRET experiments mainly due to the reason that daunomycin is highly fluorescent molecule with λ_{ex} = 480 nm and λ_{em} = 590 nm, which falls in the range of emission of attached fluorophore moieties (e.g. FAM at 5'-end and TAMRA at 3'-end of DNA), which might result in significant contribution to fluorescence intensity and pollute the "donor" fluorescence (De Cian et al., 2007). Moreover, daunomycin might interact with attached labeled compounds (e.g. FAM and TAMRA) and increase in melting might be the result of interaction with fluorescent-labeled dyes thus yielding false positives.

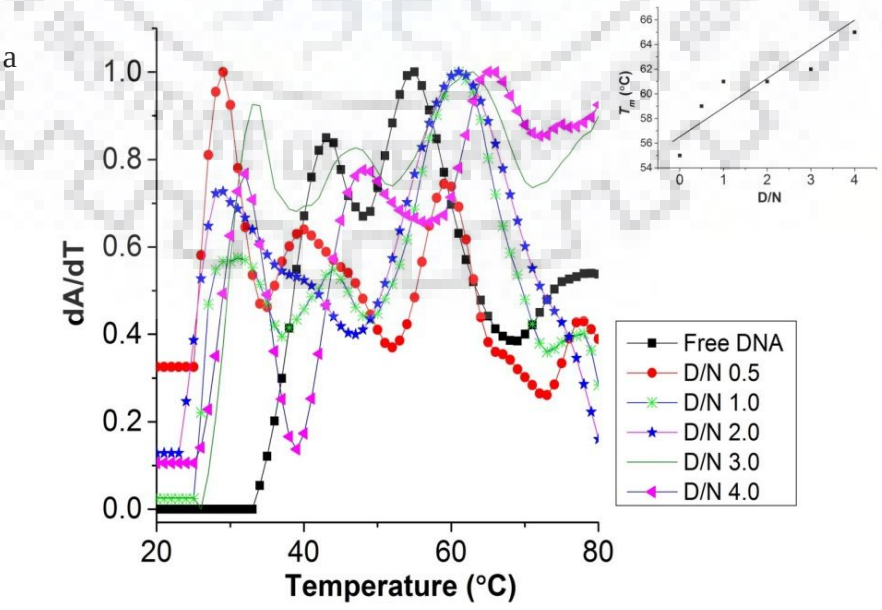

b

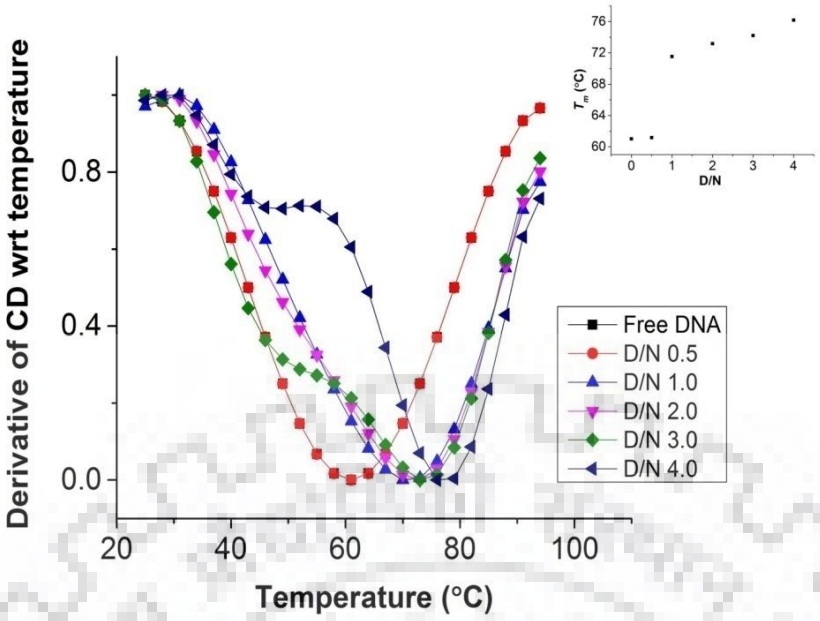

Figure 3.5 Thermal melting profiles of a) 1 µM free Tet7 and its complex with daunomycin at D/N ratio = 0.5, 1.0, 2.0, 3.0 and 4.0 showing derivative of absorbance with respect to temperature (dA/dT) as a function of temperature (T). The inset shows a plot of melting temperature (T_m) as a function of D/N ratio; b) 10 µM free Tet7 and its complex with daunomycin at D/N ratio = 0.5, 1.0, 2.0, 3.0 and 4.0 showing derivative of CD with respect to temperature as a function of temperature (T). The inset shows a plot of melting temperature (T_m) as a function of D/N ratio.

Table 3.2 Melting temperatures (T_m) of free Tet7 (1 µM) and its complex with daunomycin at D/N = 0.5, 1.0, 2.0, 3.0 and 4.0 determined through absorbance spectroscopy.

Samples	T_m (°C)	
Free DNA	55.0	
		ΔT_m
D/N 0.5	59.0	4.0
D/N 1.0	61.0	6.0
D/N2.0	61.0	6.0
D/N3.0	62.0	7.0
D/N 4.0	65.0	10.0

Table 3.3 Melting temperatures (T_m) of free Tet7 (15 µM) and its complex with daunomycin at D/N = 0.5, 1.0, 2.0, 3.0 and 4.0 determined through CD spectroscopy.

Samples	T_m (°C)	
Free DNA	61.0	
		ΔT_m
D/N 0.5	61.0	1.0
D/N 1.0	61.0	10.0
D/N2.0	70.0	13.0
D/N3.0	71.0	12.0
D/N 4.0	76.0	13.0

3.3.5 Nuclear Magnetic Resonance

The conformational analysis of free Tet7 has earlier been carried out in our laboratory (Tarikere Palakshan Pradeep & Barthwal, 2016; Padmapriya & Barthwal, 2017; Kumar & Barthwal, 2018). The NMR spectra are well characterized and show the presence of Hoogsteen base pairing among G quartets. Several intra-nucleotide and sequential inter-nucleotide NOE correlations confirm the existence of well- defined discrete tetra-molecular parallel quadruplex having right-handed B-DNA conformation with *anti* glycosidic bond rotation (Wang & Patel, 1992; Tarikere Palakshan Pradeep & Barthwal, 2016; Padmapriya & Barthwal, 2017; Kumar & Barthwal, 2018). Imino signals of four GNH protons at 10.5-11.5 ppm show that Hoogsteen base pairing among G quartets is retained in the complex. We examined the two-dimensional ^{1}H-^{1}H NOESY spectra of 2:1 daunomycin-Tet7 complex (Fig. 3.6) for short (i) intramolecular connectivities within DNA and (ii) intermolecular distance correlations between daunomycin and DNA. The details of titrations by NMR are discussed in chapter 4. Firstly, all intra molecular Nuclear Overhauser Enhancement (NOE) correlations within DNA, that is, between adjacent GNH protons (G3NH-G4NH, G4NH-G5NH, G5NH-G6NH) and sequential NOEs between GNH and preceding GH8/TH6/TCH$_3$ protons (G3NH-T2H6, G3NH-T2CH$_3$, G4NH-G3H8, G5NH-G4H8, G6NH-G5H8) were found to exist. Further sequential inter nucleotide NOE correlations, between base GH8/TH6 and deoxyribose H1'/H2'/H2" protons (sequential walk connecting H8/H6 to H2" shown with arrows in Fig. 3.6) were also present. This confirms that the overall conformation of G-quadruplex with *anti* glycosidic bond rotation is unchanged on interaction with daunomycin. The presence of all expected sequential NOEs at each step along DNA give a direct proof that there is no opening of base quartets at any step for intercalation of ligand chromophore and that daunomycin binds externally to DNA quadruplex without causing any major alteration in its conformation. Secondly, a close examination of

NOESY spectra showed several intermolecular short contacts between daunomycin and DNA protons. The NOE connectivities 5'CH_3 - G6H8; 1H - T1CH_3, T2CH_3; 3H - T2CH_3; 1H, 2H, 3H - T7CH_3; 4OCH_3 - G6H8, T7CH_3 show close proximity of ring D protons of daunomycin to G6, T7 bases, and T2 base. It also shows the involvement of 5'CH_3 of daunosamine sugar in interaction. Thus, there are apparently two binding sites, one close to G6, T7 bases and other in the proximity of T2 base. In addition, G6NH resonating at 10.89 ppm is considerably upfield shifted by 0.34 ppm (Tarikere Palakshan Pradeep & Barthwal, 2016; Padmapriya & Barthwal, 2017; Kumar & Barthwal, 2018; Phan, Kuryavyi, Gaw, & Patel, 2005). On the other hand, T7H6 and T7CH_3 resonating at 7.34 and 1.63 ppm, respectively in comparison to their corresponding position in free Tet7 (Tarikere Palakshan Pradeep & Barthwal, 2016; Padmapriya & Barthwal, 2017; Kumar & Barthwal, 2018) are downfield shifted by 0.30 and 0.21 ppm, respectively. This shows that G6 has enhanced stacking interaction while T7 is destacked on binding to daunomycin. This is inferred as end stacking with last G-quartet by displacing T7 base (Padmapriya & Barthwal, 2017; Phan et al., 2005). The external binding near T2 residue may be due to groove binding. It was also noted that inter ligand NOEs due to two daunomycin molecules lying close to each other as a stacked structure in parallel or antiparallel orientations were absent (P. Agrawal, Barthwal, et al., 2009), which shows that layers of daunomycin do not exist in the complex.

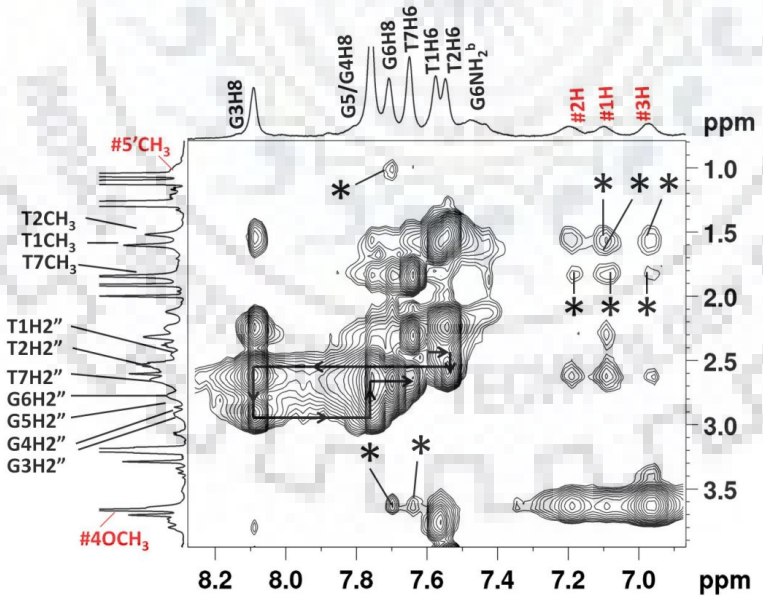

Figure 3.6 Expansion of specific region of 2D NOESY spectra of daunomycin-Tet7 complex at D/N = 3.0 at 25 °C using mixing time (τ_m) = 250 ms showing sequential walk of base H8/H6 protons with deoxyribose H2" protons (along the direction of arrows) and intermolecular cross peaks (marked as *) between daunomycin (#) and Tet7 at D/N= 3.0 at 25 °C. The NOEs shown are 5'CH_3 - G6H8; 1H - T1CH_3, T2CH_3; 3H - T2CH_3; 1H, 2H, 3H - T7CH_3; 4OCH_3 - G6H8, T7CH_3.

3.3.6 Molecular Docking

In order to get further insight into the location of binding sites, we conducted molecular docking studies of daunomycin with Tet7 using available PDB (ID: 139D). The lowest energy conformations showed the existence of 2 binding sites close to T1pT2pG3 and G6pT7 (Fig. 3.7 a,b) with binding affinities of -2.32 kcal/mol and -1.55 kcal/mol. Binding at T1pT2pG3 site was stabilized by 4 hydrogen bonds: (i) oxygen of daunosamine sugar moiety with PO_4^{2-} of T2 (2.31 Å), (ii) oxygen of glycosidic linkage with PO_4^{2-} of T2 (2.92 Å), (iii) 6OH of ring B with PO_4^{2-} of T2 (2.36 Å), and (iv) $9COCH_3$ of ring A with O2 of T1 (2.58 Å) (Fig. 3.7 c). Two other hydrogen bonds: NH_3^+ of daunosamine sugar moiety with O3' of G4 (2.87 Å) and 6OH of ring B with PO_4^{2-} of G5 (2.56 Å) stabilize binding at G6pT7 site (Fig. 3.7 d).

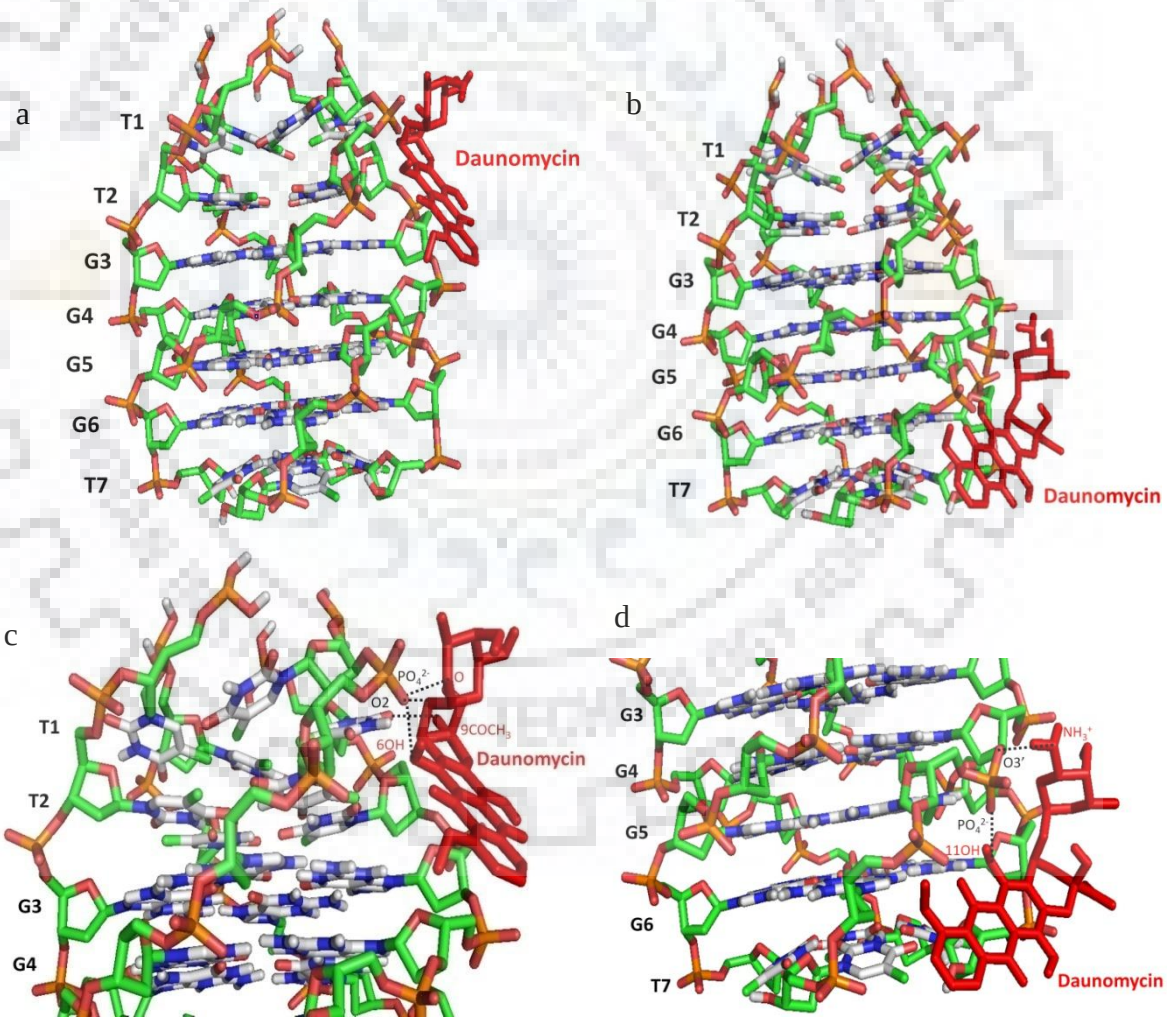

Figure 3.7 The schematic diagram of molecular docking studies showing binding of daunomycin to Tet7 (PDB ID: 139D) at; a) T1pT2pG3 site and; b) G6pT7 site. Close-up view of ligand binding sites showing hydrogen bonds (black dashed lines) at; c) T1pT2pG3 site and; d) G6pT7 sites. Both models were generated using Autodock 4.2 and visualized by PyMol.

3.3.7 Mode of Binding

In duplex DNA, generally, three modes of binding have been recognized: intercalation, groove binding, and electrostatic interaction. Intercalation of ligand between base pairs leads to a significant change in absorbance/emission accompanied by a large redshift, $\Delta\lambda_{max}$ ~20-40 nm while groove binding may show significant change but only a minor change in λ_{max} up to ~15 nm (Tarikere Palakashan Pradeep & Barthwal, 2016). The electrostatic interaction, on the other hand, may induce a smaller change in absorbance/emission with practically no change in λ_{max}. Similar results have been obtained on binding of ligands to DNA quadruplexes (Manet, Manoli, Zambelli, Andreano, Masi, Cellai, & Monti, 2011; Das, Chatterjee, & Suresh Kumar, 2017; Padmapriya & Barthwal, 2017; Kumar & Barthwal, 2018; Tarikere Palakashan Pradeep & Barthwal, 2016). Our absorbance data shows significant (55%) change in absorbance accompanied by minor red shift $\Delta\lambda_{max}$ = 3 nm, which indicates that classical intercalation is not a preferred mode of binding. The daunomycin molecule may, however, interact with DNA on binding externally. The alteration in absorbance may be due to the interaction of the π electron cloud of daunomycin and G-quadruplex DNA. The observed changes (55%) are much higher than that reported in literature (up to 29%) for 21/22-mer human telomeric DNA (Manet, Manoli, Zambelli, Andreano, Masi, Cellai, & Monti, 2011; Manet, Manoli, Zambelli, Andreano, Masi, Cellai, Ottani, et al., 2011; Das et al., 2017) which adopts hybrid structures having both parallel and antiparallel strands with loops connecting the strands. Apparently pure parallel stranded G-quadruplex with no loops, as in the present case, allows stronger external binding.

The fluorescence data shows extensive quenching on addition of daunomycin, as also observed in literature for 21/22-mer hybrid G-quadruplex structures (Manet, Manoli, Zambelli, Andreano, Masi, Cellai, & Monti, 2011; Manet, Manoli, Zambelli, Andreano, Masi, Cellai, Ottani, et al., 2011; Das et al., 2017) with a minor shift in emission maxima. Efficient quenching may be attributed to electron transfer by the proximity of daunomycin to guanines (Manet, Manoli, Zambelli, Andreano, Masi, Cellai, & Monti, 2011; Das et al., 2017) suggesting stacking on top or bottom of tetrad or close to G-tetrads along DNA backbone. The observed redshift in emission maxima, $\Delta\lambda_{em}$ = 4 nm, excludes the possibility of classical intercalation (Tarikere Palakashan Pradeep & Barthwal, 2016). The fluorescence data confirms the presence of 2 independent binding sites with the same order of binding affinity. The circular dichroism spectra show that overall conformation of DNA is unchanged with parallel stranded strands having similar stacking arrangement of base quartets as in free DNA quadruplex and right-

handed helix geometry. Accordingly, both end stacking and groove binding may be responsible for the external binding of daunomycin to DNA in the present investigations. Daunomycin dimer is completely disrupted on binding to DNA and it exists in monomeric form in the bound complex. Thus, layers of daunomycin with two daunomycin in parallel or antiparallel orientations, as observed in X-ray crystallographic structure of daunomycin-[d-(TGGGGT)]$_4$ complex (Clark et al., 2003) do not exist in solution. The thermal stabilization of DNA T_m = 10-15 °C may, therefore, be attributed to groove binding and/or end stacking modes of interaction. The change in the magnitude of induced CD band and T_m up to D/N = 4.0 shows that binding of daunomycin with DNA continues at higher D/N ratios as perhaps the two sites on DNA are not fully occupied at D/N = 2.0.

The NMR spectroscopy experiments provided knowledge of interactions at the molecular level. Proof of external binding comes from the presence of all sequential NOE connectivities along the sequence of DNA, which is in accord with the findings by absorption, fluorescence and CD spectroscopy. Presence of several NOEs gives a direct proof of the proximity of daunomycin to DNA quadruplex at two sites close to G6, T7 and T2 bases. Further the upfield shift in G6NH and downfield shift in T7H6, T7CH$_3$ suggest stacking of daunomycin chromophore with last G-quartet by displacing T7 residue. The docking results are in agreement with these observations. It may be noted that the mode of binding obtained in the present investigations in daunomycin-Tet7 complex are close to the findings based on molecular dynamics simulations (Shen et al., 2017) which show that daunomycin binds to [d(TGGGGT)]$_4$ quadruplex DNA through end stacking and groove binding with practically similar binding affinities. End stacking mode was also predicted on the basis of collision-induced dissociation in daunomycin-[d-(TGGGGT)]$_4$ complex (N. Xu et al., 2012). The results are however in sharp contrast with the crystal structure of daunomycin-[d-(TGGGGT)]$_4$ complex determined earlier (Clark et al., 2003) which shows two layers, each containing three daunomycin molecules, sandwiched between two [d-(TGGGGT)]$_4$ quadruplexes. Absence of inter ligand NOEs in present investigations also confirms the non-existence of layers of daunomycin in solution studies. Binding at grooves and end stacking were also deduced from entropy and enthalpy driven interactions, respectively in 3+1 hybrid 21-mer human telomeric DNA (Manet, Manoli, Zambelli, Andreano, Masi, Cellai, & Monti, 2011).

The present investigations also show that direct binding of daunomycin with DNA leads to thermal stabilization by 10-15 °C, which may interfere with the association of telomeric DNA with telomerase and contribute to telomere dysfunction.

3.4 Conclusion

We conclude that daunomycin binds to parallel stranded Tet7 in 1:1 and 2:1 stoichiometry with a significant decrease in absorbance, emission and magnitude of circular dichroism with practically no shift in wavelength maxima. The daunomycin dimers present in a free state in solution are disrupted on interaction with DNA. A small positive CD band at ~460 nm suggests external binding. Presence of all sequential NOE connectivities pertaining to short interproton distance contacts confirms external binding. The observed intermolecular NOEs between two interacting molecules and chemical shift changes indicate end stacking with G6 quartet by displacement of T7 base as well as groove binding. Molecular docking studies show the existence of few hydrogen bonds and end stacking and groove binding, which are in conformity with experimental results. Binding of daunomycin leads to thermal stabilization ~10-15 °C which is likely to hamper the access of telomerase to its functional site at telomeres. The present studies on the mode of action pave the way for alternate derivatives/analogs by making different chemical modifications of anthracyclines to arrive at a more potent telomerase inhibitor.

Chapter 4: NMR based solution structure of daunomycin complexed with intermolecular parallel G-quadruplex DNA 7-mer [d-(TTGGGGT)$_4$]

4.1 Introduction

The role of daunomycin/adriamycin in disruption of maintenance of telomeres has recently been evidenced (Ogretmen et al., 2001; Nakajima et al., 2003; Sabatino et al., 2010; Zhang et al., 2012). The findings demonstrate that the anthracyclines target different forms of DNA. NMR studies on the interaction of daunomycin analogs, nemorubicin, and doxorubicin, with G-quadruplex sequences containing three guanine repeats, e.g. [d-(TTAGGGT)]$_4$, showed (Scaglioni et al., 2016) that binding takes place at A3pG4 and terminal G-tetrad. There are no investigations on G4 DNA complexes comprising four guanine repeats. We have undertaken a study of the interaction of daunomycin with [d-(TTGGGGT)]$_4$ (Tet7) primarily by NMR techniques. We show real-time binding by SPR experiments. The stoichiometry of complexes is determined independently by Job Plot experiment using fluorescence spectroscopy. DOSY experiments confirm the formation of a stable complex. Detailed analysis of proton NMR spectra including direct short interproton contacts in NOESY spectra gives valuable information on specific interactions at the molecular level. Phosphorus-31 NMR has been used to give information on DNA backbone geometry. Thermal melting profiles of imino protons have been examined and correlated to DSC thermograms.

4.2 Materials and Methods

Details of the materials and methods used are given in chapter 2. For SPR experiments, 30.0-960.0 µM daunomycin solutions were used. For Job plot experiments, the relative mole fractions of quadruplex DNA Tet7 and daunomycin were varied keeping the total concentration of DNA and daunomycin constant at 7 µM. 1.16 mM of G-quadruplex DNA Tet7 was used in NMR experiments. 50 µM of free [d-(TTGGGGT)]$_4$ (corresponding to a single strand concentration of d-(TTGGGGT) as 200 µM) was scanned to obtain a melting profile of free DNA in DSC experiments. Each set of a complex with increasing daunomycin concentrations and fixed Tet7 concentration of 50 µM at D/N ratio = 0.5, 1.0, 2.0, 3.0 and 4.0 were scanned to obtain the melting profile of bound forms.

4.3 Results and Discussion

4.3.1 Surface Plasmon Resonance, Job Plot, and Diffusion Ordered Spectroscopy

The surface plasmon resonance sensograms (Fig. 4.1 a) give a direct proof of binding of daunomycin with [d-(TTGGGGT)]$_4$. The steady state response increases with a concentration in the range 30.0-960.0 μM (Fig. 4.1 b) indicating that a specific interaction of daunomycin with Tet7 indeed does take place. The binding isotherms yield affinity constant $K_b \sim 4.1 \times 10^3$ M^{-1} at 25 °C referring to the dominant mode of interaction. Direct assessment of stoichiometry of complex made by continuous variation (Job plot) analysis using fluorescence show slope change between approximately linear regions at a mole fraction of daunomycin ~0.50 and 0.66 yielding stoichiometry ratios ~1:1 and 2:1 for daunomycin: Tet7 complex (Fig. 4.1 c). We observed scatter of data at mole fraction 0.5-0.7, which may be due to the existence of multiple stoichiometric complexes although the highest stoichiometry attained in complexes appears to be 2:1.

The ^{1}H DOSY experiments showed (Fig. 4.1 d) that diffusion constant of 1H/2H/3H protons (~4.0×10^{-10} m^2/s) in free daunomycin and T7H6/G6H8 protons in free DNA (~1.5×10^{-10} m^2/s) are greater than that for bound DNA (~1.0×10^{-10} m^2/s) at D/N = 2.0 at 25 °C. This shows that ligand-bound DNA undergoes diffusion at a slower rate as a stable complex upon binding (Cocco, Hanakahi, Huber, & Maizels, 2003; Kumar & Barthwal, 2018). Due to the presence of two stoichiometries as evidenced by Job plot and perhaps two binding sites, daunomycin proton signals were broadened and could not be used for calculating diffusion constant. The DOSY spectra thus confirm the formation of a stable bound complex.

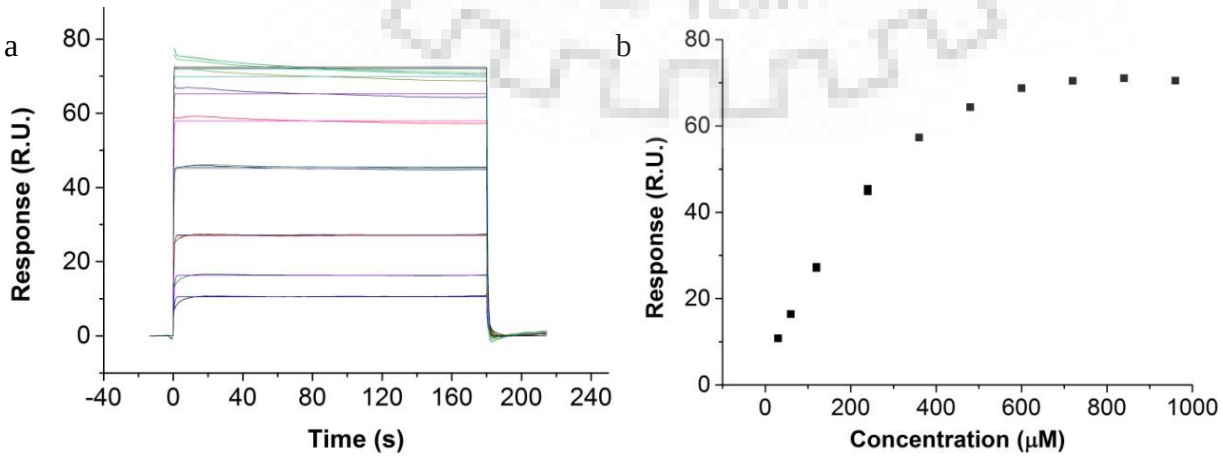

c

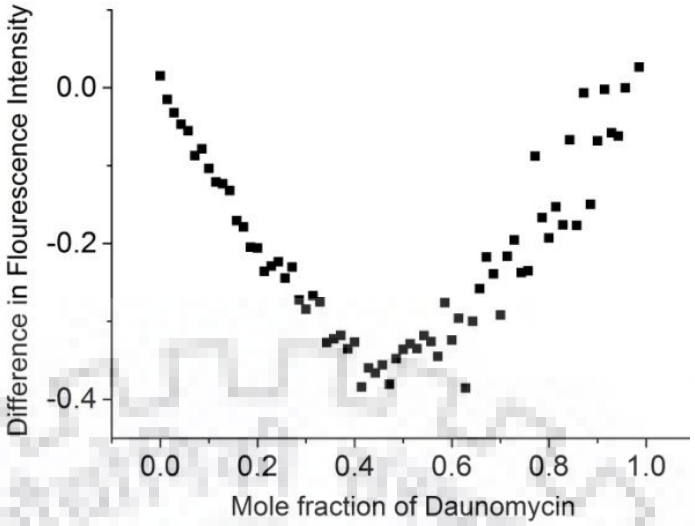

d

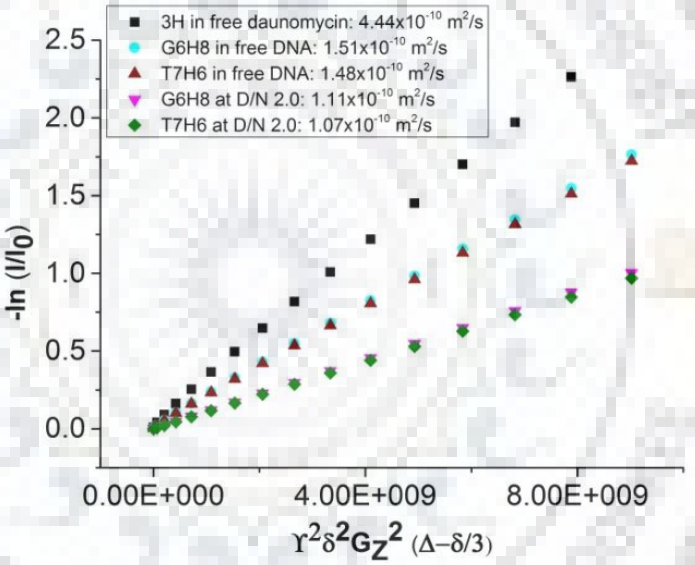

Figure 4.1 a) Results of SPR experiments for binding of daunomycin to Tet7. Sensograms obtained for free daunomycin concentration from 30 µM (bottom) to 960 µM (top), using HEPES buffer with 100 mM KCl at 25 °C; b) Binding plot of steady-state response (R.U.) versus concentration of daunomycin (µM); c) Job plot for binding of daunomycin to Tet7 showing difference in fluorescent intensity of bound and unbound daunomycin as a function of mole fraction of daunomycin; and d) Diffusion coefficient measurement obtained from DOSY spectra of free daunomycin, free Tet7 and daunomycin-Tet7complex at D/N = 2.0 at 25 °C.

4.3.2 Proton Nuclear Magnetic Resonance

The complete unambiguous assignment of all exchangeable and non-exchangeable protons in free Tte7 (Fig. 4.2 a-j) was done (Table 4.1-4.3) by rigorous analysis of 2D ^{1}H-^{1}H NOESY and ^{1}H-^{1}H COSY, ^{1}H-^{13}C HSQC spectra (Pradeep & Barthwal, 2016; Padmapriya & Barthwal, 2017; Kumar & Barthwal, 2018). Presence of imino signals of four guanines protons at 10.5-11.5 ppm show presence of Hoogsteen base pairing among G quartets, while G-quadruplex formation is further ascertained by NOE correlations between adjacent GNH protons and sequential NOEs between GNH (Fig. 4.2 g) and preceding GH8/TH6/TCH$_3$ protons (Fig. 4.2 h). A single set of GNH, GH8, TH6, and TCH$_3$ in every G-tetrad show fourfold symmetry of quadruplex Tet7. Intra nucleotide and sequential inter nucleotide NOE correlations, between base H8/H6 and deoxyribose H1'/H2'/H2" protons (Fig. 4.2 i,j), confirm the existence of tetramolecular parallel quadruplex having right-handed B-DNA conformation with predominant C2' *endo* sugar pucker and *anti* glycosidic bond rotation (Wang & Patel, 1992; Pradeep & Barthwal, 2016; Padmapriya & Barthwal, 2017; Kumar & Barthwal, 2018). The imino protons of thymine were in fast exchange with solvent and can't be ascertained for hydrogen bond formation and the existence of tetrad (Gavathiotis et al., 2003).

Table 4.1 ^{1}H Chemical shift (ppm) of protons in daunomycin-Tet7 complex (δ_b) at D/N = 4.0 in KBPES buffer containing 100 mM KCl (90% H_2O+10% D_2O solvent) at 25 °C. Δδ refers to change in chemical shift due to the binding. -ve Δδ indicates an upfield shift.

Residues	T1		T2		G3		G4	
Protons	δ_b	Δδ	δ_b	Δδ	δ_b	Δδ	δ_b	Δδ
H8/H6	7.57	-0.02	7.54	0.00	8.08	-0.06	7.74	-0.06
H1'	6.15	0.01	6.05	0.02	6.03	-0.04	6.02	-0.04
CH_3	1.60	-0.05	1.51	-0.02	-	-	-	-
NH_2^b	7.57	-0.02	7.54	0.00	9.73	-0.11	9.05	-0.12
NH_2^{nb}	-	-	-	-	6.14	-0.16	6.06	-0.14
NH	-	-	-	-	11.36	-0.15	10.97	-0.11
Residues	G5		G6		T7			
Protons	δ_b	Δδ	δ_b	Δδ	δ_b	Δδ		
H8/H6	7.74	-0.10	7.69	-0.02	7.64	0.30		
H1'	6.02	-0.06	6.27	0.03	6.20	0.15		
CH_3	-	-	-	-	1.84	0.21		
NH_2^b	9.05	-0.12	7.47	0.01	7.64	0.30		
NH_2^{nb}	7.75	-0.07	6.77	0.01	-	-		
NH	10.82	-0.12	10.55	-0.34	-	-		

Table 4.2 ^{1}H Chemical shift (ppm) of DNA protons in daunomycin-Tet7 complex (δ_b) at various Daunomycin (D) / Nucleic acid (N) ratios, D/N, in KBPES buffer containing 100 mM KCl (90% H_2O+10% D_2O) at 25 °C. $\Delta\delta$ refers to change in chemical shift due to the binding. Negative sign in $\Delta\delta$ indicates upfield shift.

D/N	RESIDUES	T1		T2		G3		G4		G5		G6		T7	
	PROTONS	δ_b	$\Delta\delta$	δ_b	$\Delta\delta$	δ_b	$\Delta\delta$	δ_b	$\Delta\delta$	δ_b	$\Delta\delta$	δ_b	$\Delta\delta$	δ_b	$\Delta\delta$
1.0	H8/H6	7.57	-0.02	7.53	-0.01	8.12	-0.02	7.78	-0.02	7.79	-0.05	7.72	0.01	7.59	0.25
	H1’	6.14	0.00	6.03	0.00	6.04	-0.03	6.05	-0.01	6.07	-0.01	6.30	0.06	6.18	0.13
	H2’	2.21	0.00	2.26	-0.01	2.64	-0.02	2.65	0.01	2.71	-0.01	2.26	0.00	2.28	0.11
	H2”	2.41	-0.01	2.58	-0.02	2.94	-0.02	2.91	-0.01	2.75	-0.02	2.66	-0.02	2.65	0.00
	H3’	4.62	-0.03	4.91	0.01	5.04	-0.02	5.06	0.01	5.06	-0.03	5.08	0.04	5.03	0.07
	H4’	4.26	-0.04	4.20	0.03	4.38	-0.02	4.29	-0.04	4.54	-0.04	4.52	-0.01	4.55	0.09
	H5’	4.08	0.01	4.06	0.00	4.14	-0.01	4.28	0.00	4.36	0.00	4.23	-0.02	4.15	0.02
	H5”	3.74	-0.03	4.02	-0.01	4.10	-0.01	4.23	0.00	4.28	-0.04	4.20	-0.01	4.08	0.01
	CH_3	1.63	-0.02	1.52	-0.01	-	-	-	-	-	-	-	-	1.80	0.17
	NH_2^b	-	-	-	-	9.81	-0.03	9.10	-0.07	9.09	-0.08	7.46	0.00	-	-
	NH_2^{nb}	-		-	-	6.16	-0.14	6.13	-0.07	7.79	-0.03	6.76	0.00	-	-
	NH	-	-	-	-	11.47	-0.04	11.04	-0.04	10.87	-0.07	10.67	-0.22	-	-
2.0	H8/H6	7.57	-0.02	7.54	0.00	8.11	-0.03	7.77	-0.03	7.77	-0.07	7.72	0.01	7.64	0.30
	H1’	6.15	0.01	6.05	0.02	6.04	-0.03	6.04	-0.02	6.04	-0.04	6.31	0.07	6.21	0.16
	H2’	2.23	0.02	2.24	-0.03	2.63	-0.03	2.66	0.02	2.70	-0.02	2.31	0.05	2.30	0.13
	H2”	2.44	0.02	2.57	-0.03	2.93	-0.03	2.85	-0.07	2.85	0.08	2.68	0.00	2.65	0.00
	H3’	4.66	0.01	4.92	0.02	5.04	-0.02	5.07	0.02	5.07	-0.02	5.08	0.04	5.06	0.10
	H4’	4.25	-0.05	4.19	0.02	4.38	-0.02	4.29	-0.04	-	-	4.54	0.01	4.57	0.11
	H5’	4.07	0.00	4.06	0.00	4.15	0.00	4.28	0.00	4.36	0.00	4.24	-0.01	4.16	0.03
	H5”	3.76	-0.01	4.02	-0.01	4.11	0.00	4.23	0.00	4.28	-0.04	4.20	-0.01	4.11	0.04
	CH_3	1.61	-0.04	1.54	0.01	-	-	-	-	-	-	-	-	1.84	0.21
	NH_2^b	-	-	-	-	9.78	-0.06	9.08	-0.09	9.09	-0.08	7.47	0.01	-	-
	NH_2^{nb}	-	-	-	-	6.18	-0.12	6.10	-0.10	7.76	-0.06	6.77	0.01	-	-
	NH	-	-	-	-	11.42	-0.09	11.01	-0.07	10.84	-0.10	10.59	-0.30	-	-

Table 4.3 ^{1}H Chemical shift (ppm) of DNA protons in daunomycin-Tet7 complex (δ_b) at various D/N ratios in KBPES buffer containing 100 mM KCl (90% H_2O+10% D_2O) at 25 °C. Δδ refers to change in chemical shift due to the binding. Negative sign in Δδ indicates upfield shift.

D/N	RESIDUES	T1		T2		G3		G4		G5		G6		T7	
	PROTONS	δ_b	Δδ	δ_b	Δδ	δ_b	Δδ	δ_b	Δδ	δ_b	Δδ	δ_b	Δδ	δ_b	Δδ
3.0	H8/H6	7.57	-0.02	7.54	0.00	8.09	-0.05	7.75	-0.05	7.75	-0.09	7.70	-0.01	7.64	0.30
	H1’	6.17	0.03	6.06	0.03	6.04	-0.03	6.04	-0.02	6.04	-0.04	6.29	0.05	6.21	0.16
	H2’	2.23	0.02	2.24	-0.03	2.62	-0.04	2.67	0.03	2.71	-0.01	2.36	0.10	2.31	0.14
	H2”	2.47	0.05	2.56	-0.04	2.91	-0.05	2.91	-0.01	2.76	-0.01	2.66	-0.02	2.63	-0.02
	H3’	4.66	0.01	4.92	0.02	5.04	-0.02	5.05	0.00	5.05	-0.04	5.08	0.04	5.07	0.11
	H4’	4.26	-0.04	4.17	0.00	4.37	-0.03	4.29	-0.04	-	-	4.54	0.01	4.56	0.10
	H5’	4.08	0.01	4.07	0.01	4.13	-0.02	4.28	0.00	4.36	0.00	4.25	0.00	4.15	0.02
	H5”	3.76	-0.01	4.03	0.00	4.10	-0.01	4.23	0.00	4.28	-0.04	4.21	0.00	4.10	0.03
	CH_3	1.60	-0.05	1.52	-0.01	-	-	-	-	-	-	-	-	1.83	0.20
	NH_2^{b}	-	-	-	-	9.76	-0.08	9.06	-0.11	9.05	-0.12	7.46	0.00	-	-
	NH_2^{nb}	-	-	-	-	6.15	-0.15	6.07	-0.13	7.75	-0.07	6.76	0.00	-	-
	NH	-	-	-	-	11.37	-0.14	10.98	-0.10	10.82	-0.12	10.55	-0.34	-	-
4.0	H8/H6	7.57	-0.02	7.54	0.00	8.08	-0.06	7.74	-0.06	7.74	-0.10	7.69	-0.02	7.64	0.30
	H1’	6.15	0.01	6.05	0.02	6.03	-0.04	6.02	-0.04	6.02	-0.06	6.27	0.03	6.20	0.15
	H2’	2.23	0.02	2.22	-0.05	2.60	-0.06	2.67	0.03	2.67	-0.05	2.28	0.02	2.30	0.13
	H2”	2.45	0.03	2.56	-0.04	2.90	-0.06	2.91	-0.01	2.79	0.02	2.65	-0.03	2.63	-0.02
	H3’	4.66	0.01	4.92	0.02	5.03	-0.03	5.05	0.00	5.05	-0.04	5.07	0.03	5.07	0.11
	H4’	4.26	-0.04	4.18	0.01	4.38	-0.02	4.28	-0.05	4.58	0.00	4.54	0.01	4.56	0.10
	H5’	4.07	0.00	4.07	0.01	4.14	-0.01	4.28	0.00	4.36	0.00	4.24	-0.01	4.15	0.02
	H5”	3.77	0.00	4.02	-0.01	4.10	-0.01	4.23	0.00	4.28	-0.04	4.20	-0.01	4.07	0.00
	CH_3	1.60	-0.05	1.51	-0.02	-	-	-	-	-	-	-	-	1.84	0.21
	NH_2^{b}	-	-	-	-	9.73	-0.11	9.05	-0.12	9.05	-0.12	7.47	0.01	-	-
	NH_2^{nb}	-	-	-	-	6.14	-0.16	6.06	-0.14	7.75	-0.07	6.77	0.01	-	-
	NH	-	-	-	-	11.36	-0.15	10.97	-0.11	10.82	-0.12	10.55	-0.34	-	-

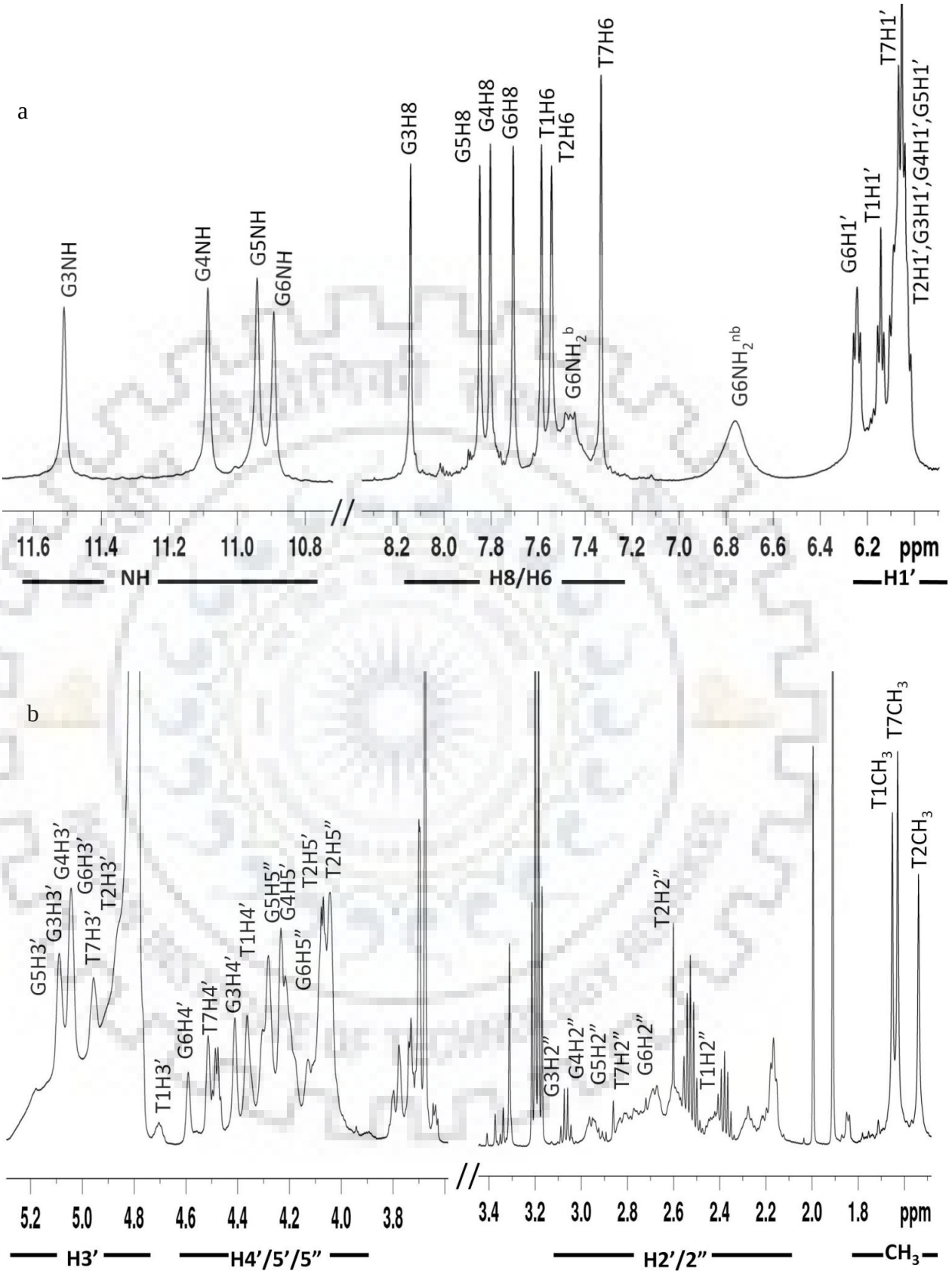
a
G3NH
G4NH
G5NH
G6NH
G3H8
G5H8
G4H8
G6H8
T1H6
T2H6
T7H6
G6NH2b
G6NH2nb
G6H1′
T1H1′
T2H1′,G3H1′,G4H1′,G5H1′
T7H1′
11.6 11.4 11.2 11.0 10.8 8.2 8.0 7.8 7.6 7.4 7.2 7.0 6.8 6.6 6.4 6.2 ppm
NH
H8/H6
H1′
b
G5H3′
G3H3′
G4H3′
G6H3′
T7H3′
T2H3′
T1H3′
G6H4′
T7H4′
G3H4′
T1H4′
G5H5″
G4H5′
G6H5″
T2H5′
T2H5″
G3H2″
G4H2″
G5H2″
T7H2″
G6H2″
T2H2″
T1H2″
T1CH3
T7CH3
T2CH3
5.2 5.0 4.8 4.6 4.4 4.2 4.0 3.8 3.4 3.2 3.0 2.8 2.6 2.4 2.2 2.0 1.8 ppm
H3′
H4′/5′/5″
H2′/2″
CH3

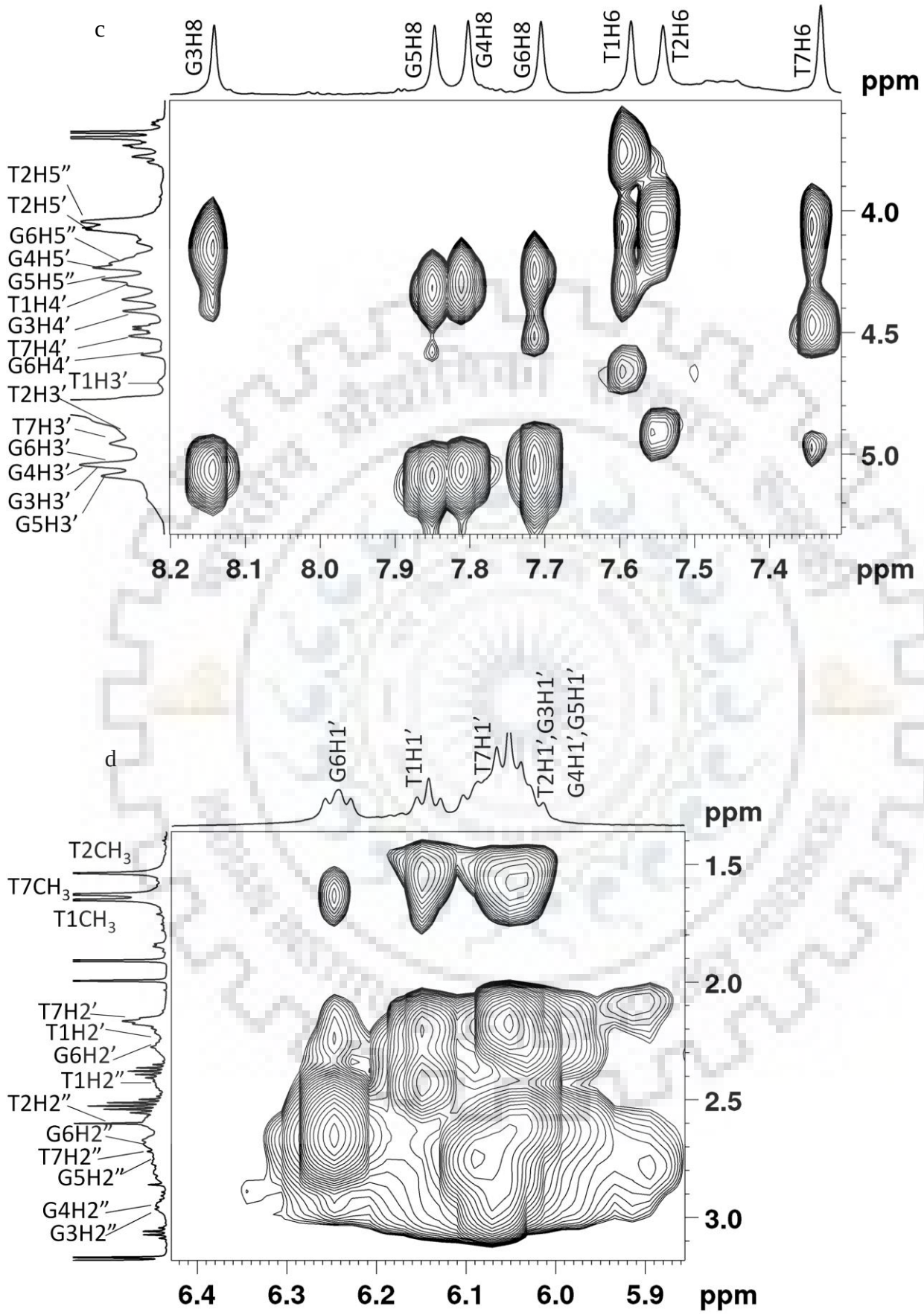
c
G3H8
G5H8
G4H8
G6H8
T1H6
T2H6
T7H6
ppm
T2H5″
T2H5′
G6H5″
G4H5′
G5H5″
T1H4′
G3H4′
T7H4′
G6H4′
T1H3′
T2H3′
T7H3′
G6H3′
G4H3′
G3H3′
G5H3′
4.0
4.5
5.0
8.2
8.1
8.0
7.9
7.8
7.7
7.6
7.5
7.4
ppm
d
G6H1′
T1H1′
T7H1′
T2H1′,G3H1′
G4H1′,G5H1′
ppm
T2CH3
T7CH3
T1CH3
T7H2′
T1H2′
G6H2′
T1H2″
T2H2″
G6H2″
T7H2″
G5H2″
G4H2″
G3H2″
1.5
2.0
2.5
3.0
6.4
6.3
6.2
6.1
6.0
5.9
ppm

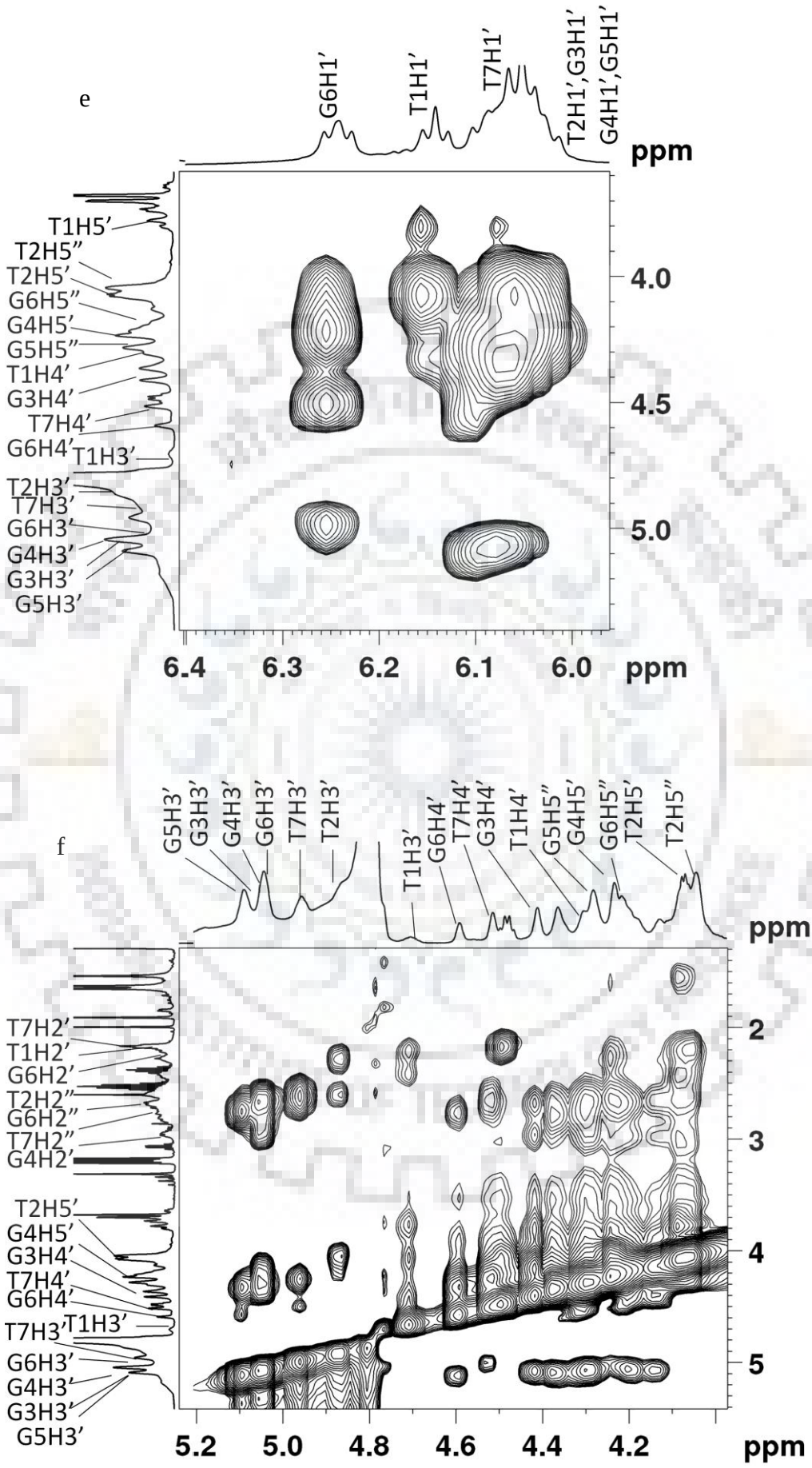
e
G6H1′
T1H1′
T7H1′
T2H1′,G3H1′
G4H1′,G5H1′
ppm
T1H5′
T2H5″
T2H5′
G6H5″
G4H5′
G5H5″
T1H4′
G3H4′
T7H4′
G6H4′
T1H3′
T2H3′
T7H3′
G6H3′
G4H3′
G3H3′
G5H3′
4.0
4.5
5.0
6.4
6.3
6.2
6.1
6.0
ppm
f
G5H3′
G3H3′
G4H3′
G6H3′
T7H3′
T2H3′
T1H3′
G6H4′
T7H4′
G3H4′
T1H4′
G5H5″
G4H5′
G6H5″
T2H5′
T2H5″
ppm
T7H2′
T1H2′
G6H2′
T2H2″
G6H2″
T7H2″
G4H2′
T2H5′
G4H5′
G3H4′
T7H4′
G6H4′
T7H3′
T1H3′
G6H3′
G4H3′
G3H3′
G5H3′
2
3
4
5
5.2
5.0
4.8
4.6
4.4
4.2
ppm

g

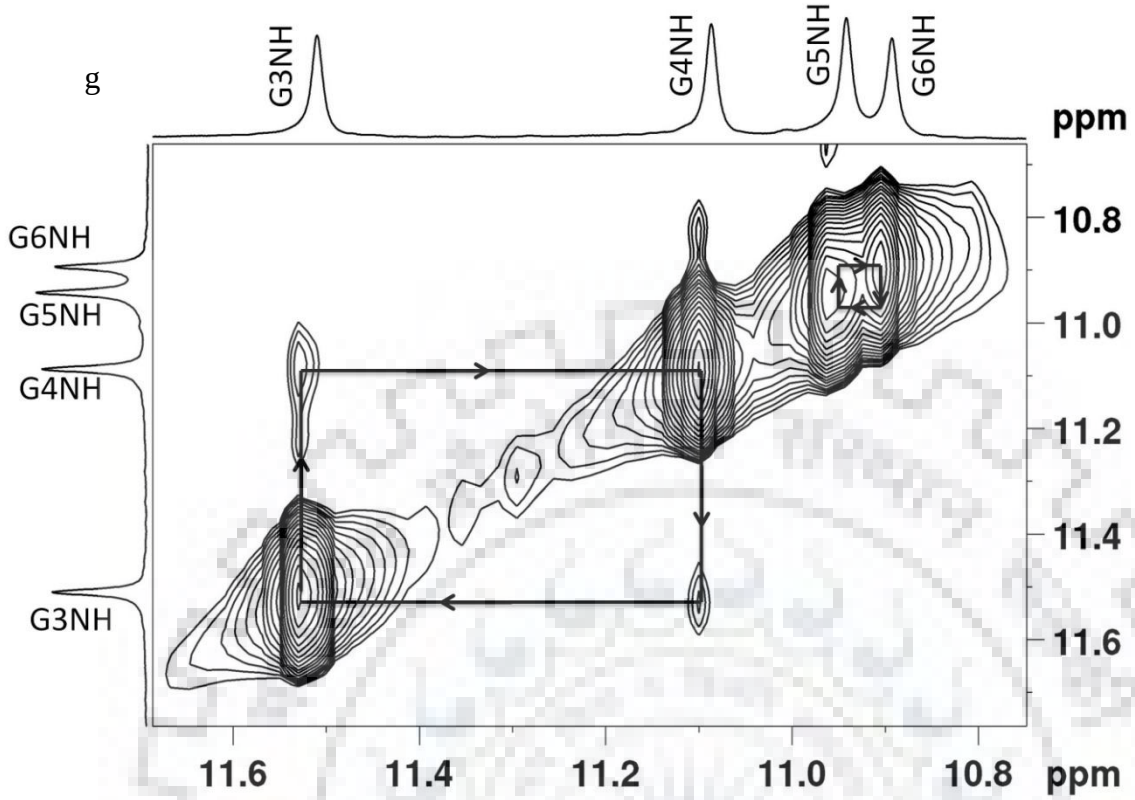
G3NH
G4NH
G5NH
G6NH
ppm
10.8
11.0
11.2
11.4
11.6
11.6
11.4
11.2
11.0
10.8
ppm

h

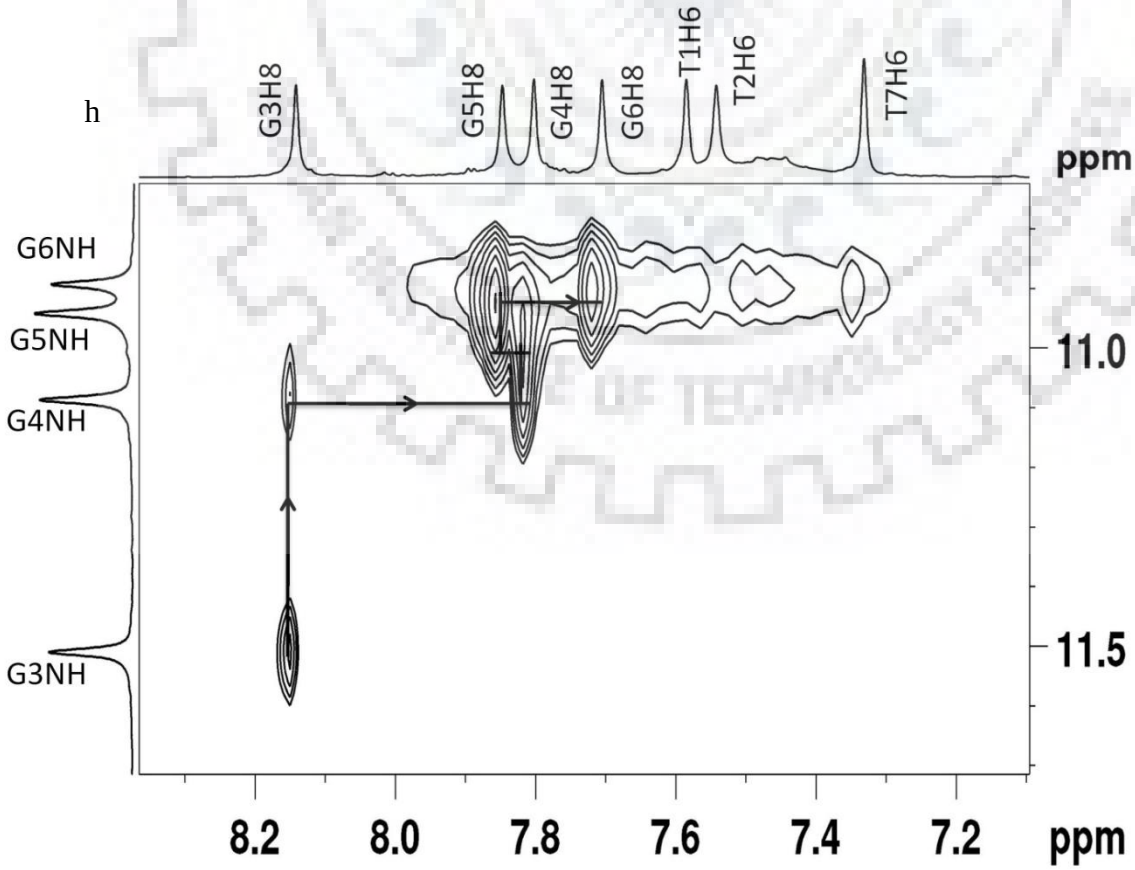
G3H8
G5H8
G4H8
G6H8
T1H6
T2H6
T7H6
ppm
G6NH
G5NH
G4NH
G3NH
11.0
11.5
8.2
8.0
7.8
7.6
7.4
7.2
ppm

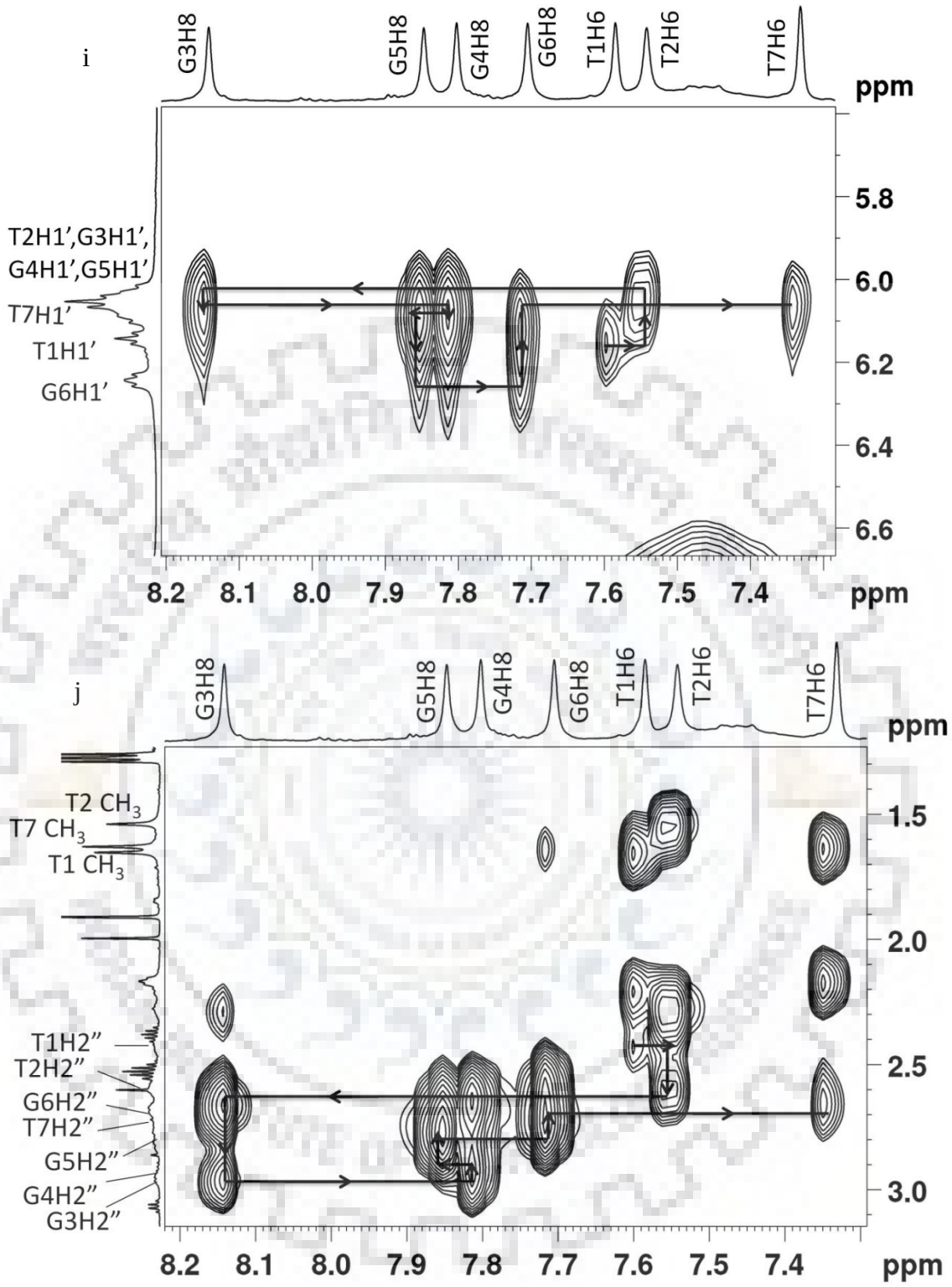

Figure 4.2 a-b) 1D-^{1}H NMR spectra of free Tet7 in KBPES buffer containing 100 mM KCl (90% H_2O+10% D_2O) at 25 °C. c-f) Expansion of specific regions ^{1}H-^{1}H 2D NOESY spectra of free Tet7 and; sequential connectivity (black arrows) between; g) imino protons; h) adjacent imino and base protons; i) base-sugar (H1') protons; and j) base-sugar (H2'/2") protons at τ_m = 250 ms in KBPES buffer (90% H_2O+10% D_2O) at 25 °C.

The quadruplex Tet7 was titrated with daunomycin at D/N = 0.0-4.0 and monitored by ^{1}H and ^{31}P NMR at several D/N ratios at 3 different temperatures, 25, 30 and 40 °C. Two dimensional ^{1}H-^{1}H NOESY, ^{1}H-^{13}C HSQC and ^{1}H-^{31}P HMBC spectra were recorded at D/N = 1.0, 2.0, 3.0 and 4.0 at 25 °C. ^{1}H-^{1}H NOESY and ^{1}H-^{13}C HSQC spectra were also recorded at 35 °C at D/N = 1.0, 2.0 and 3.0. Progressive addition of daunomycin to 1.16 mM Tet7 resulted (Fig. 4.3 a,b) in shifting and broadening of DNA proton signals along with the appearance of new signals which were subsequently assigned to daunomycin protons. A single set of sharp, well defined and intense resonances of GNH, GH8, TH6, and TCH_3 protons show that there is no loss of fourfold symmetry of Tet7 upon complexation. Unambiguous assignment of all non-exchangeable and exchangeable protons of Tet7, as well as daunomycin protons in complex at D/N = 1.0-4.0, was accomplished (Tables 4.1-4.9) by analysis of proton NMR spectra of free Tet7 (Fig. 4.2 a,b), free daunomycin (Fig. 4.4 a), daunomycin-Tet7 complex (Fig. 4.4 b,c), their corresponding ^{1}H-^{1}H NOESY (Fig. 4.2 c-j and 4.4 d-k) and ^{1}H-^{13}C HSQC (Fig. 4.5 a-d) spectra. The resonance signals of deoxyribose protons of DNA could be clearly distinguished from the daunosamine sugar and ring A/D protons signals in ^{1}H-^{13}C HSQC spectra (Fig. 4.5 a-d) in spite of spectral overlap. 1H and 3H of daunomycin (7.0-7.3 ppm) show clear distance correlation with $4OCH_3$ resonance (3.67 ppm). The carbons attached to them resonate at ~119 ppm (Fig. 4.5 a), which is far apart from ^{13}C signals of bases (133-139 ppm) and deoxyribose H1' (82-92 ppm) (Fig. 4.5 c). ^{13}C signals (63-67 ppm) of deoxyribose H5'/5" (3.7-4.4 ppm) separate out from that of $4OCH_3$, 7H, 5'H, 4'H and 3'H protons (Fig. 4.5 b). Similarly 2axH, 2eqH, 10axH, 10eqH, 8axH, 8eqH and $9COCH_3$ resonances (1.7-2.8 ppm) overlapping with deoxyribose H2'/H2" (2.2-3.0 ppm) have ^{13}C signals close to that for free drug in the range 22-35 ppm (Fig. 4.5 d), which are well separated from corresponding ^{13}C signals of H2'/H2" (36-44 ppm). The existence of a single set of resonances for both ligand and DNA shows that a well-defined stable complex is formed, which refers to the major conformer present in ligand-DNA complex.

Table 4.4 ^{1}H Chemical shift (ppm) of daunomycin protons in free daunomycin (δ_f) and daunomycin-Tet7 complex (δ_b) at D/N = 4.0 in KBPES buffer containing 100 mM KCl (90% H_2O+10% D_2O solvent) at 25 °C. Change in chemical shift of daunomycin protons due to binding, $\Delta\delta = \delta_b - \delta_f$. -ve $\Delta\delta$ indicates an upfield shift.

Protons	δ_f	δ_b	$\Delta\delta$	Protons	δ_f	δ_b	$\Delta\delta$
Ring D				Daunosamine sugar			
2H	7.71	7.20	-0.51	1'H	5.49	5.11	-0.38
1H	7.53	7.03	-0.50	2'eqH	1.99	1.81	-0.18
3H	7.43	6.93	-0.50	2'axH	1.99	1.81	-0.18
$4OCH_3$	3.94	3.60	-0.34	3'H	3.70	3.53	-0.17
Ring A				4'H	3.83	3.68	-0.15
7H	4.82	4.55	-0.27	5'H	4.27	4.05	-0.22
8eqH	2.23	1.91	-0.32	$5'CH_3$	1.30	1.05	-0.25
8axH	2.13	1.91	-0.22				
$9COCH_3$	2.45	2.28	-0.17				
10eqH	2.94	2.58	-0.36				
10axH	2.70	2.53	-0.17				

Table 4.5 ^{1}H Chemical shift (ppm) of daunomycin protons in free daunomycin (δ_f) and in daunomycin-Tet7 complex (δ_b) at various D/N ratios in KBPES buffer containing 100 mM KCl (90% H_2O+10% D_2O) at 25 °C. $\Delta\delta = \delta_b - \delta_f$, nd: not determined

Daunomycin Protons	Free Daunomycin	D/N=1.0		D/N=2.0		D/N=3.0		D/N=4.0	
	δ_f	δ_b	$\Delta\delta$	δ_b	$\Delta\delta$	δ_b	$\Delta\delta$	δ_b	$\Delta\delta$
2H	7.71	7.30	-0.41	7.26	-0.45	7.19	-0.52	7.20	-0.51
1H	7.53	7.21	-0.32	7.18	-0.35	7.09	-0.44	7.03	-0.50
3H	7.43	7.04	-0.39	7.02	-0.41	6.95	-0.48	6.93	-0.50
4OCH_3	3.94	3.70	-0.24	3.67	-0.27	3.62	-0.32	3.60	-0.34
1'H	5.49	nd	nd	4.92	-0.57	5.06	-0.43	5.11	-0.38
7H	4.82	nd	nd	4.57	-0.25	4.54	-0.28	4.55	-0.27
5'H	4.27	3.81	-0.46	3.91	-0.36	3.98	-0.29	4.05	-0.22
4'H	3.83	3.53	-0.3	3.60	-0.23	3.64	-0.19	3.68	-0.15
3'H	3.70	3.33	-0.37	3.42	-0.28	3.48	-0.22	3.53	-0.17
5'CH_3	1.30	0.74	-0.56	0.90	-0.4	1.02	-0.28	1.05	-0.25
9$COCH_3$	2.45	2.43	-0.02	2.33	-0.12	2.28	-0.17	2.28	-0.17
2'eqH	1.99	1.66	-0.33	1.77	-0.22	1.78	-0.21	1.81	-0.18
2'axH	1.99	1.56	-0.43	1.73	-0.26	1.73	-0.26	1.81	-0.18
8eqH	2.23	2.08	-0.15	1.87	-0.36	1.91	-0.32	1.91	-0.32
8axH	2.13	1.72	-0.41	1.81	-0.32	1.85	-0.28	1.91	-0.22
10eqH	2.94	2.64	-0.3	2.59	-0.35	2.56	-0.38	2.58	-0.36
10axH	2.70	2.56	-0.14	2.54	-0.16	2.53	-0.17	2.53	-0.17

* Negative sign in $\Delta\delta$ denotes upfield shift.

Table 4.6 ^{1}H Chemical shift (ppm) of methyl and imino protons in free Tet7 (δ_f) and daunomycin-Tet7complex (δ_b) at various D/N ratios in KBPES buffer containing 100 mM KCl (90% H_2O+10% D_2O) at 25 °C. $\Delta\delta = \delta_b - \delta_f$

Protons	CH_3						NH							
	T1		T2		T7		G3		G4		G5		G6	
Free DNA (δ_f)	1.65		1.53		1.63		11.51		11.08		10.94		10.89	
	δ_b	$\Delta\delta$	δ_b	$\Delta\delta$	δ_b	$\Delta\delta$	δ_b	$\Delta\delta$	δ_b	$\Delta\delta$	δ_b	$\Delta\delta$	δ_b	$\Delta\delta$
D/N=0.2	1.65	0.00	1.53	0.00	1.66	0.03	11.50	-0.01	11.07	-0.01	10.93	-0.01	10.86	-0.03
D/N=0.5	1.65	0.00	1.53	0.00	1.72	0.09	11.47	-0.04	11.06	-0.02	10.90	-0.04	10.80	-0.09
D/N=0.8	1.65	0.00	1.53	0.00	1.78	0.15	11.48	-0.03	11.05	-0.03	10.88	-0.06	10.70	-0.19
D/N=1.0	1.64	-0.01	1.53	0.00	1.80	0.17	11.47	-0.04	11.04	-0.04	10.87	-0.07	10.67	-0.22
D/N=1.5	1.63	-0.02	1.52	-0.01	1.83	0.20	11.45	-0.06	11.02	-0.06	10.85	-0.09	10.62	-0.27
D/N=2.0	1.62	-0.03	1.52	-0.01	1.84	0.21	11.42	-0.09	11.01	-0.07	10.84	-0.10	10.59	-0.30
D/N=2.5	1.61	-0.04	1.52	-0.01	1.84	0.21	11.39	-0.12	11.00	-0.08	10.83	-0.11	10.58	-0.31
D/N=3.0	1.61	-0.04	1.52	-0.01	1.84	0.21	11.37	-0.14	10.98	-0.10	10.82	-0.12	10.55	-0.34
D/N=3.5	1.60	-0.05	1.52	-0.01	1.84	0.21	11.35	-0.16	10.97	-0.11	10.82	-0.12	10.55	-0.34
D/N=4.0	1.60	-0.05	1.52	-0.01	1.84	0.21	11.36	-0.15	10.97	-0.11	10.82	-0.12	10.55	-0.34

* Negative sign in $\Delta\delta$ denotes upfield shift

Table 4.7 ^{1}H Chemical shift (ppm) of base protons in free Tet7 (δ_f) and daunomycin-Tet7 complex (δ_b) at various D/N ratios in KBPES buffer containing 100 mM KCl (90% H_2O+10% D_2O)at 25 °C. $\Delta\delta = \delta_b - \delta_f$

Protons	H8/H6													
	T1		T2		G3		G4		G5		G6		T7	
Free DNA (δ_f)	7.59		7.54		8.14		7.80		7.84		7.71		7.34	
	δ_b	$\Delta\delta$	δ_b	$\Delta\delta$	δ_b	$\Delta\delta$	δ_b	$\Delta\delta$	δ_b	$\Delta\delta$	δ_b	$\Delta\delta$	δ_b	$\Delta\delta$
D/N=0.2	7.57	-0.02	7.54	0.00	8.13	-0.01	7.80	0.00	7.83	-0.01	7.71	0.00	7.35	0.01
D/N=0.5	7.57	-0.02	7.54	0.00	8.13	-0.01	7.79	-0.01	7.82	-0.02	7.71	0.00	7.44	0.10
D/N=0.8	7.57	-0.02	7.54	0.00	8.12	-0.02	7.78	-0.02	7.8	-0.04	7.72	0.01	7.55	0.21
D/N=1.0	7.57	-0.02	7.53	-0.01	8.12	-0.02	7.78	-0.02	7.79	-0.05	7.72	0.01	7.59	0.25
D/N=1.5	7.57	-0.02	7.54	0.00	8.11	-0.03	7.78	-0.02	7.79	-0.05	7.72	0.01	7.63	0.29
D/N=2.0	7.57	-0.02	7.54	0.00	8.11	-0.03	7.77	-0.03	7.77	-0.07	7.72	0.01	7.64	0.30
D/N=2.5	7.57	-0.02	7.54	0.00	8.10	-0.04	7.76	-0.04	7.76	-0.08	7.71	0.00	7.65	0.31
D/N=3.0	7.57	-0.02	7.54	0.00	8.09	-0.05	7.75	-0.05	7.75	-0.09	7.70	-0.01	7.64	0.30
D/N=3.5	7.56	-0.03	7.54	0.00	8.07	-0.07	7.74	-0.06	7.74	-0.10	7.70	-0.01	7.64	0.30
D/N=4.0	7.57	-0.02	7.54	0.00	8.08	-0.06	7.74	-0.06	7.74	-0.10	7.69	-0.02	7.64	0.30

* Negative sign in $\Delta\delta$ denotes upfield shift.

Table 4.8 ^{1}H Chemical shift (ppm) of H1' sugar protons in free Tet7 (δ_f) and daunomycin-Tet7 complex (δ_b) at various D/N ratios in KBPES buffer containing 100 mM KCl (90% H_2O+10% D_2O) at 25 °C. $\Delta\delta = \delta_b - \delta_f$. Negative sign in $\Delta\delta$ denotes upfield shift.

Protons	H1'					
	T1		G6		T7	
Free DNA (δ_f)	6.14		6.24		6.05	
	δ_b	$\Delta\delta$	δ_b	$\Delta\delta$	δ_b	$\Delta\delta$
D/N=0.2	6.14	0.00	6.25	0.01	6.06	0.01
D/N=0.5	6.13	-0.01	6.28	0.04	6.10	0.05
D/N=0.8	6.13	-0.01	6.29	0.05	6.17	0.12
D/N=1.0	6.14	0.00	6.30	0.06	6.18	0.13
D/N=1.5	6.15	0.01	6.30	0.06	6.21	0.16
D/N=2.0	6.15	0.01	6.31	0.07	6.21	0.16
D/N=2.5	6.16	0.02	6.30	0.06	6.21	0.16
D/N=3.0	6.17	0.03	6.29	0.05	6.21	0.16
D/N=3.5	6.16	0.02	6.28	0.04	6.20	0.15
D/N=4.0	6.15	0.01	6.27	0.03	6.20	0.15

Table 4.9 ^{1}H Chemical shift (ppm) of daunomycin protons in free state (δ_f) and in daunomycin-Tet7complex (δ_b) at various D/N ratios in KBPES buffer containing 100 mM KCl (90% H_2O+10% D_2O) at 25 °C. $\Delta\delta = \delta_b - \delta_f$. Negative sign in $\Delta\delta$ denotes upfield shift.

Protons	Daunomycin							
	1H		2H		3H		5'CH_3	
Free Daunomycin (δ_f)	7.53		7.71		7.43		1.30	
	δ_b	$\Delta\delta$	δ_b	$\Delta\delta$	δ_b	$\Delta\delta$	δ_b	$\Delta\delta$
D/N=0.2	7.11	-0.42	7.20	-0.51	7.03	-0.40	0.69	-0.61
D/N=0.5	7.21	-0.32	7.30	-0.41	7.04	-0.39	0.70	-0.60
D/N=0.8	7.21	-0.32	7.30	-0.41	7.04	-0.39	0.72	-0.58
D/N=1.0	7.21	-0.32	7.30	-0.41	7.04	-0.39	0.74	-0.56
D/N=1.5	7.20	-0.33	7.29	-0.42	7.04	-0.39	0.81	-0.49
D/N=2.0	7.18	-0.35	7.26	-0.45	7.02	-0.41	0.90	-0.40
D/N=2.5	7.14	-0.39	7.22	-0.49	7.00	-0.43	0.97	-0.33
D/N=3.0	7.09	-0.44	7.19	-0.52	6.95	-0.48	1.00	-0.30
D/N=3.5	7.07	-0.46	7.17	-0.54	6.95	-0.48	1.05	-0.25
D/N=4.0	7.03	-0.50	7.16	-0.51	6.93	-0.50	1.05	-0.25

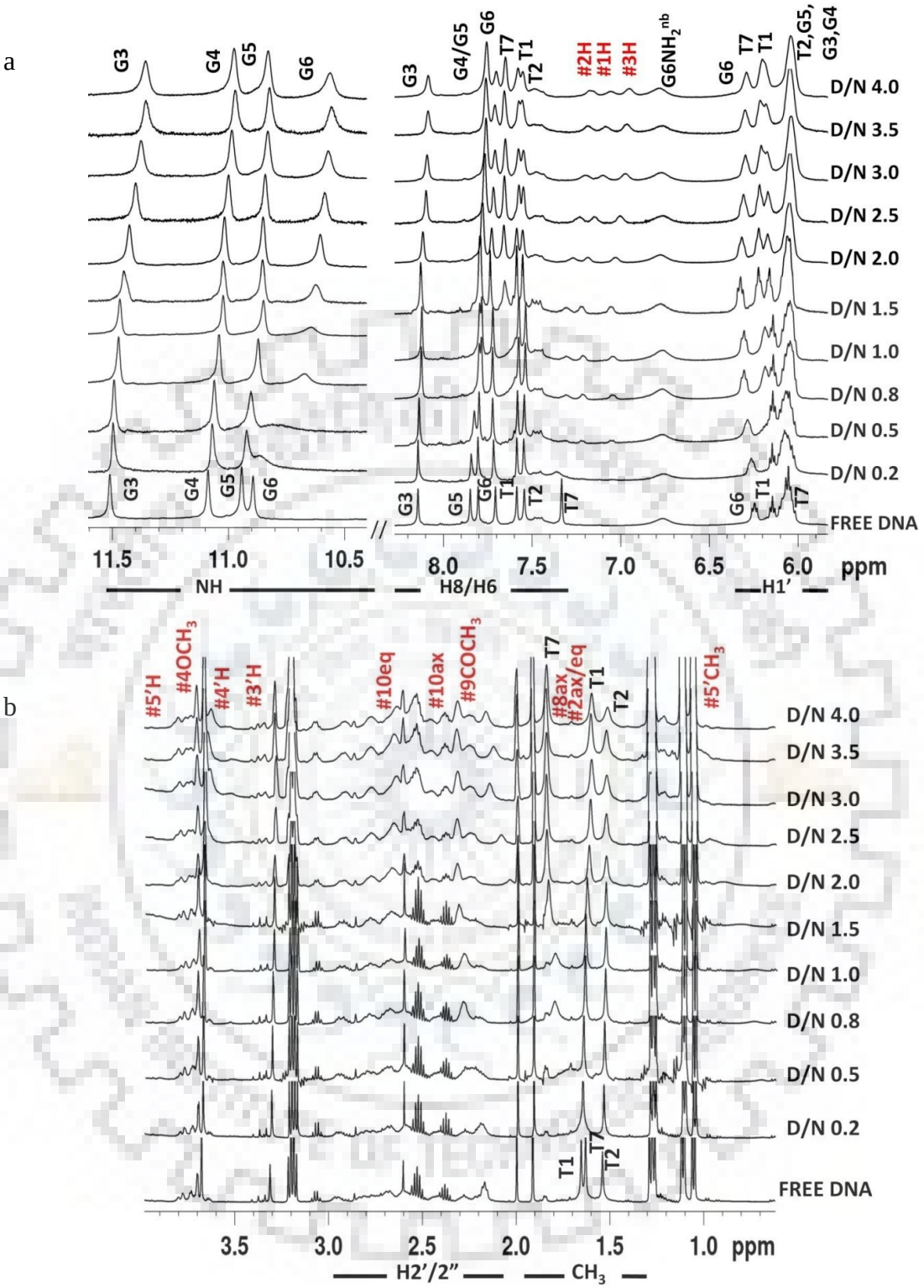

Figure 4.3 1D ^{1}H NMR spectra of 1.16 mM Tet7 and its complex upon progressive addition of daunomycin at different D/N ratios at 25 °C; a) Imino, base and sugar H1' protons along with ring D aromatic protons 1H, 2H and 3H of daunomycin; b) Deoxyribose sugar H2'/2" and methyl protons of thymine along with daunomycin protons 5'H, 4OCH_3, 4'H, 3'H, 10eqH, 10axH, 9$COCH_3$, 8axH, 2axH, 2eqH and 5'CH_3 at 25 °C. Symbol # denotes daunomycin protons.

a

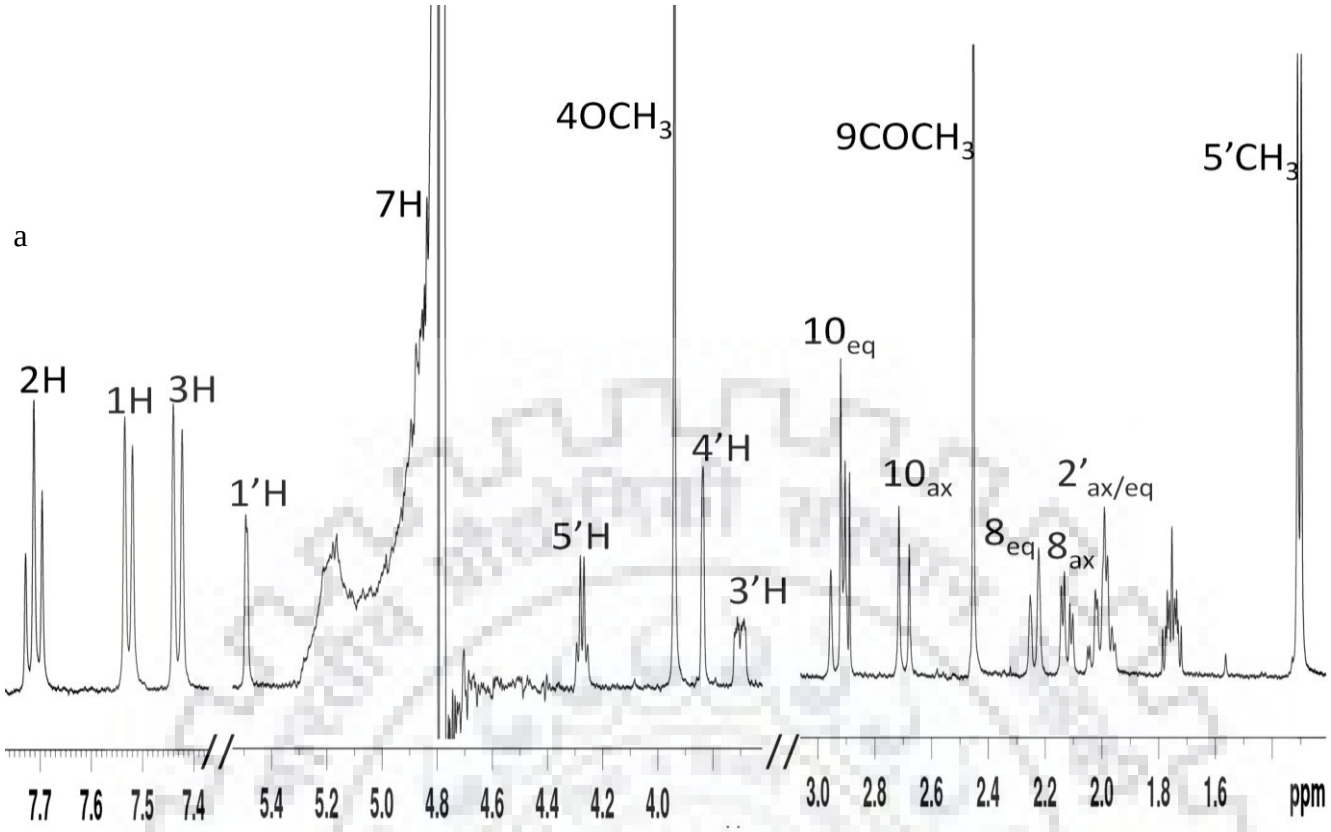
2H
1H
3H
1'H
7H
4OCH3
5'H
4'H
3'H
10eq
9COCH3
10ax
8eq
8ax
2'ax/eq
5'CH3
7.7 7.6 7.5 7.4 5.4 5.2 5.0 4.8 4.6 4.4 4.2 4.0 3.0 2.8 2.6 2.4 2.2 2.0 1.8 1.6 ppm

b

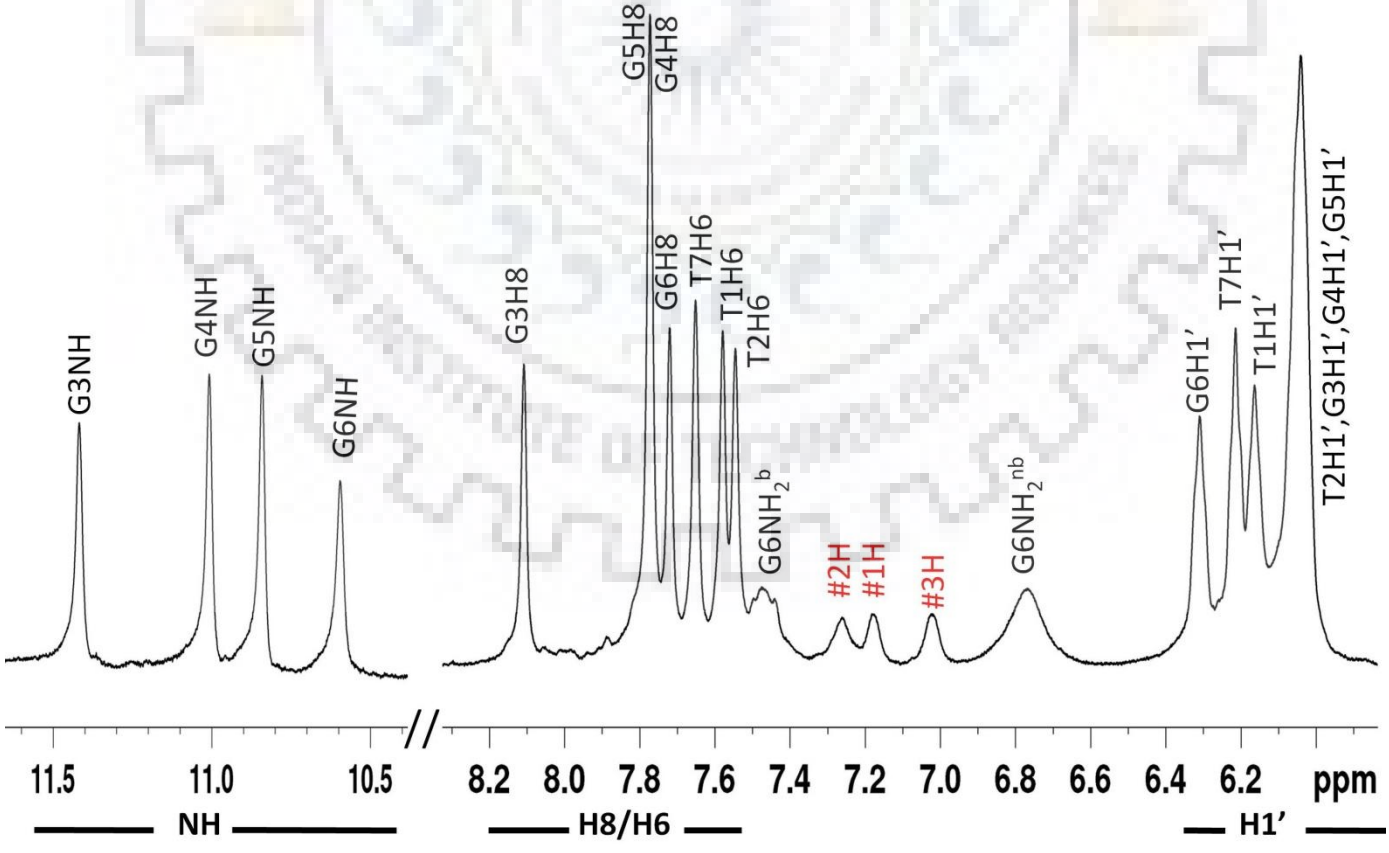
G3NH
G4NH
G5NH
G6NH
G3H8
G5H8
G4H8
G6H8
T7H6
T1H6
T2H6
G6NH2b
#2H
#1H
#3H
G6NH2nb
G6H1'
T7H1'
T1H1'
T2H1',G3H1',G4H1',G5H1'
11.5 11.0 10.5 8.2 8.0 7.8 7.6 7.4 7.2 7.0 6.8 6.6 6.4 6.2 ppm
NH
H8/H6
H1'

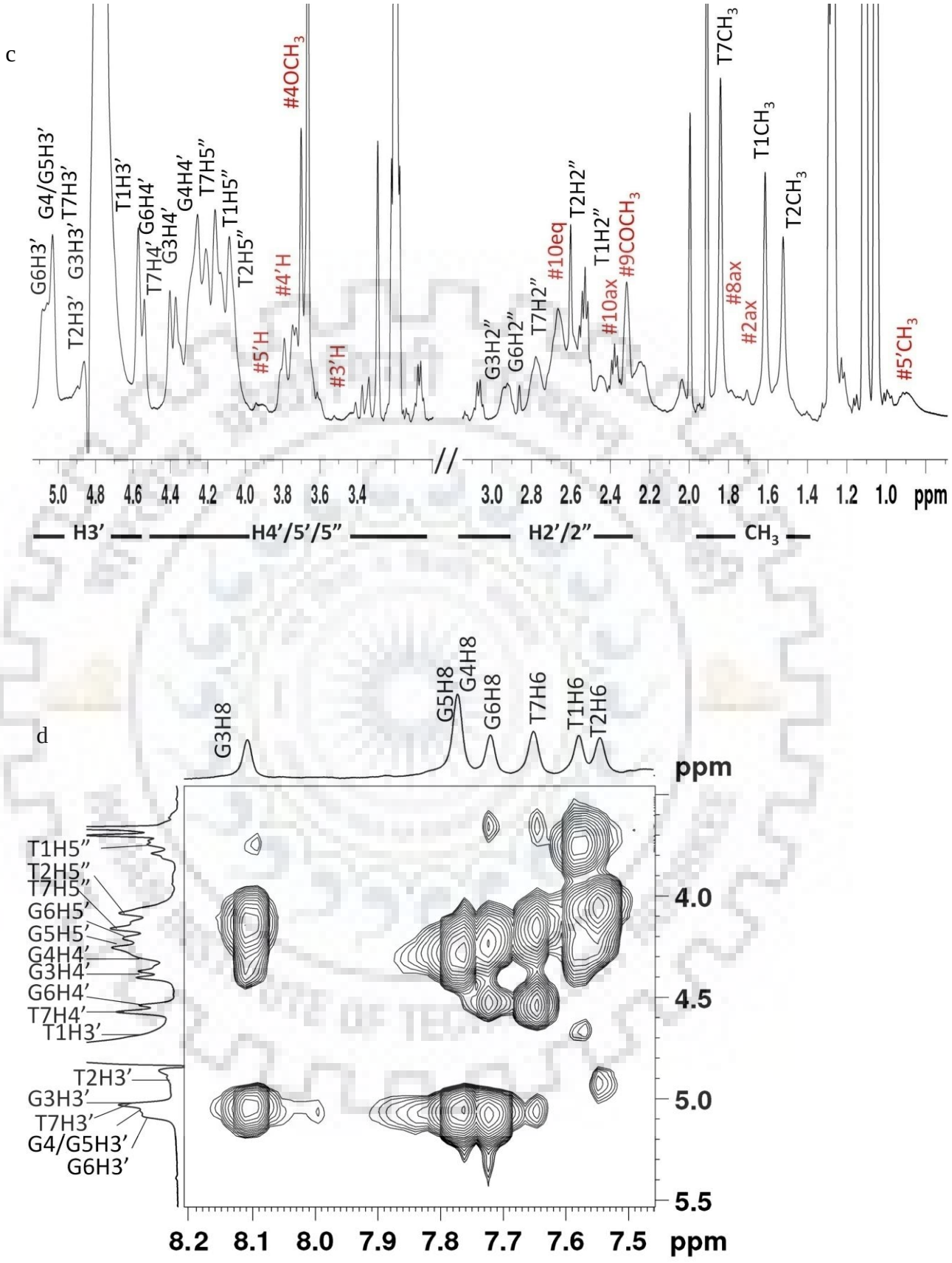
c
G6H3'
G4/G5H3'
T7H3'
G3H3'
T2H3'
T1H3'
G6H4'
T7H4'
G3H4'
G4H4'
T7H5"
T1H5"
T2H5"
#5'H
#4OCH3
#4'H
#3'H
G3H2"
G6H2"
T7H2"
#10eq
T2H2"
T1H2"
#10ax
#9COCH3
T7CH3
#8ax
#2ax
T1CH3
T2CH3
#5'CH3
5.0 4.8 4.6 4.4 4.2 4.0 3.8 3.6 3.4 3.0 2.8 2.6 2.4 2.2 2.0 1.8 1.6 1.4 1.2 1.0 ppm
H3'
H4'/5'/5"
H2'/2"
CH3
d
G3H8
G5H8
G4H8
G6H8
T7H6
T1H6
T2H6
ppm
T1H5"
T2H5"
T7H5"
G6H5'
G5H5'
G4H4'
G3H4'
G6H4'
T7H4'
T1H3'
T2H3'
G3H3'
T7H3'
G4/G5H3'
G6H3'
4.0
4.5
5.0
5.5
8.2 8.1 8.0 7.9 7.8 7.7 7.6 7.5 ppm

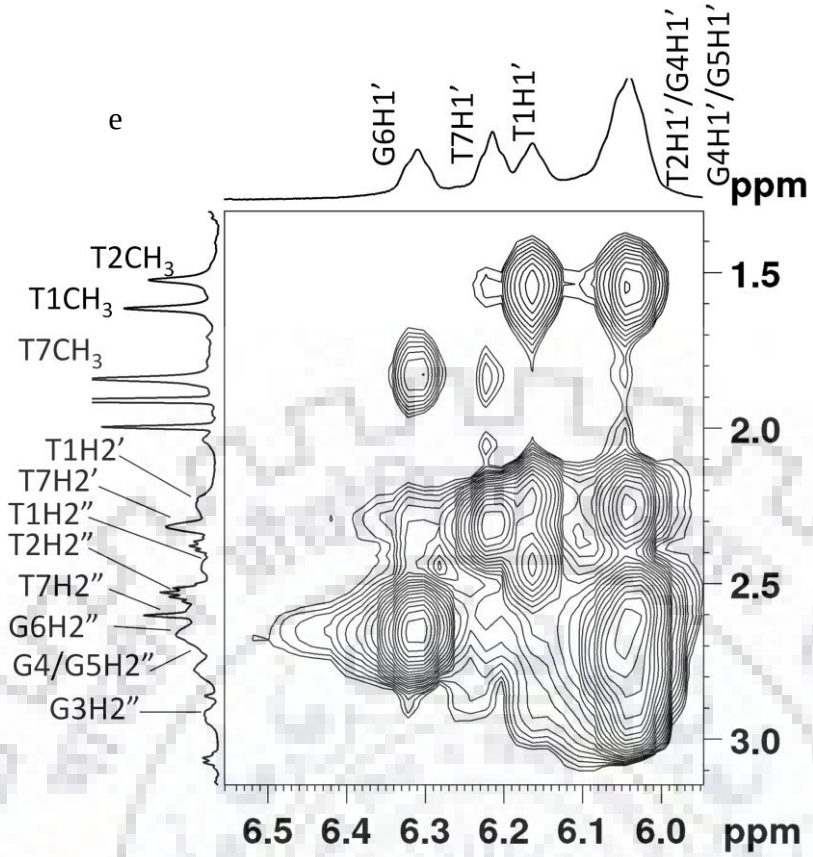
e
G6H1′
T7H1′
T1H1′
T2H1′/G4H1′
G4H1′/G5H1′
ppm
T2CH3
T1CH3
T7CH3
T1H2′
T7H2′
T1H2″
T2H2″
T7H2″
G6H2″
G4/G5H2″
G3H2″
1.5
2.0
2.5
3.0
6.5 6.4 6.3 6.2 6.1 6.0 ppm

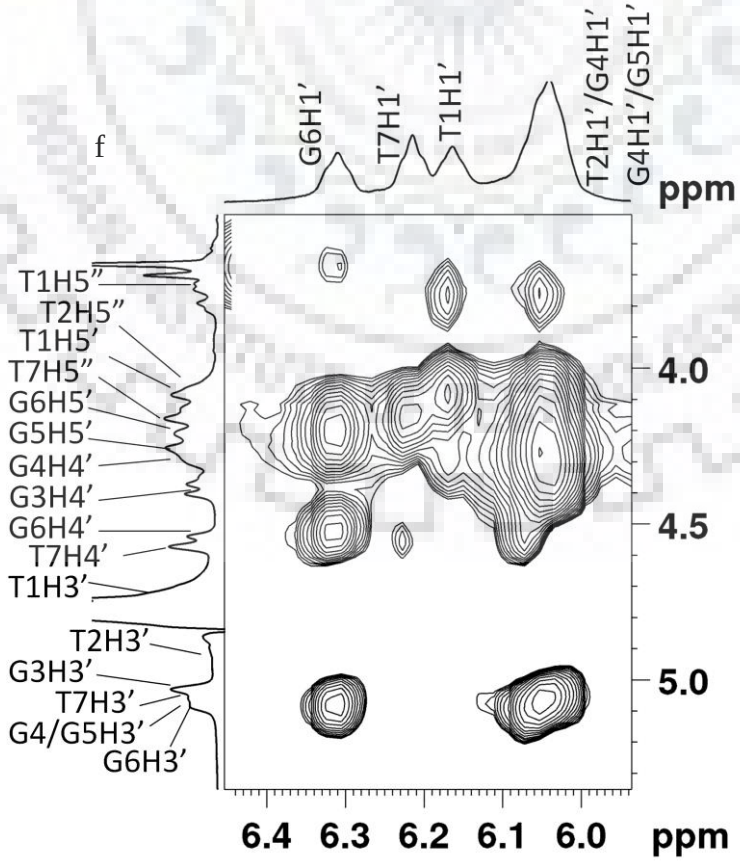
f
G6H1′
T7H1′
T1H1′
T2H1′/G4H1′
G4H1′/G5H1′
ppm
T1H5″
T2H5″
T1H5′
T7H5″
G6H5′
G5H5′
G4H4′
G3H4′
G6H4′
T7H4′
T1H3′
T2H3′
G3H3′
T7H3′
G4/G5H3′
G6H3′
4.0
4.5
5.0
6.4 6.3 6.2 6.1 6.0 ppm

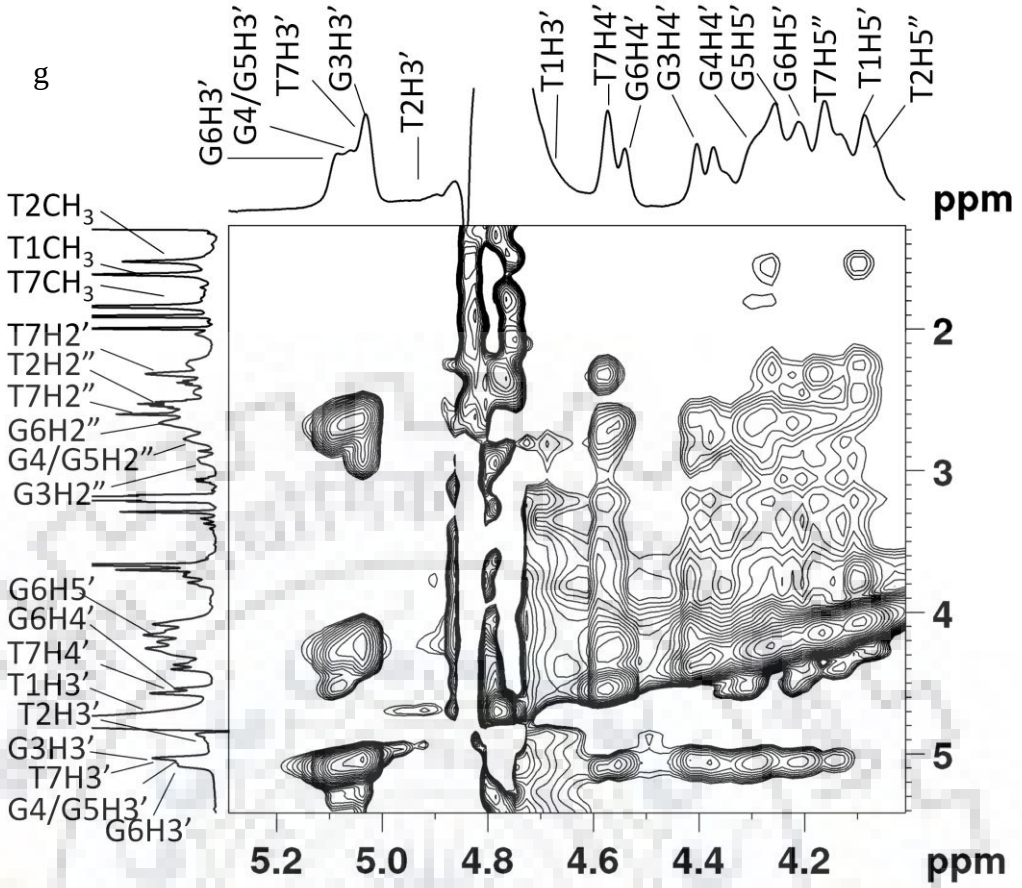
g
G6H3′
G4/G5H3′
T7H3′
G3H3′
T2H3′
T1H3′
T7H4′
G6H4′
G3H4′
G4H4′
G5H5′
G6H5′
T7H5″
T1H5′
T2H5″
ppm
T2CH3
T1CH3
T7CH3
T7H2′
T2H2″
T7H2″
G6H2″
G4/G5H2″
G3H2″
G6H5′
G6H4′
T7H4′
T1H3′
T2H3′
G3H3′
T7H3′
G4/G5H3′
G6H3′
2
3
4
5
5.2
5.0
4.8
4.6
4.4
4.2
ppm

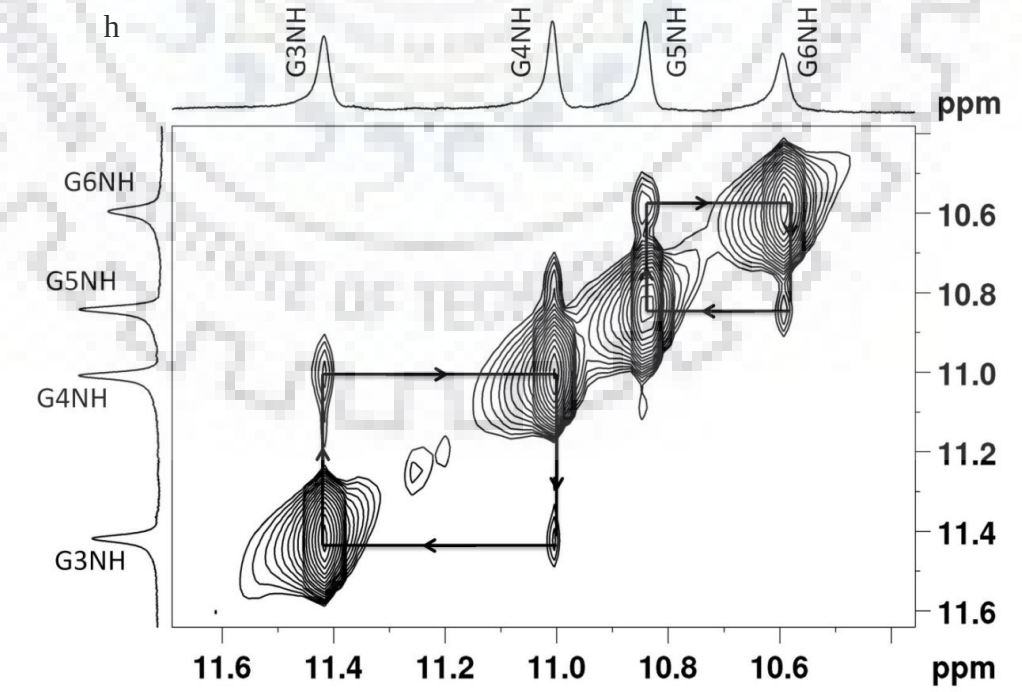
h
G3NH
G4NH
G5NH
G6NH
ppm
G6NH
G5NH
G4NH
G3NH
10.6
10.8
11.0
11.2
11.4
11.6
11.6
11.4
11.2
11.0
10.8
10.6
ppm

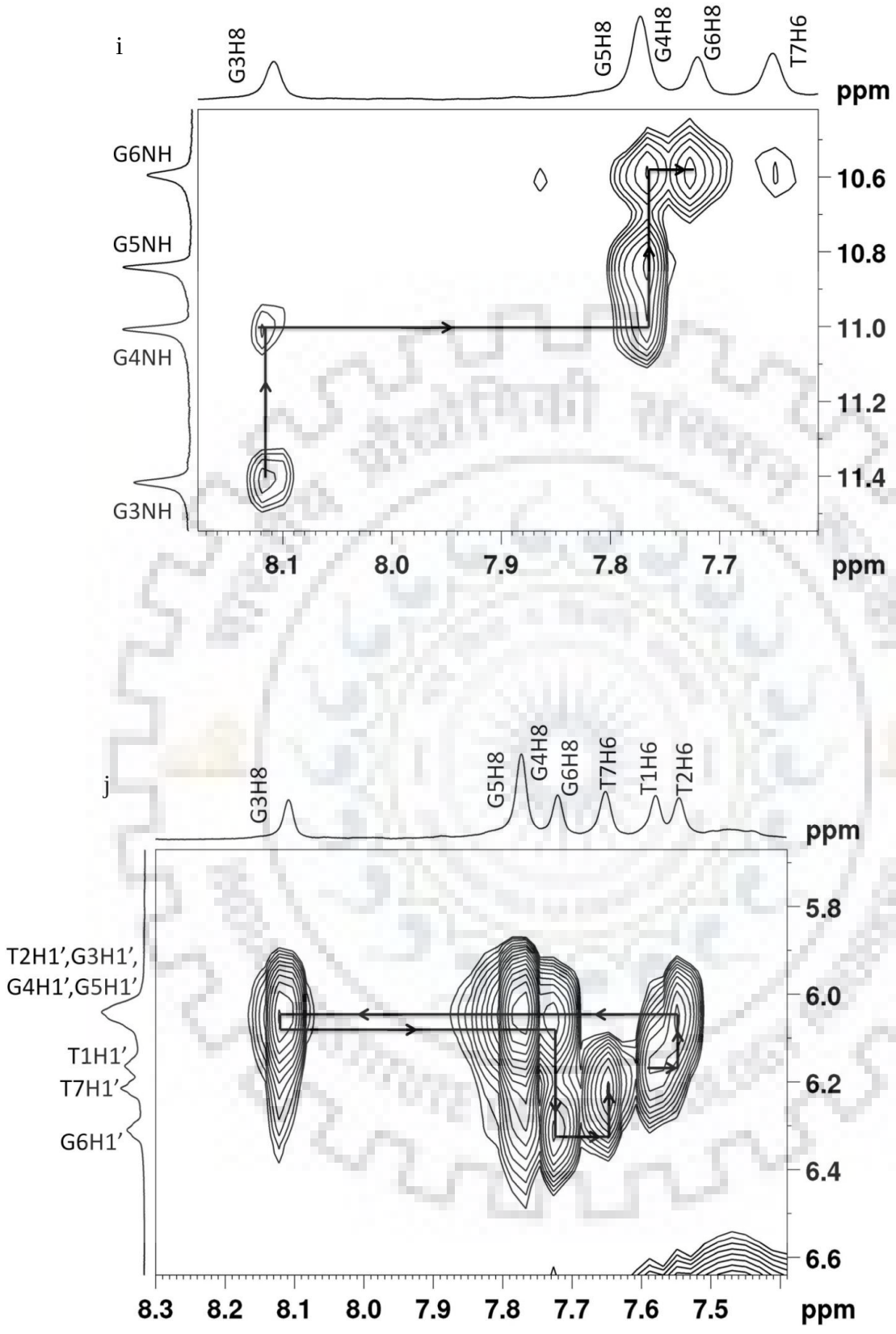
i
G3H8
G5H8
G4H8
G6H8
T7H6
ppm
G6NH
G5NH
G4NH
G3NH
10.6
10.8
11.0
11.2
11.4
8.1
8.0
7.9
7.8
7.7
ppm
j
G3H8
G5H8
G4H8
G6H8
T7H6
T1H6
T2H6
ppm
T2H1',G3H1',
G4H1',G5H1'
T1H1'
T7H1'
G6H1'
5.8
6.0
6.2
6.4
6.6
8.3
8.2
8.1
8.0
7.9
7.8
7.7
7.6
7.5
ppm

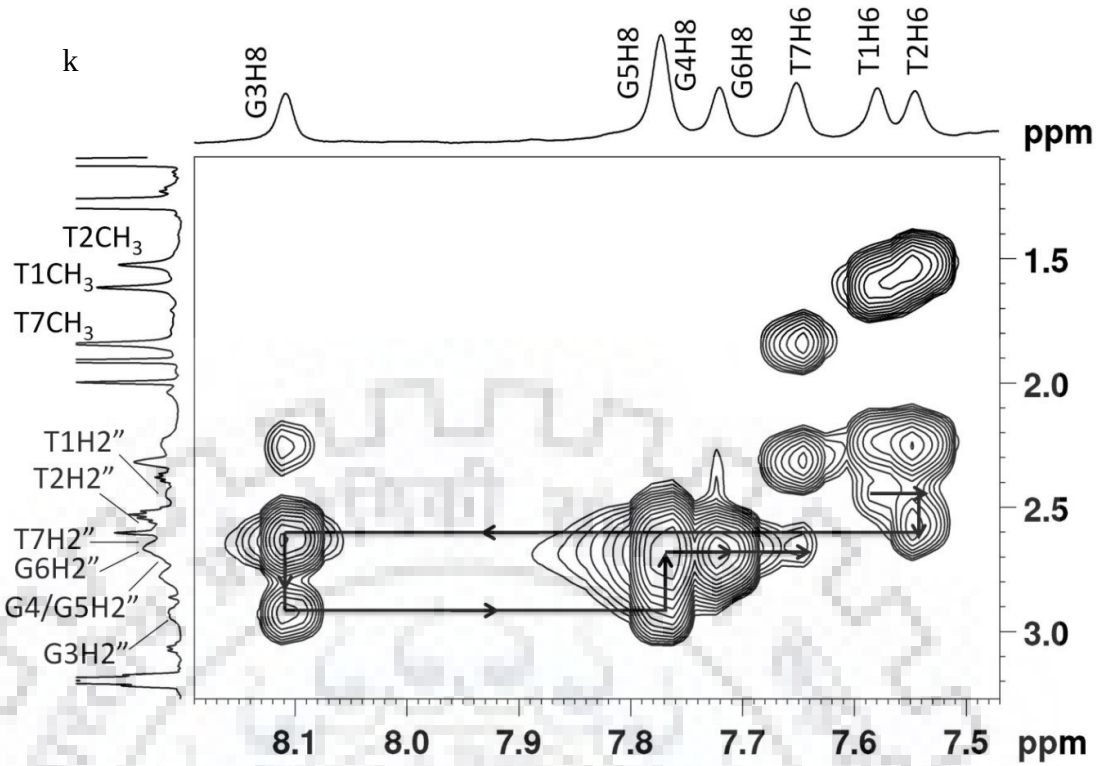

Figure 4.4 a) 1D ^{1}H NMR spectrum of free daunomycin in water (90% H_2O+10% D_2O) at 25 °C. b-c) 1D ^{1}H NMR spectrum of daunomycin-Tet7complex at D/N = 2.0 in KBPES buffer. Daunomycin protons are represented by (#); d-g) Expansion of ^{1}H-^{1}H 2D NOESY spectra of daunomycin-Tet7complex at D/N = 2.0 ; and sequential connectivity (black arrows) between h) imino protons; i) adjacent imino and base protons; j) base-sugar (H1') protons; and k) base-sugar (H2'/2") protons at τ_m = 250 ms in KBPES buffer (90% H_2O+10% D_2O) at 25 °C.

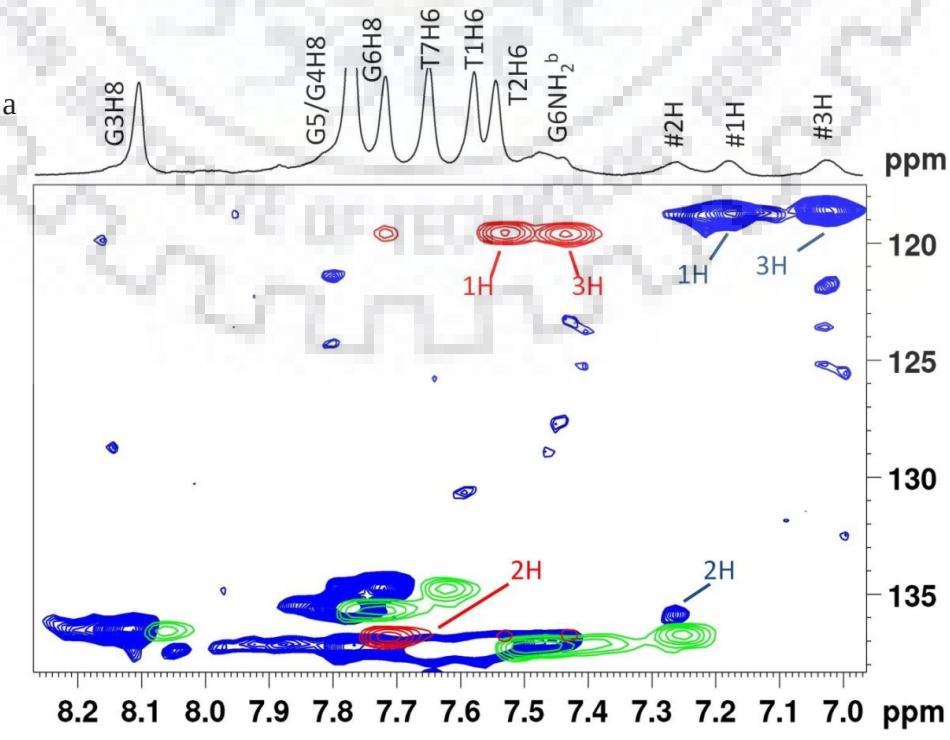

b

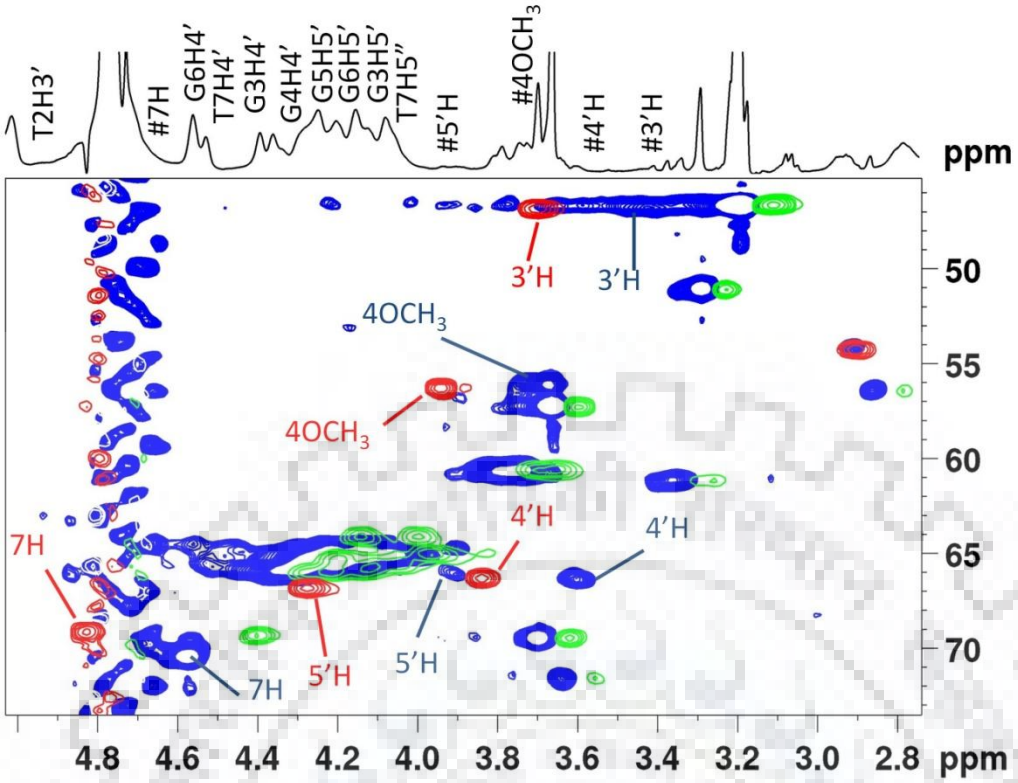
T2H3′
#7H
G6H4′
T7H4′
G3H4′
G4H4′
G5H5′
G6H5′
G3H5′
T7H5″
#5′H
#4OCH3
#4′H
#3′H
ppm
3′H
3′H
4OCH3
4OCH3
4′H
4′H
7H
5′H
5′H
7H
50
55
60
65
70
4.8
4.6
4.4
4.2
4.0
3.8
3.6
3.4
3.2
3.0
2.8
ppm

c

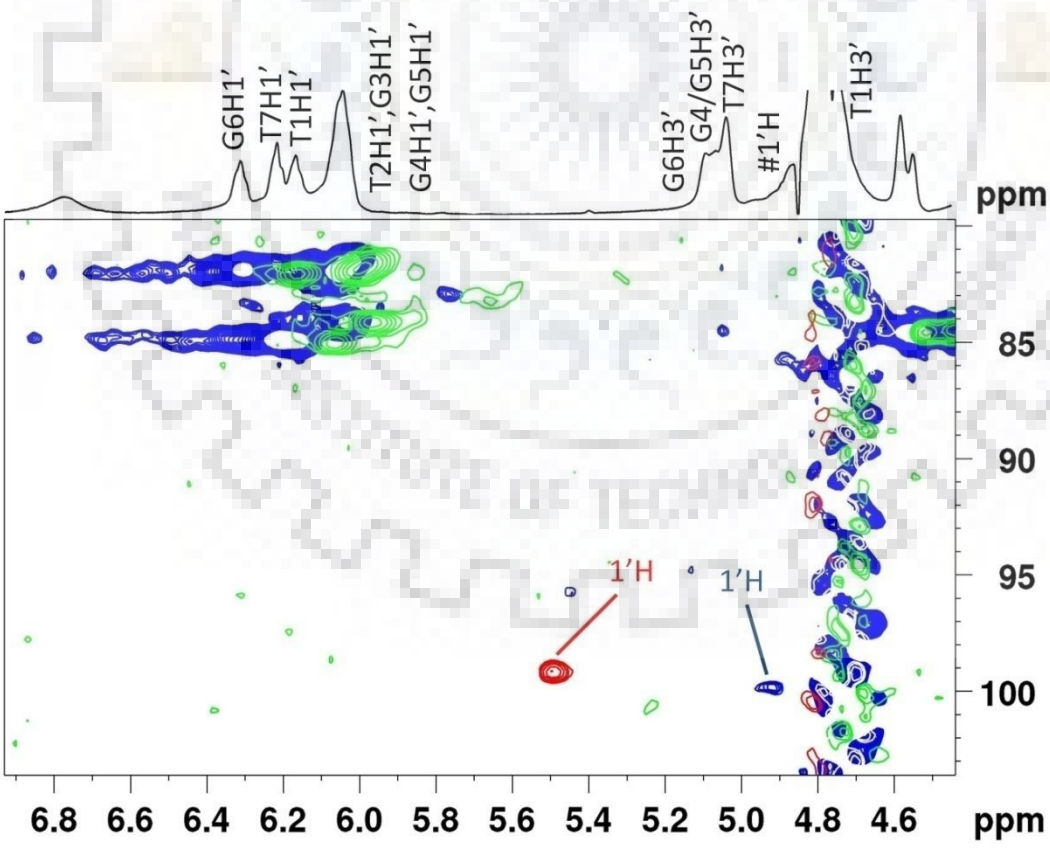
G6H1′
T7H1′
T1H1′
T2H1′,G3H1′
G4H1′,G5H1′
G6H3′
G4/G5H3′
T7H3′
#1′H
T1H3′
ppm
1′H
1′H
85
90
95
100
6.8
6.6
6.4
6.2
6.0
5.8
5.6
5.4
5.2
5.0
4.8
4.6
ppm

d

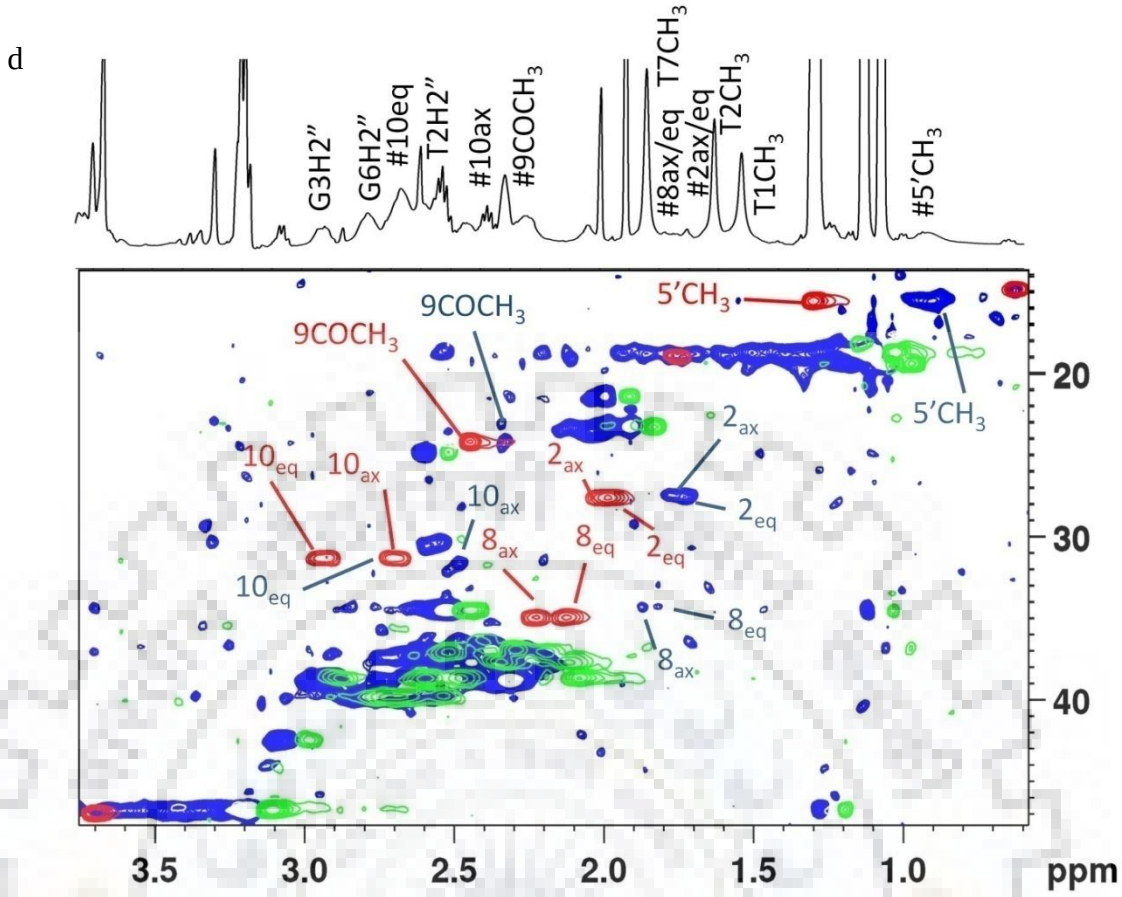

Figure 4.5 a-d) Expansion of specific region of 2D ^{1}H-^{13}C HSQC spectrum showing overlay of free daunomycin (red), free Tet7 (green) and daunomycin-Tet7complex at D/N = 2.0 (blue) in KBPES buffer (90% H_2O+10% D_2O) at 25 °C. 1D ^{1}H NMR spectrum at the top of HSQC spectra is daunomycin-Tet7 complex at D/N = 2.0.

The initial addition of 0.2 and 0.5 mole equivalents of daunomycin to Tet7 resulted in the severe broadening of G6NH, T7H6 and $T7CH_3$ (Fig. 4.3 a,b) suggestive of binding close to these bases. The broadening is maximum at D/N = 1.0. On addition of 2 mole equivalents of drug, all the three resonances become sharp and remain sharp up to D/N = 4.0, pointing towards a stoichiometry of 2:1 in daunomycin-Tet7 complex (Fedoroff et al., 1998; Cocco et al., 2003; Gavathiotis et al., 2003; Scaglioni et al., 2016; Pradeep & Barthwal, 2016; Padmapriya & Barthwal, 2017; Kumar & Barthwal, 2018). This is in accord with Job plot which uses lower concentrations of DNA but identical conditions of salt concentration and temperature. The patterns of perturbations in NMR spectra reflect the position, stability, and kinetics of binding events. The G6NH, T7H6, $T7CH_3$ and T7H1' show a continuous change in chemical shift up to D/N = 2.0-2.5 beyond which they stop drifting (Table 4.6-4.8). On the other hand $T1CH_3$, G3NH, G3H8 and G4H8 show noticeable upfield shift (0.05-0.15 ppm)

(Table 4.6-4.8) as well as broadening of signals (Fig. 4.3 a,b) at D/N>2.0-2.5. Therefore, another binding site is located close to T1-T2-G3 bases on 5'-end. The binding at 2 sites may be sequential or else simultaneous binding takes place, but binding affinity at T1-T2-G3 site is apparently lower so that the site gets occupied at relatively higher D/N ratios. G6NH shifts significantly upfield by 0.34 ppm while T7H6, T7CH_3 and T7H1' shift downfield by 0.30, 0.21 and 0.15 ppm, respectively. Sequence-specific changes in proton NMR signals of DNA rule out the existence of a non-specific adherence of daunomycin externally to DNA. Changes in the chemical shift reflect the chemical environment of interacting molecules and large upfield shift are generally indicative of stacking interactions (Scaglioni et al., 2016; Pradeep & Barthwal, 2016; Padmapriya & Barthwal, 2017; Kumar & Barthwal, 2018). Apparently, G6 base is better stacked on complexation while T7 appears to be destacked. This can occur if the ligand stacks with G6 quartet and T7 unit, which is rather flexible, is pushed away by the ligand. The change in chemical shift in T1, T2, G3 protons is relatively much lesser (Fig. 4.6), it being a maximum of 0.15 ppm in G3NH. It is possible that ligand binds near this site externally without significantly affecting DNA conformation. Also, the G4 and G5 residues show minor changes throughout the course of titrations which may be due to minor conformational adjustments in DNA as more and more of daunomycin binds.

We obtained an estimate of binding constant from variation in chemical shift of several protons with D/N ratio (Table 4.6-4.8) which gives K_b ~1.8-2.3x10^4 M^{-1} for T7H6, T7CH_3 protons, 2.3x10^3 M^{-1} for G6NH, and 1.4x10^2 M^{-1} for T1CH_3 protons, (Fig. 4.7 a-d) so that binding at G6-T7 residues has greater affinity than corresponding T1-T2-G3 site. Daunomycin protons show expected intramolecular NOE connectivities (Table 4.10) due to the proximity of pairs of protons as observed in the case of free daunomycin (P. Agrawal, Barthwal, et al., 2009). All daunomycin protons shift upfield on binding to DNA. The upfield shift in 2H, 1H, 3H, 4OCH_3, 1'H, 8eqH, and 10eqH are significant being 0.51, 0.50, 0.50, 0.34, 0.38, 0.32 and 0.39 ppm, respectively while other protons shift by 0.13-0.27 ppm at D/N = 4.0 (Fig. 4.8, Table 4.4). The change is continuous with D/N ratio in the range D/N = 0.5-4.0. Since the binding affinity at one site is relatively stronger, both sites may not be occupied at D/N = 2.0. The aromatic ring protons of ring D and those lying equatorially or close to plane ABCD of aromatic rings are upfield shifted to a large extent, perhaps due to ring current effects of nucleic acid bases. Since all sequential NOE connectivities are intact and there is no possibility of classical intercalation, the ring ABCD of daunomycin could partially stack with G6 base by destacking T7 base. Among daunosamine sugar protons, significantly large upfield shifts in 5'H and 5'CH_3 protons

(0.27-0.31 ppm) show that daunosamine sugar may interact with DNA backbone in the bound complex. Although DNA peaks sharpened at D/N = 2.0, the daunomycin peaks remained broader than the DNA base and imino signals. The existence of only one set of daunomycin signals requires the ligand to be in fast exchange among all possible bound conformations, that is, due to either of the two sites or both sites on DNA being occupied by the ligand. The hydroxyl protons at 6, 11, 9 and 4' positions were not observable in any spectra of complex even at low temperatures, that is, 5 °C.

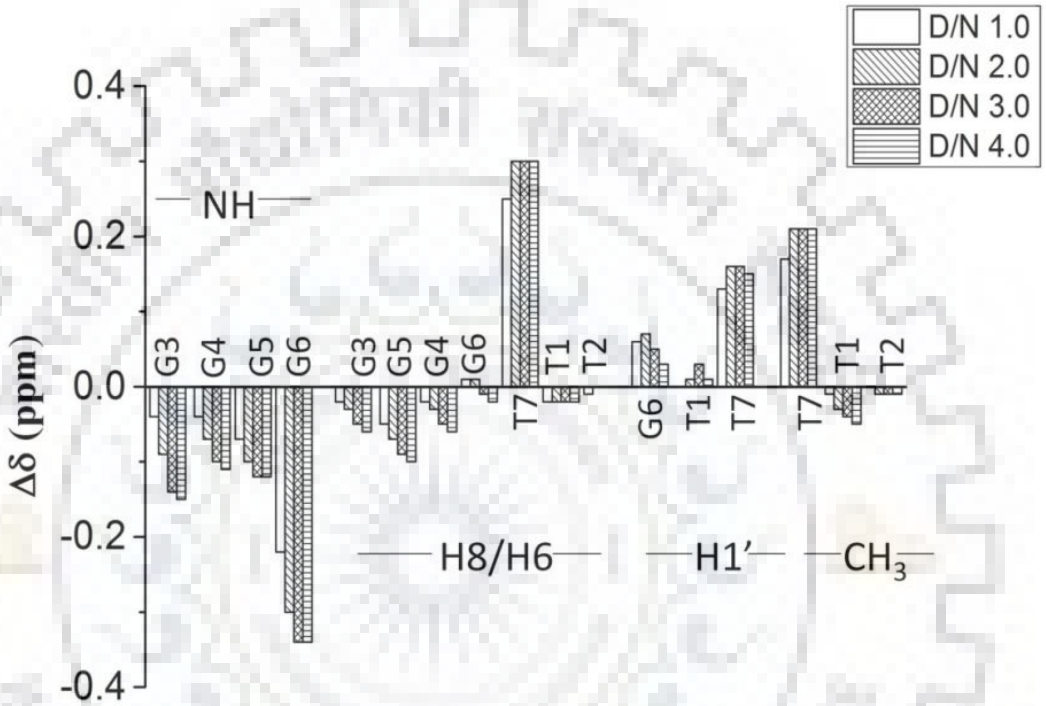

Figure 4.6 Bar diagram showing the change in ^{1}H chemical shift (Δδ) of Tet7 protons upon complex formation with daunomycin at different D/N ratios.

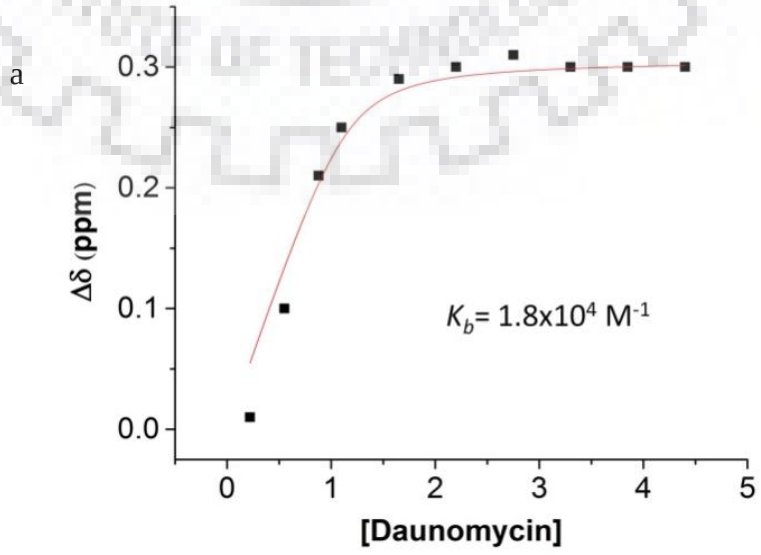

b

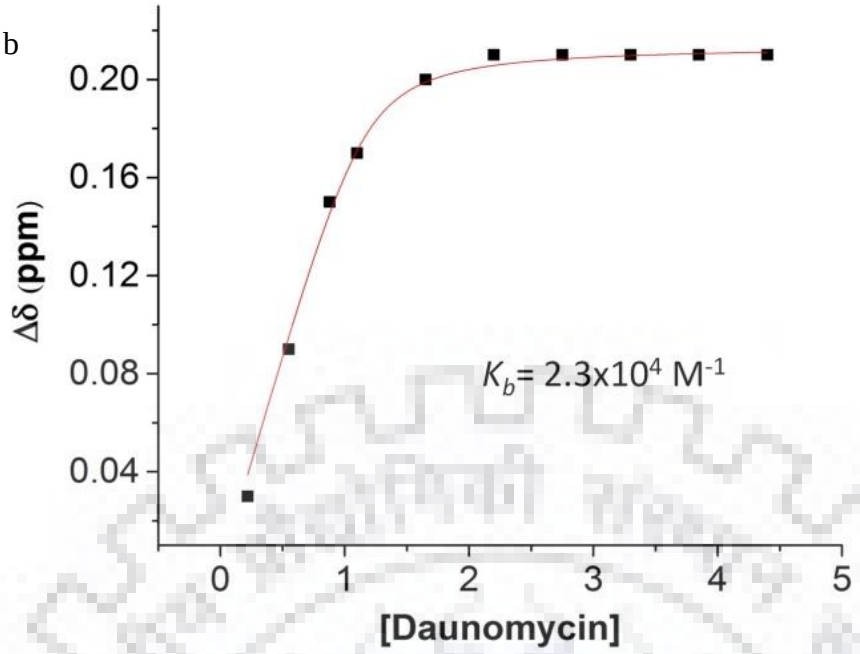
0.20
0.16
0.12
0.08
0.04
Δδ (ppm)
K_b= 2.3x10^4 M^{-1}
0
1
2
3
4
5
[Daunomycin]

c

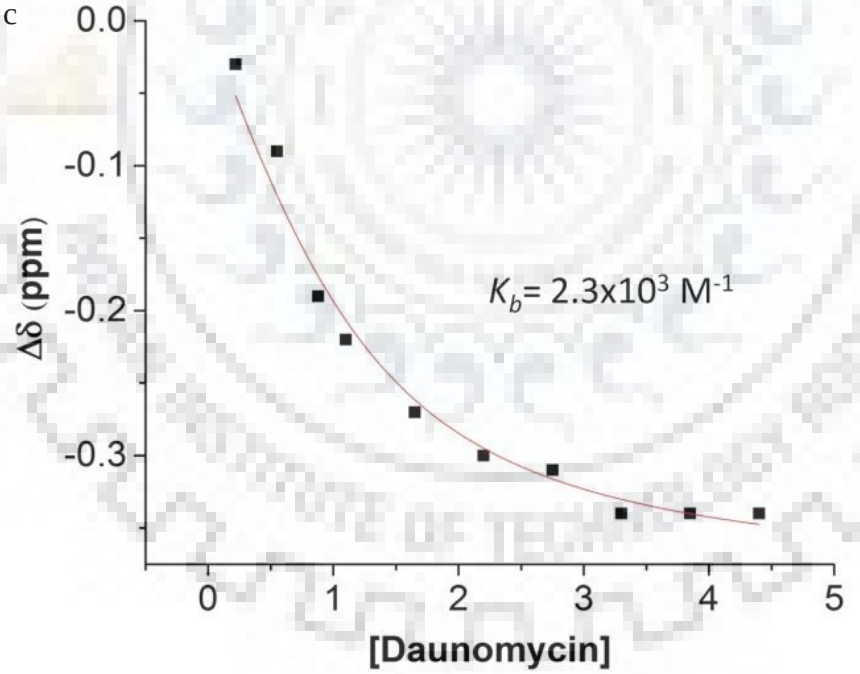
0.0
-0.1
-0.2
-0.3
Δδ (ppm)
K_b= 2.3x10^3 M^{-1}
0
1
2
3
4
5
[Daunomycin]

d

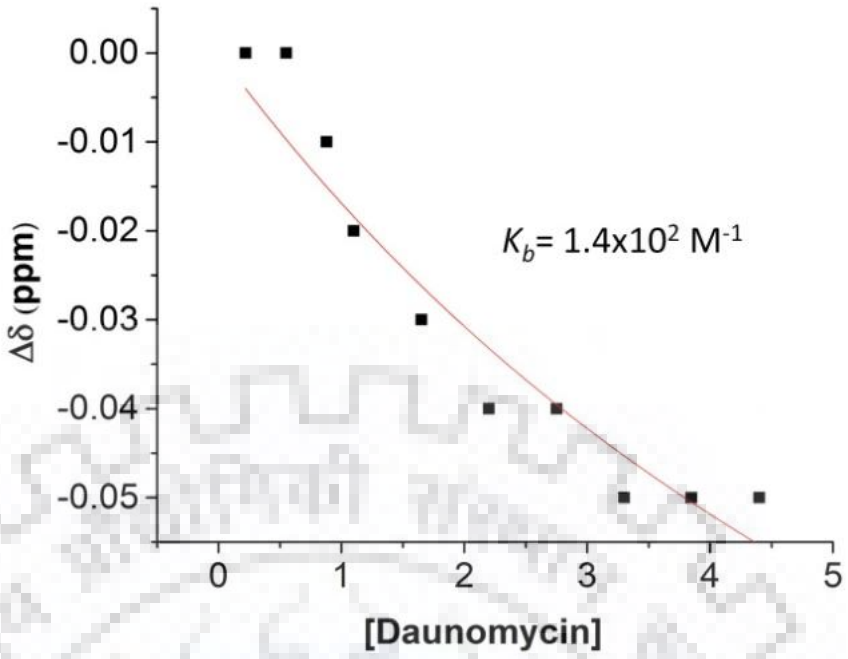

Figure 4.7 Nonlinear fitted curve (red) for simultaneous binding at two different sites in daunomycin-Tet7complex of protons a) T7H6, b) T7CH_3, c) G6NH and d) T1CH_3. Plot shows the change in chemical shift (Δδ) of protons at D/N = 0.2-4.0 as a function of daunomycin concentration (μM) showing binding constants (K_b) at 25 °C.

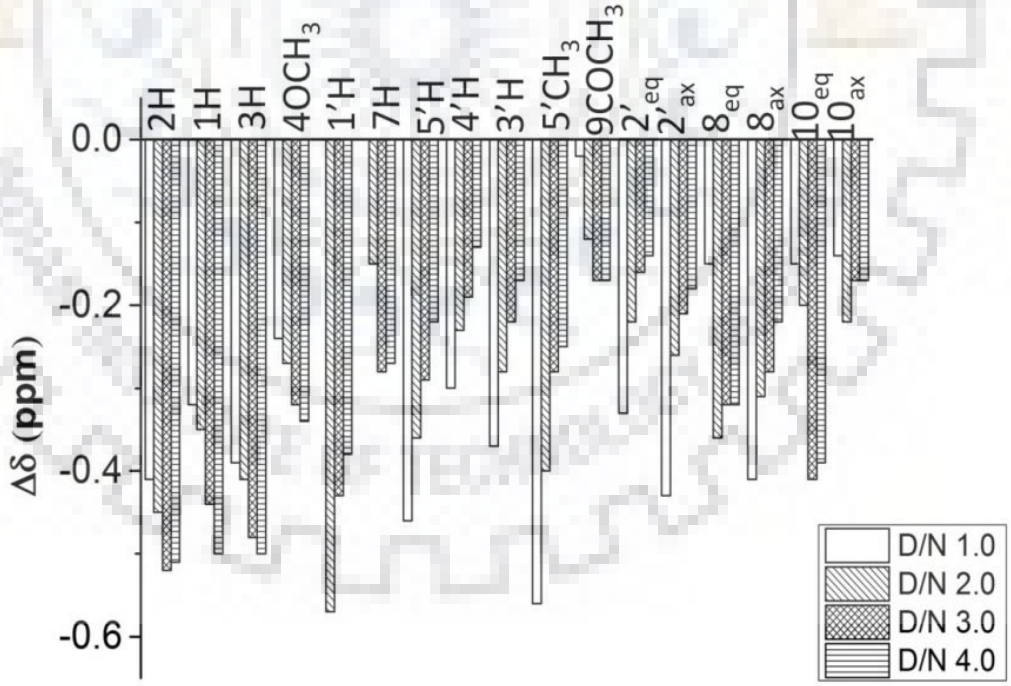

Figure 4.8 Bar diagram showing change in ^{1}H chemical shift (Δδ) of daunomycin protons on complexation at D/N = 1.0, 2.0, 3.0 and 4.0 in 10 mM phosphate buffer with 100 mM KCl (90% H_2O + 10% D_2O) at 25 °C.

Table 4.10 Intramolecular distances (Å) and relative intensities of intramolecular NOE cross peaks of daunomycin protons in daunomycin-Tet7 complex at D/N = 1.0, 2.0, 3.0 and 4.0 at τ_m = 250 ms at 25 °C. nd: not determined s - strong, m - medium, w - weak intensity; o - overlap

S.No.	Label	Intra molecular NOE correlations	Interproton distance at D/N=2.0	Intensity of NOE cross peak at D/N=1.0	Intensity of NOE cross peak at D/N=2.0	Intensity of NOE cross peak at D/N=3.0	Intensity of NOE cross peak at D/N=4.0
1	D1	5'CH_3-5'H	2.70	s	s	s	s
2	D2	5'CH_3-4'H	2.74	s	s	s	s
3	D3	5'CH_3-3'H	3.58	w	m	w	nd
4	D4	2'$_{eq}$-4'H	2.95	m	m	m	nd
5	D5	2'$_{eq}$-3'H	2.66	s	s	s	nd
6	D6	4OCH_3-2H	2.90	s	s	s	s
7	D7	4OCH_3-1H	3-4	m	m/broad	m/broad	m/broad
8	D8	4OCH_3-3H	2.20	s	s	s	s
9	D9	5'H-4'H	2.70	nd	s	nd	nd
10	D10	5'H-3'H	3.01	nd	m	m	nd
11	D11	8$_{ax}$-5'H	2.72	s	s	s	nd

4.3.3 Phosphorus-31 Nuclear Magnetic Resonance

The phosphorus-31 NMR signals were assigned using standard strategies by ^{1}H-^{31}P HMBC spectra using ^{3}J and ^{4}J coupling with $(H3')_n/(H5'/H5'')_{n+1}$ and $(H4')_n/(H4')_{n+1}$, respectively in free (Fig. 4.9 a) and complexed DNA (Fig. 4.9 b) at 25 °C (Kumar & Barthwal, 2018; Tripathi & Barthwal, 2018; Gorenstein & Kar, 1975). On progressive addition of daunomycin, the ^{31}P signal of G6pT7 shifted slightly downfield up to D/N = 1.0 then upfield up to D/N = 4.0 while all other ^{31}P signals shifted gradually upfield (Fig. 4.10, Table 4.11). The drift in resonances is sequence dependent, it being 0.27, 0.23, 0.25, 0.38, 0.39 and 0.13 ppm upfield for T1pT2, T2pG3 G3pG4, G4pG, G5pG6, and G6pT7, respectively at D/N = 4.0 and is indicative of specificity of interaction between daunomycin and G-quadruplex. It is known that ^{31}P chemical shifts vary in response to local, sequence-specific and distortions induced in DNA duplex geometry (Gorenstein & Kar, 1975). Theoretical and experimental studies in duplex DNA have shown (Gorenstein & Kar, 1975; Agrawal, Govil, & Barthwal, 2009) that switching from energetically more favourable B_I conformation ($\zeta=g^-$, $\alpha=g^-$) to more flexible B_{II} conformation ($\zeta=t$, $\alpha=g^-$) having 1 kcal/mole greater energy induces downfield shift ~1.5-2.0 ppm, which is required to open the base pairs from 3.4 to 6.8 Å to permit intercalation between two base pairs. Besides the widening and narrowing of ester O-P-O bond angle due to distortions caused in DNA backbone lead to small upfield and downfield shifts, respectively. Purely electrostatic interactions between drug and DNA in drug-DNA complexes produce small upfield shifts. The dispersion in ^{31}P chemical shifts may also result from different populations of B_I and B_{II} conformational states (Gorenstein & Kar, 1975; Agrawal, Govil, et al., 2009). The observed upfield shifts may, therefore, be attributed to the proximity of $3'NH_3^+$ moiety to phosphates of DNA or widening of the ester bond. Absence of large downfield shift completely rules out the opening of base pairs to allow classical intercalation at any step along DNA. These results clearly prove that daunomycin binds to Tet7 externally and certainly not by classical intercalation mode of binding.

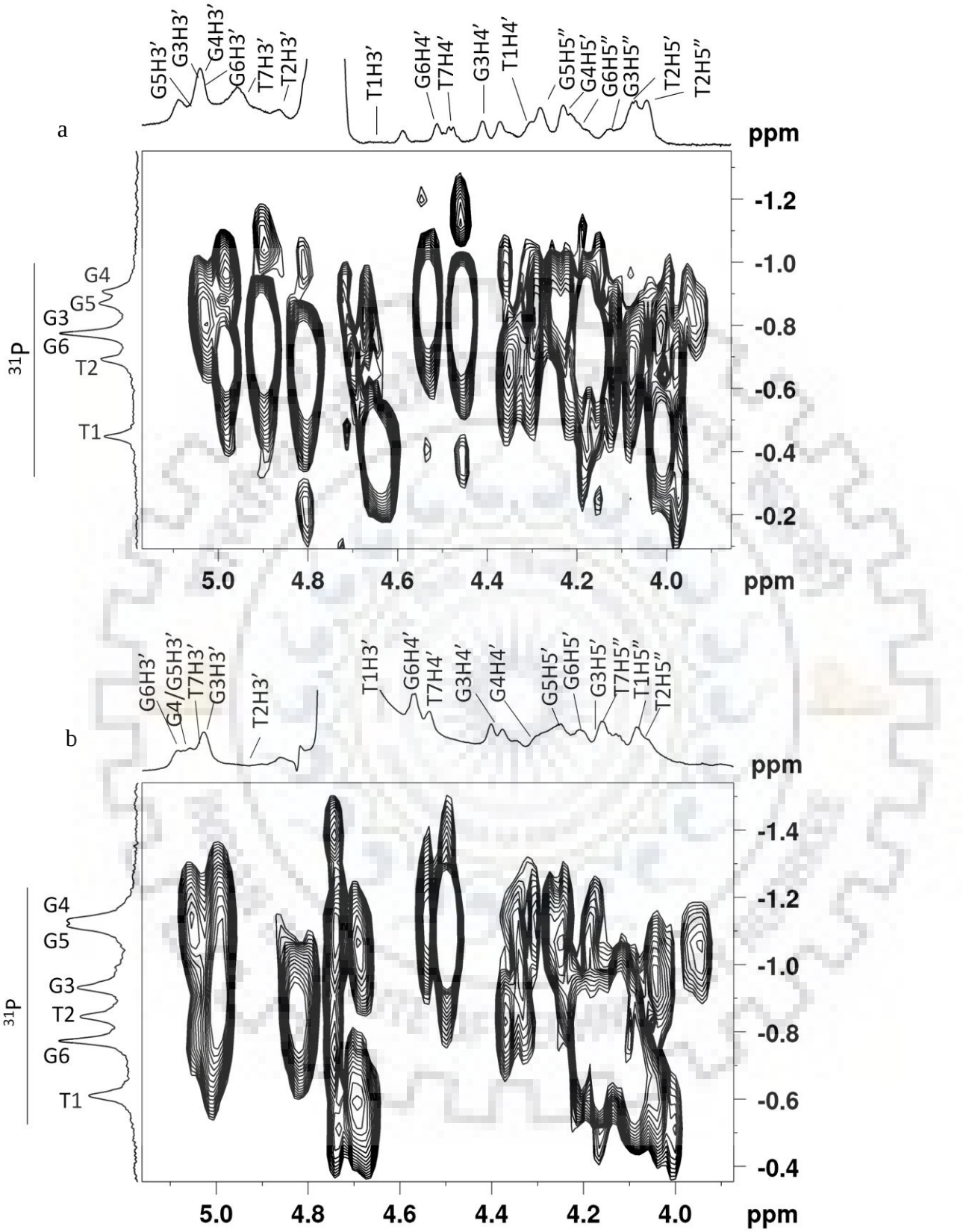

Figure 4.9 2D ^{1}H-^{31}P HMBC spectra of a) free Tet7 and b) daunomycin-Tet7 complex at D/N = 2.0 complex in KBPES buffer (90% H_2O+10% D_2O) at 25°C.

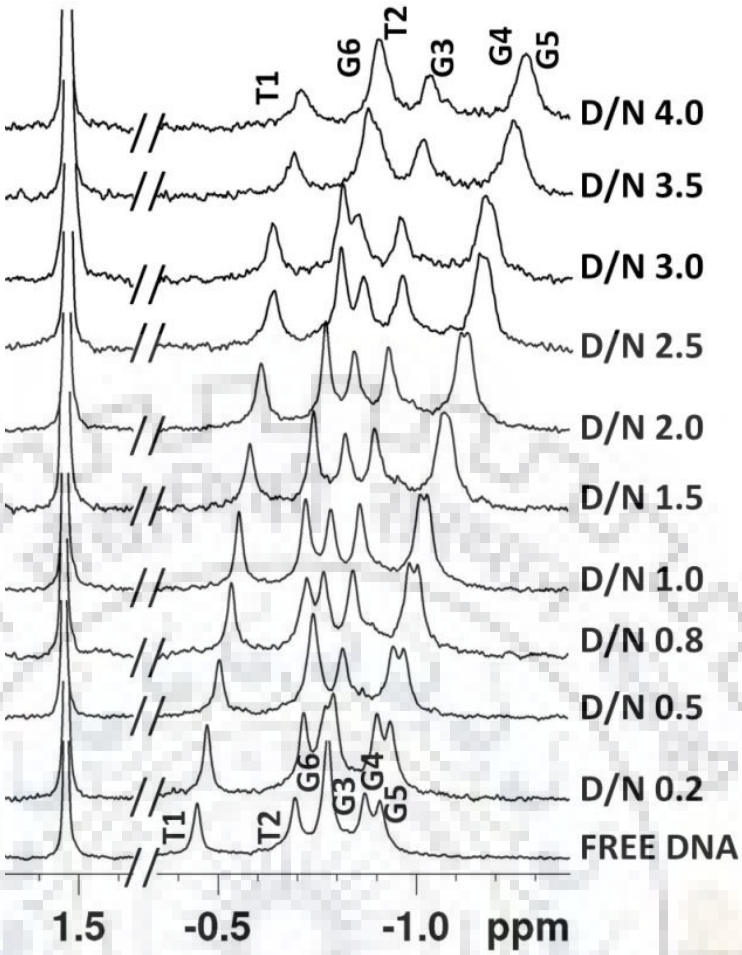

Figure 4.10 Proton decoupled ^{31}P NMR spectra of 1.16 mM Tet7 and its complex upon progressive addition of daunomycin at different D/N ratios in 10 mM phosphate buffer with 100 mM KCl (90% H_2O + 10% D_2O) at 25 °C.

Table 4.11 Chemical shift (ppm) of phosphorus (^{31}P) resonances in free Tet7 (δ_f) and daunomycin-Tet7 complex (δ_b) at various D/N ratios in KBPES buffer containing 100 mM KCl (90% H_2O+10% D_2O) at 25 °C. $\Delta\delta = \delta_b - \delta_f$

	T1pT2		T2pG3		G3pG4		G4pG5		G5pG6		G6pT7	
Free DNA (δ_f)	-0.44		-0.69		-0.78		-0.90		-0.87		-0.77	
	δ_b	$\Delta\delta$	δ_b	$\Delta\delta$	δ_b	$\Delta\delta$	δ_b	$\Delta\delta$	δ_b	$\Delta\delta$	δ_b	$\Delta\delta$
D/N=0.2	-0.47	-0.03	-0.71	-0.02	-0.79	-0.01	-0.93	-0.03	-0.90	-0.03	-0.77	0.00
D/N=0.5	-0.50	-0.06	-0.74	-0.05	-0.81	-0.03	-0.97	-0.07	-0.94	-0.07	-0.75	0.02
D/N=0.8	-0.53	-0.09	-0.77	-0.08	-0.84	-0.06	-1.01	-0.11	-0.98	-0.11	-0.73	0.04
D/N=1.0	-0.55	-0.11	-0.79	-0.10	-0.86	-0.08	-1.03	-0.13	-1.01	-0.14	-0.72	0.05
D/N=1.5	-0.58	-0.14	-0.82	-0.13	-0.89	-0.11	-1.08	-0.18	-1.07	-0.20	-0.74	0.03
D/N=2.0	-0.60	-0.16	-0.84	-0.15	-0.93	-0.15	-1.13	-0.23	-1.11	-0.24	-0.77	0.00
D/N=2.5	-0.63	-0.19	-0.86	-0.17	-0.95	-0.17	-1.17	-0.27	-1.15	-0.28	-0.80	-0.03
D/N=3.0	-0.63	-0.19	-0.84	-0.15	-0.95	-0.17	-1.18	-0.28	-1.16	-0.29	-0.80	-0.03
D/N=3.5	-0.68	-0.24	-0.89	-0.20	-1.01	-0.23	-1.25	-0.35	-1.23	-0.36	-0.87	-0.10
D/N=4.0	-0.71	-0.27	-0.92	-0.23	-1.03	-0.25	-1.28	-0.38	-1.26	-0.39	-0.90	-0.13

*Negative sign in $\Delta\delta$ denotes upfield shift.

4.3.4 NOE Correlations and Conformation of Complex

The sequential NOE cross peaks among adjacent guanine imino protons and imino to base protons (Fig. 4.4 h,i) confirm continuity between guanine bases forming G-quartets and that G-quadruplex DNA structure is intact after binding to daunomycin. The entire pattern of classical sequential connectivities of base protons to sugar H1'/H2'/H2" protons of neighboring bases at 5' end as well as among intra nucleotide protons shows that the conformation of daunomycin-Tet7 complexes closely resembles that of free Tet7 having right-handed helix and *anti* glycosidic bond rotation in all guanines. The presence of all sequential NOEs of H8/H6 with H1'/H2'/H2" (Fig. 4.4 j,k) indicates that there are no opening of base pairs from 3.4 to 6.8 Å at any 5'-3' base pair step to permit classical kind of intercalation of aromatic chromophore of daunomycin between base pairs, as observed in case of both X-ray crystallographic (Frederick, Williams, Ughetto, van der Marel, et al., 1990) and NMR solution structures (Barthwal et al., 2006; Agrawal, Govil, et al., 2009) of complexes of daunomycin with duplex DNA sequences $[d\text{-}CGATCG]_2$, $[d\text{-}TGATCA]_2$, $d\text{-}[TGTACA]_2$, etc. This gives independent evidence of the absence of any possibility of classical drug intercalation as a possible mode of interaction in DNA quadruplex.

Eleven intramolecular NOE cross peaks expected due to short distance contacts within daunomycin were observed (Fig. 4.11 a,b and Table 4.10). In addition 22 intermolecular NOE cross peaks between daunomycin and T1, T2, G6, T7 protons were observed (Fig. 4.11 a, c-e and Table 4.12) indicating presence of two distinct binding sites in DNA, that is, T1-T2 and G6-T7, corroborating stoichiometry of 1:1 and 2:1 determined independently by Job plot. The intermolecular NOEs between ring D aromatic 1H, 2H, 3H, $4OCH_3$ protons with G6NH/G6H8/T7CH_3/G6H1' show stacking of daunomycin with base quartets. The existence of these short distance contacts is in accord with the observed large upfield shifts up to 0.45 ppm in these protons (Fig. 4.8, Table 4.4). Three NOE cross peaks of 5'CH_3 of daunosamine sugar with G6H8/G6H1'/G6H2" indicate its proximity to DNA, which also showed large upfield shift ~0.40 ppm as compared to other daunosamine protons. Apart from large mixing time (400 ms), these NOEs were also seen at short mixing time (200 ms) so that chances of combination of transferred NOEs or exchange effect of two orientations of a single molecule can be excluded. There were no detectable NOEs from daunomycin to any part of the interior G4 plane and this plane, therefore, appears to have no contact with the ligand. Also, chemical shift of G3/G4/G5 protons were not significantly influenced by ligand binding although G3H8 showed line broadening. We observed some extra resonance peaks of low intensity, particularly

in 1.2-1.8 ppm range, which was apparent in NOESY spectra at D/N>2.0. Some of these signals give weakly intense intermolecular NOEs with ring D protons of daunomycin. Such NOEs, which do not match with the sharp major assigned TCH_3 peaks, were not considered for analysis. These presumably arise due to the presence of a minor conformation of the complex.

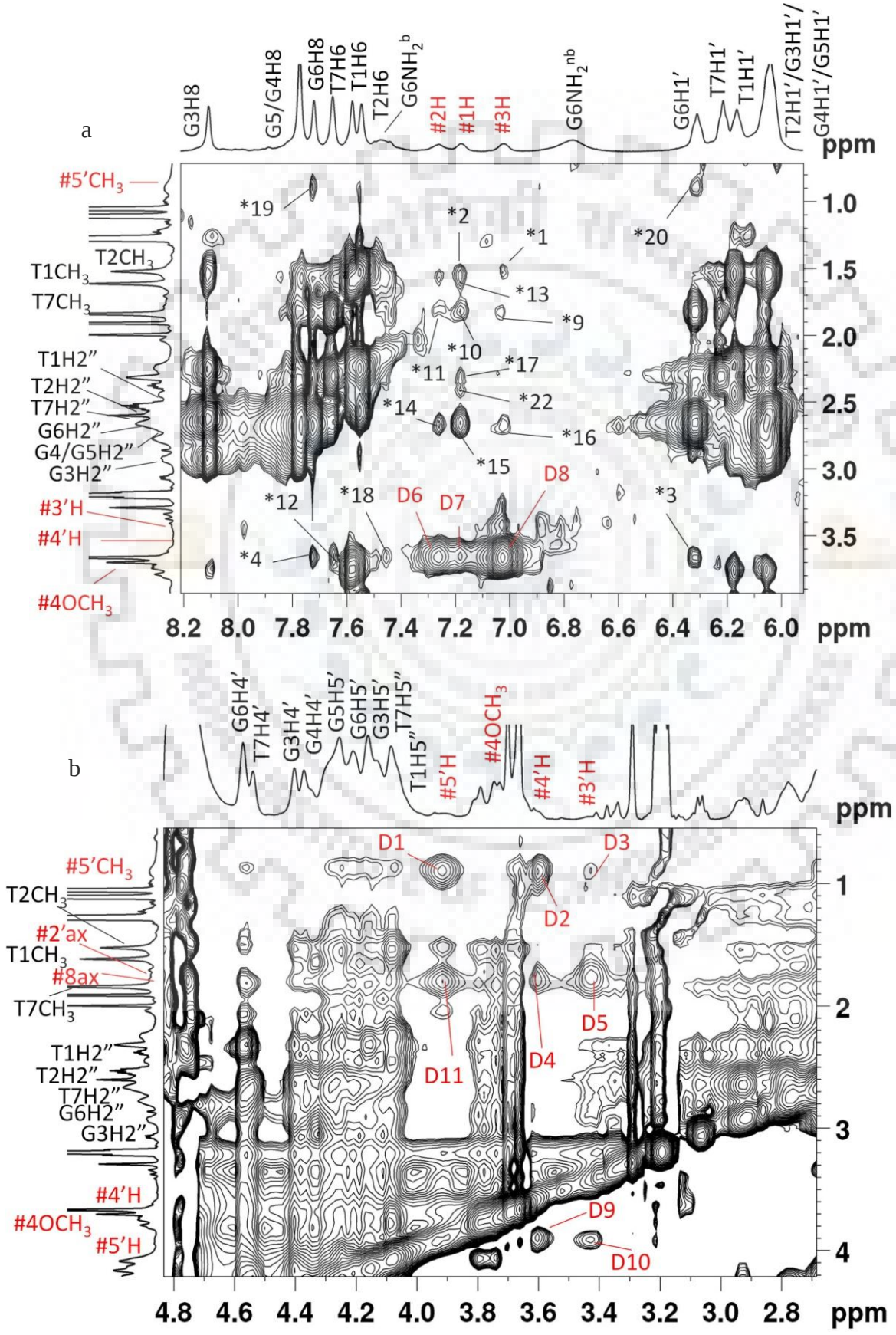

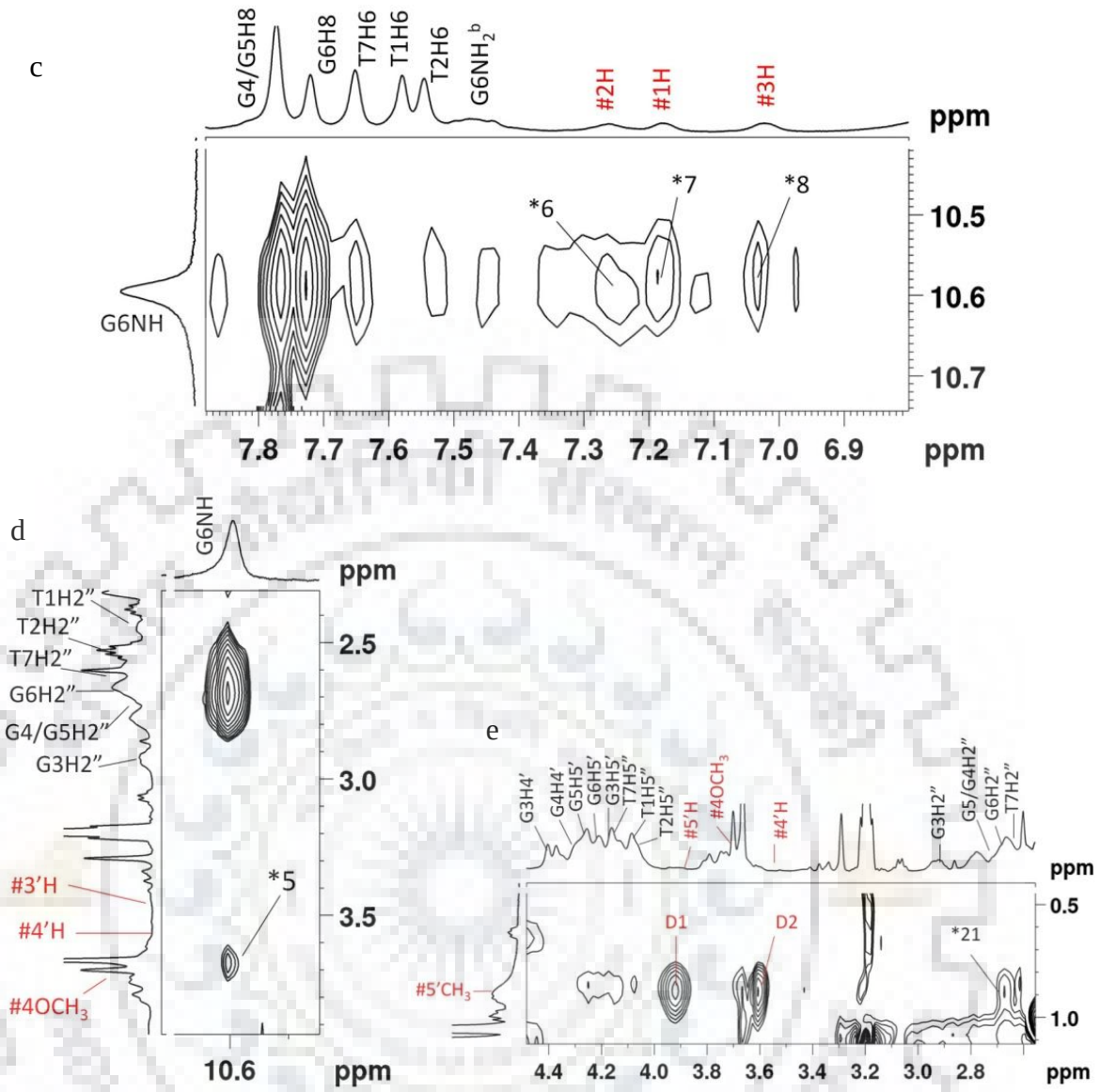

Figure 4.11 2D ^{1}H-^{1}H NOESY spectra of daunomycin-Tet7 complex at D/N = 2.0, mixing time τ_m = 250 ms at 25 °C. Expansion of specific regions of NOESY spectra showing NOE correlations between a) daunomycin protons 1H, 2H, 3H, 5'CH_3, 3'H, 4'H and 4OCH_3 and H8/H6/H1'/H2'/H2"/CH_3 protons along with intramolecular NOE cross peaks of daunomycin (D); b) daunomycin protons5'CH_3, 3'H, 4'H, 5'H, 2'$_{ax}$, and 8'$_{ax}$; c) daunomycin protons 1H, 2H, 3H and imino proton, d) daunomycin proton 4OCH_3 and imino proton, e) daunomycin proton 5'CH_3 and sugar H2" proton along with intra molecular NOE cross peaks of daunomycin (D). Symbol # denotes daunomycin protons, D denotes intramolecular cross peaks of daunomycin (D numbering as in Table 4.10) and * denotes intermolecular cross peaks between daunomycin and Tet7 protons (* numbering as in Table 4.12).

Distance restraints from 13 non-overlapping intermolecular NOEs (Table 4.12) which were found in NOESY spectra recorded at all mixing times (200-400 ms) and at each D/N ratio were used to build the model by positioning daunomycin at two independent sites close to T1pT2 and G6pT7 steps of Tet7. The restrained Molecular Dynamics (rMD) simulations approach used to arrive at a conformation that fits into observed NOE data included 138 intra-DNA and 11 intra-daunomycin (Table 4.10) distance restraints. Stacking interaction between daunomycin chromophore and G6pT7 bases was evident in the rMD structure (Fig. 4.12 a) while external binding was observed at T1pT2 site. Ring A, B, C and D of daunomycin molecule binds at the groove of T1pT2 base (Fig. 4.12 b,c). Ring D of daunomycin stacks with purine ring of terminal G6 base by the slight opening of T7 base thus bringing $4OCH_3$ close to G quartet (Fig. 4.12 d,e). A single hydrogen bond was formed between $9COCH_3$ with NH of T2 base at T1pT2 site (Fig. 4.12 b). The energy terms, restraints violations and RMSD of the obtained structure are reported in (Table 4.13). Out of total restraint violations of 3.3% (5 out of 151), 2.6% belong to T7 base so that the impact of restraint violations is minimal. The electrostatic and van der Waals energy contribution to the total energy suggests the role of stacking and electrostatic attraction of NH_3^+ of daunosamine sugar moiety with DNA backbone.

The observed intermolecular short distance NOE contacts between daunomycin and DNA as well as rMD structure provided direct confirmation of end stacking and external groove binding at G6-T7 and T1-T2 sites, respectively. This is at variance with X-ray crystallographic structure showing layers of daunomycin stacked between two quadruplexes (Clark et al., 2003) but in accord with the MD simulations in explicit solvent for daunomycin-[d-(TGGGGT)]$_4$ (Shen et al., 2017). End stacking mode was also inferred from the collision- induced fragmentation patterns in daunomycin-[d-(TGGGGT)]$_4$ complex (N. Xu et al., 2012) and NMR studies on doxorubicin-[d-(TTAGGGT)]$_4$ complex (Scaglioni et al., 2016). It has been suggested that crystal packing forces may be responsible for the observed difference in the structure of the complex. The present NMR experiments and molecular dynamics simulations (Shen et al., 2017) have been performed in explicit water solvent, which may offer structural flexibility to the DNA.

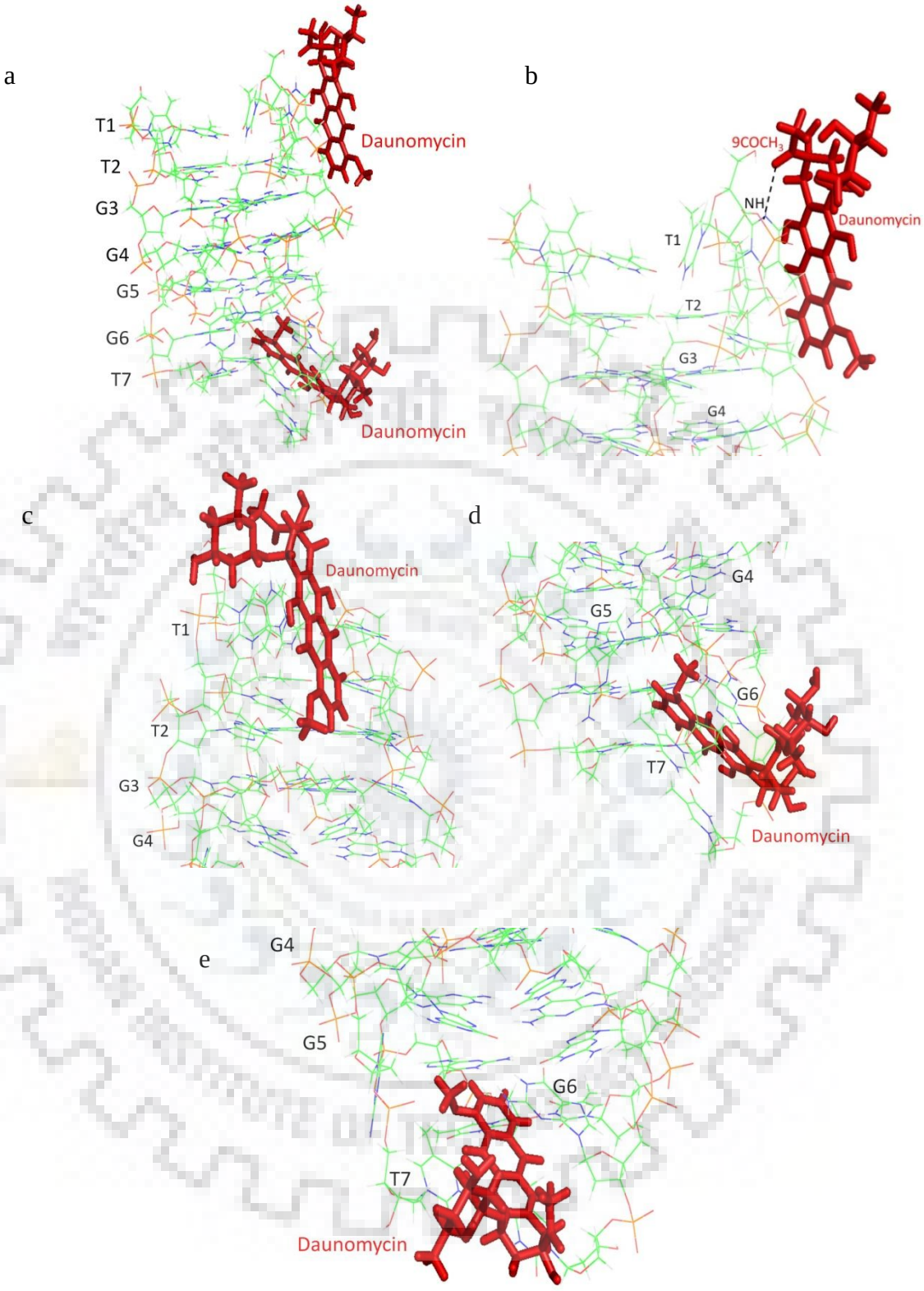

Figure 4.12 Energy minimized model of daunomycin bound to Tet7 obtained by restrained molecular dynamics simulations; a) Binding of daunomycin at two independent sites T1pT2 and G6pT7; b-c) Close up view of daunomycin binding to Tet7 at T1pT2 site and d-e) at G6pT7 site. (Hydrogen bond is represented by black dashed line).

Table 4.12 Interproton distances (Å) between daunomycin and Tet7 obtained from NOE cross peaks at D/N = 2.0, τ_m = 250 ms at 25 °C and corresponding distances (Å) in rMD model of daunomycin-Tet7complex. nd: not determined

S. No.	Intermolecular NOE correlations	Interproton distances		S. No.	Intermolecular NOE correlations	Interproton distances	
		NOESY at D/N=2.0	rMD model			NOESY at D/N=2.0	rMD model
1	3H-T2CH_3	4.22	3.44	12	4OCH_3-T7H6	4.19	4.15
2	1H-T2CH_3	4.06	3.96	13	1H-T1CH_3	3-4	5.14
3	4OCH_3-G6H1’	3.99	4.57	14	2H- G6H2”	nd	nd
4	4OCH_3-G6H8	4.20	4.83	15	1H- G6H2”	nd	nd
5	4OCH_3-G6NH	4-5	4.31	16	3H- G6H2”	nd	nd
6	2H-G6NH	3-4	4.03	17	1H-G6H2’	nd	nd
7	1H-G6NH	3.0	5.94	18	4OCH_3-G6NH_2[b]	4.16	4.75
8	3H-G6NH	3-4	2.79	19	5’CH_3-G6H8	nd	nd
9	3H-T7CH_3	4.79	4.24	20	5’CH_3-G6H1’	nd	nd
10	1H-T7CH_3	3.11	3.02	21	5’CH_3-G6H2”	nd	nd

Table 4.13 Structural data and final energy terms of daunomycin-Tet7 complex.

Experimental restraints	
Intramolecular	
Daunomycin-Daunomycin	11
DNA-DNA	138
Intermolecular	
Daunomycin-DNA	13
Total restraints	151
Average RMSD (Å)	0.35
Restraint Violations (distances >0.3 Å)	5
CVFF energy of minimized structures (kcal/mole)	
Total	-1641.98
Torsional	240.33
Electrostatic	-3163.33
van der Waals	2527.77

Further, our NMR results show that daunomycin binds as monomer at groove or stacks with terminal G-quartet unlike X-ray crystallographic structure of daunomycin-[d-(TGGGGT)]$_4$ complex (Clark et al., 2003), in which two layers of daunomycin containing 3 each of drug molecules are sandwiched between two G-quadruplexes stacked end to end. Two daunomycin molecules oriented in antiparallel orientation with respect to each other are expected to give intermolecular NOE cross peaks due to stacking of ring A protons with ring D, that is, 10axH/10eqH with 1H/2H/3H/4OCH$_3$, 8axH/8eqH with 1H/2H/3H/4OCH$_3$, 9COCH$_3$ with 2H/3H, 7H with 1H/2H/3H, 5'CH$_3$ with 1'H/2'H/3'H (Agrawal, Barthwal, et al., 2009; Evstigneev, Khomich, & Davies, 2006). On the other hand, stacking between 2 daunomycin molecules oriented parallel to each other are expected to show NOE cross peaks of ring A protons with daunosamine sugar protons, that is, 10axH/10eqH with 4'H/3'H/5'H/5'CH$_3$, 10axH/10eqH with 7H, 9COCH$_3$ with 3'H/5'H (Evstigneev et al., 2006). Some of these short contacts are evident in the X-ray crystal structure (Clark et al., 2003). NOEs of ring A protons of one daunomycin molecule with ring A protons of second daunomycin stacked over it in parallel orientation are relatively weaker in intensity than the corresponding intramolecular NOE connectivities, so that intensity of intramolecular NOE cross peaks will dominate in NOESY spectra and cannot be used to judge parallel orientation. We did not observe any drug-drug intermolecular NOE cross peak at any D/N ratio in the NOESY spectra of complexes in present investigations. Hence, neither a parallel/antiparallel dimer of daunomycin binds nor do two layers of daunomycin molecules sandwiched between two G-quadruplexes exist in the solution structure of complex, as observed in crystal structure of daunomycin-[d-(TGGGGT)]$_4$ complex (Clark et al., 2003). Besides, the stoichiometry of complex in the crystal structure (Clark et al., 2003) would be 3:1 while our Job plot shows (Fig. 4.1 c) that maximum stoichiometry that is reached is 2:1. In addition, the observed CD spectra did not exhibit any bisignate peaks (Fig. 3.4 d) which is an independent proof of the non-existence of stacked layers of daunomycin or presence of daunomycin dimer in parallel or antiparallel orientation in our solution studies. This is in accord with the findings by rMD simulations of daunomycin-[d-(TGGGGT)]$_4$ (Shen et al., 2017) complexes in which only monomer is found to bind to DNA.

4.3.5 Thermal Denaturation

Melting profiles of GNH protons in free and bound DNA at D/N = 1.0-4.0 were obtained at 25-80 °C in steps of 5 °C upon its transition from ordered to disordered state (Fig. 4.13). In free Tet7, G3NH and G6NH signals appear as low-intensity resonances at a temperature ~65 °C due to the breaking of Hoogsteen hydrogen bonds between guanines on a quartet plane and

exchange of the NH proton with solvent. But G4NH and G5NH exist as sharp well-defined resonances at 65-80 °C so that both, G3NH and G6NH disappear first (T_{m1}>65 °C) followed by G4NH, G5NH (T_{m2}). The melting of free Tet7 apparently follows a 3-state process (alternately two "two-state" melting processes) in which an intermediate conformation of G-quadruplex DNA exists which has G3NH, G6NH in unfolded form and G4NH, G5NH are still folded, so that T_{m1} ~65 °C (± 5 °C) while T_{m2} may be comparatively quite high, but could not be ascertained as data was not recorded beyond 80 °C (Kumar & Barthwal, 2018; Pradeep & Barthwal, 2016). T_m decreases in the order: G4NH, G5NH > G6NH, G3NH. On complex formation, imino protons are stabilized to higher temperatures (Fig. 4.13). G3NH signal is of relatively lower intensity at D/N = 1.0-4.0 as compared to corresponding G6NH signal. G3NH disappears at D/N = 1.0, 2.0, 3.0 and 4.0 at about > 70, 75, 80 and > 80 °C, respectively, so that T_{m1} increases with molar ratio. G6NH disappears at temperature > 80 °C at D/N = 1.0-4.0. The melting transitions, therefore, follow the 4-state process in which the first G3NH disappears (T_{m1} ~80 °C), then G6NH disappears (T_{m2} > 80 °C) followed by G4NH, G5NH protons, which appear as sharp resonances at 80 °C indicating that Tm_3 may be quite high. Thus T_m decreases in the order: G4NH, G5NH > G6NH > G3NH. The terminal G-quartets, involving G3NH and G6NH, are shielded upon binding to daunomycin which thermally stabilizes the tetramolecular G-quadruplex DNA efficiently. G6NH, which was disappearing along with G3NH in free form, is stabilized upon complex formation to a much greater extent than G3NH. This enhanced stabilization is consistent with observed large upfield shift and significant broadening of G6NH, T7H6 and T7CH_3 as compared to all other protons establishing G6pT7 as the major binding site involving π-π stacking interactions with daunomycin aromatic ring leading to an estimate of thermal stabilization of ~15 °C.

We measured the melting temperature of folded → unfolded Tet7 in free and bound form at D/N = 0.0, 0.5, 1.0, 2.0, 3.0, 3.5 and 4.0 independently using differential scanning calorimeter (Fig. 4.14 a-g and Table 4.14). The thermogram of 50 μM free [d-(TTGGGGT)]$_4$ (single strand concentration 200 μM) fitted in multiple-state model on deconvolution having melting transitions T_{m1} = 46.2 ± 0.4 °C, T_{m2} = 54.9 ± 0.7 °C, T_{m3} = 72.9 ± 0.6 °C and T_{m4} = 110.5 ± 0.1 °C (P. Kumar & Barthwal, 2018). This, in general, indicates that the species may be involved in equilibria consisting of either a single folded quadruplex to random coil transition through an intermediate or two independent species following separate pathways not involving intermediates to the same unfolded state (Antonacci, Chaires, & Sheardy, 2007). In the present case, the stepwise disappearance of imino protons with temperature (Fig. 4.13) indicates the existence of several intermediates. In free Tet7, G3NH and G6NH show melting around 65 °C (±5 °C) which may correspond to T_{m3} = 72.9 °C, observed in DSC experiments. G4NH and

G5NH form the core of G tetrad and show melting temperature well beyond 65 °C in NMR experiments which could be referred to as T_{m4} = 110.5 °C in DSC experiments (as T_{m3} = 72.9 °C appears to be less probable). The observed lower melting temperatures, T_{m1} = 46.2 °C and T_{m2} = 54.9 °C may correspond to the melting transitions of other regions of Tet7 e.g. T1/T2/T7 nucleotide residues. This may be evidenced by the fact that the imino protons of thymine are not observed, being in fast exchange with solvent (Gavathiotis et al., 2003), as mentioned earlier. NH melting transitions thus give insight into stepwise melting transitions at atomic level which cannot be deduced from DSC experiments. In all complexes at D/N = 1.0-4.0 (Fig. 4.14 b-g and Table 4.14), only three melting transitions were observed, the expected fourth transition is apparently beyond the range of temperature measurements (i.e. T_{m4}>120 °C). At D/N = 4.0, T_{m1} = 60.8 ± 1.6 °C, T_{m2} = 72.6 ± 0.4 °C and T_{m3} = 87.3 ± 0.5 °C and from the comparison of DSC thermograms (Fig. 4.14 a-c) with NH melting profiles (Fig. 4.13), it may be inferred that T_{m3} = 87.3 °C refers to disappearance G6NH while T_{m4} for G4NH, G5NH are well beyond 120 °C. Thus stabilization of G6NH and G4NH/G5NH are 14.4+1.1 °C and >10 °C, respectively. The extent of stabilization ΔT_m increases with D/N ratio (Fig. 4.14 h), which is likely to happen if both sites are not occupied at D/N = 2.0 so that binding continues as D/N approaches 4.0.

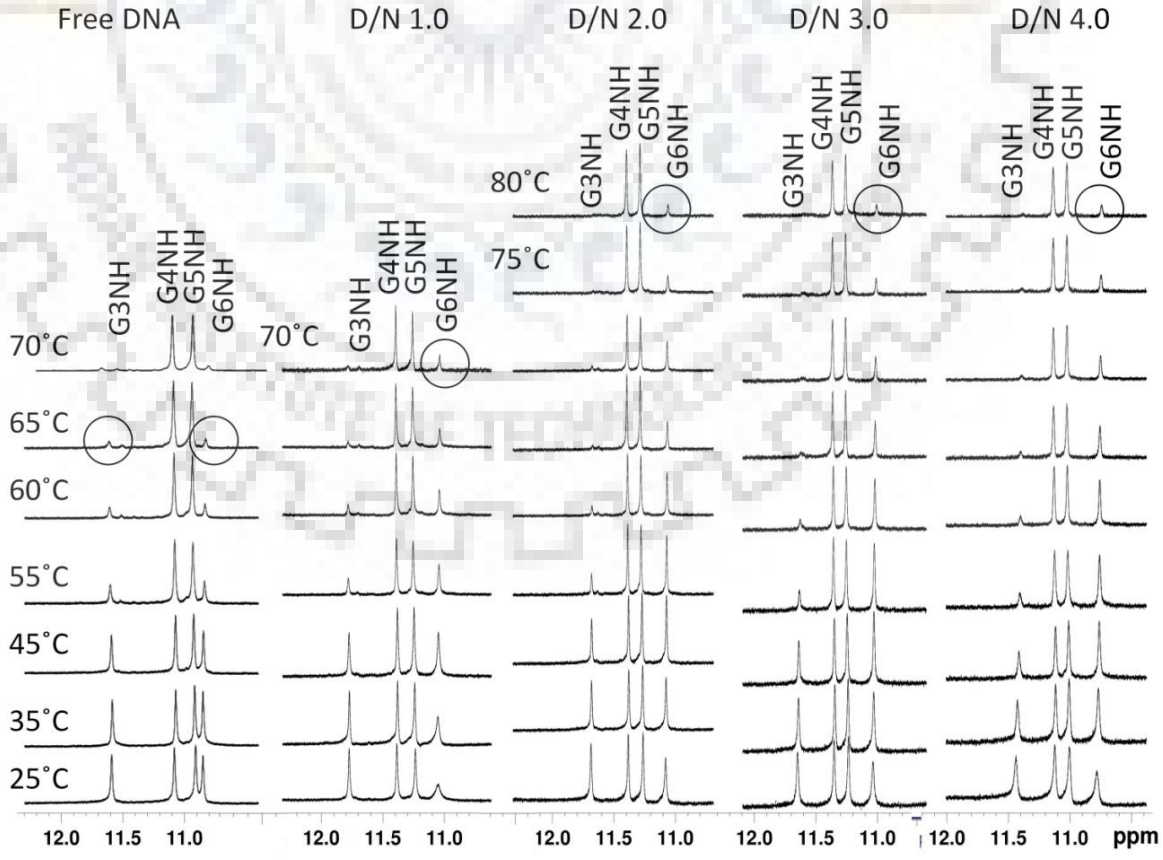

Figure 4.13 1D ^{1}H NMR spectra of imino protons showing thermal melting profile of free Tet7 and daunomycin-Tet7 complex at different D/N ratios at different temperatures.

a

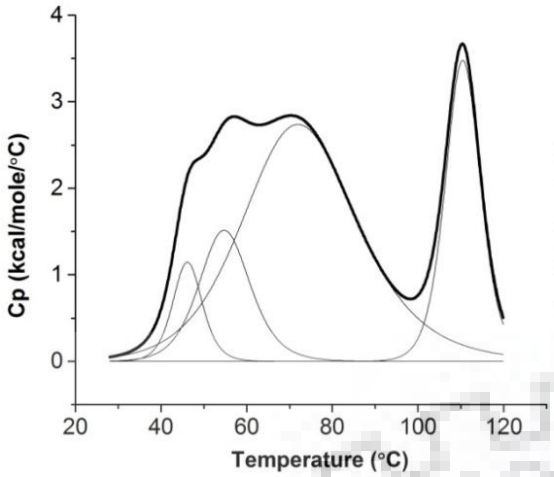
Cp (kcal/mole/°C)
Temperature (°C)

b

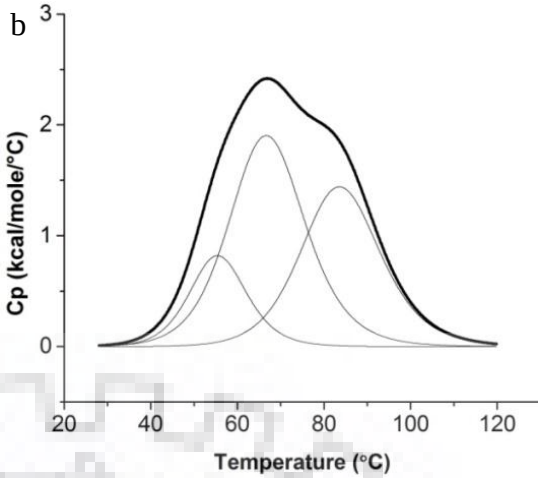
Cp (kcal/mole/°C)
Temperature (°C)

c

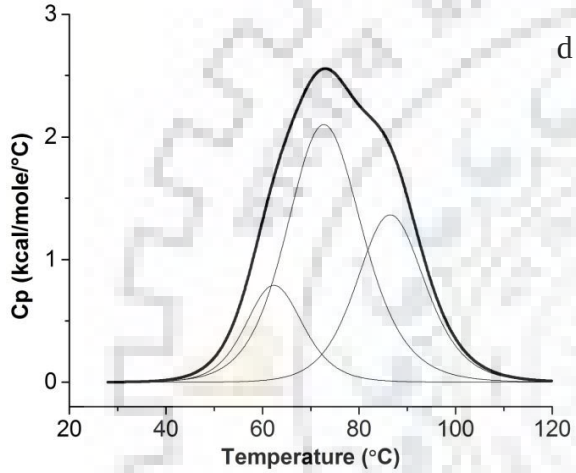
Cp (kcal/mole/°C)
Temperature (°C)

d

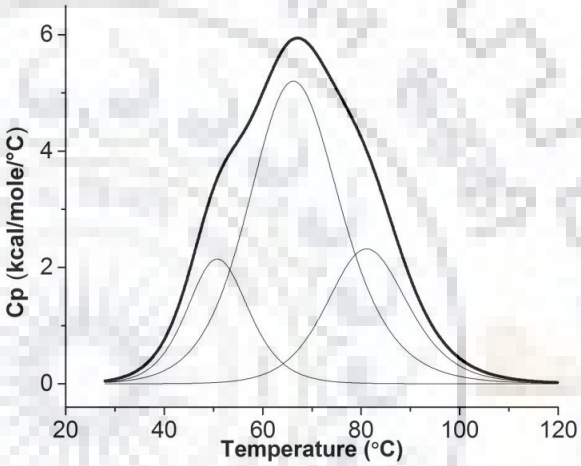
Cp (kcal/mole/°C)
Temperature (°C)

e

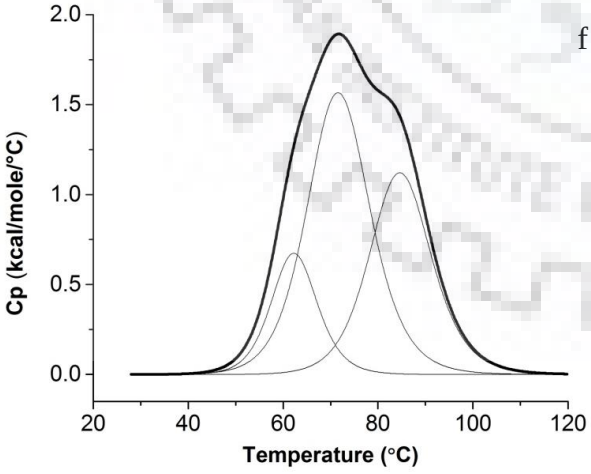
Cp (kcal/mole/°C)
Temperature (°C)

f

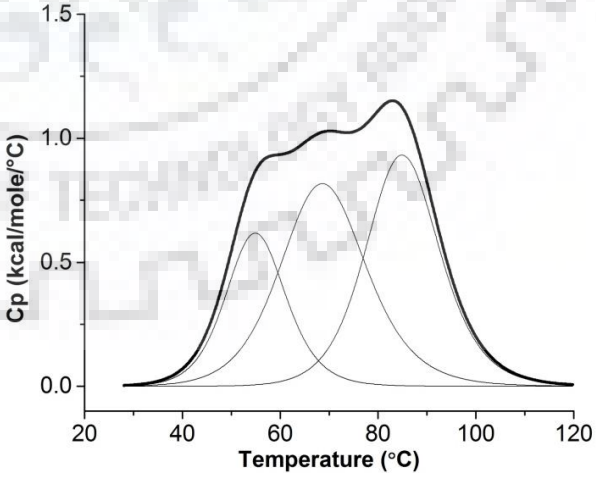
Cp (kcal/mole/°C)
Temperature (°C)

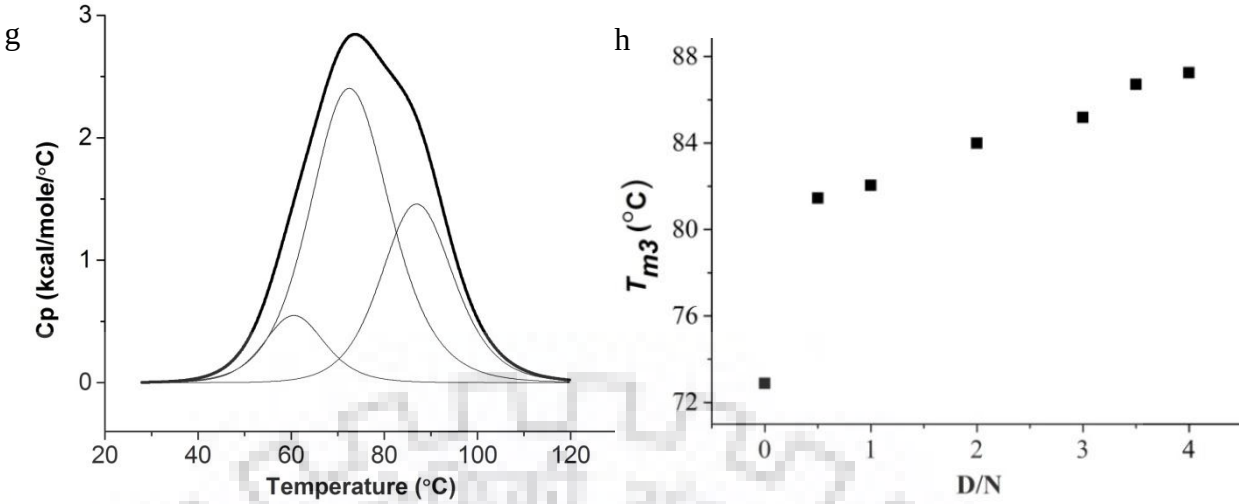

Figure 4.14 DSC thermograms showing excess heat capacity as a function of temperature for daunomycin-Tet7 complex at a) 50 µM free Tet7 b-g) D/N=0.5, 1.0, 2.0, 3.0, 3.5 and 4.0. All samples were prepared in phosphate buffer (KBPES) (pH 7.0) containing 100 mM KCl. h) Plot of melting temperature T_{m3} obtained from DSC experiments as a function of D/N ratio.

Table 4.14 Data obtained from DSC experiments showing change in melting temperature (T_m) of Tet7 upon complexation with daunomycin at different D/N ratios.

	T_{m1} (°C)		T_{m2} (°C)		T_{m3} (°C)		T_{m4} (°C)	
Free DNA	46.2±0.4		54.9±0.7		72.9±0.6		110.5±0.1	
		ΔT_m		ΔT_m		ΔT_m		ΔT_m
D/N = 0.5	51.0±0.4	4.8	66.7±0.3	11.8	81.5±0.7	8.6	-	-
D/N = 1.0	52.4±4.8	6.2	65.1±3.3	10.2	82.0±2.9	9.1	-	-
D/N = 2.0	55.7±3.3	9.5	67.1±2.3	12.2	84.0±1.3	11.1	-	-
D/N = 3.0	55.1±1.3	8.9	69.02±1.1	14.1	85.2±0.8	12.3	-	-
D/N = 3.5	62.6±1.4	16.4	73.0±0.7	18.1	86.7±0.5	13.8	-	-
D/N = 4.0	60.8±1.6	14.6	72.6±0.4	17.7	87.3±0.5	14.4	-	-

Thus, binding of daunomycin to Tet7 leads to thermal stabilization of DNA quadruplex. The observed ΔT_m ~15 °C is significantly higher than the value of 0 and 5 °C reported in literature for 21-mer human telomeric DNA in Na^+ (Manet, Manoli, Zambelli, Andreano, Masi, Cellai, Ottani, et al., 2011) and K^+ (Manet, Manoli, Zambelli, Andreano, Masi, Cellai, & Monti, 2011) rich aqueous solutions, respectively. External binding of one molecule of daunomycin to 22-mer human telomeric DNA in K^+ rich aqueous solutions yielded ΔT_m ~ 11 °C (Das et al., 2017). Apparently, in the present investigations, binding of daunomycin at two sites is

stabilizing pure parallel tetra molecular Tet7 to a greater extent (ΔT_m ~ 15 °C) than unimolecular 21-mer/22-mer human telomeric DNA having a 3+1 hybrid structure with loops.

4.4 Groove Binding Mode

Daunomycin binds to both duplex DNA as well as quadruplex DNA and has a greater affinity for duplex DNA, although the mode of binding is totally different in the two types of DNA. MD simulations show that end stacking with terminal G-tetrad and groove binding mode are energetically equally favorable, while intercalation is the preferred binding mode over groove binding in case of duplex DNA (Shen et al., 2017), as also reported for X-ray crystallographic (Frederick, Williams, Ughetto, van der Marel, et al., 1990) and NMR (Barthwal et al., 2006; Agrawal, Govil, et al., 2009) structures of complexes of daunomycin-duplex DNA. The present NMR investigations confirm groove binding and end stacking in G-quadruplex DNA in contrast to classical intercalation mode of binding. This may be attributed to high stability of G-quartets and consequently large amount of energy required to unstack them as compared to classical intercalation of daunomycin chromophore in d-CpG and d-TpG steps on binding to [d-(CGATCG)]$_2$, [d-(TGATCA)]$_2$, etc. (Agrawal, Govil, et al., 2009; Barthwal et al., 2006; Frederick et al., 1990). Groove binding is a novel mode since the chemical nature of the grooves in G-quadruplex is quite different from that of duplex DNA. A large negative electrostatic field exists in the center of G-quartets as compared to the major groove of a G-C base pair in duplex DNA. The structure of distamycin-[d-(TGGGGT)]$_4$ (Randazzo, Galeone, & Mayol, 2001) showed that all the grooves were practically same and the ligand could easily bind at two diametrically opposite grooves. This feature in G-quadruplex DNA can provide selectivity over duplex DNA, which is essential to translate G-quadruplex ligands into successful drugs and also reduce cell toxicity caused by presently used daunomycin/doxorubicin in chemotherapy. The fact that daunomycin targets the pathway of telomere maintenance by telomerase paves the way to structure-based design to produce a de novo anthracycline that acts as a more potent telomerase inhibitor. The present investigations of interactions at the molecular level by NMR contribute to the understanding of non-selective drugs such as daunomycin, which binds to both duplex and quadruplex DNA. Anthracyclines offer opportunities to have many derivatives/analogs by different chemical modifications. For instance, our studies show the involvement of 5'CH_3 group of daunosamine in binding. It will be worth investigating if epimer forms of sugar or two or more conjugated sugar rings could show enhanced insertion in grooves and better selectivity. Also, substitution on aromatic ring could affect binding affinity.

4.5 Conclusions

The present study focuses on the binding of daunomycin to parallel stranded tetra molecular Tet7 quadruplex DNA comprising telomeric DNA sequence from *Tetrahymena thermophilia*. Direct real-time binding experiments show specific interaction between two molecules. Daunomycin-Tet7 complex undergoes diffusion as a stable complex. Complexes having a stoichiometry of 1:1 and 2:1 coexist. The overall conformation of Tet7 is not significantly altered on interaction and daunomycin dimers present in free daunomycin are disrupted on binding to DNA. The NMR experiments confirm that a specific interaction between two molecules occurs. Presence of sequential NOEs along the sequence of DNA in ^{1}H-^{1}H NOESY spectra and absence of large downfield shifts in ^{31}P NMR studies give a clear proof of the absence of classical intercalation to permit stacking of aromatic chromophore of daunomycin between G-quartets of DNA. Two binding sites, G6-T7 and T1-T2, are evident from analysis of chemical shifts, line broadening and 22 short interproton NOE contacts. Ring A protons, 1H, 2H, 3H, $4OCH_3$, and daunosamine sugar protons, 5'H, $5'CH_3$ are involved in the interaction with DNA. End stacking with terminal G-tetrad G6 and groove binding close to T1-T2 bases are found to exist. The binding leads to substantial thermal stabilization of Tet7 by ΔT_m ~15 °C, which may result from enhanced stacking of G6 quartet with daunomycin chromophore at G6pT7 site, presence of hydrogen bond and specific van der Waals contacts at grooves. The findings have implications in structure-based designing of anthracycline drugs as potent telomerase inhibitors.

Chapter 5: Multispectroscopic investigation of binding of anticancer drug daunomycin with intramolecular 22-mer G-quadruplex DNA d-[GGGG(TTGGGG)$_3$]

5.1 Introduction

Apart from binding to duplex DNA, daunomycin molecules interact with G-quadruplex DNA (Ren & Chaires, 1999). Recently, few studies have been conducted to deduce the mechanistic and biophysical insights into the interaction of daunomycin with human G-quadruplex 21/22-mer DNA. The interaction of two analogues of daunomycin, doxorubicin and sabarubicin, with 21-mer human telomeric sequence in K^+ and Na^+ rich solutions showed (Manet, Manoli, Zambelli, Andreano, Masi, Cellai, Ottani, et al., 2011; Manet, Manoli, Zambelli, Andreano, Masi, Cellai, & Monti, 2011) induced positive CD band at 500 nm on binding which leads to increase in melting temperature of DNA by 5 °C (Manet, Manoli, Zambelli, Andreano, Masi, Cellai, & Monti, 2011). The interaction in Na^+ rich solution, on the other hand, did not show any stabilization of DNA although fluorescence emission and CD bands were affected significantly (Manet, Manoli, Zambelli, Andreano, Masi, Cellai, Ottani, et al., 2011). There are no studies on G-quadruplex DNA having 4 guanines, e.g. d-TTGGGGT, the telomeric DNA sequence from *Tetrahymena thermophilia*, which forms more stable structures. Henceforth, we have carried out series of experiments using SPR, absorbance, fluorescence (steady state and life time), CD and NMR spectroscopy to ascertain real time binding and mode of interaction of duanomycin with G-quadruplex 22-mer d-[GGGG(TTGGGG)$_3$] (Tet22) from *Tetrahymena thermophilia* telomeric DNA in presence of 100 mM K^+. Thermal melting profiles have been obtained using DSC to determine the extent of stabilization of DNA

5.2 Materials and Methods

Details of the materials and methods used are given in chapter 2. For SPR experiments, 3.75-960 μM of daunomycin solution was used. Increasing amounts of Tet22 were added stepwise to a fixed concentration of 7 μM daunomycin in 33 experiments conducted at mole equivalent ratios of Daunomycin (D) to Nucleic acid (N) in the range, D/N = 0.18-4.6 for titrations monitored by absorption spectroscopy. The same samples were used for fluorescence experiments. The relative mole fractions of Tet22 and daunomycin were varied keeping their total concentration constant (4 μM) for Job plot experiments. The life time values were calculated for 7 μM of free daunomycin and its complex with Tet22 at D/N = 0.3, 0.5, 1.0, 2.0, 3.0 and 4.0. Circular Dichroism experiments were performed using 10.0 μM Tet22 and

daunomycin was added progressively at mole equivalent ratios D/N = 0.1-5.0 in 31 experiments. Similarly, CD experiments were also performed using 10.0 µM d-[AGGG(TTAGGG)$_3$] and 15.0 µM d-(TTAGGG)$_4$ and titrating with daunomycin. CD samples were also prepared in buffer containing 0, 25, 150 and 200 mM KCl apart from usual 100 mM KCl concentration. In another set of experiments, Tet22 was added stepwise to 400 µM daunomycin in 11 experiments conducted at D/N = 0.5-4.9 at 25 °C. For NMR experiments, 2.30 mM of Tet22 was used. For DSC experiments, 50 µM of Tet22and daunomycin-Tet22 complexes at D/N = 0.5, 1.0, 2.0, 3.0 and 4.0 were used. Molecular docking studies were carried out using the structure of quadruplex DNA d-[(TTGGGG)$_4$] (Tet24) obtained from PDB ID: 186D. Three-dimensional (3D) conformer of a drug molecule was obtained from PubChem CID: 30323.

5.3 Results and Discussion

5.3.1 Surface Plasmon Resonance

The SPR sensograms (Fig. 5.1 a) show that the steady state response increases with an increase in daunomycin concentration in the range 3.75-960 µM (Fig. 5.1 b), thereby, confirming that a specific interaction of daunomycin with Ttel22 indeed does take place. The binding isotherms yield affinity constant K_b ~2.1x10^3 M^{-1} at 25 °C while the analysis of the kinetics of association and dissociation yields K_b ~6.9x10^3 M^{-1} (Table 5.1) giving a direct proof of interaction between two molecules.

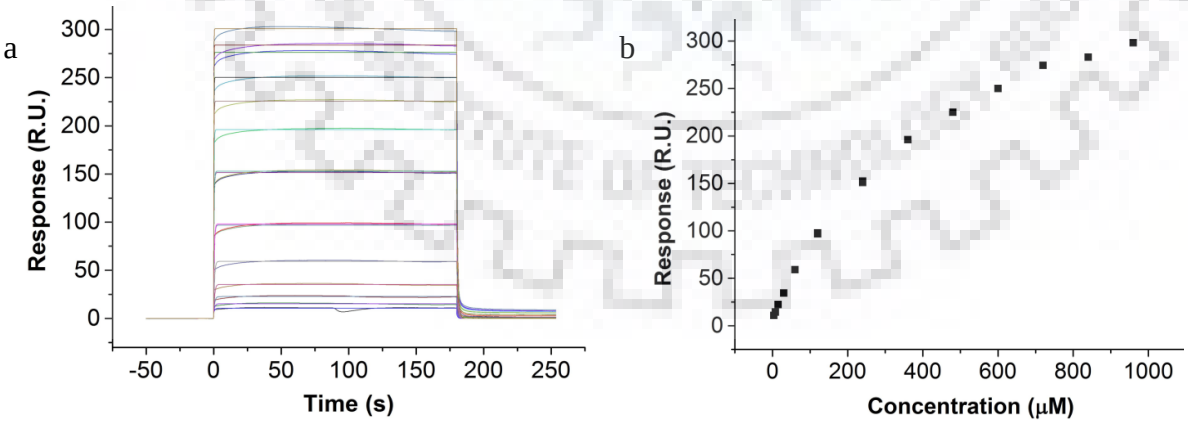

Figure 5.1 Surface Plasmon Resonance results for interaction of daunomycin with Tet22 using HEPES buffer (pH 7.4) with 100 mM KCl at 25 °C. a) Sensograms obtained for the increasing concentration of daunomycin from 3.75 µM (bottom) to 960 µM (top) and. b) Steady-state binding plot showing Response Unit (R.U.) with respect to the concentration of daunomycin (µM).

Table 5.1 Surface Plasmon Resonance (SPR) data showing equilibrium binding constants (K_b), equilibrium Dissociation constant (K_D), association rate constant (k_a) and dissociation rate constant (k_d) and maximum Response Unit (RU_{max}) obtained from the binding of daunomycin with Tet22 at 25 °C.

Experiment	Flow rate (µl/min)	RU_{max}	k_a ($M^{-1}s^{-1}$)	k_d (s^{-1})	K_D (M)	K_b (M^{-1})	χ^2
Kinetics run 1	30	195.1	$8.3x10^3$	1.2	$1.4x10^{-4}$	$6.9x10^3$	29.4
Steady State run 1	30	487.3	-	-	$5.5x10^{-4}$	$1.8x10^3$	16.9
Kinetics run 2	30	185.9	$8.2x10^3$	1.2	$1.4x10^{-4}$	$6.9x10^3$	16.4
Steady State run 2	30	433.7	-	-	$4.8x10^{-4}$	$2.1x10^3$	4.4
Kinetics run 3	30	110.8	$1.1x10^4$	1.8	$1.6x10^{-4}$	$6.2x10^3$	7.4
Steady State run 3	30	424.3	-	-	$4.8x10^{-4}$	$2.0x10^3$	2.5

5.3.2 Absorption

The titrations were monitored at ~478 nm since daunomycin shows absorption maxima at 290 and 478 nm while DNA absorbs at 260 nm. A 7 µM concentration of daunomycin used is not expected to show effects due to the self-association (Fiallo, Tayeb, Suarato, & Garnier-Suillerot, 1998; Chaires, Dattagupta, & Crothers, 1982; Agrawal, Barthwal, & Barthwal, 2009). Stepwise addition of Tet22 resulted in hypochromism of ~37% up to D/N = 0.18 at 478 nm accompanied by the redshift of $\Delta\lambda_{max}$ ~7 nm (selected data are shown in Fig. 5.2 a). The data does not show an isosbestic point in the entire range of D/N ratios so that multiple stoichiometric daunomycin-DNA complexes may exist in solution. The plots of absorbance (A) (inset of Fig. 5.2 a) and 1/A (Fig. 5.2 b) versus D/N show inflection points at D/N ~0.8 and 2.0 due to a change in slope so that stoichiometry of daunomycin-DNA complex is likely to be 1:1 or 2:1 (Bianco, Musetti, Krapcho, Palumbo, & Sissi, 2013; Dasgupta & Goldberg, 1985; Wilson, Tanious, Fernandez-Saiz, & Rigl, 1997; Dasgupta, Parrack, & Sasisekharan, 1987; Evans et al., 2007). The Scatchard plots being nonlinear and not fitting into the combination of straight lines, cannot be used to estimate affinity constant K_b with confidence (Wilson et al., 1997; Evans et al., 2007; Evans et al., 2007; Pasternack, Gibbs, & Villafranca, 1983). The intrinsic binding constant $K_b = 5.6 \times 10^4$ and $K_b = 6.1 \times 10^5$ M^{-1} at D/N = 0.18-0.33 and 0.33-4.6, respectively may be considered as a rough estimates (Fig. 5.2 c) and average of several complexes. The observed change in absorbance accompanied by minor redshift indicates that classical intercalation is not a preferred mode of binding (Manet, Manoli, Zambelli, Andreano,

Masi, Cellai, Ottani, et al., 2011; Manet, Manoli, Zambelli, Andreano, Masi, Cellai, & Monti, 2011; Padmapriya & Barthwal, 2016; Pasternack et al., 1983; Krugh & Reinhardt, 1975; Awasthi, Dogra, & Barthwal, 2013; Pradeep & Barthwal, 2016). The daunomycin molecule may, however, interacts with DNA on binding externally at ends of DNA or along grooves in the backbone of DNA. The alteration in absorbance may be due to the interaction of the π electron cloud of daunomycin and G-quadruplex DNA. Similar results have earlier been reported on binding of doxorubicin/daunomycin with 21/22-mer human telomeric DNA quadruplex in K^+ and Na^+ rich aqueous solutions (Manet, Manoli, Zambelli, Andreano, Masi, Cellai, Ottani, et al., 2011; Manet, Manoli, Zambelli, Andreano, Masi, Cellai, & Monti, 2011; Das, Chatterjee, & Suresh Kumar, 2017).

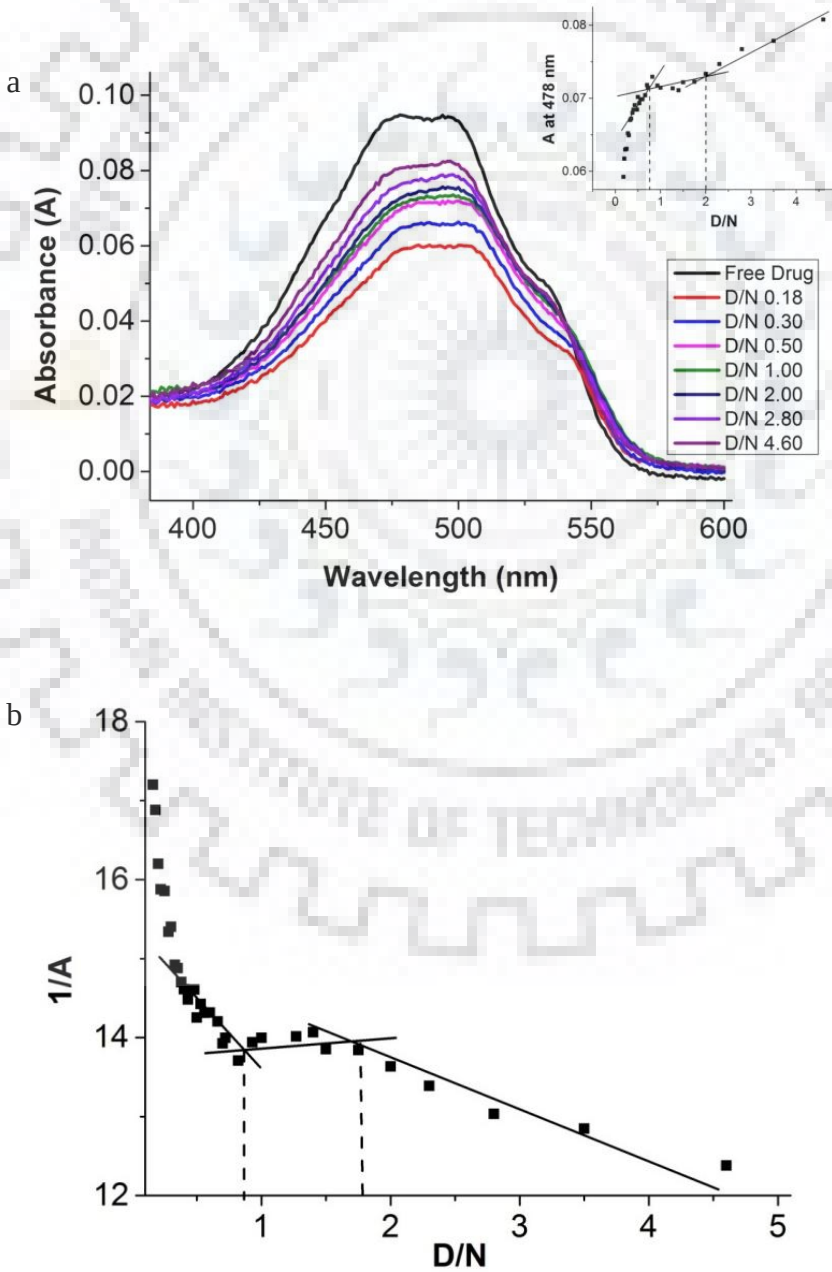

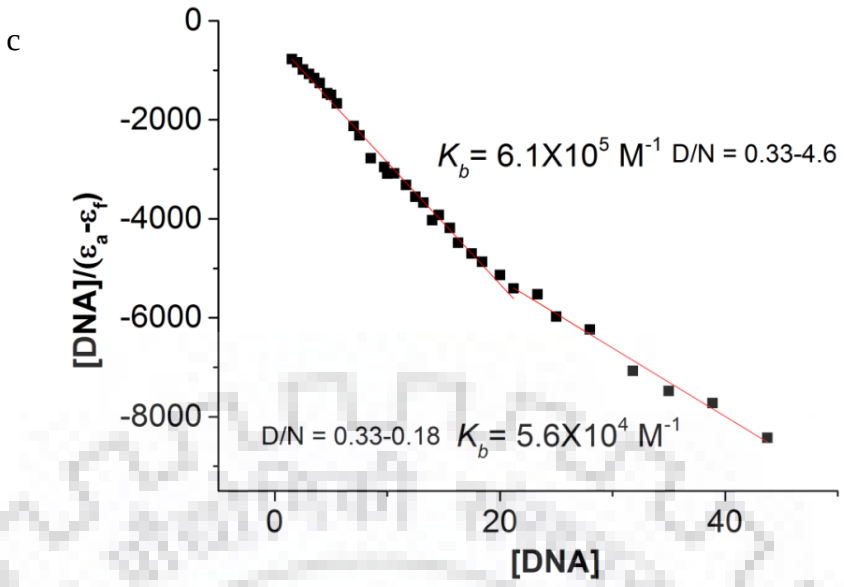

Figure 5.2 a) Absorption spectra of 7 µM free daunomycin and its complex with increasing concentration of Tet22 in 10 mM phosphate buffer containing 100 mM KCl at some selected Daunomycin (D) to Nucleic acid (N) ratios, D/N, at 25 °C. The inset shows plot of Absorbance (A) as a function of D/N ratio at 478 nm at 25 °C.; b) Plot of reciprocal of absorbance (1/A) as a function of D/N and c) Plot of [DNA] / (ε_a - ε_f) as a function of DNA concentration (µM) at 478 nm.

5.3.3 Fluorescence

Addition of Tet22 to daunomycin results in quenching of fluorescence intensity up to 99% at D/N = 0.18 with a red shift $\Delta\lambda_{em}$ = 0.5-1 nm in both the emission maxima (selected data shown in Fig. 5.3 a) indicating strong interaction. A plot of F (inset of Fig. 5.3 a) and 1/F (Fig. 5.3 b) versus D/N show inflection at D/N ~1.0 and 2.0 (Padmapriya & Barthwal, 2016; Pradeep & Barthwal, 2016; Ranjan, Andreasen, Kumar, Hyde-Volpe, & Arya, 2010; Teulade-Fichou et al., 2003). The Stern-Volmer plot showing F/F_0 versus [DNA] (Fig. 5.3 c) and plot of log $[F-F_0]$ / F versus log [DNA] (Fig. 5.3 d), respectively give (Tarikere Palakashan Pradeep & Barthwal, 2016) K_{SV} and K_b in the range 1.5-4.9x10^5 M^{-1}. The bimolecular quenching constant, *Kq* ~4x10^{14} $M^{-1}s^{-1}$ using K_{sv} = 4.0x10^5 M^{-1} and lifetime τ = 1.0 ns is much greater than collision constant of biomolecule and small molecule (Tarikere Palakashan Pradeep & Barthwal, 2016). Presence of static quenching owing to ground state interactions is also evident from the accompanying changes in absorbance and no change in fluorescence lifetime (discussed later). Efficient quenching (86-93%) may be attributed to electron transfer by the proximity of daunomycin to guanines. Similar results have been reported on binding of doxorubicin/daunomycin to 21/22-mer human telomeric DNA sequence (Manet, Manoli,

Zambelli, Andreano, Masi, Cellai, Ottani, et al., 2011; Manet, Manoli, Zambelli, Andreano, Masi, Cellai, & Monti, 2011; (Das et al., 2017). The fluorescent decay of daunomycin was mono exponential with lifetime τ = 1.03 ns (Fig. 5.3 e). The decay for several complexes at D/N = 0.3, 0.5, 1.0-4.0 remained mono exponential with lifetime τ = 0.97-1.00 ns (Fig. 5.3 e, Table 5.2), which may be due to equal lifetime for free and bound daunomycin or alternately for both complexes being non-emissive (Manet, Manoli, Zambelli, Andreano, Masi, Cellai, & Monti, 2011).

The plot of difference in fluorescence intensity as a function of mole fraction of daunomycin shows inflection points at ~0.48 and 0.67 (Fig. 5.3 f) yielding stoichiometry of 1:1 and 2:1 of daunomycin-Tet22 complex, (Tarikere Palakashan Pradeep & Barthwal, 2016) which is consistent with titration studies by absorbance and fluorescence. A scatter in data at higher values of mole fraction of daunomycin is observed.

a

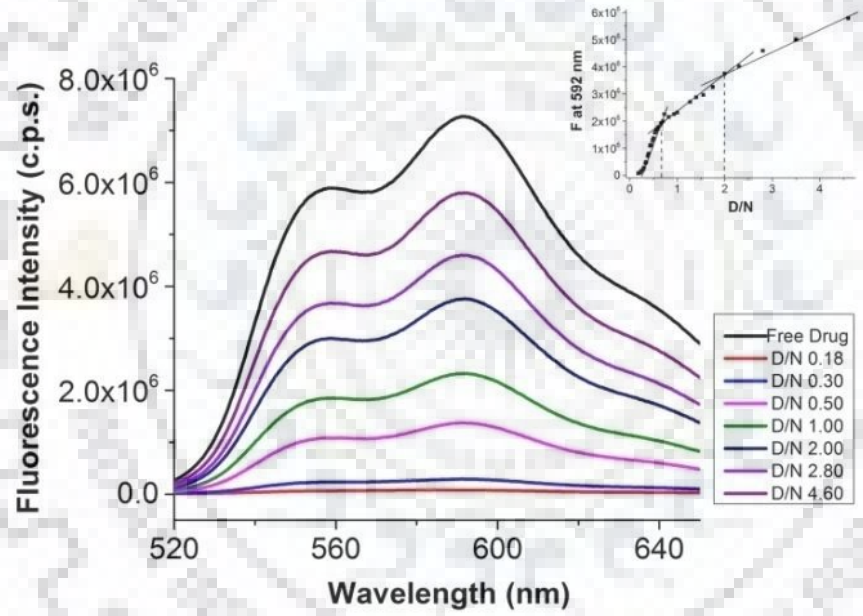

b

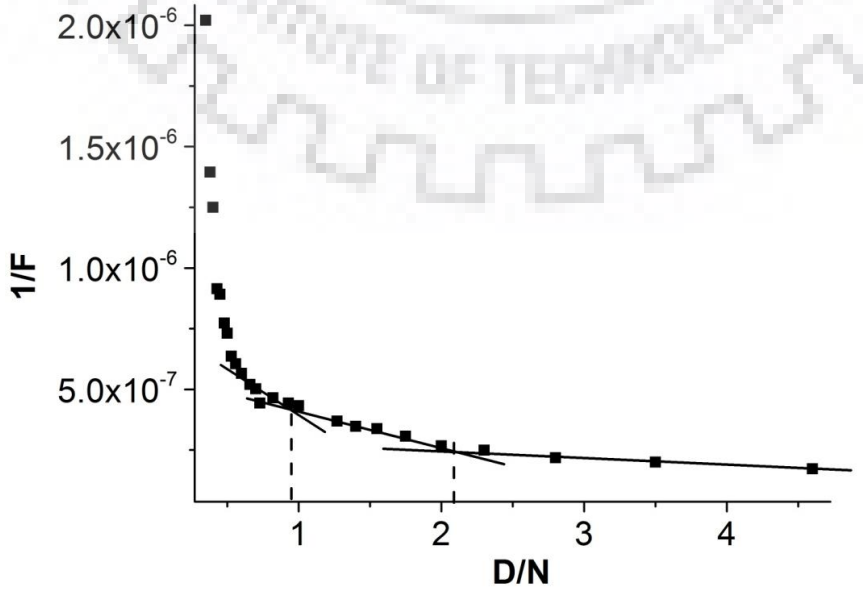

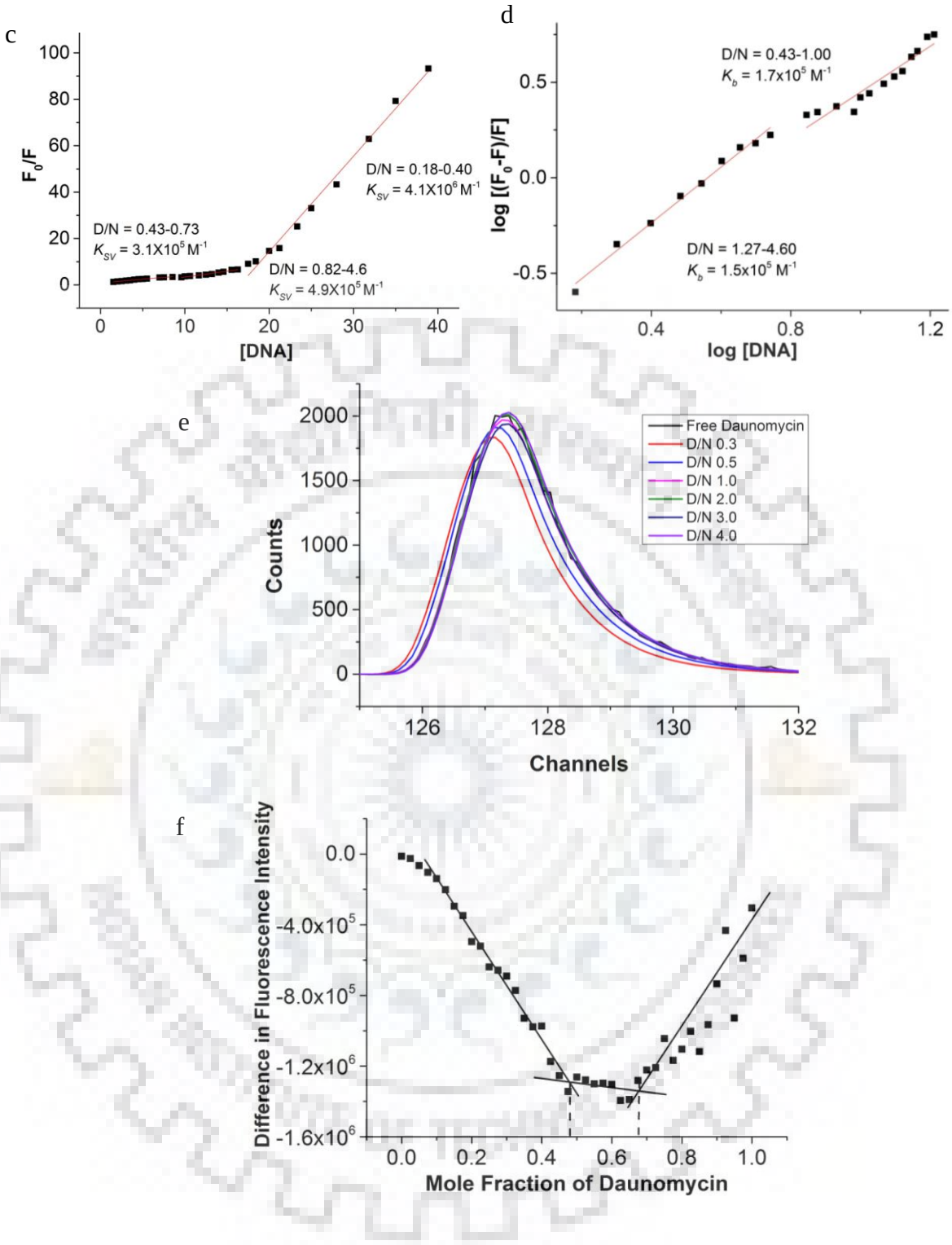

Figure 5.3 a) Fluorescence emission intensity of 7 μM free daunomycin and its complex with increasing concentration of Tet22 in 10 mM phosphate buffer containing 100 mM KCl at some selected Daunomycin (D) to Nucleic acid (N) ratios, D/N, using λ_{ex} = 480 nm at 25 °C. The inset shows the plot of Fluorescence intensity (F) as a function of D/N ratio 592 nm; b) Plot of reciprocal of Fluorescence intensity (1/F) as a function of D/N ratio; c) Plot of F_0/F with respect to DNA concentration (μM); d) Plot of log [(F_0-F)/F] as a function of log [DNA] at 592 nm; e) Fluorescence decay profiles of 7 μM free daunomycin and its complexes with Tet22 at varying D/N ratios at 25 °C; f) Job plot for binding of daunomycin to Tet22 using fluorescence.

Table 5.2 Lifetime (τ) of free daunomycin (7 μM) and daunomycin-Tet22 complex at D/N = 0.3, 0.5, 1.0, 2.0, 3.0 and 4.0 with λ_{ex} = 456 nm and λ_{em} = 590 nm at 25 °C.

	τ(ns)	%	χ^2
Free Drug	1.03	100	0.91
D/N = 0.3	0.89	100	1.35
D/N = 0.5	0.96	100	1.07
D/N = 1.0	0.98	100	0.98
D/N = 2.0	0.99	100	1.03
D/N = 3.0	0.98	100	0.99
D/N = 4.0	0.97	100	0.98

5.3.4 Circular Dichroism

The circular dichroism spectra of Tet22 in presence of 100 mM K^+ shows (Fig. 5.4 a) a well defined positive band at 265 nm indicating stacking arrangements of tetrads that is characteristic of parallel stranded G-quadruplex DNA having stacking of bases with same glycosidic bond angle (i.e. either *anti* or *syn*) and a positive band at 290 nm that is characteristic of antiparallel stranded G-quadruplex DNA showing stacking of guanosines with different glycosidic bond angle (i.e. *anti* and *syn*) (Vorlíčková et al., 2012; Hudson, Brooks, & Graves, 2009; Kypr, Kejnovská, Bednářová, & Vorlíčková, 2012; Dapić et al., 2003; Karsisiotis et al., 2011) . Parallel and antiparallel forms of G-quadruplex show a negative and positive CD bands centered around 238-240 and 240-245 nm, respectively (Vorlíčková et al., 2012; Hudson et al., 2009; Kypr et al., 2012; Dapić et al., 2003; Karsisiotis et al., 2011; Masiero et al., 2010; Gray et al., 2008). Thus, the observed negative band at 240 nm and dominant positive band at 265 nm (Fig. 5.4 a) shows that the sequence d-[GGGG(TTGGGG)$_3$] forms a mixture of 3+1 hybrid as well as parallel quadruplexes in the presence of 100 mM K^+ and the population of latter arrangement prevails (Vorlíčková et al., 2012).

The formation of G-quadruplex is influenced by K^+ concentration (Vorlíčková et al., 2012; Hudson et al., 2009; Paramasivan, Rujan, & Bolton, 2007) and we, therefore, recorded CD spectra in water, buffer containing 0 (no additional salt), 25, 150 and 200 mM K^+ (Figure. 5.4 a). It is found that in the absence of any additional K^+ ions, there are two positive CD bands of comparatively same intensities at 265 nm and 290 nm, that is, identical to CD spectra (Vorlíčková et al., 2012) of 3+1 hybrid structure of 24-mer G-quadruplex DNA sequence, [d-(T2G4)$_4$] determined by NMR in Na^+ rich solutions (Y. Wang & Patel, 1994). On adding 25

mM K^+, the 265 nm peak intensity is found to be more intense than the corresponding 295 nm peak which indicates the presence of parallel quadruplex (Vorlíčková et al., 2012). Further stepwise increase in K^+ concentration from 25 mM to 200 mM shows that the positive 260 nm CD band dominates and the spectra is characteristic of a mixture of 3+1 hybrid and parallel quadruplexes and that a significant population of latter arrangement prevails (Vorlíčková et al., 2012). Thus, K^+ promotes the formation of parallel quadruplex, as has also been observed earlier for other G-quadruplex DNA sequences (Vorlíčková et al., 2012; Hudson et al., 2009; Paramasivan et al., 2007). Further, the relative populations of two structures remains unchanged at concentration >150 mM K^+ reaching an equilibrium with respect to relative populations of two conformations.

a

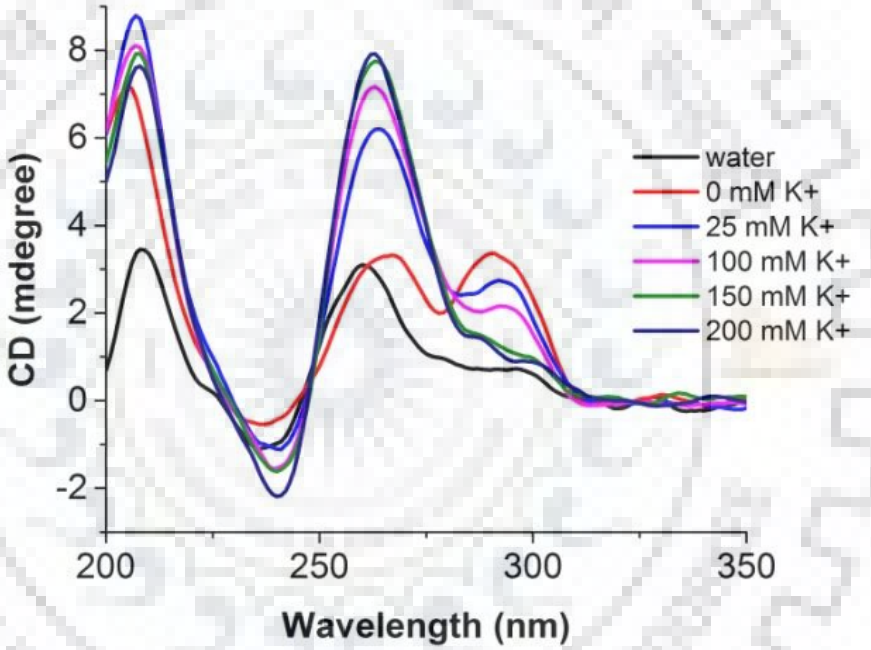

b

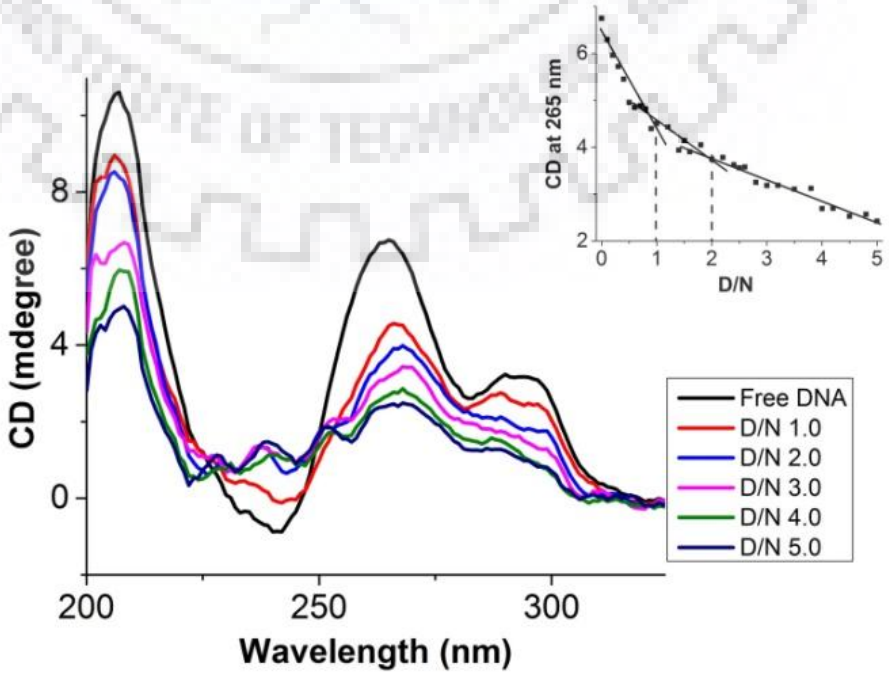

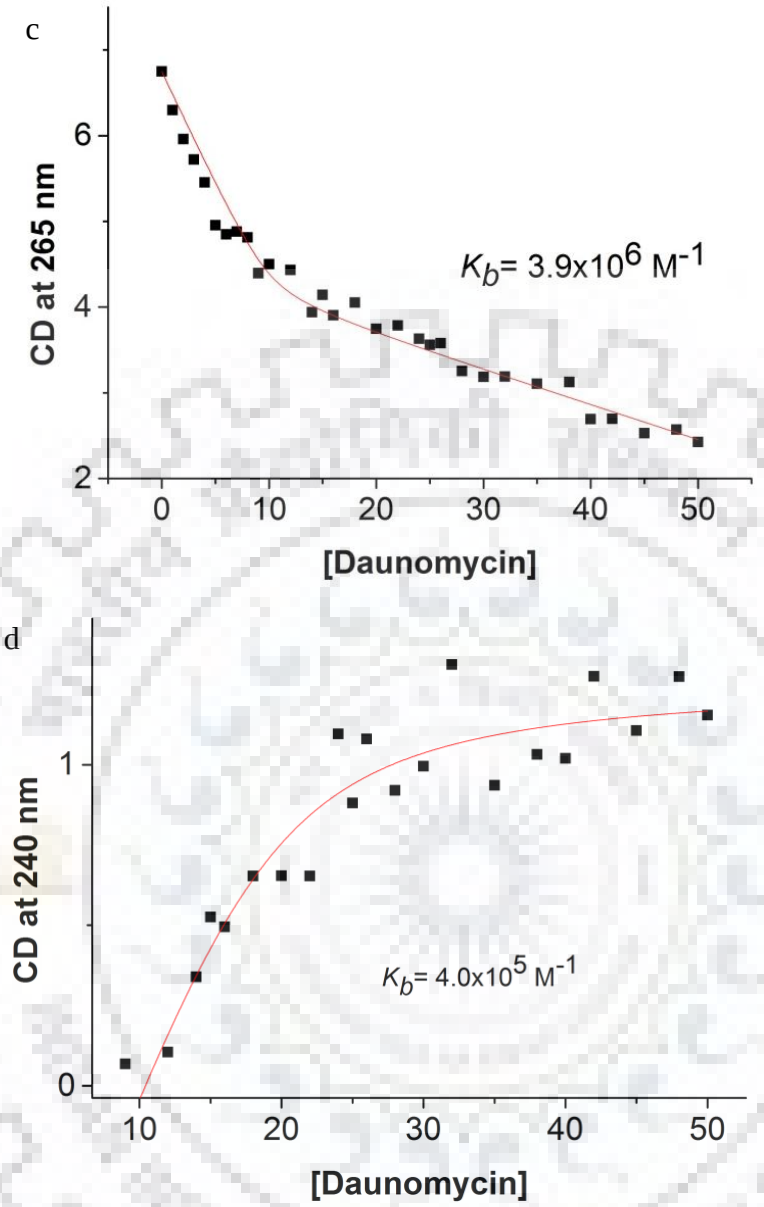

Figure 5.4 a) CD spectra of free 10 µM Tet22 in water and in KBPES buffer containing 0, 25, 100, 150 and 200 mM KCl; b) CD spectra of free 10 µM Tet22 and its complex with increasing concentration of daunomycin at some selected Daunomycin (D) to Nucleic acid (N) ratios, D/N, in 10 mM phosphate buffer with 100 mM KCl at 25 °C. The inset shows plot of CD (mdegree) at 265 nm as a function of D/N ratio; Nonlinear fitted curve of observed CD in mdegrees (red) for binding of daunomycin with Tet22 at c) 265 nm and d) 240 nm as a function of daunomycin concentration (µM) showing binding constant (K_b); d) CD spectra of 400 µM daunomycin in free form and its complex with increasing concentration of Tet22 at some selected D/N ratios. The inset shows the plot of CD (mdegree) at 458 nm as a function of D/N ratio.

Upon addition of daunomycin to 10 µM Tet22 up to D/N = 5.0 in presence of 100 mM K^+, the magnitude of 290, 265 and 240 nm bands decrease significantly by 60, 63 and 67%, respectively which perhaps reflects the change in the relative population of two G-quadruplex conformations. The binding is accompanied by a minor red shift ~1-3 nm (Fig. 5.4 b) which rules out classical intercalation and is indicative of external binding (De Cian et al., 2007). Groove binding has been shown to induce changes in the magnitude of 265 and 243 nm bands while end stacking does not show any significant change (De Cian et al., 2007). Accordingly, both end stacking and external groove binding may be occurring in present investigations. Plot of CD signal at 265 nm (inset of Fig. 5.4 a) shows inflection at D/N = 1.0 and 2.0 suggesting stoichiometry of complex as ~1:1 and 2:1 (Rezler et al., 2005), and the absence of an iso-elliptic point confirms the presence of multiple stoichiometries of complexes. Non-linear curve fitting of the plot of magnitude of CD at 265 and 243 nm as a function of daunomycin concentration (Fig. 5.4 c,d) using equation (5) yield different affinity constants, K_b = 3.9x10^6 M^{-1} and 4.0x10^5 M^{-1}, respectively, which may be due to presence of several conformations of complex which contribute differently at different wavelengths. We also carried out titrations of daunomycin with G-quadruplex DNA comprising 0, 25 and 200 mM K^+ (Fig. 5.5 a-c) and found that affinity constant at 0-25 mM K^+ is ~1.4x10^6 M^{-1} as compared to the corresponding value of 4.0 x10^6 M^{-1} at 100-200 mM K^+ (Fig. 5.6 a-f and Table 5.3). Apparently, the binding to 3+1 hybrid structure (at 0 mM K^+) has weaker affinity than the parallel G-quadruplex structure stabilized by high concentrations (100-200 mM) of K^+.

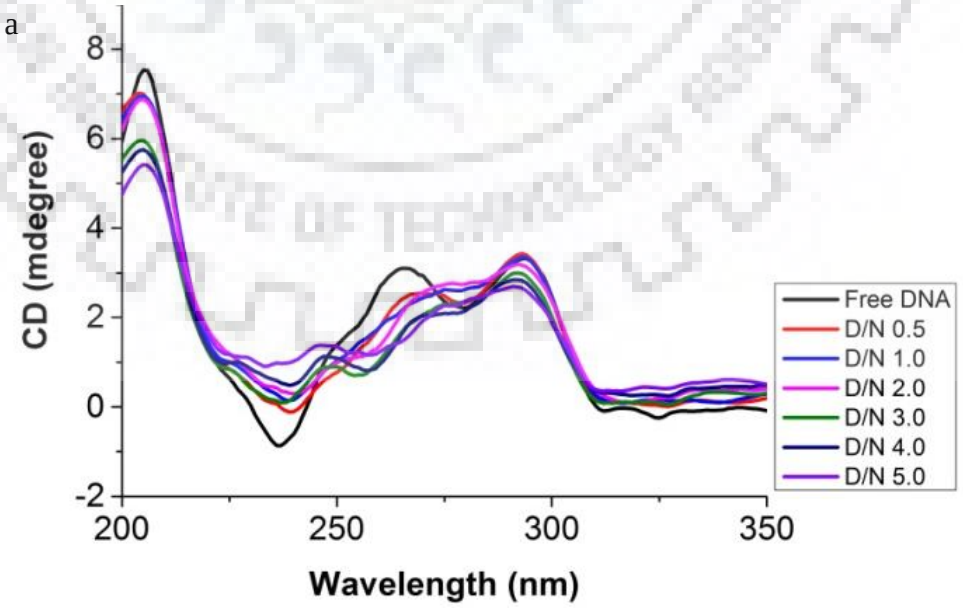

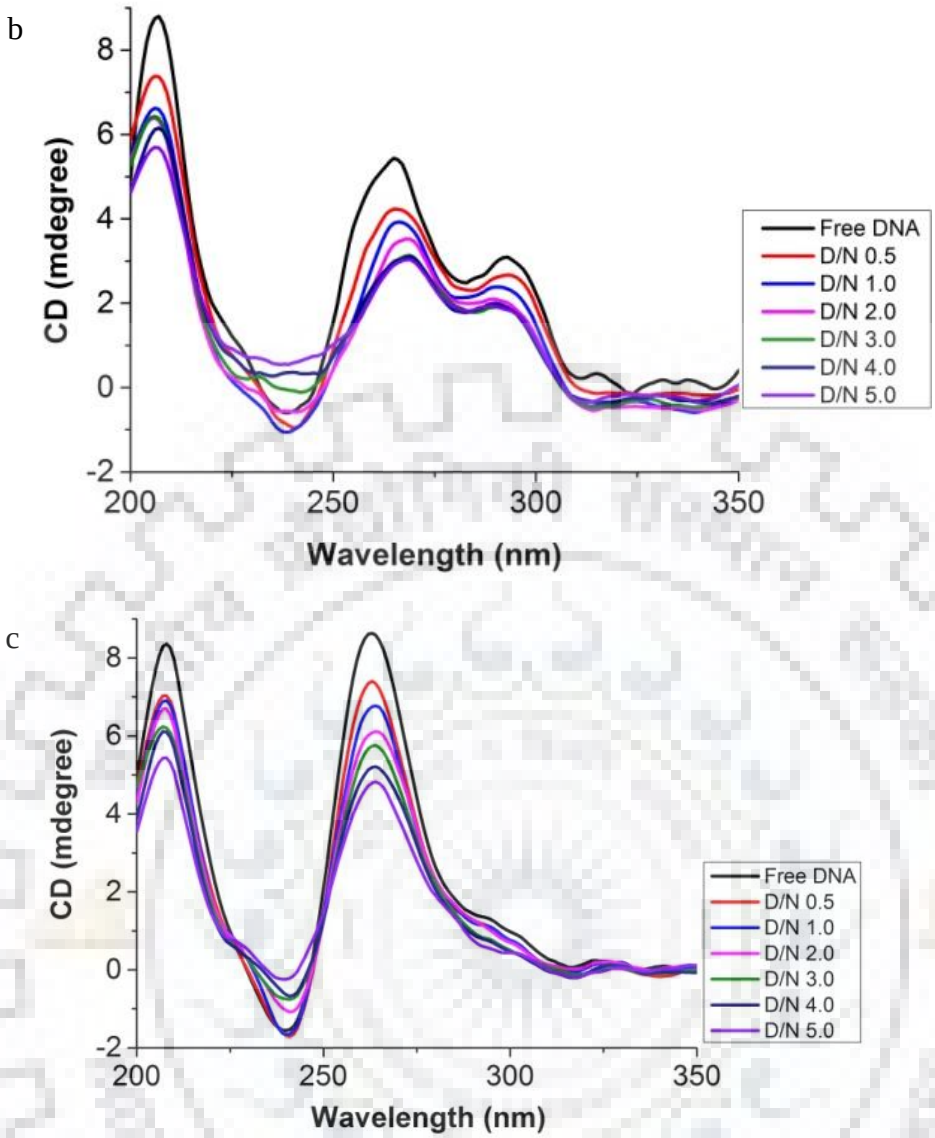

Figure 5.5 CD spectra of titration of daunomycin into 10 µM solution of Tet22 in KBPES buffer containing a) 0 mM KCl; b) 25 mM KCl and c) 200 mM KCl at 25 °C.

In order to examine the existence of induced CD bands, Tet22 was added to 400 µM daunomycin (Figure 5.6 g) in steps. The bisignate CD band characteristic of the self-associated dimeric form of daunomycin, having positive and negative peaks at 460 and 540 nm, respectively and cross over point at 500 nm, observed at high concentrations of daunomycin (Gallois et al., 1998), disappeared on interaction with DNA. This demonstrates that daunomycin binds as a monomer. A small positive band at ~460-480 nm was observed (Figure 5.6 g), which increased slightly in magnitude with D/N ratio (inset of Figure 5.4 b). The presence of small positive induced CD band has earlier been attributed to binding of ligands at grooves or end stacking with bases of DNA (Manet, Manoli, Zambelli, Andreano, Masi, Cellai, Ottani, et al., 2011; Manet, Manoli, Zambelli, Andreano, Masi, Cellai, & Monti, 2011; Bianco

et al., 2013; Rezler et al., 2005; White et al., 2007; Jain, Reddy, Paul, Muniyappa, & Bhattacharya, 2009; Paul et al., 2012; Zhao et al., 2013). On binding of adriamycin to human telomeric DNA 22-mer sequence in K^+ rich solution, end stacking was inferred (Manet, Manoli, Zambelli, Andreano, Masi, Cellai, Ottani, et al., 2011) on the basis of observed red shift of 25-30 nm in both, the absorption maxima and 350 nm CD band of adriamycin.

Table 5.3 Binding constants obtained from data of CD experiments for titration of daunomycin to Tet22 in KBPES buffer containing different concentrations of KCl at 25 °C.

Potassium ion concentration	CD at 240 nm	CD at 265 nm
	K_b (M^{-1})	K_b (M^{-1})
0 mM	4.9 x 10^5	1.6 x 10^6
25 mM	1.3 x 10^4	1.2 x 10^6
100 mM	4.0 x 10^5	3.9 x 10^6
200 mM	4.0 x 10^5	4.1 x 10^6

We did not observe significant shift in wavelength maxima of absorption (~7 nm) and emission (< 1 nm) while redshift in 350 nm CD band of daunomycin was ~13 nm, which suggests absence of stacking interactions and presumably presence of groove binding (Bianco et al., 2013; Rezler et al., 2005; Jain et al., 2009). We made an attempt to investigate the daunomycin-DNA interactions further by Nuclear Magnetic Resonance and docking studies.

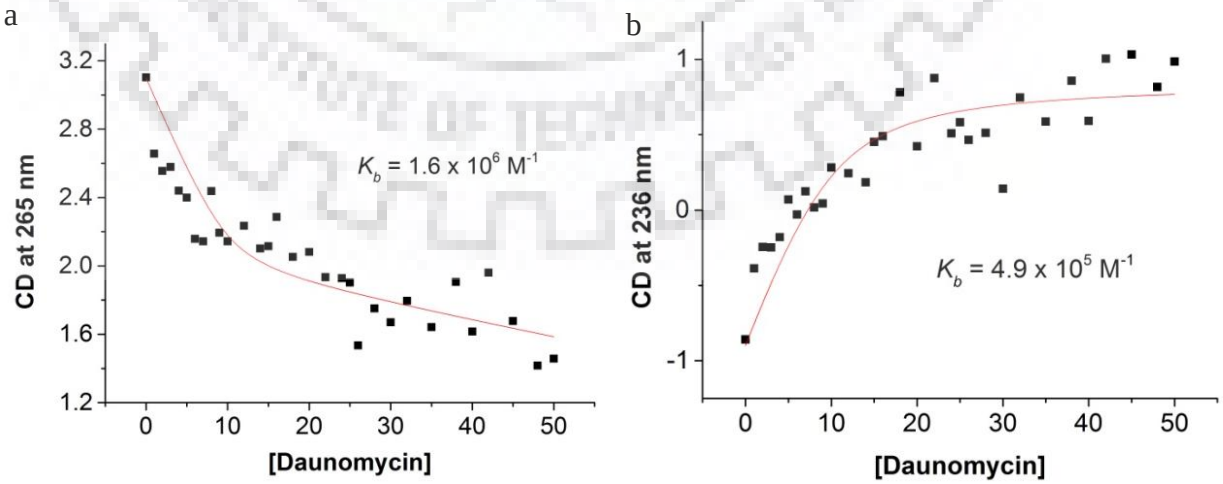

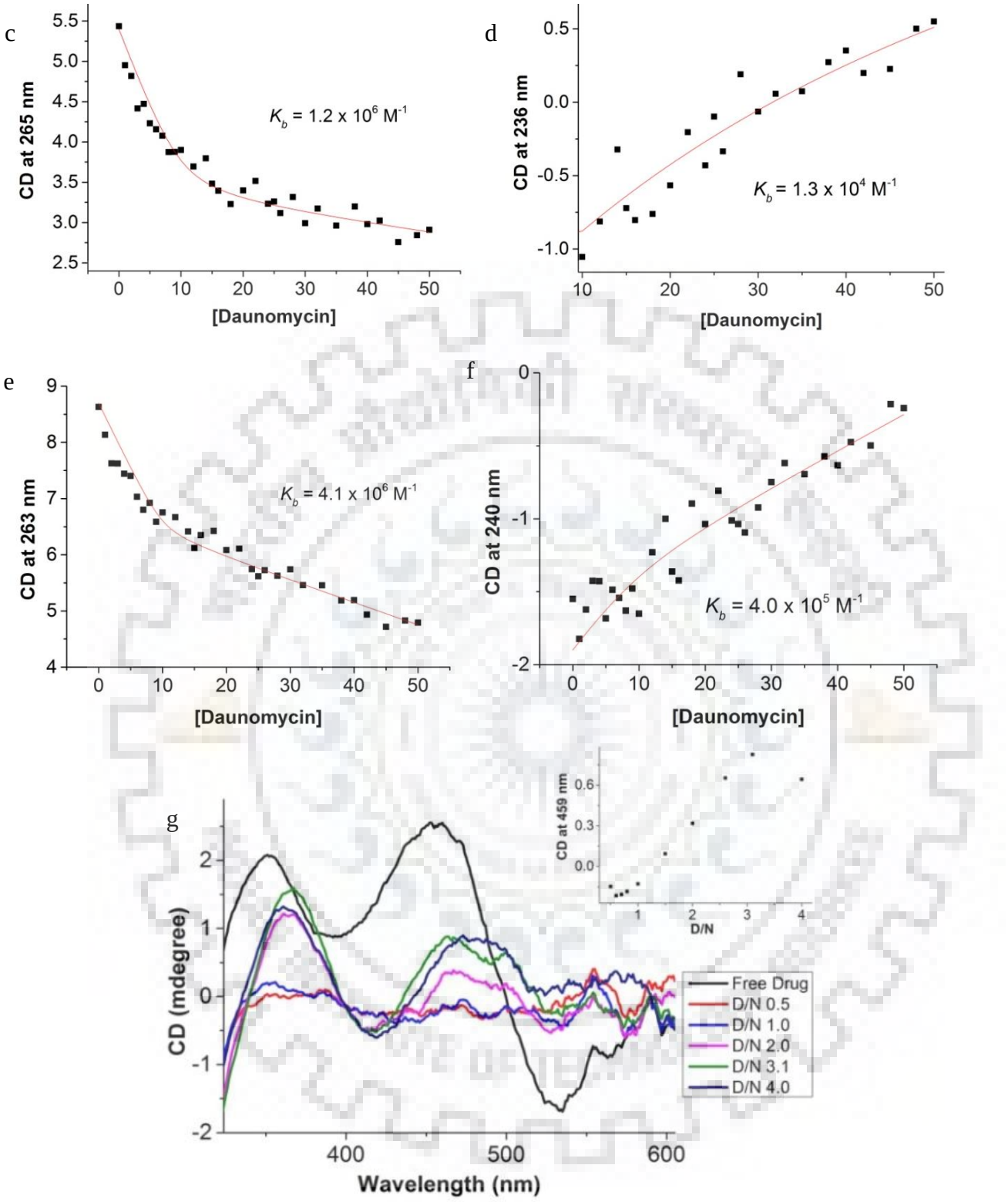

Figure 5.6 Nonlinear fitted curve of CD in mdegrees as a function of daunomycin concentration (μM) showing binding constant (K_b) for binding of daunomycin to 10 μM Tet22 in KBPES buffer containing a-b) 0 mM KCl; c-d) 25 mM KCl; and e-f) 200 mM KCl at 25 °C; g) CD spectra of 400 μM daunomycin in free form and its complex with increasing concentration of Tet22 at some selected D/N ratios in 10 mM phosphate buffer with 100 mM KCl at 25 °C. The inset shows the plot of CD (mdegree) at 458 nm as a function of D/N ratio.

5.3.5 Nuclear Magnetic Resonance

The ^{1}H NMR spectra of Tet22 in K^+ rich aqueous solution (Fig. 5.7 a-c) show that chemical shift positions of several resonances are same (Table 5.4) as that of NMR spectra of 24-mer d-$(T2G4)_4$ sequence in Na^+ rich solution (Wang & Patel, 1994; E. Henderson, Hardin, Walk, Tinoco, & Blackburn, 1987; Hardin, Corregan, Lieberman, & Brown II, 1997) although the spectral lines are significantly broadened. In addition, several extra resonance peaks are observed which suggest existence of other quadruplex structure besides the 3+1 hybrid structure found in Na^+ rich solution, (Seenisamy et al., 2004) which may be attributed to presence of parallel quadruplex structure as evidenced by the observed prominent 265 nm CD band (Fig. 5.4 a) (Vorlíčková et al., 2012). ^{31}P NMR spectra (Fig. 5.7 d) also show similarities (Table 5.5) and broadening of signals as compared to that in Na^+ rich solution (Henderson et al., 1987; Hardin et al., 1997). The signals spread over a range of ~1.5 ppm as expected due to heterogeneity in phopho-diester conformations, as have been found to exist in Z-DNA (Henderson et al., 1987; Hardin et al., 1997; Hall, Cruz, Tinoco, Jovin, & van de Sande, 1984) due to presence of both *anti* and *syn* conformations of glycosidic bond rotation.

a

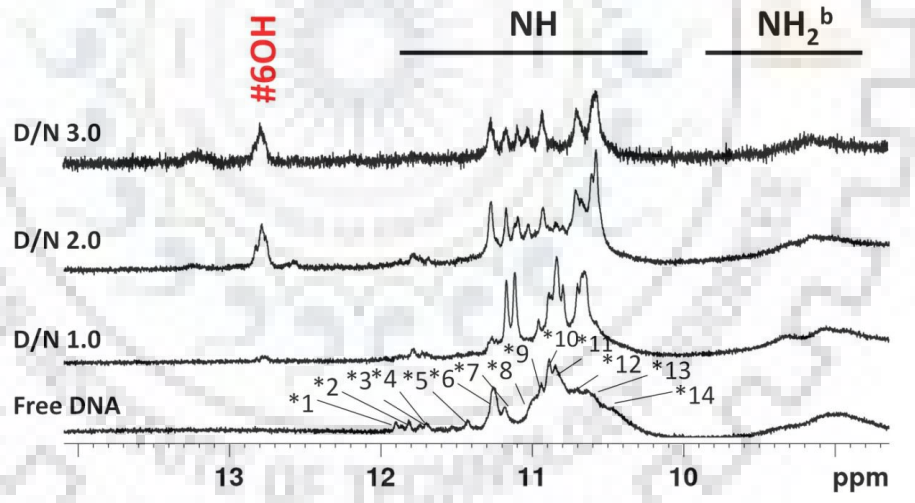

b

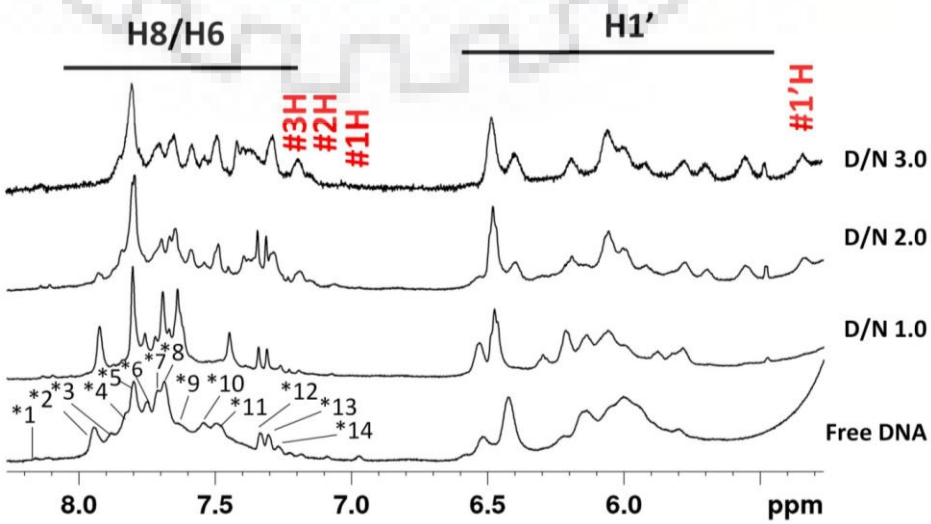

c

d

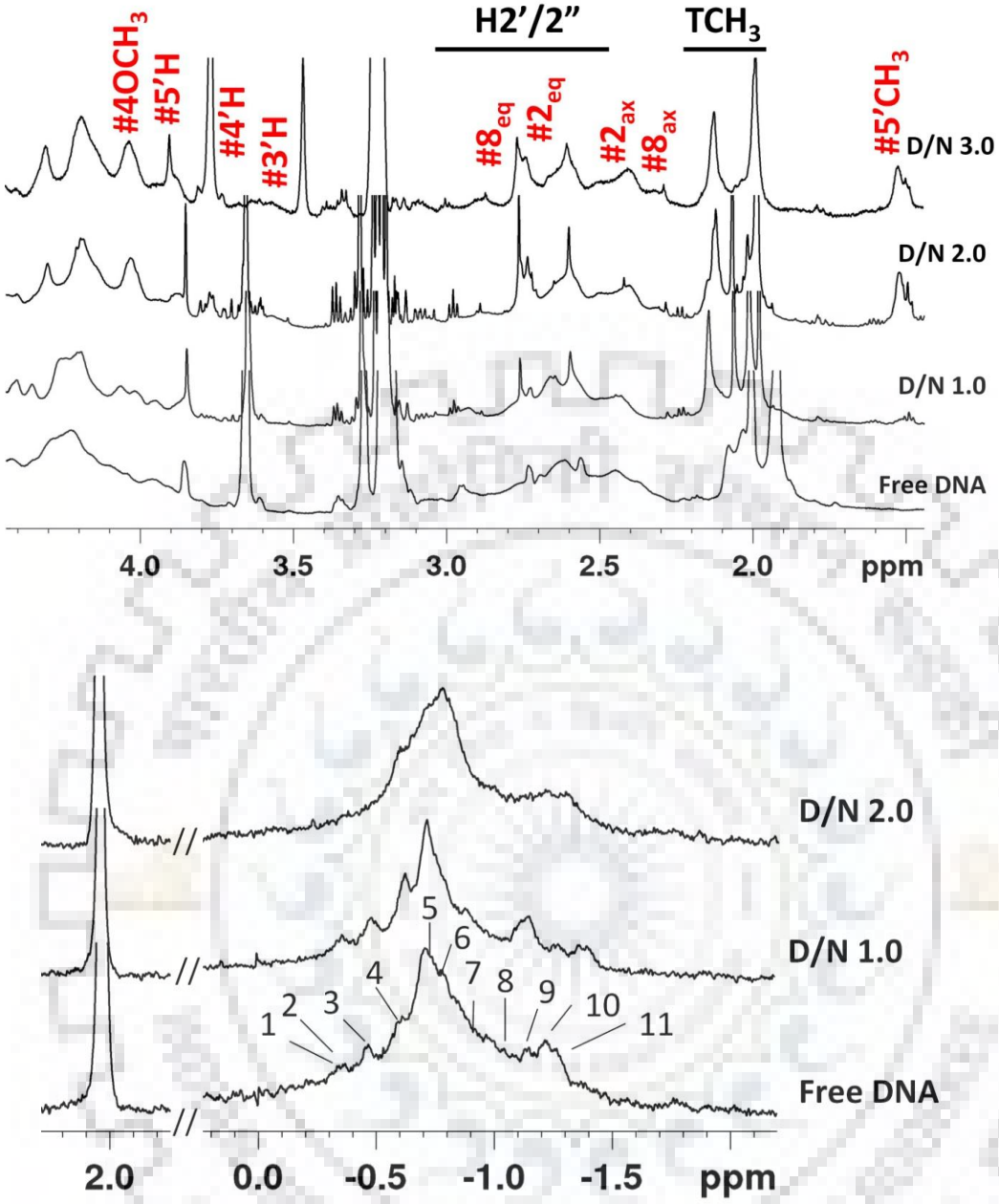

Figure 5.7 1D ^{1}H and ^{31}P NMR spectra of 2.3 mM of Tet22 and its complex upon progressive addition of daunomycin to DNA at different D/N ratios at 25 °C (90% H_2O + 10%D_2O solvent); a) Imino protons and 6OH protons of daunomycin; b) base and sugar H1′ protons of DNA and ring D protons 1H, 2H and 3H of daunomycin; c) Sugar H2′/2″ and methyl protons of thymine and daunomycin protons 5′H, 4OCH_3,4′H, 3′H, 2axH, 2eqH, 8axH, 8eqH and 5′CH_3 at 25 °C; and d) ^{31}P NMR spectra of free Tet22 and its complex with daunomycin at D/N =1.0 and 2.0. Symbol # refers to daunomycin proton signals and * denotes proton signals which appear at the same position as that in NMR structure in Na^+ rich solution (Wang & Patel, 1994).

Table 5.4 ^{1}H Chemical shift (ppm) of protons in Tet22 in KBPES buffer containing 100 mM KCl (90% H_2O + 10% D_2O solvent) at 25 °C and that reported in the literature by Wang and Patel (1994).

Protons	Present Work		Wang and Patel (1994)		
Residues	NH	H8/H6	Residues	NH	H8/H6
1	11.90	8.14	T1	-	7.59
2	11.81	7.95	T2	11.89	7.46
3	11.69	7.89	G3	11.93	7.25
4	11.49	7.83	G4	12.18	8.14
5	11.42	7.80	G5	11.35	7.84
6	11.28	7.75	G6	-	7.95
7	11.15	7.70	T7	-	7.63
8	11.05	7.68	T8	-	7.03
9	10.94	7.64	G9	-	7.32
10	10.88	7.51	G10	11.23	7.14
11	10.85	7.48	G11	11.11	7.52
12	10.70	7.33	G12	11.09	8.14
13	10.62	7.30	T13	-	7.81
14	10.45	7.26	T14	-	7.12
			G15	11.05	7.82
			G16	11.15	7.64
			G17	10.94	7.48
			G18	10.87	7.70
			T19	-	7.83
			T20	-	7.89
			G21	11.49	7.16
			G22	11.28	7.39
			G23	11.45	7.95
			G24	-	7.85

On adding daunomycin at D/N ratio = 1.0, 2.0 and 3.0, a single set of daunomycin protons are observed (Fig. 5.7 a-c). At D/N=3.0, although the daunomycin spectral lines have increased intensity and become more prominent, they apparently show line broadening, which may be due to the formation of more than one stoichiometric complex. Several daunomycin protons could be assigned unambiguously by following standard method using ^{1}H-^{1}H NOESY (Fig. 5.8 a-d and 5.9 a-c) (Barthwal, Mujeeb, Srivastava, & Sharma, 1996). The expected intra molecular NOE connectivities within the daunomycin molecule (Table 5.6 and 5.7) confirm the assignment (Barthwal et al., 1996; Barthwal et al., 2008).

Table 5.5 ^{31}P Chemical shift (ppm) of phosphorous in Tet22 in KBPES buffer containing 100 mM KCl (90% H_2O + 10% D_2O solvent) at 25 °C and those reported in the literature by Wang and Patel (1994) and Henderson et al. (1987).

Present Work		Henderson et al. (1987)		Wang and Patel (1994)	
Residue	Chemical Shift	Residue	Chemical Shift	Residue	Chemical Shift
1	-0.33	1	-3.60	T1	-4.39
2	-0.36	2	-3.75	T2	-4.25
3	-0.45	3	-3.80	G3	-3.81
4	-0.60	4	-3.85	G4	-4.29
5	-0.71	5	-4.10	G5	-4.11
6	-0.77	6	-4.20	G6	-4.56
7	-0.96	7	-4.30	T7	-5.17
8	-1.04	8	-4.40	T8	-4.09
9	-1.12	9	-4.55	G9	-3.28
10	-1.15	10	-4.60	G10	-4.0 to -4.5
11	-1.21	11	-4.75	G11	-
				G12	-2.89
				T13	-4.96
				T14	-4.30
				G15	-4.0 to -4.5
				G16	-4.0 to -4.5
				G17	-4.55
				G18	-4.0 to -4.5
				T19	-4.99
				T20	-5.38
				G21	-4.35
				G22	-4.39
				G23	-4.54
				G24	-

The 6OH, 1H, 2H, 3H, 7H and 1'H shift upfield by -0.23 to -1.08 ppm while 4OCH_3, 5'CH_3 2'axH, 2'eqH, 8axH, 8eqH, etc. shift downfield up to 0.63 ppm (Table 5.8 and 5.9). It is notable that 6OH which is not easily observed in spectra of daunomycin in aqueous solution (Barthwal et al., 1996; Barthwal et al., 2008) are observable in spectra of complex (Fig. 5.7 a). This is presumably due to shielding from solvent water in the structure of complex, implicating its direct involvement in the interaction between daunomycin and quadruplex DNA.

Several intermolecular NOEs are observed in the NOESY spectra of complex (Fig. 5.8 a-d and 5.9 a-c) showing the proximity of protons of daunomycin to that of DNA (Table 5.10 and 5.11).

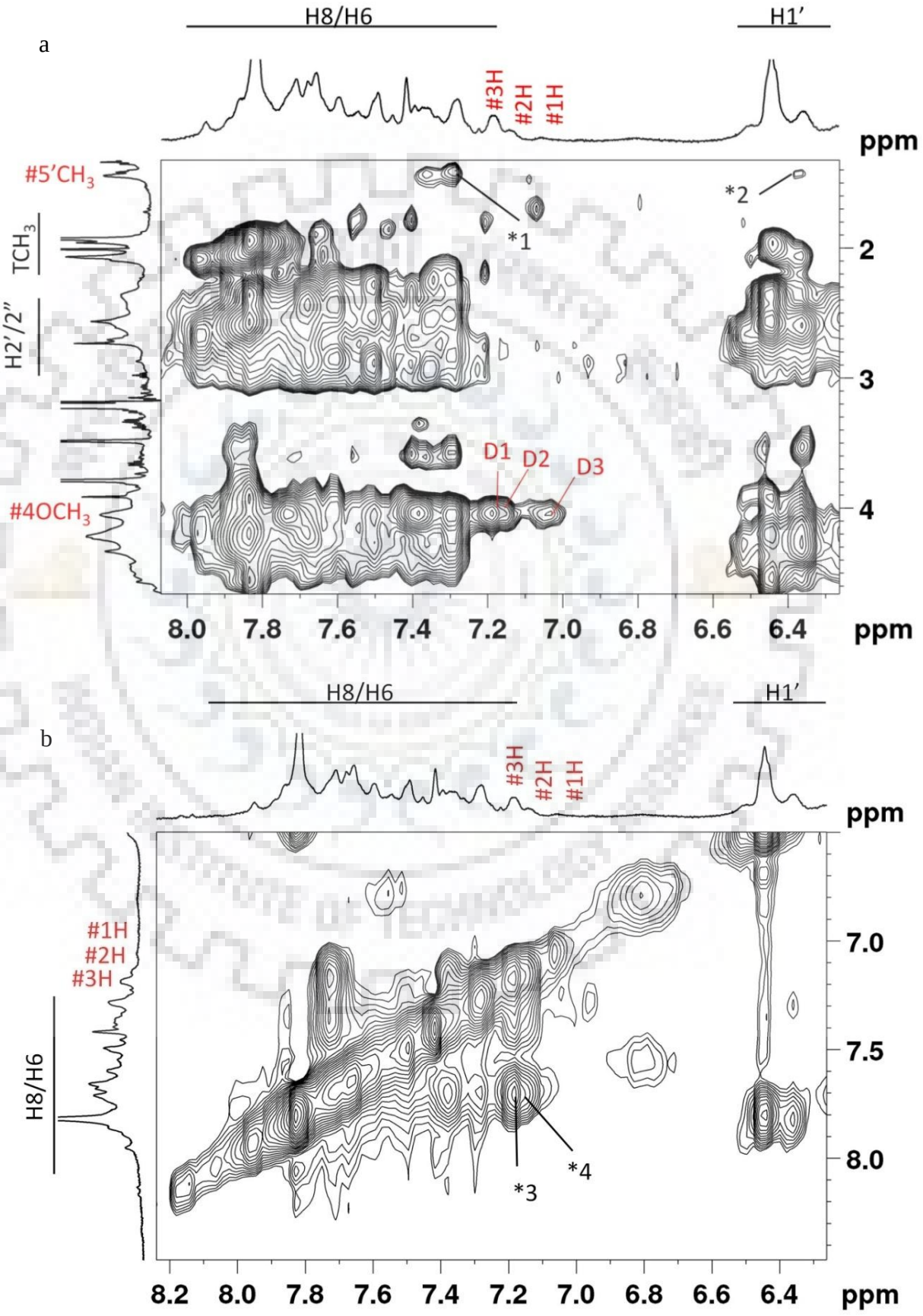

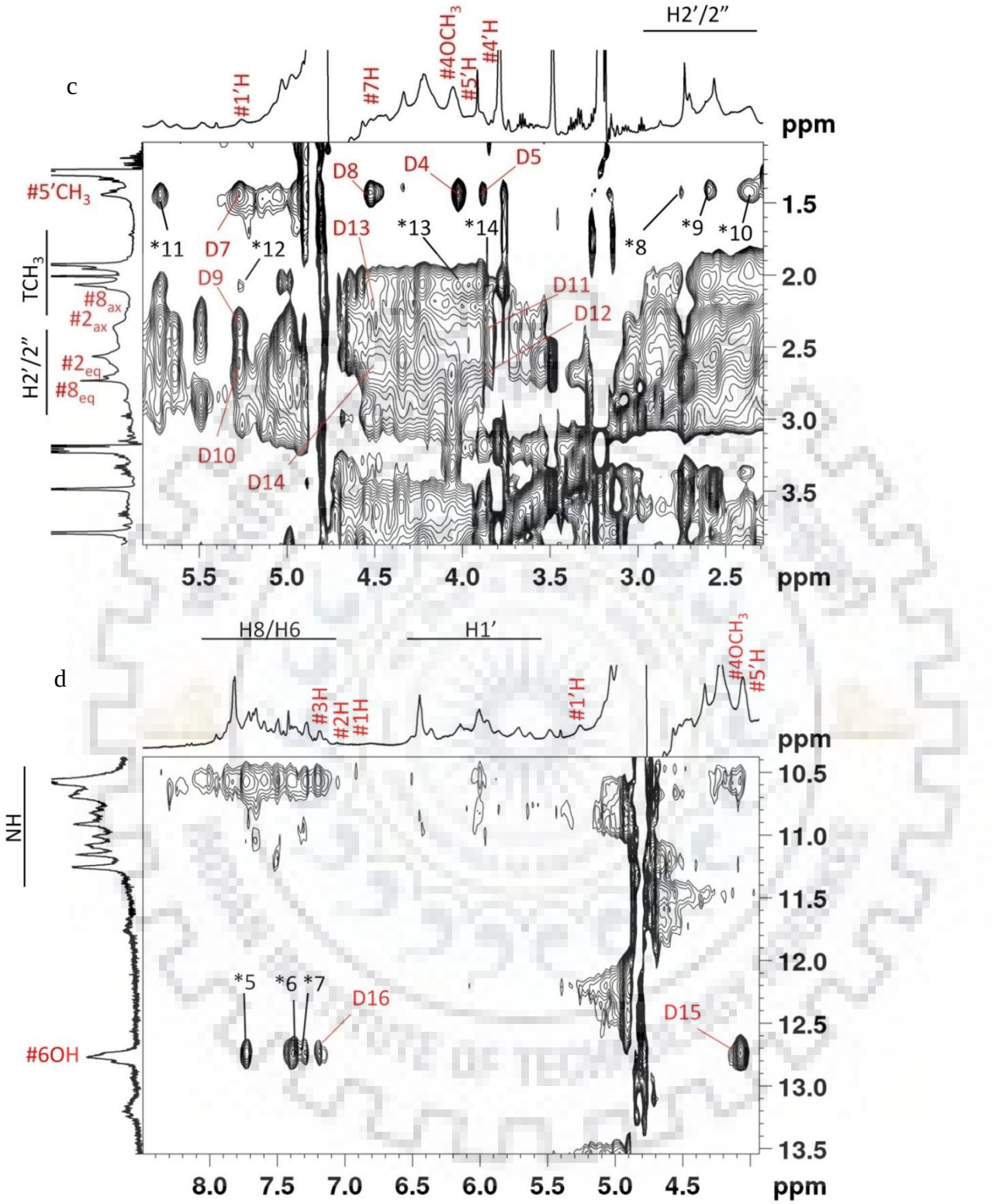

Figure 5.8 2D ^{1}H-^{1}H NOESY spectra of daunomycin-Tet22 complex at D/N = 2.0, mixing time τ_m = 300 ms at 25 °C (90% H_2O + 10% D_2O solvent). Expansion of specific regions of NOESY spectra showing NOE correlations between a) 5'CH_3 and H8/H6/H1' protons; b) 3H, 2H and H8/H6 protons; c) 5'CH_3 and deoxyribose sugar H2'/2"/H3' protons, 5'H, 4'H, 1'H, and TCH_3 protons; d) 6OH and H8/H6 protons. Symbol # denotes daunomycin protons, D denotes intra molecular cross peaks within daunomycin (numbering as in Table 5.6) and * denotes inter molecular cross peaks between daunomycin and DNA protons (numbering as in Table 5.10).

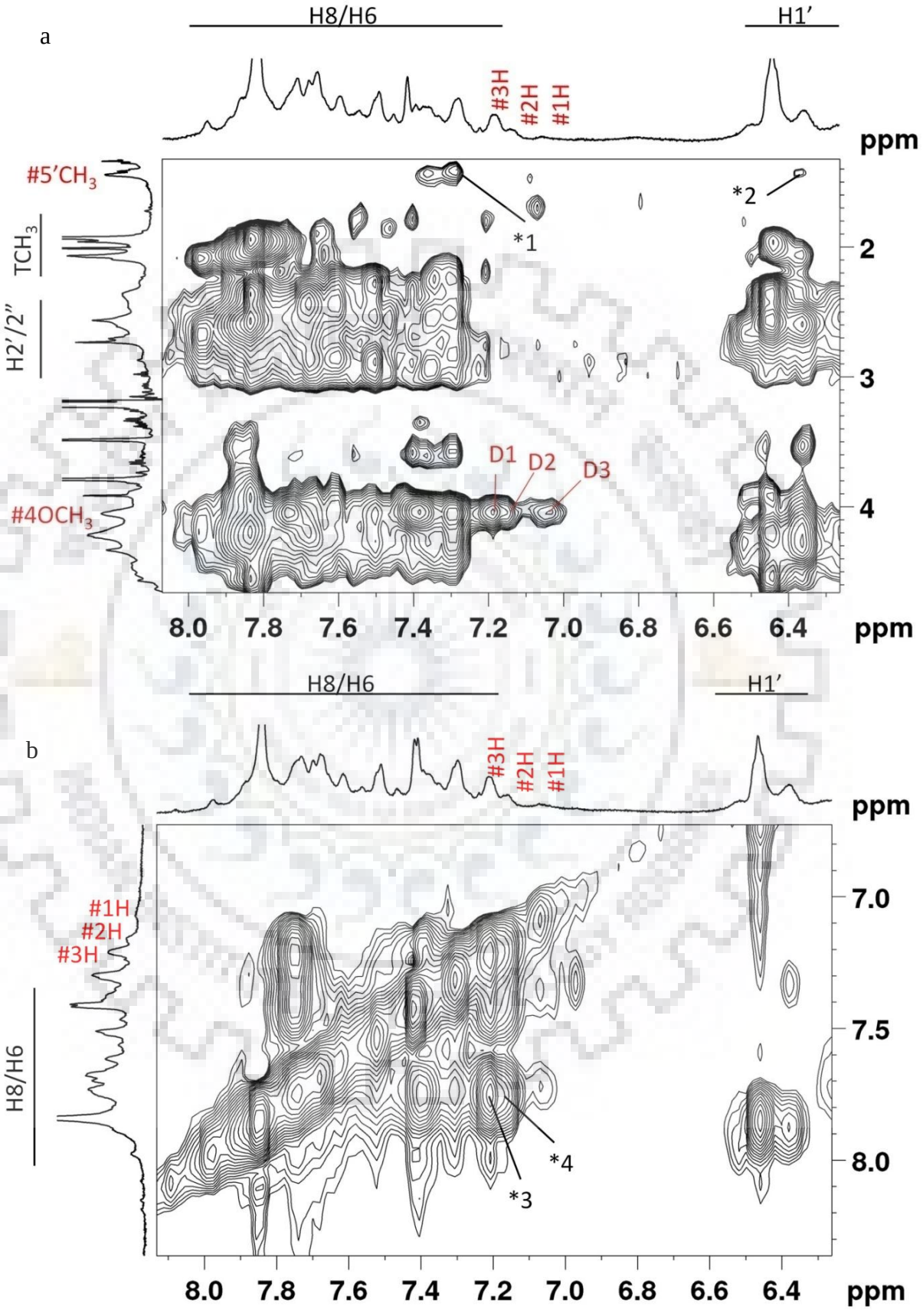
a
H8/H6
H1'
#3H
#2H
#1H
ppm
#5'CH3
TCH3
H2'/2''
#4OCH3
*1
*2
D1
D2
D3
2
3
4
8.0
7.8
7.6
7.4
7.2
7.0
6.8
6.6
6.4
ppm
b
H8/H6
H1'
#3H
#2H
#1H
ppm
#1H
#2H
#3H
H8/H6
*4
*3
7.0
7.5
8.0
8.0
7.8
7.6
7.4
7.2
7.0
6.8
6.6
6.4
ppm

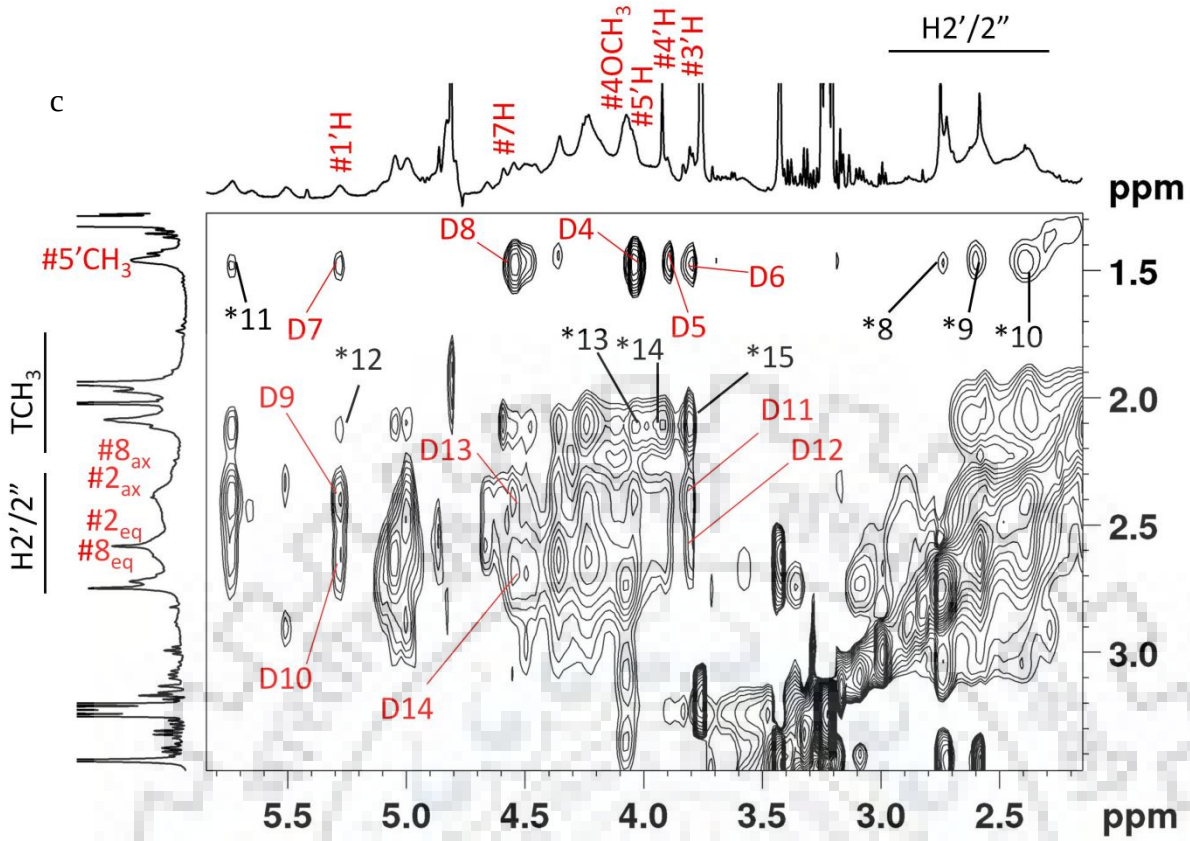

Figure 5.9 2D ^{1}H-^{1}H NOESY spectra of daunomycin-Tet22 complex at D/N = 2.0, mixing time τ_m = 300 ms at 25 °C (100% D_2O solvent). Expansion of specific regions of NOESY spectra showing NOE correlations between a) daunomycin proton 5'CH_3 and H8/H6/H1' protons along with intra molecular NOE cross peaks of daunomycin, b) daunomycin protons 3H, 2H and H8/H6 protons, c) daunomycin protons 5'CH_3, 5'H, 4'H, 3'H with sugar H2'/2"/H3' and TCH_3 protons along with intra molecular NOE cross peaks of daunomycin. Symbol # denotes daunomycin protons, D denotes intra molecular cross peaks of daunomycin (numbering as in Table 5.7) and * denotes inter molecular cross peaks between daunomycin and DNA protons (numbering as in Table 5.11).

Notable among these are 1H, 2H, 3H and 6OH protons with base H8/H6 resonances, which may be due to the stacking of daunomycin ring partially with the G/T aromatic bases. In addition, 5'CH_3 which appears as a broad resonance line is in the proximity of base H8/H6, deoxyribose H1', H2', H2'', H3' protons. The phosphorus NMR signals get broadened on the addition of daunomycin and show shifts ~0.2 ppm, which may be attributed to electrostatic interaction or widening/narrowing of the phosphodiester bond (Gorenstein & Kar, 1975). We did not observe any large downfield shifts ~1.6 ppm expected on the transition of backbone torsional angle from gauche to trans conformation to allow the opening of base pairs (Gorenstein, 1992; Agrawal, Govil, & Barthwal, 2009). This excludes any possibility of

classical intercalation of the aromatic ring of daunomycin between any of the base planes at any step along the sequence. Due to the formation of more than one stoichiometric complex and presence of both, antiparallel and parallel G-quadruplexes, it is not possible to get the NMR based structure of complex unambiguously from distance restraints. However, NMR spectra confirm the formation of a complex involving specific interactions, in particular, the involvement of 6OH and 5'CH_3 protons, ring D protons in partial stacking and external binding without opening of base quartets.

Table 5.6 Intra molecular NOE correlations between daunomycin-daunomycin protons (D) obtained from NOESY experiment (τ_m = 300 ms) at D/N = 2.0 in KBPES buffer containing 100 mM KCl (90% H_2O + 10% D_2O solvent) at 25 °C.

S. No.	Intra molecular NOE correlations	S. No.	Intra molecular NOE correlations
1	4OCH_3-3H	9	1'H-2axH
2	4OCH_3-2H	10	1'H-2eqH
3	4OCH_3-1H	11	3'H-2axH
4	5'CH_3-5'H	12	3'H-2eqH
5	5'CH_3-4'H	13	7H-8axH
6	5'CH_3-3'H	14	7H-8eqH
7	5'CH_3-1'H	15	6OH-4OCH_3
8	5'CH_3-7H	16	6OH-3H

Table 5.7 Intra molecular NOE correlations between daunomycin-daunomycin protons (D) obtained from NOESY experiment (τ_m = 300 ms) at D/N = 2.0 in KBPES buffer containing 100 mM KCl (100% D_2O solvent) at 25 °C. na: not available

S. No.	Intra molecular NOE correlations	S. No.	Intra molecular NOE correlations
1	4OCH_3-3H	9	1'H-2axH
2	4OCH_3-2H	10	1'H-2eqH
3	4OCH_3-1H	11	3'H-2axH
4	5'CH_3-5'H	12	3'H-2eqH
5	5'CH_3-4'H	13	7H-8axH
6	na	14	7H-8eqH
7	5'CH_3-1'H	15	na
8	5'CH_3-7H	16	na

Table 5.8 ^{1}H Chemical shift (ppm) of daunomycin protons in daunomycin (δ_f) and daunomycin Tet22 complex (δ_b) at D/N = 2.0 in KBPES buffer containing 100 mM KCl (90% H_2O + 10% D_2O solvent) at 25 °C. Change in chemical shift of daunomycin protons due to binding, $\Delta\delta = \delta_b - \delta_f$. -ve $\Delta\delta$ indicates upfield shift; nd: not determined

Protons	δ_f	δ_b	$\Delta\delta$	Protons	δ_f	δ_b	$\Delta\delta$
Ring D/B				Daunosamine sugar			
2H	7.71	7.14	-0.57	1'H	5.49	5.26	-0.23
1H	7.53	7.04	-0.49	2'eqH	1.99	2.62	0.63
3H	7.43	7.18	-0.25	2'axH	1.99	2.36	0.37
4OCH_3	3.94	4.04	0.10	3'H	3.70	3.76	0.06
6OH	13.85	12.77	-1.08	4'H	3.83	3.88	0.05
11OH	13.17	nd	nd	5'H	4.27	4.02	-0.25
Ring A				5'CH_3	1.30	1.46	0.16
7H	4.82	4.52	-0.30				
8eqH	2.23	2.64	0.41				
8axH	2.13	2.38	0.25				
9$COCH_3$	2.45	nd	nd				
10eqH	2.94	nd	nd				
10axH	2.70	nd	nd				

Table 5.9 ^{1}H Chemical shift (ppm) of daunomycin protons in free daunomycin (δ_f) and daunomycin-Tet22 complex (δ_b) at D/N = 2.0 in KBPES buffer containing 100 mM KCl (100% D_2O solvent) at 25 °C. Change in chemical shift of daunomycin protons due to binding, $\Delta\delta = \delta_b - \delta_f$. -ve $\Delta\delta$ indicates an upfield shift. nd: not determined; na: not available

Protons	δ_f	δ_b	$\Delta\delta$	Protons	δ_f	δ_b	$\Delta\delta$
Ring D/B				Daunosamine sugar			
2H	7.71	7.16	-0.55	1'H	5.49	5.28	-0.21
1H	7.53	7.06	-0.47	2'eqH	1.99	2.61	0.62
3H	7.43	7.21	-0.22	2'axH	1.99	2.40	0.31
4OCH_3	3.94	4.08	0.14	3'H	3.70	3.79	0.09
6OH	13.85	na	na	4'H	3.83	3.88	0.05
11OH	13.17	na	na	5'H	4.27	4.03	-0.24
Ring A				5'CH_3	1.30	1.48	0.18
7H	4.82	4.54	-0.28				
8eqH	2.23	2.67	0.44				
8axH	2.13	2.40	0.27				
9$COCH_3$	2.45	nd	nd				
10eqH	2.94	nd	nd				
10axH	2.70	nd	nd				

Table 5.10 Inter molecular NOE correlations between daunomycin and Tet22 protons (*) obtained from NOESY spectra (τ_m = 300 ms) at D/N = 2.0 in KBPES buffer containing 100 mM KCl (90% H_2O + 10% D_2O solvent) at 25 °C. Chemical shift values (ppm) are shown in brackets. The strong (s), medium (m) and weakly (w) intense cross peaks correspond approximately to distance of 2.0–3.0, 3.0–4.0, and 4.0–5.0 Å, respectively

S. No.	Inter molecular DNA-daunomycin NOE correlations	Intensity of NOE cross peaks
1	H8/H6 (7.28) - 5'CH_3 (1.46)	m
2	H1' (6.37) - 5'CH_3 (1.46)	w
3	H8/H6 (7.71) - 3H (7.18)	s
4	H8/H6 (7.70) - 2H (7.14)	s
5	H8/H6 (7.72) - 6OH (12.77)	s
6	H8/H6 (7.38) - 6OH (12.77)	s
7	H8/H6 (7.29) - 6OH (12.77)	w
8	H2'/2"(2.75) - 5'CH_3 (1.46)	w
9	H2'/2" (2.59) - 5'CH_3 (1.46)	w
10	H2'/2" (2.36) - 5'CH_3 (1.46)	m
11	H1'(5.72) - 5'CH_3 (1.46)	m
12	TCH_3(2.11) - 1'H(5.26)	w
13	TCH_3(2.11) - 5'H(4.27)	w
14	TCH_3(2.11) - 4'H(3.83)	w

Table 5.11 Inter molecular NOE correlations between daunomycin and Tet22 protons (*) obtained from NOESY experiment (τ_m = 300 ms) at D/N = 2.0 in KBPES buffer containing 100 mM KCl (100% D_2O solvent) at 25 °C. Chemical shift values (ppm) are shown in brackets. The strong (s), medium (m) and weakly (w) intense cross peaks correspond to the distance of 2.0–3.0, 3.0–4.0, and 4.0–5.0 Å, respectively. na: not available

S. No.	Inter molecular DNA-daunomycin NOE correlations	Intensity of NOE cross peaks
1	H8/H6 (7.28)-5'CH_3 (1.48)	m
2	H1' (6.37)-5'CH_3 (1.48)	w
3	H8/H6 (7.71)-3H (7.21)	s
4	H8/H6 (7.70)-2H (7.16)	s
5	na	na
6	na	na
7	na	na
8	H2'/2"(2.75)-5'CH_3 (1.48)	w
9	H2'/2" (2.59)-5'CH_3 (1.48)	w
10	H2'/2" (2.36)-5'CH_3 (1.48)	m
11	H1'(5.72)-5'CH_3 (1.48)	m
12	TCH_3(2.11) - 1'H(5.26)	w
13	TCH_3(2.11) - 5'H(4.27)	w
14	TCH_3(2.11) - 4'H(3.83)	w
15	TCH_3(2.11) - 3'H(3.70)	w

5.3.6 Thermal denaturation

The change in melting temperature (ΔT_m) of folded → unfolded free Tet22 quadruplex DNA and its complex with daunomycin at D/N = 0.5, 1.0, 2.0, 3.0 and 4.0 in presence of 100 mM K^+ were obtained using differential scanning calorimeter. The data of 50 µM free Tet22 fits into two "two state" model (alternately referred to as three state melting process) showing two major transitions, T_{m1} and T_{m2}, centered at 76.0 ± 0.25 and 90.0 ± 0.1 ºC (Fig. 5.10 a), respectively indicating existence of intermediate species in melting pathway (Ghosh, Pradhan, Kar, Chowdhury, & Dasgupta, 2013; Hardin, Henderson, Watson, & Prosser, 1991). These T_m values of free quadruplex, are comparable to that reported in the literature for similar quadruplex sequences (Ghosh et al., 2013; Hardin et al., 1991). The broad and non-symmetric nature of DSC curves suggests the presence of perhaps more than one conformation in equilibrium with each other so that observed T_m value may be referred to as "apparent melting temperature". The melting profiles of complexes show stabilization of DNA and T_m increases with D/N ratio (Fig. 5.10 b-g and Table 5.12). The T_{m2} increases to 100 °C at D/N = 4.0 yielding total thermal stabilization ΔT_m ~10 °C, which may be attributed to the specific interaction between daunomycin and DNA. The extent of stabilization ΔT_m increases with D/N ratio which is likely to happen if both sites are not occupied at D/N = 2.0 so that binding continues as D/N approaches 4.0. Stabilization of ΔT_m = 0, 5 and 11 °C have earlier been obtained on binding of doxorubicin/daunomycin to 21/22-mer human telomeric DNA in Na^+ rich (Manet, Manoli, Zambelli, Andreano, Masi, Cellai, Ottani, et al., 2011), and K^+ rich aqueous solutions (Manet, Manoli, Zambelli, Andreano, Masi, Cellai, & Monti, 2011; Das et al., 2017).

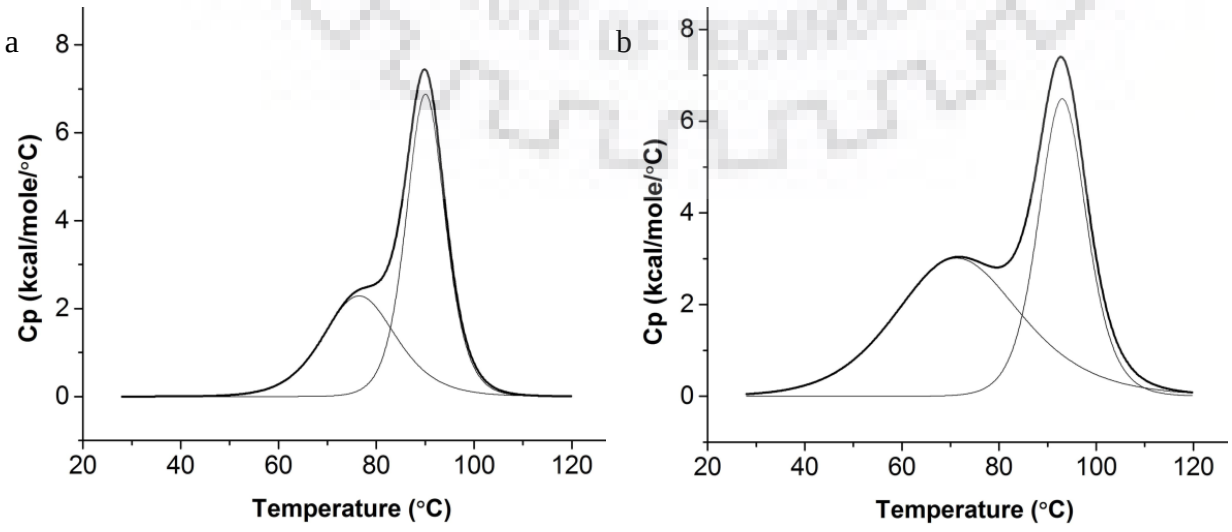

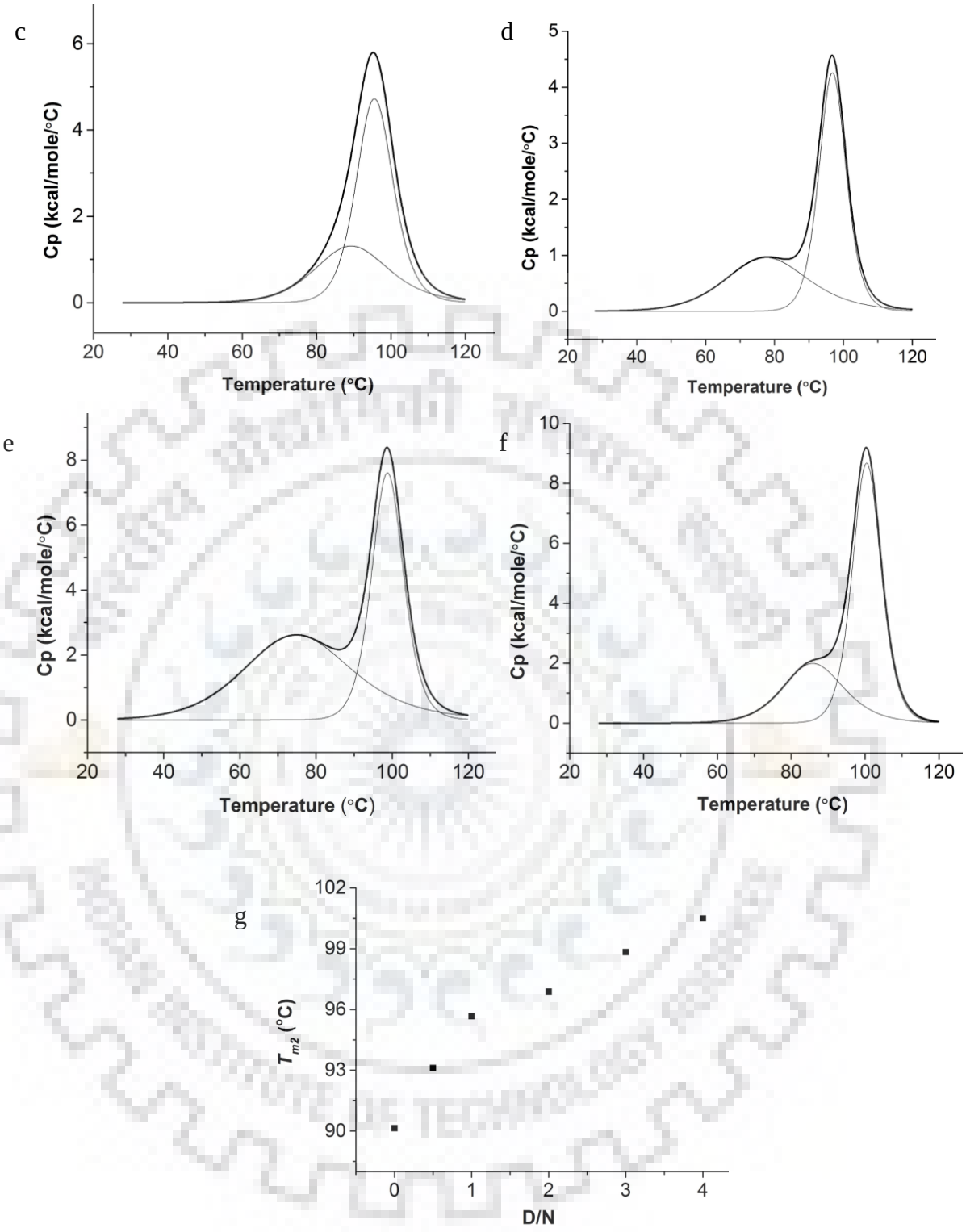

Figure 5.10 Differential Scanning Calorimetry thermograms showing excess heat capacity as a function of the temperature of a) free 50 µM Tet22 and b-f) daunomycin-Tet22 complexes at Daunomycin (D) to Nucleic acid (N) ratios, D/N = 0.5, 1.0, 2.0, 3.0 and 4.0. The observed raw data (thick black lines) have been deconvoluted into "two-state" processes (thin grey lines), respectively using Origin 7.0. All samples were prepared in phosphate buffer (KBPES) (pH 7.0) containing 100 mM KCl. g) Plot of melting temperature T_{m2} obtained from DSC experiments as a function of D/N ratio.

Table 5.12 Data obtained from DSC experiments showing the change in melting temperature (T_m) of Tet22 (50μM) upon complexation with daunomycin at different drug(D)/nucleotide(N) ratios.

D/N	T_m (°C)	
Free DNA	90.1 ± 0.1	
	T_m (°C)	ΔT_m (°C)
D/N = 0.5	93.1 ± 0.1	3.0
D/N = 1.0	95.6 ± 0.1	5.5
D/N = 2.0	96.8± 0.1	6.7
D/N = 3.0	98.8 ± 0.1	8.7
D/N = 4.0	100.5 ± 0.1	10.4

5.3.7 Molecular docking

In order to get insight into the mode of binding, we conducted molecular docking studies of daunomycin with 24-mer sequence d-[$(TTGGGG)_4$], having 3+1 hybrid structure obtained in Na^+ containing solution (Y. Wang & Patel, 1994), using available PDB (ID:186D). The CD spectra of this NMR based solution structure has two equally intense bands at 260 and 295 nm (Vorlíčková et al., 2012). The observed CD spectra of Tet22 which is 22-mer sequence d-[$GGGG(TTGGGG)_3$] lacking TT bases at 5'end is obtained in 100 mM K^+ solution. The differences in flanking bases and cation identity contribute to changes in the conformation of Tet22 with more number of guanines having *anti* conformations resulting in increased intensity of 265 nm band (Fig. 5.4 b) as compared to that for the 24-mer sequence in Na^+ rich solution. The overall structure and shape of CD bands at 260 and 295 nm in 22-mer in K^+ rich solution, however, remains unaltered. Thus, Tet22 G-quadruplex DNA has parallel form mixed with 3+1 hybrid structure (Vorlíčková et al., 2012; Karsisiotis et al., 2011; Masiero et al., 2010; Gray et al., 2008). Since, no structure of *Tetrahymena* telomeric DNA in K^+ rich solution is available in the database, we have chosen the structure of 24-mer d-[$TTGGGG(TTGGGG)_3$] (Tet24) as the nearest available model for our docking studies (Y. Wang & Patel, 1994).

Molecular docking studies yield negative binding energy confirming the formation of bound complex. The lowest energy conformation of the complex showed the existence of binding site at G9, G18, G22, G23 step of Tet24 (Fig. 5.11 a-d) with the binding energy of -5.56 kcal/mol.

Binding at G9, G18, G22, G23 site was stabilized by 9 hydrogen bonds: (a) $4OCH_3$ with PO_4^{2-} of G23 (3.26 Å), (b) 5O of ring C with PO_4^{2-} of G23 (3.14 Å) and O3' of G22 (2.84 Å), (c) 6OH of ring B with O3' of G22 (3.04 Å), (d) NH_3^+ of daunosamine sugar moiety with O5' of G22 (2.63 Å) and PO_4^{2-} of G22 (2.62 Å), (e) 4'OH of daunosamine sugar moiety with PO_4^{2-} of G22 (2.84 Å), (f) oxygen of ring of daunosamine sugar moiety with PO_4^{2-} of G22 (3.17 Å) and (g) $9COCH_3$ of ring A with N7 of G9 (2.87 Å). The conformation of complex thus obtained may be considered as a representative study of the binding of daunomycin to the 3+1 hybrid structure of *Tetrahymena* DNA and has limitations due to the absence of explicit solvent, ions and conformational flexibility in DNA. Nevertheless, it is consistent with observed NMR spectra showing changes in chemical shift (Table 5.8) and short intermolecular contacts (Fig. 5.8 a-d, Table 5.10) involving daunosamine sugar protons resulting from the proximity of daunosamine sugar to DNA in the bound complex (Fig. 5.11 a-d).

It may be noted that the experimental studies refer to a mixed population of parallel and 3+1 hybrid conformation of G-quadruplex (Fig. 5.4 b). Two binding sites have been inferred from spectroscopy studies (Fig. 5.3-5.6). It is speculated that another site of daunomycin binding may pertain to parallel G-quadruplex in which the ring D of daunomycin may partially stack with bases of DNA resulting in substantial upfield shifts in these protons (Table 5.8).

a

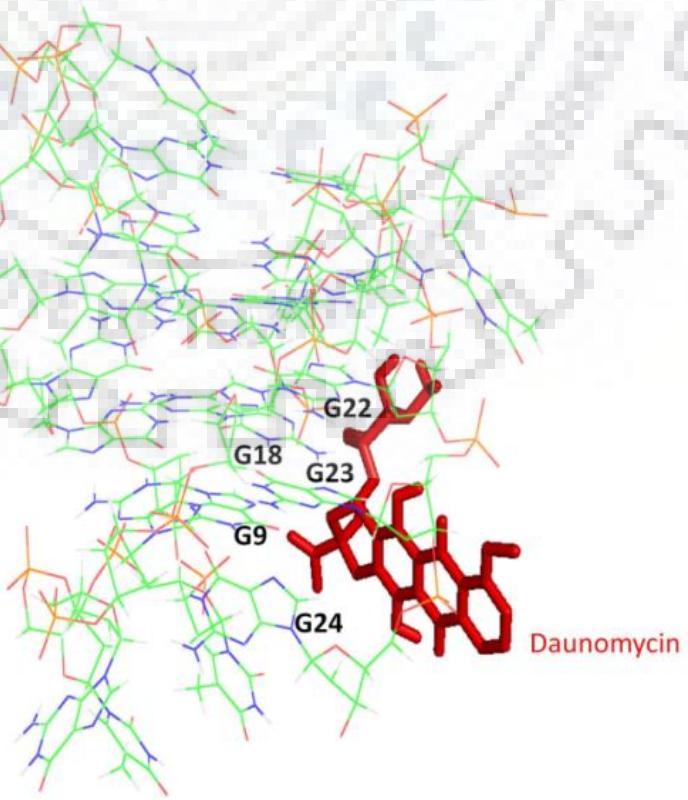

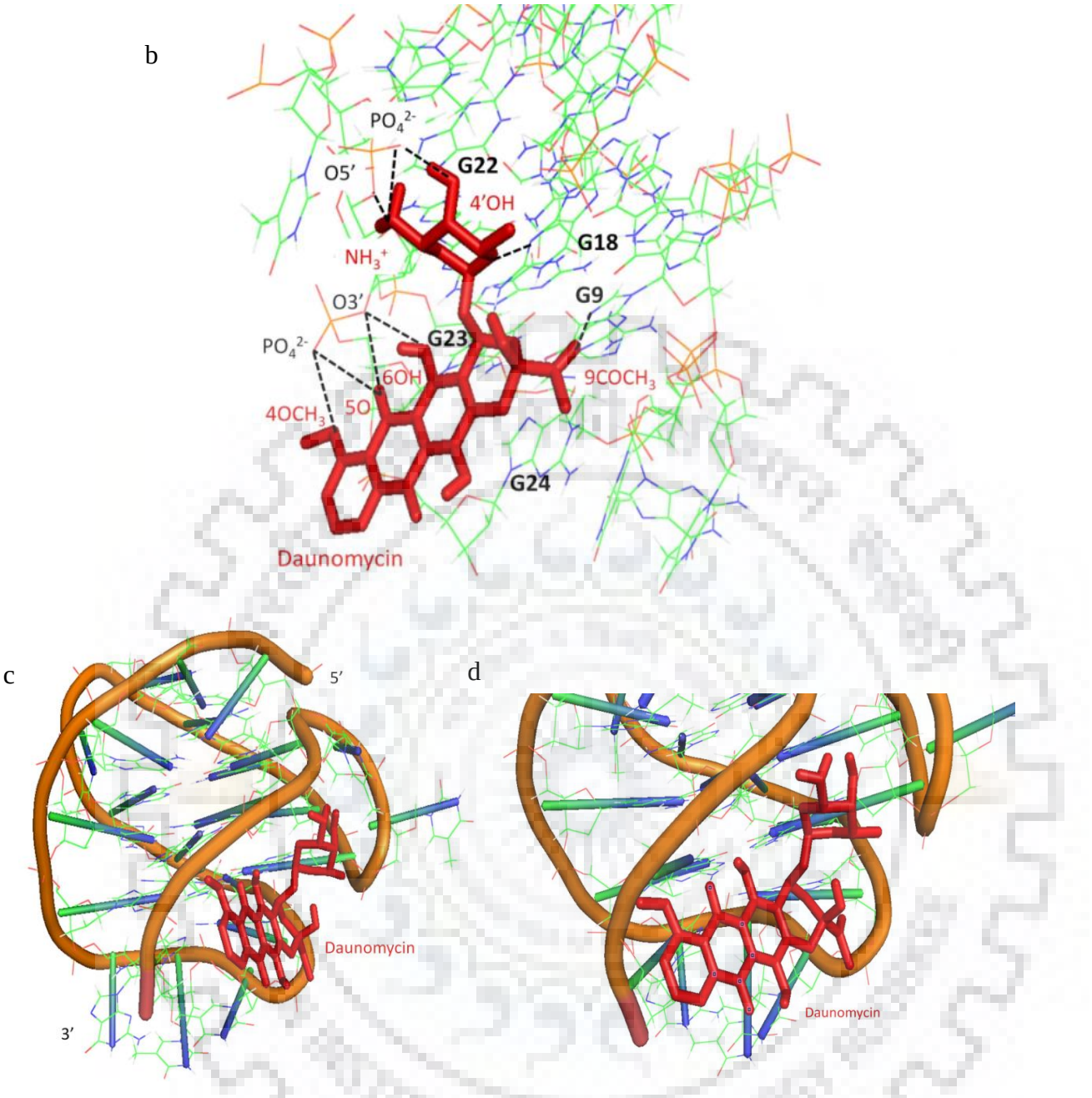

Figure 5.11 The schematic diagram of molecular docking studies representing binding of daunomycin to Tet24 (PDB ID: 186D) at a) G18, G22 and G23 site, b) Close-up view of ligand binding site showing hydrogen bonds (black dashed lines). c) Ribbon representation of G quadruplex DNA docked with daunomycin and d) Ribbon representation of G quadruplex DNA showing close up view of the binding site. The model was generated using Autodock 4.2 and visualized by PyMol.

5.4 Binding to other G-quadruplex sequences

We have earlier shown that binding of daunomycin to 7-mer intermolecular parallel G-quadruplex Tet7 takes place with an affinity constant K_b = 4x10^5 M^{-1} (Chapter 4). We investigated the binding of daunomycin to 7-mer intermolecular parallel G-quadruplex [d-(TTAGGGT)]$_4$ and 22-mer intramolecular d-[AGGG(TTAGGG)$_3$] comprising human telomeric DNA sequence TTAGGG by CD spectroscopy. It was observed (Fig. 5.12 a) that binding to 7-mer pure parallel form of G-quadruplex (Tripathi, Pradeep, & Barthwal, 2016; Kumar & Barthwal, 2018) leads to reduction in magnitude of both 243 and 264 nm CD bands and yields affinity constant K_b = 4.3x10^4 M^{-1} (Fig. 5.12 b). The 22-mer sequence in K$^+$ rich solutions is known to adopt a 3+1 hybrid structure with mixed parallel and antiparallel orientations of the phosphate backbone resulting in both parallel and antiparallel characteristics. The CD spectra thus show a maximum at 290 nm representing antiparallel portion, a shoulder at 265 nm and minimum at 238 nm corresponding to the parallel portions of the quadruplex structure (Hudson et al., 2009; Paramasivan et al., 2007; Ambrus et al., 2006; Bessi et al., 2012). Further the 3+1 hybrid structure exists as a mixture of two isoforms, form 1 and form 2, which differ by loop arrangements: the double chain reversal loop is formed by the first and third linker in form 1 and form 2, respectively (Wang & Patel, 1993; Ambrus et al., 2006; Bessi et al., 2012; Lin et al., 2018). Binding of daunomycin to 22-mer G-quadruplex sequence also leads to a decrease in the magnitude of CD bands (Fig. 5.13 a) and yielded K_b = 9.2x10^4 M^{-1} (Fig. 5.13 b). These results suggest that binding to human telomeric DNA sequences containing three G-tetrads are weaker than that to DNA telomeric sequences derived from *Tetrahymena thermophilia* containing four G-tetrads stacked over each other. In an independent study, it was shown (Das et al., 2017) that daunomycin binds to intramolecular 22-mer d-[AGGG(TTAGGG)$_3$] in K$^+$ rich solution with an affinity constant of 1.8x10^6 M^{-1} although measurements were carried out only at low daunomycin to DNA mole ratios up to 1:1 only. Also, one dimensional NMR studies have shown (Phan et al., 2005) that daunomycin binds to Pu24I sequence d-[TGAGGGTGGIGAGGGTGGGGAAGG] in which imino protons of G4 and G13 residues were shifted upfield by ~0.25 ppm and broadened. It was inferred that daunomycin binds near top G-tetrad formed by G4, G8, G13, G17 residues but the detailed structural analysis was not carried out. This is at variance with present docked structure which shows that daunomycin binds externally making short contacts with G9, G18, G22, G23 residues (Fig. 5.11). Thus, binding of daunomycin to G-quadruplex DNA is sequence dependent. There are no studies in the literature to show if they bind to G-quadruplex sequences from promoters of oncogenes

(e.g. ckit, bcl-2, K-ras, etc) or potential quadruplex-forming sequences present in the bacterial/viral genome.

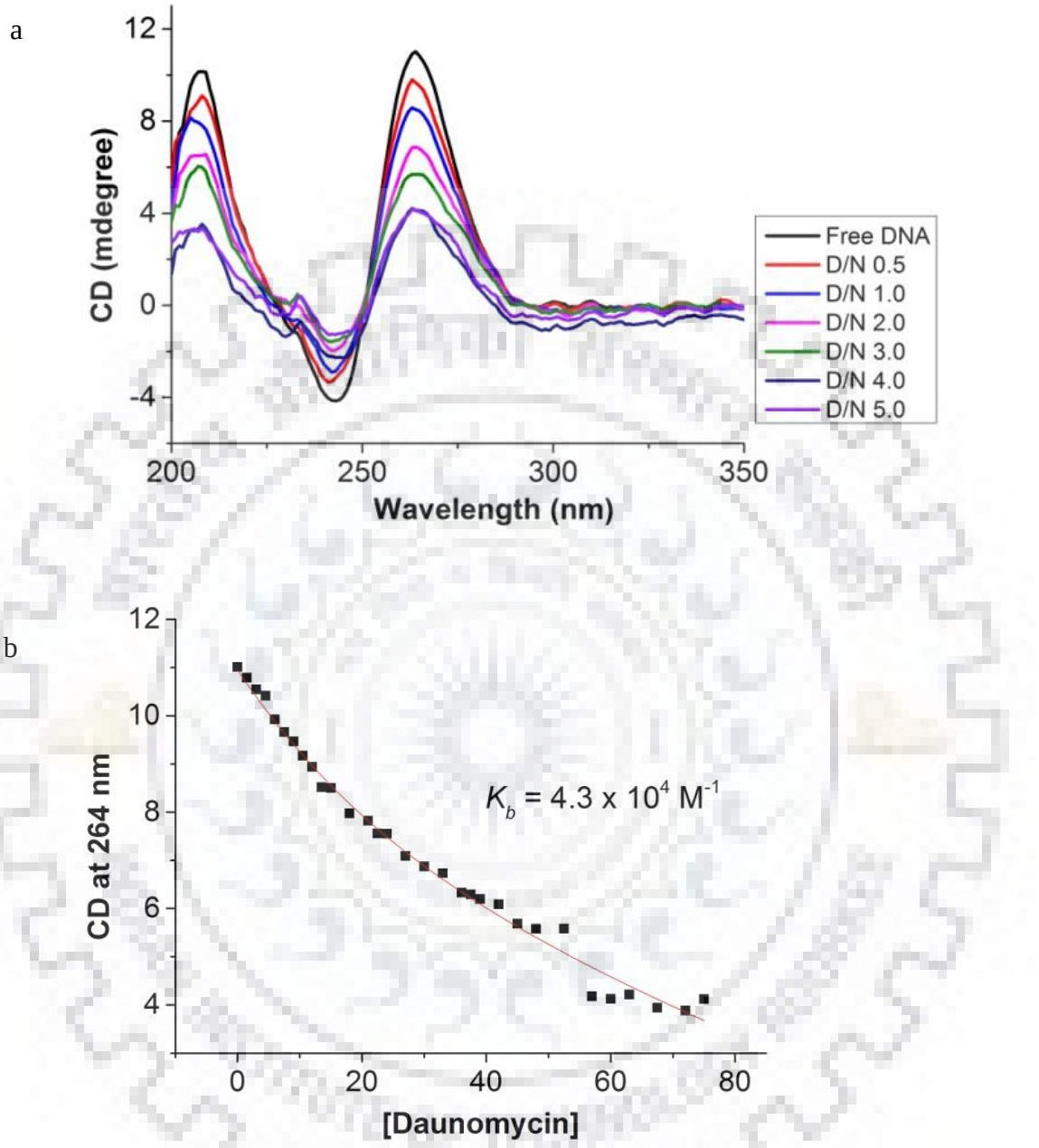

Figure 5.12 a) CD spectra of titration of daunomycin solution in 15 µM of [d-(TTAGGGT)]$_4$ in 10 mM phosphate buffer containing 100 mM KCl at 25 °C; b) Nonlinear fitted curve of CD in mdegrees as a function of daunomycin concentration (µM) showing binding constant (K_b) for binding of daunomycin.

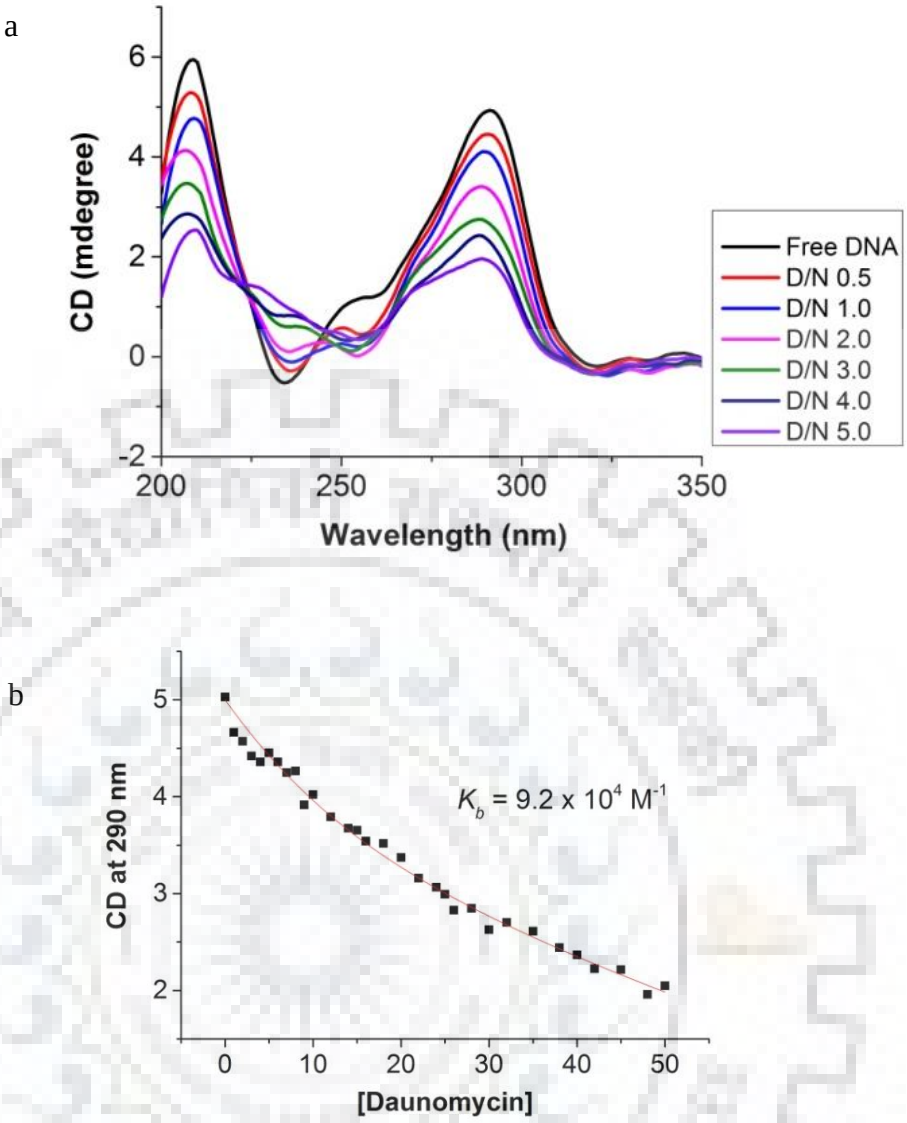

Figure 5.14 a) CD spectra of titration of daunomycin solution in 10 μM of d-[AGGG(TTAGGG)$_3$] in 10 mM phosphate buffer containing 100 mM KCl at 25 °C; b) Nonlinear fitted curve of CD in mdegrees as a function of daunomycin concentration (μM) showing binding constant (K_b) for binding of daunomycin.

Nevertheless, the present investigations show that daunomycin binds to telomeric DNA sequence from human and *Tetrahymena thermophilia* containing TTAGGG and TTGGGG sequence and cause thermal stability of G-quadruplex DNA. It has been argued that although daunomycin has higher affinity towards DNA duplex as compared to G-quadruplex DNA (Ren & Chaires, 1999), it exerts its anticancer activity through multiple pathways involving interaction with G-quadruplex (Ogretmen et al., 2001; Zhang et al., 2012; Elmore et al., 2002; Nakajima et al., 2003; Hussner et al., 2012). The binding induced thermal stabilization of G-quadruplex DNA may hamper association of telomerase enzyme to telomeres resulting in telomere dysfunction (Elmore et al., 2002) and other processes enhancing apoptosis (Ogretmen

et al., 2001; Zhang et al., 2012; Elmore et al., 2002; Nakajima et al., 2003; Hussner et al., 2012). It is worth noting that the conformation of daunomycin bound G-quadruplex DNA involving different DNA sequences are quite different and depend upon finer structural details involving specific contacts and hydrogen bond formation (Das et al., 2017; Shen, Mulholland, Zheng, & Wu, 2017; Clark, Pytel, Squire, & Neidle, 2003) which may ultimately be responsible for different binding affinities in different complexes. It has recently been reported that structural modifications in daunosamine sugar moiety of doxorubicin (an analog of daunomycin having $9CH_2OH$ in place of the $9COCH_3$ group at ring A in Figure 3.1) is a key towards the effectiveness of anticancer activity (Denel-bobrowska & Marczak, 2017). In this regard, we are investigating binding characteristics of epirubicin, an analog, in which H and OH groups are reversed in orientation at 4'position of daunosamine sugar. There is indeed an immense scope in the modification of binding moieties of anthracyclines for better therapeutic applications.

5.5 Conclusion

Surface plasmon resonance experiments establish the formation of a specific bound complex of daunomycin with 22-mer telomeric DNA sequence from *Tetrahymena*. Change in absorbance and fluorescence accompanied by minor shift in wavelength rule out classical intercalation as a mode of binding. Efficient quenching of fluorescence demonstrates the proximity of daunomycin to DNA. Circular dichroism spectra confirm external binding of daunomycin in monomeric form. Molecular docking studies confirm complex formation with negative binding energy. NMR studies exhibit specificity of interaction with direct evidence of short intermolecular contacts between two interacting molecules. The interaction leads to substantial thermal stabilization, ΔT_m = 10° C of G-quadruplex which may interfere with the access of telomeres to the telomerase enzyme resulting in telomere dysfunction. Anthracyclines afford enormous possibilities of substitutions at the aromatic rings as well as the daunosamine sugar moiety, some of which are expected to make very specific contacts through hydrogen bonding or hydrophobic interactions. Groove/external binding suggested by present investigations also offers scope for better selectivity towards quadruplex DNA in comparison to duplex DNA since grooves in DNA quadruplex are quite different in size and electrostatic nature from that in duplex DNA. The selectivity towards quadruplex structures would result in reduced cell toxicity, which is very much desirable. Our findings pave the way for possible modifications as well as the need to conduct structural studies to evaluate the molecular basis of action and contribute to novel drug development based on telomerase inhibition by anthracyclines.

6.1 Introduction

Recent investigations in literature point towards the role of adriamycin in disruption of maintenance of telomeres (Elmore et al., 2002; Ogretmen et al., 2001; Nakajima et al., 2003; Sabatino et al., 2010; Zhang et al., 2012; Hussner et al., 2012) speculating that adriamycin and its analogs may bind to different forms of DNA, e.g. G-quadruplex DNA sequences. The interactions involved and the role of anthracyclines in the ultimate process of apoptosis of cancerous cells is however not understood. We have monitored titrations of 4'-epiadriamycin (Fig. 6.1 a) and adriamycin (Fig. 6.1 b), two analogs of daunomycin, with [d-(TTGGGGT)]$_4$ (Tet7) by absorbance, steady state & lifetime fluorescence and CD spectroscopy. We have also obtained melting profiles of daunomycin-DNA complexes at varying Drug (D) to Nucleic acid (N) ratios (D/N). The findings have been supplemented by two-dimensional ^{1}H-^{1}H Nuclear Overhauser Enhancement SpectroscopY (NOESY) experiments which give short interproton distance contacts. The docking of 4'epiadriamycin/adriamycin with Tet7 has also been carried out.

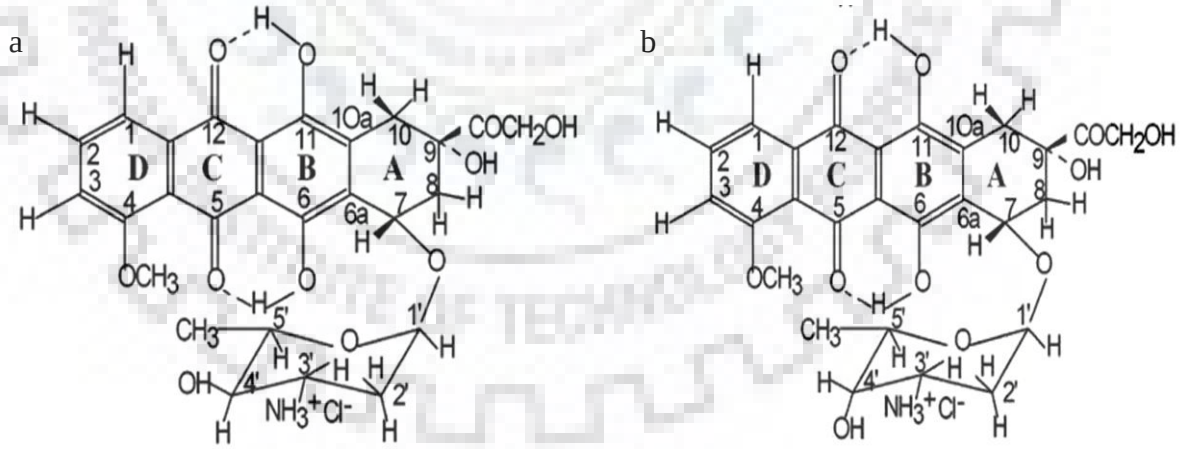

Figure 6.1 Chemical structure of a) 4'-epiadriamycin (or epirubicin) and b) adriamycin

6.2 Materials and Methods

Details of Materials and Methods are given in Chapter 2. For absorbance measurements, increasing amounts of Tet7 were added to 7 μM 4'-epiadriamycin/adriamycin to obtain Drug (D) to DNA (N) molar ratios D/N = 0.15-4.60 in a set of 26 samples. 1 μM of free quadruplex

DNA Tet7, corresponding to 4 μM single strand concentration of [d-(TTGGGGT)], was used to obtain a melting profile of free DNA by measuring absorbance at 260 nm. Appropriate amounts of 4'-epiadriamycin/adriamycin were added to it to get samples of complex at D/N = 0.5, 1.0, 2.0, 3.0, and 4.0 and each sample was scanned from 20-90 °C with a scan rate of 1°C/min at 260 nm to get absorbance as a function of temperature. Fluorescence measurements were performed on same samples as that used in absorption spectroscopy studies by exciting 4'-epiadriamycin/adriamycin at λ_{ex} = 480 nm and the emission spectra were recorded in the wavelength range of 520-650 nm at 25 °C. The lifetime values were calculated for 7 μM 4'-epiadriamycin/adriamycin and its complexes at D/N = 0.3, 0.5, 1.0, 2.0, 3.0 and 4.0 using λ_{ex} = 456 nm and λ_{em}= 590 nm. For titrations monitored by CD spectroscopy, 4'-epiadriamycin/adriamycin was added progressively to Tet7 (15.0 μM) at D/N = 0.1-5.0 in a set of 31 samples. In another set of experiments, Tet7 was added stepwise to 400 μM 4'epiadriamycin/adriamycin at D/N = 0.5-4.0 in a set of 8 samples at 25 °C. Thermal melting studies of 10 μM of free Tet7 its complex with 4'-epiadriamycin/adriamycin at D/N = 0.5, 1.0, 2.0, 3.0 and 4.0 were performed in temperature range 25-90 °C by heating at the rate of 1 °C/min in steps of 3 °C and measuring CD at 265 nm. For molecular docking studies, the structure of Tet7 was obtained from PDB ID: 139D. Three-dimensional (3D) conformer of 4'-epiadriamycin and adriamycin was obtained from PubChem CID: 41867 and 31703, respectively. 1.03 mM and 1.15 mM of Tet7 was used for titration with 4'-epiadriamycin and adriamycin at D/N = 4.0, respectively for NMR studies.

6.3 Result and Discussion

6.3.1 Absorption

The two anthracycline-based ligands, 4'-epiadriamycin (or epirubicin) and adriamycin, show absorption maxima at 290 and 481/482 nm, which have been attributed to $^1A \rightarrow {}^1L_a$ and $^1A \rightarrow {}^1L_b$ π-π^* transitions polarized along the short and long axis of the chromophore, respectively. The band at 481/482 nm is sensitive to self-aggregation (Manet, Manoli, Zambelli, Andreano, Masi, Cellai, & Monti, 2011), therefore ligand concentration of 7 μM was chosen so that formation of the dimer is minimal. Stepwise addition of Tet7 to 4'-epiadriamycin in the range D/N = 0.15 to 4.60 (selected data are shown in Fig. 6.2 a) results in hypochromism of ~56% at 481 nm accompanied by redshift $\Delta\lambda_{max}$ ~7 nm. A plot of absorbance (A) versus D/N (inset of Fig. 6.2 a) and 1/A versus D/N (Fig. 6.2 b) show change in slope at D/N = 0.59, 1.00, 2.24 and D/N = 0.54, 1.01 and 2.03, respectively so that stoichiometry of 0.5:1, 1:1 and 2:1 may exist in

ligand-DNA complexes. The data shows no isobestic point in the entire range of D/N indicating the presence of multiple stoichiometry complexes. Similar results for adriamycin conducted in the range D/N = 0.15 to 4.60 (selected data are shown in Fig. 6.2 c) show hypochromism of ~49% at 482 nm accompanied by redshift $\Delta\lambda_{max}$~10 nm. A plot of A versus D/N (inset of Fig. 6.2 c) and 1/A versus D/N (Fig. 6.2 d) show change in slope at D/N = 0.42, 1.20, 1.88 and D/N = 0.43, 1.11 and 2.01, respectively reflecting stoichiometry of 0.5:1, 1:1 and 2:1 in ligand-DNA complexes. In 4'-epiadriamycin-Tet7 complex, we get intrinsic binding constant K_b = 1.1x10^5 M^{-1} at D/N = 0.15-0.30 and K_b = 2.8x10^5 M^{-1} at D/N = 0.35-4.60 using equation (1) (Fig. 6.2 e). The corresponding intrinsic binding constant values of adriamycin-Tet7 complex are K_b = 7.0x10^4 M^{-1} at D/N = 0.15-0.30 and K_b = 4.9x10^5 M^{-1} at D/N = 0.35-4.60 (Fig. 6.2 f). The Scatchard plots are nonlinear and do not fit into a straight line; therefore the observed affinity constant K_b may be considered an average value.

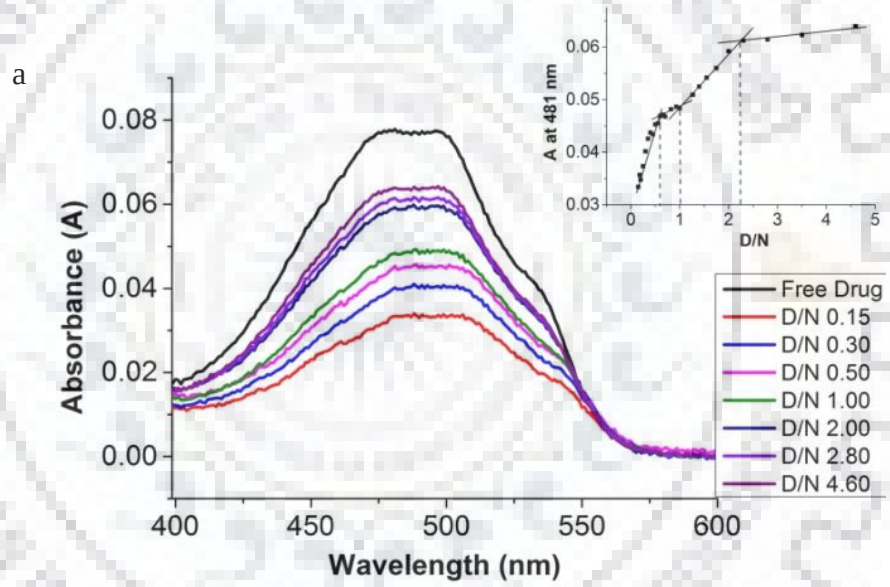

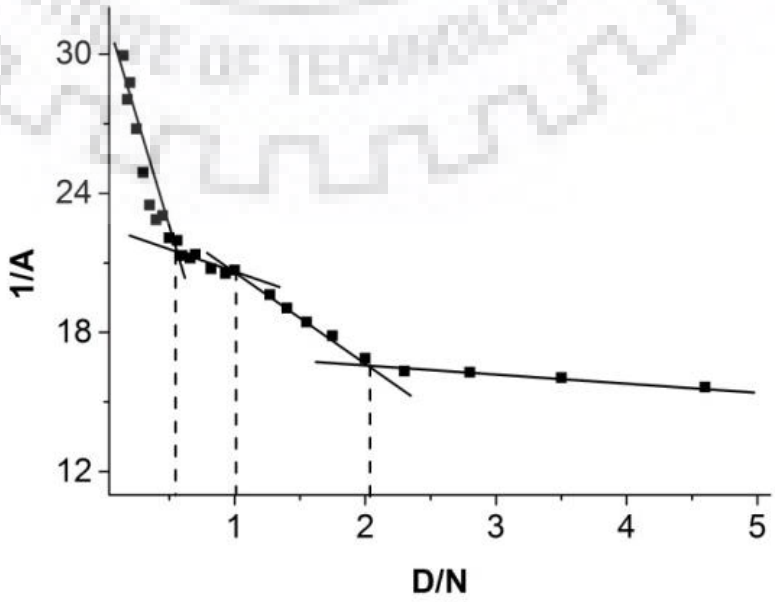

c

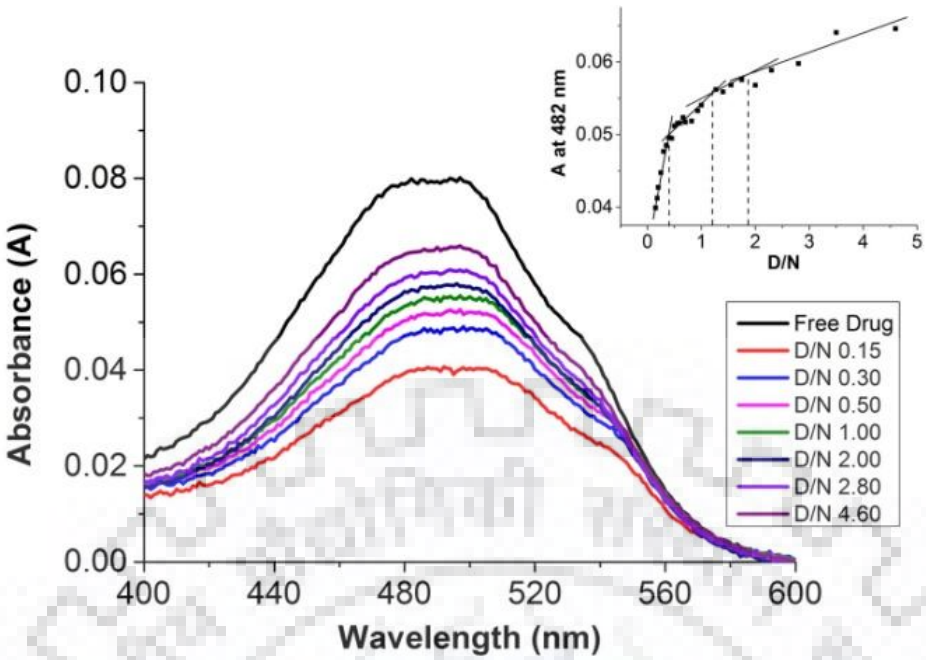
Absorbance (A)
Wavelength (nm)
Free Drug
D/N 0.15
D/N 0.30
D/N 0.50
D/N 1.00
D/N 2.00
D/N 2.80
D/N 4.60
A at 482 nm
D/N

d

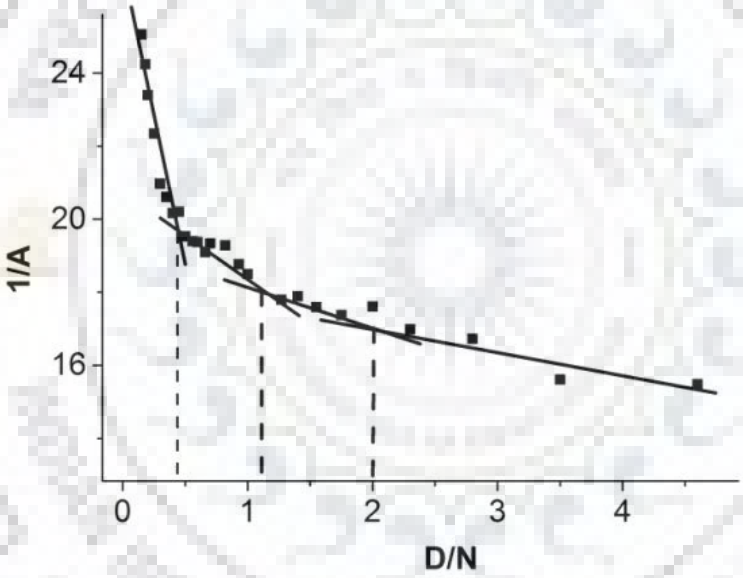
1/A
D/N

e

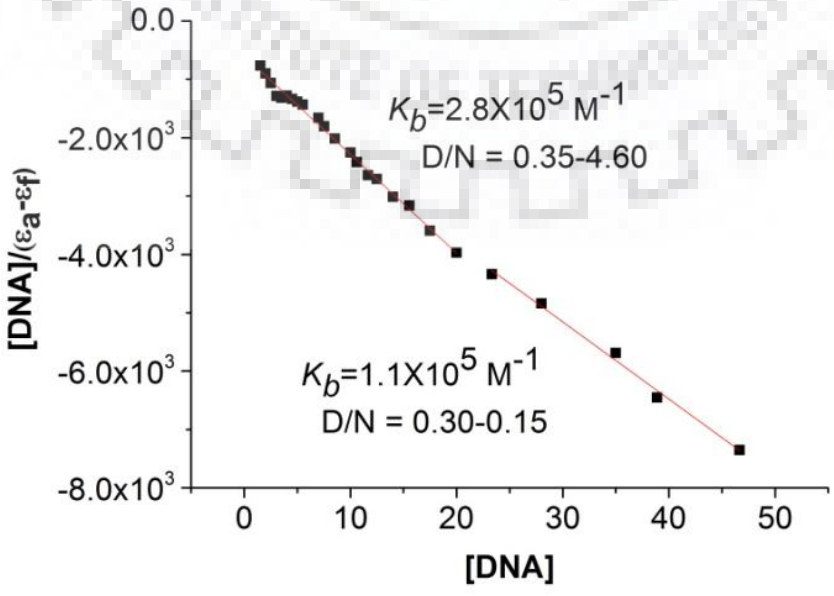
[DNA]/(εa-εf)
[DNA]
Kb=2.8X10^5 M^-1
D/N = 0.35-4.60
Kb=1.1X10^5 M^-1
D/N = 0.30-0.15

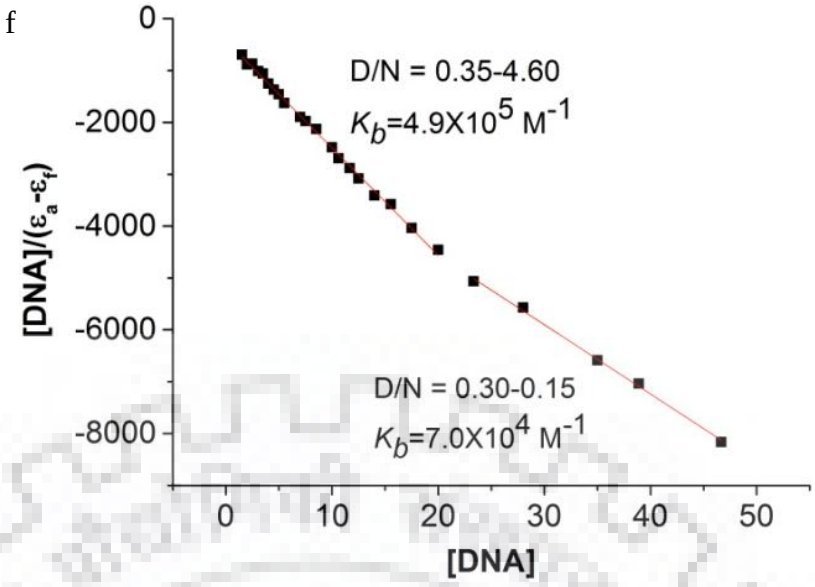

Figure 6.2 a) Titrations of 7 μM 4'-epiadriamycin with increasing concentration of Tet7 at D/N = 0.15-4.6 (data at some selected D/N ratios shown). The inset shows plot of absorbance (A) at 481 nm as a function of D/N ratio; b) Plot of reciprocal of absorbance (1/A) as a function of D/N ratio at 481 nm; c) Titrations of 7 μM adriamycin with increasing concentration of Tet7 at D/N = 0.15-4.6 (data at some selected D/N ratios shown). The inset shows the plot of absorbance (A) at 482 nm as a function of D/N ratio; d) Plot of reciprocal of absorbance (1/A) as a function of D/N ratio at 481 nm; e-f) Plot of [DNA]/(ε_a-ε_f) as a function of concentration of DNA, [DNA], in μM at 481 nm for D/N = 0.48-4.6 and D/N = 0.16-0.46 yielding value of binding constants (K_b).

6.3.2 Fluorescence

Excitation of 4'-epiadriamycin and adriamycin at 480 nm results in intense emission having maxima at 556 and 592 nm which has been assigned to $^1A \rightarrow {}^1L_b$ transition (Manet, Manoli, Zambelli, Andreano, Masi, Cellai, & Monti, 2011). Addition of Tet7 to 4'-epiadrimaycin (7 μM) results in quenching of fluorescence intensity (F) by 95% at D/N = 0.15 accompanied by a redshift $\Delta\lambda_{em}$ = 2-4 nm in both the emission maxima (selected data shown in Fig. 6.3 a) indicating strong interaction with DNA. A plot of F versus D/N (inset of Fig. 6.3 a) and 1/F versus D/N (Fig. 6.3 b) shows inflection at D/N = 0.52, 1.28, 2.23 and D/N = 0.52, 1.01 and 2.00, respectively. The Stern-Volmer plot showing F_0 / F versus concentration of DNA (Fig. 6.3 c) and plot of log [(F_0 - F) / F] versus log [DNA] (Fig. 6.3 d) using equations (2) and (3), respectively give K_{SV} and K_b in the range 1.4-16.0x10^5 M^{-1}. The bimolecular quenching constant, Kq~8×10^{14} $M^{-1}s^{-1}$ obtained by using K_{sv} = 8.0x10^5 M^{-1} and fluorescence lifetime τ = 1.0 ns is much greater than collision constant for a biomolecule and small molecule as a ligand,

i.e. 2×10^{10} $M^{-1}s^{-1}$, excluding the possibility of dynamic quenching. Static quenching is also evident from the accompanying changes in absorbance and no change in fluorescence lifetime. Non-linear curve fitting of fluorescence data at 592 nm in two independent binding sites using equation (4) (Thordarson, 2011; Hargrove, Zhong, Sessler, & Anslyn, 2010) yield binding constants K_{b1} = 9.2x10^5 M^{-1} and K_{b2} = 4.3x10^4 M^{-1} (Fig. 6.3 e).

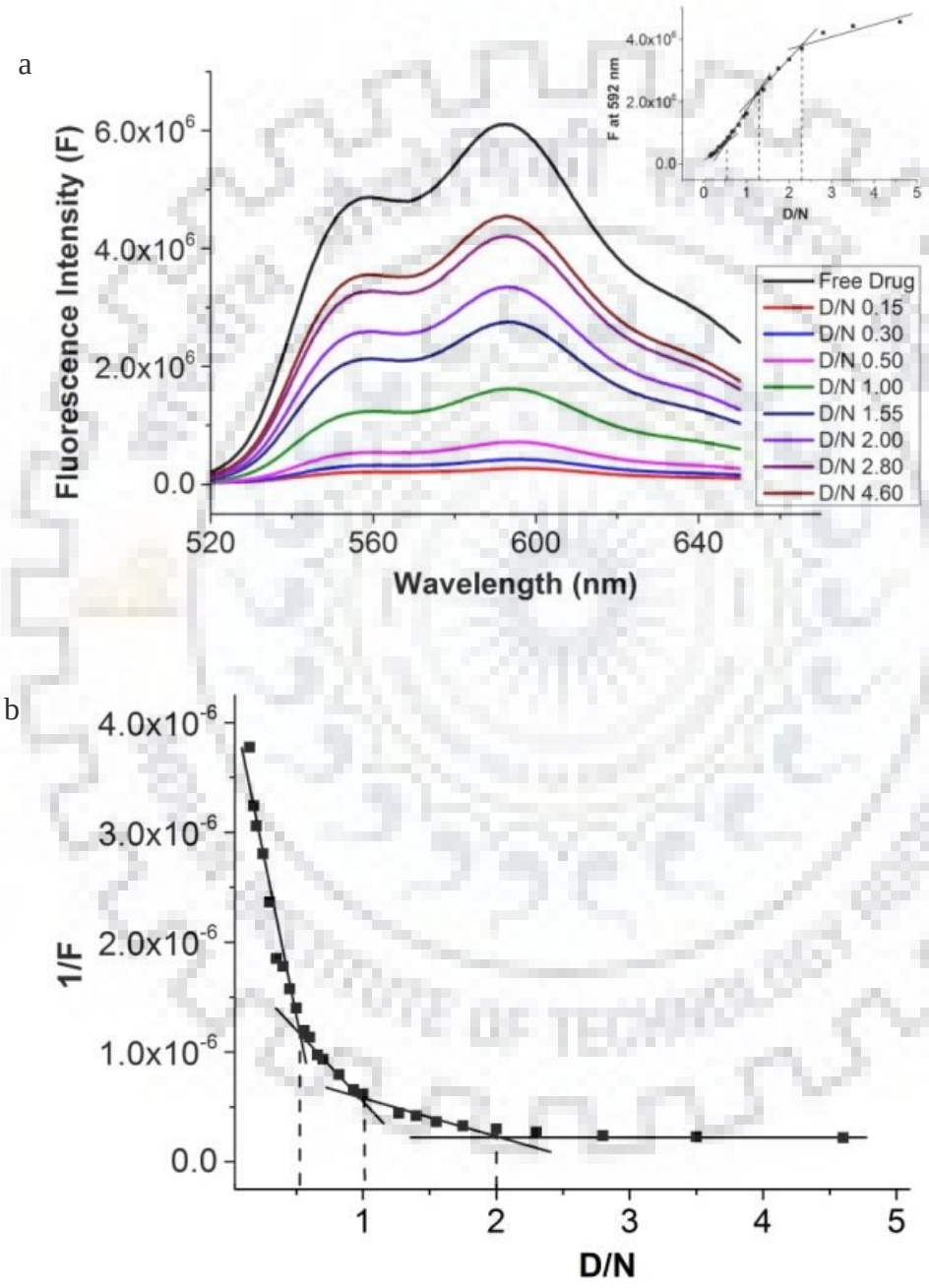

c

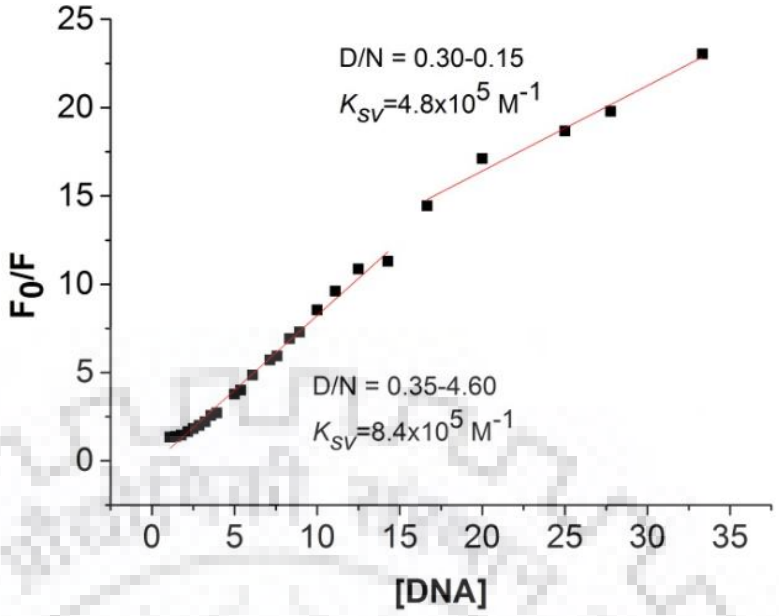
D/N = 0.30-0.15
K_{sv}=4.8x10^5 M^{-1}
D/N = 0.35-4.60
K_{sv}=8.4x10^5 M^{-1}
F_0/F
[DNA]

d

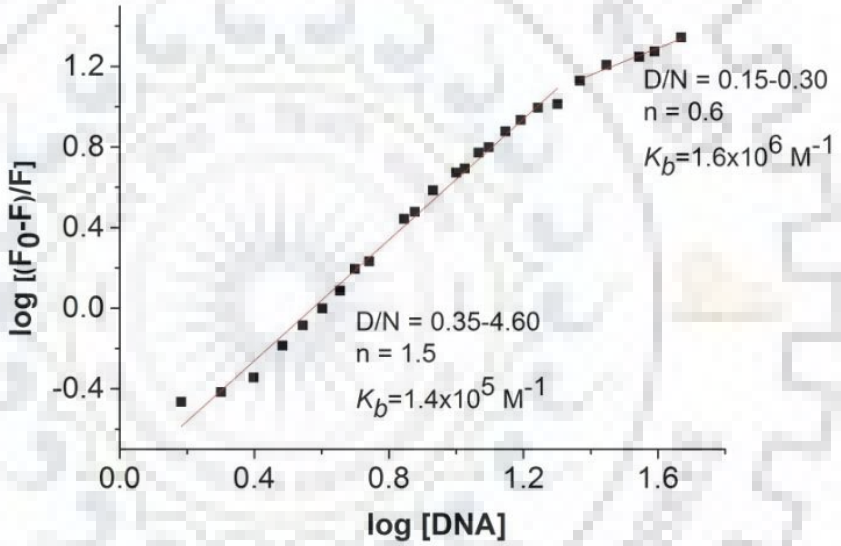
D/N = 0.15-0.30
n = 0.6
K_b=1.6x10^6 M^{-1}
D/N = 0.35-4.60
n = 1.5
K_b=1.4x10^5 M^{-1}
log [(F$_0$-F)/F]
log [DNA]

e

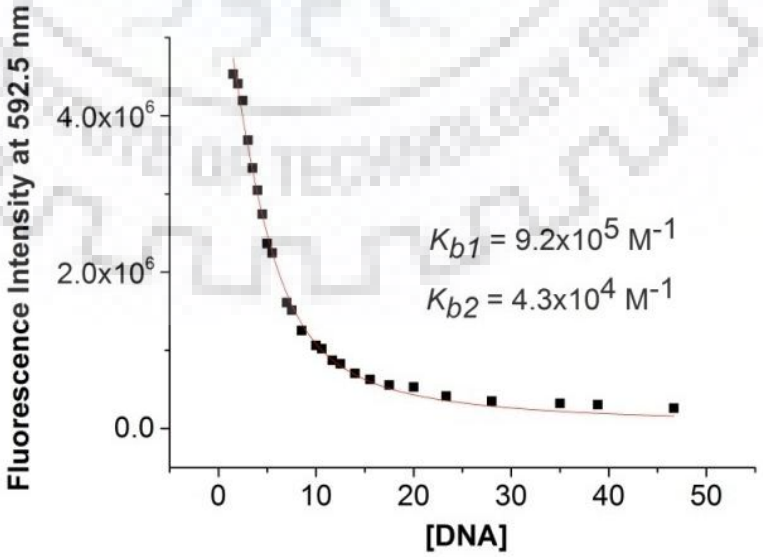
K_{b1} = 9.2x10^5 M^{-1}
K_{b2} = 4.3x10^4 M^{-1}
Fluorescence Intensity at 592.5 nm
[DNA]

f

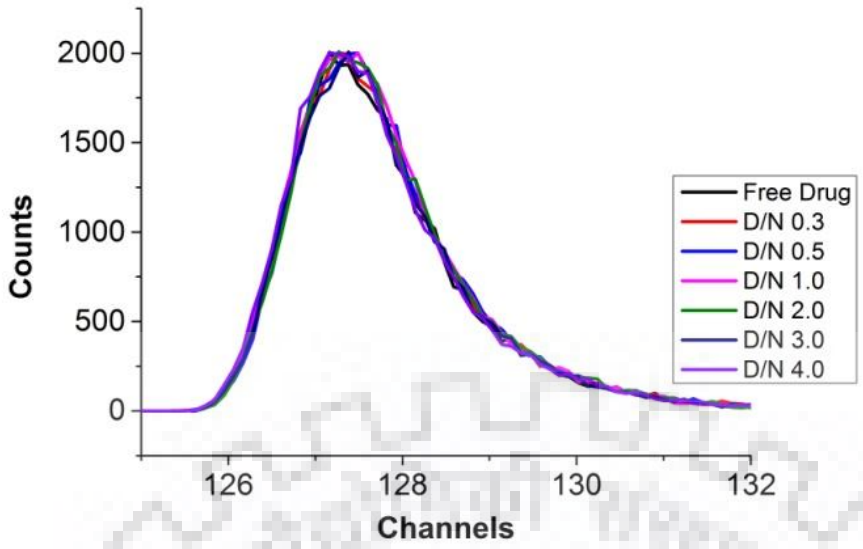

Figure 6.3 a) Fluorescence emission spectra of 7 μM 4'-epiadriamycin with increasing concentration of Tet7 (data at some selected D/N ratios shown). The inset shows plot of fluorescence intensity (F) at 592 nm as a function of D/N ratio; b) Plot of reciprocal of fluorescence intensity (1/F) at 592 nm as a function of D/N ratio; c) Plot of F_0/F versus DNA concentration (μM) at 592 nm giving Stern Volmer constant (K_{sv}); d) Plot of log (F_0-F/F) versus log [DNA] at 592 nm showing binding constants (K_b) and stoichiometry (n); e) Nonlinear fitted curve (red) for binding at two binding sites for observed fluorescence emission intensity at 592 nm as a function of DNA concentration (μM) showing two binding constants (K_{b1} and K_{b2}); f) Fluorescence decay profiles of free 4'-epiadriamycin and 4'-epiadriamycin-Tet7 complexes at varying D/N ratios.

The fluorescence decay of 4'-epiadriamycin at 7 μM and its complexes at D/N = 1.0-4.0 were measured by time-correlated single photon counting using $\Delta\lambda_{ex}$ = 456 nm and $\Delta\lambda_{em}$ = 590 nm at 25 °C. The decay was mono exponential with lifetime τ ~1.00 ns. The decay for several complexes at D/N = 0.3, 0.5, 1.0-4.0 remained monoexponential with lifetime τ = 0.96-1.02 ns (Fig. 6.3 f) (Table 6.1). This shows that lifetime for both free 4'-epiadriamycin and its complexes are the same. It has been shown that bound complex is non-emissive (Manet, Manoli, Zambelli, Andreano, Masi, Cellai, & Monti, 2011) and in that case, the observed lifetime is due to free 4'-epiadriamycin itself.

Table 6.1 Lifetime (τ) of free 4'-epiadriamycin (7 μM) and 4'-epiadriamycin-Tet7 complex at D/N = 0.3, 0.5, 1.0, 2.0, 3.0 and 4.0 with λ_{ex} = 456 nm and λ_{em} = 590 nm at 25 °C.

Samples	τ (ns)	%	χ^2
Free 4'-epiadriamycin	1.00	100	1.24
D/N 0.3	1.02	100	1.20
D/N 0.5	1.00	100	0.99
D/N 1.0	0.96	100	0.99
D/N 2.0	0.96	100	1.07
D/N 3.0	1.00	100	1.02
D/N 4.0	0.96	100	0.99

Similar results have been found for the binding adriamycin with Tet7 quenches fluorescence intensity up to 93% accompanied by the redshift of $\Delta\lambda_{em}$ = 3-4 nm in both the emission maxima (selected data shown in Fig. 6.4 a). A plot of F versus D/N (inset of Fig. 6.4 a) and 1/F versus D/N (Fig. 6.4 b) shows inflection at D/N = 0.56, 0.93, 2.13 and D/N = 0.51, 1.15 and 2.15, respectively. The Stern-Volmer plot showing F_0 / F versus concentration of DNA (Fig. 6.4 c) and plot of log [(F_0 - F) / F] versus log [DNA] (Fig. 6.4 d) using equation (2) and (3), respectively give K_{SV} and K_b in the range 2.2-7.2x10^5 M^{-1}. The bimolecular quenching constant, Kq~4×10^{14} $M^{-1}s^{-1}$, obtained by using K_{sv} = 4.0x10^5 M^{-1} and fluorescence lifetime τ = 1.0 ns is much greater than collision constant for a biomolecule and small molecule as a ligand, i.e. 2×10^{10} $M^{-1}s^{-1}$, excluding the possibility of any dynamic quenching. Static quenching is also evident from the accompanying changes in absorbance and no change in fluorescence lifetime. Non-linear curve fitting of fluorescence data at 592 nm in two independent binding sites using equation (4) yield binding constants K_{b1} = 4.2x10^5 M^{-1} and K_{b2} = 2.4x10^5 M^{-1} (Fig. 6.4 e).

a

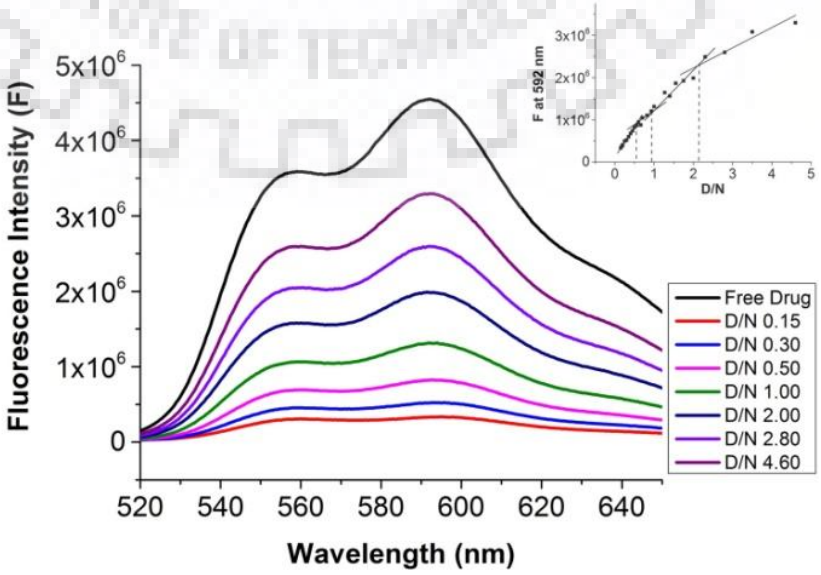

b

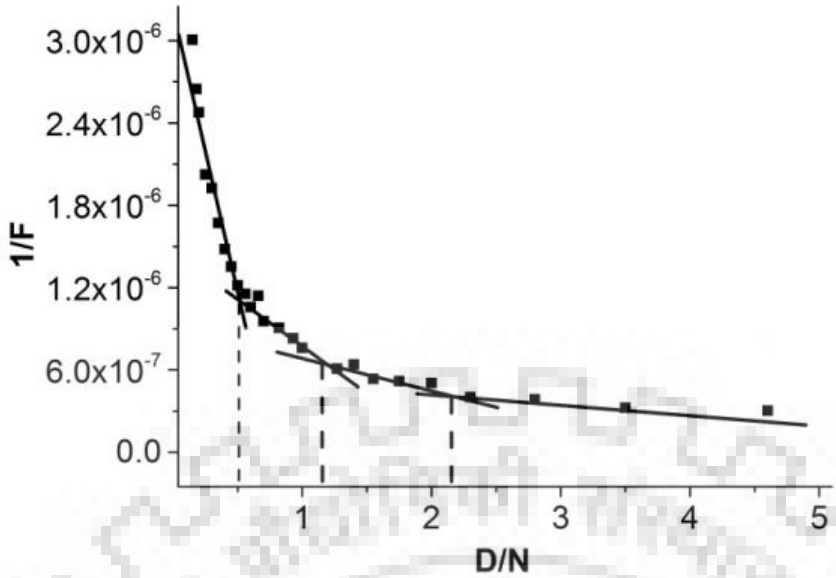
3.0x10-6
2.4x10-6
1.8x10-6
1.2x10-6
6.0x10-7
0.0
1/F
1
2
3
4
5
D/N

c

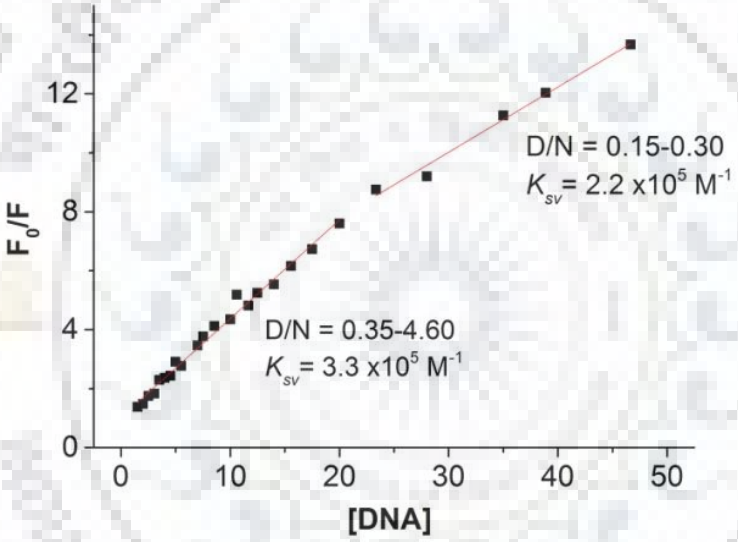
12
8
4
0
F0/F
D/N = 0.15-0.30
Ksv = 2.2 x10^5 M^-1
D/N = 0.35-4.60
Ksv = 3.3 x10^5 M^-1
0
10
20
30
40
50
[DNA]

d

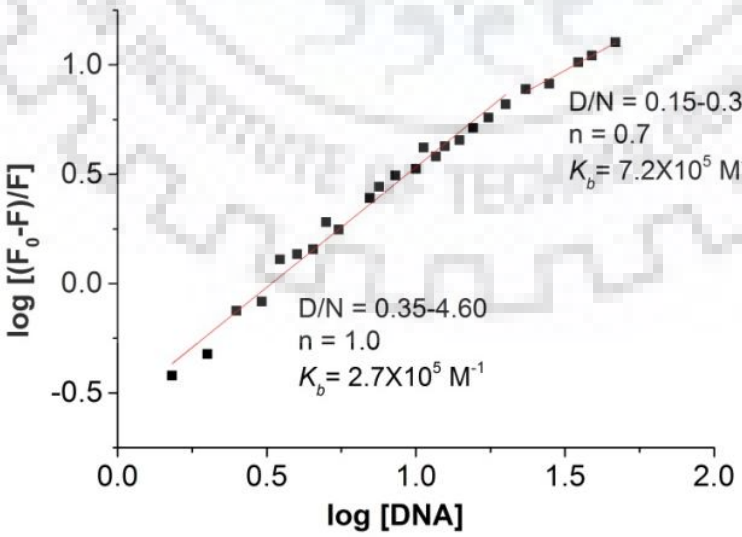
1.0
0.5
0.0
-0.5
log [(F0-F)/F]
D/N = 0.15-0.30
n = 0.7
Kb = 7.2X10^5 M^-1
D/N = 0.35-4.60
n = 1.0
Kb = 2.7X10^5 M^-1
0.0
0.5
1.0
1.5
2.0
log [DNA]

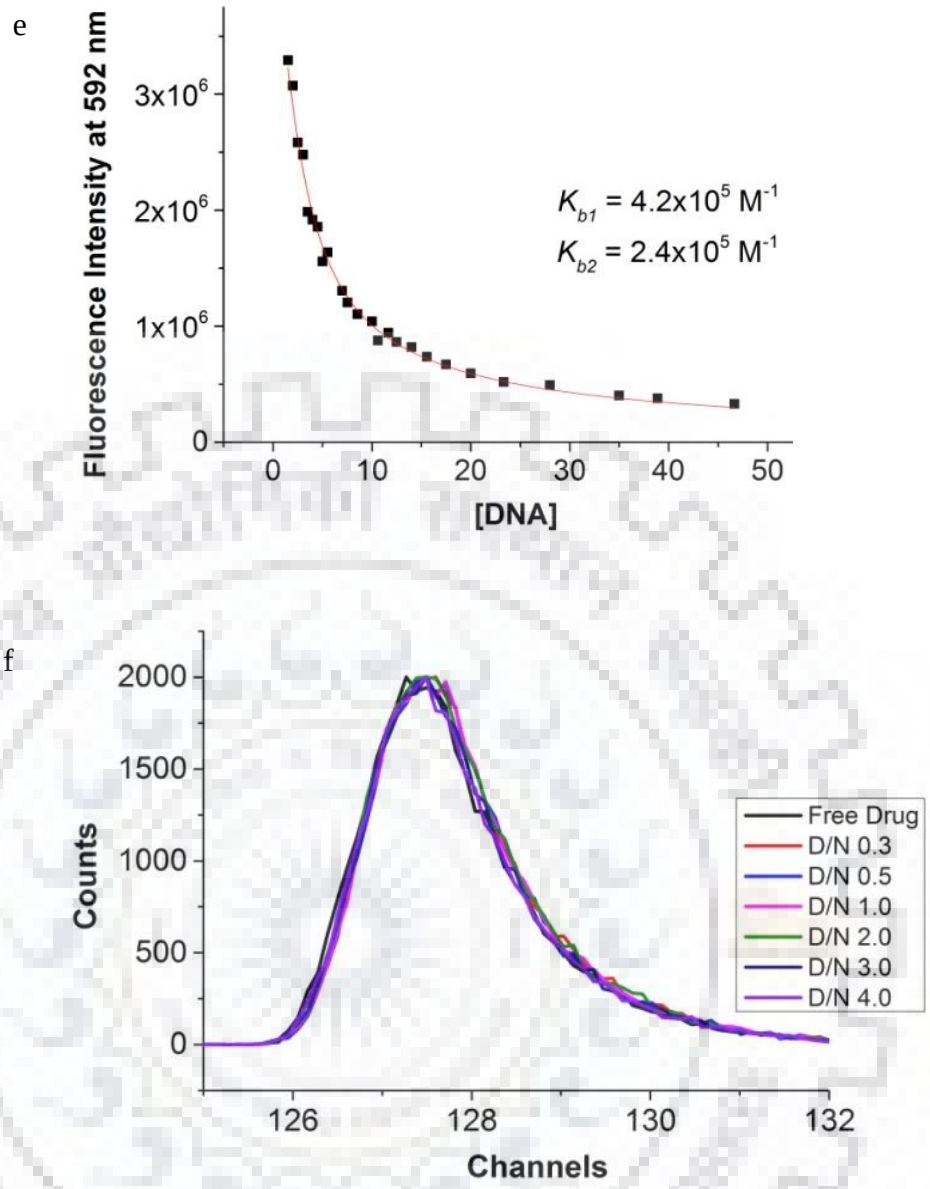

Figure 6.4 a) Fluorescence emission spectra of 7 µM adriamycin with increasing concentration of Tet7 (data at some selected D/N ratios shown). The inset shows plot of fluorescence intensity (F) at 592 nm as a function of D/N ratio; b) Plot of reciprocal of fluorescence intensity (1/F) at 592 nm as a function of D/N ratio; c) Plot of F_0/F versus DNA concentration (µM) at 592 nm giving Stern Volmer constant (K_{sv}); d) Plot of log (F_0-F/F) versus log [DNA] at 592 nm showing binding constants (K_b) and stoichiometry (n); e) Nonlinear fitted curve (red) for binding at two binding sites for observed fluorescence emission intensity at 592 nm as a function of DNA concentration (µM) showing two binding constants (K_{b1} and K_{b2}); f) Fluorescence decay profiles of free adriamycin and adriamycin-Tet7 complexes at varying D/N ratios.

The fluorescence decay measurement of adriamycin and its complexes at D/N = 1.0-4.0 were measured using time-correlated single photon counting using $\Delta\lambda_{ex}$ = 456 nm and $\Delta\lambda_{em}$ = 590 nm at 25 °C. The decay was monoexponential with lifetime τ ~0.99 ns. The decay for several complexes at D/N = 0.3, 0.5, 1.0-4.0 remained monoexponential with lifetime τ = 0.96-1.03 ns (Fig. 6.4 f) (Table 6.2). This shows that lifetime for both free adriamycin and its complexes are non-emissive (Manet, Manoli, Zambelli, Andreano, Masi, Cellai, & Monti, 2011) and the observed lifetime is due to free adriamycin itself.

Table 6.2 Lifetime (τ) of free adriamycin (7 μM) and adriamycin- Tet7 complex at D/N = 0.3, 0.5, 1.0, 2.0, 3.0 and 4.0 with λ_{ex} = 456 nm and λ_{em} = 590 nm at 25 °C.

Samples	τ (ns)	%	χ^2
Free adriamycin	0.99	100	1.18
D/N 0.3	0.99	100	1.01
D/N 0.5	0.97	100	0.98
D/N 1	1.03	100	1.00
D/N 2	1.01	100	1.03
D/N 3	0.96	100	1.03
D/N 4	0.98	100	1.02

6.3.3 Circular Dichroism

Circular Dichroism of Tet7 show well defined positive band at 264 nm indicating stacking arrangements of tetrads that is characteristic of parallel stranded G-quadruplex DNA with *anti* conformation of glycosidic bond rotation along with a negative band at 244 nm representing right-handed helicity of DNA (Karsisiotis et al., 2011; Dapić et al., 2003; Esposito, Virgilio, Randazzo, Galeone, & Mayol, 2005; Petraccone et al., 2007; Masiero et al., 2010) (Fig. 6.5 a). The positive CD band at 210 nm, characteristic of G4 structures confirms the formation of G quadruplex DNA. Upon progressive addition of 4'-epiadriamycin to Tet7 (15 μM), the CD bands at 264 nm and 244 nm diminish by 61% and 62%, respectively with a shift Δλ~1 nm in both CD bands (part of data shown in Fig. 6.5 a) at D/N = 5.0. This shows a strong interaction between ligand and DNA. No overall change in the shape of CD bands and minor shift in wavelength maxima are indicative of external binding of 4'-epiadriamycin to Tet7 (Tarikere Palakashan Pradeep & Barthwal, 2016; White et al., 2007). A plot of CD at 265 nm versus D/N (inset of Fig. 6.5 a) shows inflection at D/N = 1.0 and 2.0 indicating stoichiometry of complex as 1:1 and 2:1 in ligand-DNA complexes. Non-linear curve fitting of the plots of magnitude of

CD at 264 nm as a function of 4'-epiadriamycin concentration (Fig. 6.5 b) using equation (6) yield affinity constant K_b = 2.1x10^5 M^{-1}. The data fitted well in a single binding site which is understandable if two K_b values are of same order and are not distinguishable in CD spectra. CD spectra of 400 μM 4'-epiadriamycin shows bisignate CD bands which is characteristic of a dimer with positive and negative peaks at 454 and 519 nm, respectively and cross over point at 493 nm (Gallois et al., 1998). On progressive addition of DNA at D/N = 0.5-4.0, the CD bands at 454 and 519 nm decrease by ~99% and 64%, respectively whereas that at 350 nm decreases by 93% accompanied by the redshift of 10 nm (Fig. 6.5 c).

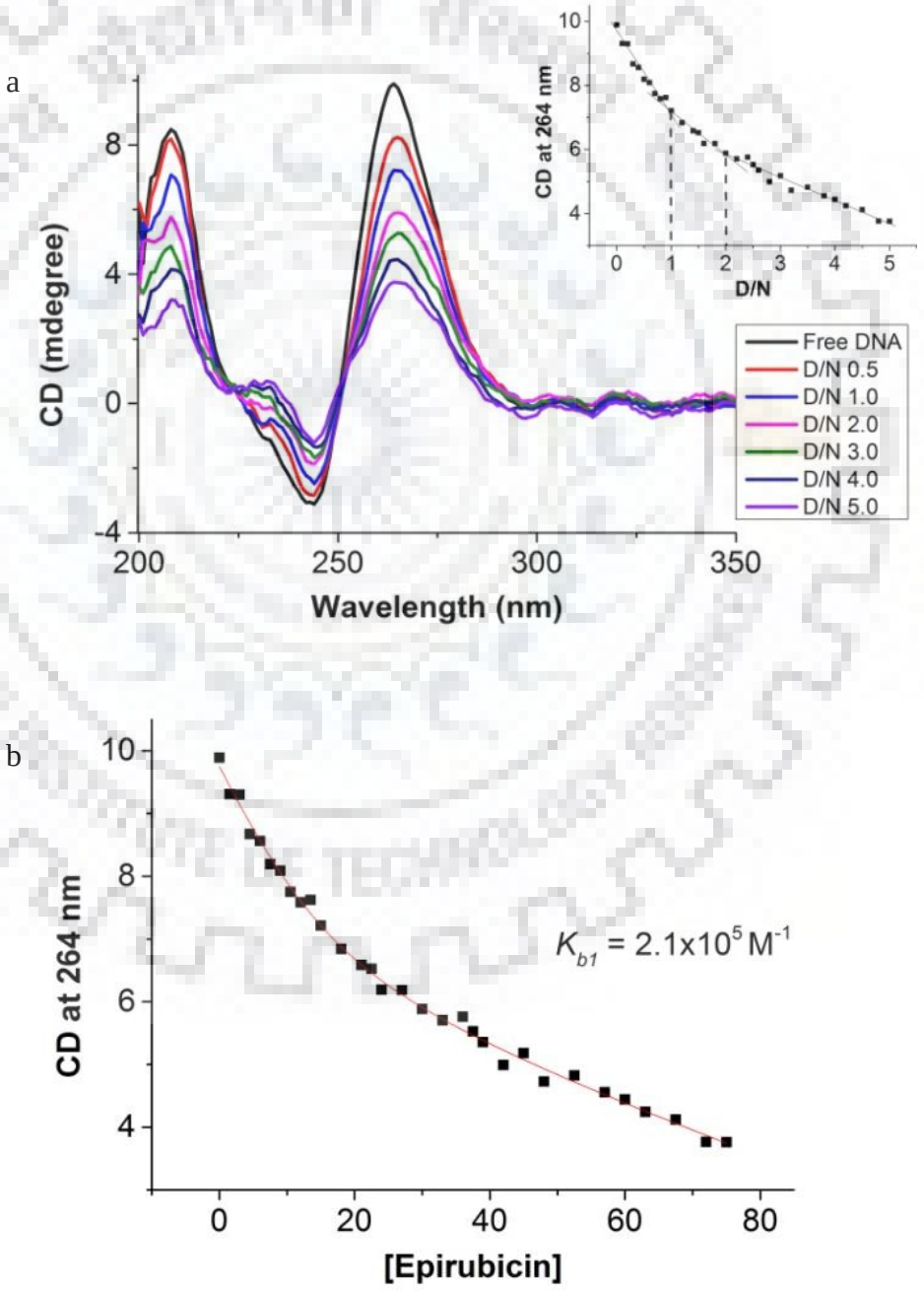

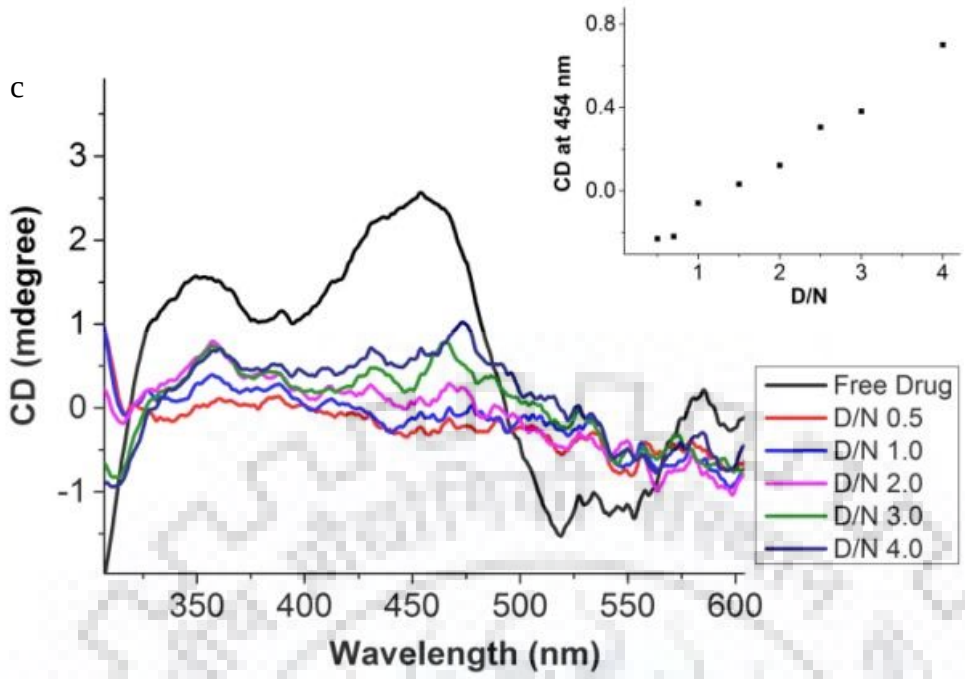

Figure 6.5 a) CD spectra of 15 µM free Tet7 and its complex on progressive addition of 4'-epiadriamycin at D/N ratio = 0.1-5.0 (data at some selected D/N shown). The inset shows the plot of CD (mdegree) at 264 nm as a function of drug concentration (µM) at 25 °C; b) Nonlinear fitted curve (red) for binding at two sites in 4'-epiadriamycin-Tet7 complexes for the observed CD (mdegree) at 264 nm as a function of drug concentration (µM) showing binding constants (K_b); c) CD spectra of 4'-epiadriamycin (400 µM) in free form and its complex with increasing concentration of Tet7 at D/N = 0.5-4.9 (data at some selected D/N shown). The inset shows the plot of CD (mdegree) at 454 nm as a function of D/N ratio.

Similar experiments with adriamycin show decrease in intensity of CD bands at 264 nm and 242 nm by 58% and 75%, respectively accompanied by the redshift of 1-3 nm (part of data shown in Fig. 6.6 a) at D/N = 5.0. A plot of CD at 265 nm versus D/N (inset of Fig. 6.6 a) shows inflection at D/N = 1.0 and 2.1 indicating stoichiometry of complex as 1:1 and 2:1. The estimated K_b value from the nonlinear curve fitting of CD at 264 nm as a function of adriamycin concentration (Fig. 6.6 b) using equation (6) is 3.8×10^4 M^{-1}. CD spectra of 400 µM free adriamycin show bisignate CD bands with positive and negative peaks at 445/466 and 518/543 nm, respectively and cross over point at 496 nm which is characteristic of a dimer (Gallois et al., 1998). Addition of Tet7 up to D/N = 0.5, decreases CD at 350, 466 and 543 nm by 60%, 93%, and 100%, respectively accompanied by a redshift of ~8 nm (Fig. 6.6 c). The CD data shows that both, 4'-epiadriamycin and adriamycin, bind externally in the monomeric form to Tet7.

a

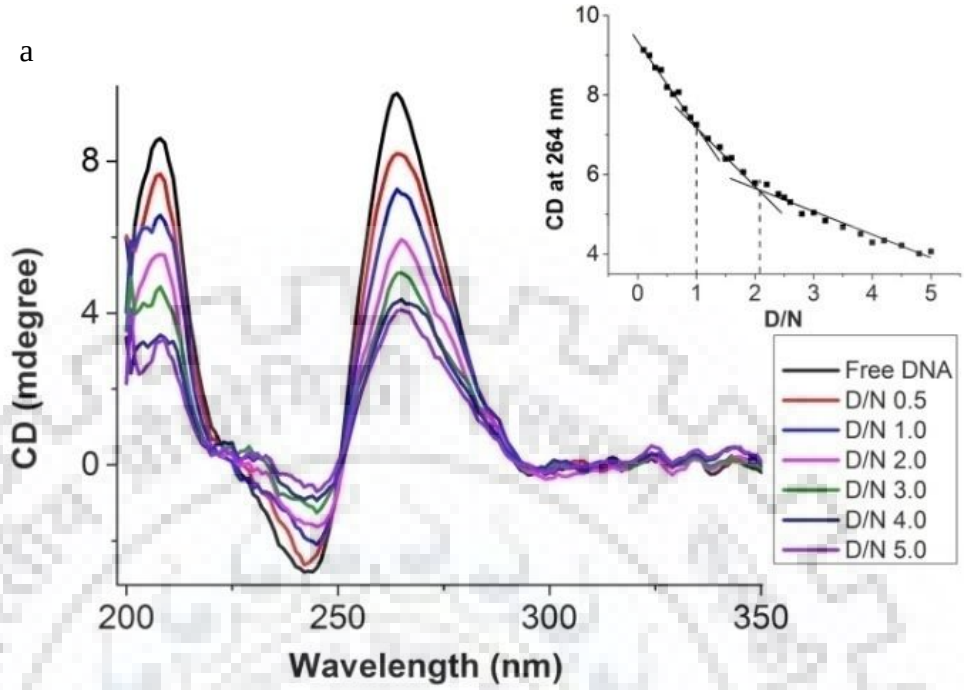
CD (mdegree)
Wavelength (nm)
CD at 264 nm
D/N
Free DNA
D/N 0.5
D/N 1.0
D/N 2.0
D/N 3.0
D/N 4.0
D/N 5.0

b

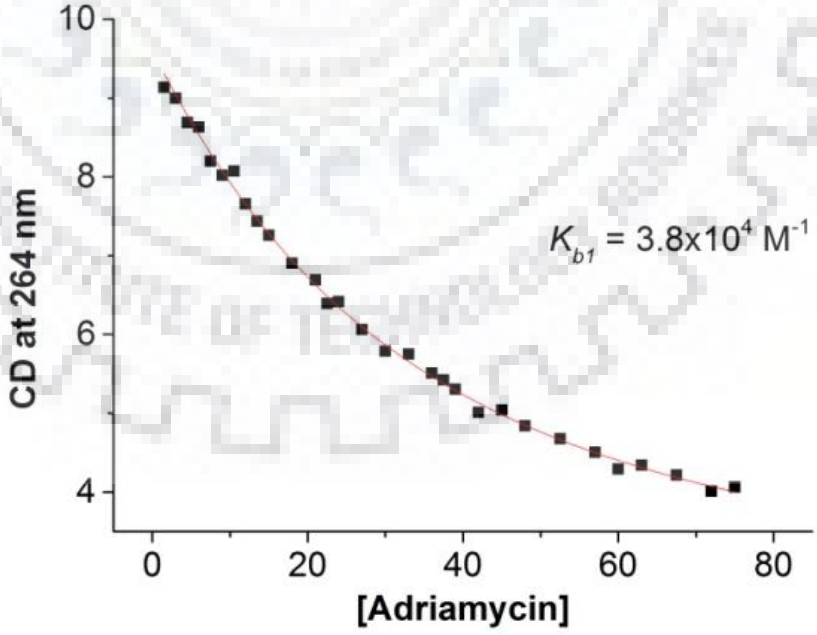
CD at 264 nm
[Adriamycin]
K_{b1} = 3.8x10^4 M^{-1}

c

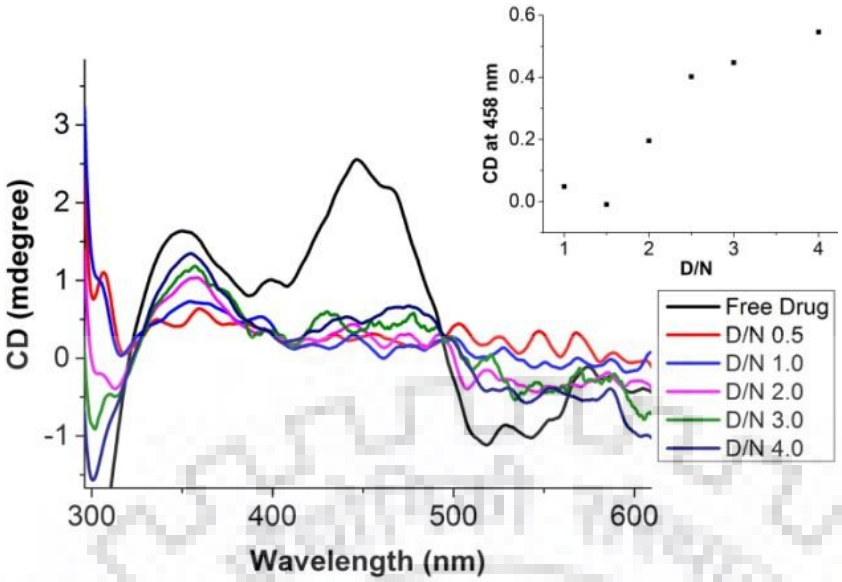

Figure 6.6 a) CD spectra free Tet7 and its complex with adriamycin at D/N ratio = 0.1-5.0 (data at some selected D/N shown). The inset shows the plot of CD (mdegree) at 264 nm as a function of drug concentration; b) Nonlinear fitted curve (red) for binding at two sites in adriamycin-Tet7 complexes for the observed CD (mdegree) at 264 nm as a function of drug concentration (μM) showing binding constants (K_b); c) CD spectra of adriamycin (400 μM) in free form and its complex with Tet7 at D/N = 0.5-4.9 (data at some selected D/N shown). The inset shows the plot of CD (mdegree) at 458 nm as a function of D/N ratio.

6.3.4 Thermal Denaturation

The change in melting temperature (ΔT_m) of folded → unfolded Tet7 and its complex with 4'-epiadriamycin and adriamycin at D/N = 0.5, 1.0, 2.0, 3.0 and 4.0 were obtained using absorbance at 260 nm (Fig. 6.7 a,b and Table 6.3, 6.4) (E. Henderson, Hardin, Walk, Tinoco, & Blackburn, 1987; Hardin, Corregan, Lieberman, & Brown II, 1997). Reversible absorbance measurements at 295 nm allow precise monitoring of "intramolecular" G-quartet formation and dissociation as compared to that at 260 nm (which leads to uncertainty) (Mergny et al., 1998). However, the "intermolecular" G4 DNA involving four independent strands, e.g. $[d\text{-}(TGGGG)]_4$, are usually parallel stranded with all guanines in *anti* conformation and do not show CD peak at 295 nm. Also, the absorbance versus wavelength plot is dominated by 260 nm peak and the transitions at 295 nm were not found so that 260 nm peak has since been used to get an estimate of T_m (Henderson et al., 1987; Hardin et al., 1997). Free DNA shows a melting transition at 55 ± 1 °C which gets stabilized on the binding of 4'-epiadriamycin. The T_m increases with D/N ratio (inset of Fig. 6.7 a) and is ~67 °C at D/N = 4.0 yielding total thermal

stabilization, ΔT_m = 12 ± 1 °C. In case of the adriamycin-Tet7 complex the increase in T_m with D/N (inset of Fig. 6.7 b) is similar to 4'-epiadriamycin-Tet7 complex with total stabilization of ΔT_m = 11 ± 1 °C.

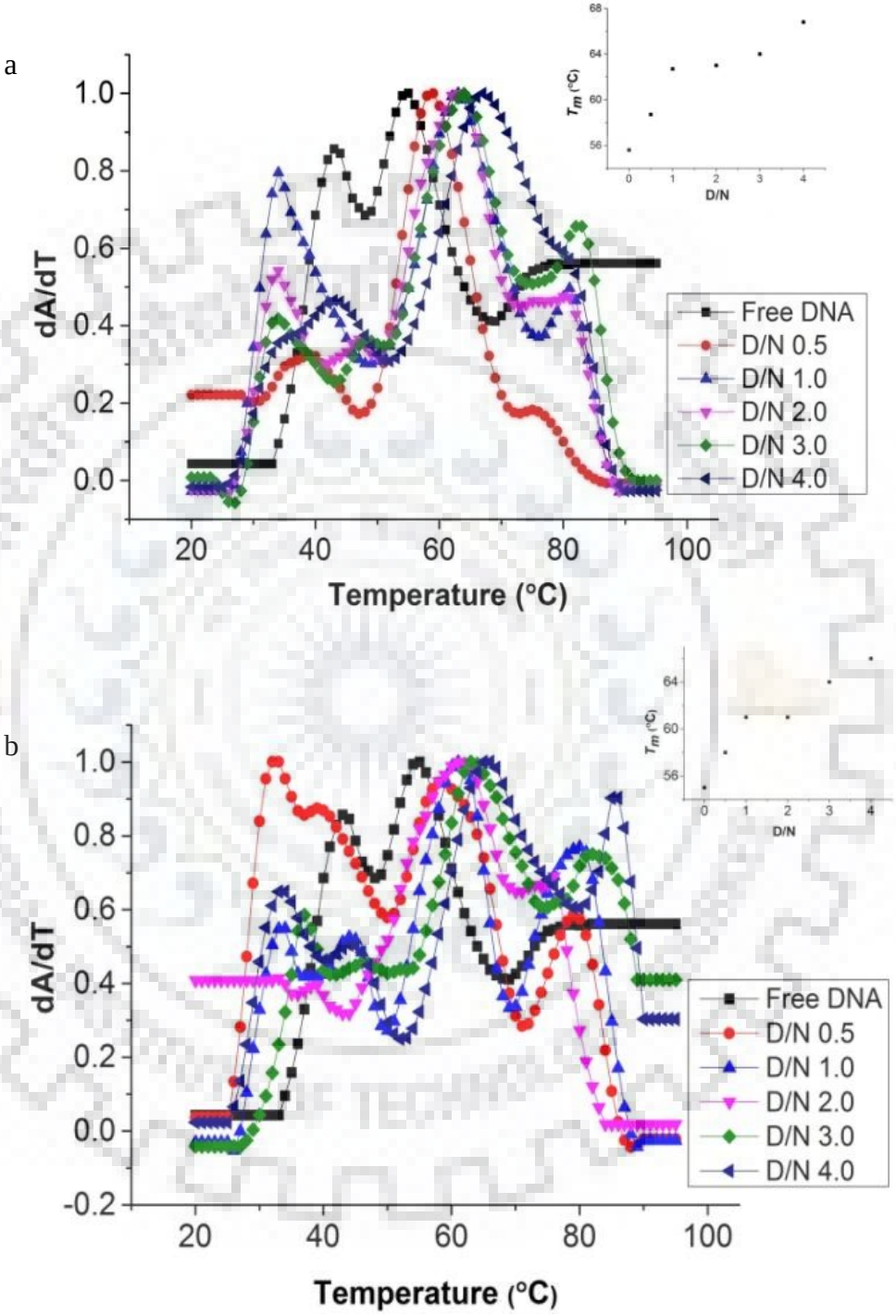

Figure 6.7 Thermal melting profiles of 1 µM free Tet7 and its complex with a) 4'-epiadriamycin and b) adriamycin at D/N ratio = 0.5, 1.0, 2.0, 3.0 and 4.0 showing derivative of absorbance with respect to temperature (dA/dT) as a function of temperature (T). The inset shows the plot of melting temperature (T_m) as a function of D/N ratio.

Table 6.3 Melting temperatures (T_m) of free Tet7 (1 µM) and its complex with 4'-epiadriamycin at D/N = 0.5, 1.0, 2.0, 3.0 and 4.0 determined through absorbance spectroscopy.

Samples	T_m (°C)	
Free DNA	55.0	
		ΔT_m
D/N 0.5	58.0	3.0
D/N 1.0	62.0	7.0
D/N 2.0	63.0	8.0
D/N 3.0	64.0	9.0
D/N 4.0	67.0	12.0

Table 6.4 Melting temperatures (T_m) of free Tet7 (1 µM) and its complex with adriamycin at D/N = 0.5, 1.0, 2.0, 3.0 and 4.0 determined through absorbance spectroscopy.

Samples	T_m (°C)	
Free DNA	55.0	
		ΔT_m
D/N 0.5	58.0	3.0
D/N 1.0	61.0	6.0
D/N 2.0	61.0	6.0
D/N 3.0	64.0	9.0
D/N 4.0	66.0	11.0

Thermal transitions from folded → unfolded form of Tet7 and its complexes with 4'-epiadriamycin and adriamycin was measured independently using CD measurements at 265 nm (Fig. 6.8 a,b and Table 6.5, 6.6). In "intermolecular" G-quadruplex, CD measurements at ~260/265 nm are more reliable as CD has single positive band at ~260 nm with no contribution at 295 nm (Dapić et al., 2003; Esposito et al., 2005; Petraccone et al., 2007; Masiero et al., 2010). Free Tet7 shows a melting transition at 61 ± 3 °C. The melting temperature increases with D/N (inset of Fig. 6.8 a,b) and total thermal stabilization ΔT_m = 13 °C ± 3 °C and 16 °C ± 3 °C was obtained in case of adriamycin and 4'-epiadriamycin-Tet7 complexes, respectively at D/N = 4.0. The measurement using Förster Resonance Energy Transfer (FRET) could not be carried out as 4'-epiadriamycin and adriamycin are fluorescent molecules with λ_{ex} = 480 nm and λ_{em} = 592 nm which falls in the range of emission of attached fluorophore moieties (e.g. Fluorescein amidite (FAM) at 5'-end and tetramethylrhodamine **(**TAMRA) at 3'-end of DNA), which might result in significant contribution to fluorescence intensity and pollute the "donor"

fluorescence (De Cian et al., 2007). Moreover, these drugs may interact with labeled dyes (e.g. FAM and TAMRA) yielding false positives.

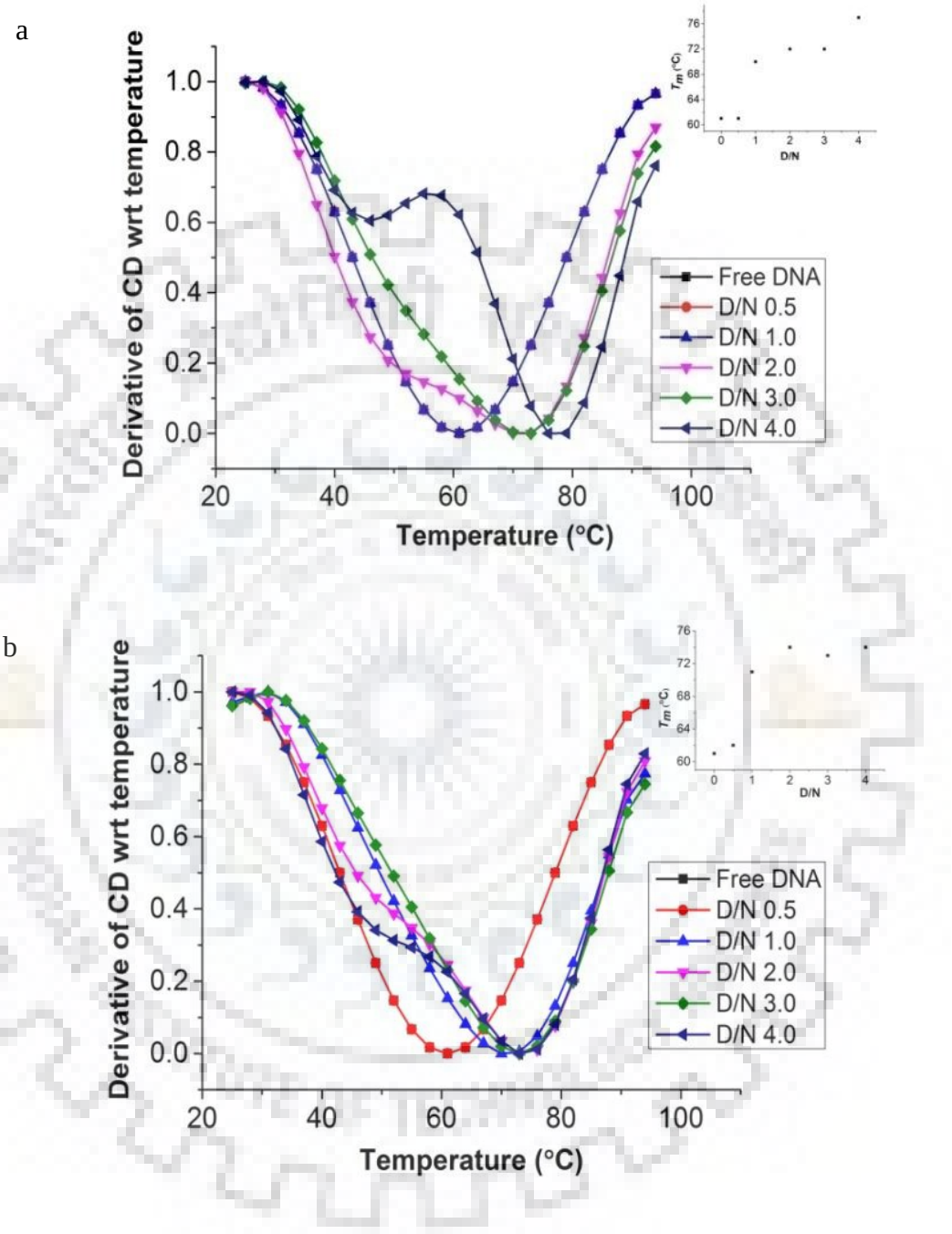

Figure 6.8 Thermal melting profiles of 10 µM free Tet7 and its complex with a) 4'-epiadriamycin and b) adriamycin at D/N ratio = 0.5, 1.0, 2.0, 3.0 and 4.0 showing derivative of CD with respect to temperature as a function of temperature (T). The inset shows a plot of melting temperature (T_m) as a function of D/N ratio.

Table 6.5 Melting temperatures (T_m) of free Tet7 (15 µM) and its complex with 4'-epiadriamycin at D/N = 0.5, 1.0, 2.0, 3.0 and 4.0 determined through CD spectroscopy.

Samples	T_m (°C)	
Free DNA	61.0	
		ΔT_m
D/N 0.5	61.0	0.0
D/N 1.0	70.0	9.0
D/N 2.0	72.0	11.0
D/N 3.0	72.0	11.0
D/N 4.0	77.0	16.0

Table 6.6 Melting temperatures (T_m) of free Tet7 (15 µM) and its complex with adriamycin at D/N = 0.5, 1.0, 2.0, 3.0 and 4.0 determined through CD spectroscopy.

Samples	T_m (°C)	
Free DNA	61.0	
		ΔT_m
D/N 0.5	62.0	1.0
D/N 1.0	71.0	10.0
D/N 2.0	74.0	13.0
D/N 3.0	73.0	12.0
D/N 4.0	74.0	13.0

6.3.5 Nuclear Magnetic Resonance

Conformational analysis of Tet7 (Tarikere Palakshan Pradeep & Barthwal, 2016; Padmapriya & Barthwal, 2017; Kumar & Barthwal, 2018) and its complex with daunomycin has earlier been carried out (Chapter 4). Similar studies with 2:1 complex of 4'-epiadriamycin-Tet7 and adriamycin-Tet7 (discussed in detail in next Chapter 7) showed that DNA exists in G-quadruplex form having Hoogsteen base pairing among G-quartets and right-handed B-DNA conformation with *anti* glycosidic bond rotation. Presence of sequential NOE at all base steps along sequence showed that there is no opening of base pairs to permit intercalation of ligand chromophores. Both ligands bind externally without causing any major alteration in Tet7. In addition, intermolecular short NOE contacts between 4'-epiadriamycin / adriamycin and Tet7 protons were observed. The NOE connectivities: 1H - T1CH_3 / T2CH_3 / T2H2' / T7CH_3 / G6H2", 2H - T1CH_3 / T2CH_3 / T2H2' / T7CH_3 / G6H2", 3H - T1CH_3 / T2CH_3 / T2H2'/ G6H2" and 4OCH_3 - G6H1' / G6H8 show proximity of ring D protons to T1, T2 and G6, T7 bases

(Fig. 6.9 a,b). Further G6NH is found to be significantly shifted upfield by 0.36 ppm while T7H1' and $T7CH_3$ are downfield shifted by 0.20 ppm and 0.17 ppm, respectively from their corresponding position in free Tet7. This suggests that the G6 experiences enhanced stacking interaction involving ring D of ligands while T7 gets relatively destacked. T1/T2 site appears to be occupied externally by the ligands. There were no short contacts between ligand-ligand which may occur on the formation of stacked dimers in parallel or antiparallel orientation as observed in X-ray structure of daunomycin-[d-(TGGGGT)]$_4$ complex (Clark et al., 2003).

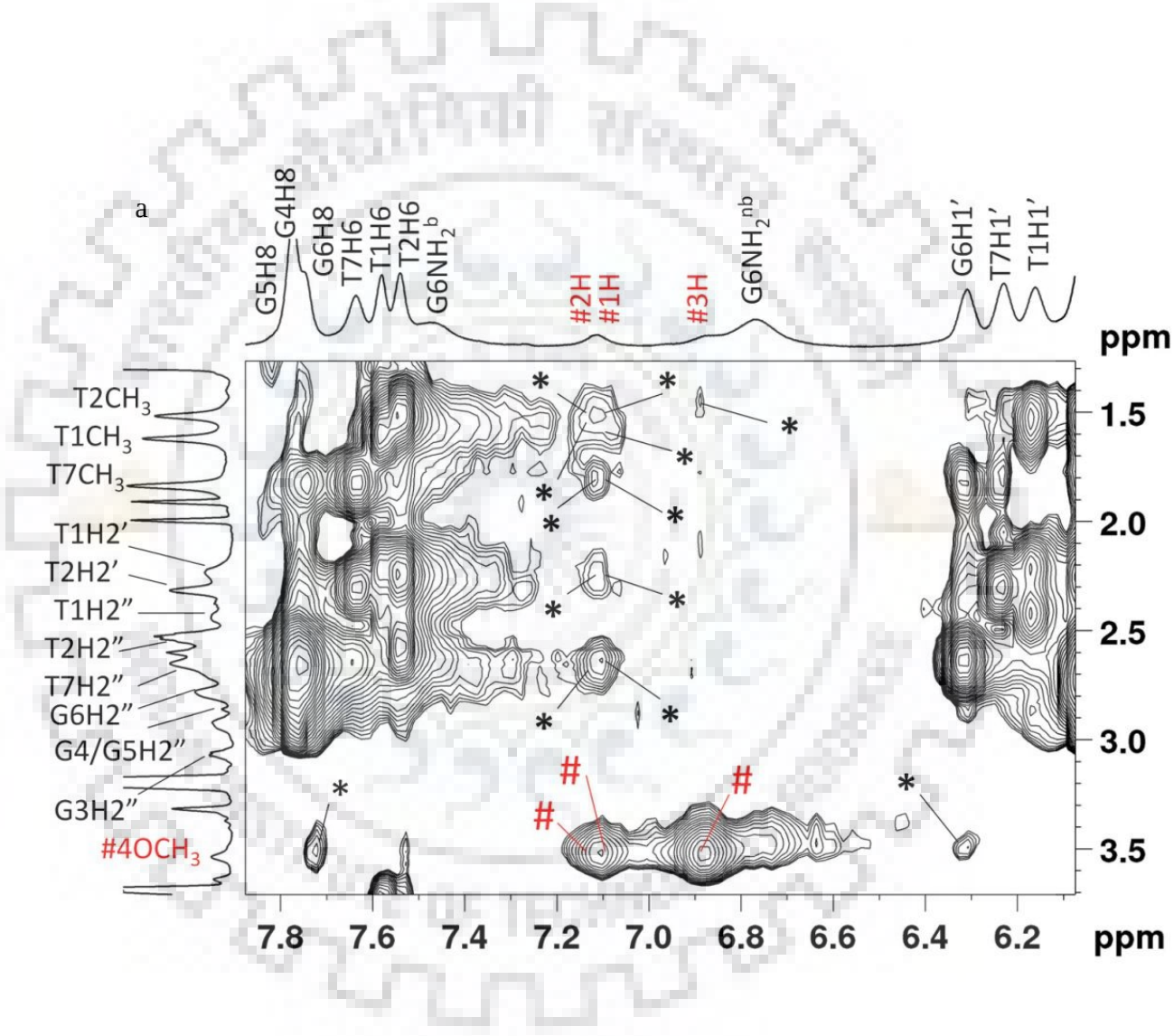

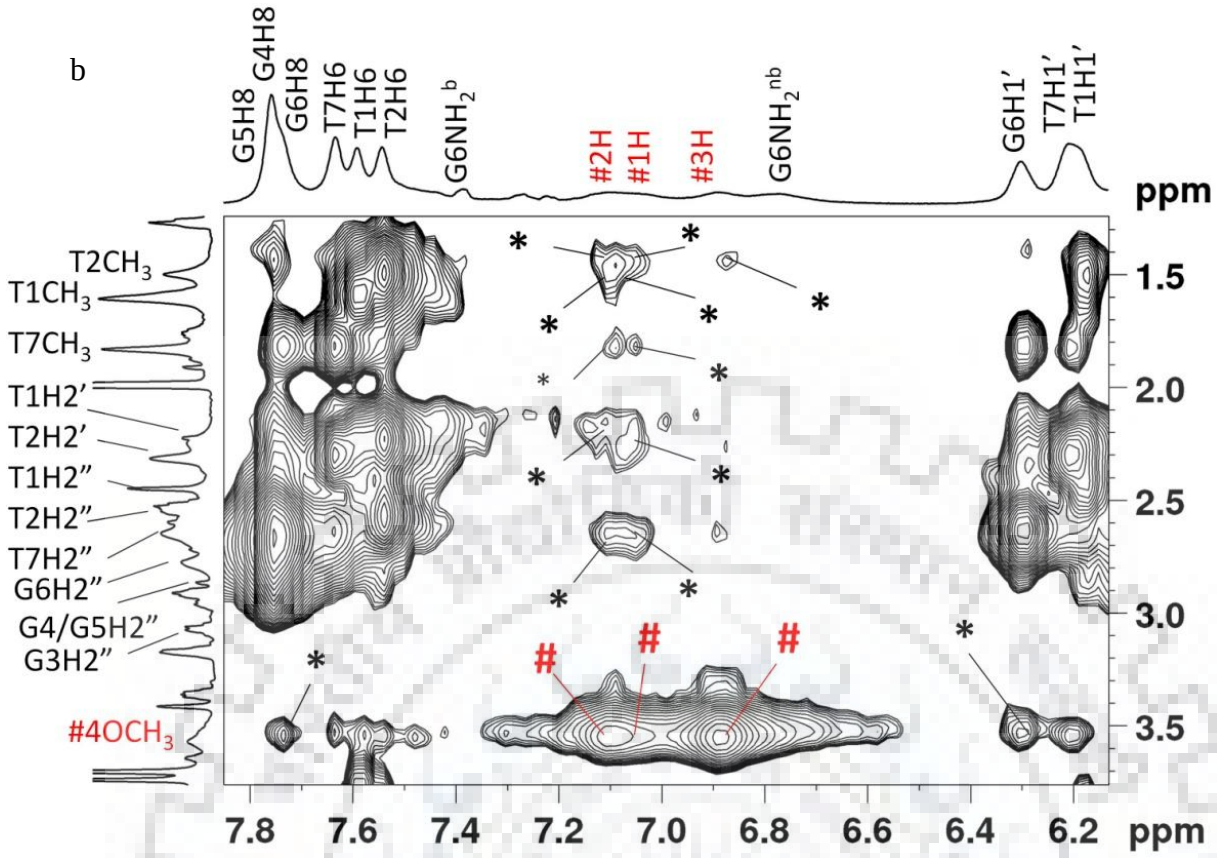

Figure 6.9 Expansion of specific region of 2D NOESY spectra of a) 4'epiadriamycin-Tet7 complex and; b) adriamycin-Tet7 complex at D/N = 4.0 at 25 °C using mixing time (τ_m) = 250 ms showing intermolecular cross peaks (marked as *) between drug and Tet7 and intramolecular drug-drug cross peaks (marked as #).

6.3.6 Molecular Docking

We performed molecular docking studies of 4'-epiadriamycin and adriamycin with Tet7 using available PDB (ID: 139D) in order to get insight into the location of binding sites. In 4'-epiadriamycin-Tet7 complex the lowest energy conformations showed the existence of 2 binding sites close to T1pT2pG3 and G6pT7 (Fig. 6.10 a,b) with binding affinities of -6.88 kcal/mol and -6.42 kcal/mol. Binding at T1pT2pG3 site was stabilized by 9 hydrogen bonds: (a) NH_3^+ of daunosamine sugar moiety with PO_4^{2-} of T2 (2.74 Å), (b) 5O of ring C with PO_4^{2-} of T2 (3.23 Å), (c) 6OH of ring B with PO_4^{2-} of T2 (3.20 Å), (d) 12O of ring C with O2 of T2 (3.10 Å), (e) 12O of ring C with N9 of G3 (3.08 Å), (f) 12O of ring C with O4' of G3 (2.32 Å), (g) 11OH of ring B with NH of G3 (2.62 Å), (h) $9COCH_2OH$ with PO_4^{2-} of G3 (1.92 Å), (i) $9COCH_2OH$ with O3' of G4 (2.86 Å) (Fig. 6.10 c). Six other hydrogen bonds: (a) NH_3^+ of daunosamine sugar moiety with PO_4^{2-} of G5 (2.52 Å), (b) 4'H of daunosamine sugar moiety with PO_4^{2-} of G5 (2.79 Å), (c) 4'H of daunosamine sugar moiety with NH_2 of G6 (2.88 Å), (d)

9OH of ring A with O3' of T7 (2.54 Å), (e) 6OH of ring B with PO_4^{2-} of T7 (3.42 Å), (f) 5O of ring C with PO_4^{2-} of T7 (2.43 Å) stabilize binding at G6pT7 site (Fig. 6.10 d).

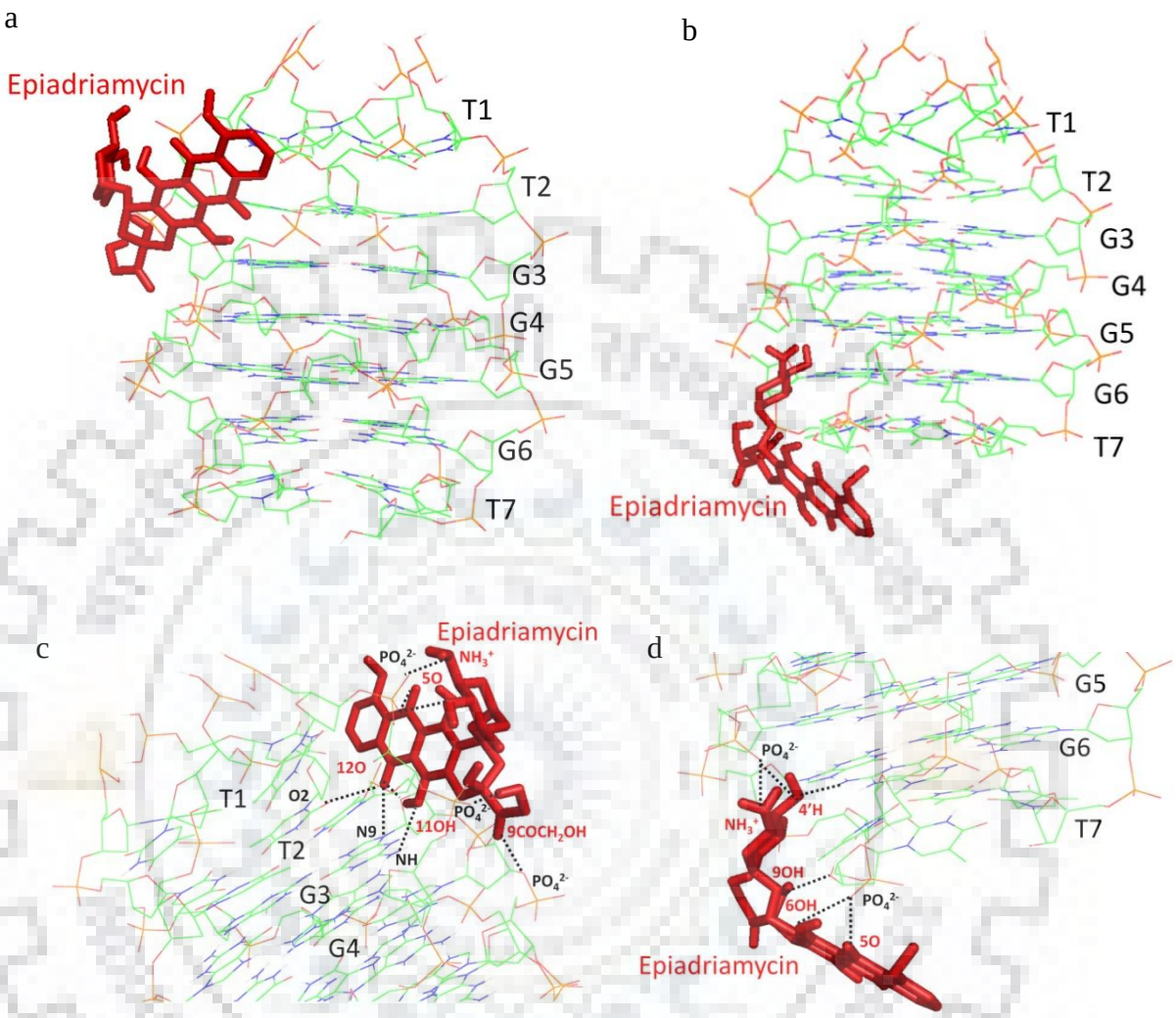

Figure 6.10 The schematic diagram of molecular docking studies showing binding of 4'-epiadriamycin to Tet7 (PDB ID: 139D) at; a) T1pT2pG3 site and; b) G6pT7 site. Close-up view of ligand binding sites showing hydrogen bonds (black dashed lines) at; c) T1pT2pG3 site and; d) G6pT7 sites. Both models were generated using Autodock 4.2 and visualized by PyMol.

Similarly for adriamycin-Tet7 complex the lowest energy conformations similar binding sites close to T1pT2pG3 and G6pT7 (Fig. 6.11 a-d) with binding affinities of -6.27 kcal/mol and -5.78 kcal/mol. Binding at T1pT2pG3 site was stabilized by 5 hydrogen bonds: (a) 5O of ring C with O3' of T1 (3.48 Å), (b) 5O of ring C with PO_4^{2-} of T2 (3.50 Å), (c) 6OH of ring C with PO_4^{2-} of T2 (2.57 Å), (d) oxygen of daunosamine sugar moiety with PO_4^{2-} of T2 (2.91 Å), (e) 4'OH of daunosamine sugar moiety with PO_4^{2-} of G3 (2.28 Å) (Fig. 6.11 c). However,

binding at G6pT7 site is stabilized by three hydrogen bonds: (a) 12O of ring C with N1 of T7 (3.17 Å), (b) NH_3^+ of daunosamine sugar moiety with O5' of T7 (3.31 Å), (c) NH_3^+ of daunosamine sugar moiety with PO_4^{2-} of T7 (2.63 Å) (Fig. 6.11 d).

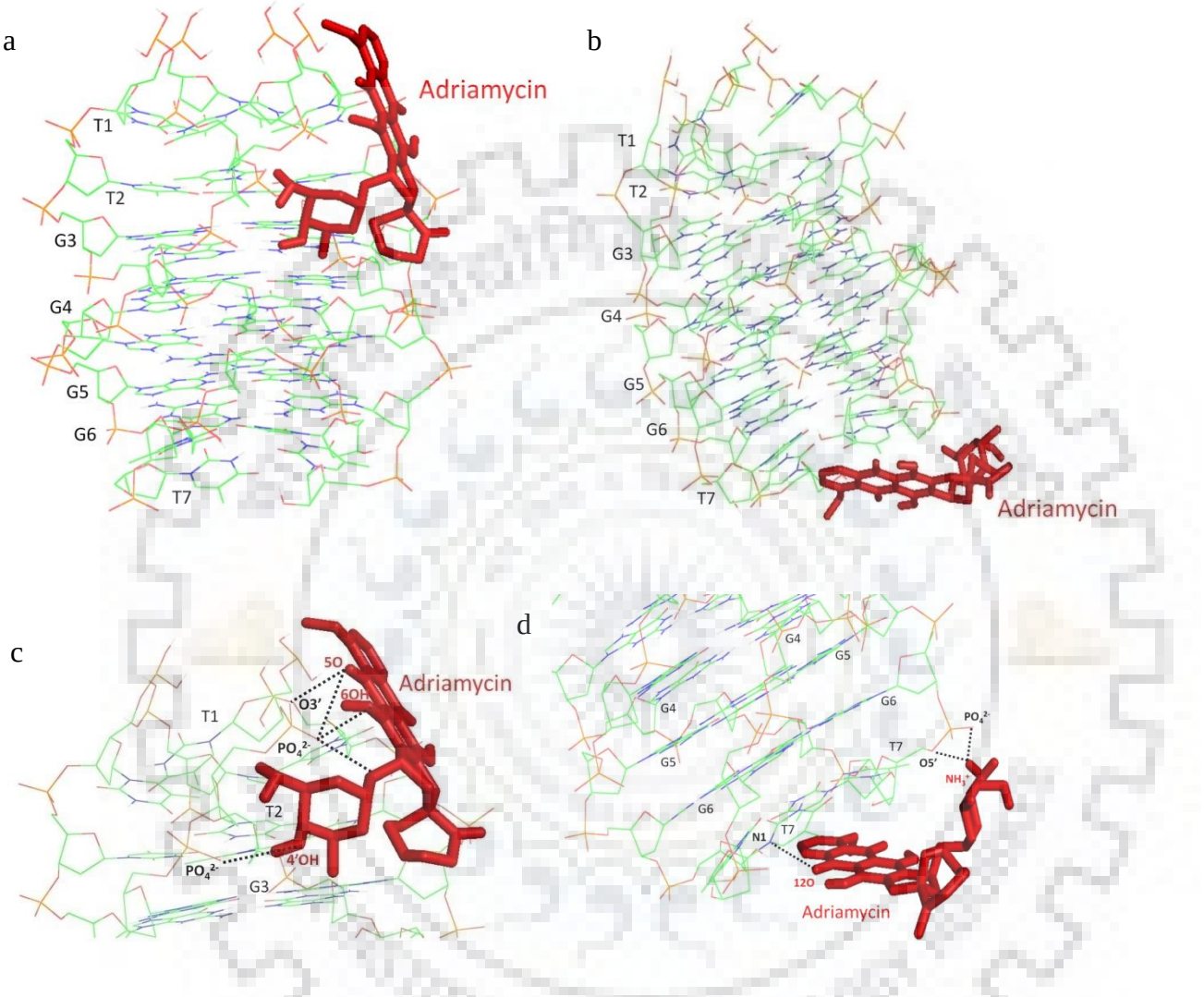

Figure 6.11 The schematic diagram of molecular docking studies showing binding of adriamycin to Tet7 (PDB ID: 139D) at; a) T1pT2pG3 site and; b) G6pT7 site. Close-up view of ligand binding sites showing hydrogen bonds (black dashed lines) at; c) T1pT2pG3 site and; d) G6pT7 sites. Both models were generated using Autodock 4.2 and visualized by PyMol.

6.4 Conclusion

We conclude that the anthracycline drugs adriamycin and 4'-epiadriamycin binds to tetramolecular parallel G-quadruplex DNA Tet7 forming 1:1 and 2:1 complexes in the solution. Extreme quenching of fluorescence intensity of drugs upon binding to Tet7 indicates good proximity and orientation of drugs to guanines residues for efficient transfer of electrons. Spectroscopic results suggest binding of these drugs takes place externally via groove and end stacking mode of interaction. CD experiments show disruption of drug dimers upon addition of Tet7 and binding to DNA takes place as a monomer. NMR and molecular docking studies show binding of these drugs takes place at two distinct sites namely, T1pT2pG3 and G6pT7 along with the formation of hydrogen bonds. Also, the interaction of these drugs with Tet7 leads to thermal stabilization of 11-16 °C which might inhibit telomerase activity in cancer cells.

Chapter 7: NMR based solution structure of 4'-epiadriamycin and adriamycin complexed with intermolecular parallel G-quadruplex DNA 7-mer [d-(TTGGGGT)]$_4$

7.1 Introduction

The anthracyclines target different forms of DNA. Nuclear Magnetic Resonance (NMR) studies on the interaction of daunomycin analogs, nemorubicin, and adriamycin, with G-quadruplex sequences containing three/four guanine repeats, have been investigated (Scaglioni et al., 2016). There are no such investigations on G4 DNA complexes comprising four guanine repeats. We have undertaken a study of the interaction of 4'epiadriamycin (or epirubicin) and adriamycin with [d(TTGGGGT)]$_4$ (Tet7) primarily by NMR techniques. We show real-time binding by SPR experiments. The stoichiometry of complexes is determined independently by Job Plot using fluorescence. DOSY experiments confirm the formation of a stable complex. Detailed analysis of proton NMR spectra including direct short interproton contacts in NOESY spectra gives information on specific interactions at molecular level. Phosphorus-31 NMR has been used to give information on DNA backbone geometry. Thermal melting profiles of imino protons have been examined and correlated to DSC thermograms.

7.2 Material and Methods

Details of materials and methods used are given in chapter 2. For Surface Plasmon Resonance experiments, 1.87-240 μM 4'epiadriamycin/adriamycin solutions were used. For Job plot experiments, the relative mole fractions of quadruplex DNA Tet7 and 4'epiadriamycin/adriamycin were varied keeping total concentration of DNA and 4'epiadriamycin/adriamycin constant at 4 μM. 1.03 mM and 1.15 mM of G-quadruplex DNA Tet7 were used in NMR experiments for titration with 4'-epiadriamycin and adriamycin, respectively. 50 μM of free [d-(TTGGGGT)]$_4$ (corresponding to single strand concentration of d-(TTGGGGT) as 200 μM) was scanned to obtain melting profile of free DNA in DSC experiments. Each set of complex with increasing 4'epiadriamycin/adriamycin concentrations and fixed Tet7 concentration of 50 μM at D/N ratio = 0.5, 1.0, 2.0, 3.0 and 4.0 were scanned to obtain melting profile of bound forms.

7.3. Results and Discussion

7.3.1 Surface Plasmon Resonance (SPR)

SPR gives a direct proof of binding of 4'-epiadriamycin (Fig. 7.1 a) and adriamycin (Fig. 7.1 b) with Tet7. The steady state response increases with concentration in the range 1.87-240 μM (Fig. 7.1 c,d) indicating specific binding indeed does takes place. The binding isotherms yield affinity constant K_b~ 6.6-7.6x10^3 M^{-1} for 4'-epiadriamycin-Tet7 (Table 7.1) and K_b~ 0.9-1.5x10^4 M^{-1} for adriamycin-Tet7 (Table 7.2) at 25 °C. The binding affinity of adriamycin for Tet7 is similar to 4'-epiadriamycin as well as daunomycin (Chapter 4).

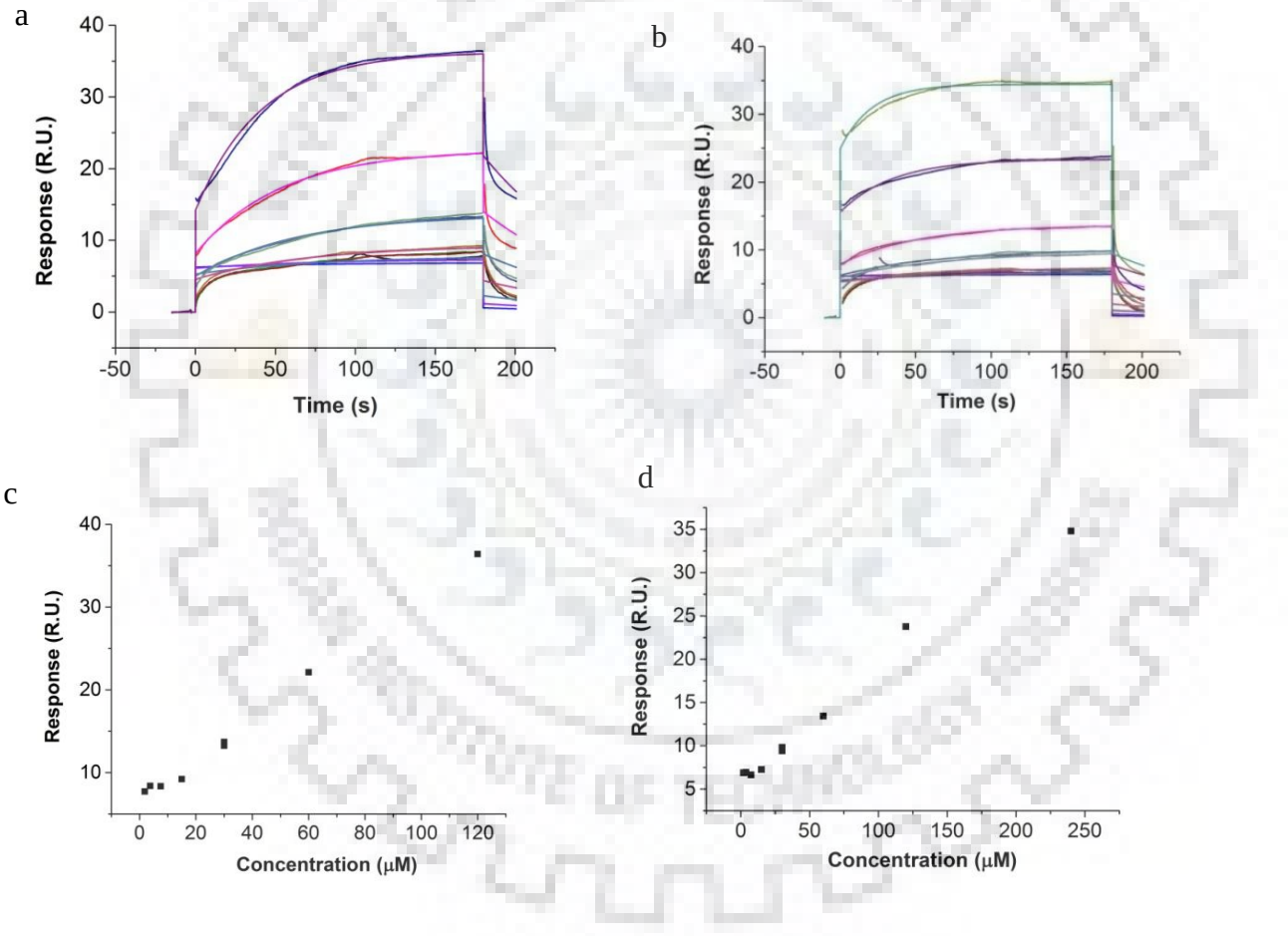

Figure 7.1 Results of SPR experiments for binding of a) 4'-epiadriamycin and b) adriamycin to Tet7. Sensograms obtained for 4'-epiadriamycin/adriamycin concentration from 1.87 μM (bottom) to 240 μM (top), using HEPES buffer with 100 mM KCl at 25 °C; Binding plot of steady-state response (R.U.) versus concentration of c) 4'-epiadriamycin (μM); and d) adriamycin.

Table 7.1 Surface Plasmon Resonance (SPR) data showing equilibrium binding constants (K_b), equilibrium dissociation constant (K_D), association rate constant (k_a) and dissociation rate constant (k_d) and maximum Response Unit (RU_{max}) obtained from binding of 4'-epiadriamycin with Tet7 at 25 °C.

Experiment	Flow rate (µl/min)	RU_{max}	k_a ($M^{-1}s^{-1}$)	k_d (s^{-1})	K_D (M)	K_b (M^{-1})	χ^2
Kinetics run 1	30	46.3	96.8	0.01	$1.3x10^{-4}$	$7.6x10^{3}$	0.7
Steady State run 1	30	$1.5x10^{6}$	-	-	6.2	0.16	0.7
Kinetics run 2	30	53.8	84.5	0.01	$1.5x10^{-4}$	$6.6x10^{3}$	0.8
Steady State run 2	30	$3.0x10^{6}$	-	-	12.7	0.07	0.9

Table 7.2 Surface Plasmon Resonance (SPR) data showing equilibrium binding constants (K_b), equilibrium dissociation constant (K_D), association rate constant (k_a) and dissociation rate constant (k_d) and maximum Response Unit (RU_{max}) obtained from binding of adriamycin with Tet7 at 25 °C.

Experiment	Flow rate (µl/min)	RU_{max}	k_a ($M^{-1}s^{-1}$)	k_d (s^{-1})	K_D (M)	K_b (M^{-1})	χ^2
Kinetics run 1	30	12.0	156.4	$1.0x10^{-2}$	$6.4x10^{-5}$	$1.5x10^{4}$	0.5
Steady State run 1	30	135.5	-	-	$8.6x10^{-4}$	$1.1x10^{3}$	1.1
Kinetics run 2	30	17.5	138.5	$1.5x10^{-2}$	$1.1x10^{-4}$	$9.0x10^{3}$	0.9
Steady State run 2	30	125.8	-	-	$8.5x10^{-4}$	$1.1x10^{3}$	2.1

7.3.2 Job plot

Direct determination of stoichiometry of 4'-epiadriamycin/adriamycin-Tet7 complexes was made by continuous variation (Job plot) analysis using fluorescence. The slope change between approximately linear regions at mole fraction of 4'-epiadriamycin (~0.48 and 0.64) and adriamycin (~0.49 and 0.65) yields stoichiometry ratios ~1:1 and 2:1 for 4'-epiadriamycin-Tet7 (Fig. 7.2 a) and adriamycin-Tet7 complexes (Fig. 7.2 b), respectively. We observed scatter of data at mole fraction 0.5-0.7, which may be due to the existence of multiple stoichiometries as

well as multiple conformations in complexes although the highest stoichiometry attained in complexes appears to be 2:1 in both the cases.

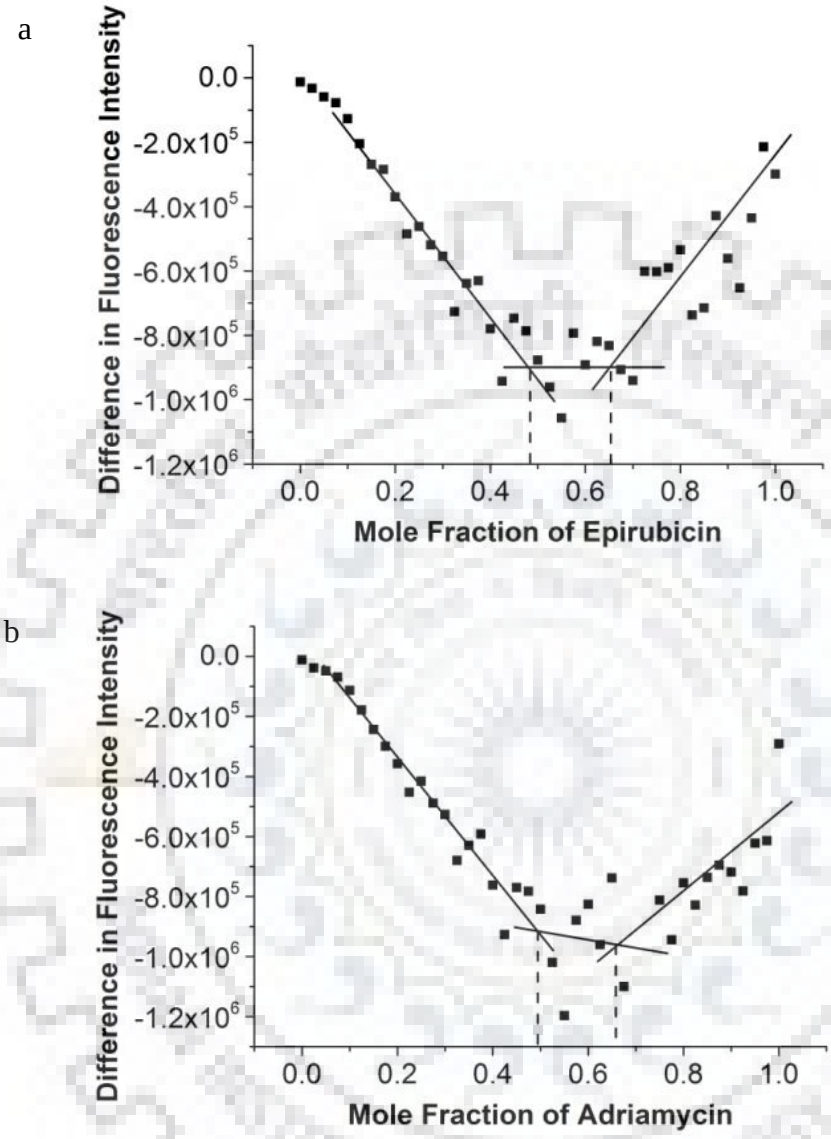

Figure 7.2 Job plot for binding of a) 4'-epiadriamycin and b) adriamycin to Tet7 showing difference in fluorescent intensity of bound and unbound drug as a function of mole fraction of drug.

7.3.3 Diffusion Ordered Spectroscopy (DOSY)

The ^{1}H DOSY experiments show (Fig. 7.3 a) that diffusion constant of $4OCH_3$ protons ($2.7x10^{-10}$ m^2/s) in free 4'-epiadriamycin and G6H8 protons in free Tet7 ($1.5x10^{-10}$ m^2/s) are greater than that for bound Tet7 ($1.3x10^{-10}$ m^2/s) at D/N = 2.0 at 25 °C. This shows that drug bound Tet7 undergoes diffusion at a slower rate as a stable complex upon binding (Cocco, Hanakahi, Huber, & Maizels, 2003; Kumar & Barthwal, 2018). Drug proton signals were

broadened and could not be used for calculating diffusion constants. The DOSY spectra thus confirm the formation of a stable bound complex. Similar results showing slower diffusion constant were obtained on addition of adriamycin to Tet7 (Fig. 7.3 b).

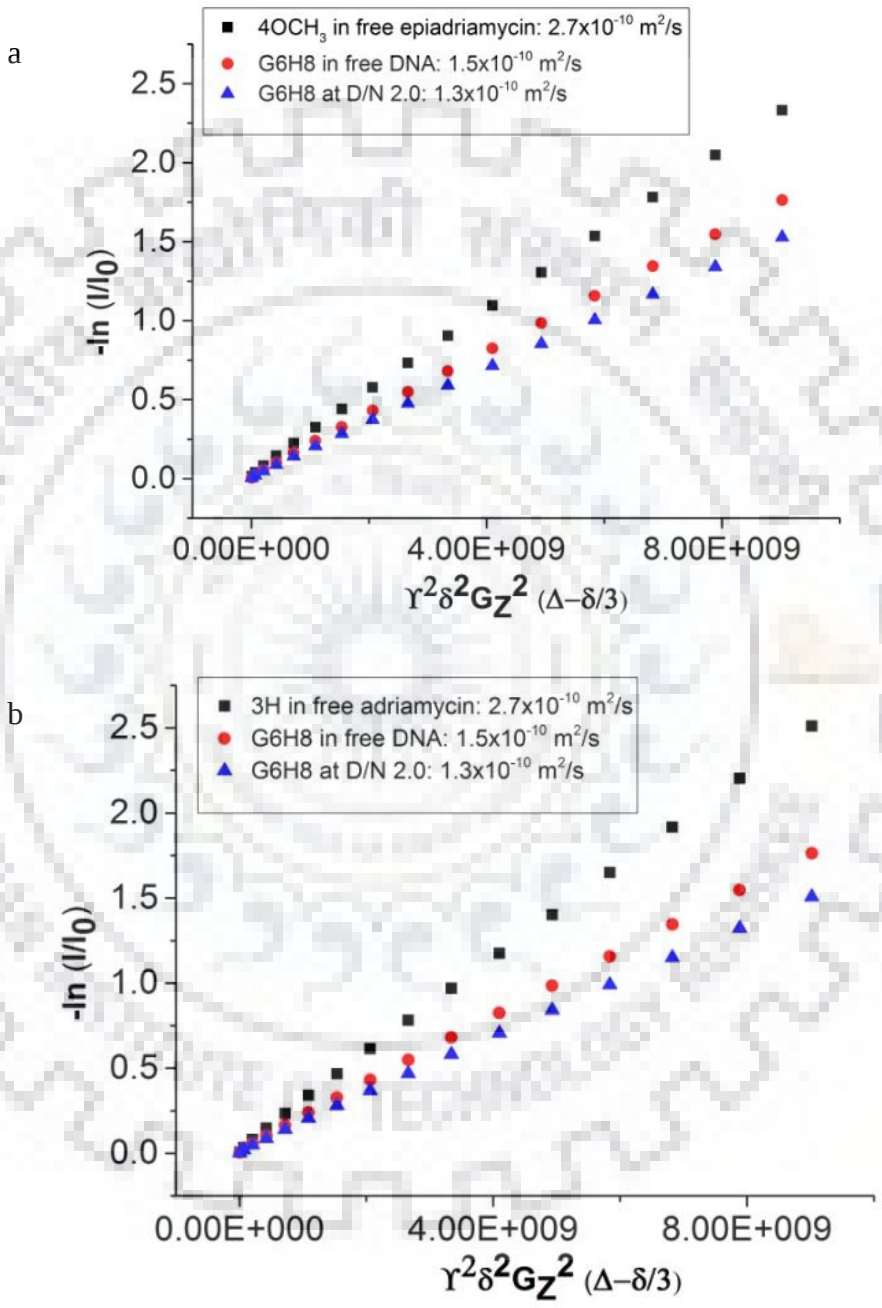

Figure 7.3 Diffusion coefficient measurement obtained from DOSY spectra of a) free 4'-epiadriamycin, free Tet7 and 4'-epiadriamycin-Tet7 complex and b) free adriamycin, free Tet7 and adriamycin-Tet7 complex at D/N = 2.0 at 25 °C.

7.3.4 Proton Nuclear Magnetic Resonance

The complete unambiguous assignment of all exchangeable and non-exchangeable protons in Tet7 (Fig. 7.4 a-j) was made by rigorous analysis of 2D ^{1}H-^{1}H NOESY and ^{1}H-^{13}C HSQC spectra (Pradeep & Barthwal, 2016; Padmapriya & Barthwal, 2017; Kumar & Barthwal, 2018). The presence of four imino signals at 10.6-11.6 ppm shows existence of Hoogsteen base pairing among G quartets. NOE correlations between adjacent GNH protons and sequential NOEs between GNH (Fig. 7.4 g) and preceding GH8/TH6 protons (Fig. 7.4 h) further ascertain G-quadruplex formation. A single set of GNH, GH8, TH6, and TCH_3 in every G-tetrad shows four-fold symmetry of Tet7. The relative intensities of intra nucleotide and sequential inter nucleotide NOE correlations between base H8/H6 and deoxyribose sugar H1'/H2'/H2" protons (Fig. 7.4 i-j) and intra nucleotide deoxyribose sugar protons show formation of tetramolecular parallel quadruplex having right-handed B-DNA conformation with predominant C2' *endo* sugar pucker and *anti* glycosidic bond rotation (Wang & Patel, 1992; Pradeep & Barthwal, 2016; Padmapriya & Barthwal, 2017; Kumar & Barthwal, 2018). Thymine imino protons were not ascertained as they show fast exchange with solvent (Gavathiotis et al., 2003).

a

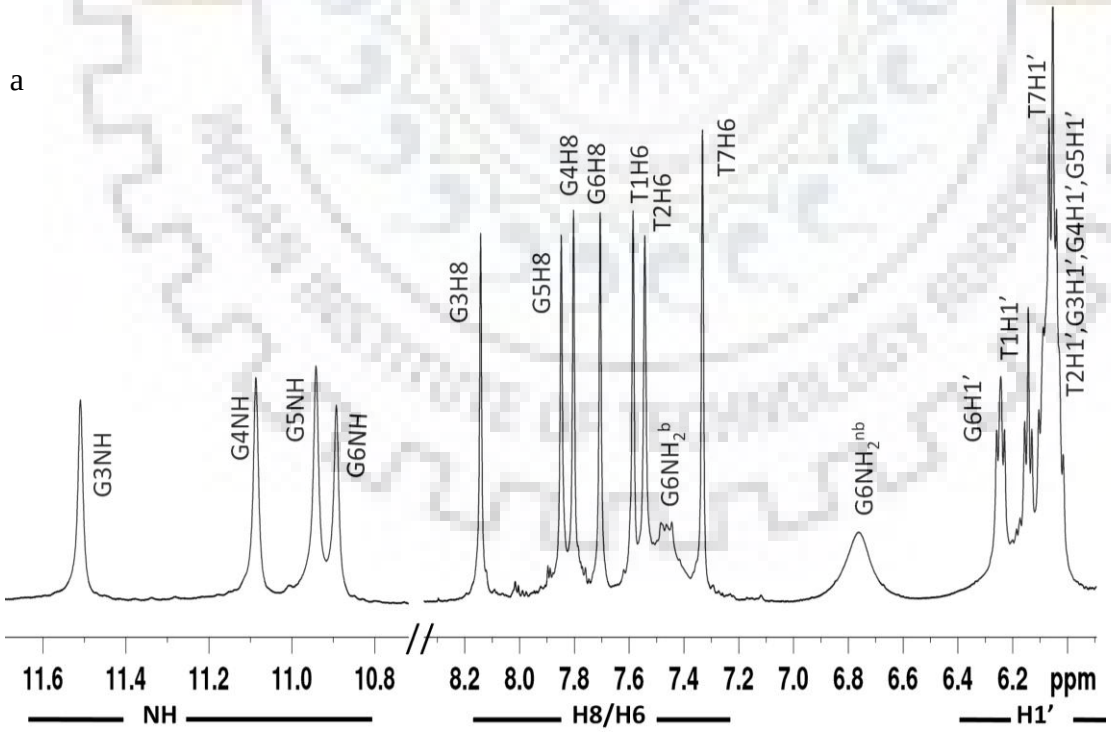

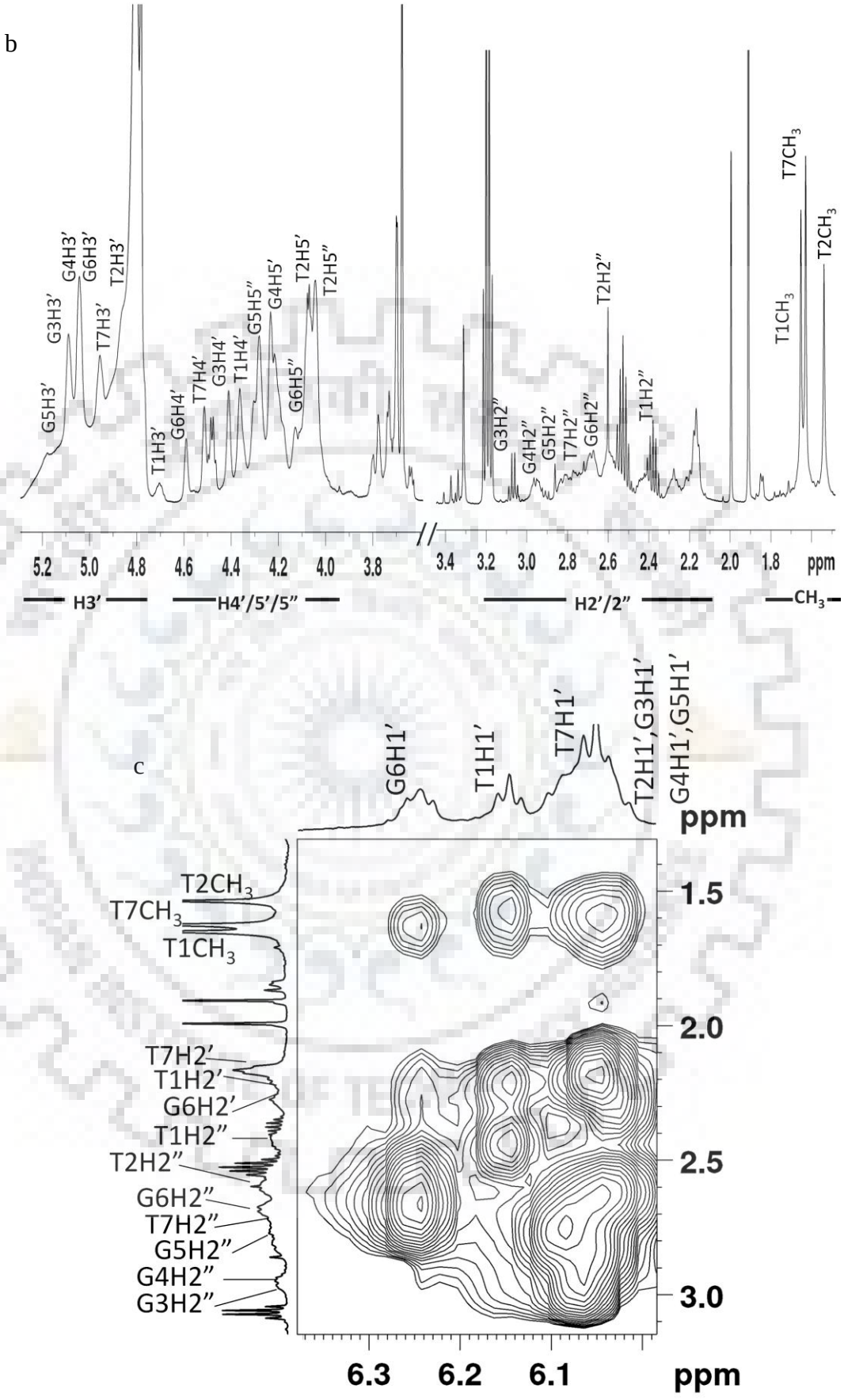
b
G5H3′
G3H3′
G4H3′
G6H3′
T7H3′
T2H3′
T1H3′
G6H4′
T7H4′
G3H4′
T1H4′
G5H5″
G4H5′
G6H5″
T2H5′
T2H5″
G3H2″
G4H2″
G5H2″
T7H2″
G6H2″
T2H2″
T1H2″
T1CH3
T7CH3
T2CH3
5.2 5.0 4.8 4.6 4.4 4.2 4.0 3.8 3.4 3.2 3.0 2.8 2.6 2.4 2.2 2.0 1.8 ppm
H3′
H4′/5′/5″
H2′/2″
CH3
c
G6H1′
T1H1′
T7H1′
T2H1′,G3H1′
G4H1′,G5H1′
ppm
T2CH3
T7CH3
T1CH3
T7H2′
T1H2′
G6H2′
T1H2″
T2H2″
G6H2″
T7H2″
G5H2″
G4H2″
G3H2″
1.5
2.0
2.5
3.0
6.3 6.2 6.1 ppm

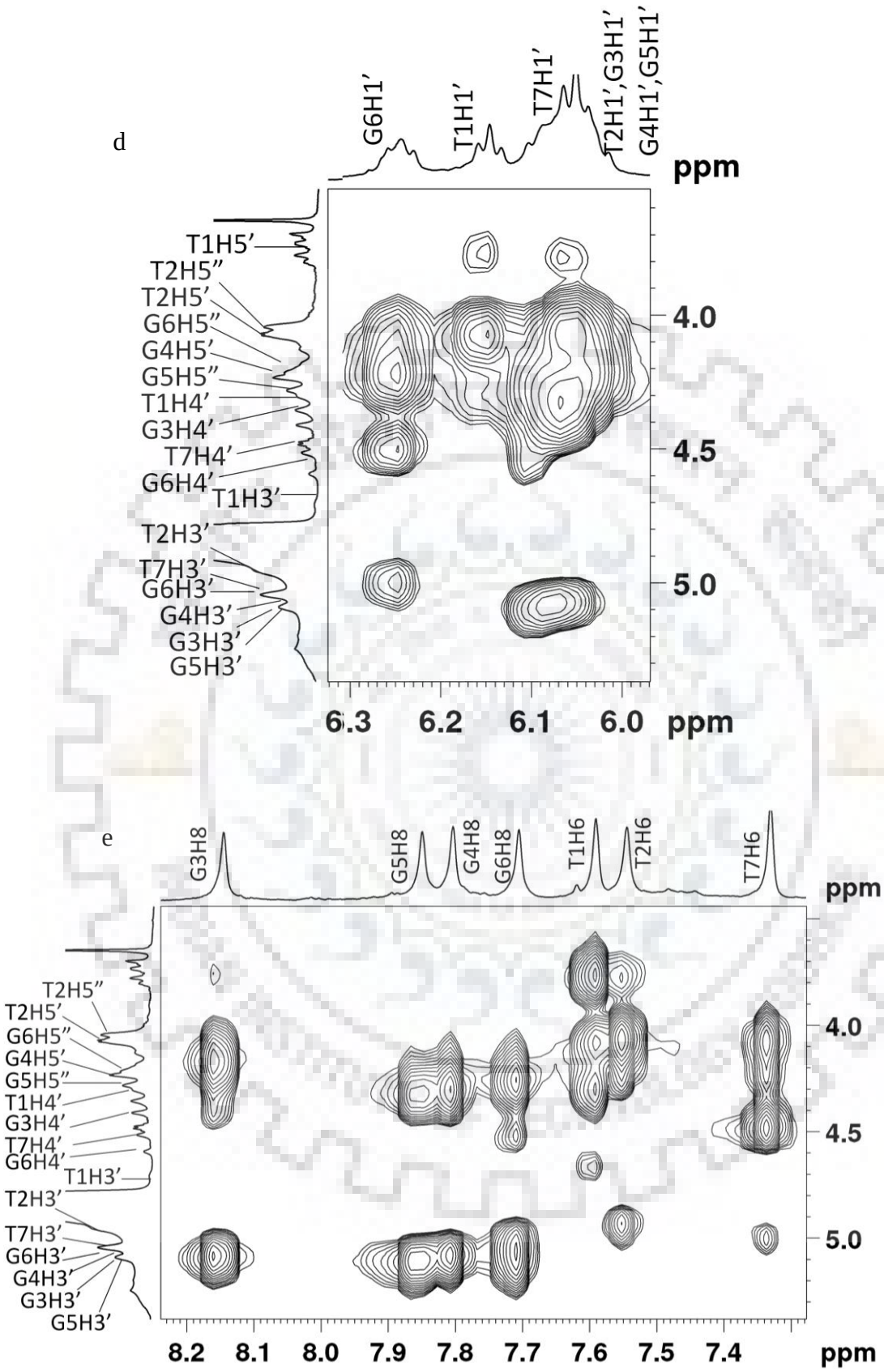
d
G6H1′
T1H1′
T7H1′
T2H1′,G3H1′
G4H1′,G5H1′
ppm
T1H5′
T2H5″
T2H5′
G6H5″
G4H5′
G5H5″
T1H4′
G3H4′
T7H4′
G6H4′
T1H3′
T2H3′
T7H3′
G6H3′
G4H3′
G3H3′
G5H3′
4.0
4.5
5.0
6.3
6.2
6.1
6.0
ppm
e
G3H8
G5H8
G4H8
G6H8
T1H6
T2H6
T7H6
ppm
T2H5″
T2H5′
G6H5″
G4H5′
G5H5″
T1H4′
G3H4′
T7H4′
G6H4′
T1H3′
T2H3′
T7H3′
G6H3′
G4H3′
G3H3′
G5H3′
4.0
4.5
5.0
8.2
8.1
8.0
7.9
7.8
7.7
7.6
7.5
7.4
ppm

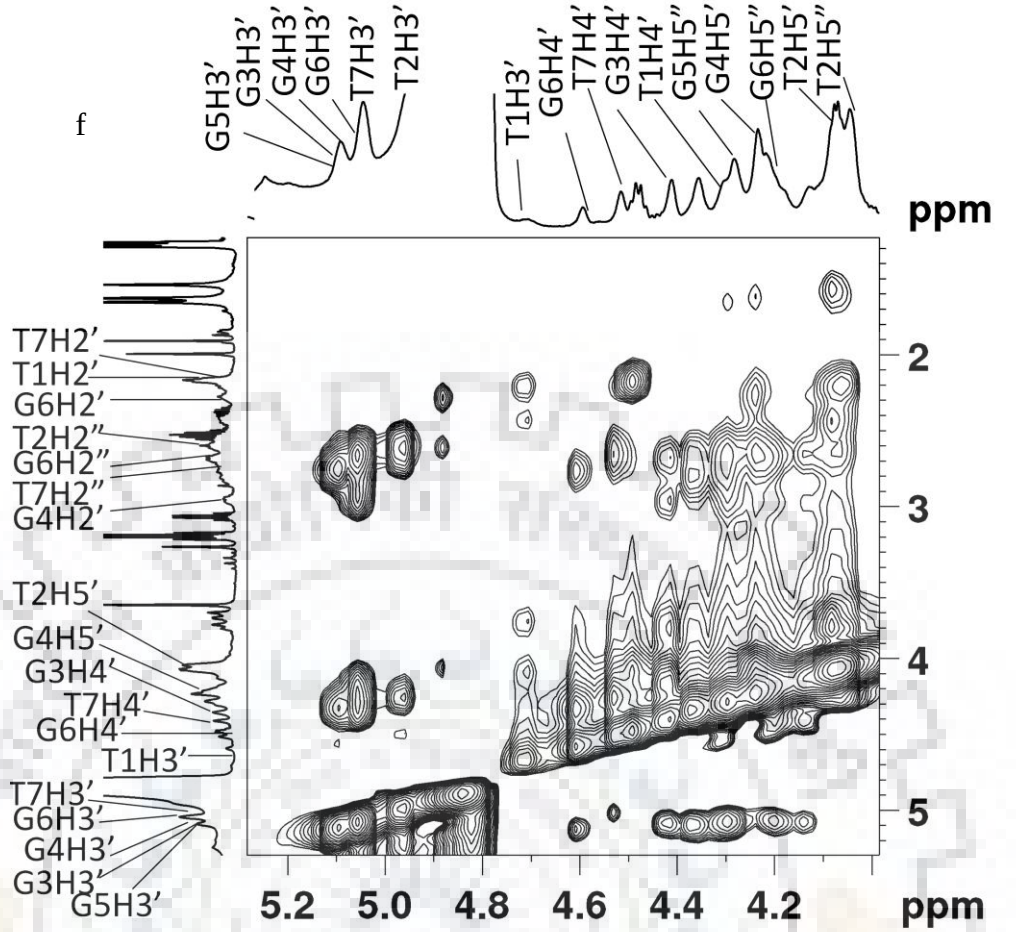
f
G5H3′
G3H3′
G4H3′
G6H3′
T7H3′
T2H3′
T1H3′
G6H4′
T7H4′
G3H4′
T1H4′
G5H5″
G4H5′
G6H5″
T2H5′
T2H5″
ppm
T7H2′
T1H2′
G6H2′
T2H2″
G6H2″
T7H2″
G4H2′
T2H5′
G4H5′
G3H4′
T7H4′
G6H4′
T1H3′
T7H3′
G6H3′
G4H3′
G3H3′
G5H3′
2
3
4
5
5.2
5.0
4.8
4.6
4.4
4.2
ppm

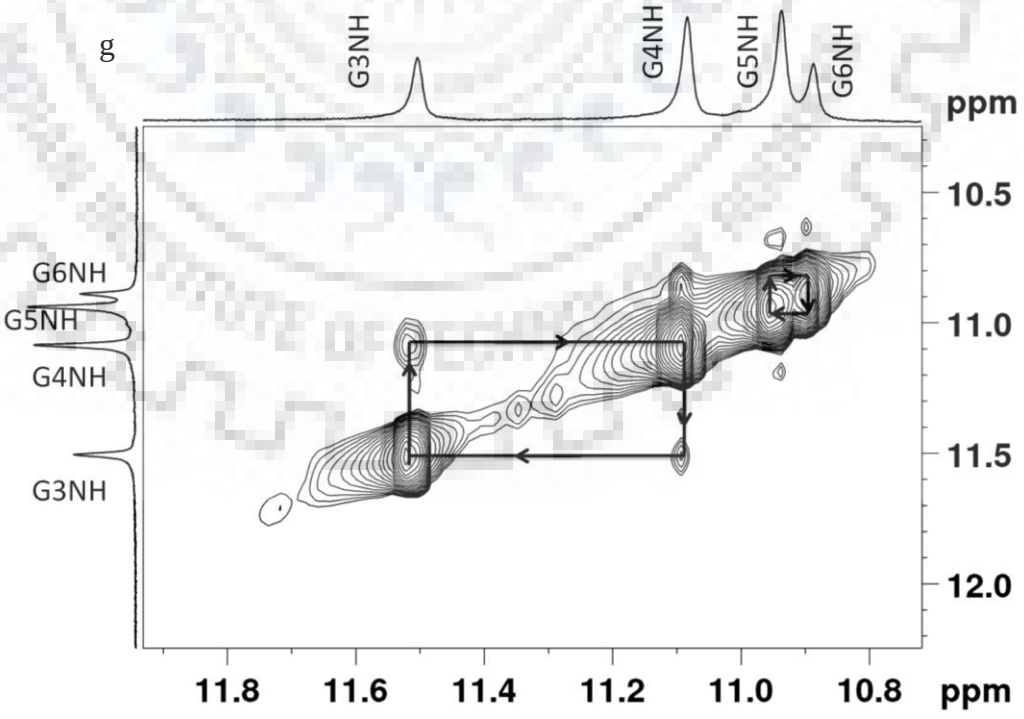
g
G3NH
G4NH
G5NH
G6NH
ppm
G6NH
G5NH
G4NH
G3NH
10.5
11.0
11.5
12.0
11.8
11.6
11.4
11.2
11.0
10.8
ppm

h

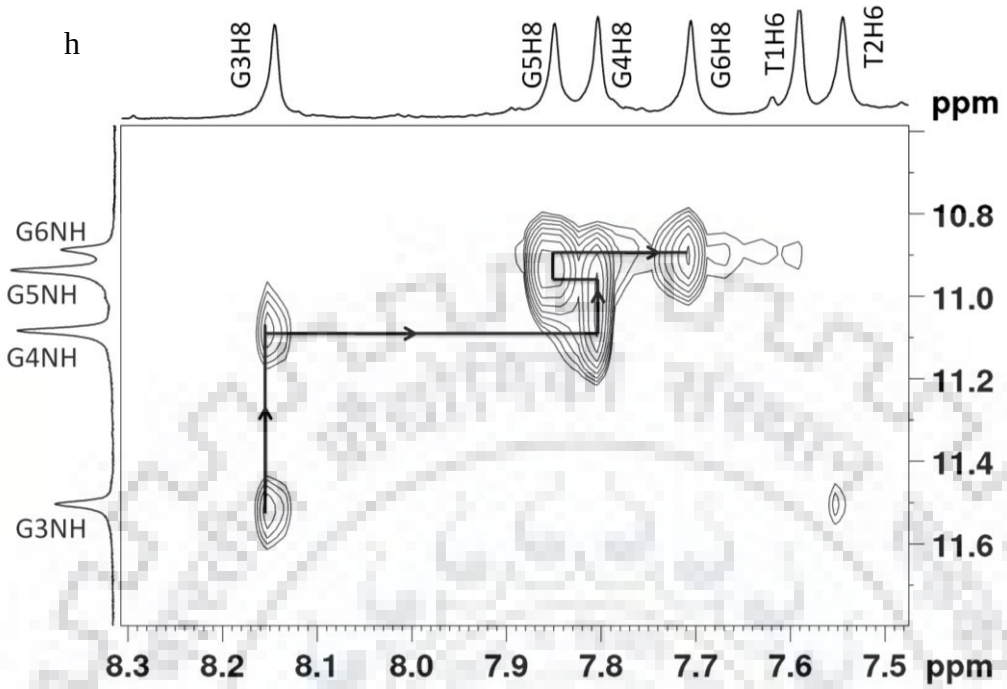
G3H8
G5H8
G4H8
G6H8
T1H6
T2H6
ppm
G6NH
G5NH
G4NH
G3NH
10.8
11.0
11.2
11.4
11.6
8.3
8.2
8.1
8.0
7.9
7.8
7.7
7.6
7.5
ppm

i

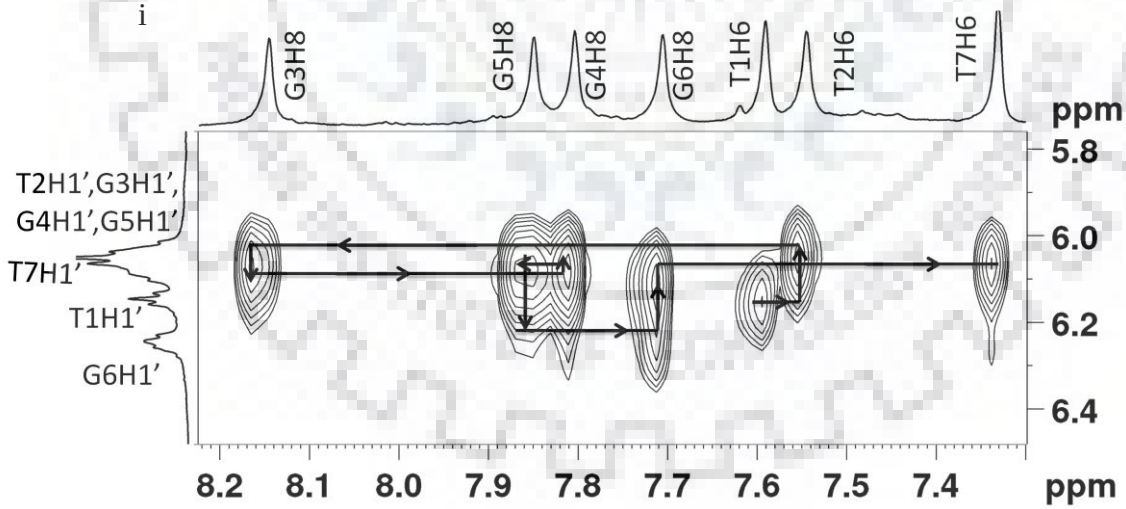
G3H8
G5H8
G4H8
G6H8
T1H6
T2H6
T7H6
ppm
T2H1',G3H1',
G4H1',G5H1'
T7H1'
T1H1'
G6H1'
5.8
6.0
6.2
6.4
8.2
8.1
8.0
7.9
7.8
7.7
7.6
7.5
7.4
ppm

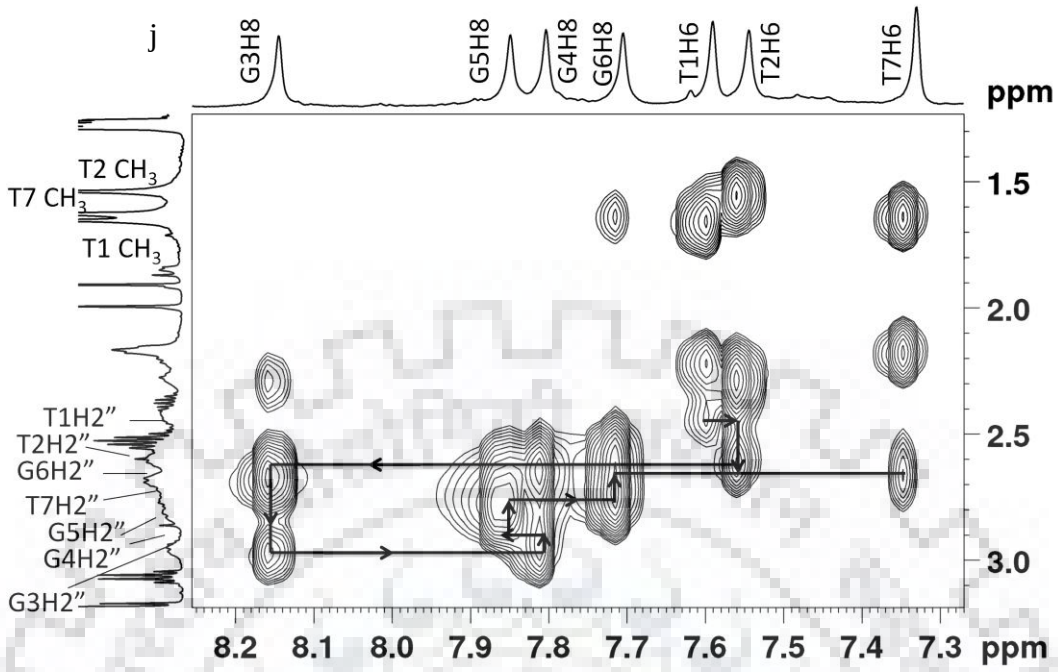

Figure 7.4 a-b) 1D-^{1}H NMR spectra of free Tet7 in KBPES buffer containing 100 mM KCl (90% H_2O+10% D_2O) at 25 °C; c-f) Expansion of ^{1}H-^{1}H 2D NOESY spectra of free Tet7 and; sequential connectivity (black arrows) between; g) imino protons; h) adjacent imino and base protons; i) base-sugar (H1') protons; and j) base-sugar (H2'/2") protons at τ_m = 250 ms in KBPES buffer (90% H_2O+10% D_2O) at 25 °C.

Tet7 (1.03 mM) was titrated with 4'-epiadriamycin at D/N = 0.0-4.0 and monitored at Drug (D) to Nucleotide (N) ratio, D/N = 0.0-4.0 by ^{1}H and ^{31}P NMR at three temperatures, 25 °C, 30 °C and 40 °C. Two dimensional ^{1}H-^{1}H NOESY and ^{1}H-^{13}C HSQC were recorded at D/N = 1.0, 2.0, 3.0 and 4.0 whereas ^{1}H-^{31}P HMBC was recorded at D/N = 2.0 at 25 °C. The progressive addition of 4'-epiadriamycin causes shifting and broadening of DNA proton signals. New proton signals appeared in the range 1.0-2.5 ppm, 3.0-3.7 ppm, and 6.8-7.2 ppm, which were subsequently assigned to 4'-epiadriamycin protons. A single set of well defined and intense resonances of base protons shows that there is no loss of four-fold symmetry of Tet7 upon complexation. Unambiguous assignment of all non-exchangeable and exchangeable protons of Tet7 and 4'-epiadriamycin protons was accomplished (Tables 7.3-7.9) by analysis of proton NMR spectra of free Tet7 (Fig. 7.4 a-j), free 4'-epiadriamycin (Fig 7.5 a), 4'-epiadriamycin-Tet7 complex (Fig. 7.5 b-e), their corresponding ^{1}H-^{1}H NOESY (Fig. 7.5 f-m) and ^{1}H-^{13}C HSQC (Fig. 7.6 a-d) spectra. The 1H, 2H and 3H protons of 4'-epiadriamycin (6.8-7.2 ppm) show clear distance correlation with a 4OCH_3 proton (3.52 ppm) in ^{1}H-^{1}H NOESY spectra. Carbon attached to 1H and 3H resonate around 120 ppm (Fig. 7.5 a) which is far apart from ^{13}C

signals of bases (133-139 ppm) and deoxyribose H1' (81-88 ppm) (Fig. 7.5 b). ^{13}C signals of deoxyribose H5'/5" (64-66 ppm) separate out from that of $4OCH_3$ (56 ppm), 5'H (68 ppm), 4'H (72 ppm) and 3'H (50 ppm) (Fig. 7.5 c). Similarly 2'axH, 2'eqH, 8axH, 8eqH 10axH, and 10eqH resonances (1.7-2.5 ppm) that overlap with that of deoxyribose H2'/H2" (2.2-3.0 ppm) have ^{13}C signals close to that for free drug in the range 32-35 ppm (Fig. 7.5 d) and are well separated from corresponding ^{13}C signals of H2'/H2" resonating at 37-41 ppm. The single set of resonances of both ligand and DNA show that a well defined stable complex is formed which may be referred to as the major conformer present in ligand-DNA complex.

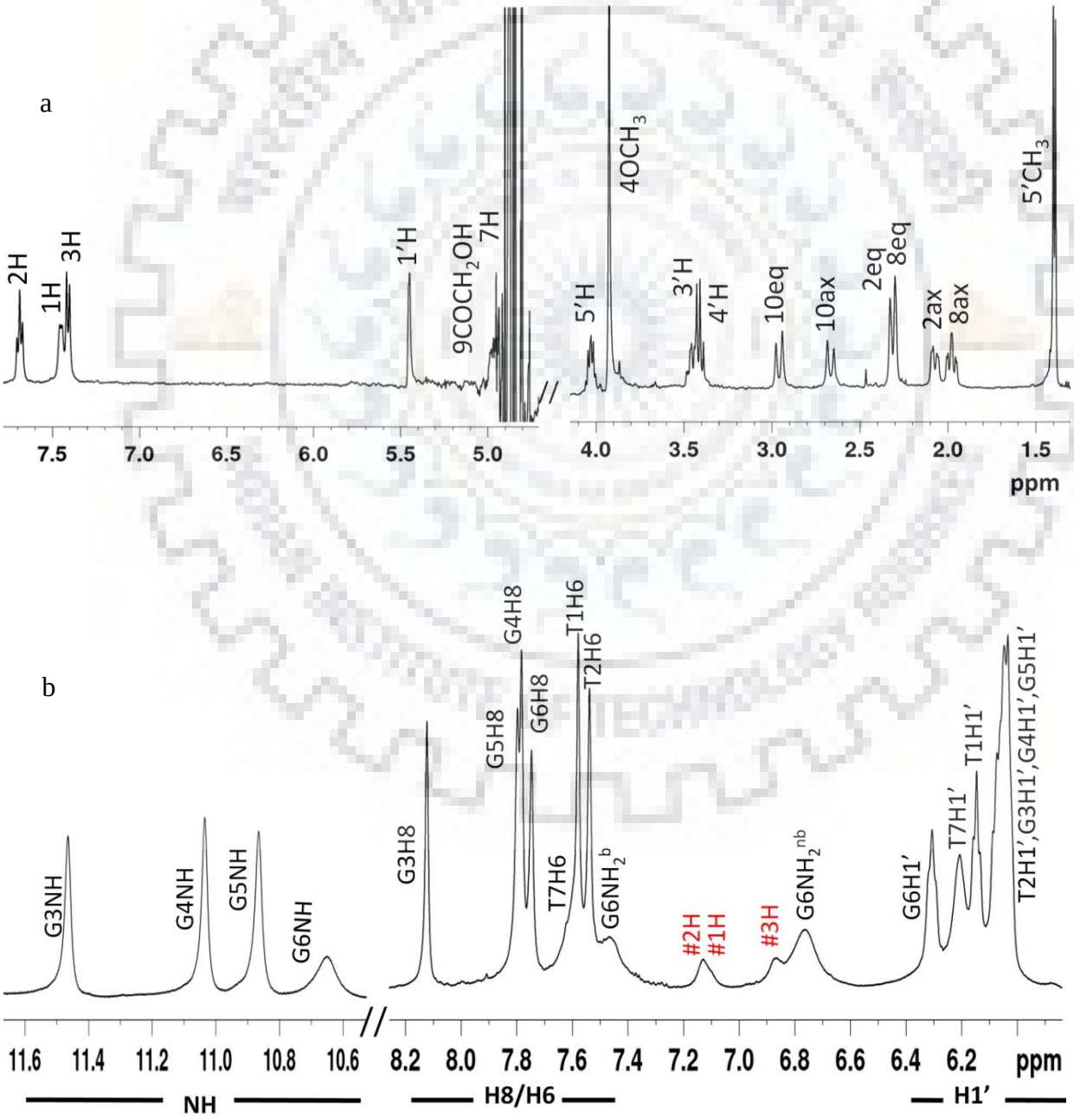

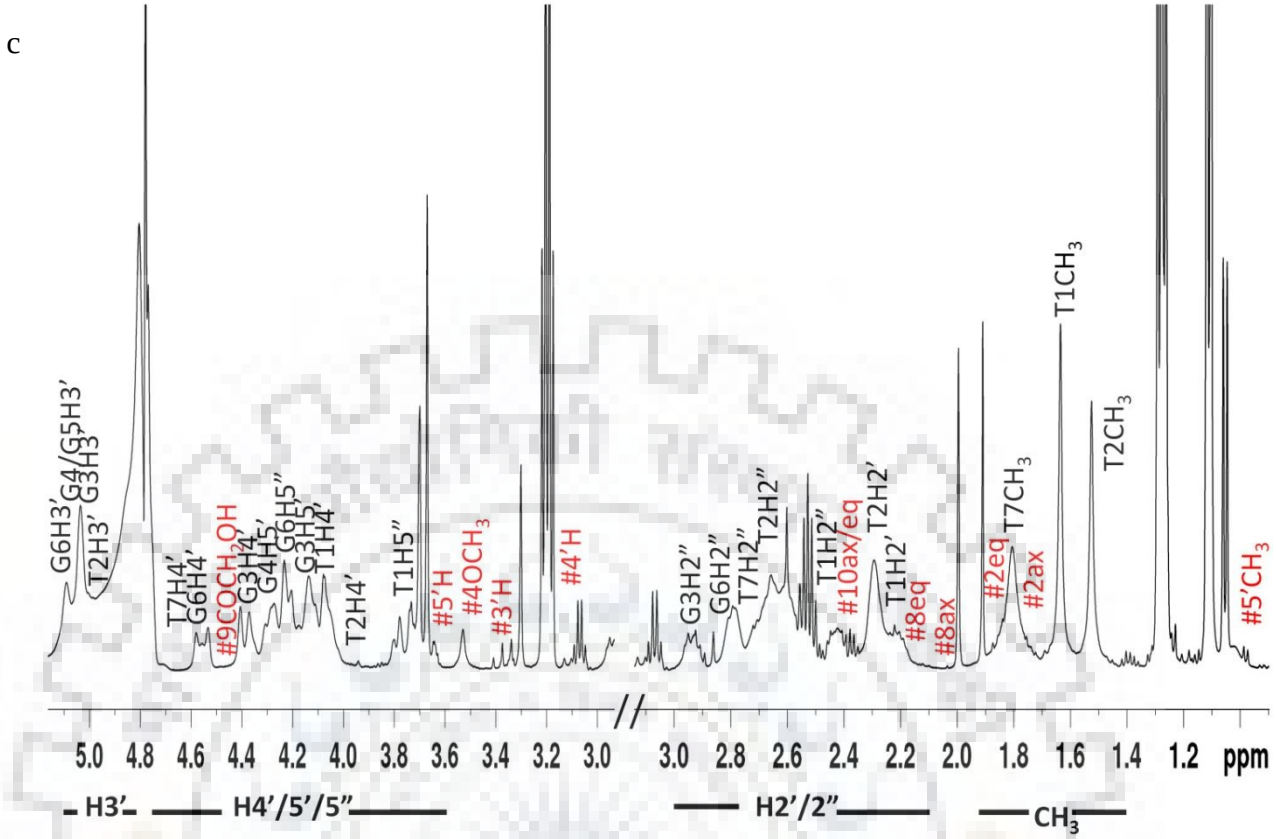
c
G6H3'
G4/G5H3'
G3H3'
T2H3'
T7H4'
G6H4'
#9COCH2OH
G3H4'
G4H5'
G6H5"
G3H5'
T1H4'
T2H4'
T1H5"
#5'H
#4OCH3
#3'H
#4'H
G3H2"
G6H2"
T7H2"
T2H2"
T1H2"
#10ax/eq
T2H2'
T1H2'
#8eq
#8ax
#2eq
T7CH3
#2ax
T1CH3
T2CH3
#5'CH3
5.0 4.8 4.6 4.4 4.2 4.0 3.8 3.6 3.4 3.2 3.0 3.0 2.8 2.6 2.4 2.2 2.0 1.8 1.6 1.4 1.2 ppm
H3'
H4'/5'/5"
H2'/2"
CH3

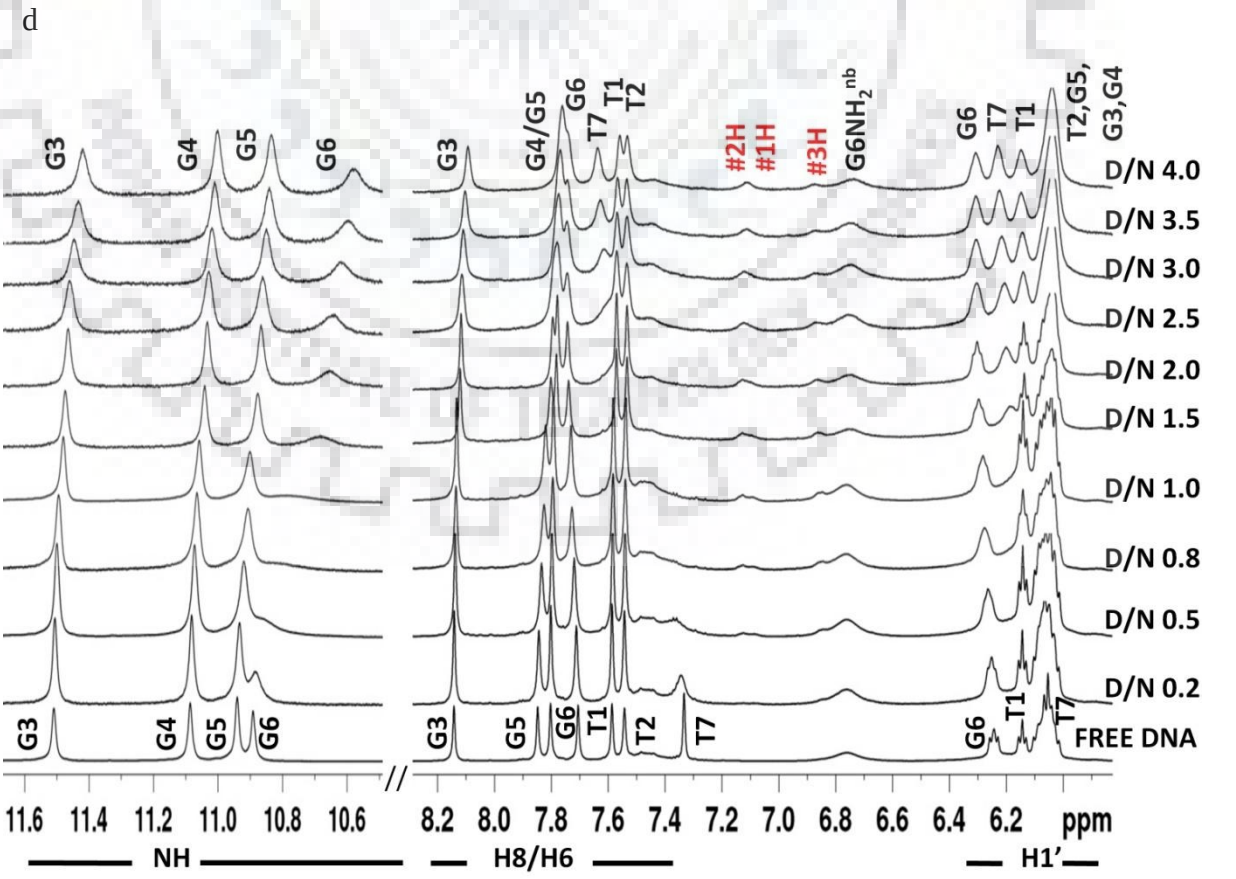
d
G3
G4
G5
G6
G4/G5
T7
T1
T2
#2H
#1H
#3H
G6NH2nb
T2,G5,
G3,G4
D/N 4.0
D/N 3.5
D/N 3.0
D/N 2.5
D/N 2.0
D/N 1.5
D/N 1.0
D/N 0.8
D/N 0.5
D/N 0.2
FREE DNA
11.6 11.4 11.2 11.0 10.8 10.6
8.2 8.0 7.8 7.6 7.4 7.2 7.0 6.8 6.6 6.4 6.2 ppm
NH
H8/H6
H1'

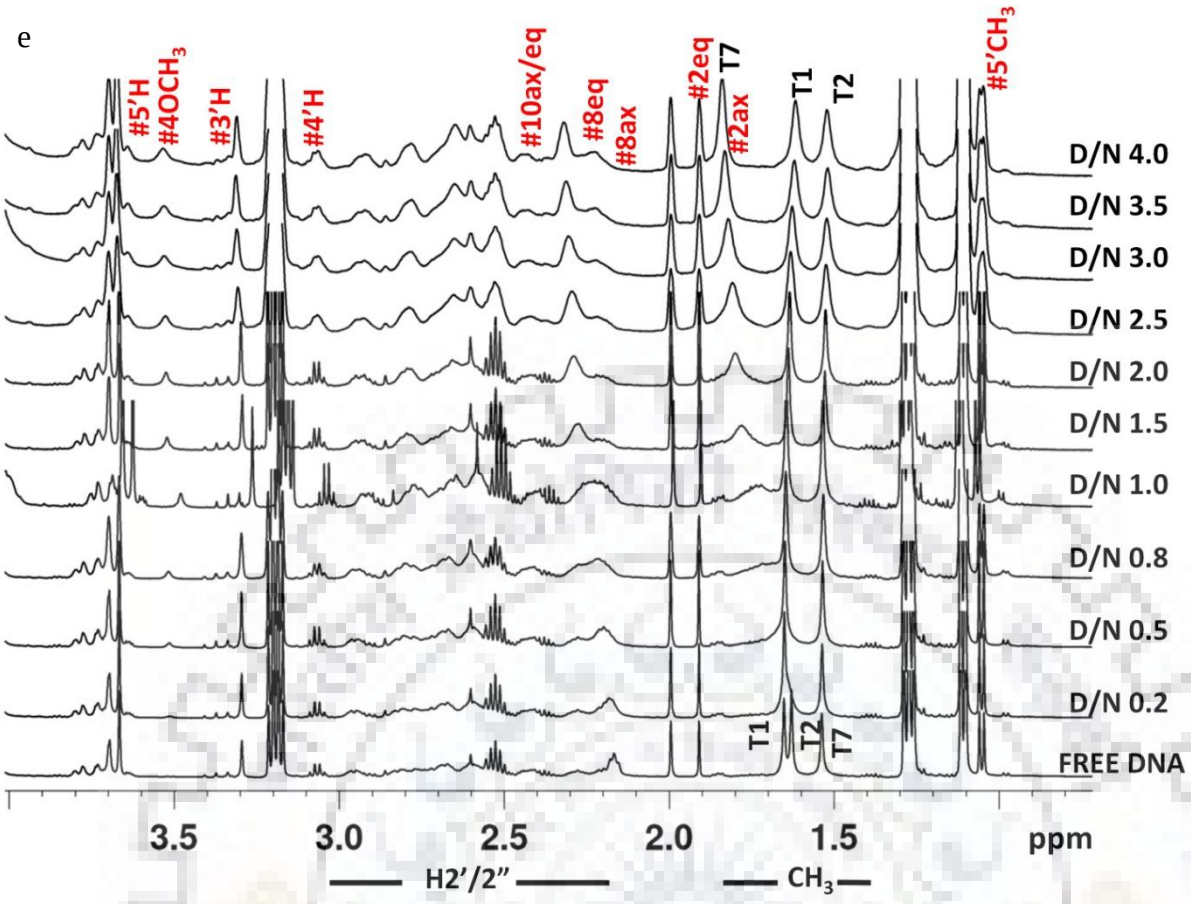
e
#5'H
#4OCH3
#3'H
#4'H
#10ax/eq
#8eq
#8ax
#2eq
T7
#2ax
T1
T2
#5'CH3
D/N 4.0
D/N 3.5
D/N 3.0
D/N 2.5
D/N 2.0
D/N 1.5
D/N 1.0
D/N 0.8
D/N 0.5
D/N 0.2
FREE DNA
T1
T2
T7
3.5
3.0
2.5
2.0
1.5
ppm
H2'/2"
CH3

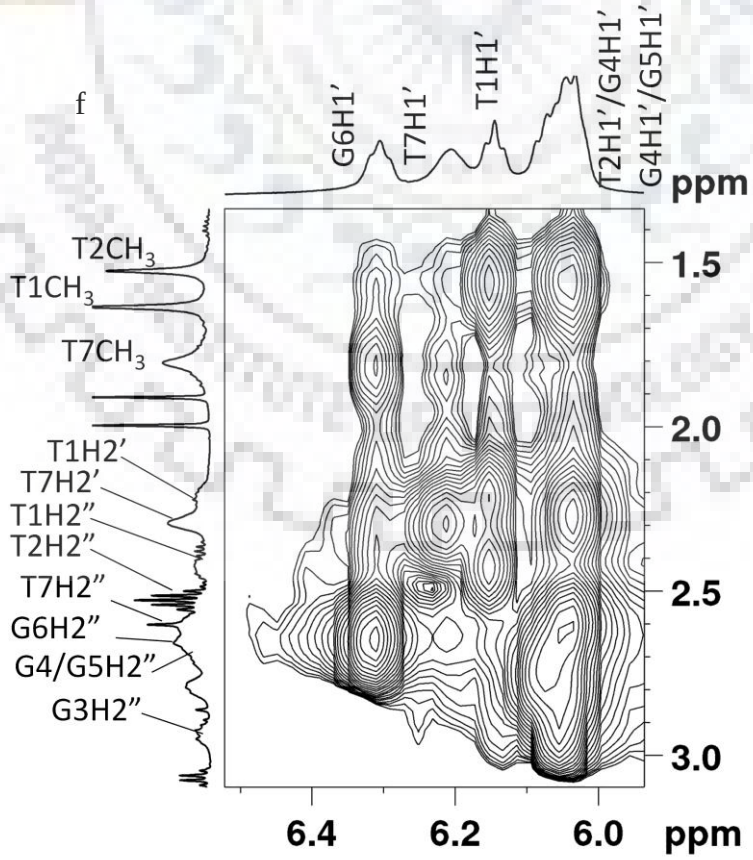
f
G6H1'
T7H1'
T1H1'
T2H1'/G4H1'
G4H1'/G5H1'
ppm
T2CH3
T1CH3
T7CH3
T1H2'
T7H2'
T1H2"
T2H2"
T7H2"
G6H2"
G4/G5H2"
G3H2"
1.5
2.0
2.5
3.0
6.4
6.2
6.0
ppm

g

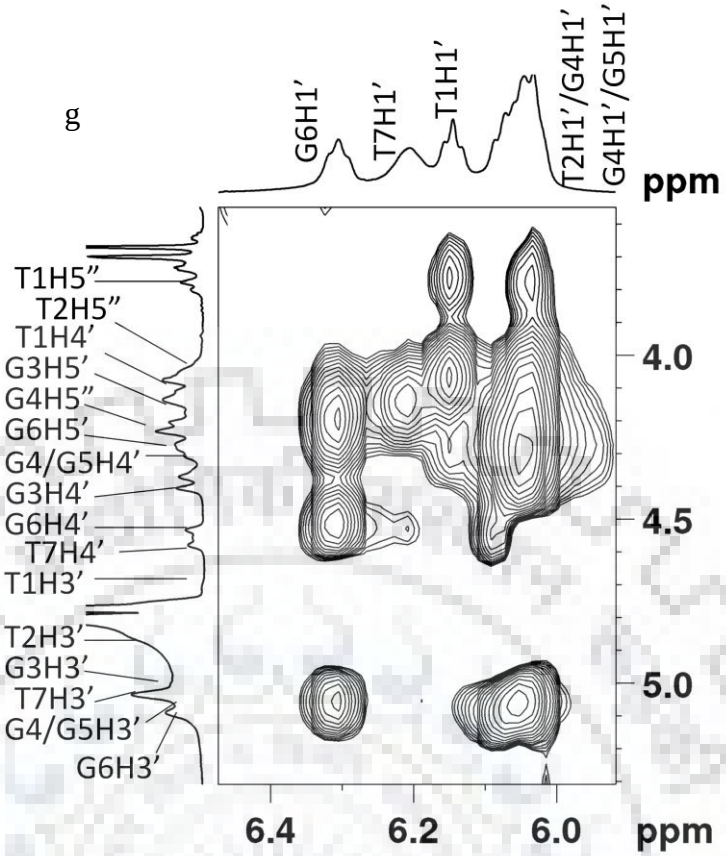
G6H1'
T7H1'
T1H1'
T2H1'/G4H1'
G4H1'/G5H1'
ppm
T1H5"
T2H5"
T1H4'
G3H5'
G4H5"
G6H5'
G4/G5H4'
G3H4'
G6H4'
T7H4'
T1H3'
T2H3'
G3H3'
T7H3'
G4/G5H3'
G6H3'
4.0
4.5
5.0
6.4
6.2
6.0
ppm

h

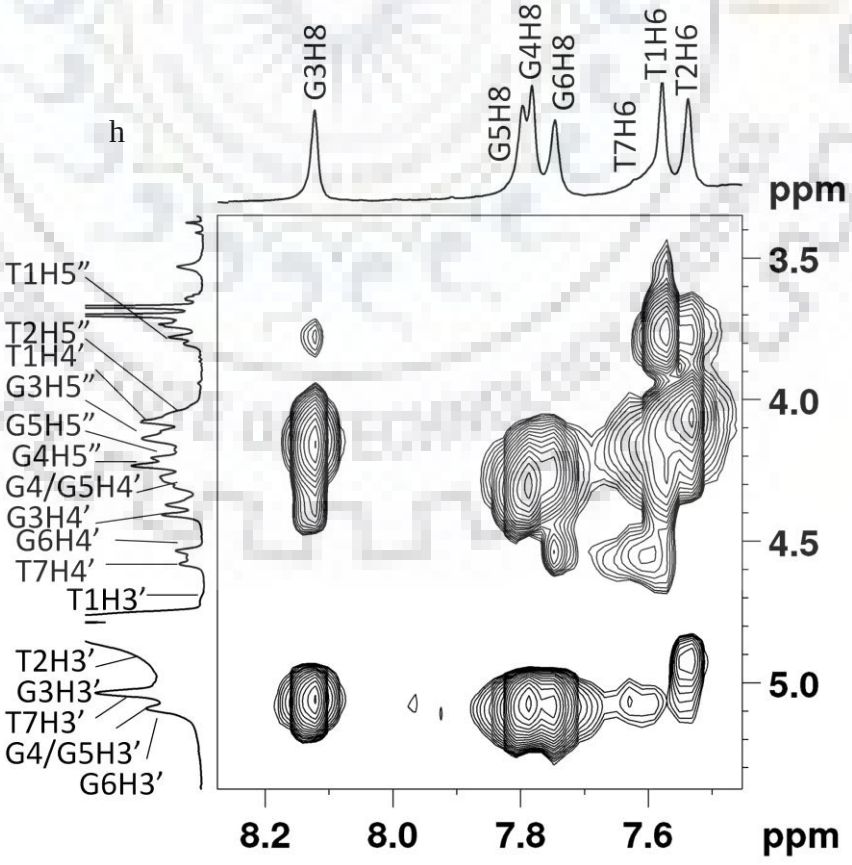
G3H8
G5H8
G4H8
G6H8
T7H6
T1H6
T2H6
ppm
T1H5"
T2H5"
T1H4'
G3H5"
G5H5"
G4H5"
G4/G5H4'
G3H4'
G6H4'
T7H4'
T1H3'
T2H3'
G3H3'
T7H3'
G4/G5H3'
G6H3'
3.5
4.0
4.5
5.0
8.2
8.0
7.8
7.6
ppm

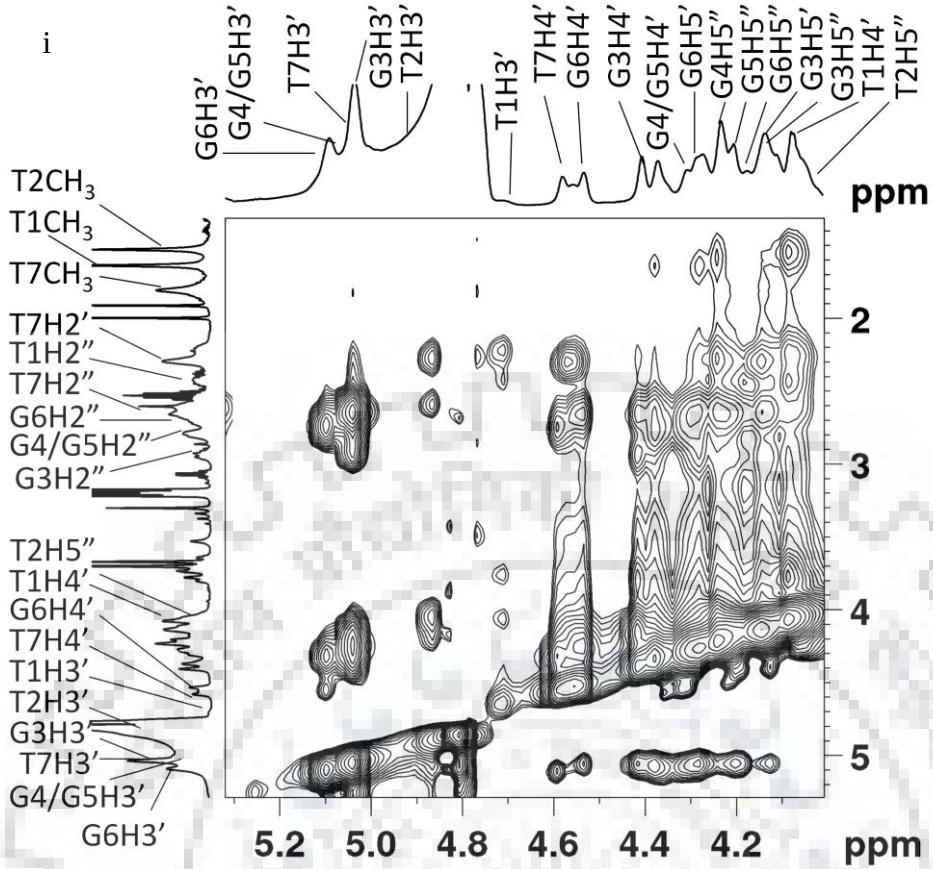
i
G6H3′
G4/G5H3′
T7H3′
G3H3′
T2H3′
T1H3′
T7H4′
G6H4′
G3H4′
G4/G5H4′
G6H5′
G4H5″
G5H5″
G6H5″
G3H5′
G3H5″
T1H4′
T2H5″
ppm
T2CH3
T1CH3
T7CH3
T7H2′
T1H2″
T7H2″
G6H2″
G4/G5H2″
G3H2″
T2H5″
T1H4′
G6H4′
T7H4′
T1H3′
T2H3′
G3H3′
T7H3′
G4/G5H3′
G6H3′
2
3
4
5
5.2
5.0
4.8
4.6
4.4
4.2
ppm

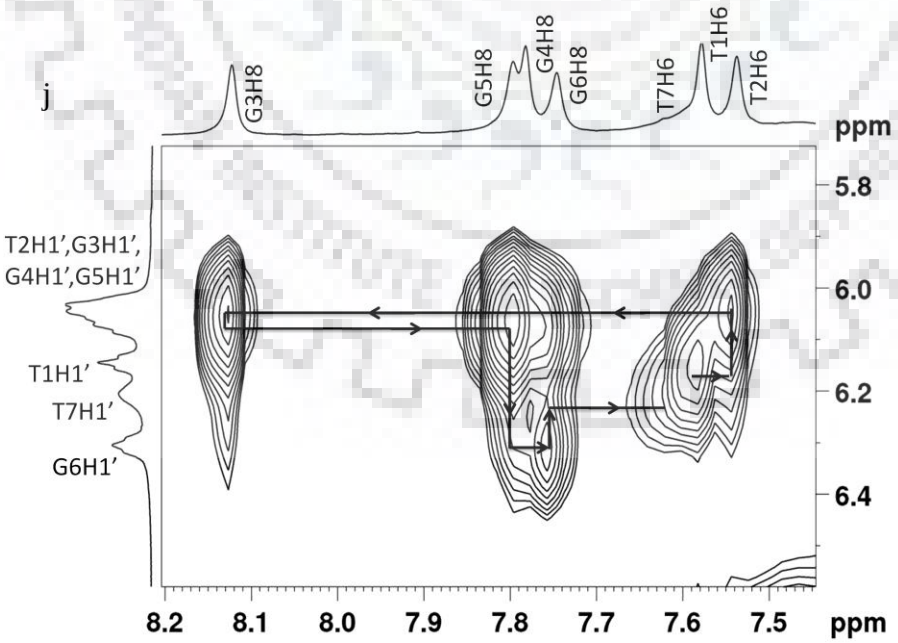
j
G3H8
G5H8
G4H8
G6H8
T7H6
T1H6
T2H6
ppm
T2H1′,G3H1′,
G4H1′,G5H1′
T1H1′
T7H1′
G6H1′
5.8
6.0
6.2
6.4
8.2
8.1
8.0
7.9
7.8
7.7
7.6
7.5
ppm

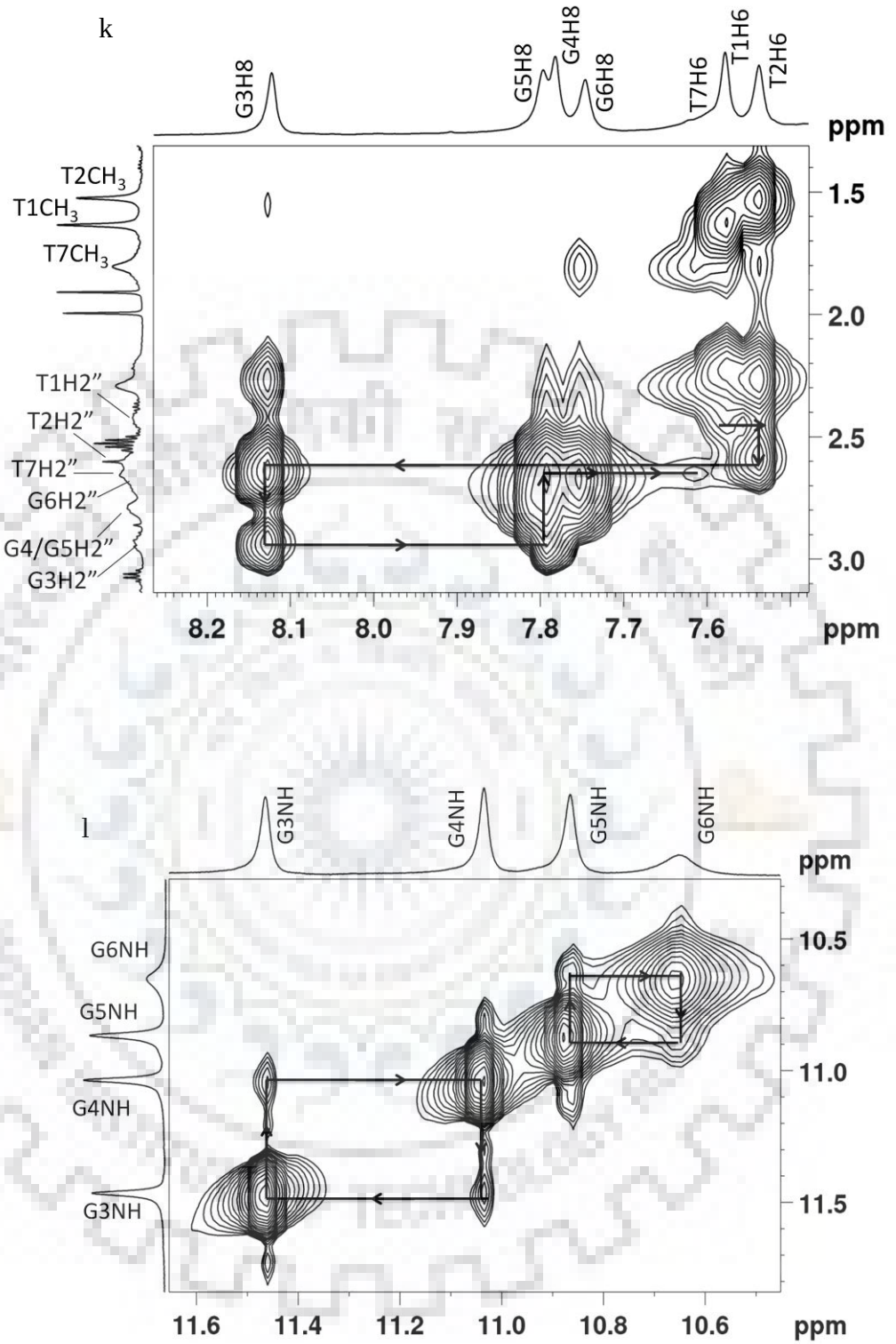
k
G3H8
G5H8
G4H8
G6H8
T7H6
T1H6
T2H6
ppm
T2CH3
T1CH3
T7CH3
T1H2″
T2H2″
T7H2″
G6H2″
G4/G5H2″
G3H2″
1.5
2.0
2.5
3.0
8.2
8.1
8.0
7.9
7.8
7.7
7.6
ppm
l
G3NH
G4NH
G5NH
G6NH
ppm
G6NH
G5NH
G4NH
G3NH
10.5
11.0
11.5
11.6
11.4
11.2
11.0
10.8
10.6
ppm

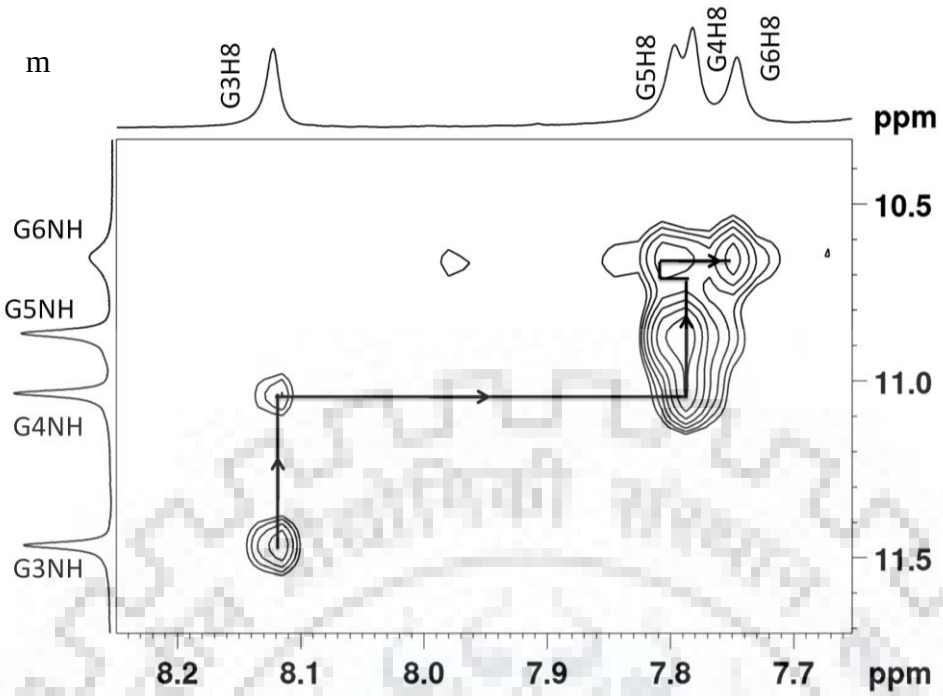

Figure 7.5 a) 1D ^{1}H NMR spectrum of free 4'-epiadriamycin in water (90% H_2O+10% D_2O) at 25 °C. b-c) ^{1}H NMR spectrum of 4'-epiadriamycin-Tet7 complex at D/N = 2.0 in KBPES buffer; ^{1}H NMR spectra of Tet7 and its complex upon progressive addition of 4'-epiadriamycin to DNA at different D/N ratios showing d) Imino, base and sugar H1' protons along with ring D aromatic protons 1H, 2H and 3H; e) Deoxyribose sugar H2'/2" and methyl protons of thymine along with drug protons at 25 °C. Symbol # denotes 4'-epiadriamycin protons. f-i) Expansion of ^{1}H-^{1}H 2D NOESY spectra of 4'-epiadriamycin-Tet7 complex complex at D/N = 2.0 ; and sequential connectivity (black arrows) between j) imino protons; k) adjacent imino and base protons; l) base-sugar (H1') protons; and m) base-sugar (H2'/2") protons at τ_m = 250 ms in KBPES buffer (90% H_2O+10% D_2O) at 25 °C.

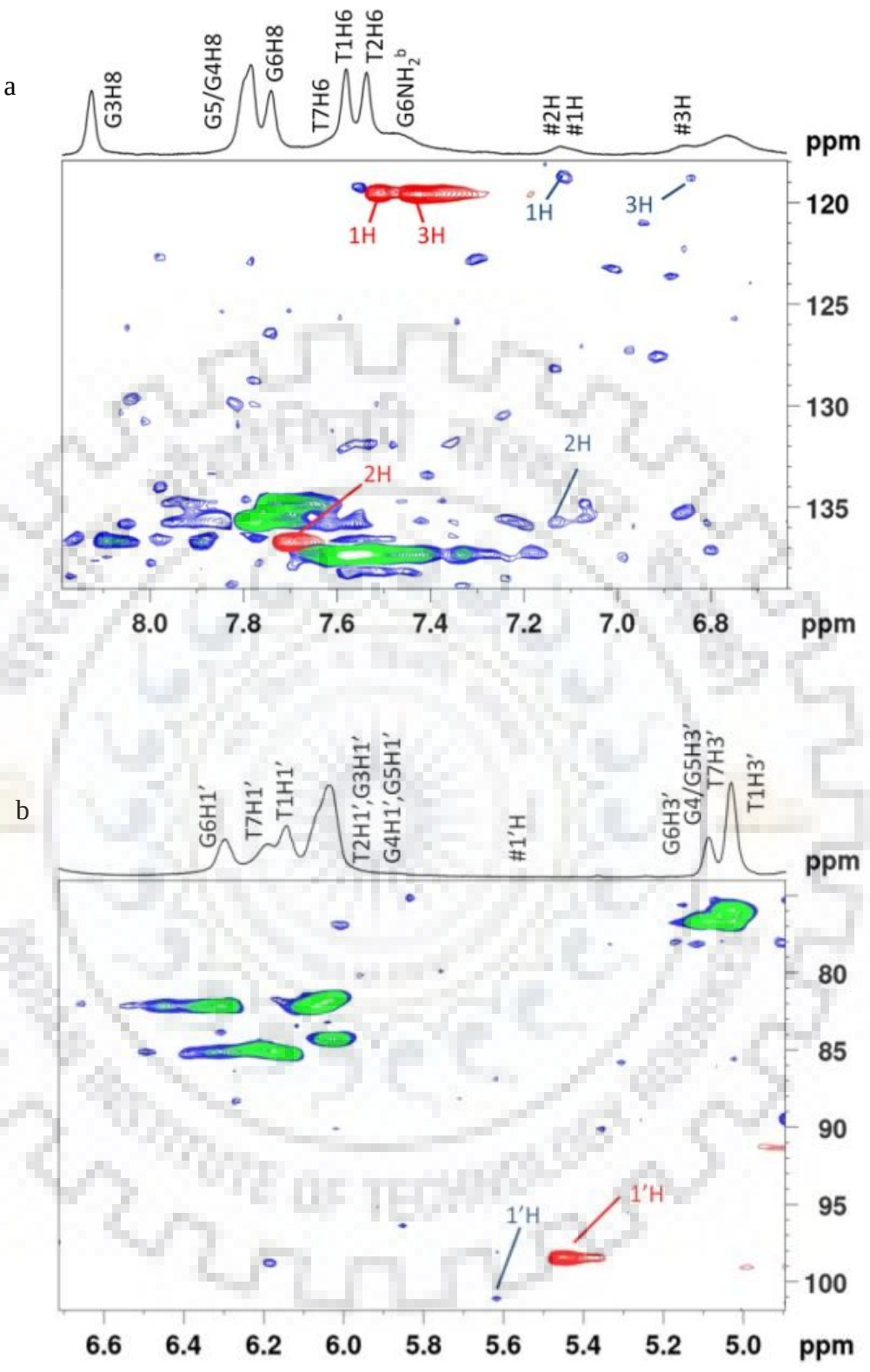
a
G3H8
G5/G4H8
G6H8
T7H6
T1H6
T2H6
G6NH2 b
#2H
#1H
#3H
ppm
1H
3H
1H
3H
120
125
130
135
2H
2H
8.0
7.8
7.6
7.4
7.2
7.0
6.8
ppm
b
G6H1'
T7H1'
T1H1'
T2H1',G3H1'
G4H1',G5H1'
#1'H
G6H3'
G4/G5H3'
T7H3'
T1H3'
ppm
80
85
90
95
100
1'H
1'H
6.6
6.4
6.2
6.0
5.8
5.6
5.4
5.2
5.0
ppm

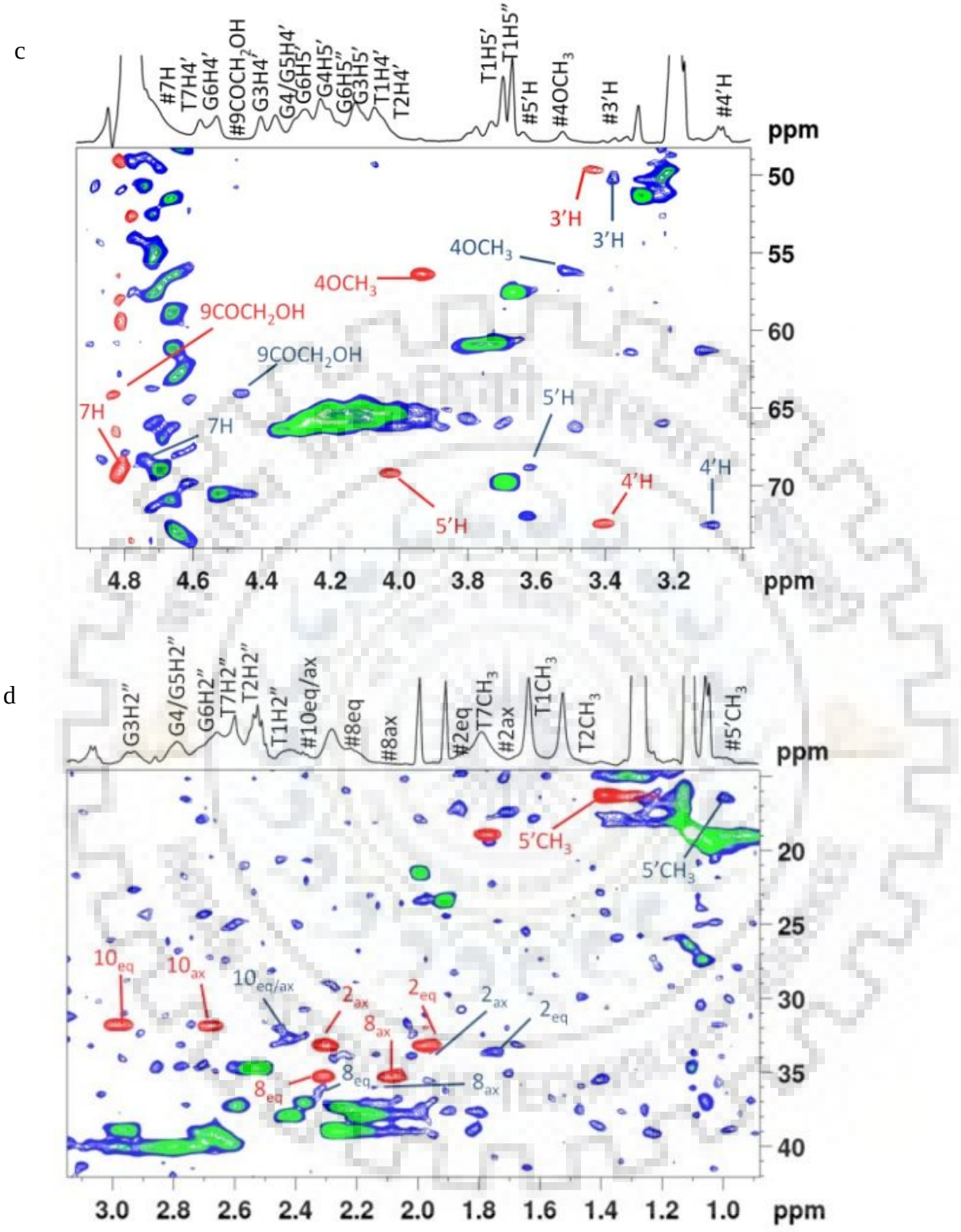

Figure 7.6 a-d) Expansion of specific region of 2D ^{1}H-^{13}C HSQC spectrum showing overlay of free 4'-epiadriamycin (red), free Tet7 (green) and 4'-epiadriamycin-Tet7complex at D/N = 2.0 (blue) in KBPES buffer (90% H_2O+10% D_2O) at 25 °C.1D ^{1}H NMR spectrum at the top of HSQC spectra is 4'-epiadriamycin-Tet7 complex at D/N = 2.0.

Table 7.3 ^{1}H Chemical shift (ppm) of 4'-epiadriamycin protons in free 4'-epiadriamycin (δ_f) and in 4'-epiadriamycin-Tet7complex (δ_b) at various D/N ratios in KBPES buffer containing 100 mM KCl (90% H_2O+10% D_2O) at 25 °C. $\Delta\delta = \delta_b - \delta_f$, nd: not determined.

Protons	Free Epiadriamycin	D/N=1.0		D/N=2.0		D/N=3.0		D/N=4.0	
	δ_f	δ_b	$\Delta\delta$	δ_b	$\Delta\delta$	δ_b	$\Delta\delta$	δ_b	$\Delta\delta$
2H	7.69	7.08	-0.61	7.11	-0.58	7.11	-0.58	7.10	-0.59
1H	7.49	7.12	-0.37	7.08	-0.41	7.11	-0.38	7.12	-0.37
3H	7.41	6.85	-0.56	6.87	-0.54	6.87	-0.54	6.88	-0.53
4OCH_3	3.93	3.52	-0.41	3.52	-0.41	3.53	-0.40	3.53	-0.40
1'H	5.45	5.61	0.16	5.61	0.16	nd	nd	nd	nd
7H	4.82	nd	-	4.74	-0.08	4.66	-0.16	4.68	-0.14
5'H	4.02	3.63	-0.39	3.62	-0.40	3.66	-0.36	3.69	-0.33
4'H	3.39	3.12	-0.27	3.08	-0.31	3.17	-0.22	3.16	-0.23
3'H	3.42	3.37	-0.05	3.37	-0.05	3.41	-0.01	3.38	-0.04
5'CH_3	1.38	0.99	-0.39	1.00	-0.38	1.01	-0.37	1.08	-0.30
9$COCH_2OH$	4.83	4.46	-0.37	4.46	-0.37	4.48	-0.35	4.53	-0.30
2'axH	1.96	1.64	-0.32	1.75	-0.21	1.71	-0.25	1.79	-0.17
2'eqH	2.29	1.94	-0.35	1.95	-0.34	1.97	-0.32	1.93	-0.36
8eqH	2.30	nd	nd	2.31	0.01	2.37	0.07	nd	nd
8axH	2.07	2.17	0.10	2.14	0.07	2.20	0.13	nd	nd
10eqH	2.97	2.50	-0.47	2.45	-0.52	2.47	-0.5	2.50	-0.47
10axH	2.66	2.50	-0.16	2.45	-0.21	2.47	-0.19	2.50	-0.16

Table 7.4 ^{1}H Chemical shift (ppm) of protons in 4'epiadriamycin-Tet7complex (δ_b) at various D/N ratios in KBPES buffer containing 100 mM KCl (90% H_2O+10% D_2O) at 25 °C. $\Delta\delta = \delta_b - \delta_f$. Negative sign in $\Delta\delta$ denotes upfield shift.

D/N	RESIDUES	T1		T2		G3		G4		G5		G6		T7	
	PROTONS	δ_b	$\Delta\delta$	δ_b	$\Delta\delta$	δ_b	$\Delta\delta$	δ_b	$\Delta\delta$	δ_b	$\Delta\delta$	δ_b	$\Delta\delta$	δ_b	$\Delta\delta$
1.0	H8/H6	7.57	-0.01	7.53	-0.01	8.14	0.00	7.79	-0.01	7.82	-0.02	7.73	0.03	7.49	0.16
	H1'	6.14	0.00	6.04	0.00	6.06	0.01	6.07	-0.01	6.08	-0.05	6.28	0.05	6.18	0.13
	H2'	2.20	0.00	2.28	0.01	2.66	0.01	2.63	0.04	2.74	0.02	2.63	0.08	2.26	0.11
	H2"	2.43	0.02	2.61	0.01	2.95	0.00	2.69	0.00	2.79	0.00	2.69	0.02	2.24	0.07
	H3'	4.66	0.01	4.91	0.01	5.06	0.01	5.06	0.00	5.07	-0.01	5.08	0.04	4.51	0.05
	H4'	4.07	0.01	4.02	-0.01	4.41	0.01	4.30	0.01	4.31	0.01	4.54	0.03	-	-
	H5'	3.78	0.01	4.07	0.01	4.16	0.01	4.23	0.00	4.38	0.01	4.28	-0.01	-	-
	H5"	3.72	0.01	4.04	0.01	4.12	0.01	4.26	-0.02	4.28	0.01	4.18	-0.01	-	-
	CH_3	1.63	-0.02	1.54	0.01	-	-	-	-	-	-	-	-	1.73	0.11
	NH_2^{b}	-	-	-	-	9.83	-0.02	9.14	-0.05	9.24	0.07	7.46	-0.01	-	-
	NH_2^{nb}	-		-	-	6.22	-0.06	6.16	-0.04	6.16	-0.08	6.76	0.00	-	-
	NH	-	-	-	-	11.50	-0.01	11.06	-0.02	10.90	-0.04	10.77	-0.12	-	-
2.0	H8/H6	7.59	0.01	7.54	0.00	8.12	-0.02	7.78	-0.02	7.80	-0.04	7.75	0.05	7.62	0.29
	H1'	6.16	0.02	6.04	0.00	6.05	0.00	6.07	-0.01	6.08	-0.05	6.32	0.09	6.21	0.16
	H2'	2.24	0.04	2.27	0.00	2.65	0.00	2.61	0.02	2.68	-0.04	2.64	0.09	2.30	0.15
	H2"	2.42	0.01	2.59	-0.01	2.95	0.00	2.71	0.02	2.80	0.01	2.70	0.03	2.65	0.48
	H3'	4.68	0.03	4.92	0.02	5.05	0.00	5.07	0.01	5.08	0.00	5.09	0.05	5.06	0.60
	H4'	4.08	0.02	4.05	0.02	4.40	0.00	4.29	0.00	4.30	0.00	4.53	0.02	4.55	0.49
	H5'	3.76	-0.01	4.06	0.00	4.14	-0.01	4.23	0.00	4.37	0.00	4.29	0.00	-	-
	H5"	3.74	0.03	4.03	0.00	4.12	0.01	4.28	0.00	4.27	0.00	4.19	0.00	-	-
	CH_3	1.64	-0.01	1.54	0.01	-	-	-	-	-	-	-	-	1.81	0.19
	NH_2^{b}	-	-	-	-	9.82	-0.03	9.18	-0.01	9.10	-0.07	7.46	-0.01	-	-
	NH_2^{nb}	-	-	-	-	6.20	-0.08	6.13	-0.07	6.13	-0.11	6.76	0.00	-	-
	NH	-	-	-	-	11.47	-0.04	11.04	-0.04	10.86	-0.08	10.65	-0.24	-	-

Table 7.5 ^{1}H Chemical shift (ppm) of protons in 4'epiadriamycin-Tet7complex (δ_b) at various D/N ratios in KBPES buffer containing 100 mM KCl (90% H_2O+10% D_2O) at 25 °C. $\Delta\delta = \delta_b - \delta_f$. Negative sign in $\Delta\delta$ denotes upfield shift.

D/N	RESIDUES	T1		T2		G3		G4		G5		G6		T7	
	PROTONS	δ_b	$\Delta\delta$	δ_b	$\Delta\delta$	δ_b	$\Delta\delta$	δ_b	$\Delta\delta$	δ_b	$\Delta\delta$	δ_b	$\Delta\delta$	δ_b	$\Delta\delta$
3.0	H8/H6	7.58	0.00	7.54	0.00	8.12	-0.02	7.79	-0.01	7.78	-0.06	7.75	0.05	7.62	0.29
	H1'	6.15	0.01	6.05	0.01	6.04	-0.01	6.06	-0.02	6.07	-0.06	6.31	0.08	6.22	0.17
	H2'	2.22	0.02	2.26	-0.01	2.63	-0.02	2.64	0.05	2.77	0.05	2.63	0.08	2.25	0.10
	H2"	2.46	0.05	2.59	-0.01	2.93	-0.02	2.73	0.04	2.86	0.07	2.70	0.03	2.30	0.13
	H3'	4.62	-0.03	4.92	0.02	5.04	-0.01	5.05	-0.01	5.06	-0.02	5.08	0.04	4.54	0.08
	H4'	4.08	0.02	4.01	-0.02	4.39	-0.01	4.29	0.00	4.30	0.00	4.52	0.01	4.17	0.11
	H5'	3.76	-0.01	4.05	-0.01	4.15	0.00	4.23	0.00	4.37	0.00	4.29	0.00	-	-
	H5"	3.72	0.01	4.06	0.03	4.11	0.00	4.28	0.00	4.27	0.00	4.19	0.00	-	-
	CH_3	1.62	-0.03	1.53	0.00	-	-	-	-	-	-	-	-	1.82	0.20
	NH_2^{b}	-	-	-	-	9.82	-0.03	9.08	-0.11	9.14	-0.03	7.46	-0.01	-	-
	NH_2^{nb}	-	-	-	-	6.21	-0.07	6.11	-0.09	6.11	-0.13	6.76	0.00	-	-
	NH	-	-	-	-	11.45	-0.06	11.03	-0.05	10.85	-0.09	10.62	-0.27	-	-
4.0	H8/H6	7.58	0.00	7.54	0.00	8.12	-0.02	7.78	-0.02	7.77	-0.07	7.74	0.04	7.63	0.30
	H1'	6.16	0.02	6.04	0.00	6.03	-0.02	6.05	-0.03	6.08	-0.05	6.30	0.07	6.22	0.17
	H2'	2.22	0.02	2.26	-0.01	2.63	-0.02	2.64	0.05	2.77	0.05	2.63	0.08	2.25	0.10
	H2"	2.46	0.05	2.59	-0.01	2.93	-0.02	2.73	0.04	2.86	0.07	2.70	0.03	2.30	0.13
	H3'	-	-	4.88	-0.02	5.04	-0.01	5.05	-0.01	5.06	-0.02	5.08	0.04	4.52	0.06
	H4'	4.08	0.02	4.03	0.00	4.37	-0.03	4.29	0.00	4.30	0.00	4.51	0.00	4.06	0.00
	H5'	3.77	0.00	4.06	0.00	4.15	0.00	4.23	0.00	4.37	0.00	4.29	0.00	4.15	0.06
	H5"	3.72	0.01	4.03	0.00	4.11	0.00	4.28	0.00	4.27	0.00	4.19	0.00	4.08	0.04
	CH_3	1.62	-0.03	1.52	-0.01	-	-	-	-	-	-	-	-	1.82	0.20
	NH_2^{b}	-	-	-	-	9.80	-0.05	9.07	-0.12	9.12	-0.05	7.46	-0.01	-	-
	NH_2^{nb}	-	-	-	-	6.19	-0.09	6.09	-0.11	6.09	-0.15	6.76	0.00	-	-
	NH	-	-	-	-	11.44	-0.07	11.02	-0.06	10.84	-0.10	10.60	-0.29	-	-

Table 7.6 ^{1}H Chemical shift (ppm) of methyl and imino protons in free Tet7 (δ_f) and 4'epiadriamycin-Tet7 complex (δ_b) at various D/N ratios in KBPES buffer containing 100 mM KCl (90% H_2O+10% D_2O) at 25 °C. $\Delta\delta = \delta_b - \delta_f$. Negative sign in $\Delta\delta$ denotes upfield shift.

Protons	CH_3						NH							
	T1		T2		T7		G3		G4		G5		G6	
Free DNA (δ_f)	1.65		1.53		1.62		11.51		11.08		10.94		10.89	
	δ_b	$\Delta\delta$	δ_b	$\Delta\delta$	δ_b	$\Delta\delta$	δ_b	$\Delta\delta$	δ_b	$\Delta\delta$	δ_b	$\Delta\delta$	δ_b	$\Delta\delta$
D/N=0.2	1.65	0.00	1.53	0.00	1.64	0.02	11.50	-0.01	11.08	0.00	10.93	-0.01	10.88	-0.01
D/N=0.5	1.65	0.00	1.53	0.00	1.65	0.03	11.50	-0.01	11.07	-0.01	10.92	-0.02	10.85	-0.04
D/N=0.8	1.65	0.00	1.53	0.00	1.71	0.09	11.49	-0.02	11.06	-0.02	10.90	-0.04	10.81	-0.08
D/N=1.0	1.63	-0.02	1.54	0.01	1.73	0.11	11.50	-0.01	11.06	-0.02	10.90	-0.04	10.77	-0.12
D/N=1.5	1.64	-0.01	1.53	0.00	1.78	0.16	11.47	-0.04	11.04	-0.04	10.87	-0.07	10.68	-0.21
D/N=2.0	1.64	-0.01	1.54	0.01	1.81	0.19	11.47	-0.04	11.04	-0.04	10.86	-0.08	10.65	-0.24
D/N=2.5	1.63	-0.02	1.52	-0.01	1.80	0.18	11.46	-0.05	11.03	-0.05	10.86	-0.08	10.64	-0.25
D/N=3.0	1.62	-0.03	1.53	0.00	1.82	0.2	11.45	-0.06	11.03	-0.05	10.85	-0.09	10.62	-0.27
D/N=3.5	1.62	-0.03	1.52	-0.01	1.83	0.21	11.43	-0.08	11.01	-0.07	10.84	-0.10	10.60	-0.29
D/N=4.0	1.62	-0.03	1.52	-0.01	1.82	0.20	11.44	-0.07	11.02	-0.06	10.84	-0.10	10.60	-0.29

Table 7.7 ^{1}H Chemical shift (ppm) of base protons in free Tet7 (δ_f) and 4'-epiadriamycin-Tet7complex (δ_b) at various D/N ratios in KBPES buffer containing 100 mM KCl (90% H_2O+10% D_2O)at 25 °C. $\Delta\delta = \delta_b - \delta_f$. Negative sign in $\Delta\delta$ denotes upfield shift.

Protons	H8/H6													
	T1		T2		G3		G4		G5		G6		T7	
Free DNA (δ_f)	7.58		7.54		8.14		7.80		7.84		7.70		7.33	
	δ_b	$\Delta\delta$	δ_b	$\Delta\delta$	δ_b	$\Delta\delta$	δ_b	$\Delta\delta$	δ_b	$\Delta\delta$	δ_b	$\Delta\delta$	δ_b	$\Delta\delta$
D/N=0.2	7.58	0.00	7.54	0.00	8.14	0.00	7.80	0.00	7.84	0.00	7.71	0.01	7.34	0.01
D/N=0.5	7.58	0.00	7.54	0.00	8.14	0.00	7.79	-0.01	7.83	-0.01	7.72	0.02	7.36	0.03
D/N=0.8	7.58	0.00	7.54	0.00	8.13	-0.01	7.79	-0.01	7.82	-0.02	7.72	0.02	7.39	0.06
D/N=1.0	7.57	-0.01	7.53	0.01	8.14	0.00	7.79	-0.01	7.82	-0.02	7.73	0.03	7.49	0.16
D/N=1.5	7.57	-0.01	7.53	-0.01	8.12	-0.02	7.78	-0.02	7.80	-0.04	7.73	0.03	7.52	0.19
D/N=2.0	7.59	0.01	7.54	0.00	8.12	-0.02	7.78	-0.02	7.80	-0.04	7.75	0.05	7.62	0.29
D/N=2.5	7.57	-0.01	7.53	-0.01	8.11	-0.03	7.78	-0.02	7.79	-0.05	7.74	0.04	7.61	0.28
D/N=3.0	7.58	0.00	7.54	0.00	8.12	-0.02	7.79	-0.01	7.78	-0.06	7.75	0.05	7.62	0.29
D/N=3.5	7.57	-0.01	7.53	-0.01	8.10	-0.04	7.77	-0.03	7.77	-0.07	7.74	0.04	7.63	0.30
D/N=4.0	7.58	0.00	7.54	0.00	8.12	-0.02	7.78	-0.02	7.77	-0.07	7.74	0.04	7.63	0.30

Table 7.8 ^{1}H Chemical shift (ppm) of H1' sugar protons in free Tet7 (δ_f) and 4'-epiadriamycin-Tet7 complex (δ_b) at various D/N ratios in KBPES buffer containing 100 mM KCl (90% H_2O+10% D_2O) at 25 °C. $\Delta\delta = \delta_b - \delta_f$. Negative sign in $\Delta\delta$ denotes upfield shift.

Protons	H1'					
	T1		G6		T7	
Free DNA (δ_f)	6.14		6.23		6.05	
	δ_b	$\Delta\delta$	δ_b	$\Delta\delta$	δ_b	$\Delta\delta$
D/N=0.2	6.14	0.00	6.25	0.02	6.08	0.03
D/N=0.5	6.14	0.00	6.26	0.03	6.09	0.04
D/N=0.8	6.14	0.00	6.27	0.04	6.09	0.04
D/N=1.0	6.14	0.00	6.28	0.05	6.18	0.13
D/N=1.5	6.14	0.00	6.29	0.06	6.19	0.14
D/N=2.0	6.16	0.02	6.32	0.09	6.21	0.16
D/N=2.5	6.14	0.00	6.30	0.07	6.21	0.16
D/N=3.0	6.15	0.01	6.31	0.08	6.22	0.17
D/N=3.5	6.15	0.01	6.30	0.07	6.22	0.17
D/N=4.0	6.16	0.02	6.30	0.07	6.22	0.17

Table 7.9 ^{1}H Chemical shift (ppm) of 4'-epiadriamycin protons in a free state (δ_f) and in 4'-epiadriamycin-Tet7 complex (δ_b) at various D/N ratios in KBPES buffer containing 100 mM KCl (90% H_2O+10% D_2O) at 25 °C. $\Delta\delta = \delta_b - \delta_f$. Negative sign in $\Delta\delta$ denotes upfield shift.

Protons	Epiadriamycin							
	1H		2H		3H		5'CH_3	
Free Epiadriamycin (δ_f)	7.49		7.69		7.41		1.38	
	δ_b	$\Delta\delta$	δ_b	$\Delta\delta$	δ_b	$\Delta\delta$	δ_b	$\Delta\delta$
D/N=0.2	7.08	-0.41	7.12	-0.57	6.84	-0.57	0.85	-0.53
D/N=0.5	7.08	-0.41	7.12	-0.57	6.84	-0.57	0.89	-0.49
D/N=0.8	7.08	-0.41	7.12	-0.57	6.84	-0.57	0.98	-0.40
D/N=1.0	7.08	-0.41	7.12	-0.57	6.85	-0.56	0.99	-0.39
D/N=1.5	7.10	-0.39	7.12	-0.57	6.86	-0.55	1.00	-0.38
D/N=2.0	7.11	-0.38	7.11	-0.58	6.87	-0.54	1.02	-0.36
D/N=2.5	7.12	-0.37	7.13	-0.56	6.87	-0.54	1.05	-0.33
D/N=3.0	7.11	-0.38	7.11	-0.58	6.87	-0.54	1.01	-0.37
D/N=3.5	7.11	-0.38	7.11	-0.58	6.87	-0.54	1.05	-0.33
D/N=4.0	7.12	-0.37	7.10	-0.59	6.88	-0.53	1.08	-0.30

a

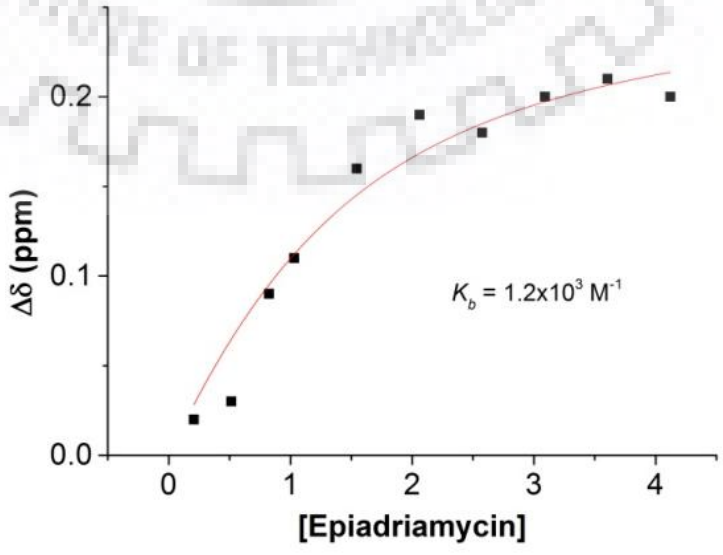

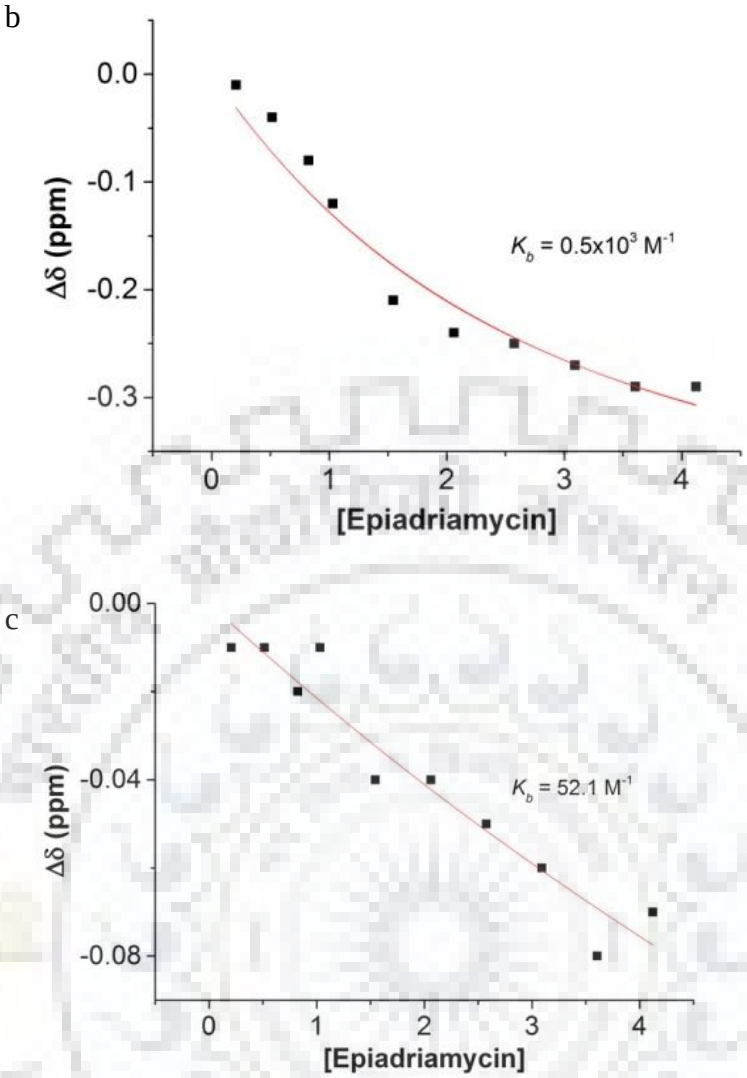

Figure 7.7 Nonlinear fitted curve (red) for simultaneous binding at two different sites in 4'-epiadriamycin-Tet7 complex of protons a) $T7CH_3$, b) G6NH and c) G3NH. The plot shows a change in chemical shift (Δδ) of protons at D/N = 0.2-4.0 as a function of 4'-epiadriamycin concentration (μM) showing binding constants (K_b) at 25 °C.

The initial addition of 0.2, 0.5, 0.8 and 1.0 mole equivalent of 4'-epiadriamycin to Tet7 resulted in a severe broadening of G6NH, T7H6, and $T7CH_3$ suggesting binding close to G6/T7 bases (Fig 7.5 b,c). Broadening is maximum at D/N = 0.8-1.0 and upon further addition of 4'-epiadriamycin, these spectral lines become sharp at D/N >2.5, perhaps due to a stoichiometry of ~2:1 in 4'-epiadriamycin-DNA complex (Fedoroff et al., 1998; Cocco et al., 2003; Gavathiotis et al., 2003; Scaglioni et al., 2016; Pradeep & Barthwal, 2016; Padmapriya & Barthwal, 2017; Kumar & Barthwal, 2018). T1H1' triplet appears as a sharp resonance as compared to the corresponding G6H1', T7H1' up to D/N =1.0 and shows line broadening

similar to G6H1', T7H1' at D/N>2.5. Similarly, T1CH_3, T2CH_3, and G3NH remain sharp resonance at initial stages of titration and show slight broadening at D/N >2.5 (Fig 7.5 b,c). Chemical shift perturbation in NMR spectra gives information of position, stability, and kinetics of binding events (Scaglioni et al., 2016; Pradeep & Barthwal, 2016; Padmapriya & Barthwal, 2017; Kumar & Barthwal, 2018). G6NH, T7CH_3, T7H1', T7H6 show significant chemical shift changes which drift continuously up to D/N = 2.0 beyond which they drift slightly. The upfield shift in GNH protons decreased in following order G6 (0.29 ppm) > G5 (0.10 ppm) > G3, G4 (0.07 ppm) (Table 7.4-7.6). The shift in G4NH/G5NH is minimal at earlier stages and is noticeable at D/N >2.0. It may be noted the G6NH shifts upfield by 0.29 ppm whereas T7H6, T7CH_3 and T7H1' shift downfield by 0.30 ppm, 0.20 ppm, and 0.17 ppm, respectively (Fig 7.5 b,c and Table 7.4-7.8). G6 base appears to experience better stacking interactions on complexation while T7 base may be destacked and the ligand may be binding at G6pT7 sites during the initial course of titration. The shifts in H6, H1' and methyl protons of T1/T2 are relatively much lesser. The shift in G3NH is apparent only at D/N >2.0. This suggests ligand binding near T1pT2pG3 sites at higher D/N values without significantly affecting DNA conformation. An estimate of the binding constant from the variation in the chemical shifts in G6NH, and T7CH_3 protons gives K_b ~0.5-1.2x10^3 M^{-1}. The change in G3NH proton yields much lower K_b ~5.2x10^1 M^{-1} so that binding at G6pT7 residues has higher affinity than at T1pT2pG3 sites (Fig. 7.7 a-c). The aromatic ring D protons (1H, 2H, 3H) of 4'-epiadriamycin show significant upfield shift up to 0.59 ppm. The shifts 10eq protons (0.47 ppm) are larger than corresponding shifts in 10ax protons. Such large upfield shifts may be due to the stacking of ring D and ring A with bases of Tet7. A significant upfield shift in 5'CH_3, 5'H, 4'H, and 2'eqH protons points towards the involvement of daunosamine sugar in binding (Table 7.3). Since all sequential NOE connectivities of base and deoxyribose sugar protons (Fig. 7.5 l,m) are intact, there is no possibility of classical intercalation. 4'-epiadriamycin protons remain broad which may be due to fast exchange among possible conformations at two sites on DNA which may be partially or fully occupied.

Progressive addition of adriamycin to 1.15 mM Tet7 in a separate experiment showed drift and broadening in specific proton signals of DNA with the appearance of new proton signals, which were assigned to protons of adriamycin. Unambiguous assignment of all Tet7 and adriamycin protons was achieved (Tables 7.3-7.9) by using proton NMR spectra of free Tet7 (Fig. 7.4 a-j), free 4'-adriamycin (Fig 7.8 a), adriamycin-Tet7 complex (Fig. 7.8 b-e), their corresponding ^{1}H-^{1}H NOESY (Fig. 7.8 f-m) and ^{1}H-^{13}C HSQC (Fig. 7.9 a-d) spectra. The overall trend of

shifts and broadening in DNA and drug protons was similar to that found in case of 4'-epiadriamycin although the magnitude of changes were different (Tables 7.10-7.15 and Fig. 7.8 b-e). G6NH is severely broadened and is observable only at D/N > 1.5. Unlike in the case of 4'-epiadriamycin, G3NH and G4NH also get broadened in initial stages of titration. T7H6, and $T7CH_3$ signals are severely broadened and appears as a distinct signal only at D/N = 2.0 (Fig. 7.8 d,e). On the other hand, $T2CH_3$ remains as sharp peak up to D/N = 2.0 and broadening is clearly apparent at D/N = 3.0-4.0. The changes in G6NH, $T7CH_3$, T7H6, G6H8, T7H1', and G6H1' get saturated at D/N = 2.0 (Tables 7.13-15). On the other hand shifts in $T1CH_3$ and $T2CH_3$ are apparent only at higher D/N values. The chemical shift of imino protons decreases in order of G6 (0.36 ppm) > G5,G3 (0.15 ppm) > G4 (0.12 ppm) (Tables 7.13). The aromatic protons of adriamycin 1H, 2H, 3H, 8eqH, 10eqH, 1'H and 7H which lie in the plane of ring ABCD show large upfield shifts (0.22-0.59 ppm) (Tables 7.10). Two binding sites may exist, one in which ring ABCD stacks with G6 base on pushing away T7 base and other along with T1pT2pG3 bases. The stacking with G6 base is however much stronger (G6NH, $\Delta\delta$ = 0.36 ppm) than that in case of 4'-epiadriamycin (G6NH, $\Delta\delta$ = 0.29 ppm). The binding constants obtained from chemical shift changes in G6NH, $T7CH_3$ ($2.3\text{-}5.7\times10^3$ M^{-1}) and G3NH (9.9×10^1 M^{-1}) protons (Fig. 7.10 a-c) are also slightly higher as compared to that in case of 4'-epiadriamycin (Fig. 7.7 a-c).

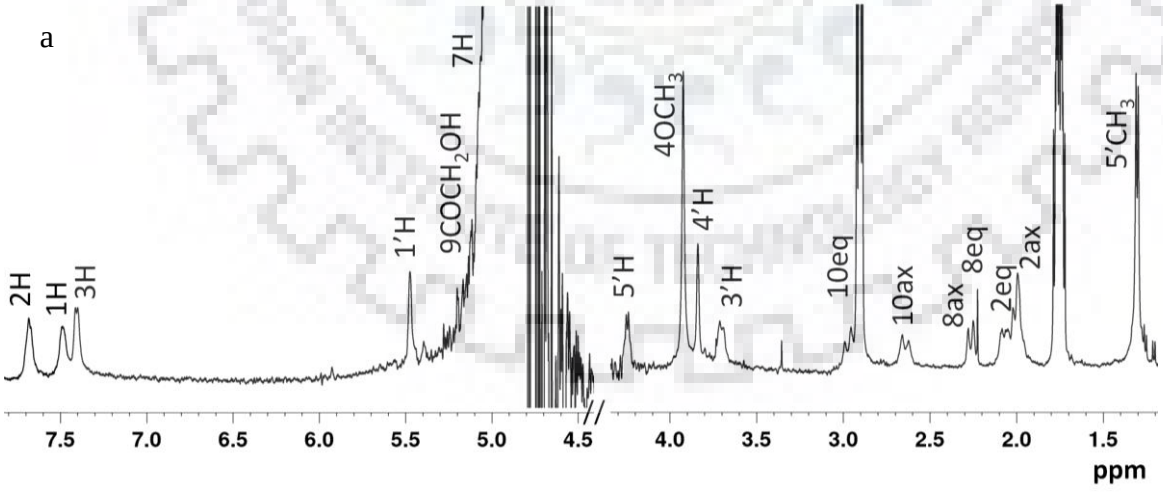

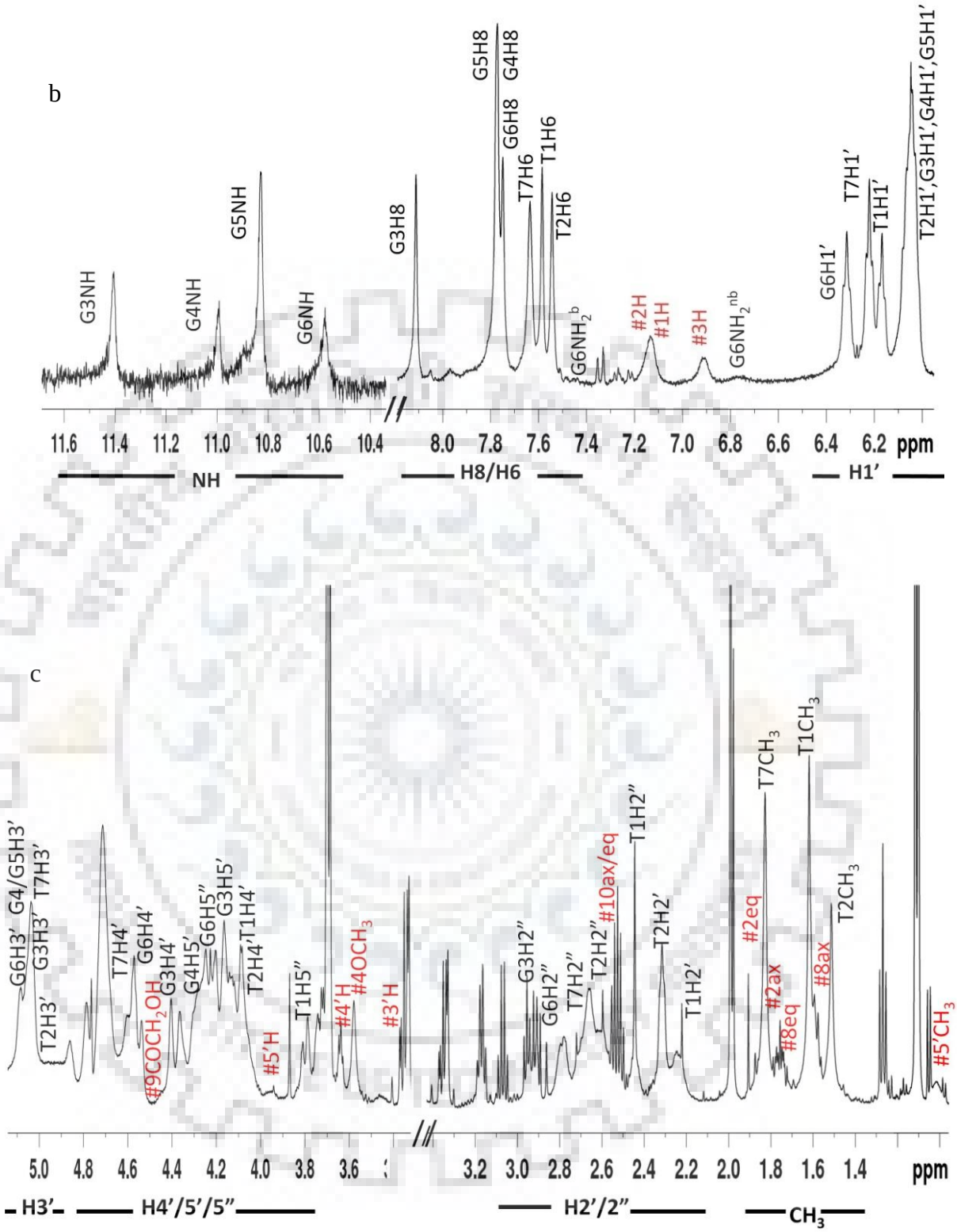
b
G3NH
G4NH
G5NH
G6NH
G3H8
G5H8
G4H8
G6H8
T7H6
T1H6
T2H6
G6NH2b
#2H
#1H
#3H
G6NH2nb
G6H1′
T7H1′
T1H1′
T2H1′,G3H1′,G4H1′,G5H1′
11.6 11.4 11.2 11.0 10.8 10.6 10.4 8.0 7.8 7.6 7.4 7.2 7.0 6.8 6.6 6.4 6.2 ppm
NH
H8/H6
H1′
c
G6H3′ G4/G5H3′ T7H3′
G3H3″
T2H3′
T7H4′
G6H4′
#9COCH2OH
G3H4′
G4H5′
G6H5″
G3H5′
T1H4′
T2H4′
#5′H
T1H5″
#4′H
#4OCH3
#3′H
G3H2″
G6H2″
T7H2″
T2H2″
#10ax/eq
T1H2″
T2H2′
T1H2′
#2eq
#2ax
#8eq
#8ax
T7CH3
T1CH3
T2CH3
#5′CH3
5.0 4.8 4.6 4.4 4.2 4.0 3.8 3.6 3.2 3.0 2.8 2.6 2.4 2.2 2.0 1.8 1.6 1.4 ppm
H3′
H4′/5′/5″
H2′/2″
CH3

d

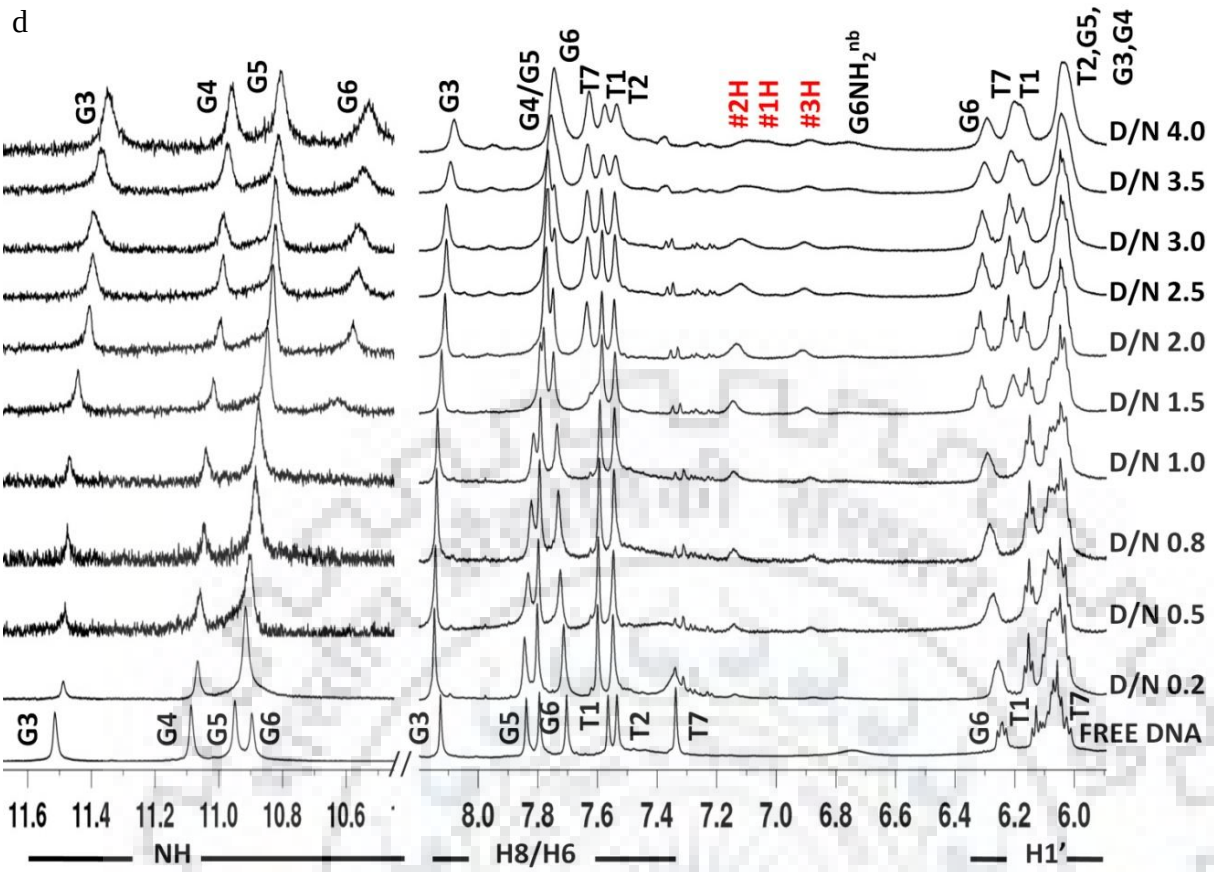
G3
G4
G5
G6
G4/G5
T7
T1
T2
#2H
#1H
#3H
G6NH2nb
T2,G5,
G3,G4
D/N 4.0
D/N 3.5
D/N 3.0
D/N 2.5
D/N 2.0
D/N 1.5
D/N 1.0
D/N 0.8
D/N 0.5
D/N 0.2
FREE DNA
11.6 11.4 11.2 11.0 10.8 10.6
8.0 7.8 7.6 7.4 7.2 7.0 6.8 6.6 6.4 6.2 6.0
NH
H8/H6
H1'

e

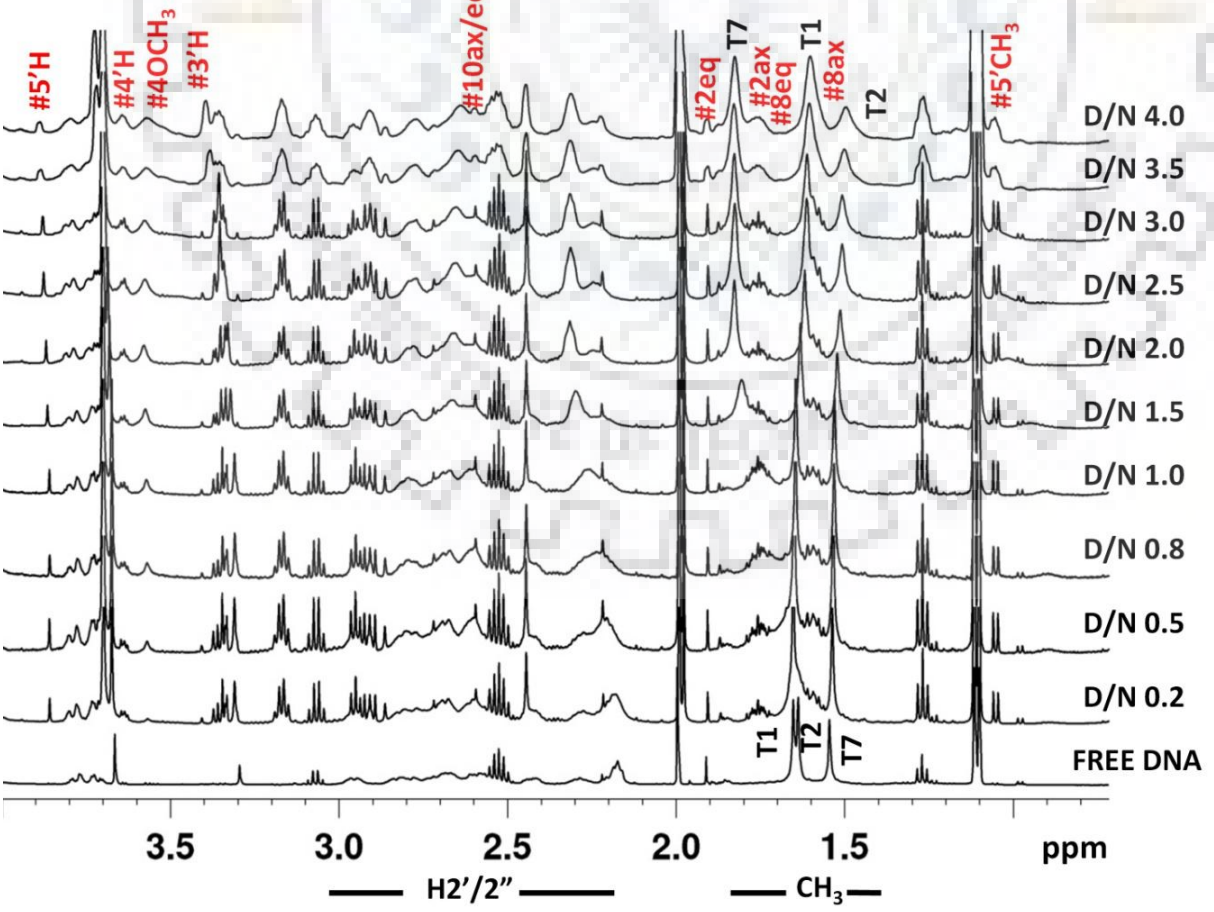
#5'H
#4'H
#4OCH3
#3'H
#10ax/eq
#2eq
T7
#2ax
#8eq
T1
#8ax
T2
#5'CH3
D/N 4.0
D/N 3.5
D/N 3.0
D/N 2.5
D/N 2.0
D/N 1.5
D/N 1.0
D/N 0.8
D/N 0.5
D/N 0.2
FREE DNA
3.5 3.0 2.5 2.0 1.5
ppm
H2'/2"
CH3

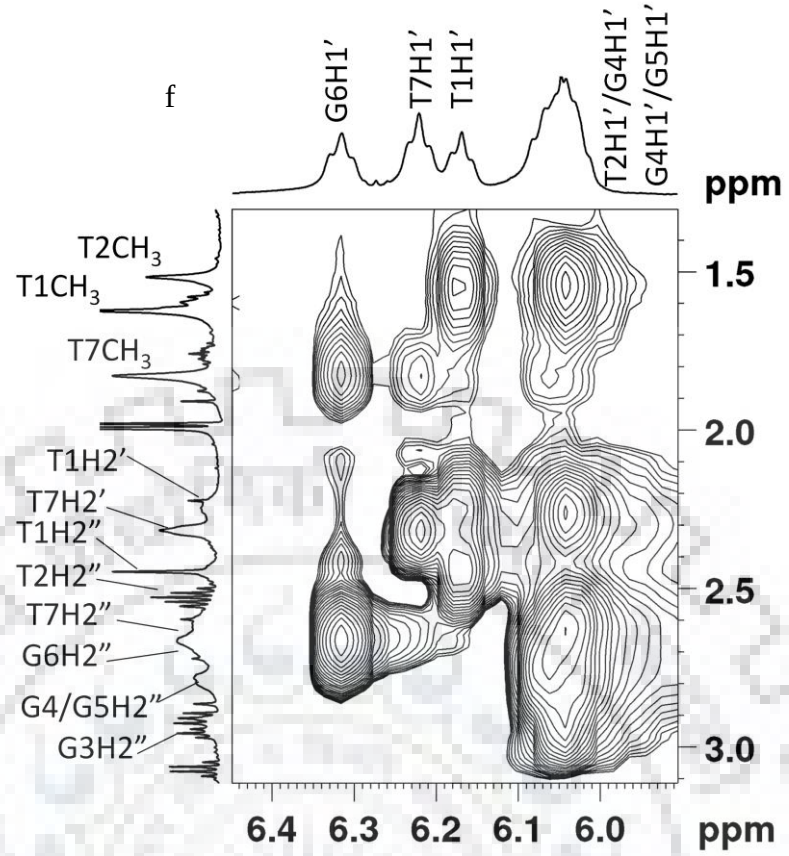
f
G6H1′
T7H1′
T1H1′
T2H1′/G4H1′
G4H1′/G5H1′
ppm
T2CH3
T1CH3
T7CH3
T1H2′
T7H2′
T1H2″
T2H2″
T7H2″
G6H2″
G4/G5H2″
G3H2″
1.5
2.0
2.5
3.0
6.4 6.3 6.2 6.1 6.0
ppm

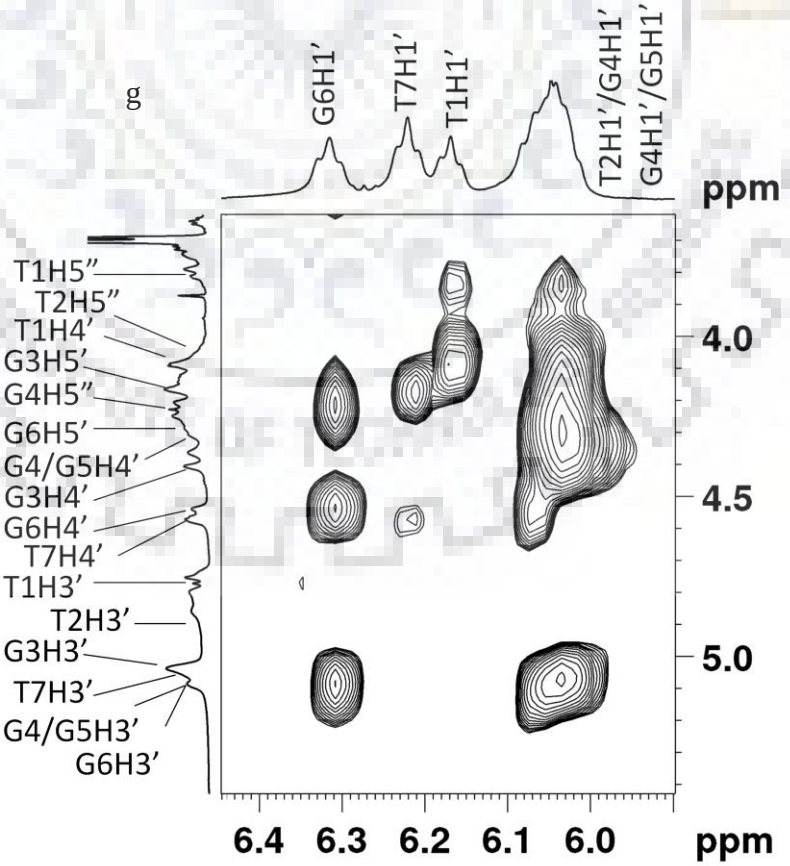
g
G6H1′
T7H1′
T1H1′
T2H1′/G4H1′
G4H1′/G5H1′
ppm
T1H5″
T2H5″
T1H4′
G3H5′
G4H5″
G6H5′
G4/G5H4′
G3H4′
G6H4′
T7H4′
T1H3′
T2H3′
G3H3′
T7H3′
G4/G5H3′
G6H3′
4.0
4.5
5.0
6.4 6.3 6.2 6.1 6.0
ppm

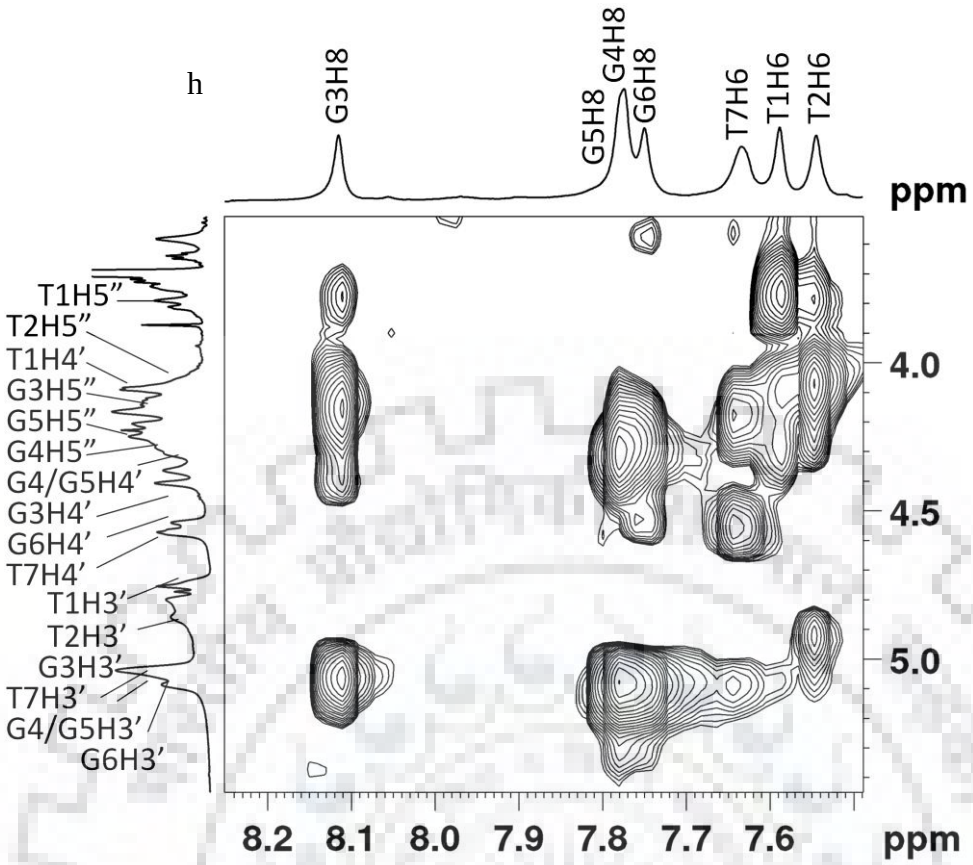
h
G3H8
G5H8
G4H8
G6H8
T7H6
T1H6
T2H6
ppm
T1H5″
T2H5″
T1H4′
G3H5″
G5H5″
G4H5″
G4/G5H4′
G3H4′
G6H4′
T7H4′
T1H3′
T2H3′
G3H3′
T7H3′
G4/G5H3′
G6H3′
4.0
4.5
5.0
8.2 8.1 8.0 7.9 7.8 7.7 7.6 ppm

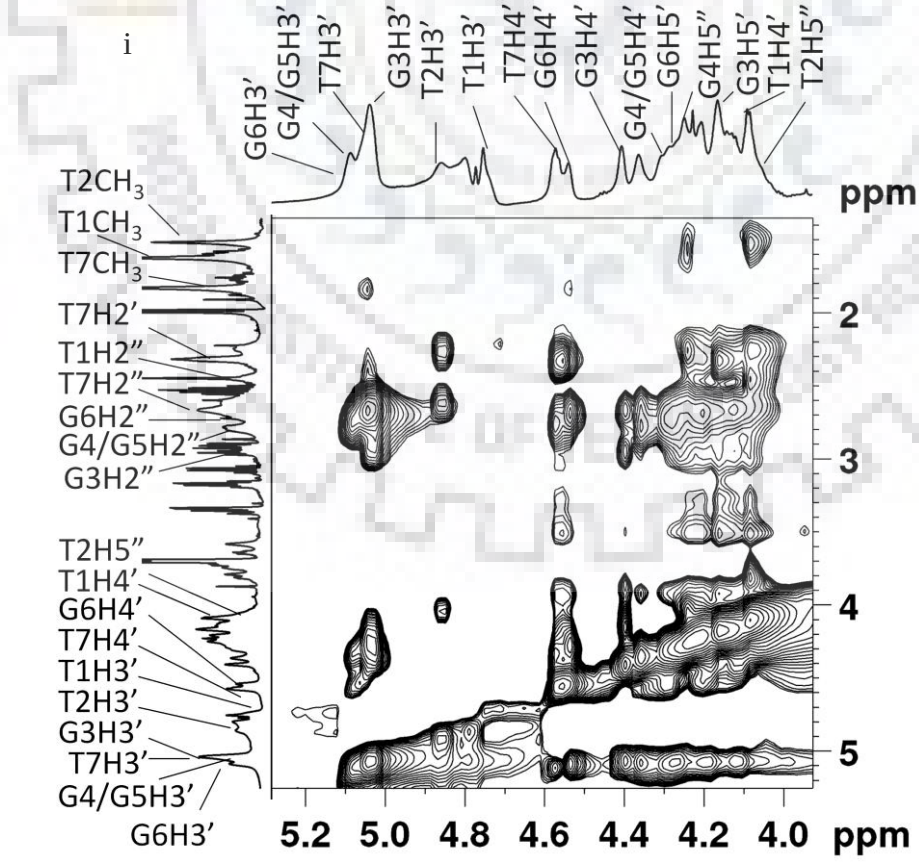
i
G6H3′
G4/G5H3′
T7H3′
G3H3′
T2H3′
T1H3′
T7H4′
G6H4′
G3H4′
G4/G5H4′
G6H5′
G4H5″
G3H5′
T1H4′
T2H5″
ppm
T2CH3
T1CH3
T7CH3
T7H2′
T1H2″
T7H2″
G6H2″
G4/G5H2″
G3H2″
T2H5″
T1H4′
G6H4′
T7H4′
T1H3′
T2H3′
G3H3′
T7H3′
G4/G5H3′
G6H3′
2
3
4
5
5.2 5.0 4.8 4.6 4.4 4.2 4.0 ppm

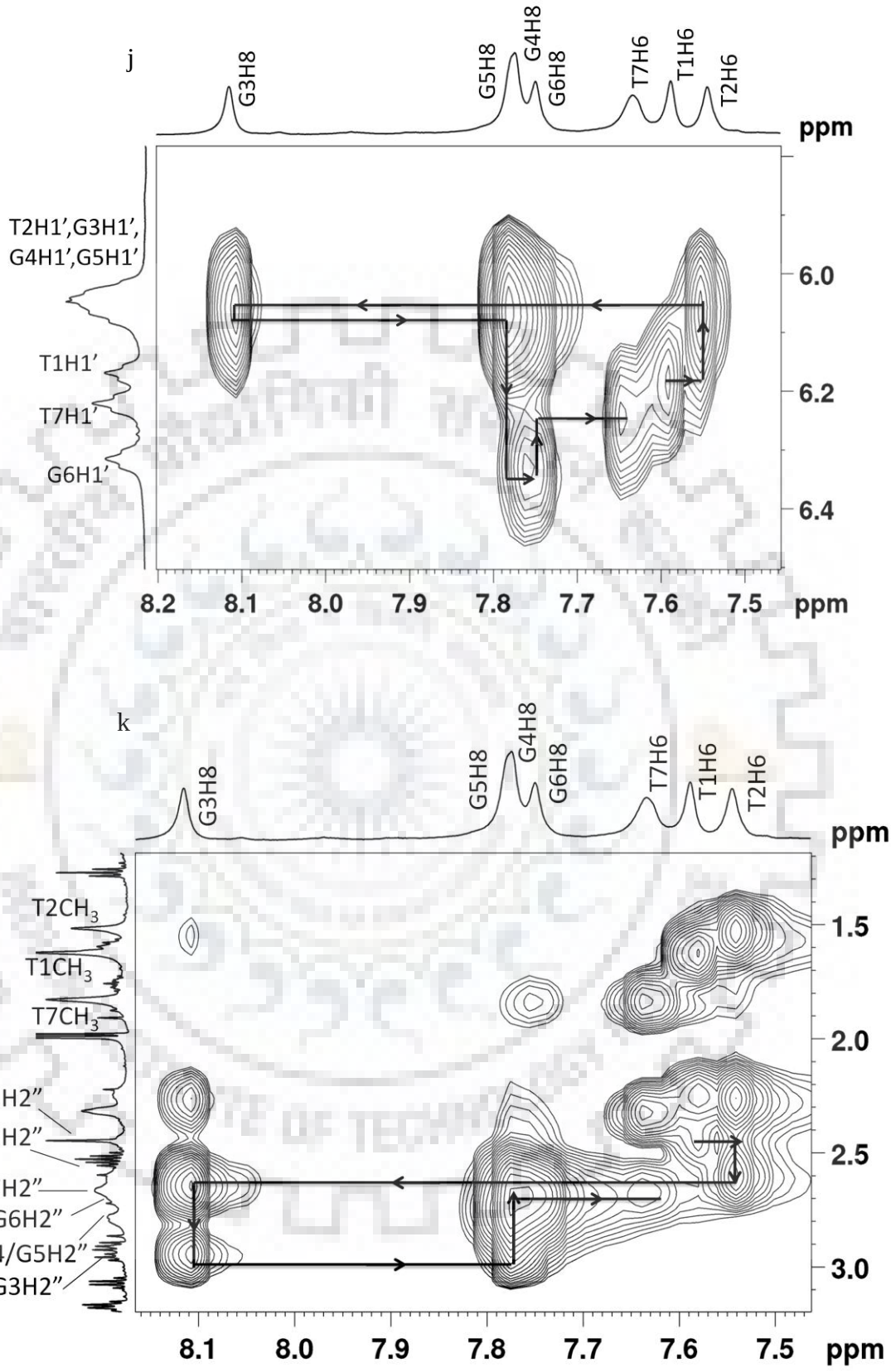
j
G3H8
G5H8
G4H8
G6H8
T7H6
T1H6
T2H6
ppm
T2H1',G3H1',
G4H1',G5H1'
T1H1'
T7H1'
G6H1'
6.0
6.2
6.4
8.2
8.1
8.0
7.9
7.8
7.7
7.6
7.5
ppm
k
G3H8
G5H8
G4H8
G6H8
T7H6
T1H6
T2H6
ppm
T2CH3
T1CH3
T7CH3
T1H2"
T2H2"
T7H2"
G6H2"
G4/G5H2"
G3H2"
1.5
2.0
2.5
3.0
8.1
8.0
7.9
7.8
7.7
7.6
7.5
ppm

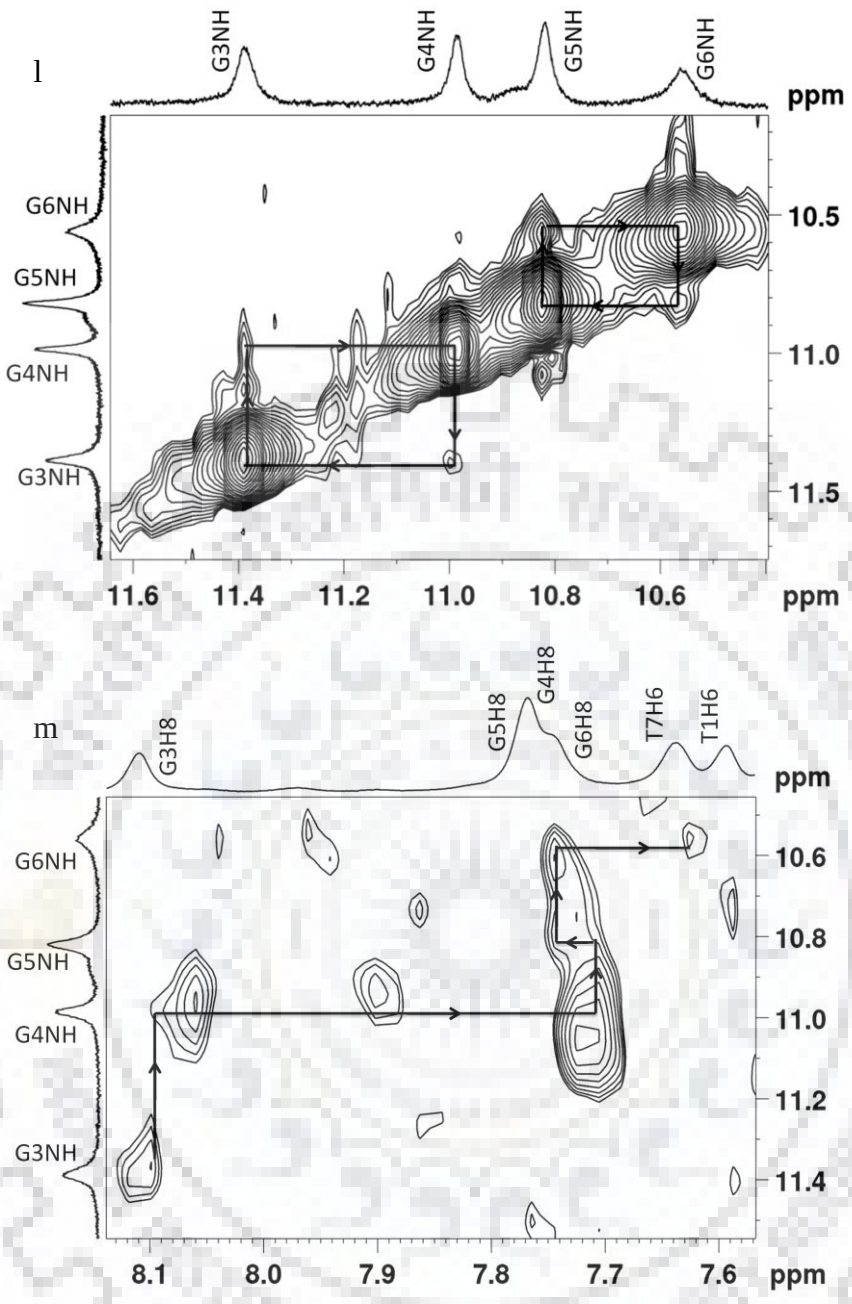

Figure 7.8 a) 1D ^{1}H NMR spectrum of free adriamycin in water (90% H_2O+10% D_2O) at 25 °C. b-c) ^{1}H NMR spectrum of the adriamycin-Tet7 complex at D/N = 2.0 in KBPES buffer.; ^{1}H NMR spectra of Tet7 and its complex upon progressive addition of adriamycin to Tet7 at different D/N ratios showing d) Imino, base and sugar H1' protons along with ring D aromatic protons 1H, 2H and 3H; e) Deoxyribose sugar H2'/2" and methyl protons of thymine along with drug protons at 25 °C. Symbol # denotes adriamycin protons. f-i) Expansion of ^{1}H-^{1}H 2D NOESY spectra of adriamycin-Tet7 complex complex at D/N = 2.0 and; sequential connectivity (black arrows) between j) imino protons; k) adjacent imino and base protons; l) base-sugar (H1') protons; and m) base-sugar (H2'/2") protons at τ_m = 250 ms in KBPES buffer (90% H_2O+10% D_2O) at 25 °C.

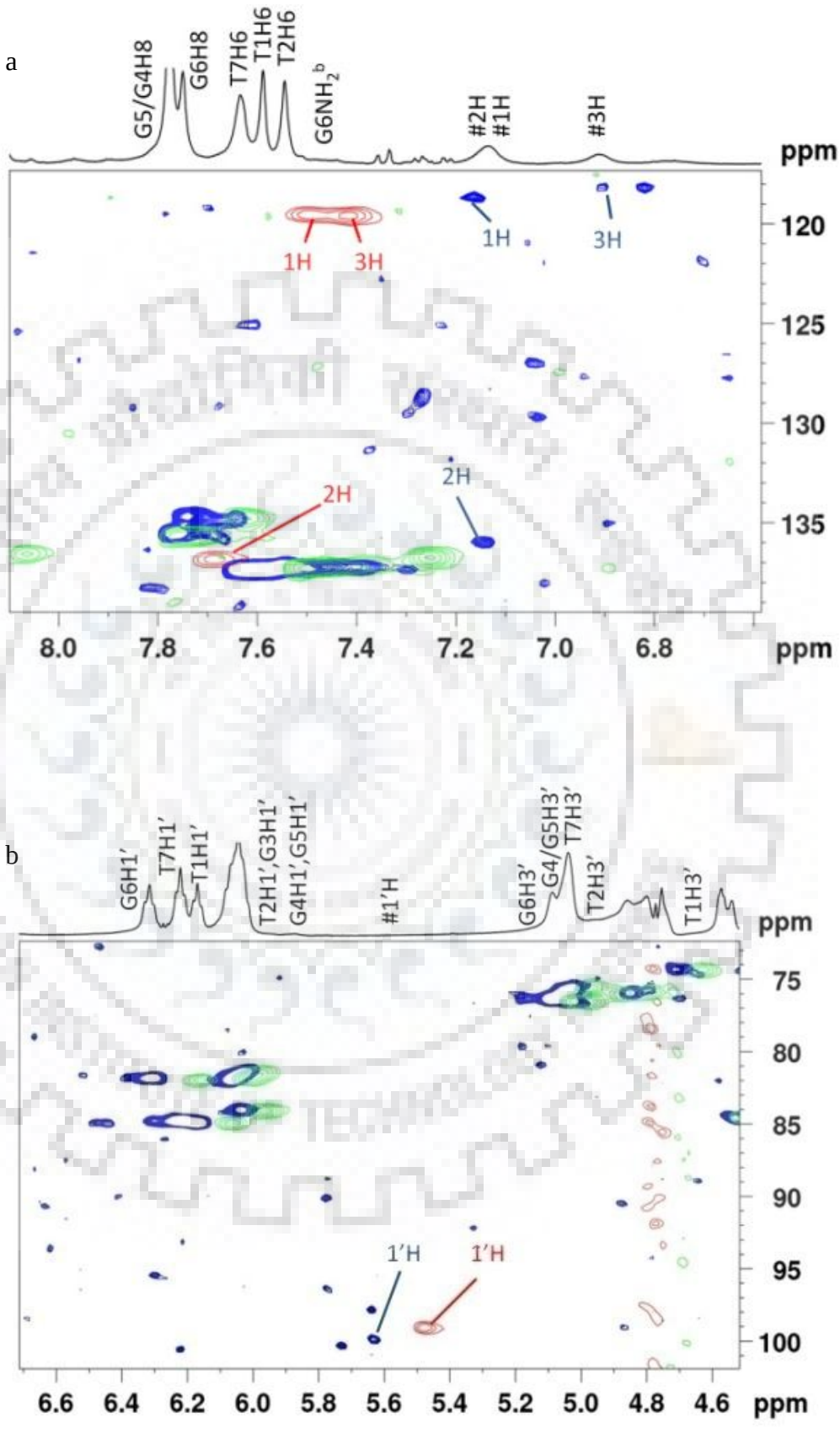
a
G5/G4H8
G6H8
T7H6
T1H6
T2H6
G6NH2b
#2H
#1H
#3H
ppm
1H
3H
1H
3H
2H
2H
120
125
130
135
8.0
7.8
7.6
7.4
7.2
7.0
6.8
ppm
b
G6H1'
T7H1'
T1H1'
T2H1',G3H1'
G4H1',G5H1'
#1'H
G6H3'
G4/G5H3'
T7H3'
T2H3'
T1H3'
ppm
75
80
85
90
95
100
1'H
1'H
6.6
6.4
6.2
6.0
5.8
5.6
5.4
5.2
5.0
4.8
4.6
ppm

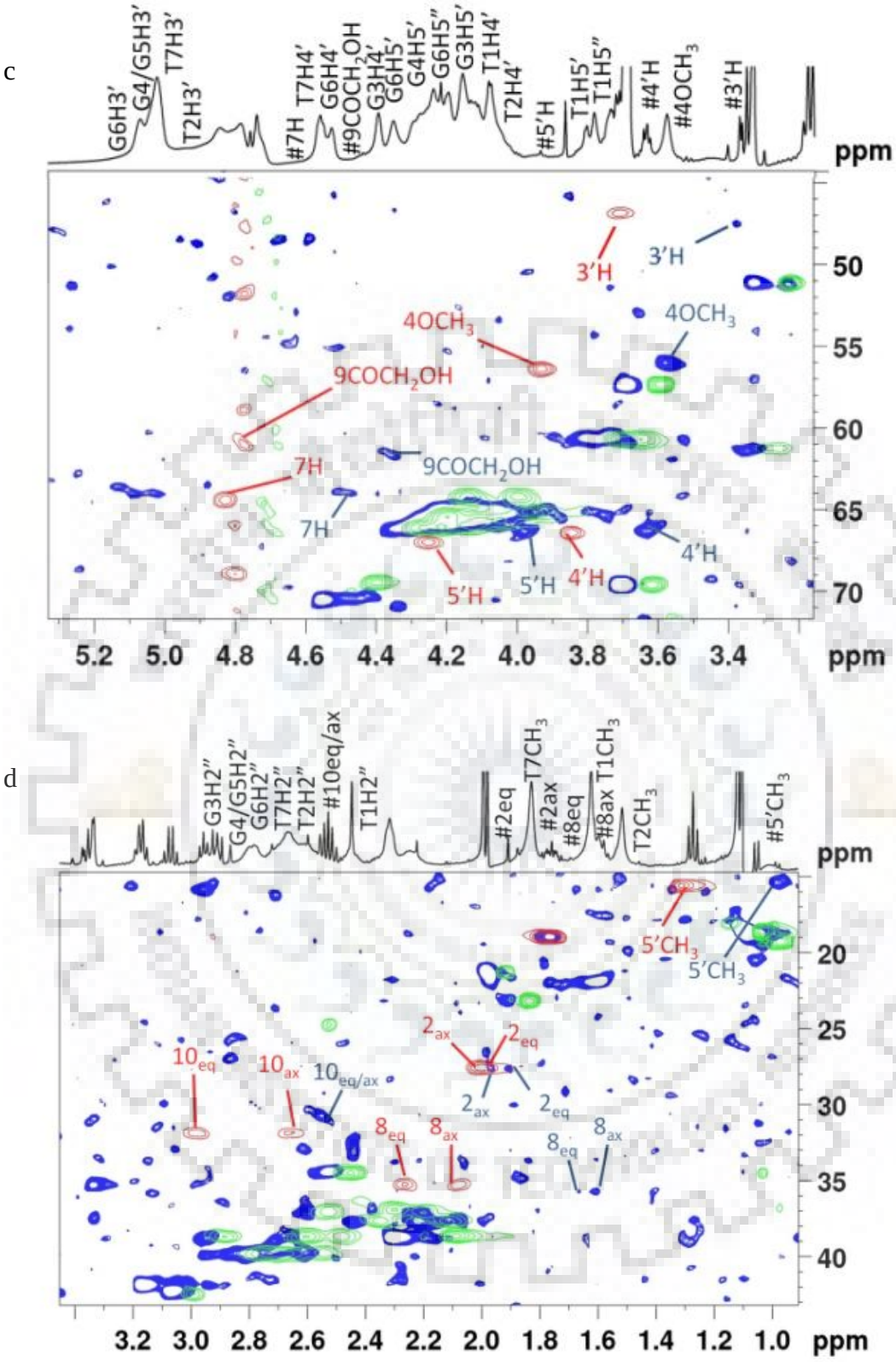

Figure 7.9 a-d) Expansion of specific region of 2D ^{1}H-^{13}C HSQC spectrum showing overlay of free adriamycin (red), free Tet7 (green) and adriamycin-Tet7complex at D/N = 2.0 (blue) in KBPES buffer (90% H_2O+10% D_2O) at 25 °C.1D ^{1}H NMR spectrum at the top of HSQC spectra is adriamycin-Tet7 complex at D/N = 2.0.

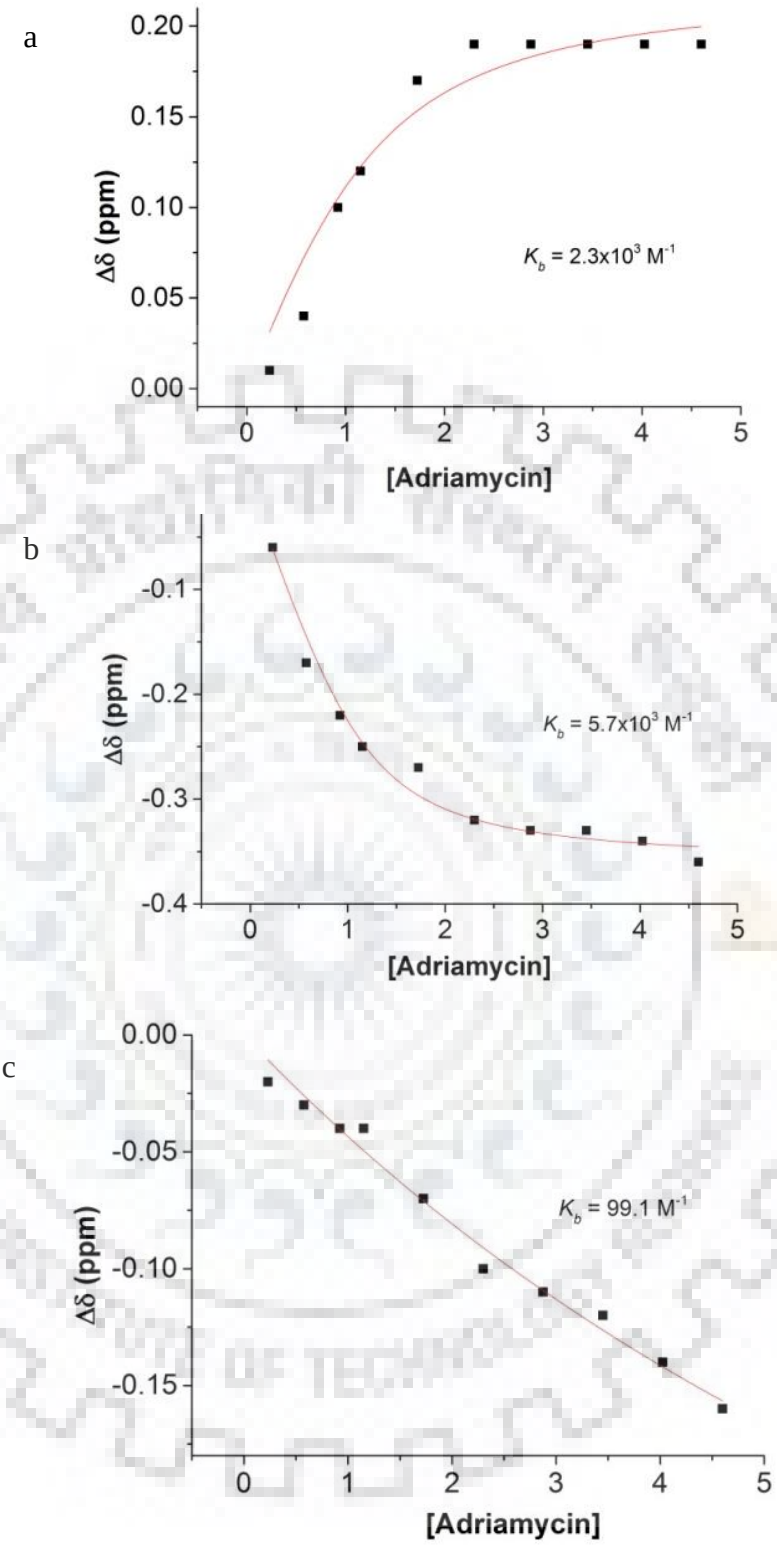

Figure 7.10 Nonlinear fitted curve (red) for simultaneous binding at two different sites in adriamycin-Tet7complex of protons a) $T7CH_3$, b) G6NH and c) G3NH. The plot shows a change in chemical shift (Δδ) of protons at D/N = 0.2-4.0 as a function of adriamycin concentration (μM) showing binding constants (K_b) at 25 °C.

Table 7.10 ^{1}H Chemical shift (ppm) of adriamycin protons in free adriamycin (δ_f) and in the adriamycin-Tet7 complex (δ_b) at various D/N ratios in KBPES buffer containing 100 mM KCl (90% H_2O+10% D_2O) at 25 °C. $\Delta\delta = \delta_b - \delta_f$, nd: not determined.

Protons	Free adriamycin	D/N=1.0		D/N=2.0		D/N=3.0		D/N=4.0	
	δ_f	δ_b	$\Delta\delta$	δ_b	$\Delta\delta$	δ_b	$\Delta\delta$	δ_b	$\Delta\delta$
2H	7.68	7.14	-0.54	7.13	-0.55	7.12	-0.56	7.09	-0.59
1H	7.49	7.14	-0.35	7.13	-0.36	7.12	-0.37	7.06	-0.43
3H	7.41	6.87	-0.54	6.91	-0.50	6.91	-0.50	6.88	-0.53
4OCH_3	3.93	3.57	-0.36	3.57	-0.36	3.57	-0.36	3.56	-0.37
1’H	5.47	5.79	0.32	5.63	0.16	5.50	0.03	5.25	-0.22
7H	4.80	4.51	-0.29	4.64	-0.16	4.80	0.00	4.52	-0.28
5’H	4.25	3.86	-0.39	3.97	-0.28	4.00	-0.25	4.01	-0.24
4’H	3.84	3.57	-0.27	3.63	-0.21	3.66	-0.18	3.69	-0.15
3’H	3.70	3.39	-0.31	3.36	-0.34	3.46	-0.24	3.50	-0.20
5’CH_3	1.30	0.90	-0.40	1.02	-0.28	1.06	-0.24	1.05	-0.25
9$COCH_2OH$	4.83	4.43	-0.40	4.50	-0.33	4.50	-0.33	4.53	-0.30
2’axH	1.98	1.77	-0.21	1.90	-0.08	1.90	-0.08	1.93	-0.05
2’eqH	2.01	1.84	-0.17	1.96	-0.05	1.87	-0.14	1.95	-0.06
8eqH	2.26	1.71	-0.55	1.60	-0.66	1.61	-0.65	1.93	-0.33
8axH	2.08	1.97	-0.11	1.66	-0.42	1.61	-0.47	1.87	-0.21
10eqH	2.98	2.56	-0.42	2.55	-0.43	2.55	-0.43	2.54	-0.44
10axH	2.66	2.66	0.00	2.55	-0.11	2.55	-0.11	2.54	-0.12

Table 7.11 ^{1}H Chemical shift (ppm) of protons in adriamycin-Tet7complex (δ_b) at various D/N ratios in KBPES buffer containing 100 mM KCl (90% H_2O+10% D_2O) at 25 °C. $\Delta\delta = \delta_b - \delta_f$. Negative sign in $\Delta\delta$ denotes upfield shift.

D/N	RESIDUES	T1		T2		G3		G4		G5		G6		T7	
	PROTONS	δ_b	$\Delta\delta$	δ_b	$\Delta\delta$	δ_b	$\Delta\delta$	δ_b	$\Delta\delta$	δ_b	$\Delta\delta$	δ_b	$\Delta\delta$	δ_b	$\Delta\delta$
1.0	H8/H6	7.59	0.01	7.55	0.01	8.13	-0.01	7.79	-0.01	7.81	-0.03	7.72	0.02	7.52	0.19
	H1’	6.15	0.01	6.04	0.00	6.05	0.00	6.06	-0.02	6.09	-0.04	6.30	0.07	6.12	0.07
	H2’	2.21	0.01	2.26	-0.01	2.65	0.00	2.60	0.01	2.71	-0.01	2.26	-0.29	2.27	0.12
	H2”	2.43	0.02	2.59	-0.01	2.95	0.00	2.70	0.01	2.75	-0.04	2.66	-0.01	2.63	0.46
	H3’	4.63	-0.02	4.90	0.00	5.05	0.00	5.06	0.00	5.07	-0.01	5.08	0.04	4.53	0.07
	H4’	4.06	0.00	4.01	-0.02	4.39	-0.01	4.29	0.00	4.28	-0.02	4.52	0.01	4.08	0.02
	H5’	3.76	-0.01	4.07	0.01	4.14	-0.01	4.23	0.00	4.35	-0.02	4.23	-0.06	4.12	0.03
	H5”	3.70	-0.01	4.05	0.02	4.12	0.01	4.28	0.00	4.26	-0.01	4.20	0.01	4.06	0.02
	CH_3	1.64	-0.01	1.53	-0.01	-	-	-	-	-	-	-	-	1.75	0.13
	NH_2^{b}	-	-	-	-	9.79	-0.06	9.13	-0.06	9.14	-0.03	7.45	-0.02	-	-
	NH_2^{nb}	-		-	-	6.29	0.01	6.13	-0.07	6.20	-0.04	6.77	0.01	-	-
	NH	-	-	-	-	11.47	-0.04	11.04	-0.04	10.87	-0.07	10.64	-0.25	-	-
2.0	H8/H6	7.58	0.02	7.54	0.00	8.11	-0.02	7.77	-0.03	7.77	-0.07	7.75	0.05	7.64	0.30
	H1’	6.17	0.03	6.04	0.00	6.04	-0.01	6.05	-0.03	6.06	-0.07	6.31	0.07	6.22	0.17
	H2’	2.24	0.04	2.26	-0.01	2.65	0.00	2.60	0.01	2.68	-0.03	2.58	0.03	2.32	0.17
	H2”	2.44	0.03	2.60	0.00	2.95	0.00	2.68	-0.01	2.74	-0.05	2.66	-0.01	2.67	0.50
	H3’	4.66	0.01	4.92	0.02	5.05	0.00	5.06	0.00	5.07	-0.01	5.08	0.04	5.09	0.63
	H4’	4.09	0.03	4.01	-0.02	4.37	-0.03	4.28	-0.01	4.31	0.01	4.53	0.02	4.55	0.49
	H5’	3.76	-0.01	4.07	0.01	4.14	-0.01	4.26	0.03	4.38	0.01	4.26	-0.03	4.18	0.09
	H5”	3.72	0.01	4.05	0.02	4.10	-0.01	4.30	0.02	4.28	0.01	4.15	-0.04	4.12	0.08
	CH_3	1.62	-0.03	1.51	-0.03	-	-	-	-	-	-	-	-	1.82	0.19
	NH_2^{b}	-	-	-	-	9.80	-0.05	9.11	-0.08	9.19	0.02	7.45	-0.02	-	-
	NH_2^{nb}	-	-	-	-	6.29	0.01	6.08	-0.12	6.22	-0.02	6.76	0.00	-	-
	NH	-	-	-	-	11.41	-0.10	10.99	-0.09	10.83	-0.12	10.57	-0.32	-	-

Table 7.12 ^{1}H Chemical shift (ppm) of protons in adriamycin-Tet7complex (δ_b) at various D/N ratios in KBPES buffer containing 100 mM KCl (90% H_2O+10% D_2O) at 25 °C. $\Delta\delta = \delta_b - \delta_f$. Negative sign in $\Delta\delta$ denotes upfield shift.

D/N	RESIDUES	T1		T2		G3		G4		G5		G6		T7	
	PROTONS	δ_b	$\Delta\delta$	δ_b	$\Delta\delta$	δ_b	$\Delta\delta$	δ_b	$\Delta\delta$	δ_b	$\Delta\delta$	δ_b	$\Delta\delta$	δ_b	$\Delta\delta$
3.0	H8/H6	7.58	0.02	7.54	0.00	8.11	-0.03	7.77	-0.03	7.77	-0.07	7.75	0.05	7.64	0.31
	H1’	6.17	0.03	6.04	0.00	6.03	-0.02	6.05	-0.03	6.05	-0.08	6.31	0.08	6.22	0.17
	H2’	2.25	0.05	2.24	-0.03	2.62	-0.03	2.60	0.01	2.67	-0.05	2.58	0.03	2.31	0.16
	H2”	2.46	0.05	2.58	-0.02	2.92	-0.03	2.65	-0.04	2.73	-0.06	2.67	0.00	2.65	0.48
	H3’	4.62	-0.03	5.03	0.13	5.04	-0.01	5.06	0.00	5.06	-0.02	5.07	0.03	5.06	0.60
	H4’	4.10	0.04	4.02	-0.01	4.37	-0.03	4.28	-0.01	4.33	0.03	4.52	0.01	4.54	0.48
	H5’	3.75	-0.02	4.07	0.01	4.16	0.01	4.20	-0.03	4.35	-0.02	4.24	-0.05	4.16	0.07
	H5”	3.72	0.01	4.03	0.00	4.10	-0.01	4.27	-0.01	4.28	0.01	4.15	-0.04	4.11	0.07
	CH_3	1.61	-0.04	1.51	-0.03	-	-	-	-	-	-	-	-	1.82	0.20
	NH_2^b	-	-	-	-	9.78	-0.07	9.06	-0.13	9.20	0.03	7.47	0.00	-	-
	NH_2^{nb}	-	-	-	-	6.19	-0.09	6.08	-0.12	6.20	-0.04	6.76	0.00	-	-
	NH	-	-	-	-	11.39	-0.12	10.98	-0.10	10.82	-0.12	10.56	-0.33	-	-
4.0	H8/H6	7.57	-0.01	7.53	-0.01	8.08	-0.06	7.75	-0.05	7.75	-0.09	7.74	0.04	7.63	0.30
	H1’	6.17	0.03	6.04	0.00	6.03	-0.02	6.04	-0.04	6.04	-0.09	6.29	0.06	6.21	0.16
	H2’	2.24	0.04	2.23	-0.04	2.62	-0.03	2.60	0.01	2.68	-0.04	2.58	0.03	2.31	0.16
	H2”	2.50	0.09	2.57	-0.03	2.92	-0.03	2.67	-0.02	2.74	-0.05	2.65	-0.02	2.64	0.47
	H3’	4.60	-0.05	4.91	0.01	5.04	-0.01	5.06	0.00	5.06	-0.02	5.06	0.02	5.07	0.61
	H4’	4.10	0.04	4.02	-0.01	4.35	-0.05	4.28	-0.01	4.34	0.04	4.51	0.00	4.54	0.48
	H5’	3.78	0.01	4.07	0.01	4.15	0.00	4.20	-0.03	4.35	-0.02	4.24	-0.05	4.16	0.07
	H5”	3.74	0.03	4.03	0.00	4.10	-0.01	4.27	-0.01	4.28	0.01	4.16	-0.03	4.10	0.06
	CH_3	1.60	-0.05	1.50	-0.04	-	-	-	-	-	-	-	-	1.82	0.20
	NH_2^b	-	-	-	-	9.74	-0.11	9.04	-0.15	9.18	0.01	7.45	-0.02	-	-
	NH_2^{nb}	-	-	-	-	6.16	-0.12	6.07	-0.13	6.18	-0.06	6.77	0.01	-	-
	NH	-	-	-	-	11.35	-0.16	10.96	-0.12	10.80	-0.14	10.53	-0.36	-	-

Table 7.13 ^{1}H Chemical shift (ppm) of methyl and imino protons in free Tet7 (δ_f) and adriamycin-Tet7complex (δ_b) at various D/N ratios in KBPES buffer containing 100 mM KCl (90% H_2O+10% D_2O) at 25 °C. $\Delta\delta = \delta_b - \delta_f$. Negative sign in $\Delta\delta$ denotes upfield shift.

Protons	CH_3						NH							
	T1		T2		T7		G3		G4		G5		G6	
Free DNA (δ_f)	1.65		1.54		1.63		11.51		11.08		10.95		10.89	
	δ_b	$\Delta\delta$	δ_b	$\Delta\delta$	δ_b	$\Delta\delta$	δ_b	$\Delta\delta$	δ_b	$\Delta\delta$	δ_b	$\Delta\delta$	δ_b	$\Delta\delta$
D/N=0.2	1.65	0.00	1.53	-0.01	1.64	0.01	11.49	-0.02	11.07	-0.01	10.91	-0.04	10.83	-0.06
D/N=0.5	1.65	0.00	1.53	-0.01	1.67	0.04	11.48	-0.03	11.06	-0.02	10.90	-0.05	10.72	-0.17
D/N=0.8	1.64	-0.01	1.53	-0.01	1.73	0.10	11.47	-0.04	11.05	-0.03	10.88	-0.07	10.67	-0.22
D/N=1.0	1.64	-0.01	1.53	-0.01	1.75	0.12	11.47	-0.04	11.04	-0.04	10.87	-0.08	10.64	-0.25
D/N=1.5	1.63	-0.02	1.52	-0.02	1.80	0.17	11.44	-0.07	11.02	-0.06	10.84	-0.11	10.62	-0.27
D/N=2.0	1.62	-0.03	1.51	-0.03	1.82	0.19	11.41	-0.10	10.99	-0.09	10.83	-0.12	10.57	-0.32
D/N=2.5	1.61	-0.04	1.52	-0.02	1.82	0.19	11.40	-0.11	10.99	-0.09	10.82	-0.13	10.56	-0.33
D/N=3.0	1.61	-0.04	1.51	-0.03	1.82	0.19	11.39	-0.12	10.98	-0.1	10.82	-0.13	10.56	-0.33
D/N=3.5	1.60	-0.05	1.50	-0.04	1.82	0.19	11.37	-0.14	10.97	-0.11	10.81	-0.14	10.55	-0.34
D/N=4.0	1.60	-0.05	1.50	-0.04	1.82	0.19	11.35	-0.16	10.96	-0.12	10.80	-0.15	10.53	-0.36

Table 7.14 ^{1}H Chemical shift (ppm) of base protons in free Tet7 (δ_f) and adriamycin-Tet7 complex (δ_b) at various D/N ratios in KBPES buffer containing 100 mM KCl (90% H_2O+10% D_2O) at 25 °C. $\Delta\delta = \delta_b - \delta_f$. Negative sign in $\Delta\delta$ denotes upfield shift.

Protons	H8/H6													
	T1		T2		G3		G4		G5		G6		T7	
Free DNA (δ_f)	7.56		7.54		8.13		7.80		7.84		7.70		7.34	
	δ_b	$\Delta\delta$	δ_b	$\Delta\delta$	δ_b	$\Delta\delta$	δ_b	$\Delta\delta$	δ_b	$\Delta\delta$	δ_b	$\Delta\delta$	δ_b	$\Delta\delta$
D/N=0.2	7.60	0.04	7.55	0.01	8.14	0.01	7.80	0.00	7.84	0.00	7.71	0.01	7.34	0.00
D/N=0.5	7.59	0.03	7.55	0.01	8.14	0.01	7.80	0.00	7.83	-0.01	7.72	0.02	7.39	0.05
D/N=0.8	7.59	0.03	7.55	0.01	8.14	0.01	7.79	-0.01	7.82	-0.02	7.73	0.03	7.46	0.12
D/N=1.0	7.59	0.03	7.55	0.01	8.13	0.00	7.79	-0.01	7.81	-0.03	7.72	0.02	7.52	0.18
D/N=1.5	7.58	0.02	7.54	0.00	8.12	-0.01	7.78	-0.02	7.79	-0.05	7.75	0.05	7.61	0.27
D/N=2.0	7.58	0.02	7.54	0.00	8.11	-0.02	7.77	-0.03	7.77	-0.07	7.75	0.05	7.64	0.30
D/N=2.5	7.58	0.02	7.54	0.00	8.11	-0.02	7.77	-0.03	7.77	-0.07	7.75	0.05	7.64	0.30
D/N=3.0	7.58	0.02	7.54	0.00	8.11	-0.02	7.77	-0.03	7.77	-0.07	7.75	0.05	7.64	0.30
D/N=3.5	7.58	0.02	7.54	0.00	8.09	-0.04	7.75	-0.05	7.76	-0.08	7.75	0.05	7.64	0.30
D/N=4.0	7.57	0.01	7.53	-0.01	8.08	-0.05	7.75	-0.05	7.75	-0.09	7.74	0.04	7.63	0.29

Table 7.15 ^{1}H Chemical shift (ppm) of sugar protons in free Tet7 (δ_f) and adriamycin-Tet7 complex (δ_b) at various D/N ratios in KBPES buffer containing 100 mM KCl (90% H_2O+10% D_2O) at 25 °C. $\Delta\delta = \delta_b - \delta_f$. Negative sign in $\Delta\delta$ denotes upfield shift.

Protons	H1'					
	T1		G6		T7	
Free DNA (δ_f)	6.14		6.24		6.05	
	δ_b	$\Delta\delta$	δ_b	$\Delta\delta$	δ_b	$\Delta\delta$
D/N=0.2	6.15	0.01	6.25	0.01	6.08	0.03
D/N=0.5	6.15	0.01	6.26	0.02	6.09	0.04
D/N=0.8	6.15	0.01	6.27	0.03	6.09	0.04
D/N=1.0	6.15	0.01	6.30	0.06	6.12	0.07
D/N=1.5	6.16	0.02	6.31	0.07	6.20	0.15
D/N=2.0	6.17	0.03	6.31	0.07	6.22	0.17
D/N=2.5	6.17	0.03	6.31	0.07	6.22	0.17
D/N=3.0	6.17	0.03	6.31	0.07	6.22	0.17
D/N=3.5	6.17	0.03	6.30	0.06	6.22	0.17
D/N=4.0	6.17	0.03	6.29	0.05	6.21	0.16

Table 7.16 ^{1}H Chemical shift (ppm) of adriamycin protons in a free state (δ_f) and in the adriamycin-Tet7 complex (δ_b) at various D/N ratios in KBPES buffer containing 100 mM KCl (90% H_2O+10% D_2O) at 25 °C. $\Delta\delta = \delta_b - \delta_f$. Negative sign in $\Delta\delta$ denotes upfield shift.

Protons	Adriamycin							
	1H		2H		3H		5'CH_3	
Free Adriamycin (δ_f)	7.49		7.68		7.41		1.30	
	δ_b	$\Delta\delta$	δ_b	$\Delta\delta$	δ_b	$\Delta\delta$	δ_b	$\Delta\delta$
D/N=0.2	7.11	-0.38	7.14	-0.54	6.87	-0.54	0.89	-0.41
D/N=0.5	7.12	-0.37	7.14	-0.54	6.87	-0.54	0.90	-0.4
D/N=0.8	7.13	-0.36	7.14	-0.54	6.87	-0.54	0.90	-0.4
D/N=1.0	7.14	-0.35	7.14	-0.54	6.87	-0.54	0.90	-0.4
D/N=1.5	7.14	-0.35	7.14	-0.54	6.90	-0.51	0.95	-0.35
D/N=2.0	7.13	-0.36	7.13	-0.55	6.91	-0.5	1.02	-0.28
D/N=2.5	7.12	-0.37	7.12	-0.56	6.91	-0.5	1.03	-0.27
D/N=3.0	7.12	-0.37	7.12	-0.56	6.91	-0.5	1.06	-0.24
D/N=3.5	7.08	-0.41	7.11	-0.57	6.89	-0.52	1.05	-0.25
D/N=4.0	7.06	-0.43	7.09	-0.59	6.88	-0.53	1.05	-0.25

7.3.5. Phosphorous-31 NMR

The phosphorus-31 NMR signals were assigned by following standard strategies using ^{3}J and ^{4}J coupling of phosphorus signals with $(H3')_n/(H5'/H5'')_{n+1}$ and $(H4')_n/(H4')_{n+1}$, respectively in free (Fig 7.11 a) and complexed DNA (Fig 7.11 b,c) in ^{1}H-^{31}P HMBC spectra at 25 °C (Kumar & Barthwal, 2018; Tripathi & Barthwal, 2018; Gorenstein & Kar, 1975). On progressive addition of 4'-epiadriamycin, all ^{31}P signals shifted downfield (Table 7.17 and Fig 7.12 a). The drift in resonance is sequence dependant, it being 0.28 ppm and 0.19 ppm for G6pT7 and T1pT2, respectively. The shifts in other ^{31}P signals are lesser and are indicative of specificity of the interaction. This shift also suggests that the binding site is close to G6pT7 and T1pT2 sites. ^{31}P chemical shift vary in response to DNA duplex geometry. Classical intercalation between base pair of duplex DNA by aromatic rings result in change of dihedral angle ζ=C3'-O3'-P-O5' from *gauche* (g^-) to *trans* (t) conformation which increases distance between base pair to 6.8 Å resulting in downfield shift of ~1.5 ppm (Gorenstein & Kar, 1975; Agrawal, Govil, & Barthwal, 2009). Pure electrostatic interactions between drug and DNA cause the small upfield shift. On the other hand, widening and narrowing of O-P-O ester bond angle leads to small upfield and downfield shift, respectively (Gorenstein & Kar, 1975; Agrawal, Govil, & Barthwal, 2009). Dispersion in ^{31}P chemical shift also results from the relative composition of B_I and B_{II} conformational states. Lower dispersion of ^{31}P signals (~0.4 ppm) suggests *anti* conformation of DNA (Henderson et al., 1987; Hardin et al., 1997; Hall, Cruz, Tinoco, Jovin, & van de Sande, 1984) in parallel stranded Tet7. Absence of large downfield shift of the order of 1.5 ppm rules out classical intercalation. The downfield shift of 0.28 ppm and 0.19 ppm in G6pT7 and T1pT2 signals, respectively may be induced by the distortion of DNA upon binding of 4'-epiadriamycin externally to Tet7.

The ^{31}P chemical shift perturbations in Tet7 on the binding of adriamycin are much larger than that in 4'-epiadriamycin indicating the greater extent of induced distortions. All ^{31}P signals shifts continuously up to D/N = 4.0 (Table 7.18 and Fig. 7.12 b). These shifts are maximum in G6pT7 and T1pT2 being 0.60 ppm and 0.57 ppm, respectively. The shifts in the other four signals T2pG3, G3pG4, G4pG5, and G5pG6 are also large being up to 0.51 ppm. Classical intercalation of adriamycin with bases is completely ruled out by the absence of downfield shift ~1.5 ppm as observed in case duplex DNA (P. Agrawal, Govil, et al., 2009). The ^{31}P NMR spectra clearly point towards difference in conformation of 4'-epiadriamycin and adriamycin bound complexes formed on binding to the same Tet7.

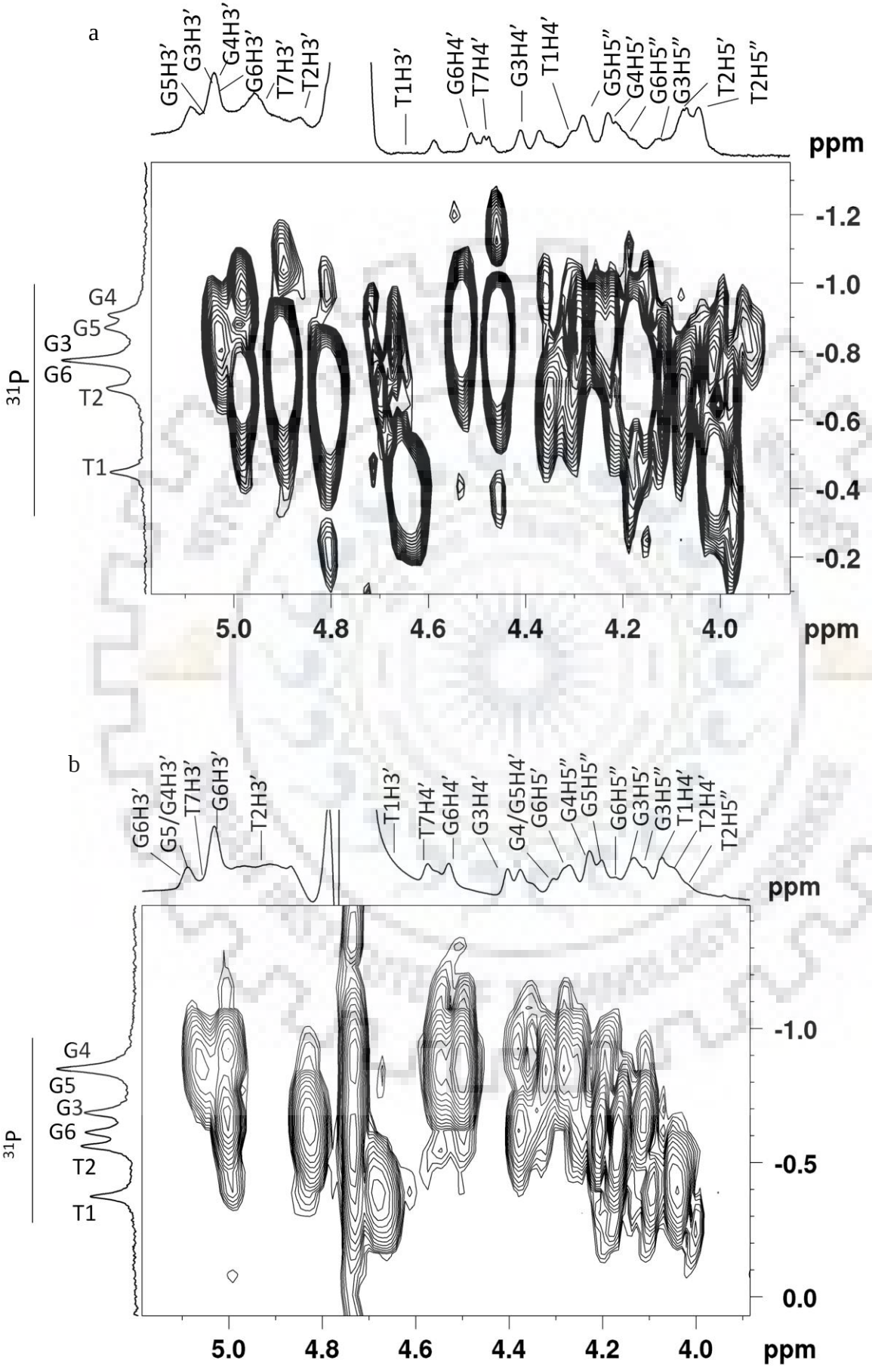
a
G5H3′
G3H3′
G4H3′
G6H3′
T7H3′
T2H3′
T1H3′
G6H4′
T7H4′
G3H4′
T1H4′
G5H5″
G4H5′
G6H5″
G3H5″
T2H5′
T2H5″
ppm
-1.2
-1.0
-0.8
-0.6
-0.4
-0.2
31P
G4
G5
G3
G6
T2
T1
5.0
4.8
4.6
4.4
4.2
4.0
ppm
b
G6H3′
G5/G4H3′
T7H3′
G6H3′
T2H3′
T1H3′
T7H4′
G6H4′
G3H4′
G4/G5H4′
G6H5′
G4H5″
G5H5″
G6H5″
G3H5′
G3H5″
T1H4′
T2H4′
T2H5″
ppm
-1.0
-0.5
0.0
31P
G4
G5
G3
G6
T2
T1
5.0
4.8
4.6
4.4
4.2
4.0
ppm

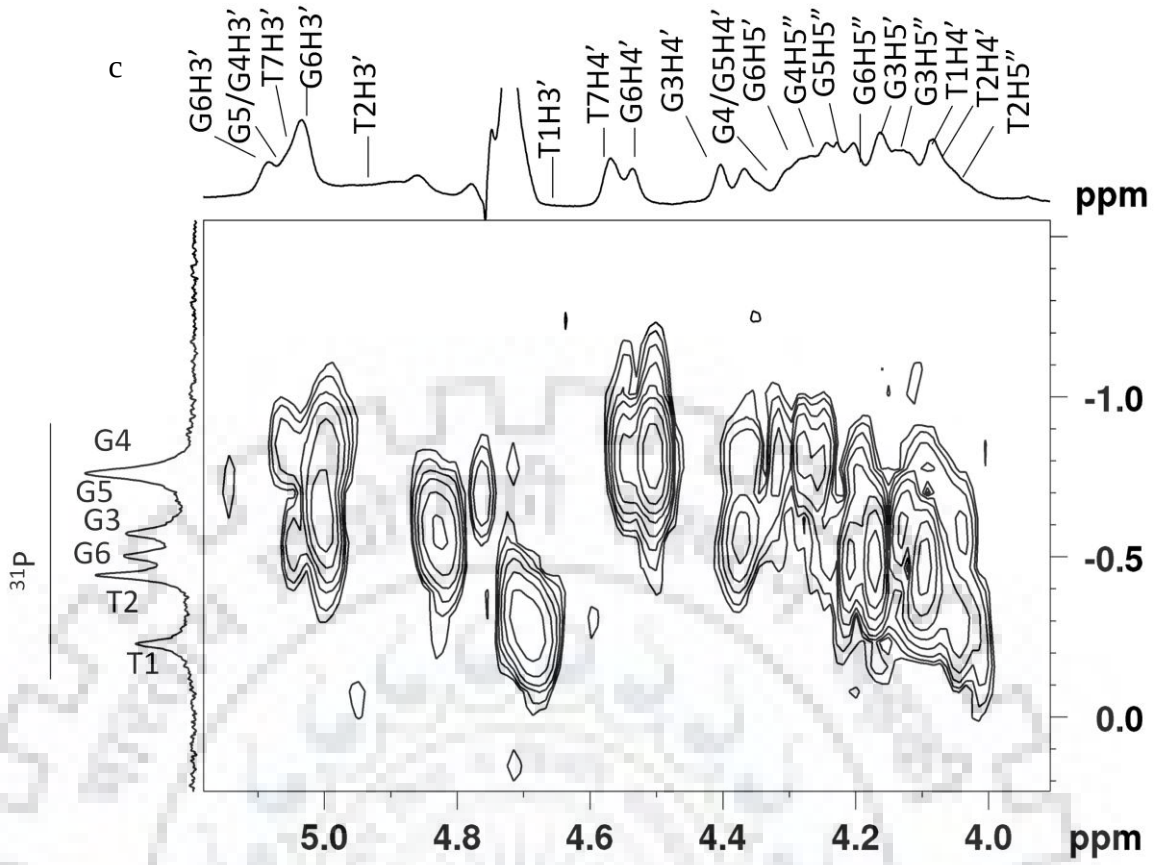

Figure 7.11 2D ^{1}H-^{31}P HMBC spectra of a) free Tet7 ; b) 4'-epiadriamycin-Tet7complex and c) adriamycin-Tet7complex at D/N = 2.0 complex in KBPES buffer (90% H_2O+10% D_2O) at 25°C.

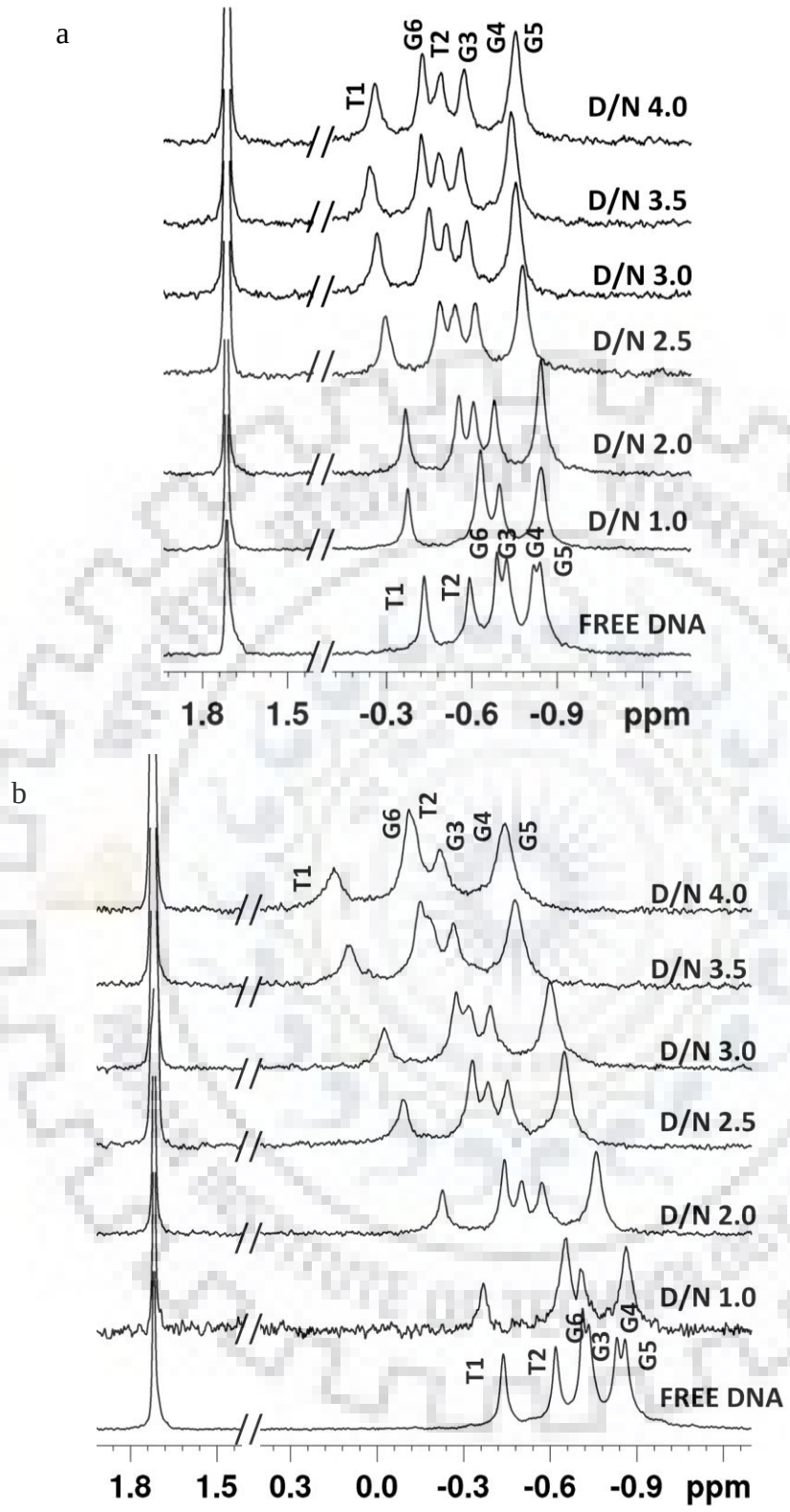

Figure 7.12 Proton decoupled ^{31}P NMR spectra of 1.16 mM Tet7 and its complex upon progressive addition of a) 4'-epiadriamycin and b) adriamycin at different D/N ratios in 10 mM phosphate buffer with 100 mM KCl (90% H_2O + 10% D_2O) at 25 °C.

Table 7.17 Chemical shift (ppm) of phosphorus (^{31}P) resonances in free Tet7 (δ_f) and 4'-epiadriamycin-Tet7 complex (δ_b) at various D/N ratios in KBPES buffer containing 100 mM KCl (90% H_2O+10% D_2O) at 25 °C. $\Delta\delta = \delta_b - \delta_f$. Positive sign in $\Delta\delta$ show downfield shift.

	T1pT2		T2pG3		G3pG4		G4pG5		G5pG6		G6pT7	
Free DNA (δ_f)	-0.43		-0.59		-0.72		-0.84		-0.81		-0.69	
	δ_b	$\Delta\delta$	δ_b	$\Delta\delta$	δ_b	$\Delta\delta$	δ_b	$\Delta\delta$	δ_b	$\Delta\delta$	δ_b	$\Delta\delta$
D/N=1.0	-0.36	0.07	-0.62	-0.03	-0.69	0.03	-0.84	0.00	-0.82	-0.01	-0.62	0.07
D/N=2.0	-0.30	0.13	-0.58	0.01	-0.63	0.09	-0.80	0.04	-0.79	0.02	-0.53	0.16
D/N=2.5	-0.29	0.14	-0.54	0.05	-0.61	0.11	-0.78	0.06	-0.77	0.04	-0.48	0.21
D/N=3.0	-0.26	0.17	-0.51	0.08	-0.58	0.14	-0.75	0.09	-0.74	0.07	-0.44	0.25
D/N=3.5	-0.24	0.19	-0.48	0.11	-0.55	0.17	-0.74	0.10	-0.73	0.08	-0.41	0.28
D/N=4.0	-0.24	0.19	-0.48	0.11	-0.55	0.17	-0.74	0.10	-0.73	0.08	-0.41	0.28

Table 7.18 Chemical shift (ppm) of phosphorus (^{31}P) resonances in free Tet7 (δ_f) and adriamycin-Tet7 complex (δ_b) at various D/N ratios in KBPES buffer containing 100 mM KCl (90% H_2O+10% D_2O) at 25 °C. $\Delta\delta = \delta_b - \delta_f$. Positive sign in $\Delta\delta$ show downfield shift.

	T1pT2		T2pG3		G3pG4		G4pG5		G5pG6		G6pT7	
Free DNA (δ_f)	-0.43		-0.62		-0.73		-0.85		-0.83		-0.71	
	δ_b	$\Delta\delta$	δ_b	$\Delta\delta$	δ_b	$\Delta\delta$	δ_b	$\Delta\delta$	δ_b	$\Delta\delta$	δ_b	$\Delta\delta$
D/N=1.0	-0.36	0.07	-0.65	-0.03	-0.70	0.03	-0.86	-0.01	-0.86	-0.03	-0.65	0.06
D/N=2.0	-0.22	0.21	-0.50	0.12	-0.57	0.16	-0.75	0.10	-0.75	0.08	-0.44	0.27
D/N=2.5	-0.07	0.36	-0.37	0.25	-0.44	0.29	-0.63	0.22	-0.63	0.20	-0.31	0.40
D/N=3.0	-0.03	0.40	-0.32	0.30	-0.39	0.34	-0.60	0.25	-0.60	0.23	-0.27	0.44
D/N=3.5	0.09	0.52	-0.19	0.43	-0.26	0.47	-0.49	0.36	-0.48	0.35	-0.15	0.56
D/N=4.0	0.14	0.57	-0.13	0.49	-0.22	0.51	-0.45	0.40	-0.43	0.40	-0.11	0.60

7.3.6. NOE Correlations and Conformation of Complex

2D ^{1}H-^{1}H NOESY spectra of 4'epiadriamycin-Tet7complex at D/N = 2.0 show sequential inter nucleotide connectivities of G3NH-G4NH, G4NH-G5NH, G5NH-G6NH and G3NH-G3H8, G3H8-G4NH, G4NH-G5H8, G5H8-G6NH and G6NH-G6H8 (Fig. 7.5 j,k) indicating connectivity forming G-quartets after binding of the drug. The sequential NOE correlation between base H8/H6 and sugar H1'/H2'/2" protons e.g. T2H6-T1H1'/T1H2", G3H8-T2H1'/T2H2" and several similar NOEs at other base steps (Fig. 7.5 l,m) were also present. This rules out opening of base pairs from 3.4-6.8 Å at any 5'-3' base pair step to permit classical intercalation of 4'-epiadriamycin between bases as observed in X- ray crystallography (D'Estaintot et al., 1992) and NMR solution structure of 4'-epiadriamycin with duplex DNA sequence d-$(CGATCG)_2$ (P. Agrawal, Govil, et al., 2009). This gives independent evidence of absence of intercalation as a possible mode of interaction in Tet7. The relative intensity of base H8/H6 to sugar H1'/H2'/H2" NOE cross peaks (Fig. 7.5 l,m) establish right-handed B-DNA conformation with the *anti* glycosidic bond rotation of all guanines is retained in 4'-epiadriamycin-Tet7 complex. Relative intensities of NOE cross peaks of protons within deoxyribose, that is, intra sugar protons NOE connectivities reveal that C2' *endo* conformation is prevalent in sugar (Wang & Patel, 1992; Pradeep & Barthwal, 2016; Padmapriya & Barthwal, 2017; Kumar & Barthwal, 2018). Typical intra molecular short NOE contacts within 4'-epiadriamycin were found to be present (Table 7.19 and Fig. 7.13 a-c). The ^{1}H-^{1}H NOESY spectra of complex show several intermolecular NOE cross peak between 4'-epiadriamycin and Tet7 protons (Table 7.20 and Fig. 7.13 a-f). Nineteen intermolecular NOE cross peaks clearly depict binding at two different sites. 1H and 2H protons of ring D are close to T1CH_3, T2CH_3, and T7CH_3 while the 3H proton is spatially close to T2CH_3, and T7CH_3. This confirms the presence of two distinct sites in DNA close to G6pT7 and T1pT2 corroborating stoichiometry of 1:1 and 2:1 determined independently by Job Plot experiments. Interaction of ring D protons with T7CH_3, G6H8, and G6H1' reflects partial stacking of ring D with bases. Presence of NOE correlation of 5'CH_3 with Tet7 protons suggests the involvement of daunosamine sugar protons in the bound complex (Table 7.20 and Fig. 7.13 a). There are no detectable NOE cross peaks of 4'epiadriamycin with any of G3, G4 or G5 protons.

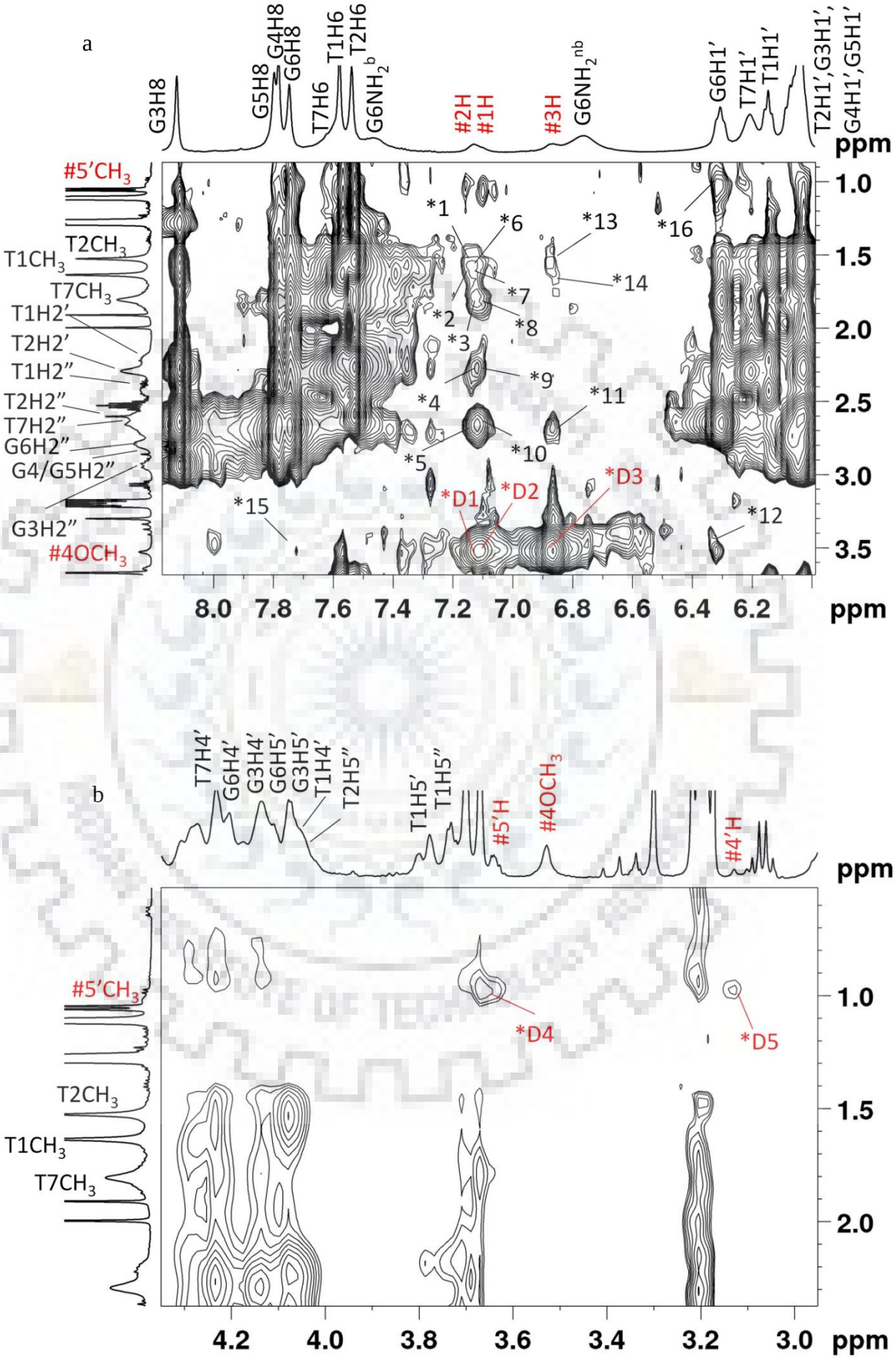
a
G3H8
G5H8
G4H8
G6H8
T7H6
T1H6
T2H6
G6NH2b
#2H
#1H
#3H
G6NH2nb
G6H1'
T7H1'
T1H1'
T2H1',G3H1',
G4H1',G5H1'
ppm
#5'CH3
T2CH3
T1CH3
T7CH3
T1H2'
T2H2'
T1H2"
T2H2"
T7H2"
G6H2"
G4/G5H2"
G3H2"
#4OCH3
*1
*2
*3
*4
*5
*6
*7
*8
*9
*10
*11
*12
*13
*14
*15
*16
*D1
*D2
*D3
8.0 7.8 7.6 7.4 7.2 7.0 6.8 6.6 6.4 6.2
ppm
1.0
1.5
2.0
2.5
3.0
3.5
b
T7H4'
G6H4'
G3H4'
G6H5'
G3H5'
T1H4'
T2H5"
T1H5'
T1H5"
#5'H
#4OCH3
#4'H
ppm
#5'CH3
T2CH3
T1CH3
T7CH3
*D4
*D5
4.2 4.0 3.8 3.6 3.4 3.2 3.0
ppm
1.0
1.5
2.0

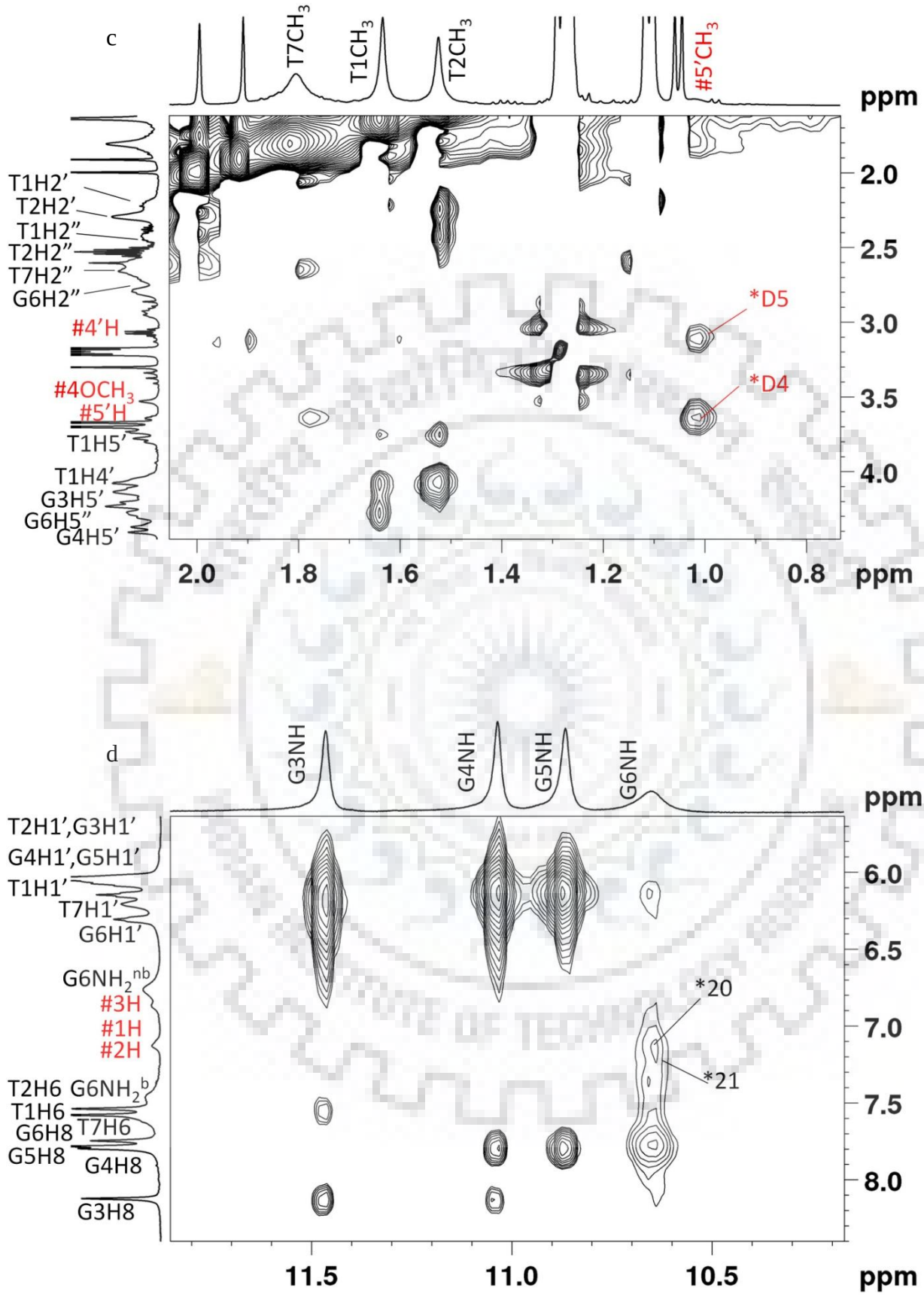
c
T7CH3
T1CH3
T2CH3
#5'CH3
ppm
T1H2'
T2H2'
T1H2"
T2H2"
T7H2"
G6H2"
#4'H
#4OCH3
#5'H
T1H5'
T1H4'
G3H5'
G6H5"
G4H5'
*D5
*D4
2.0
2.5
3.0
3.5
4.0
2.0
1.8
1.6
1.4
1.2
1.0
0.8
ppm
d
G3NH
G4NH
G5NH
G6NH
ppm
T2H1',G3H1'
G4H1',G5H1'
T1H1'
T7H1'
G6H1'
G6NH2nb
#3H
#1H
#2H
T2H6 G6NH2b
T1H6
G6H8 T7H6
G5H8
G4H8
G3H8
*20
*21
6.0
6.5
7.0
7.5
8.0
11.5
11.0
10.5
ppm

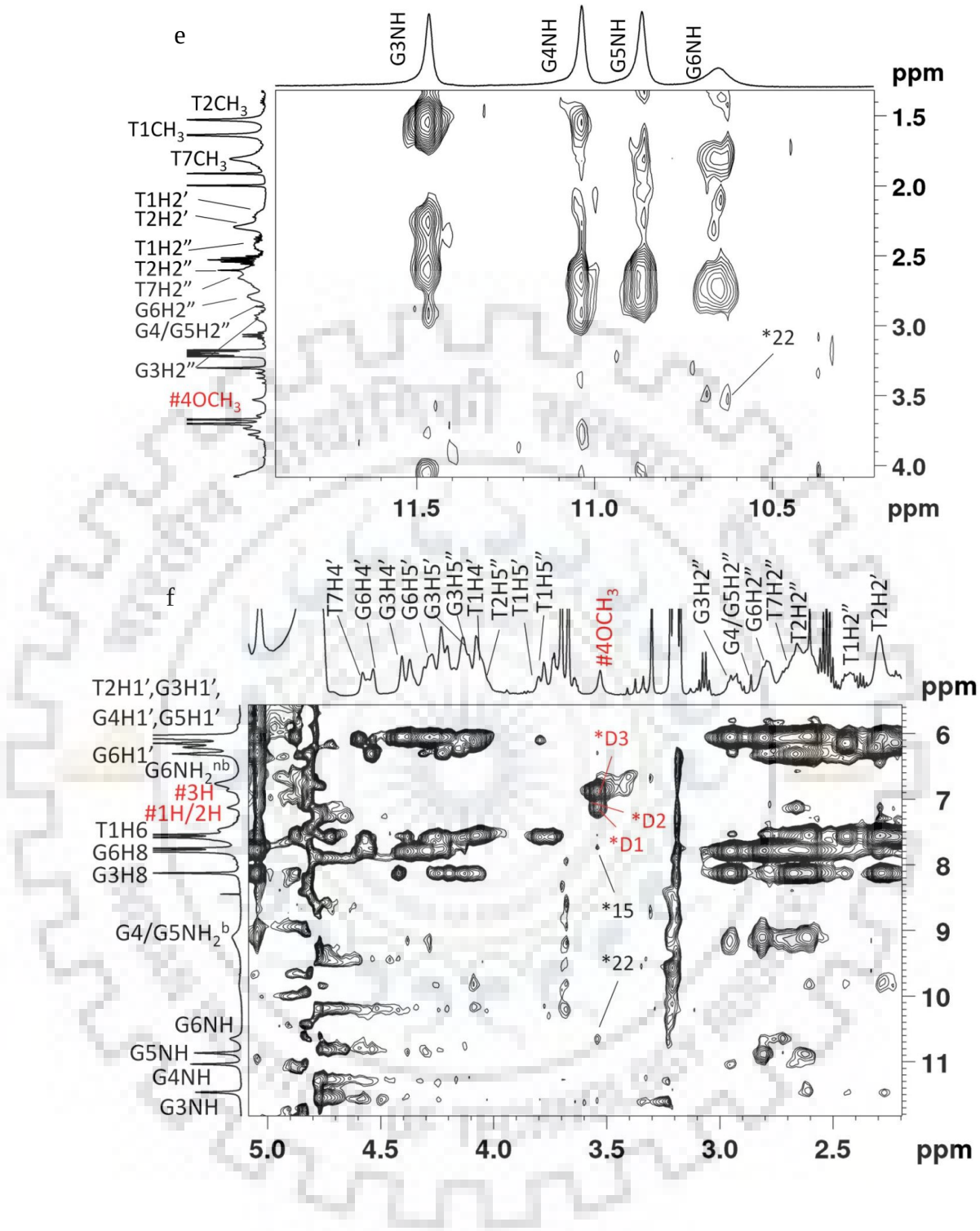

Figure 7.13 a-f) Expansion of specific regions of 2D ^{1}H-^{1}H NOESY spectra of 4'-epiadriamycin-Tet7 complex at D/N = 2.0, mixing time τ_m = 250 ms at 25 °C showing NOE correlations between 4'-epiadriamycin protons and Tet7 protons along with intramolecular NOE cross peaks of 4'-epiadriamycin (D). Symbol # denotes 4'-epiadriamycin protons, *D denotes intramolecular cross peaks of 4'-epiadriamycin (D numbering as in Table 7.19) and * denotes intermolecular cross peaks between 4'-epiadriamycin and Tet7 protons (* numbering as in Table 7.20).

Table 7.19 Intramolecular distances (Å) and relative intensities of intramolecular NOE cross peaks of 4'-epiadriamycin protons in 4'-epiadriamycin-Tet7 complex at D/N = 1.0, 2.0, 3.0 and 4.0 at τ_m=250 ms at 25 °C. nd: not determined s - strong, m - medium, w - weak intensity; o - overlap

S.No.	Label	Intra molecular NOE correlations	Inter proton distance at D/N=2.0	Intensity of NOE cross peak at D/N=1.0	Intensity of NOE cross peak at D/N=2.0	Intensity of NOE cross peak at D/N=3.0	Intensity of NOE cross peak at D/N=4.0
1	D1	4OCH_3-1H	2.9	o	o	o	o
2	D2	4OCH_3-2H	2.9	o	o	o	o
3	D3	4OCH_3-3H	2.1	s	s	s	s
4	D4	5'CH_3-5'H	2.7	m	m	nd	nd
5	D5	5'CH_3-4'H	2.8	m	m	nd	nd

Table 7.20 Interproton distances (Å) between 4'-epiadriamycin and Tet7 obtained from NOE cross peaks at D/N = 2.0, τ_m = 250 ms at 25 °C and corresponding distances (Å) in rMD model of 4'-epiadriamycin-Tet7 complex. nd: not determined; na: not available

S. No.	Inter molecular NOE correlations	Inter proton distances		S. No.	Inter molecular NOE correlations	Inter proton distances	
		NOESY at D/N=2.0	rMD model			NOESY at D/N=2.0	rMD model
1	2H-T2CH_3	4.3	7.7	12	4OCH_3-G6H1'	4.1	5.7
2	2H-T1CH_3	4.3	3.9	13	3H-T2CH_3	4.0	5.2
3	2H-T7CH_3	3.7	3.1	14	3H-T7CH_3	3.5	2.4
4	2H-T2H2'	4.1	6.3	15	4OCH_3-G6H8	4.5	6.1
5	2H-G6H2"	3.4	3.6	16	5'CH_3-G6H1'	3.7	nd
6	1H-T2CH_3	4.3	9.0	17	5'CH_3-T1H1'	na	na
7	1H-T1CH_3	4.3	5.0	18	5'CH_3-T2H1'	na	na
8	1H-T7CH_3	3.7	3.4	19	5'CH_3-G6H8	na	na
9	1H-T2H2'	4.1	8.6	20	2H-G6NH	3.5	6.8
10	1H-G6H2"	3.4	4.1	21	1H-G6NH	3.5	6.8
11	3H- G6H2"	4.5	3.9	22	4OCH_3-G6NH	4.0	3.6

Distance restraints from five non-overlapping intermolecular NOEs recorded at 250/200 ms at each D/N ratio (D/N = 1.0, 2.0, 3.0 and 4.0) were used to build the model by positioning 4'-epiadriamycin at two independent sites close to T1pT2 and G6pT7 steps. The restraint molecular dynamics (rMD) approach was used to arrive at a conformation of the complex using intramolecular DNA-DNA, intramolecular 4'-epiadriamycin-4'-epiadriamycin and intermolecular 4'-epiadriamycin-Tet7 distance restraints (Table 7.19-7.20 and Fig. 7.14 a-c). At G6pT7 site ring BCD stacks with G6 base while T7 is pushed away. In addition three hydrogen bonds, that is, 5O of ring C with O6 of G6 (2.96 Å), 5O of ring C with N1 of G6 (2.74 Å) and 6OH of ring B with O6 of G6 (3.18 Å) were observed which cannot be independently ascertained as 6OH signal was not obtained (Fig. 7.14 c). At T1pT2 sites the 4'-epiadriamycin binds externally showing four hydrogen bonds (Fig. 7.14 b), that is, 6OH of ring B with PO_4^{2-} of G3 (3.23 Å), 5O of ring C with PO_4^{2-} of G3 (3.44 Å), 12O of ring C with O2 of T2 (2.79 Å), $9COCH_2OH$ of ring A with O4 of G3 (1.87 Å). A total of 7% distance restraint violations (11 out of 148) were found in which 4% belong to terminal T7 residue so that the restraint violation was minimal (Table 7.21). The electrostatic contribution to the total energy is found to be significant. Thus we observe stacking and external binding at G6pT7 and T1pT2 sites, respectively.

a

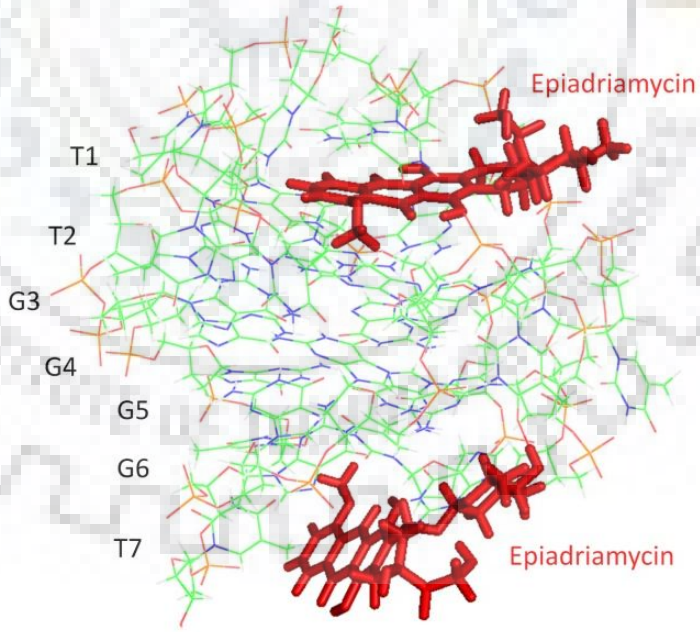

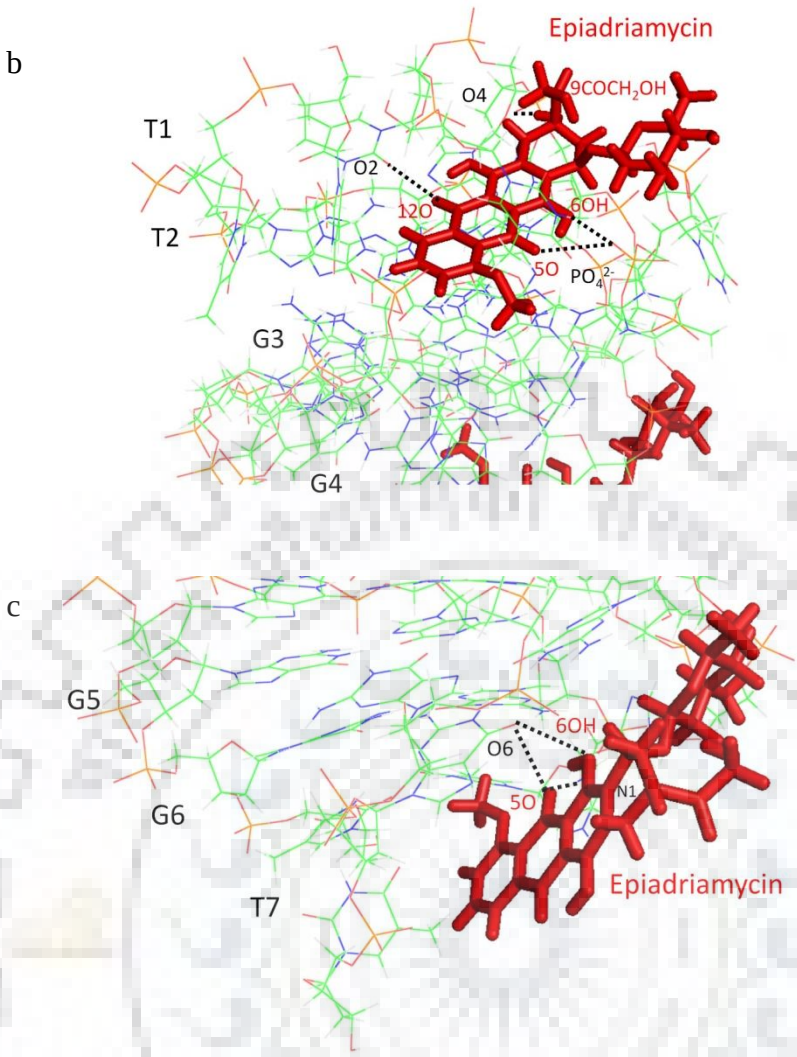

Figure 7.14 Energy minimized model of 4'-epiadriamycin bound to Tet7 obtained by restrained molecular dynamics simulations; a) Binding of 4'-epiadriamycin at two independent sites T1pT2 and G6pT7; b) Close up view of 4'-epiadriamycin binding to Tet7 at T1pT2 site and c) at G6pT7 site. (Hydrogen bond is represented by black dashed line).

Table 7.21 Structural data and final energy terms of 4’-epiadriamycin-Tet7 complex.

Experimental restraints	
Intramolecular	
Epiadriamycin-Epiadriamycin	5
DNA-DNA	138
Intermolecular	
Epiadriamycin-DNA	5
Total restraints	148
Average RMSD (Å)	0.86
Restraint Violations (distances >0.8 Å)	11
CVFF energy of minimized structures (kcal/mole)	
Total	-1617.04
Torsional	267.12
Electrostatic	-3190.39
van der Waals	2583.77

Daunomycin, an anthracycline analog, differs from 4'-epiadriamycin by having $9COCH_3$ in ring A in place of $9COCH_2OH$ and reverse orientation of H/OH groups in daunosamine sugar at 4’ position. The observed conformation of 4’-epiadriamycin-Tet7 complex showing external binding at 2 sites is similar to that found earlier in daunomycin-Tet7 complex (Chapter 4) but is in contrast to X-ray crystallographic structure in which layers of daunomycin (an analog) are stacked between G quadruplex DNA $[d\text{-}(TGGGGT)]_4$ (Clark et al., 2003). Crystal packing forces may be responsible for the difference in conformations. The observed conformation is in accord with molecular dynamics simulations of daunomycin-$[d\text{-}(TGGGGT)]_4$ complex in explicit solvent (Shen et al., 2017). End stacking mode of binding has also been inferred through ESI-MS on daunomycin to $[d\text{-}(TGGGGT)]_4$ (N. Xu et al., 2012) and NMR studies on doxorubicin-$[d\text{-}(TTAGGT)]_4$ complex (Scaglioni et al., 2016). Two 4’-epiadriamycin molecules stacked in parallel orientation are expected to give NOE cross peaks of ring A protons with daunosamine sugar and ring D protons. We did not observe intermolecular NOE connectivities expected on the formation of 4’-epiadriamycin dimer in parallel orientation, that is, 10eq-5’CH_3, 10ax-5’CH_3, 10ax-4’H, 10ax-3’H, and 7H-10eq (Agrawal, Barthwal, & Barthwal, 2009; Evstigneev, Khomich, & Davies, 2006). Further the intermolecular NOE cross peaks expected in two 4'-epiadriamycin stacked in antiparallel orientation (ring A with ring D and daunosamine sugar protons), that is, 10ax-1H, 10ax-2H, 10ax-3H, 10ax-$4OCH_3$, $9COCH_2OH$-1H, $9COCH_2OH$-2H, and $9COCH_2OH$-3H were also not present (Agrawal, Barthwal, & Barthwal, 2009; Evstigneev, Khomich, & Davies, 2006). This indicates that 4’-

epiadriamycin binds to Tet7 as a monomer although it exists as stacked dimer in free form in solution.

The NOESY spectra of the adriamycin-Tet7 complex show that sequential NOE cross peaks between NH-NH, NH-H8, base-H1'/H2'/2" are all intact (Fig. 7.8 j-m) at D/N = 2.0 indicating that adriamycin does not intercalate at any base pair step. Relative intensities of the NOE correlations between base protons H8/H6 with sugar protons H2'/2"/H1' and intra sugar protons confirms that the right-handed DNA helix with *anti* glycosidic bond rotations and C2' *endo* deoxyribose sugar conformation. Six prominent intra molecular drug-drug short contacts were observed (Table 7.22 and Fig. 7.15 a-c). In addition twenty-one intermolecular NOE cross peaks between drug and DNA protons were observed (Table 7.12 b and Fig. 7.15 a-f). A comparison of intermolecular NOEs with that of 4'-epiadriamycin-Tet7 complex (Table 7.20) shows that these NOE correlations match (Table 7.23) except that $4OCH_3$-G6NH is missing and 5'CH3-T1H1'/T2H2'/G6H8 are present in the adriamycin-Tet7 complex. However, there is a significant difference in the intensity of intermolecular NOE cross peaks, e.g. 1H and 2H protons are much closer to $T1CH_3$ and $T2CH_3$ protons while the same in 4'-epiadriamycin-Tet7 complex are in the range 4.3-5.0 Å. The intermolecular contacts of 2H with $T7CH_3$ and 1H, 3H with G6H2" are also shorter in the adriamycin-Tet7 complex as compared to 4'-epiadriamycin-Tet7 complex (Table 7.20).

Table 7.22 Intramolecular distances (Å) and relative intensities of intramolecular NOE cross peaks of adriamycin protons in the adriamycin-Tet7 complex at D/N = 1.0, 2.0, 3.0 and 4.0 at τ_m=250 ms at 25 °C. nd: not determined s - strong, m - medium, w - weak intensity; o - overlap

S.No.	Label	Intra molecular NOE correlations	Interproton distance at D/N=2.0	Intensity of NOE cross peak at D/N=1.0	Intensity of NOE cross peak at D/N=2.0	Intensity of NOE cross peak at D/N=3.0	Intensity of NOE cross peak at D/N=4.0
1	D1	$4OCH_3$-1H	2.3	o	o	o	o
2	D2	$4OCH_3$-2H	2.3	o	o	o	o
3	D3	$4OCH_3$-3H	1.6	s	s	s	s
4	D4	5'CH_3-5'H	2.0	s	s	s	s
5	D5	5'CH_3-4'H	1.9	s	s	s	s
6	D6	5'CH_3-3'H	2.9	m	m	nd	nd

Table 7.23 Interproton distances (Å) between adriamycin and Tet7 obtained from NOE cross peaks at D/N = 2.0, τ_m = 250 ms at 25 °C and corresponding distances (Å) in rMD model of adriamycin-Tet7complex. nd: not determined; na: not available

S. No.	Inter molecular NOE correlations	Interproton distances		S. No.	Intermolecular NOE correlations	Interproton distances	
		NOESY at D/N=2.0	rMD model			NOESY at D/N=2.0	rMD model
1	2H-T2CH_3	2.7	5.9	12	$4OCH_3$-G6H1'	3.5	3.0
2	2H-T1CH_3	2.7	8.6	13	3H-T2CH_3	3.2	5.0
3	2H-T7CH_3	2.9	6.2	14	3H-T7CH_3	3.5	4.9
4	2H-T2H2'	3.0	5.0	15	$4OCH_3$-G6H8	4.0	4.3
5	2H-G6H2"	2.5	7.4	16	5'CH_3-G6H1'	3.7	8.3
6	1H-T2CH_3	2.7	9.4	17	5'CH_3-T1H1'	3.7	nd
7	1H-T1CH_3	2.7	5.7	18	5'CH_3-T2H1'	4.0	nd
8	1H-T7CH_3	2.9	6.1	19	5'CH_3-G6H8	3.5	7.1
9	1H-T2H2'	3.0	3.2	20	2H-G6NH	4.5	4.8
10	1H-G6H2"	2.5	7.9	21	1H-G6NH	4.5	3.5
11	3H- G6H2"	3.5	5.4	22	$4OCH_3$-G6NH	na	na

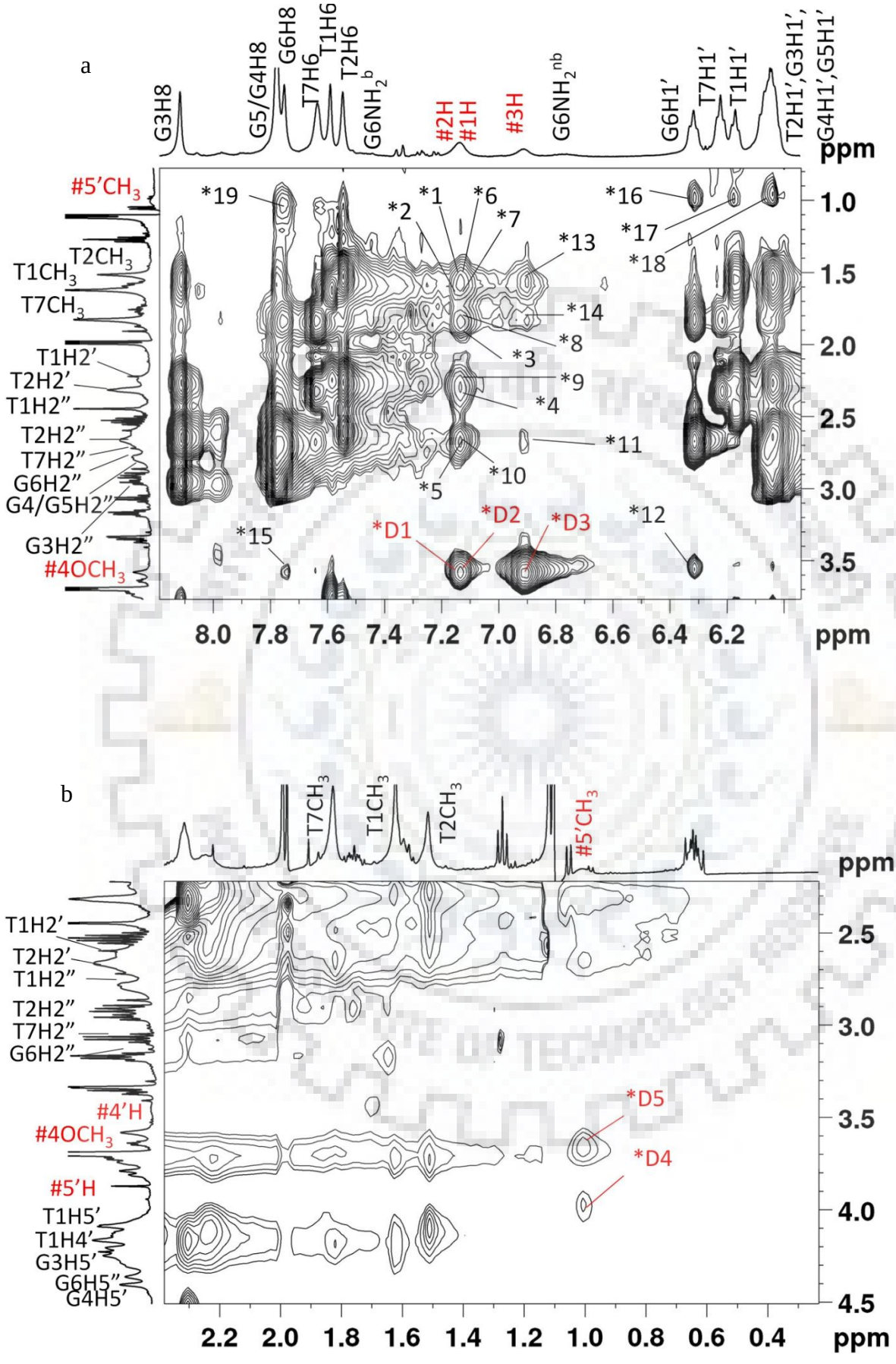
a
G3H8
G5/G4H8
G6H8
T7H6
T1H6
T2H6
G6NH2b
#2H
#1H
#3H
G6NH2nb
G6H1'
T7H1'
T1H1'
T2H1',G3H1',
G4H1',G5H1'
ppm
#5'CH3
T2CH3
T1CH3
T7CH3
T1H2'
T2H2'
T1H2"
T2H2"
T7H2"
G6H2"
G4/G5H2"
G3H2"
#4OCH3
*19
*2
*1
*6
*7
*13
*16
*17
*18
*14
*8
*3
*9
*4
*11
*10
*5
*15
*D1
*D2
*D3
*12
1.0
1.5
2.0
2.5
3.0
3.5
8.0 7.8 7.6 7.4 7.2 7.0 6.8 6.6 6.4 6.2
ppm
b
T7CH3
T1CH3
T2CH3
#5'CH3
ppm
T1H2'
T2H2'
T1H2"
T2H2"
T7H2"
G6H2"
#4'H
#4OCH3
#5'H
T1H5'
T1H4'
G3H5'
G6H5"
G4H5'
*D5
*D4
2.5
3.0
3.5
4.0
4.5
2.2 2.0 1.8 1.6 1.4 1.2 1.0 0.8 0.6 0.4
ppm

c

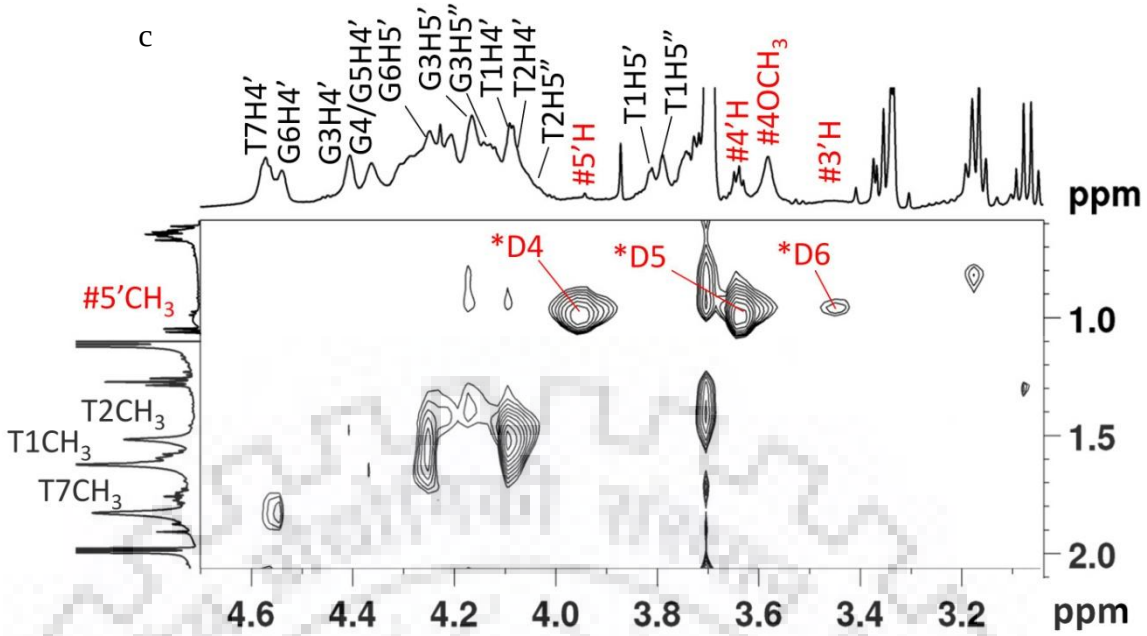
T7H4′
G6H4′
G3H4′
G4/G5H4′
G6H5′
G3H5′
G3H5″
T1H4′
T2H4′
T2H5″
#5′H
T1H5′
T1H5″
#4′H
#4OCH3
#3′H
ppm
*D4
*D5
*D6
#5′CH3
T2CH3
T1CH3
T7CH3
1.0
1.5
2.0
4.6
4.4
4.2
4.0
3.8
3.6
3.4
3.2
ppm

d

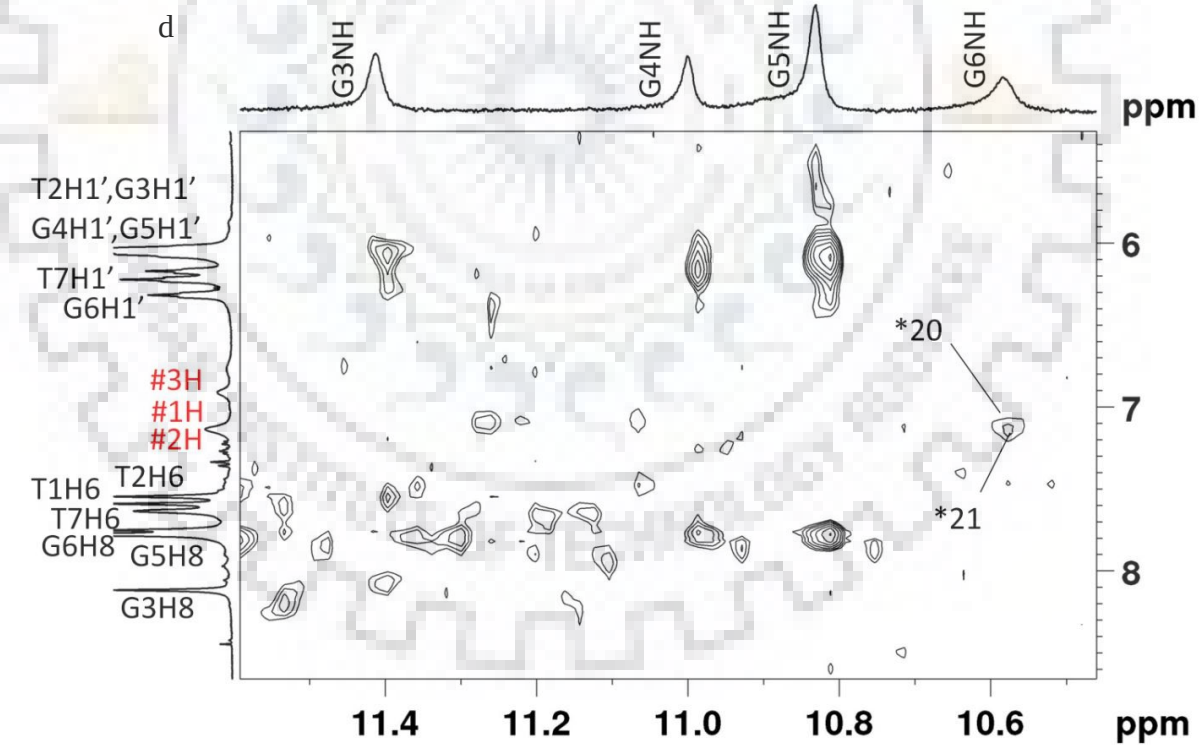
G3NH
G4NH
G5NH
G6NH
ppm
T2H1′,G3H1′
G4H1′,G5H1′
T7H1′
G6H1′
#3H
#1H
#2H
T1H6
T2H6
T7H6
G6H8
G5H8
G3H8
*20
*21
6
7
8
11.4
11.2
11.0
10.8
10.6
ppm

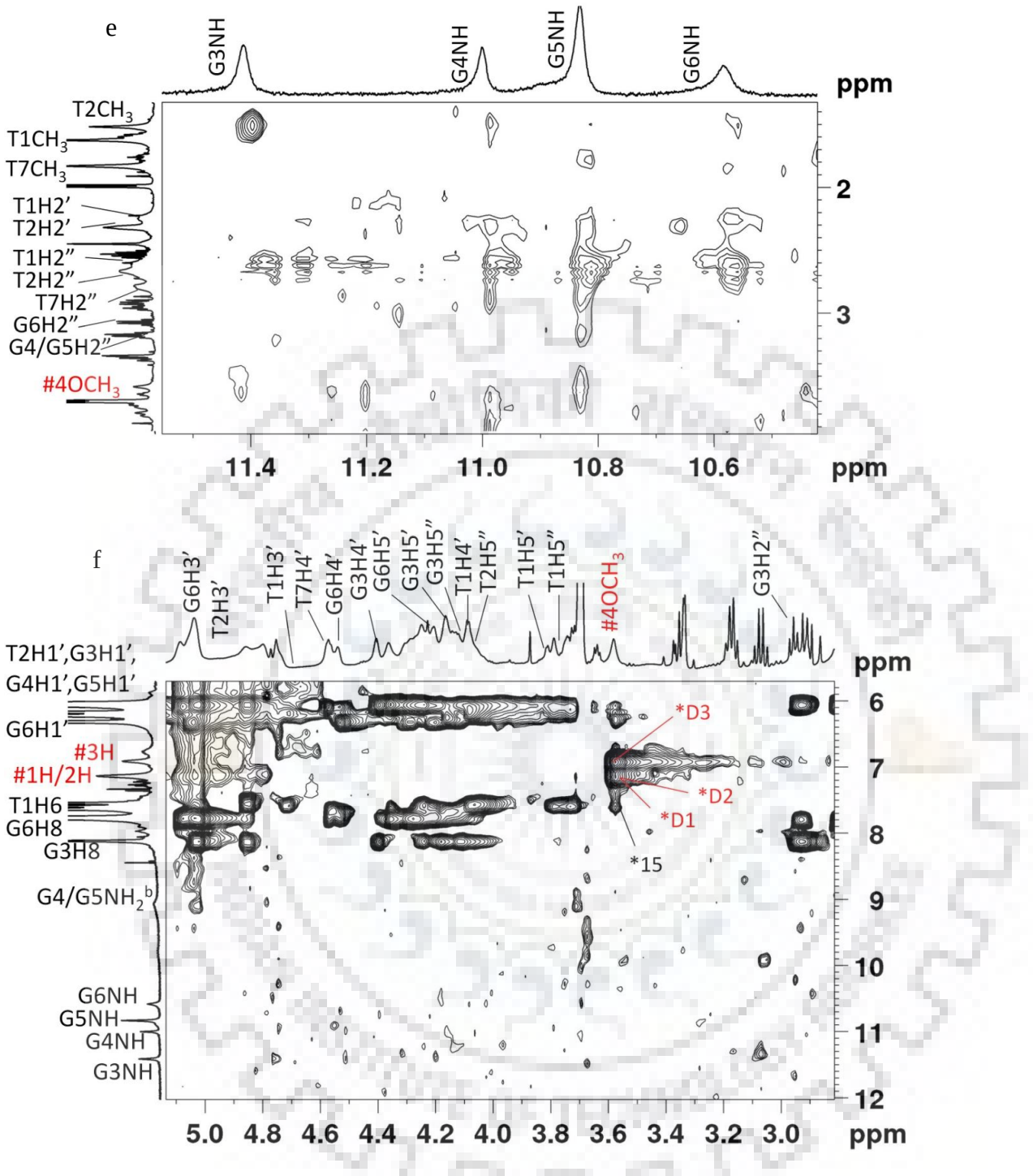

Figure 7.15 a-f) Expansion of specific regions of 2D ^{1}H-^{1}H NOESY spectra of the adriamycin-Tet7 complex at D/N = 2.0, mixing time τ_m = 250 ms at 25 °C showing NOE correlations between adriamycin protons and DNA protons along with intra molecular NOE cross peaks of adriamycin (D). Symbol # denotes adriamycin protons, *D denotes intramolecular cross peaks of adriamycin (D numbering as in Table 7.22) and * denotes intermolecular cross peaks between adriamycin and Tet7 protons (* numbering as in Table 7.23).

The conformation of complex obtained from rMD simulations using five non-overlapping short drug-DNA contacts (Table 7.23) shows the specific orientation of adriamycin at T1pT2 and G6pT7 sites (Fig. 7.16 a-c). This interaction leads to the formation of five hydrogen bonds, that is, 9COCH$_2$OH of ring A with O2 of T2 (2.92 Å), 9COCH$_2$OH of ring A with N3 of T2 (3.09 Å), 12O of ring C with PO_4^{2-} of G3 (3.03 Å), 5O of ring C with PO_4^{2-} of G5 (3.10 Å), 5O of ring C with O5 of G5 (3.33 Å) at T1pT2 site (Fig. 7.16 b) and three hydrogen bonds, that is, 5O of ring C with O5 of T7 (2.97 Å), 6OH of ring B with O5 of T7 (3.03 Å) and 4'OH of daunosamine sugar moiety with PO_4^{2-} of T7 (2.84 Å) at G6pT7 sites (Fig. 7.16 c). Total of 7% distance restraint violations (10 out of 141) were found in case of adriamycin-Tet7 complex out of which 3% belongs to T7 residue so that the restraint violation was minimal (Table 7.24). The orientation of daunosamine sugar is different from that in the case of 4'-epiadriamycin. We also looked for intermolecular drug-drug NOE contacts expected on the binding of adriamycin in the dimeric state (Agrawal, Barthwal, & Barthwal, 2009; Evstigneev, Khomich, & Davies, 2006). Absence of all such intermolecular NOE connectivities of adriamycin dimer in parallel and antiparallel orientation (ring A with ring D/daunosamine sugar protons) confirms binding in monomeric form. Several of these short NOE contacts are expected in X-ray structure (Clark et al., 2003) in which layers of daunomycin exist. Thus, NMR results show that 4'-epiadriamycin and adriamycin bind as a monomer at either site, unlike X-ray structure in which two layers of daunomycin are stacked between two G quadruplex DNA [d-(TGGGGT)]$_4$ end to end. The maximum stoichiometry reached is 2:1 and negates layers of 4'-epiadriamycin/adriamycin which will yield stoichiometry of 3:1.

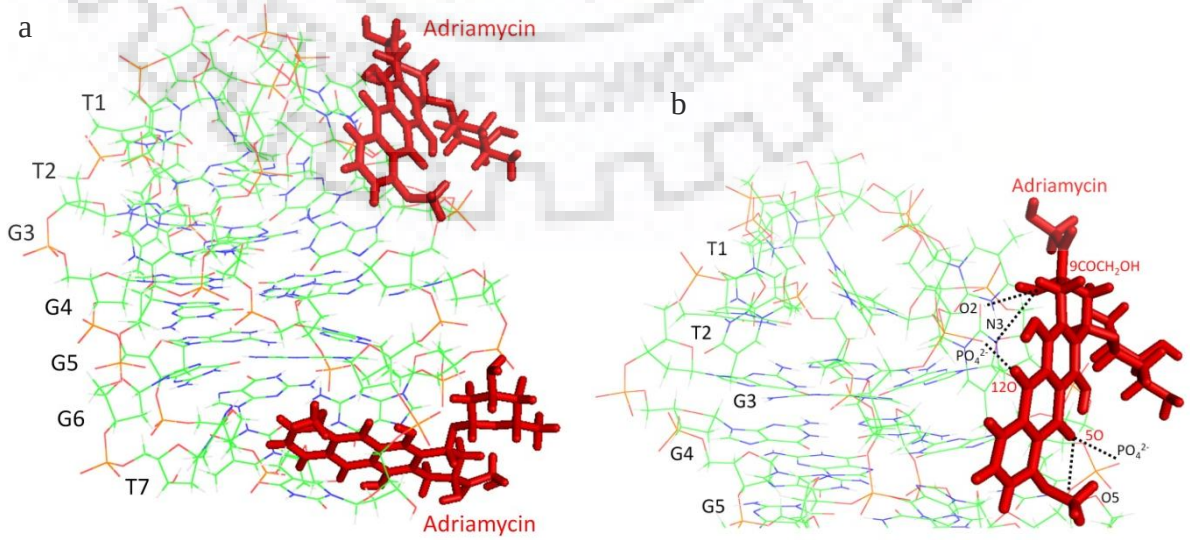

c

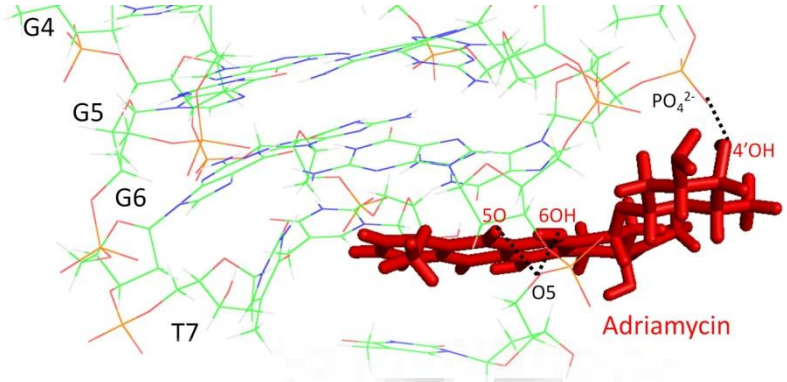

Figure 7.16 Energy minimized model of adriamycin bound to Tet7 obtained by restrained molecular dynamics simulations; a) Binding of adriamycin at two independent sites T1pT2 and G6pT7; b) Close up view of adriamycin binding to Tet7 at T1pT2 site and c) at G6pT7 site. (Hydrogen bond is represented by black dashed line).

Table 7.24 Structural data and final energy terms of adriamycin-Tet7 complex.

Experimental restraints	
Intramolecular	
adriamycin-adriamycin	6
DNA-DNA	130
Intermolecular	
adriamycin-DNA	5
Total restraints	141
Average RMSD (Å)	0.96
Restraint Violations (distances >0.8 Å)	10
CVFF energy of minimized structures (kcal/mole)	
Total	-1664.42
Torsional	256.40
Electrostatic	-3217.47
van der Waals	2612.97

7.3.7. Thermal denaturation

Melting profile of imino protons of guanine bases of free Tet7 and 4'-epiadriamycin-Tet7 complex at D/N = 1.0-4.0 were obtained at 25-85 °C in steps of 5 °C upon its transition from ordered to disordered state (Fig. 7.17). In free Tet7, G3NH and G6NH are visible at 65 °C and disappear at 70 °C due to breaking of Hoogsteen hydrogen bonds between guanines on a

quartet plane and exchange of the NH proton with solvent. However, G4NH and G5NH remain sharp at 70 °C. The melting of free Tet7 apparently follows a three-state process (alternately two "two-state" melting processes) so that intermediates of Tet7 with partially unfolded form exist. The melting temperature (T_{m1}) is about 65-70 °C and T_{m2} may be quiet high and beyond 70 °C (Kumar & Barthwal, 2018; Pradeep & Barthwal, 2016). The T_m decreases in the order: G4NH, G5NH > G6NH, G3NH. In 4'-epiadriamycin- Tet7 complex at D/N = 1.0-4.0 it is seen that G6NH is still intact at D/N = 4.0, G3NH is visible and G4NH/G5NH are well defined sharp peaks at 85 °C. The melting transition, therefore, follows four state processes so that T_m decreases in order: G4NH, G5NH > G6NH > G3NH. Thermal stabilization of G3NH is 15 °C and that for G6NH is > 20 °C. It may be noted that the terminal G6NH which was disappearing along with G3NH in free Tet7 is much more stabilized than G3NH in the complex. The enhanced stabilization is consistent with significant broadening and large upfield/downfield shift of G6/T7 protons thus confirming G6pT7 as a dominant binding site while the second binding site may be close to G3.

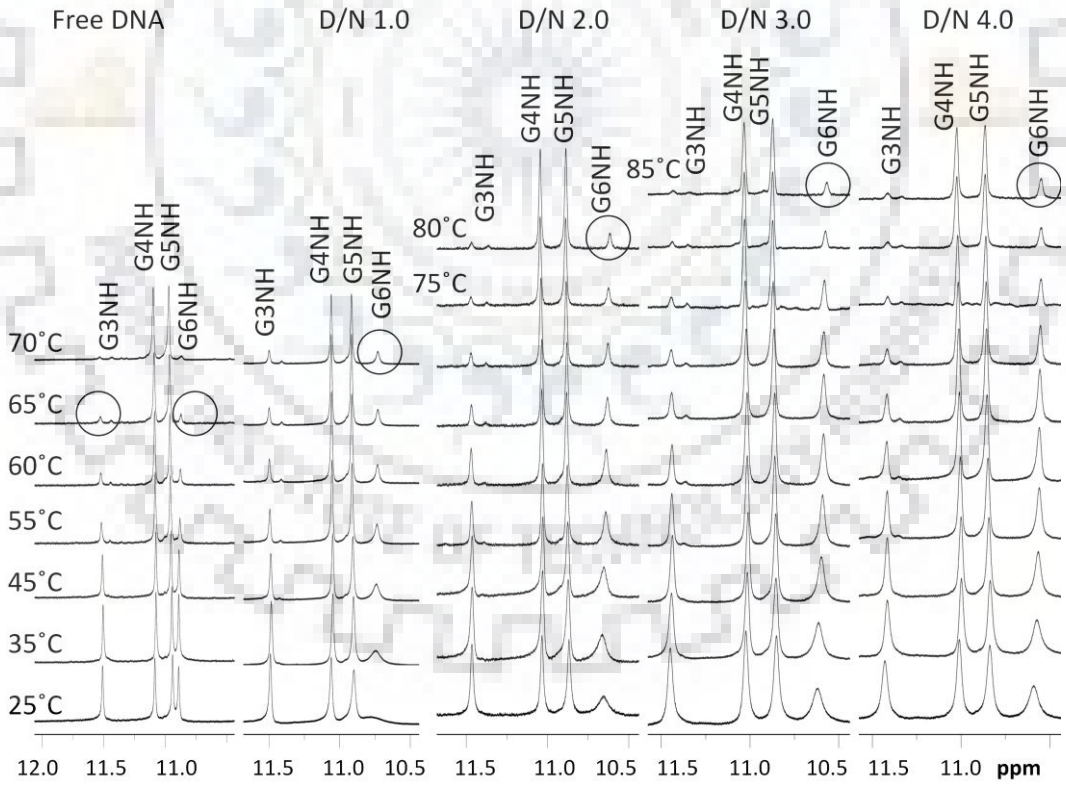

Figure 7.17 1D ^{1}H NMR spectra of imino protons showing thermal melting profile of free Tet7 and 4'-epiadriamycin- Tet7 complex at different D/N ratios at different temperatures.

We observed melting transition of folded→unfolded of free Tet7 and of 4'-epiadriamycin- Tet7 complex at D/N = 1.0-4.0 independently using differential scanning calorimeter (Fig. 7.18 a-f

and Table 7.25). DSC thermogram of 50 μM free Tet7 was fitted in multiple state model of deconvolution having melting transitions T_{m1} = 46.2±0.4 °C, T_{m2} = 54.9±0.7 °C, T_{m3} = 72.9±0.6 °C and T_{m4} = 110.5 ±0.1 °C (P. Kumar & Barthwal, 2018). This in general indicates that the species may be involved in equilibria consisting of either a single-folded quadruplex to random coil transition through an intermediate, or two independent single-folded quadruplex to random coil transition through an intermediate, or two independent species following separate pathways not involving intermediates to the same unfolded state (Antonacci et al., 2007). The stepwise disappearance of imino protons with temperature (Fig. 7.17) indicates the existence of several intermediates. The disappearance of G3NH and G6NH at 70 °C (±5 °C) may corresponds to T_{m3} = 72.9 °C in DSC experiments. Accordingly, the disappearance of G4NH and G5NH forming the central core of G tetrad could correspond to T_{m3} = 110.5 °C. The observed lower melting temperatures, T_{m1} = 46.2 °C and T_{m2} = 54.9 °C, may corresponds to the melting transitions of other regions of Tet7, e.g. T1/T2/T7 residues. In complex, it is found that T_m increases with D/N (Fig. 7.18 g) and saturates at D/N = 3.0. T_{m3} increases by 18-19 °C till D/N = 4.0. The T_{m4} value which corresponds to G4NH and G5NH are beyond the range of measurement (> 120 °C). The extent of stabilization of G3NH and G6NH may be taken as 19 °C. Further, both the sites are likely to be occupied at D/N = 3.0 so that no further stabilization occurs at D/N = 4.0.

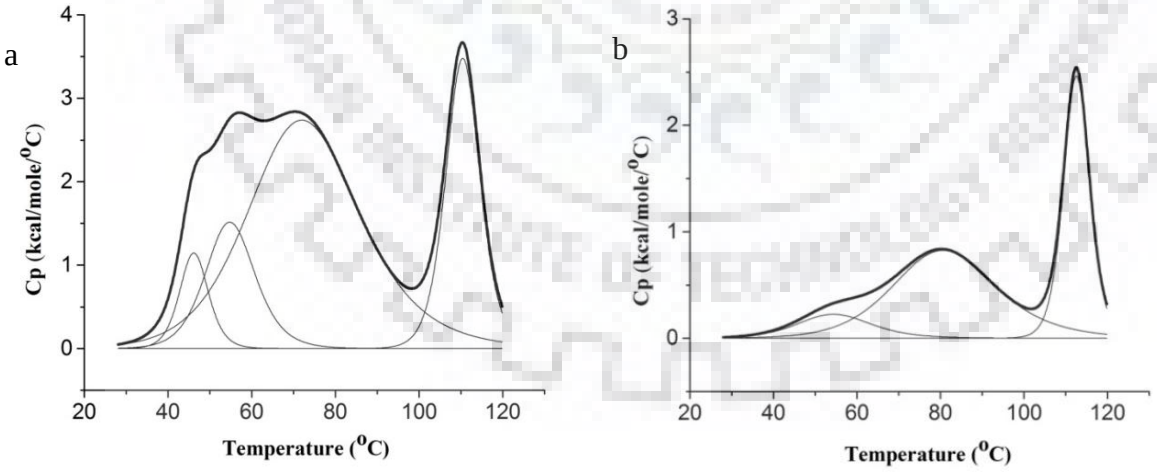

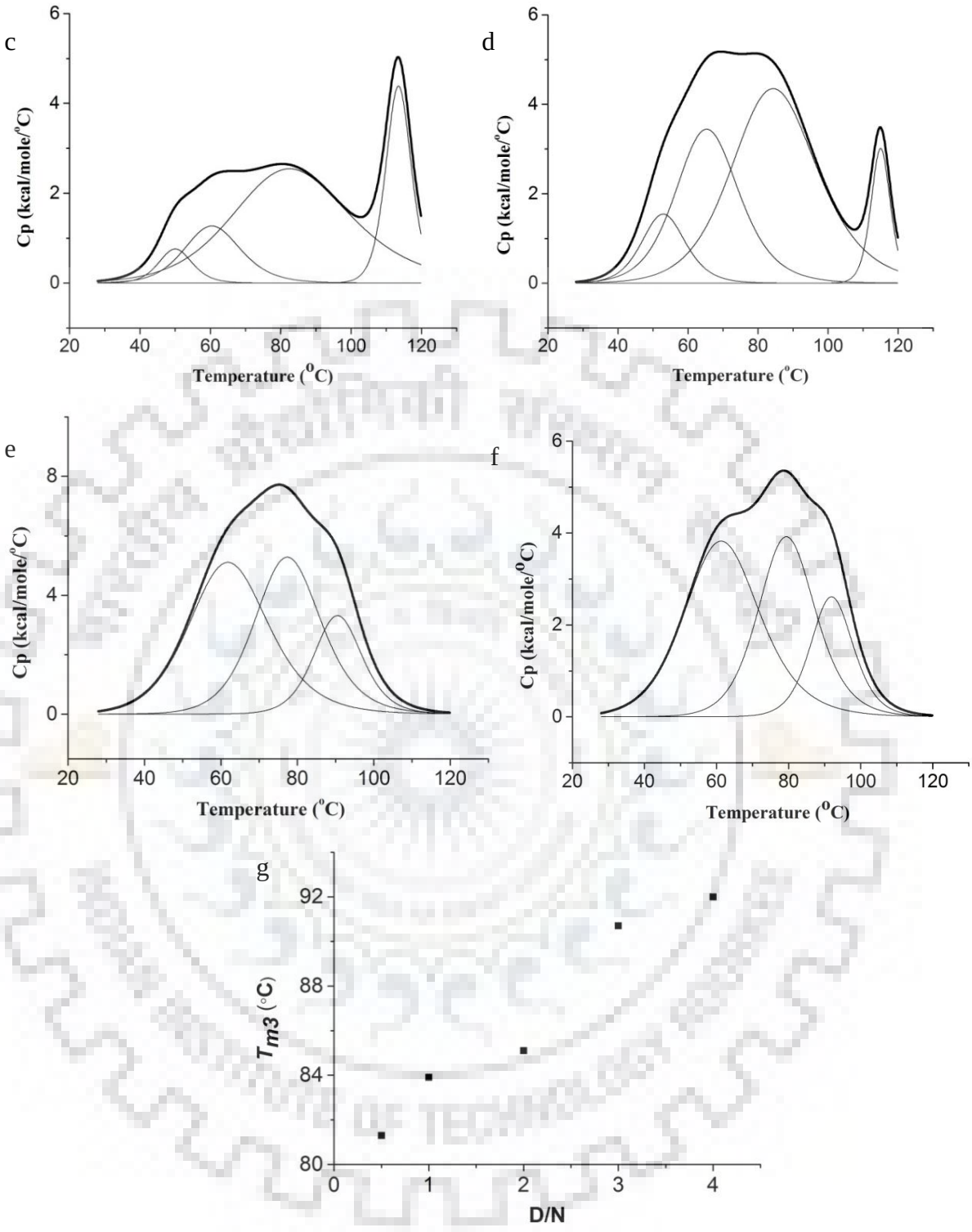

Figure 7.18 DSC thermograms showing excess heat capacity as a function of temperature for 4'-epiadriamycin-Tet7 complex at a) 50 µM free Tet7 b-f) D/N=0.5, 1.0, 2.0, 3.0, 3.5 and 4.0. All samples were prepared in phosphate buffer (KBPES) (pH 7.0) containing 100 mM KCl. g) Plot of melting temperature T_{m3} obtained from DSC experiments as a function of D/N ratio.

Table 7.25 Data obtained from DSC experiments showing change in melting temperature (T_m) of Tet7 upon complexation with 4'-epiadriamycin at different D/N ratios.

	T_{m1} (°C)		T_{m2} (°C)		T_{m3} (°C)		T_{m4}(°C)	
Free DNA	46.2±0.4		54.9±0.7		72.9±0.6		110.5±0.1	
Complex		ΔT_{m1}		ΔT_{m2}		ΔT_{m3}		ΔT_{m4}
D/N=0.5	nd	nd	54.9±0.9	0.0	81.3±0.3	8.4	112.6±0.1	2.1
D/N=1.0	50.1±0.9	3.9	60.8±1.3	5.9	83.9±1.1	11.0	113.5±0.1	3.0
D/N=2.0	53.1±0.5	6.9	65.7±0.4	10.8	85.1±0.4	12.2	115.0±0.1	4.5
D/N=3.0	62.3±1.8	16.1	77.7±1.1	22.8	90.7±1.0	17.8	nd	nd
D/N=4.0	61.8±2.7	15.6	79.7±2.4	24.8	92.0±2.0	19.1	nd	nd

Melting profiles of free Tet7 and adriamycin-Tet7 complexes were obtained at 25-80 °C in steps of 5 °C showing transition from ordered to disordered state (Fig. 7.19). This complex also shows three T_m values. The T_m decreases in the following order: G4NH, G5NH > G6NH > G3NH. G3NH which practically disappears at 75 °C at D/N = 3.0. G6NH is visible at 80 °C with low-intensity signal and G4NH/G5NH are sharp resonant peaks even at 80 °C at D/N = 4.0. At D/N = 1.0-2.0, T_m decreases in the order: G5 > G4 > G6 > G3 and at D/N = 3.0-4.0, T_m decreases in the order: G5, G4 > G6 > G3. Thermal stabilization of G6NH is > 15 °C and G6NH is more stabilized than G3NH (Fig. 7.19). DSC thermograms (Fig. 7.20 a-e) reveal that T_{m3} gets stabilized by 16 °C while T_{m4} may be beyond 120 °C at D/N = 4.0 (Table 7.26). T_{m3} may corresponds to G6NH while G4/G5NH might represent T_{m4} >120 °C. T_m increases with D/N (Fig. 7.20 f) and saturates at D/N = 2.0 showing that both sites are occupied at D/N = 2.0 in comparison to 4'-epiadriamycin- Tet7 complex in which saturation occurs at D/N = 3.0. This is in accord with observed sharpening and saturation of G6NH and T7H6 signals at D/N = 2.0 and D/N = 3.0 in adriamycin-Tet7 complex and 4'-epiadriamycin-Tet7 complex, respectively (Fig. 7.5 d and 7.8 d).

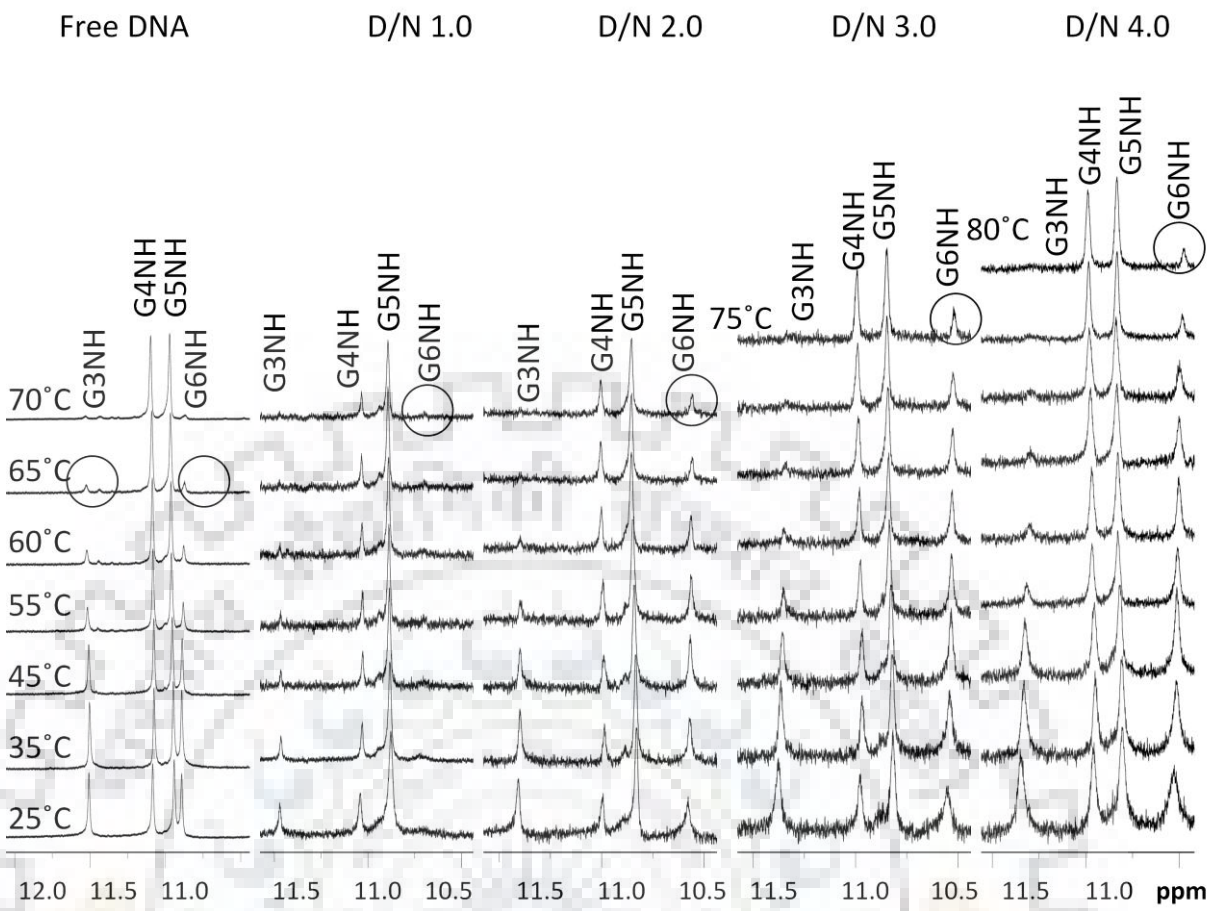

Figure 7.19 1D ^{1}H NMR spectra of imino protons showing thermal melting profiles of free Tet7 and adriamycin-Tet7 complex at different D/N ratios at different temperatures.

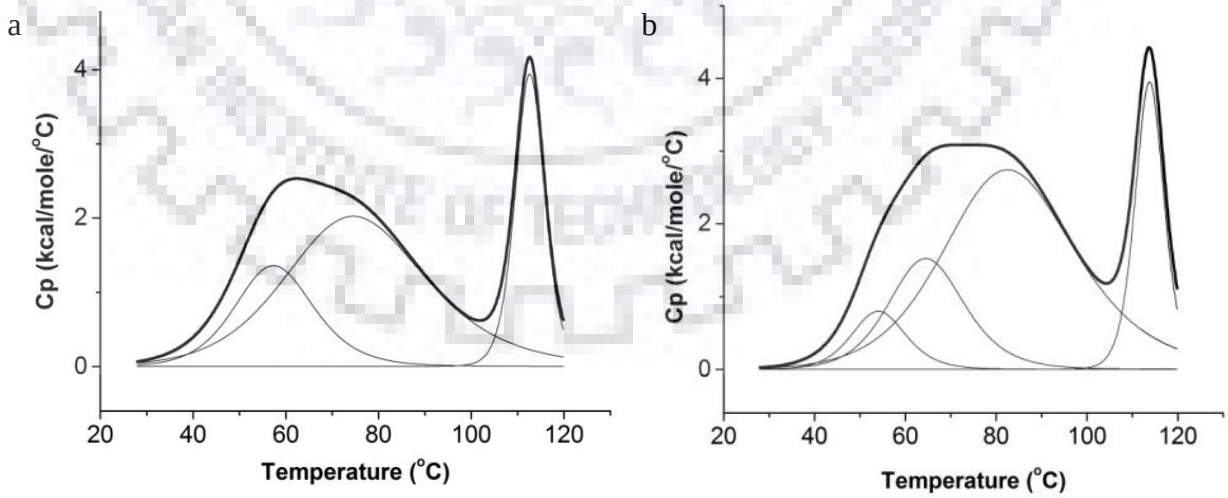

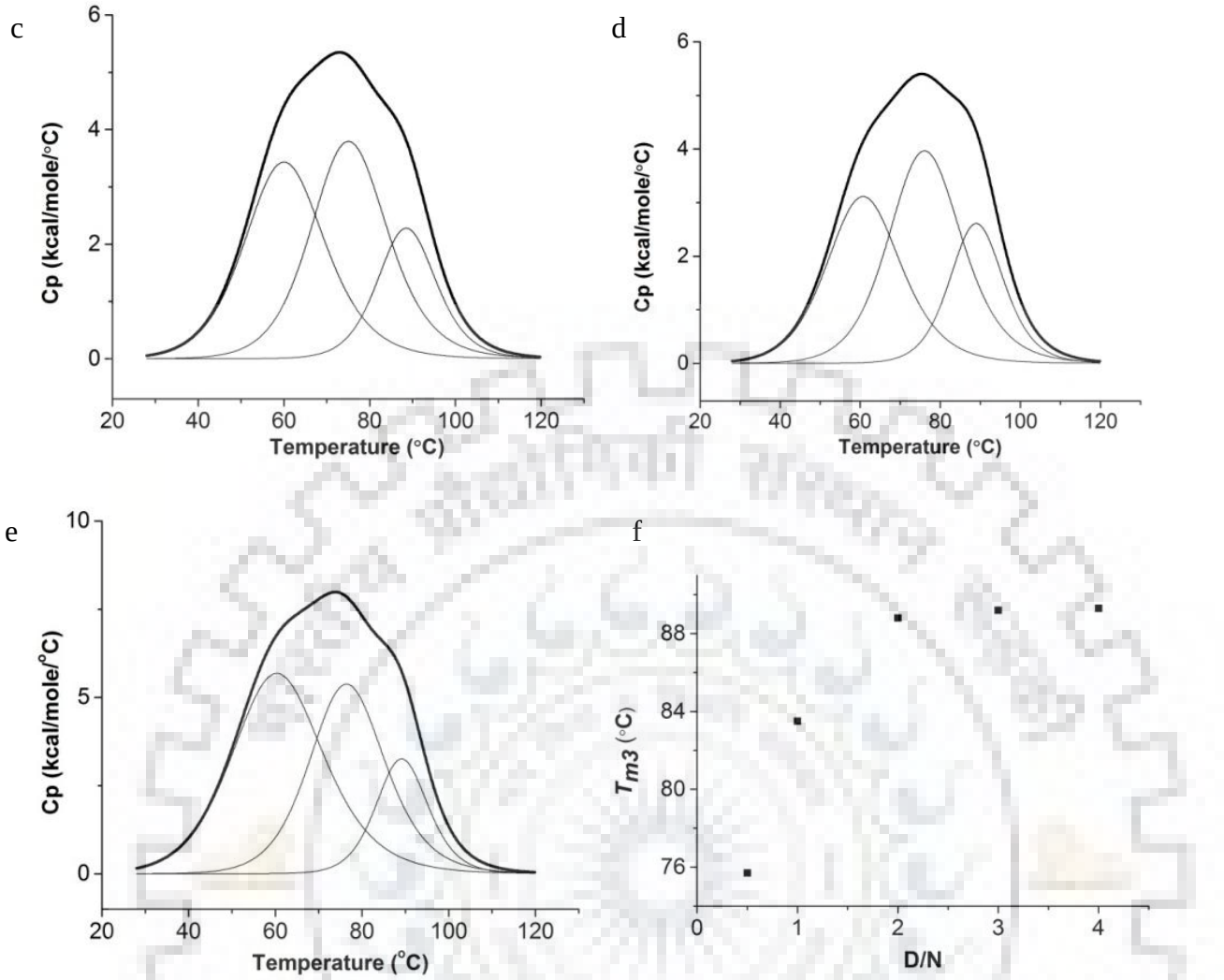

Figure 7.20 DSC thermograms showing excess heat capacity as a function of temperature for adriamycin-Tet7 complex at a-e) D/N=0.5, 1.0, 2.0, 3.0 and 4.0. All samples were prepared in phosphate buffer (KBPES) (pH 7.0) containing 100 mM KCl. f) Plot of melting temperature T_{m3} obtained from DSC experiments as a function of D/N ratio.

Table 7.26 Data obtained from DSC experiments showing change in melting temperature (T_m) of Tet7 upon complexation with adriamycin at different D/N ratios.

	T_{m1} (°C)		T_{m2} (°C)		T_{m3} (°C)		T_{m4}(°C)	
Free DNA	46.2±0.4		54.9±0.7		72.9±0.6		110.5±0.1	
Complex		ΔT_{m1}		ΔT_{m2}		ΔT_{m3}		ΔT_{m4}
D/N=0.5			57.7±0.6	2.8	75.7±1.4	2.8	112.7±0.1	2.2
D/N=1.0	54.2±1.7	8.0	64.8±1.6	9.9	83.5±1.4	10.6	113.8±0.1	3.3
D/N=2.0	60.5±1.4	14.3	75.5±1.1	20.6	88.8±1.1	15.9		
D/N=3.0	61.2±0.8	15.0	76.5±0.8	21.6	89.2±0.5	16.3		
D/N=4.0	60.9±2.2	14.7	76.8±1.9	21.9	89.3±1.4	16.4		

7.4. Conclusion

We conclude that adriamycin and 4'-epiadriamycin binds to Tet7 as a monomer at two distinct sites namely, T1pT2 and G6pT7 sites. Both the drug molecules end stacks at G6pT7 site by pushing away T7 and binds externally at T1pT2 site. No classical intercalation of either of the two drugs is evident as the sequential NOE connectivity among DNA protons remains intact (Fig.7.5 j-m and Fig. 7.8 j-m). Binding of both the drugs to Tet7 leads to thermal stabilization of T_m ~15-20 °C. However, thermal stabilization of Tet7 is slightly higher upon complexation with 4'-epiadriamycin than adriamycin (Table 6.3-6.6, 7.25-7.26 and Fig. 7.17, 7.19). Also, binding energy and number of hydrogen bond formation are higher in 4'-epiadriamycin-Tet7 complex than adriamycin-Tet7 complex (Chapter 6) which indicates slightly better stabilization and higher T_m values on binding of 4'-epiadriamycin to Tet7. Interestingly, a saturation of T_m occurs at D/N = 3.0 in 4'-epiadriamycin-Tet7 complex while in adriamycin-Tet7 complex saturation occurs at D/N = 2.0 (Fig. 7.18 g and 7.20 f). This is in accordance with sharpening and saturation of G6NH and T7H6 signals at D/N = 2.0 and 3.0 for adriamycin-Tet7 and 4'-epiadriamycin-Tet7 complexes, respectively (Fig 7.5 d and 7.8 d). This might be due to partial filling of Tet7 sites at D/N = 2.0 in case of binding of 4'-epiadriamycin and binding continues at D/N >2.0 following saturation at D/N = 3.0, as opposed to adriamycin binding to Tet7 where sites are fully occupied at D/N = 2.0.

It is important to note that daunosamine sugar protons namely 5'H, 4'H, 2'axH, and 2'eqH are more upfield shifted in 4'-epiadriamycin-Tet7 complex than in adriamycin-Tet7 complex at D/N = 4.0 (Table 7.10 and 7.3) which suggests greater interaction of sugar ring of 4'-epiadriamycin with Tet7. It must be due to the difference in orientation of the hydroxyl group present at 4' position in adriamycin and 4'-epiadriamycin. Daunosamine sugar moiety is known to interact with the groove and backbone of G-quadruplex DNA (Clark et al., 2003) and the only difference at 4' position of 4'-epiadriamycin along with greater interaction of sugar moiety to DNA might impart slightly higher thermal stabilization. These findings can be correlated from the differences in ^{31}P spectra of both the complexes. ^{31}P spectra is more broadened and downfield shifted in adriamycin-Tet7 complex than 4'-epiadriamycin-Tet7 complex (Fig. 7.12 a,b and Table 7.17-7.18) indicating the greater extent of distortion or effect on phosphate backbone of DNA in adriamycin-Tet7 complex which might result in slightly lower thermal stabilization. This effect of daunosamine sugar ring over the phosphate backbone of DNA might explain the slightly high T_m values, binding energies and number of hydrogen bonds in 4'-epiadriamycin-Tet7 complex compared to adriamycin-Tet7 complex. Although the

greater upfield shift of GNH protons in the adriamycin-Tet7 complex is observed compared to 4'-epiadriamycin-Tet7 but the upfield shift of ring D protons of adriamycin or 4'-epiadriamycin remains same in 4'-epiadriamycin/adriamycin-Tet7 complexes. These findings indicate the greater insertion of ring D of adriamycin at G6pT7 step of Tet7 as compared to 4'-epiadriamycin which is also clearly evident from intermolecular distances (Table 7.20 and 7.23) and the rMD models of both the complexes (Fig. 7.14 and 7.16). Although structurally similar ring D of both the drugs is involved in the interaction with DNA but slightly high T_m and binding energies in case 4'-epiadriamycin-Tet7 complex suggest a greater role of daunosamine sugar moiety on thermal stabilization. Therefore, we conclude that these findings will have implications in better understanding of anthracycline-G quadruplex DNA interactions.

8.1 Introduction

Apart from binding to duplex DNA, anthracyclines interact with G-quadruplex DNA (Ren & Chaires, 1999). The interaction of adriamycin (doxorubicin) and sabarubicin with 21-mer/22-mer human telomeric sequence in K^+ and Na^+ rich solutions showed (Manet, Manoli, Zambelli, Andreano, Masi, Cellai, Ottani, et al., 2011; Manet, Manoli, Zambelli, Andreano, Masi, Cellai, & Monti, 2011) co-existence of 1:1 and 2:1 ligand:DNA complexes. There are no studies on G-quadruplex DNA having 4 guanines, e.g. d-TTGGGGT, the telomeric DNA sequence from *Tetrahymena thermophilia*, which forms more stable structures. Henceforth, we have carried out series of experiments using SPR, absorbance, fluorescence (steady state and lifetime) and CD spectroscopy to ascertain real-time binding and mode of interaction of 4'epiadriamycin and adriamycin with G-quadruplex 22-mer d-[GGGG(TTGGGG)$_3$] (Tet22) from *Tetrahymena thermophilia* telomeric DNA in presence of 100 mM K^+. Thermal melting profiles have been obtained using DSC to determine the extent of stabilization of DNA.

8.2 Materials and Methods

Details of the materials and methods used are given in chapter 2. For SPR experiments, 1.87-240 μM of 4'epiadriamycin/adriamycin solution was used. Increasing amounts of Tet22 were added stepwise to a fixed concentration of 7 μM 4'epiadriamycin/adriamycin in 22 experiments conducted at mole equivalent ratios of Drug (D) to Nucleic acid (N) in the range, D/N = 0.3-4.6 for titrations monitored by absorption spectroscopy. The same samples were used for fluorescence experiments. The relative mole fractions of Tet22 and 4'epiadriamycin/adriamycin were varied keeping their total concentration constant (4 μM) for Job plot experiments. The fluorescence lifetime values were calculated for 7 μM of free 4'epiadriamycin/adriamycin and its complex with Tet22 at D/N = 0.3, 0.5, 1.0, 2.0, 3.0 and 4.0. CD experiments were performed using Tet22 (10.0 μM) and 4'epiadriamycin/adriamycin was added progressively at mole equivalent ratios D/N = 0.3-5.0 in 31 experiments. In another set of experiments, Tet22 was added stepwise to 4'epiadriamycin/adriamycin (400 μM) in 8/9 experiments conducted at D/N = 0.5-4.0 at 25 °C. For DSC experiments, 50 μM of Tet22 and 4'epiadriamycin/adriamycin-Tet22 complexes at D/N = 0.5, 1.0, 2.0, 3.0 and 4.0 were used. Molecular docking studies were carried out using the structure of quadruplex DNA d-

[$(TTGGGG)_4$] (Tet24) obtained from PDB ID: 186D. Three-dimensional (3D) conformers of 4'-epiadriamycin and adriamycin were obtained from PubChem CID: 41867 and 31703, respectively.

8.3 Results and Discussion

8.3.1 Surface Plasmon Resonance

SPR sensograms (Fig. 8.1 a,b) show interaction of 4'-epiadriamycin and adriamycin with Tet22. The steady state response increases with a concentration in the range 1.87-240 μM (Fig. 8.1 c, d) and the binding isotherms yields affinity constant $K_b \sim 4.1 \times 10^3$ M^{-1} at 25 °C while the analysis of the kinetics of association and dissociation yield $K_b \sim 10.0 \times 10^3$ M^{-1}. The corresponding values of the adriamycin-Tet22 complex are $K_b \sim 1.1 \times 10^3$ M^{-1} and $K_b \sim 1.5 \times 10^3$ M^{-1} from steady-state binding isotherms and analysis of the kinetics of association and dissociation, respectively. The results of real-time binding (Table 8.1 and 8.2) gives a direct proof of interaction of 4'epiadriamycin/adriamycin and Tet22 DNA sequence. The increase in steady-state response with concentration also indicates that binding of Tet22 with these molecules involves specific interactions.

a

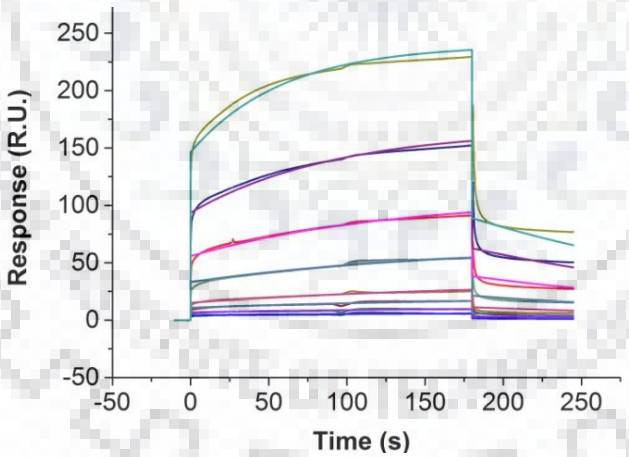

b

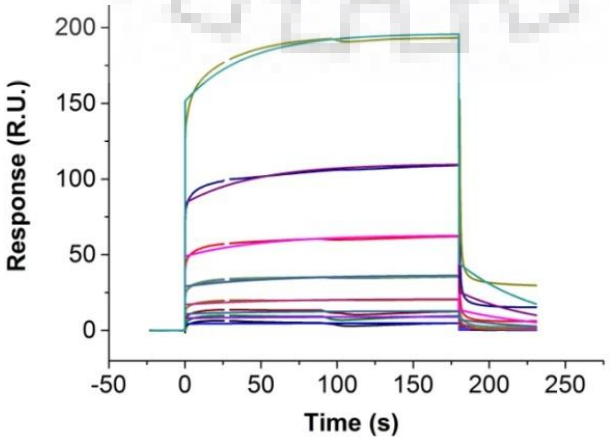

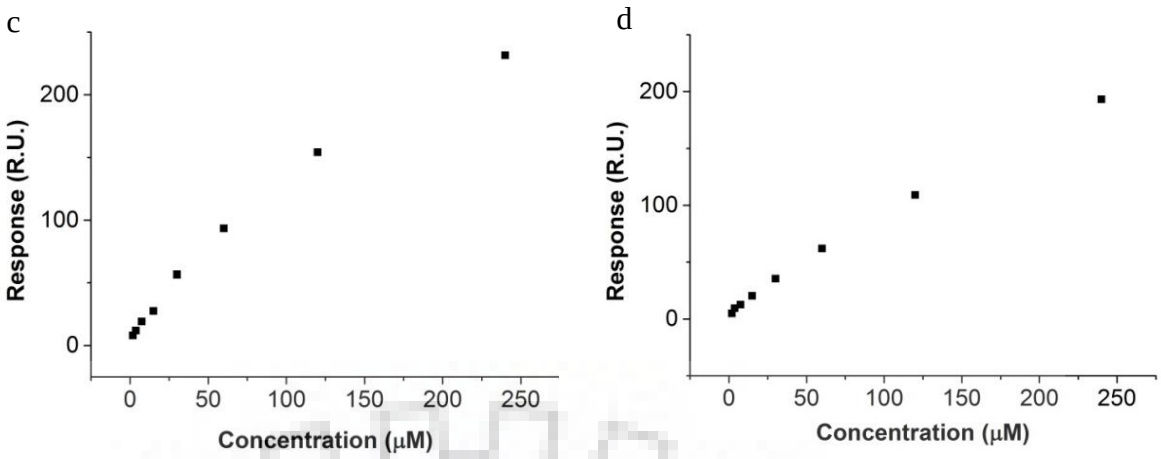

Figure 8.1 SPR sensograms obtained from the interaction of a) 4'-epiadriamycin and b) adriamycin with Tet22 using HEPES buffer (pH 7.4) with 100 mM KCl at 25 °C. Sensograms were obtained for increasing concentration of drugs from 1.87 μM (bottom) to 240 μM (top); Steady-state binding plot showing Response Unit (R.U.) with respect to the concentration of c) 4'-epiadriamycin and d) adriamycin.

Table 8.1 SPR data showing equilibrium binding constants (K_b), equilibrium dissociation constant (K_D), association rate constant (k_a) and dissociation rate constant (k_d) and maximum Response Unit (RU_{max}) obtained from the binding of 4'-epiadriamycin with Tet22 at 25 °C.

Experiment	Flow rate (μl/min)	RU_{max}	k_a ($M^{-1}s^{-1}$)	k_d (s^{-1})	K_D (M)	K_b (M^{-1})	χ^2
Kinetics run 1	30	129.7	51.0	$4.7x10^{-3}$	$9.3x10^{-5}$	$1.0x10^{4}$	8.4
Steady State run 1	30	460.4	-	-	$2.4x10^{-4}$	$4.1x10^{3}$	3.9
Kinetics run 2	30	186.9	50.5	$1.1x10^{-2}$	$2.2x10^{-4}$	$4.5x10^{3}$	10.9
Steady State run 2	30	487.1	-	-	$2.7x10^{-4}$	$3.7x10^{3}$	2.5

Table 8.2 SPR data showing equilibrium binding constants (K_b), equilibrium dissociation constant (K_D), association rate constant (k_a) and dissociation rate constant (k_d) and maximum Response Unit (RU_{max}) obtained from the binding of adriamycin with Tet22 at 25 °C.

Experiment	Flow rate (µl/min)	RU_{max}	k_a ($M^{-1}s^{-1}$)	k_d (s^{-1})	K_D (M)	K_b (M^{-1})	χ^2
Kinetics run 1	30	164.0	28.7	$1.8x10^{-2}$	$6.3x10^{-4}$	$1.5x10^{3}$	5.0
Steady State run 1	30	846.5	-	-	$8.4x10^{-4}$	$1.1x10^{3}$	1.7
Kinetics run 2	30	1098	7.3	$3.5x10^{-2}$	$4.8x10^{-3}$	$2.0x10^{2}$	4.5
Steady State run 2	30	1075	-	-	$1.1x10^{-3}$	$9.0x10^{2}$	0.8
Kinetics run 3	30	1459	4.4	$2.7x10^{-2}$	$6.2x10^{-3}$	$1.6x10^{2}$	5.2
Steady State run 3	30	994.1	-	-	$1.0x10^{-3}$	$1.0x10^{3}$	0.5

8.3.2 Absorption

4'-epiadriamycin (or epirubicin) and adriamycin show absorption maxima at 290 and 481/482 nm. The absorption band at 481/482 nm is sensitive to self-aggregation and at concentration >10 µM self aggregation occurs (Fiallo, Tayeb, Suarato, & Garnier-Suillerot, 1998; Chaires, Dattagupta, & Crothers, 1982; Agrawal, Barthwal, & Barthwal, 2009) therefore 7 µM of 4'-epiadriamycin/adriamycin was used to carry out titration with Tet22. Stepwise addition of Tet22 to 4'-epiadriamycin in the range D/N = 0.30 to 4.60 (selected data are shown in Fig. 8.2 a) resulted in hypochromism of ~32% at 482 nm accompanied by redshift $\Delta\lambda_{max}$ ~8 nm. A plot of A versus D/N (inset of Fig. 8.2 a) and 1/A versus D/N (Fig. 8.2 b) show change in slope at D/N = 0.72 and 2.09 and D/N = 1.08 and 1.78, respectively so that stoichiometry of 1:1 and 2:1 in ligand-DNA complex may exist. Data does not show any isobestic point indicating the presence of several conformations of 4'-epiadriamycin-Tet22 complex. We get intrinsic binding constant $K_b = 9.0 \times 10^4$ M^{-1} at D/N = 0.30-0.45 and $K_b = 3.2 \times 10^6$ M^{-1} at D/N = 0.50-4.60 using equation (1) (Fig. 8.2 c) which may be considered as a rough estimate only. Similarly, titrations of adriamycin with Tet22 conducted in the range D/N = 0.30 to 4.60 (selected data are shown in Fig. 8.3 a) show hypochromism of ~34 % at 482 nm accompanied by redshift $\Delta\lambda_{max}$ ~7 nm. The plot of A versus D/N (inset of Fig. 8.3 a) and 1/A versus D/N (Fig. 8.3 b) show change in slope at D/N = 0.84 and 1.92 and D/N = 0.81 and 2.00, respectively so that stoichiometry may be 1:1 and 2:1. The corresponding intrinsic binding constant values of adriamycin-Tet22 complex are $K_b = 1.5 \times 10^5$ M^{-1} at D/N = 0.30-0.45 and $K_b = 1.6 \times 10^6$ M^{-1} at D/N = 0.50-4.60

using equation (1) (Fig. 8.3 c). Existence of 2 binding sites has earlier been reported on binding of adriamycin with 22-mer human telomeric DNA quadruplex at D/N = 0.3-10.0 in K^+ and Na^+ rich aqueous solutions with K_b = 5.4x10^5 M^{-1} and 4.0x10^5 M^{-1} accompanied by red shift in absorption maxima, $\Delta\lambda_{max}$ ~25 and 10-15 nm, resulting in 27% and 17% hypochromism, respectively (Manet, Manoli, Zambelli, Andreano, Masi, Cellai, Ottani, et al., 2011; Manet, Manoli, Zambelli, Andreano, Masi, Cellai, & Monti, 2011). In another experiment on the binding of daunomycin to human telomeric 22-mer DNA at D/N = 0.07-1.0, it was observed that K_b = 1.8x10^6 M^{-1} and $\Delta\lambda_{max}$ ~5 nm resulting in 29% hypochromism with a single binding site (Das, Chatterjee, & Suresh Kumar, 2017). Our results show significant changes in hypochromism with a minor redshift which indicates intercalation is not present and ligand binds externally involving interaction of π electrons in Tet22 (Manet, Manoli, Zambelli, Andreano, Masi, Cellai, Ottani, et al., 2011; Manet, Manoli, Zambelli, Andreano, Masi, Cellai, & Monti, 2011; Padmapriya & Barthwal, 2016; Pasternack et al., 1983; Krugh & Reinhardt, 1975; Awasthi, Dogra, & Barthwal, 2013; Pradeep & Barthwal, 2016).

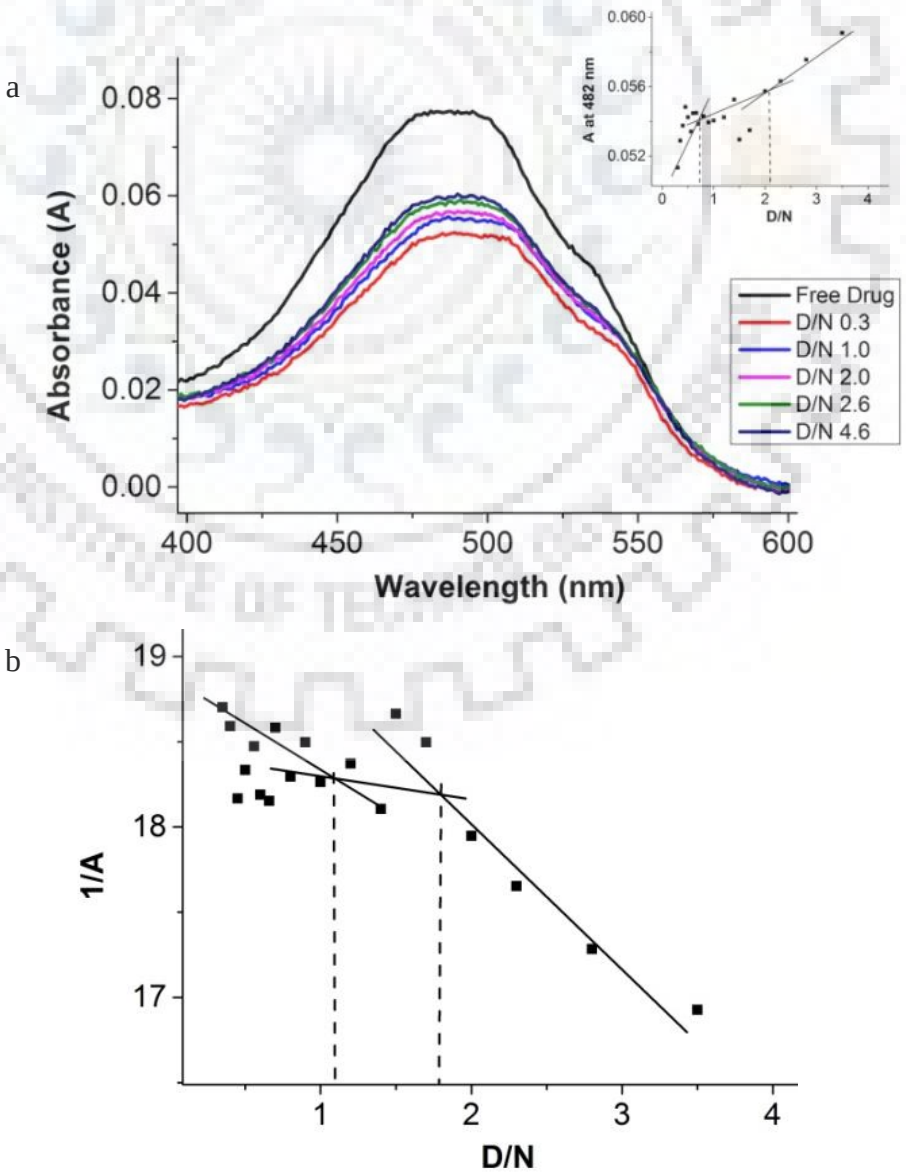

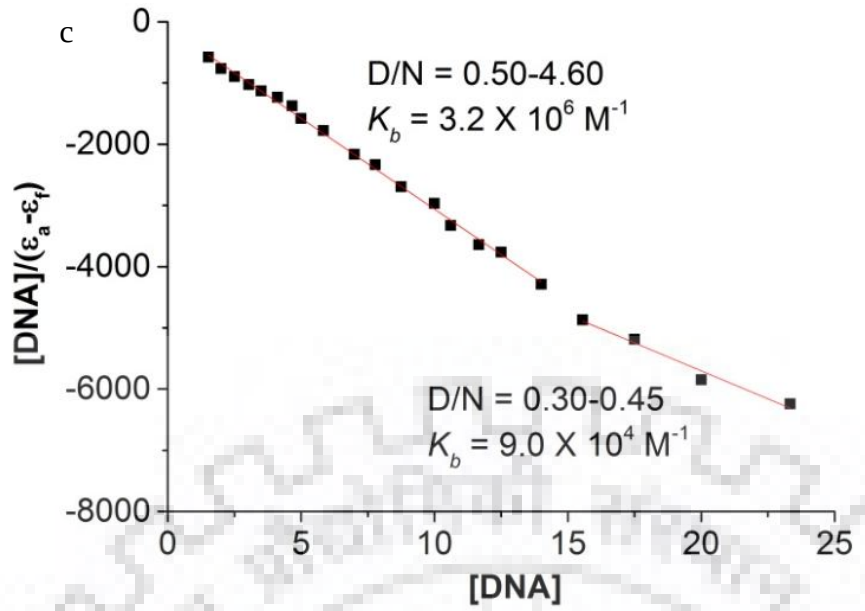

Figure 8.2 a) Absorption spectra of 7 μM free 4'-epiadriamycin and its complex with increasing concentration of Tet22 in 10 mM phosphate buffer containing 100 mM KCl at some selected Daunomycin (D) to Nucleic acid (N) ratios, D/N, at 25 °C. The inset shows plot of Absorbance (A) as a function of D/N ratio at 482 nm; b) Plot of reciprocal of absorbance (1/A) as a function of D/N and c) Plot of [DNA] / (ε_a - ε_f) as a function of DNA concentration (μM) at 482 nm.

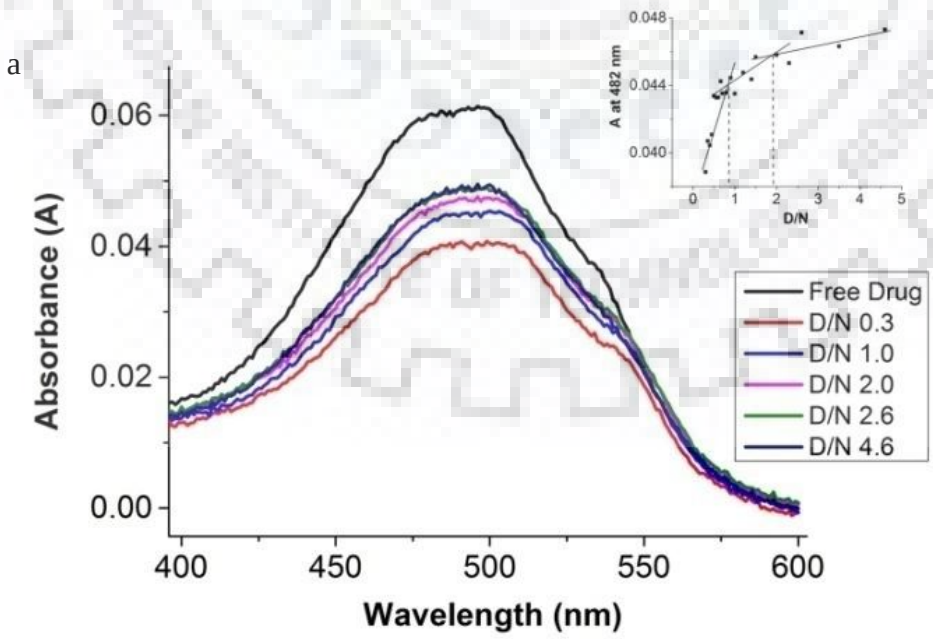

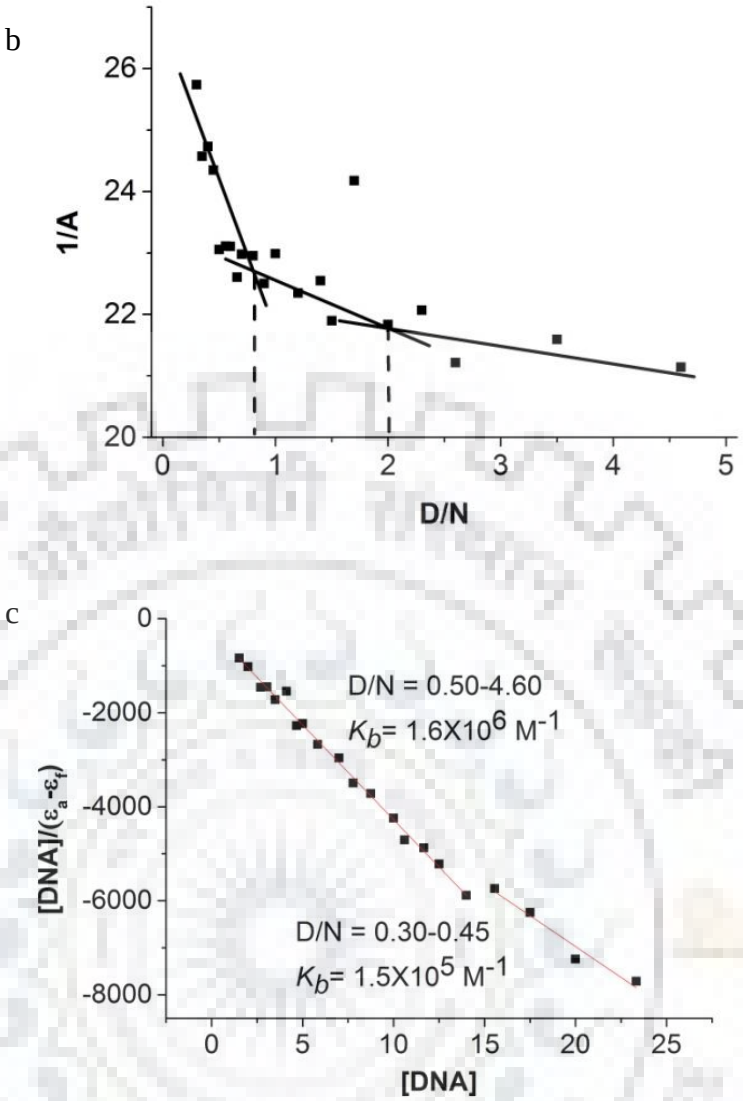

Figure 8.3 a) Absorption spectra of 7 µM free adriamycin and its complex with increasing concentration of Tet22 in 10 mM phosphate buffer containing 100 mM KCl at some selected D/N ratios at 25 °C. The inset shows plot of Absorbance (A) as a function of D/N ratio at 482 nm; b) Plot of reciprocal of absorbance (1/A) as a function of D/N and c) Plot of [DNA] / (ε_a - ε_f) as a function of DNA concentration (µM) at 482 nm.

8.3.3. Fluorescence

Stepwise addition of Tet22 to 7 µM of 4'-epiadrimaycin and adriamycin in separate experiments results in 96-97% quenching of fluorescence intensity up to D/N = 0.15 accompanied by a redshift $\Delta\lambda_{em}$ = 8 and 5.5 nm in 4'-epiadriamycin and adriamycin complexes, respectively (selected data shown in Fig. 8.4 a and Fig. 8.5 a) indicating strong interaction with DNA. A plot of F versus D/N (inset of Fig. 8.4 a and Fig. 8.4 a) shows inflection at D/N = 0.81, 2.26 and D/N = 0.91, 2.27 in 4'-epiadriamycin and adriamycin complexes, respectively

whereas, 1/F versus D/N (Fig. 8.4 b and Fig. 8.4 b) shows inflection at D/N = 1.08, 2.00 and D/N = 0.94, 1.85 in 4'-epiadriamycin and adriamycin complexes, respectively (Padmapriya & Barthwal, 2016; Pradeep & Barthwal, 2016; Ranjan, Andreasen, Kumar, Hyde-Volpe, & Arya, 2010; Teulade-Fichou et al., 2003). The Stern-Volmer plot showing F_0 / F versus concentration of DNA (Fig. 8.4 c and Fig. 8.4 c) and plot of log [(F_0 - F) / F] versus log [DNA] (Fig. 8.4 d and Fig. 8.4 d) using equations (2) and (3), respectively give (Tarikere Palakashan Pradeep & Barthwal, 2016) K_{SV} and K_b in the range of 0.23-12.0x10^6 M^{-1}. The bimolecular quenching constant, K_q ~6×10^{15} $M^{-1}s^{-1}$, obtained by using K_{sv} = 6.0x10^6 M^{-1} and fluorescence lifetime τ = 1.0 ns is much greater than collision constant for a biomolecule and small molecule as a ligand, i.e. 2×10^{10} $M^{-1}s^{-1}$, excluding the possibility of any dynamic quenching (Tarikere Palakashan Pradeep & Barthwal, 2016). The accompanying changes in absorbance and no change in fluorescence lifetime too suggest static quenching. Non linear curve fitting of fluorescence data at 592 nm in two independent binding sites using equation (4) (Thordarson, 2011; Hargrove, Zhong, Sessler, & Anslyn, 2010) yield binding constants K_{b1} = 1.9x10^6 M^{-1} and K_{b2} = 2.3x10^5 M^{-1} in 4'-epiadrimaycin-Tet22 complex (Fig. 8.4 e) and K_{b1} = 1.7x10^6 M^{-1} and K_{b2} = 8.1x10^5 M^{-1} in adriamycin-Tet22 complex (Fig. 8.5 e). The data does not show iso-emissive point due to the existence of multiple complexes. Efficient quenching may be due to electron transfer by the proximity of ligands to guanines. Binding of adriamycin to 21-mer human telomeric sequence has earlier been reported with similar binding affinity constant and with 86-93% quenching of fluorescence at D/N = 0.3-10.0 (Manet, Manoli, Zambelli, Andreano, Masi, Cellai, Ottani, et al., 2011; Manet, Manoli, Zambelli, Andreano, Masi, Cellai, & Monti, 2011).

The fluorescence decay of 4'-epiadriamycin/adriamycin and its complexes at D/N = 1.0-4.0 were measured using time-correlated single photon counting using $\Delta\lambda_{ex}$ = 456 nm and $\Delta\lambda_{em}$ = 590 nm at 25 °C. The decay was found to be monoexponential with lifetime τ = 0.85-1.04 ns at D/N = 0.0-4.0 in 4'-epiadriamycin (Fig. 8.4 f) and adriamycin (Fig. 8.5 f) complexes (Table 8.3 and 8.4). It has been suggested that the equal lifetimes in free and bound complexes may be due to the fact that complexes are non-emissive (Manet, Manoli, Zambelli, Andreano, Masi, Cellai, & Monti, 2011).

Since absorbance and fluorescence data suggested the possibility of two stoichiometries, we used an independent method of continuous variation (Job plot) to get a direct estimate of stoichiometry. The plot of the difference in fluorescence intensity as a function of mole fraction of 4'-epiadriamycin shows inflection points at ~0.48 and 0.67 (Fig. 8.4 g) yielding stoichiometry of 1:1 and 2:1 of 4'-epiadriamycin-Tet22 complex. Similar results were obtained

for adriamycin-Tet22 complex showing inflection points at ~0.49 and 0.65 (Fig. 8.5 g) showing stoichiometry of 1:1 and 2:1.

a

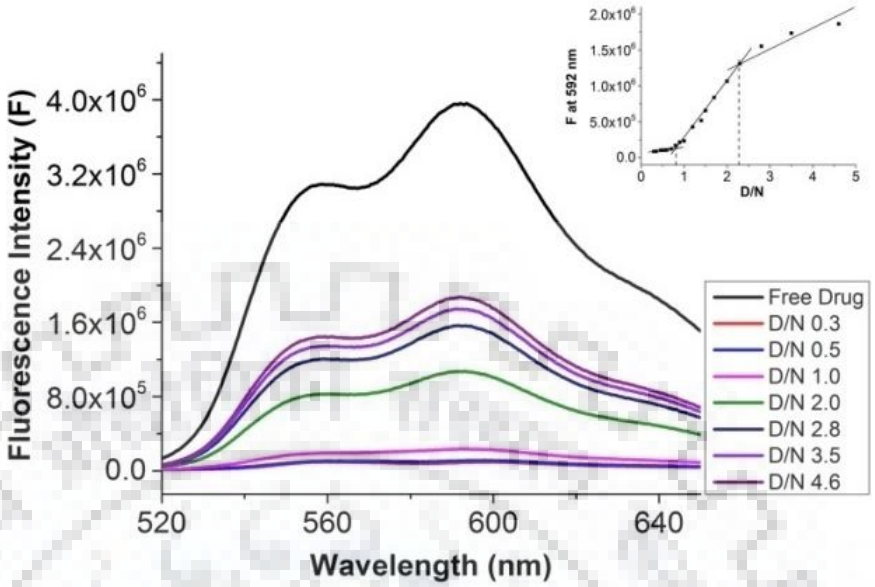

b

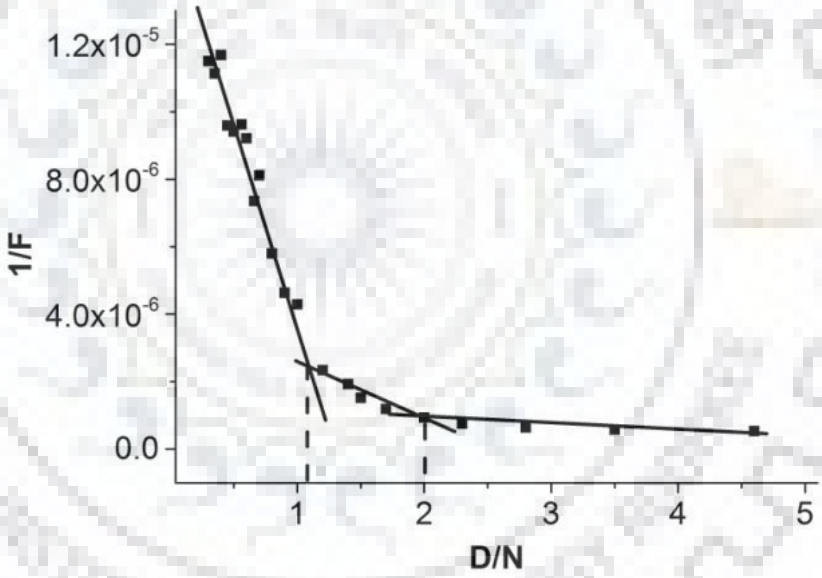

c

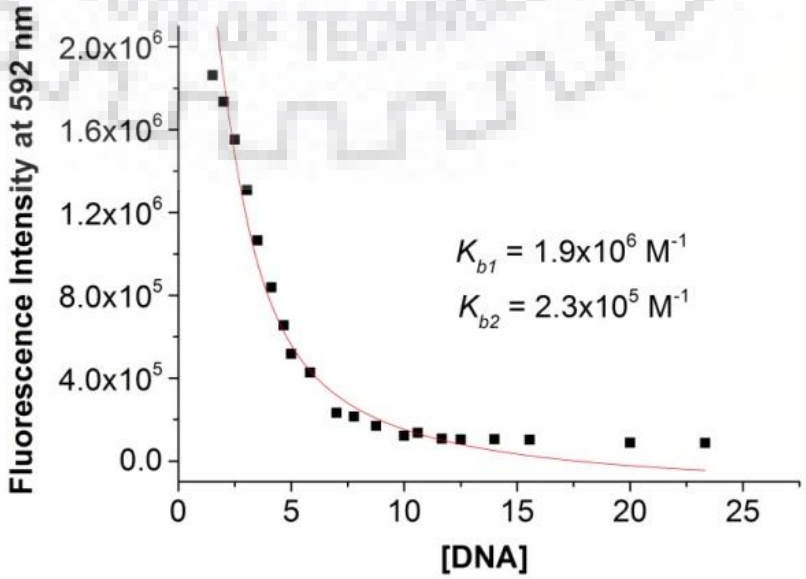

d

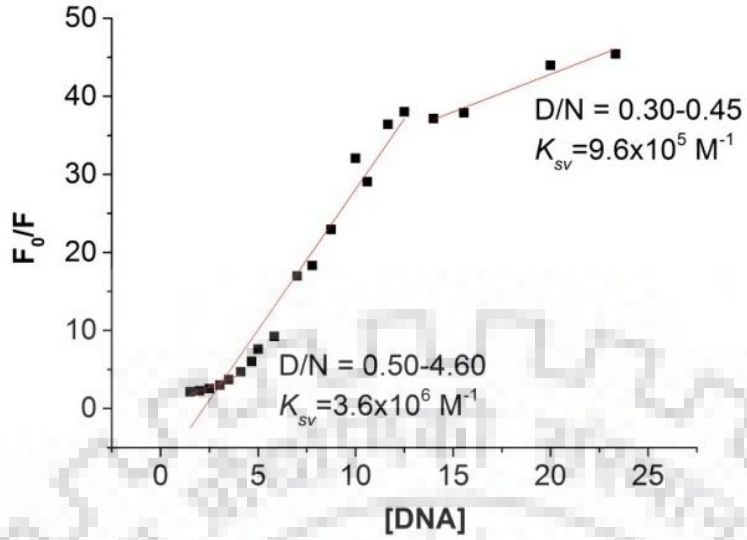
D/N = 0.30-0.45
K_{sv}=9.6x10^5 M^{-1}
D/N = 0.50-4.60
K_{sv}=3.6x10^6 M^{-1}
F_0/F
[DNA]

e

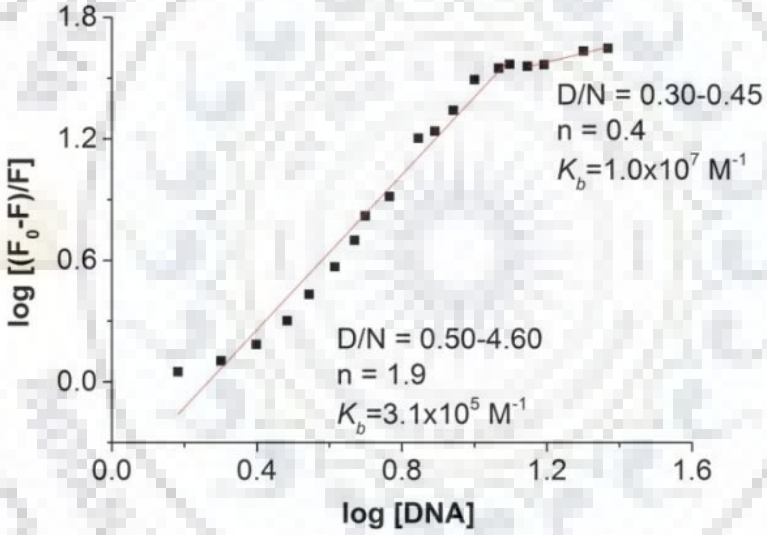
D/N = 0.30-0.45
n = 0.4
K_b=1.0x10^7 M^{-1}
D/N = 0.50-4.60
n = 1.9
K_b=3.1x10^5 M^{-1}
log [(F_0-F)/F]
log [DNA]

f

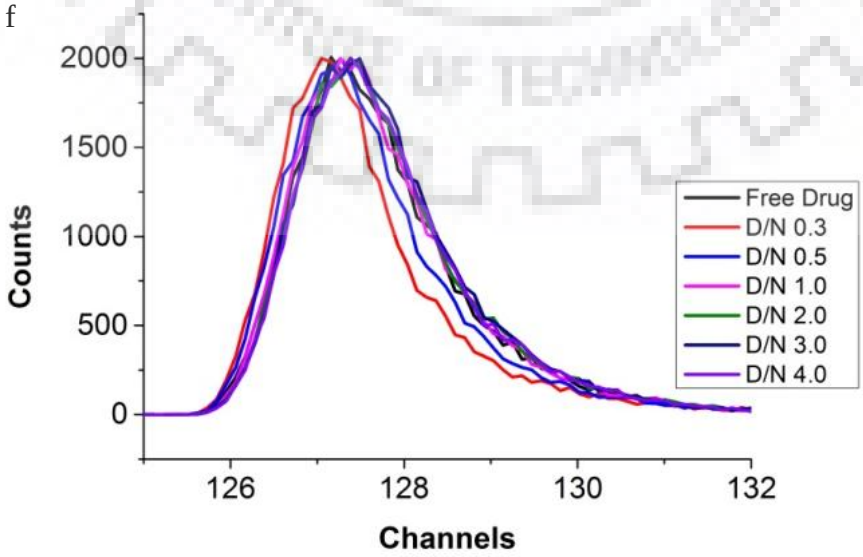
Free Drug
D/N 0.3
D/N 0.5
D/N 1.0
D/N 2.0
D/N 3.0
D/N 4.0
Counts
Channels

g

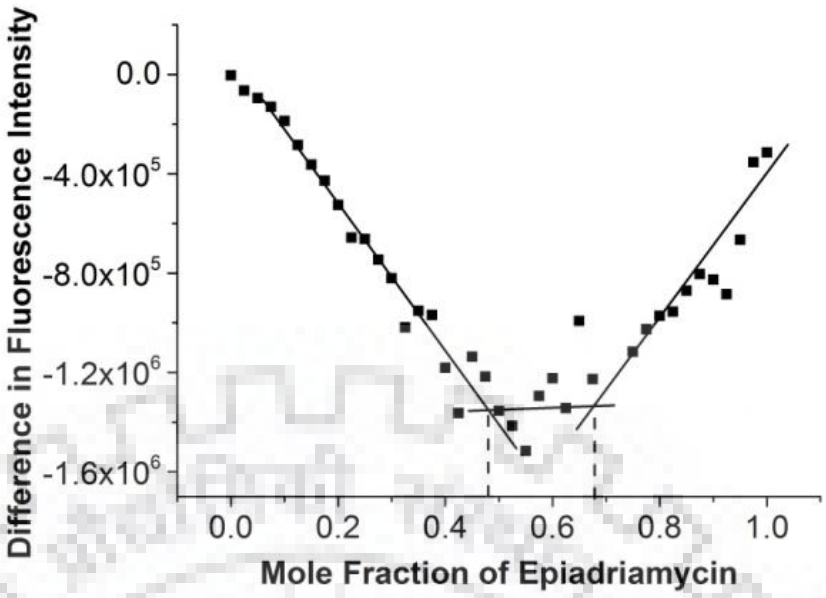

Figure 8.4 a) Fluorescence emission intensity of 7 μM free 4'-epiadriamycin and its complex with increasing concentration of Tet22 at some selected D/N ratios using λ_{ex} = 480 nm at 25 °C. The inset shows a plot of Fluorescence intensity (F) as a function of D/N ratio 592 nm; b) Plot of reciprocal of Fluorescence intensity (1/F) as a function of D/N ratio; c) Nonlinear fitted curve (red) for binding at two binding sites for observed fluorescence emission intensity at 592 nm as a function of DNA concentration (μM) showing two binding constants (K_{b1} and K_{b2}); d) Plot of F_0/F with respect to DNA concentration (μM); e) Plot of log $[(F_0-F)/F]$ as a function of log [DNA] at 592 nm; f) Fluorescence decay profiles of 7 μM free 4'-epiadriamycin and its complexes with Tet22 at varying D/N ratios at 25 °C; g) Job plot for binding of 4'-epiadriamycin to DNA using fluorescence.

a

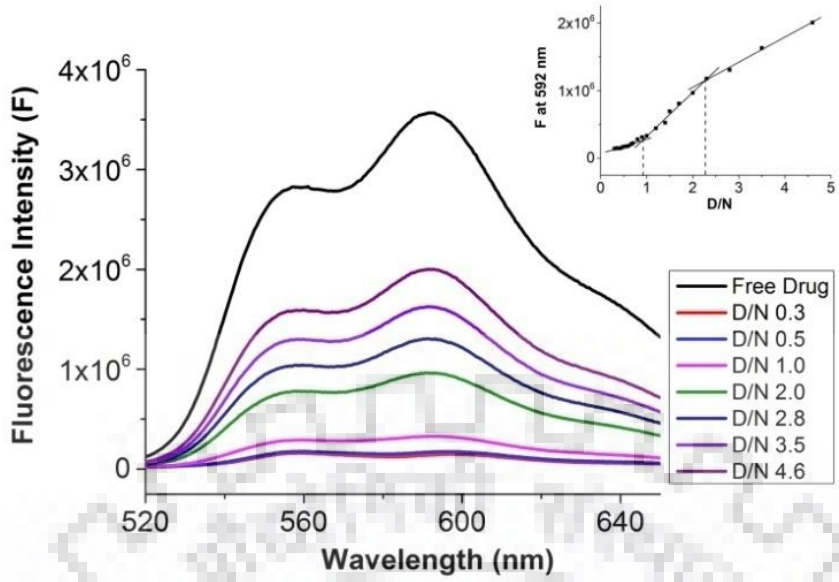
Fluorescence Intensity (F)
4x10^6
3x10^6
2x10^6
1x10^6
0
520
560
600
640
Wavelength (nm)
Free Drug
D/N 0.3
D/N 0.5
D/N 1.0
D/N 2.0
D/N 2.8
D/N 3.5
D/N 4.6
F at 592 nm
2x10^6
1x10^6
0
0
1
2
3
4
5
D/N

b

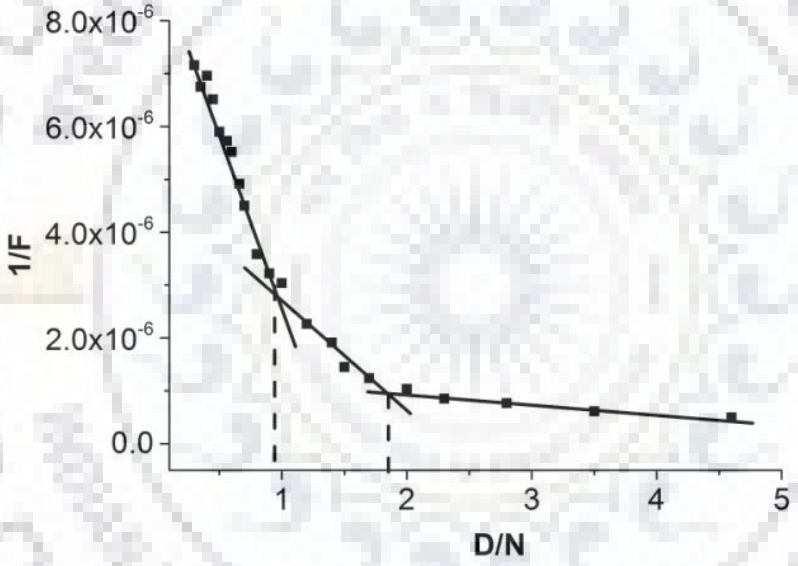
1/F
8.0x10^-6
6.0x10^-6
4.0x10^-6
2.0x10^-6
0.0
1
2
3
4
5
D/N

c

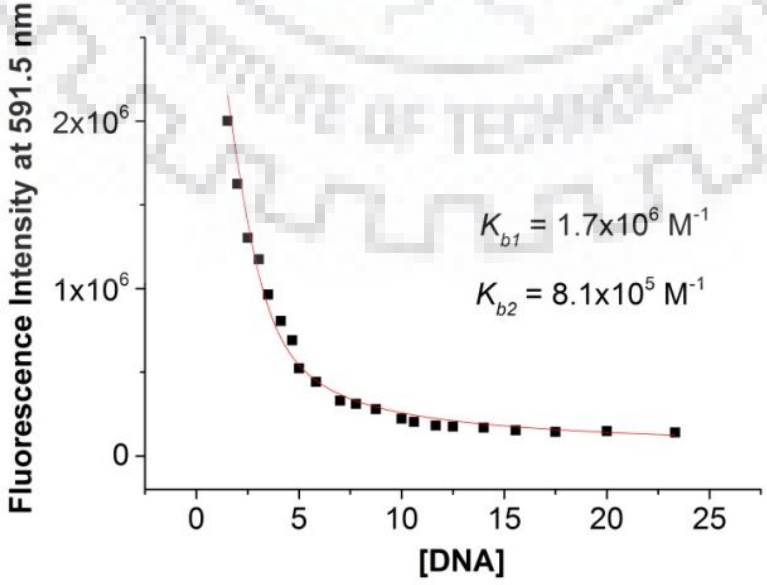
Fluorescence Intensity at 591.5 nm
2x10^6
1x10^6
0
0
5
10
15
20
25
[DNA]
K_b1 = 1.7x10^6 M^-1
K_b2 = 8.1x10^5 M^-1

d

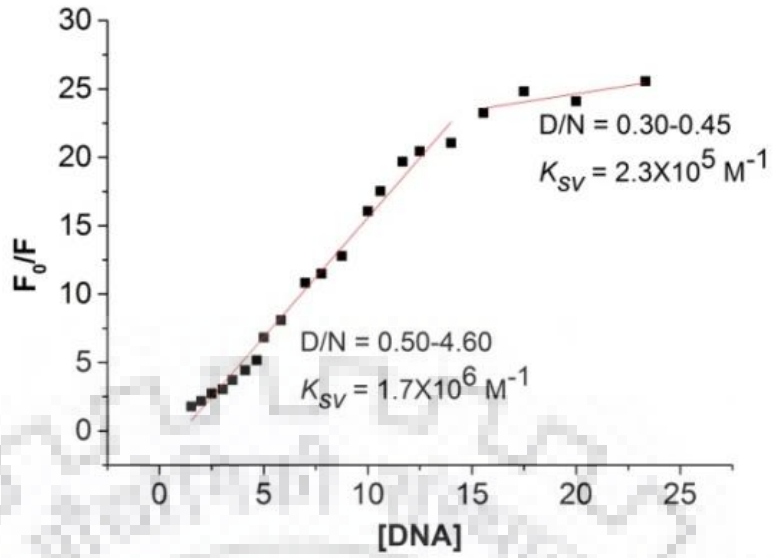
30
25
20
15
10
5
0
F_0/F
0
5
10
15
20
25
[DNA]
D/N = 0.30-0.45
K_{sv} = 2.3X10^5 M^{-1}
D/N = 0.50-4.60
K_{sv} = 1.7X10^6 M^{-1}

e

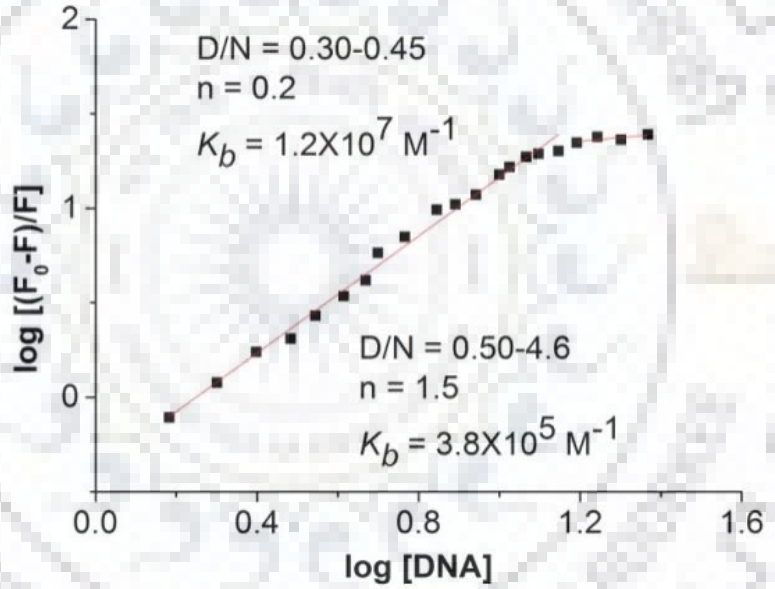
2
1
0
log [(F_0-F)/F]
0.0
0.4
0.8
1.2
1.6
log [DNA]
D/N = 0.30-0.45
n = 0.2
K_b = 1.2X10^7 M^{-1}
D/N = 0.50-4.6
n = 1.5
K_b = 3.8X10^5 M^{-1}

f

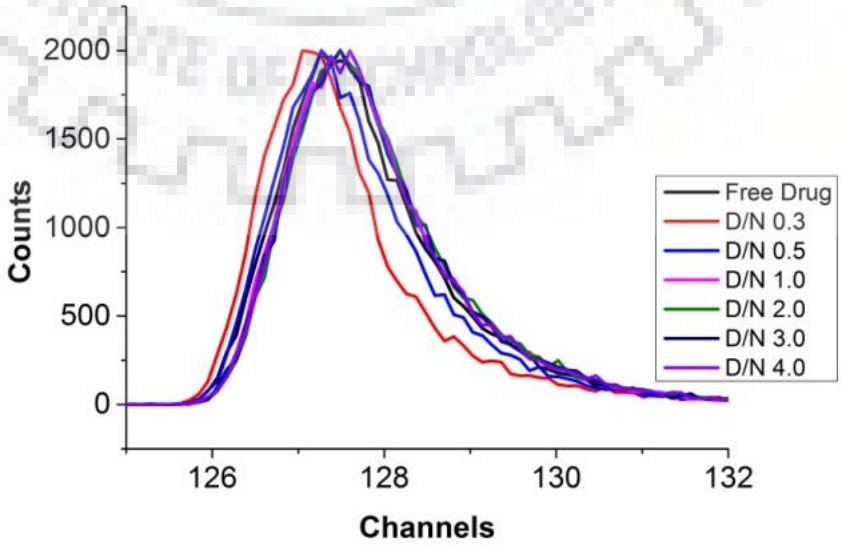
2000
1500
1000
500
0
Counts
126
128
130
132
Channels
Free Drug
D/N 0.3
D/N 0.5
D/N 1.0
D/N 2.0
D/N 3.0
D/N 4.0

g

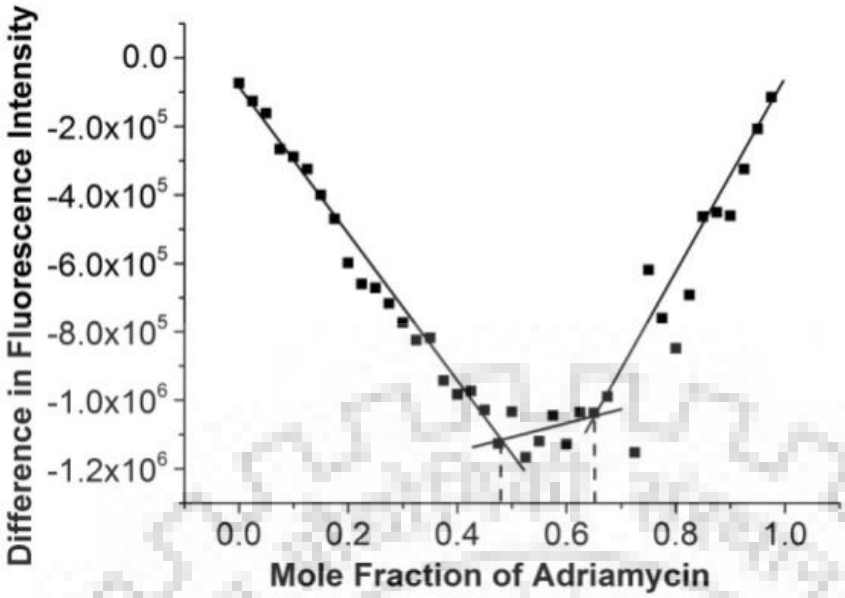

Figure 8.5 a) Fluorescence emission intensity of 7 μM free adriamycin and its complex with increasing concentration of Tet22 at some selected D/N ratios using λ_{ex} = 480 nm at 25 °C. The inset shows a plot of Fluorescence intensity (F) as a function of D/N ratio 592 nm; b) Plot of reciprocal of Fluorescence intensity (1/F) as a function of D/N ratio; c) Nonlinear fitted curve (red) for binding at two binding sites for observed fluorescence emission intensity at 592 nm as a function of DNA concentration (μM) showing two binding constants (K_{b1} and K_{b2}); d) Plot of F_0/F with respect to DNA concentration (μM); e) Plot of log $[(F_0-F)/F]$ as a function of log [DNA] at 592 nm; f) Fluorescence decay profiles of 7 μM free adriamycin and its complexes with Tet22 at varying D/N ratios at 25 °C; g) Job plot for binding of adriamycin to DNA using fluorescence.

Table 8.3 Lifetime (τ) of free 4'-epiadriamycin (7 μM) and 4'-epiadriamycin-Tet22 complex at D/N = 0.3, 0.5, 1.0, 2.0, 3.0 and 4.0 with λ_{ex} = 456 nm and λ_{em} = 590 nm at 25 °C.

Samples	τ (ns)	%	χ^2
Free 4'-epiadriamycin	1.00	100	1.24
D/N 0.3	0.85	100	1.53
D/N 0.5	0.93	100	0.98
D/N 1.0	1.02	100	1.14
D/N 2.0	1.04	100	1.27
D/N 3.0	0.95	100	1.23
D/N 4.0	0.99	100	1.05

Table 8.4 Lifetime (τ) of free adriamycin (7 μM) and adriamycin-Tet22 complex at D/N = 0.3, 0.5, 1.0, 2.0, 3.0 and 4.0 with λ_{ex} = 456 nm and λ_{em} = 590 nm at 25 °C.

Samples	τ (ns)	%	χ^2
Free adriamycin	0.99	100	1.18
D/N 0.3	0.99	100	1.60
D/N 0.5	1.03	100	1.17
D/N 1.0	0.96	100	1.04
D/N 2.0	1.02	100	1.01
D/N 3.0	0.96	100	1.08
D/N 4.0	0.98	100	1.08

8.3.4 Circular Dichroism

The observed circular dichroism spectra of Tet22 in 100 mM K^+ rich solution show (Fig. 8.6 a and 8.7 a) a well defined positive band at 265 nm and 295 nm, which are characteristic of stacking arrangements of tetrads in parallel stranded G-quadruplex DNA with same glycosidic bond angle (i.e. either *anti* or *syn*) and antiparallel stranded G-quadruplex DNA with different glycosidic bond angle (i.e. *anti* and *syn*), respectively (Vorlíčková et al., 2012; Hudson, Brooks, & Graves, 2009; Kypr, Kejnovská, Bednářová, & Vorlíčková, 2012; Dapić et al., 2003; Karsisiotis et al., 2011). Parallel and antiparallel forms of G-quadruplex show a negative and positive CD bands centered around 238-240 and 240-245 nm, respectively (Vorlíčková et al., 2012; Hudson et al., 2009; Kypr et al., 2012; Dapić et al., 2003; Karsisiotis et al., 2011; Masiero et al., 2010; Gray et al., 2008). Thus, the observed negative band at 240 nm and dominant positive band at 265 nm (Fig 8.6 a and 8.7 a) show that a mixture of 3+1 hybrid and parallel quadruplexes in the presence of 100 mM K^+ and the population of latter arrangement dominates (Vorlíčková et al., 2012).

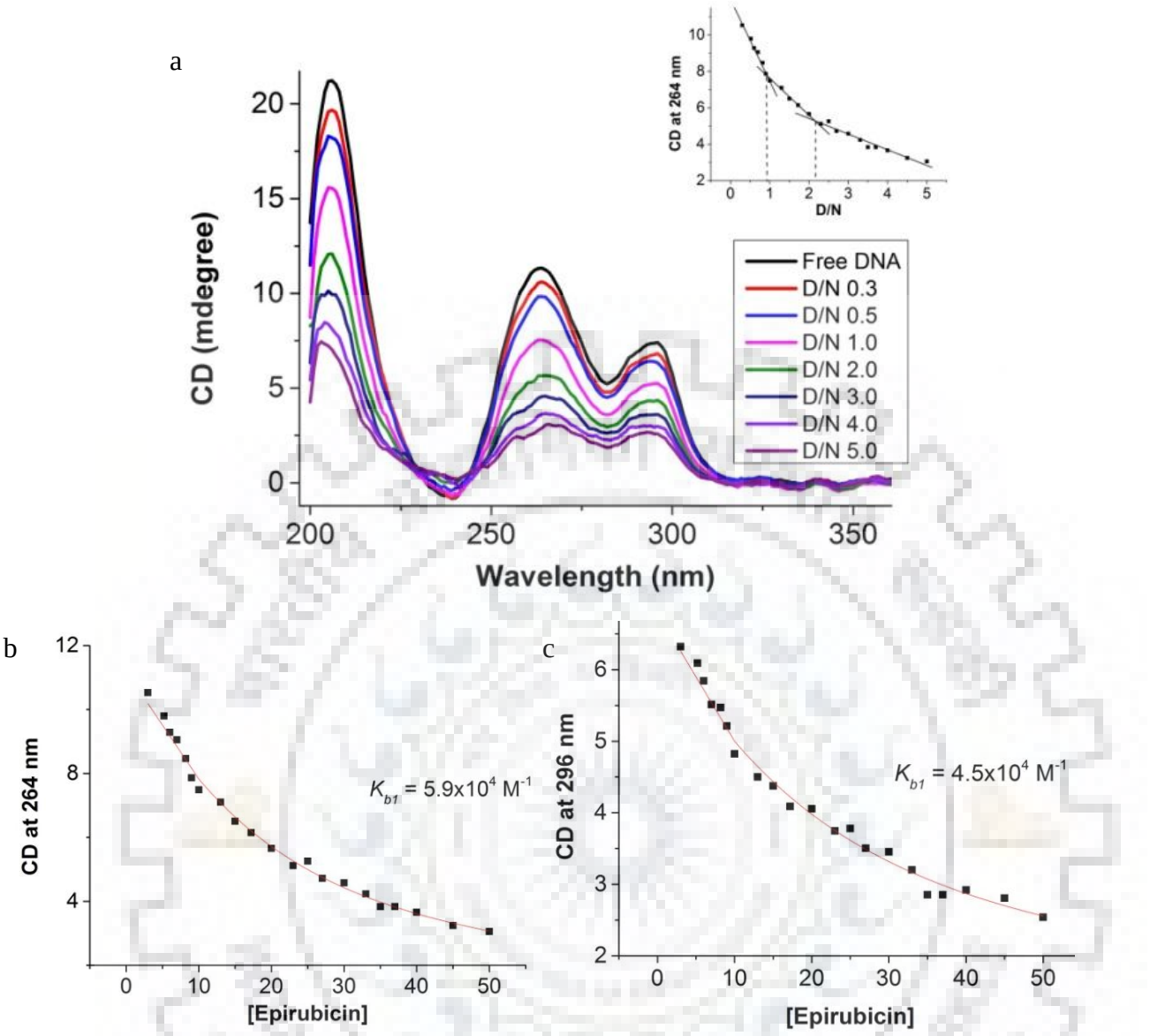

Figure 8.6 a) CD spectra of free 10 μM Tet22 and its complex with increasing concentration of 4'-epiadriamycin at some selected D/N ratios at 25 °C. The inset shows plot of CD (mdegree) at 264 nm as a function of D/N ratio; Nonlinear fitted curve of observed CD in mdegrees (red) for binding of 4'-epiadriamycin with Tet22 at b) 264 nm and c) 296 nm as a function of 4'-epiadriamycin concentration (μM) showing binding constant (K_b).

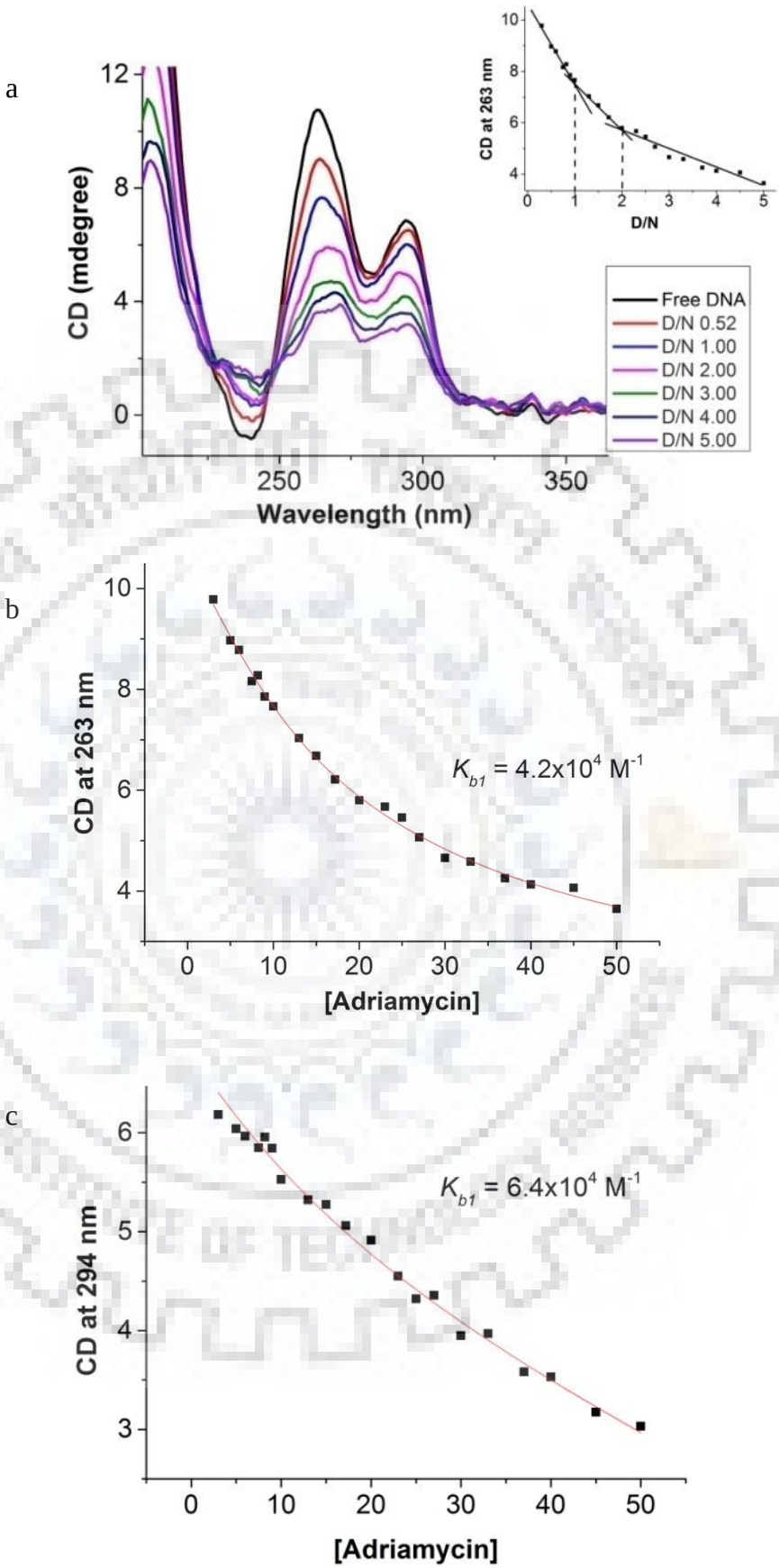

Figure 8.7 a) CD spectra of free 10 µM Tet22 and its complex with increasing concentration of adriamycin at some selected D/N ratios at 25 °C. The inset shows plot of CD (mdegree) at 263 nm as a function of D/N ratio; Nonlinear fitted curve of observed CD in mdegrees (red) for

binding of adriamycin with Tet22 at b) 263 nm and c) 294 nm as a function of adriamycin concentration (μM) showing binding constant (K_b).

Upon progressive addition of 4'-epiadriamycin to 10 μM Tet22 up to D/N = 5.0 the magnitude of 264, 296 and 239 nm bands decrease significantly by 73%, 64%, and 78%, respectively (Fig. 8.6 a) which may be due to the relative change in the conformation of two forms of G quadruplex. The binding is accompanied by 2-3 nm red shift which rules out classical intercalation and is indicative of external binding. Since groove binding has shown to induce changes in CD while end stacking does not show any significant change (De Cian et al., 2007). Therefore, both end stacking and external groove binding may be occurring in present cases. Changes in CD versus D/N show inflection point at D/N = 0.9 and 2.2 (inset of Fig. 8.6 a) indicating stoichiometry of 1:1 and 2:1 (Rezler et al., 2005). Absence of isoelliptic point shows the presence of more than one stoichiometry. Non-linear curve fitting of the plot of the magnitude of CD at 264 and 296 nm as a function of 4'-epiadriamycin concentration (Fig. 8.6 b,c) using equation (6) yield affinity constants, $K_b = 5.9 \times 10^4$ M^{-1} and 4.5×10^4 M^{-1}, respectively. The titration of Tet22 with adriamycin show similar result of a decrease in CD band by 64%, 53% and 100% at 263, 290 and 240 nm, respectively (Fig. 8.7 a). CD at 263 nm versus D/N (inset of Fig 8.7 a) shows slope change at D/N = 1.0 and 2.0 indicating stoichiometry of 1:1 and 2:1. Non-linear curve fitting of the plots of the magnitude of CD at 263 and 290 nm as a function of adriamycin concentration (Fig. 8.6 b,c) using equation (6) yield affinity constants, $K_b = 4 \times 10^4$ M^{-1} and $K_b = 6.4 \times 10^4$ M^{-1}, respectively. In order to find induced CD bands, 400 μM of 4'-epiadriamycin/adriamycin (Fig. 8.8 a,b) were taken and Tet22 DNA was added in the range D/N = 0.5-4.0.

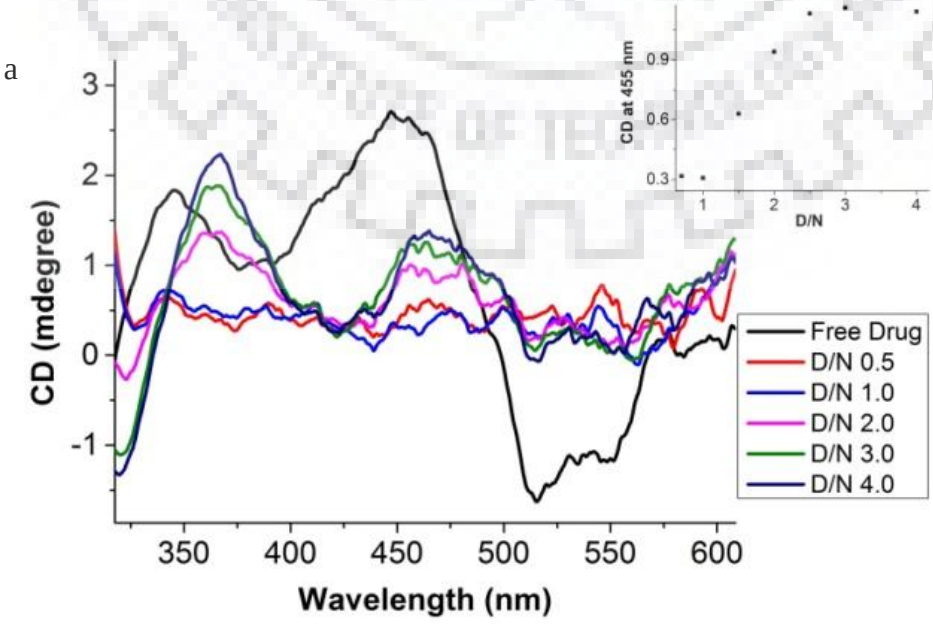

b

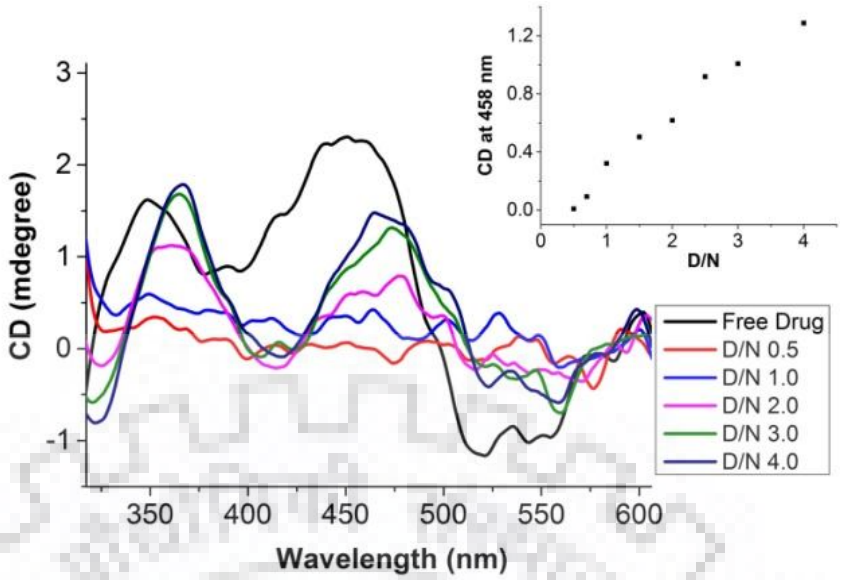

Figure 8.8 CD spectra of 400 μM a) 4'-epiadriamycin and b) adriamycin in free form and its complex with increasing concentration of Tet22 at some selected D/N ratios. The inset shows the plot of CD (mdegree) at 455/458 nm as a function of D/N ratio.

It was found that the bisignate bands of 4'-epiadriamycin/adriamycin having positive and negative peaks at ~460 and ~540 nm, respectively and cross over point at 500 nm (Gallois et al., 1998) disappear on the addition of Tet22 so that ligands bind as a monomer. The 345/340 nm band decreases by 64% and 78% at D/N = 1.0 along with redshift $\Delta\lambda$ = 15 and 5 nm in 4'-epiadriamycin-Tet22 and adriamycin-Tet22 complexes, respectively (Fig. 8.8 a,b). Further, the induce CD band at 460-480 nm is a small positive band which increases slightly with D/N. The results suggest external binding of ligands, maybe with partial stacking with bases (Manet, Manoli, Zambelli, Andreano, Masi, Cellai, Ottani, et al., 2011; Manet, Manoli, Zambelli, Andreano, Masi, Cellai, & Monti, 2011; Bianco et al., 2013; Rezler et al., 2005; White et al., 2007; Jain, Reddy, Paul, Muniyappa, & Bhattacharya, 2009; Paul et al., 2012; Zhao et al., 2013).

8.3.5 Thermal Denaturation

The change in melting temperature (ΔT_m) of folded → unfolded Tet22 DNA and its complex with 4'-epiadriamycin and adriamycin at D/N = 0.5, 1.0, 2.0, 3.0 and 4.0 were obtained using differential scanning calorimeter (Fig. 8.9 a-f and 8.10 a-e).

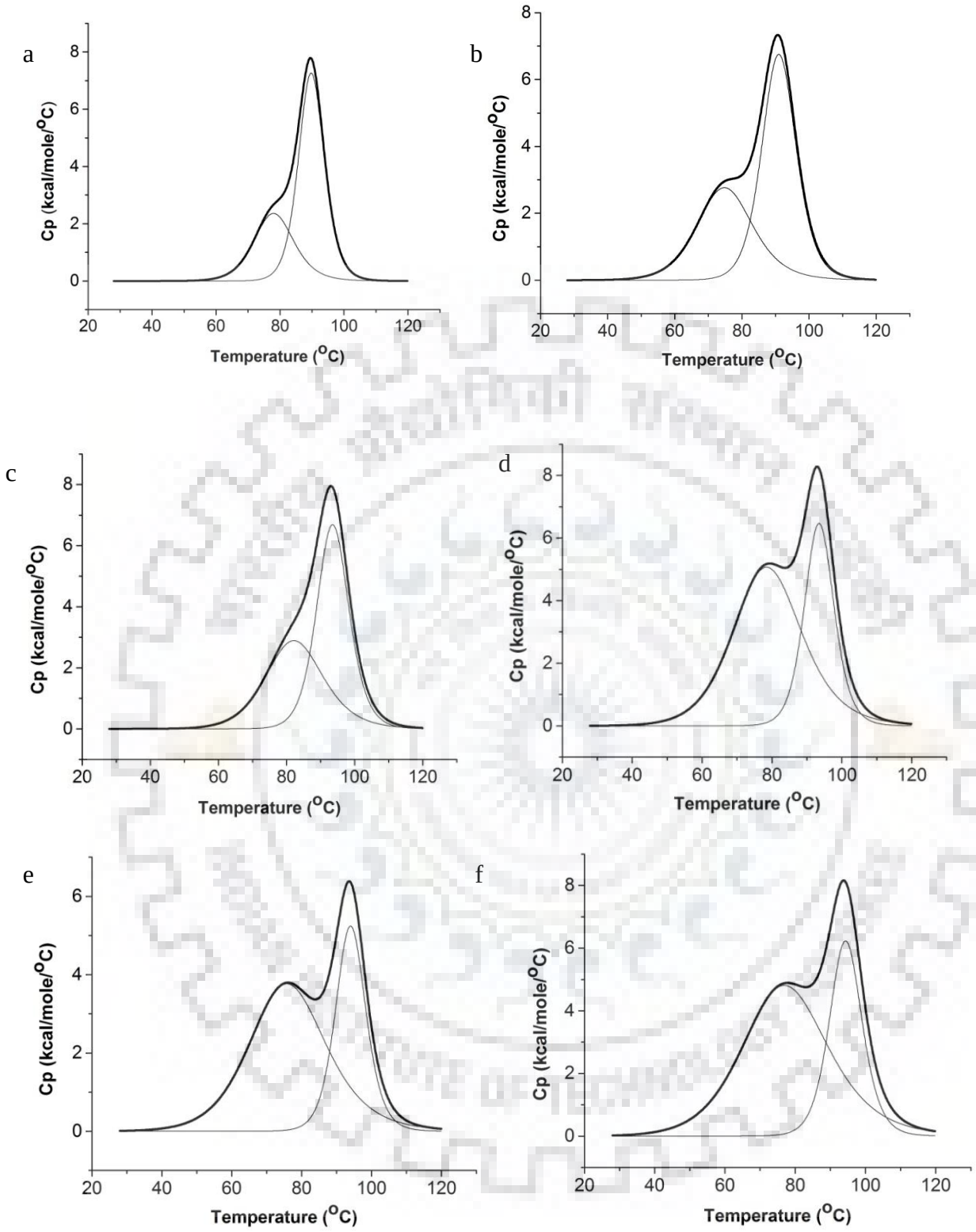
a
b
c
d
e
f
Cp (kcal/mole/^{O}C)
Temperature (^{O}C)

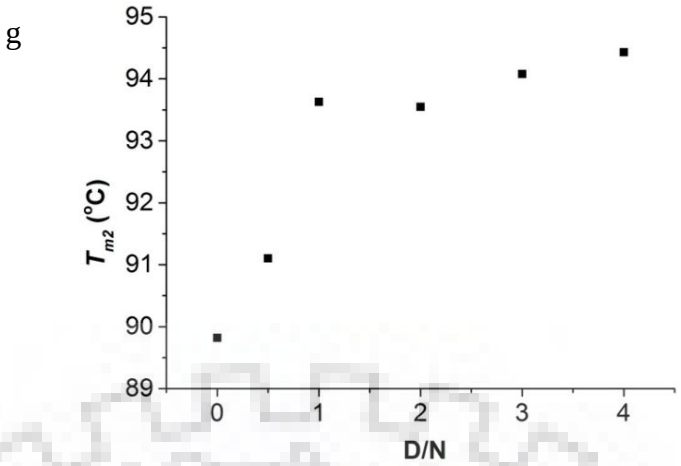

Figure 8.9 DSC thermograms showing excess heat capacity as a function of temperature of a) free 50 µM Tet22 and b-f) 4'epiadriamycin-Tet22 complexes at D/N = 0.5, 1.0, 2.0, 3.0 and 4.0. The observed raw data (thick black lines) have been deconvoluted into "two-state" processes (thin grey lines), respectively using Origin 7.0. All samples were prepared in phosphate buffer (KBPES) (pH 7.0) containing 100 mM KCl; g) Plot of melting temperature T_{m2} obtained from DSC experiments as a function of D/N ratio.

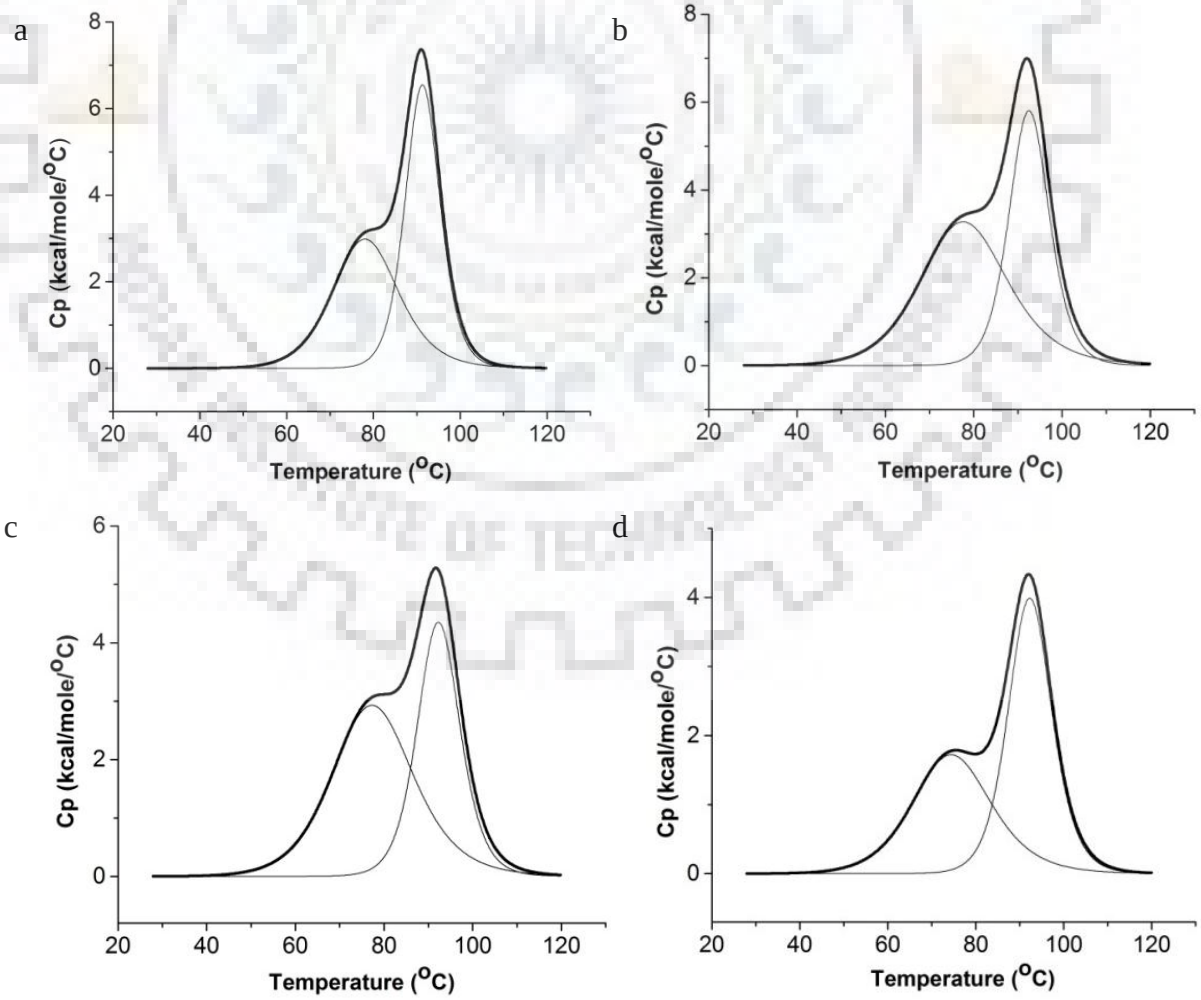

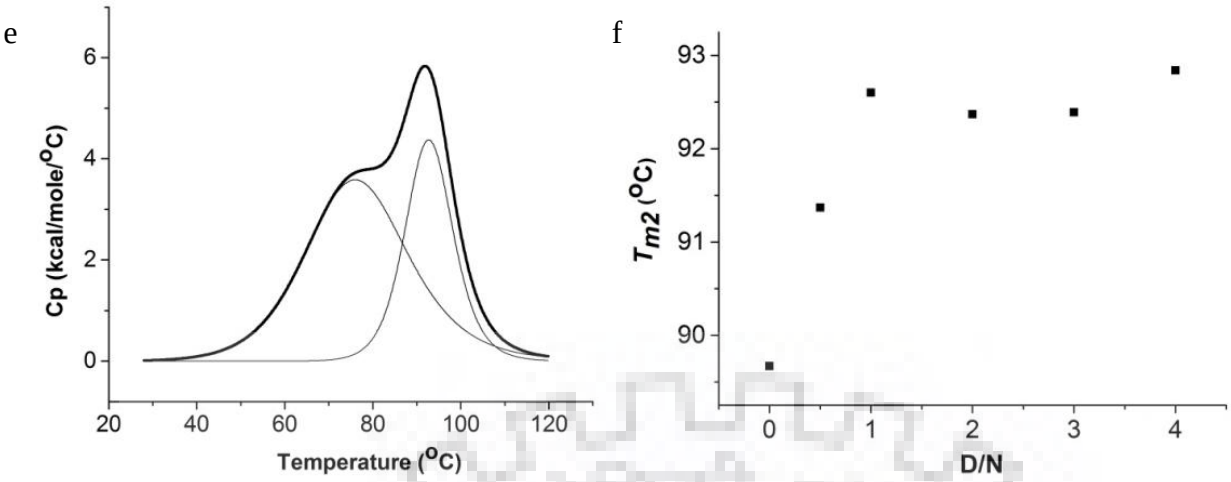

Figure 8.10 DSC thermograms showing excess heat capacity as a function of temperature of a-e) adriamycin-Tet22 complexes at D/N = 0.5, 1.0, 2.0, 3.0 and 4.0. The observed raw data (thick black lines) have been deconvoluted into "two-state" processes (thin grey lines), respectively using Origin 7.0; f) Plot of melting temperature T_{m2} obtained from DSC experiments as a function of D/N ratio.

The data of 50 μM free Tet22 DNA fits into two "two-state" model (alternately referred to as three state melting process) showing two major transitions centered at T_{m1} = 78.0 ± 0.2 ºC and T_{m2} = 90.0 ± 0.1 ºC (Fig. 8.9 a) indicating existence of intermediate species in melting pathway (Ghosh, Pradhan, Kar, Chowdhury, & Dasgupta, 2013; Hardin, Henderson, Watson, & Prosser, 1991). Since DSC curves are broad, more than one conformation may be present in equilibrium with each other. The melting profiles of complexes show stabilization of DNA and T_m increases with D/N ratio which appears to saturate at D/N = 1.0/2.0 (Fig. 8.9 g and Fig. 8.10 f). The extent of stabilization is about 4.6 °C and 3.1 °C for 4'-epiadriamycin and adriamycin Tet22 complexes, respectively at D/N = 4.0 (Table 8.5 and 8.6). Stabilization of ΔT_m = 0, 5 and 11 °C have earlier been obtained on binding of adriamycin/daunomycin to 21-mer human telomeric DNA in Na^+ rich (Manet, Manoli, Zambelli, Andreano, Masi, Cellai, Ottani, et al., 2011), K^+ rich aqueous solutions (Manet, Manoli, Zambelli, Andreano, Masi, Cellai, & Monti, 2011) and 22-mer human telomeric DNA (Das et al., 2017). The thermal stabilization of DNA ΔT_m ~3-5 °C may, therefore, be attributed to the observed specific interaction between 4'-epiadriamycin/adriamycin to Tet22 DNA.

Table 8.5 Data obtained from DSC experiments showing the change in melting temperature (T_m) of Tet22 (50μM) upon complexation with 4'-epiadriamycin at different D/N ratios.

Sample	T_m (°C)	ΔT_m (°C)
Free DNA	89.8 ± 0.1	0.0
D/N 0.5	91.1 ± 0.1	1.3
D/N 1.0	93.6 ± 0.1	3.8
D/N 2.0	93.5 ± 0.1	3.7
D/N 3.0	94.1 ± 0.3	4.3
D/N 4.0	94.4 ± 0.1	4.6

Table 8.6 Data obtained from DSC experiments showing the change in melting temperature (T_m) of Tet22 (50μM) upon complexation with adriamycin at different D/N ratios.

Sample	T_m (°C)	ΔT_m (°C)
Free DNA	89.7 ± 0.1	0.0
D/N 0.5	91.4 ± 0.1	1.7
D/N 1.0	92.6 ± 0.1	2.9
D/N 2.0	92.4 ± 0.1	2.7
D/N 3.0	92.3 ± 0.1	2.6
D/N 4.0	92.8 ± 0.1	3.1

8.3.6 Molecular Docking

In order to get insight into the mode of binding, we conducted molecular docking studies of 4'-epiadriamycin/adriamycin with 24-mer telomeric DNA sequence from *Tetrahymena* d-[(TTGGGG)$_4$] (Tet24), having 3+1 hybrid structure obtained in Na^+ containing solution, (Y. Wang & Patel, 1994) using available PDB (ID:186D). It has been shown that the CD spectra of this NMR based solution structure has two equally intense bands at 260 and 295 nm (Vorlíčková et al., 2012). We have recorded CD spectra of Tet22 lacking TT bases at 5'end in 100 mM K^+ solution which shows the dominant positive band at 265 nm and another positive band at 295 nm. The differences in flanking bases and cation identity contribute to changes in conformation. Apparently, the larger number of guanines having *anti* conformations results in increased intensity of 265 nm band (Fig 8.6 a and 8.7 a) as compared to that of the 24-mer sequence in Na^+ rich solution. The overall structure and shape of CD bands at 265 and 295 nm spectra in 22-mer in K^+ rich solution, however, remains unaltered. Thus, Tet22 G-quadruplex

DNA presumably has parallel form mixed with 3+1 hybrid structure (Vorlíčková et al., 2012; Karsisiotis et al., 2011; Masiero et al., 2010; Gray et al., 2008). Since no structure of *Tetrahymena* telomeric DNA in K^+ rich solution is available in the database, we have chosen the structure of Tet24 sequence d-[TTGGGG(TTGGGG)$_3$] as the nearest available model for our docking studies (Y. Wang & Patel, 1994).

Molecular docking studies of Tet24 with 4'-epiadriamycin and adriamycin yields negative binding energy confirming the formation of bound complex. The lowest energy conformations of 4'-epiadriamycin-Tet24 complex showed the existence of two different binding sites at G3, G4, T13, T14 step, and T8, G9, G18, G22 of Tet24 DNA (Fig. 8.11 a-d) with the binding energy of -7.40 and -6.24 kcal/mol, respectively. Binding at G3, G4, T13, T14 site was stabilized by 4 hydrogen bonds (Fig. 8.11 b): (a) 11OH of ring B with PO_4^{2-} of G4 (2.86 Å), (b) 12O of ring C with N9 of G3 (3.19 Å), (c) NH_3^+ of daunosamine sugar moiety with PO_4^{2-} of T13 (2.39 Å), (d) 4OCH_3 of ring D with PO_4^{2-} of T14 (2.88 Å). Also binding at T8, G9, G18, G22 site was stabilized by 7 hydrogen bonds (Fig. 8.11 d): (a) 12O of ring C with O3' of G22 (3.56 Å), (b) 5O of ring C with NH of G18 (3.19 Å), (c) NH_3^+ of daunosamine sugar moiety with PO_4^{2-} of G9 (2.62 Å), (d) oxygen of daunosamine sugar moiety with O2 of T8 (2.59 Å), (e) 9COCH_2OH with O2 of T8 (2.68 Å), (f) 9COCH_2OH with N3 of T8 (2.73 Å), (g) 9OH of ring A with O2 of T8 (3.35 Å).

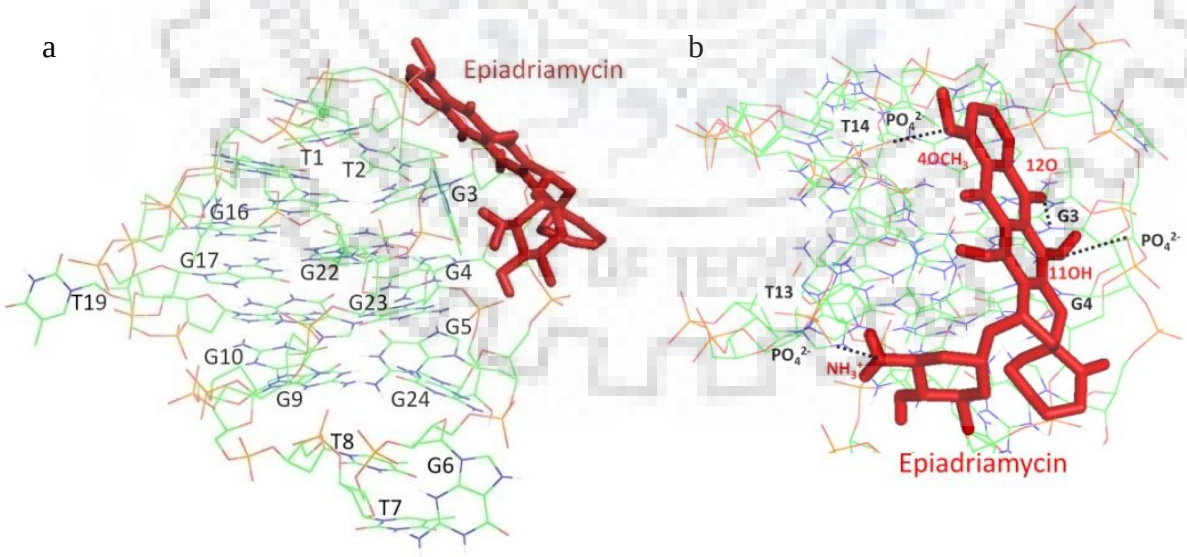

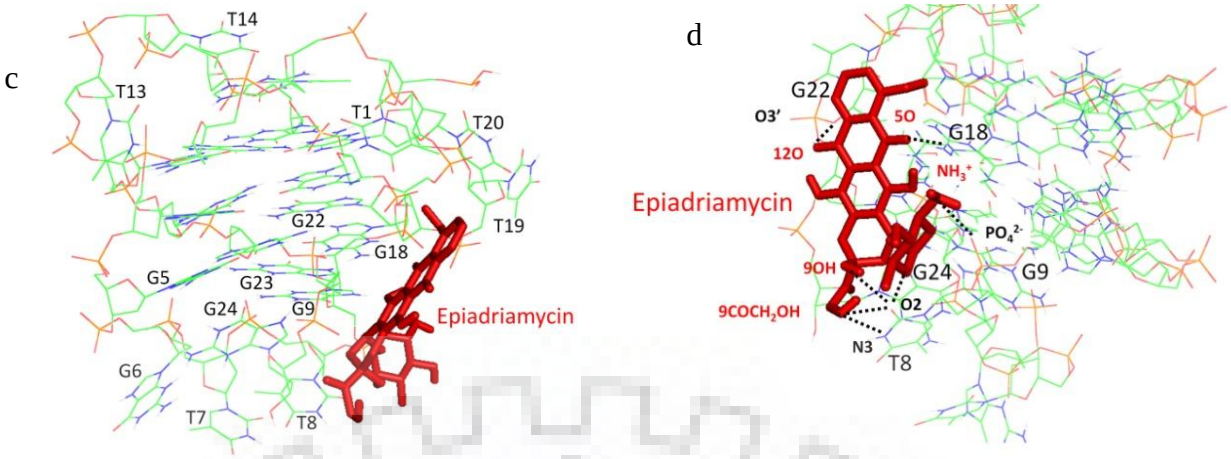

Figure 8.11 The schematic diagram of molecular docking studies representing binding of 4'-epiadriamycin to Tet24 (PDB ID: 186D); a) G3, G4, T13, T14 site; b) Close-up view of ligand binding site G3, G4, T13, T14 showing hydrogen bonds (black dashed lines); c) T8, G9, G18, G22 site; d) Close-up view of ligand binding site T8, G9, G18, G22 showing hydrogen bonds (black dashed lines). The model was generated using Autodock 4.2 and visualized by PyMol.

Similarly in case of the adriamycin-Tet24 complex we observed two different binding sites at G3, G4, T13, T14 step, and G4, G5, T7, G12, T13 step (Fig 8.12 a-d) with the binding energy of -7.72 and -5.95 kcal/mol, respectively. Binding at G3, G4, T13, T14 site was stabilized by 5 hydrogen bonds (Fig. 8.12 b): (a) $4OCH_3$ of ring D with PO_4^{2-} of T14 (3.26 Å), (b) 5O of ring C with PO_4^{2-} of T14 (3.48 Å), (c) NH_3^+ of daunosamine sugar moiety with PO_4^{2-} of T13 (2.44 Å), (d) 11OH of ring B with PO_4^{2-} of G4 (2.86 Å), (e) 12O of ring C with N9 of G3 (3.14 Å). Also binding at G4, G5, T7, G12, T13 site is stabilized by 9 hydrogen bonds (Fig. 8.12 d): (a) 12O of ring C with O4 of T13 (2.28 Å), (b) 12O of ring C with O3' of G4 (3.00 Å), (c) 12O of ring C with NH of G4 (3.29 Å), (d) 11OH of ring B with NH of G4 (3.06 Å), (e) $9COCH_2OH$ with NH of G5 (3.36 Å), (f) $9COCH_2OH$ with NH_2 of G5 (2.84 Å), (g) $9COCH_2OH$ with PO_4^{2-} of T7 (2.74 Å), (h) 4'OH of daunosamine sugar moiety with PO_4^{2-} of G12 (3.18 Å), (i) NH_3^+ of daunosamine sugar moiety with PO_4^{2-} of T13 (2.75 Å). The conformation of complex thus obtained may be considered as a representative study of the binding of 4'-epiadriamycin and adriamycin to Tet24 DNA and has limitations due to the absence of explicit solvent, ions and conformational flexibility in DNA.

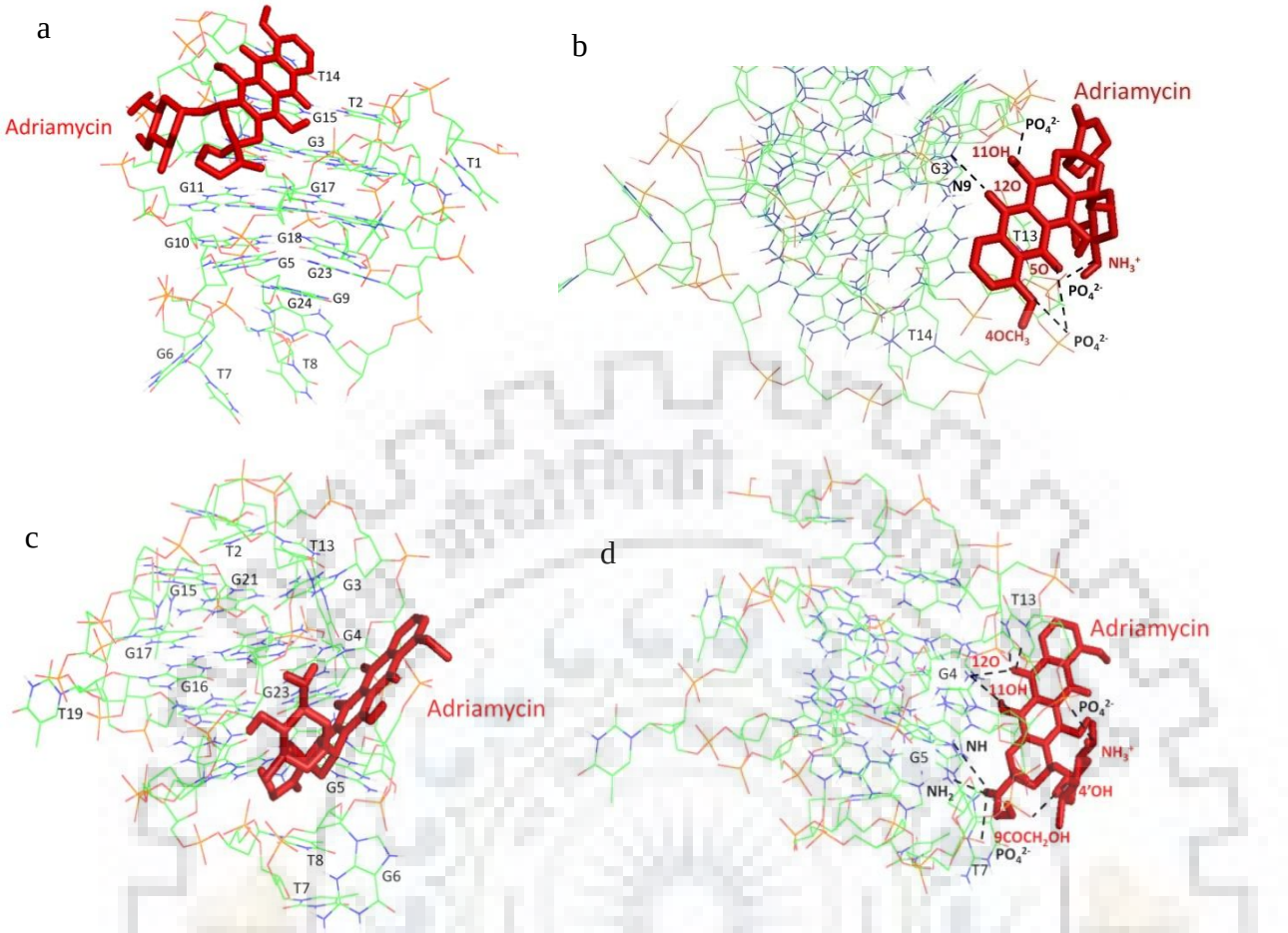

Figure 8.12 The schematic diagram of molecular docking studies representing binding of adriamycin to Tet24 (PDB ID: 186D); a) G3, G4, T13, T14 site; b) Close-up view of ligand binding site G3, G4, T13, T14 showing hydrogen bonds (black dashed lines); c) G4, G5, T7, G12, T13 site; d) Close-up view of ligand binding site G4, G5, T7, G12, T13 showing hydrogen bonds (black dashed lines). Model was generated using Autodock 4.2 and visualized by PyMol.

8.4. Conclusion

We conclude that the binding of adriamycin and 4'-epiadriamycin to Tet22 occurs as a monomer through external interactions. Extreme quenching of fluorescence indicates the proximity of chromophores of drug molecules to guanines residues for efficient transfer of electrons. Spectroscopic studies confirm the absence of classical intercalation as a mode of binding. The binding of these drugs to Tet22 results in thermal stabilization of ΔT_m 3-5 °C. Thus, our study contributes more towards the understanding of the mode of binding of anthracylines towards G-quadruplex DNA for development of better derivatives having lower cellular toxicity.

Anthracyclines are well established anticancer drugs which act through intercalation between base pairs of duplex DNA resulting in inhibition of DNA duplication, DNA dependent RNA synthesis as well as inhibition of topoisomerase II enzyme. They cause severe cardiotoxicity due to the generation of free radicals and inactivation of selenium-dependent GSH-peroxidase-1 (GSH-Px1) in cardiomyocytes. It has been demonstrated that anthracylines (doxorubicin and epirubicin) disrupt telomere maintenance through degradation of PINX1 protein which is responsible for disassociation of telomerase onto telomeres (B. Zhang et al., 2012). Thus, anthracyclines bind to both duplex and G4 DNA, and they exert their action by other possible mechanisms. Intercalation between duplex DNA base pairs has been well established by X-ray (Frederick, Williams, Ughetto, Marel, et al., 1990) and NMR (Barthwal, Mujeeb, & Govil, 1994) studies. The competition dialysis experiment by Chaires et al. showed that daunomycin binds to G-quadruplex DNA although with lesser binding affinity than that to duplex DNA (Ren & Chaires, 1999). Clark et al. visualized the crystal structure of daunomycin-$[d(TGGGGT)]_4$ complex which showed two layers of three daunomycin molecules sandwiched between two molecules of G-quadruplex DNA (Clark, Pytel, Squire, & Neidle, 2003). Yet, in another NMR based study, Scaglioni et al. determined that anthracyclines, doxorubicin, and nemorubicin, binds to several G-quadruplex sequences and c-MYC promoter element Pu22 (Scaglioni, Mondelli, Artali, Sirtori, & Mazzini, 2016). Recently, molecular dynamics simulations showed that groove binding and end stacking of daunomycin are energetically equally favorable in $[d-(TGGGGT)]_4$ while intercalation is the preferred binding mode in duplex DNA (Shen, Mulholland, Zheng, & Wu, 2017). However, there are no biophysical or structural studies on G4 DNA complexes comprising four or more guanine repeats from *Tetrahymena* telomeric DNA sequence. Therefore, we have done the detailed investigation on the binding affinity, stoichiometry, thermal stabilization and solution structure of anthracyclines with the G-quadruplex DNA. The present study emphasizes similarities and differences in the conformation of G-quadruplex DNA upon complex formation.

A comparison of NMR based structure of the three drugs namely daunomycin, adriamycin and 4'-epiadriamycin with 7 mer intermolecular G quadruplex DNA $[d-(TTGGGGT)]_4$ shows that there are two distinct binding sites, one close to T1pT2 base and other close to G6pT7 site. This is evident from the severe broadening of proton signals G6NH, $T7CH_3$, T7H6, $T1CH_3$, and $T2CH_3$. The T7 base is flipped away in bound DNA in order to accommodate drug in its vicinity in all the three structures. This leads to a downfield shift of $T7CH_3$ and T7H6 protons

by 0.20 and 0.30 ppm, respectively in all the three complexes. However, the structure clearly shows that in adriamycin complex the chromophore is better stacked with terminal (G6) quartet. This corroborates with the observed maximum upfield shift of G6NH (0.36 ppm) in adriamycin complex as compared to that in 4'-epiadriamycin complex, in which relatively lesser shift in G6NH (0.29 ppm) is observed. The binding of these drugs also affects the ^{31}P NMR signals. Apparently, adriamycin stacking in adriamycin complex has resulted in greater perturbations in the phosphate backbone at both the sites. This has resulted in greater downfield shifts of G6pT7 and T1pT2 signals (0.67 and 0.57 ppm) as compared to that in 4'-epiadriamycin complex (0.19 and 0.28 ppm). It is also noted that broadening of signals adriamycin complex is much more than the 4'-epiadriamycin complex in which all the signals remains sharp even after complexation. The shifts in daunosamine sugar protons in adriamycin and daunomycin complexes is practically the same whereas in 4'-epiadriamycin complex they are significantly different. Both adriamycin and daunomycin have same daunosamine sugar moiety and give rise to similar shifts. However, daunosamine sugar protons in 4'-epiadriamycin complex show different aspects of binding due to the inversion of H and OH group of carbon at 4' position. We observed a larger extent of upfield shift of 5'H, 4'H, and 5'CH_3, it being 0.33, 0.23 and 0.30 ppm, respectively. The shift in 3'H was 0.04 ppm which is much less than that of adriamycin and daunomycin complexes. Thus, the effect of the relative orientation of daunosamine sugar moiety is clearly evident from the chemical shift differences.

In the final NMR based structure, it is found that there is a large difference between the daunomycin complex and adriamycin/4'-epiadriamycin complex. In both adriamycin and 4'-epiadriamycin complexes the 5O and 6OH are in close proximity of DNA bases. In adriamycin complex 9$COCH_2OH$ also makes close contact with N3 and O2 of T2 base. On the other hand, in the daunomycin complex, the participation of 5O and 6OH does not exist and the 9$COCH_3$ group is close to NH of T2 base. It may be noted that 9$COCH_3$ being hydrophobic does not make direct contacts with phosphate backbone which is polar in nature. Water-mediated contacts of 9$COCH_2OH$ with phosphate of DNA has earlier been observed in X-ray crystallographic studies with duplex DNA (Frederick, Williams, Ughetto, Marel, et al., 1990). Our analysis indicates that the three complexes show different binding properties with the same G-quadruplex DNA. These differences may be responsible for different affinity constants as determined independently in real time mode by SPR experiments. The following is the order of affinity constant for complexes of $[d\text{-}(TTGGGGT)]_4$ with adriamycin > 4'-epiadriamycin > daunomycin. The greater extent of redshift in adriamycin complex as compared to the other complexes may be attributed to better stacking interactions with G6pT7 site.

Spectroscopic and computational studies suggested binding of these three drugs to Tet22 externally as a monomer, forming 1:1 and 2:1 complexes, in K^+ solution. No classical intercalation is observed upon binding of the three drugs to Tet22. However, there is a marked difference in thermal stabilization of Tet22 upon interaction with daunomycin and adriamycin/4'-epiadriamycin. Binding of daunomycin to Tet22 leads to higher ΔT_m = 10 °C as compared to that by adriamycin or 4'-epiadriamycin, which is ΔT_m = 3-5 °C (Chapter 5 and 8). Adriamycin imparts no thermal stabilization to the antiparallel structure (Manet, Manoli, Zambelli, Andreano, Masi, Cellai, Ottani, et al., 2011) and hence, effective stabilization is perhaps only through binding to parallel structures present in the solution of Tet22 (in K^+) containing a mixture of parallel and antiparallel conformations.

The difference in binding characteristics and structures of the complexes reflects that these drugs are expected to behave differently upon interaction with telomeric G quadruplex DNA. Since thermal stabilization is likely to disrupt the association of telomerase on to telomeres, the net effect of these drugs on telomere dysfunction is likely to be different. Anthracylines offers a great opportunity for modifications in sugar moiety and substituents in ring A/D. Recently, it is shown that modification in daunosamine sugar moiety at C3' position with proper formamidine system affects the ability of anticancer action (Denel-bobrowska & Marczak, 2017). Our findings through structural and biophysical studies are a step toward understanding the interaction of anthracylines with G-quadruplex DNA. This study paves a way for the development of novel derivatives through chemical modifications in daunosamine sugar moiety or in ring A/D which might cause lesser toxicity and greater specificity towards different G-quadruplex DNA sequences and inhibits telomerase enzyme leading to drug induce apoptosis.

References

Agrawal, H., Kumar, A., Bal, N. C., Siddiqi, M. I., & Arora, A. (2007). Ligand based virtual screening and biological evaluation of inhibitors of chorismate mutase (Rv1885c) from Mycobacterium tuberculosis H37Rv. *Biorganic and Medicinal Chemistry Letters*, *17*, 3053–3058. https://doi.org/10.1016/j.bmcl.2007.03.053

Agrawal, P., Barthwal, S. K., & Barthwal, R. (2009). Studies on self-aggregation of anthracycline drugs by restrained molecular dynamics approach using nuclear magnetic resonance spectroscopy supported by absorption, fluorescence, diffusion ordered spectroscopy and mass spectrometry. *European Journal of Medicinal Chemistry*, *44*(4), 1437–1451. https://doi.org/10.1016/j.ejmech.2008.09.037

Agrawal, P., Govil, G., & Barthwal, R. (2009). Studies on drug-DNA complexes, adriamycin-d-(TGATCA)2 and 4′-epiadriamycin-d-(CGATCG)2, by phosphorus-31 nuclear magnetic resonance spectroscopy. *Magnetic Resonance in Chemistry*, *47*(5), 390–397. https://doi.org/10.1002/mrc.2398

Altona, C., & Sundaralingam, M. (1972). Conformational Analysis of the Sugar Ring in Nucleosides and Nucleotides. A New Description Using the Concept of Pseudorotation. *Journal of the American Chemical Society*, *94*(23), 8205–8212. https://doi.org/10.1021/ja00778a043

Ambrus, A., Chen, D., Dai, J., Bialis, T., Jones, R. A., & Yang, D. (2006). Human telomeric sequence forms a hybrid-type intramolecular G-quadruplex structure with mixed parallel/antiparallel strands in potassium solution. *Nucleic Acids Research*, *34*(9), 2723–2735. https://doi.org/10.1093/nar/gkl348

Anand, R., Ottani, S., Manoli, F., Manet, I., & Monti, S. (2012). A close-up on doxorubicin binding to γ-cyclodextrin: an elucidating spectroscopic, photophysical and conformational study. *RSC Advances*, *2*(6), 2346–2357. https://doi.org/10.1039/c2ra01221a

Anantha, N. V., Azam, M., & Sheardy, R. D. (1998). Porphyrin Binding to Quadruplexed T4G4. *Biochemistry*, *37*(9), 2709–2714. https://doi.org/10.1021/bi973009v

Antonacci, C., Chaires, J. B., & Sheardy, R. D. (2007). Biophysical Characterization of the Human Telomeric (TTAGGG)4 Repeat in a Potassium Solution. *Biochemistry*, *46*(15), 4654–4660. https://doi.org/10.1021/bi602511p

Arinaga, S., Akiyoshi, T., & Tsuji, H. (1986). Augmentation of the Generation of Cell-mediated Cytotoxicity after a Single Dose of Adriamycin in Cancer Patients. *Cancer Research*, *46*, 4213–4216.

References

Awasthi, P., Dogra, S., & Barthwal, R. (2013). Multispectroscopic methods reveal different modes of interaction of anti cancer drug mitoxantrone with Poly (dG-dC). Poly (dG-dC) and Poly (dA-dT). Poly (dA-dT). *Journal of Photochemistry & Photobiology, B: Biology*, *127*, 78–87. https://doi.org/10.1016/j.jphotobiol.2013.07.023

Balagurumoorthy, P., & Brahmachari, S. K. (1994). Structure and stability of human telomeric sequence. *The Journal of Biological Chemistry*, *269*(34), 21858–21869.

Balasubramanian, S., & Neidle, S. (2009). G-quadruplex nucleic acids as therapeutic targets. *Current Opinion in Chemical Biology*, *13*(3), 345–353. https://doi.org/10.1016/j.cbpa.2009.04.637.G-quadruplex

Barthwal, R., Agrawal, P., Tripathi, A. N., Sharma, U., Jagannathan, N. R., & Govil, G. (2008). Structural elucidation of 4'-epiadriamycin by nuclear magnetic resonance spectroscopy and comparison with adriamycin and daunomycin using quantum mechanical and restrained molecular dynamics approach. *Archives of Biochemistry and Biophysics*, *474*(1), 48–64. https://doi.org/10.1016/j.abb.2008.02.039

Barthwal, R., Mujeeb, A., & Govil, G. (1994). Interaction of daunomycin with deoxydinucleotide d-CpG by two-dimensional proton magnetic resonance techniques. *Archives of Biochemistry and Biophysics*, *313*(2), 189–205.

Barthwal, R., Mujeeb, A., Srivastava, N., & Sharma, U. (1996). A proton nuclear magnetic resonance investigation of the conformation of daunomycin. *Chemico-Biological Interactions*, *100*, 125–139.

Barthwal, R., Sharma, U., Srivastava, N., Jain, M., Awasthi, P., Kaur, M., … Govil, G. (2006). Structure of daunomycin complexed to d-TGATCA by two-dimensional nuclear magnetic resonance spectroscopy. *European Journal of Medicinal Chemistry*, *41*(1), 27–39. https://doi.org/10.1016/j.ejmech.2005.09.005

Bax, A., & Subramanian, S. (1986). Sensitivity-Enhanced Two-Dimensional Heteronuclear Shift Correlation NMR Spectroscopy. *Journal of Magnetic Resonance*, *67*, 565–569.

Beal, P. A., & Dervan, P. B. (1991). Second Structural Motif for Recognition of DNA by Oligonucleotide-Directed Triple- Helix Formation. *Science*, *251*, 1360–1363.

Bessi, I., Bazzicalupi, C., Richter, C., Jonker, H. R. A., Saxena, K., Sissi, C., … Gratteri, P. (2012). Spectroscopic, molecular modeling, and NMR-spectroscopic investigation of the binding mode of the natural alkaloids berberine and sanguinarine to human telomeric G-quadruplex DNA. *ACS Chemical Biology*, *7*, 1109–1119. https://doi.org/10.1021/cb300096g

Bhadra, K., & Kumar, G. S. (2011). Interaction of berberine, palmatine, coralyne, and sanguinarine to quadruplex DNA: A comparative spectroscopic and calorimetric study. *Biochimica et Biophysica Acta - General Subjects*, *1810*(4), 485–496. https://doi.org/10.1016/j.bbagen.2011.01.011

Bhardwaj, N. (2007). Harnessing the immune system to treat cancer. *The Journal of Clinical Investigation*, *117*(5), 1130–1136. https://doi.org/10.1172/JCI32136.1130

Bhattacharjee, S., Chakraborty, S., Sengupta, P. K., & Bhowmik, S. (2016). Exploring the Interactions of the Dietary Plant Flavonoids Fisetin and Naringenin with G‐Quadruplex and Duplex DNA, Showing Contrasting Binding Behavior: Spectroscopic and Molecular Modeling Approaches. *The Journal of Physical Chemistry B*, *120*, 8942–8952. https://doi.org/10.1021/acs.jpcb.6b06357

Bianco, S., Musetti, C., Krapcho, A. P., Palumbo, M., & Sissi, C. (2013). Ni2+ and Cu2+ complexes of a phenanthroline-based ligand bind to G-quadruplexes at non-overlapping sites. *Chemical Communications*, *49*(73), 8057–8059. https://doi.org/10.1039/c3cc44382e

Biffi, G., Tannahill, D., McCafferty, J., & Balasubramanian, S. (2013). Quantitative visualization of DNA G-quadruplex structures in human cells. *Nature Chemistry*, *5*(3), 182–186. https://doi.org/10.1038/nchem.1548

Binaschi, M., Bigioni, M., Cipollone, A., C, R., C, G., C A, M., … F, A. (2001). Anthracyclines : Selected New Developments. *Current Medicinal Chemistry Anti Cancer Agents*, *1*, 113–130. https://doi.org/10.2174/1568011013354723

Blackburn, E H, & Szostak, J. W. (1984). THE MOLECULAR STRUCTURE OF CENTROMERES AND TELOMERES. *Annual Review of Biochemistry*, *53*, 163–194.

Blackburn, Elizabeth H. (1991). Structure and function of telomeres. *Nature*, *350*, 569–573. https://doi.org/10.1038/350569a0

Bryan, T. M., Englezou, A., Dalla-Pozza, L., Dunham, M. A., & Reddel, R. R. (1997). Evidence for an alternative mechanism for maintaining telomere length in human tumors and tumor-derived cell lines. *Nature Medicine*, *3*(11), 1271–1274.

Buket, O., Clement, L., & Danzhou, Y. (2014). DNA G-quadruplex and its potential as anticancer drug target. *Science China Chemistry*, *57*(12), 1605–1614. https://doi.org/10.1177/0963721414541462.Self-Control

Byrne, K. J. O., Thomas, A. L., Sharma, R. A., Decatris, M., Shields, F., Beare, S., & Steward, W. P. (2002). A phase I dose-escalating study of DaunoXome , liposomal daunorubicin , in metastatic breast cancer. *British Journal of Cancer*, *87*, 15–20. https://doi.org/10.1038/sj.bjc.6600344

Campbell, N. H., Parkinson, G. N., Reszka, A. P., & Neidle, S. (2008). Structural Basis of DNA Quadruplex Recognition by an Acridine Drug. *Journal of American Chemical Society*, *130*, 6722–6724.

Cash, D. D., Cohen-zontag, O., Kim, N., Shefer, K., Brown, Y., Ulyanov, N. B., … Feigon, J. (2013). Pyrimidine motif triple helix in the Kluyveromyces lactis telomerase RNA pseudoknot is essential for function in vivo. *Proceedings of the National Academy of Sciences*, *110*(27), 10970–10975. https://doi.org/10.1073/pnas.1309590110

Chaires, J. B., Dattagupta, N., & Crothers, D. M. (1982). Self-Association of Daunomycin. *Biochemistry*, *21*(17), 3927–3932. https://doi.org/10.1021/bi00260a004

Chaires, J. B., Fox, K. R., Herrera, J. E., Britt, M., & Waring, M. J. (1987). Site and Sequence Specificity of the Daunomycin-DNA Interaction. *Biochemistry*, *26*, 8227–8236.

Changenet-Barret, P., Gustavsson, T., Markovitsi, D., & Manet, I. (2016). Ultrafast Electron Transfer in Complexes of Doxorubicin with Human Telomeric G-Quadruplexes and GC Duplexes Probed by Femtosecond Fluorescence Spectroscopy. *ChemPhysChem*, *17*(9), 1264–1272. https://doi.org/10.1002/cphc.201501091

Chaudhuri, S., Pahari, B., & Sengupta, P. K. (2009). Ground and excited state proton transfer and antioxidant activity of 7-hydroxyflavone in model membranes : Absorption and fluorescence spectroscopic studies. *Biophysical Chemistry*, *139*(1), 29–36. https://doi.org/10.1016/j.bpc.2008.09.018

Clark, G. R., Pytel, P. D., & Squire, C. J. (2012). The high-resolution crystal structure of a parallel intermolecular DNA G-4 quadruplex/drug complex employing syn glycosyl linkages. *Nucleic Acids Research*, *40*(12), 5731–5738. https://doi.org/10.1093/nar/gks193

Clark, G. R., Pytel, P. D., Squire, C. J., & Neidle, S. (2003). Structure of the first parallel DNA quadruplex-drug complex. *Journal of the American Chemical Society*, *125*(14), 4066–4067. https://doi.org/10.1021/ja0297988

Cocco, M. J., Hanakahi, L. A., Huber, M. D., & Maizels, N. (2003). Specific interactions of distamycin with G-quadruplex DNA. *Nucleic Acids Research*, *31*(11), 2944–2951. https://doi.org/10.1093/nar/gkg392

Crnugelj, M., Hud, N. V., & Plavec, J. (2002). The Solution Structure of d (G4T4G3)2 : a Bimolecular G-quadruplex with a Novel Fold. *Journal of Molecular Biology*, *320*(5), 911–924. https://doi.org/10.1016/S0022-2836(02)00569-7

D'Estaintot, B. L., Gallois, B., Brown, T., & Hunter, W. N. (1992). The molecular structure of a 4'-epiadriamycin complex with d (TGATCA) at 1 . 7A resolution : comparison with the structure of 4 ' -epiadriamycin d (TGTACA) and d (CGATCG) complexes. *Nucleic Acids Research*, *20*(14), 3561–3566.

Dahm, R. (2008). Discovering DNA : Friedrich Miescher and the early years of nucleic acid research. *Human Genetics*, *122*, 565–581. https://doi.org/10.1007/s00439-007-0433-0

Dai, J., Carver, M., Punchihewa, C., Jones, R. A., & Yang, D. (2007). Structure of the Hybrid-2 type intramolecular human telomeric G-quadruplex in K+ solution : insights into structure polymorphism of the human telomeric sequence. *Nucleic Acids Research*, *35*(15), 4927–4940. https://doi.org/10.1093/nar/gkm522

Dai, J., Carver, M., & Yang, D. (2008). Polymorphism of human telomeric quadruplex structures. *Biochimie*, *90*(8), 1172–1183. https://doi.org/10.1016/j.biochi.2008.02.026

Dai, J., Hatzakis, E., Hurley, L. H., & Yang, D. (2010). I-Motif Structures Formed in the Human c-MYC Promoter Are Highly Dynamic – Insights into Sequence Redundancy and I-Motif Stability. *PLoS ONE*, *5*(7), 1–8. https://doi.org/10.1371/journal.pone.0011647

Dapić, V., Abdomerović, V., Marrington, R., Peberdy, J., Rodger, A., Trent, J. O., & Bates, P. J. (2003). Biophysical and biological properties of quadruplex oligodeoxyribonucleotides. *Nucleic Acids Research*, *31*(8), 2097–2107. https://doi.org/10.1093/nar/gkg316

Das, A., Bhadra, K., Achari, B., Chakraborty, P., & Kumar, G. S. (2011). Interaction of aristololactam- β - D -glucoside and daunomycin with poly (A): Spectroscopic and calorimetric studies. *Biophysical Chemistry*, *155*(1), 10–19. https://doi.org/10.1016/j.bpc.2011.01.011

Das, A., Bhadra, K., & Kumar, G. S. (2011). Targeting RNA by Small Molecules : Comparative Structural and Thermodynamic Aspects of Aristololactam- β -D-glucoside and Daunomycin Binding to tRNA phe. *PLoS ONE*, *6*(8), 1–11. https://doi.org/10.1371/journal.pone.0023186

Das, A., Chatterjee, S., & Suresh Kumar, G. (2017). Targeting human telomeric G-quadruplex DNA with antitumour natural alkaloid aristololactam-β-D-glucoside and its comparison with daunomycin. *Journal of Molecular Recognition*, *e2639*(2639), 1–11. https://doi.org/10.1002/jmr.2639

Das, A., & Kumar, G. S. (2013). Binding of the plant alkaloid aristololactam- β - D -glucoside and antitumor antibiotic daunomycin to single stranded polyribonucleotides. *Biochimica et Biophysica Acta General Subjects*, *1830*(10), 4708–4718. https://doi.org/10.1016/j.bbagen.2013.06.001

Dasgupta, D., & Goldberg, I. H. (1985). Mode of Reversible Binding of Neocarzinostatin Chromophore to DNA : Evidence for Binding via the Minor Groove. *Biochemistry*, *24*(24), 6913–6920. https://doi.org/10.1021/bi00345a025

Dasgupta, D., Parrack, P., & Sasisekharan, V. (1987). Interaction of Synthetic Analogues of Distamycin with Poly(dA-dT): Role of the Conjugated N-Methylpyrrole System. *Biochemistry*, *26*(20), 6381–6386. https://doi.org/10.1021/bi00394a011

De Cian, A., Guittat, L., Kaiser, M., Saccà, B., Amrane, S., Bourdoncle, A., … Mergny, J. L. (2007). Fluorescence-based melting assays for studying quadruplex ligands. *Methods*, *42*(2), 183–195. https://doi.org/10.1016/j.ymeth.2006.10.004

De Cian, A., Lacroix, L., Douarre, C., Temime-Smaali, N., Trentesaux, C., Riou, J. F., & Mergny, J. L. (2008). Targeting telomeres and telomerase. *Biochimie*, *90*(1), 131–155. https://doi.org/10.1016/j.biochi.2007.07.011

Denel-bobrowska, M., & Marczak, A. (2017). Structural modifications in the sugar moiety as a key to improving the anticancer effectiveness of doxorubicin. *Life Sciences*, *178*, 1–8. https://doi.org/10.1016/j.lfs.2017.04.009

Doroshow, J. H., Locker, G. Y., & Myers, C. E. (1980). Enzymatic Defenses of the Mouse Heart Against Reactive Oxygen Metabolites ALTERATIONS PRODUCED BY DOXORUBICIN. *Journal of Clinical Investigation*, *65*, 128–135.

Dunkern, T. R., Wedemeyer, I., Baumgärtner, M., Fritz, G., & Kaina, B. (2003). Resistance of p53 knockout cells to doxorubicin is related to reduced formation of DNA strand breaks rather than impaired apoptotic signaling. *DNA Repair*, *2*, 49–60.

Ehrke, M. J., Ryoyama, K., & Cohen, S. A. (1984). Cellular Basis for Adriamycin-induced Augmentation of Cell-mediated Cytotoxicity in Culture. *Cancer Research*, *44*, 2497–2504.

Elmore, L. W., Rehder, C. W., Di, X., McChesney, P. A., Jackson-Cook, C. K., Gewirtz, D. A., & Holt, S. E. (2002). Adriamycin-induced senescence in breast tumor cells involves functional p53 and telomere dysfunction. *The Journal of Biological Chemistry*, *277*(38), 35509–35515. https://doi.org/10.1074/jbc.M205477200

Emwas, A.-H., Luchinat, C., Turano, P., Tenori, L., Roy, R., Salek, R. M., … Wishart, D. S. (2015). Standardizing the experimental conditions for using urine in NMR-based metabolomic studies with a particular focus on diagnostic studies : a review. *Metabolomics*, *11*, 872–894. https://doi.org/10.1007/s11306-014-0746-7

Esposito, V., Virgilio, A., Randazzo, A., Galeone, A., & Mayol, L. (2005). A new class of DNA quadruplexes formed by oligodeoxyribonucleotides containing a 3'-3' or 5'-5' inversion of polarity site. *ChemComm*, (31), 3953–3955. https://doi.org/10.1039/b504455c

Evans, S. E., Mendez, M. A., Turner, K. B., Keating, L. R., Grimes, R. T., Melchoir, S., & Szalai, V. A. (2007). End-stacking of copper cationic porphyrins on parallel-stranded guanine quadruplexes. *Journal of Biological Inorganic Chemistry*, *12*(8), 1235–1249. https://doi.org/10.1007/s00775-007-0292-0

Evstigneev, M. P., Khomich, V. V., & Davies, D. B. (2006). Self-association of daunomycin antibiotic in various buffer solutions. *Russian Journal of Physical Chemistry*, *80*(5), 741–746. https://doi.org/10.1134/S003602440605013X

Fedoroff, O. Y., Salazar, M., Han, H., Chemeris, V. V., Kerwin, S. M., & Hurley, L. H. (1998). NMR-based model of a telomerase-inhibiting compound bound to G-quadruplex DNA. *Biochemistry*, *37*(36), 12367–12374. https://doi.org/10.1021/bi981330n

Fernando, H., Reszka, A. P., Huppert, J., Ladame, S., Rankin, S., Venkitaraman, A. R., … Balasubramanian, S. (2006). A Conserved Quadruplex Motif Located in a Transcription Activation Site of the Human c-kit Oncogene. *Biochemistry*, *45*(25), 7854–7860. https://doi.org/10.1021/bi0601510.A

Ferreira, Ruben, Artali, R., Benoit, A., Gargallo, R., Eritja, R., Ferguson, D. M., … Mazzini, S. (2013). Structure and Stability of Human Telomeric G-Quadruplex with Preclinical 9-Amino Acridines. *PLoS ONE*, *8*(3), 1–15. https://doi.org/10.1371/journal.pone.0057701

Ferreira, Rubén, Artali, R., Farrera-sinfreu, J., Albericio, F., Royo, M., Eritja, R., & Mazzini, S. (2011). Acridine and quindoline oligomers linked through a 4-aminoproline backbone prefer G-quadruplex structures. *Biochimica et Biophysica Acta- General Subjects*, *1810*(8), 769–776. https://doi.org/10.1016/j.bbagen.2011.04.013

Fiallo, M. M. L., Tayeb, H., Suarato, A., & Garnier-Suillerot, A. (1998). Circular Dichroism Studies on Anthracycline Antitumor Compounds. Relationship between the Molecular Structure and the Spectroscopic Data. *Journal of Pharmaceutical Sciences*, *87*(8), 967–975. https://doi.org/10.1021/js970436l

Frederick, C. A., Williams, L. D., Ughetto, G., Marel, G. A. Van Der, Boom, J. H. Van, Rich, A., & Wang, A. H.-J. (1990). Structural Comparison of Anticancer Drug-DNA Complexes : Adriamycin and Daunomycin. *Biochemistry*, *29*, 2538–2549. https://doi.org/10.1021/bi00462a016

Frederick, C. A., Williams, L. D., Ughetto, G., van der Marel, G. A., van Boom, H. J., Rich, A., & Wang, A. H.-J. (1990). Structural Comparison of Anticancer Drug-DNA Complexes: Adriamycin and Daunomycin. *Biochemistry*, *29*(10), 2538–2549. https://doi.org/10.1021/bi00462a016

Gai, W., Yang, Q., Xiang, J., Jiang, W., Li, Q., Sun, H., … Tang, Y. (2013). A dual-site simultaneous binding mode in the interaction between parallel-stranded G-quadruplex [d(TGGGGT)]4 and cyanine dye 2,2'-diethyl-9- methyl-selenacarbocyanine bromide. *Nucleic Acids Research*, *41*(4), 2709–2722. https://doi.org/10.1093/nar/gks1328

Gallois, L., Fiallo, M., & Garnier-Suillerot, A. (1998). Comparison of the interaction of doxorubicin, daunorubicin, idarubicin and idarubicinol with large unilamellar vesicles circular dichroism study. *Biochimica et Biophysica Acta - Biomembranes*, *1370*(1), 31–40. https://doi.org/10.1016/S0005-2736(97)00241-1

Gavathiotis, E., Heald, R. A., Stevens, M. F. G., & Searle, M. S. (2003). Drug recognition and stabilisation of the parallel-stranded DNA quadruplex d(TTAGGGT)4 containing the human telomeric repeat. *Journal of Molecular Biology*, *334*(1), 25–36. https://doi.org/10.1016/j.jmb.2003.09.018

Gehring, K., Leroy, J.-L., & Guéron, M. (1993). A tetrameric DNA structure with protonated cytosine.cytosine base pairs. *Letters to Nature*, *363*, 561–565.

Gellert, M., Lipsett, M. N., & Davies, D. R. (1962). Helix Formation By Guanylic Acid. *Proceedings of the National Academy of Sciences*, *48*, 2013–2018. https://doi.org/10.1145/3084381.3084430

Ghosh, S., Pradhan, S. K., Kar, A., Chowdhury, S., & Dasgupta, D. (2013). Molecular basis of recognition of quadruplexes human telomere and c-myc promoter by the putative anticancer agent sanguinarine. *Biochimica et Biophysica Acta - General Subjects*, *1830*(8), 4189–4201. https://doi.org/10.1016/j.bbagen.2013.03.027

Gille, L., & Nohl, H. (1997). ANALYSES OF THE MOLECULAR MECHANISM OF ADRIAMYCIN-INDUCED CARDIOTOXICITY. *Free Radical Biology and Medicine*, *23*(5), 775–782.

Gorenstein, D. G. (1992). 31P NMR of DNA. *Spectroscopic Methods for Analysis of DNA*, *211*, 254–286.

Gorenstein, D. G., & Kar, D. (1975). 31P chemical shifts in phosphate diester monoanions. Bond angle and torsional angle effects. *Biochemical and Biophysical Research Communications*, *65*(3), 1073–1080. https://doi.org/10.1016/S0006-291X(75)80495-5

Gornall, K. C., Samosorn, S., Talib, J., Bremner, J. B., & Beck, J. L. (2007). Selectivity of an indolyl berberine derivative for tetrameric G-quadruplex DNA. *Rapid Communications in Mass Spectrometry*, *21*, 1759–1766. https://doi.org/10.1002/rcm

Gowan, S. M., Heald, R., Stevens, M. F. G., & Kelland, L. R. (2001). Potent Inhibition of Telomerase by Small-Molecule Pentacyclic Acridines Capable of Interacting with G-Quadruplexes. *Molecular Pharmacology*, *60*(5), 981–988.

Gray, D. M., Wen, J., Gray, C. W., Repges, R., Repges, C., Raabe, G., & Fleischhauer, J. (2008). Measured and Calculated CD Spectra of G-Quartets Stacked with the Same or Opposite Polarities. *Chirality*, *20*, 431–440. https://doi.org/10.1002/chir

Gurbani, D., Kukshal, V., Laubenthal, J., Kumar, A., Pandey, A., Tripathi, S., … Dhawan, A. (2012). Mechanism of Inhibition of the ATPase Domain of Human Topoisomerase IIa by 1,4-Benzoquinone, 1,2-Naphthoquinone, 1,4-Naphthoquinone, and 9,10-Phenanthroquinone. *Toxicological Sciences*, *126*(2), 372–390. https://doi.org/10.1093/toxsci/kfr345

Hahn, W. C., Stewart, S. A., Brooks, M. W., York, S. G., Eaton, E., Kurachi, A., … Weinberg, R. A. (1999). Inhibition of telomerase limits the growth of human cancer cells. *Nature Medicine*, *5*(10), 1164–1170.

Hall, K., Cruz, P., Jr., I. T., Jovin, T. M., & van de Sande, J. H. (1984). 'Z-RNA'-a left handed RNA double helix. *Letters to Nature*, *311*(October), 584–586.

Hamilton, P. L., & Arya, D. P. (2012). Natural product DNA major groove binders. *Natural Product Reports*, *29*(2), 134–143. https://doi.org/10.1039/c1np00054c

Han, H., & Hurley, L. H. (2000). G-quadruplex DNA: A potential target for anti-cancer drug design. *Trends in Pharmacological Sciences*, *21*(4), 136–142. https://doi.org/10.1016/S0165-6147(00)01457-7

Hardin, C. C., Corregan, M. J., Lieberman, D. V., & Brown II, B. A. (1997). Allosteric interactions between DNA strands and monovalent cations in DNA quadruplex assembly: Thermodynamic evidence for three linked association pathways. *Biochemistry*, *36*(49), 15428–15450. https://doi.org/10.1021/bi970488p

Hardin, C. C., Henderson, E., Watson, T., & Prosser, J. K. (1991). Monovalent Cation Induced Structural Transitions in Telomeric DNAs: G-DNA Folding Intermediates. *Biochemistry*, *30*(18), 4460–4472. https://doi.org/10.1021/bi00232a013

Hargrove, A. E., Zhong, Z., Sessler, J. L., & Anslyn, E. V. (2010). Algorithms for the determination of binding constants and enantiomeric excess in complex host: guest equilibria using optical measurements. *New Journal of Chemistry*, *34*(2), 348–354. https://doi.org/10.1039/b9nj00498j

Hayflick, L. (1965). The Limited In Vitro Lifetime of Human Diploid Cell Strains. *Experimental Cell Research*, *37*, 614–636.

Hayflick, L., & Moorhead, P. S. (1961). The serial cultivation of human diploid cell strains. *Experimental Cell Research*, *25*, 585–621.

Henderson, A., Wu, Y., Huang, Y. C., Chavez, E. A., Platt, J., Johnson, F. B., … Lansdorp, P. M. (2014). Detection of G-quadruplex DNA in mammalian cells. *Nucleic Acids Research*, *42*(2), 860–869. https://doi.org/10.1093/nar/gkt957

Henderson, E., Hardin, C. C., Walk, S. K., Jr., I. T., & Blackburn, E. H. (1987). Telomeric DNA oligonucleotides form novel intramolecular structures containing guanine.guanine base pairs. *Cell*, *51*(6), 899–908. https://doi.org/10.1016/0092-8674(87)90577-0

Hershey, A. D., & Chase, M. (1952). Independent Functions Of Viral Protein and Nucleic Acid In Growth of Bacteriophage. *The Journal of General Physiology*, 39–56. https://doi.org/10.1085/jgp.36.1.39

Houghtaling, B. R., Cuttonaro, L., Chang, W., & Smith, S. (2004). A Dynamic Molecular Link between the Telomere Length Regulator TRF1 and the Chromosome End Protector TRF2. *Current Biology*, *14*, 1621–1631. https://doi.org/10.1016/j

Huang, H.-S., Chen, I.-B., Huang, K.-F., Lu, W.-C., Shieh, F.-Y., Huang, Y.-Y., … Lin, J.-J. (2007). Synthesis and human telomerase inhibition of a series of regioisomeric disubstituted amidoanthraquinones. *Chemical & Pharmaceutical Bulletin*, *55*(2), 284–292. https://doi.org/10.1248/cpb.55.284

Huang, H. S., Chou, C. L., Guo, C. L., Yuan, C. L., Lu, Y. C., Shieh, F. Y., & Lin, J. J. (2005). Human telomerase inhibition and cytotoxicity of regioisomeric disubstituted amidoanthraquinones and aminoanthraquinones. *Bioorganic and Medicinal Chemistry*, *13*(5), 1435–1444. https://doi.org/10.1016/j.bmc.2004.12.036

Hudson, J. S., Brooks, S. C., & Graves, D. E. (2009). Interactions of Actinomycin D with Human Telomeric G-Quadruplex DNA. *Biochemistry*, *48*, 4440–4447. https://doi.org/10.1021/bi900203z

Hussner, J., Ameling, S., Hammer, E., Herzog, S., Steil, L., Schwebe, M., … Bien, S. (2012). Regulation of Interferon-Inducible Proteins by Doxorubicin via Interferon γ-Janus Tyrosine Kinase-Signal Transducer and Activator of Transcription Signaling in Tumor Cells. *Molecular Pharmacology*, *81*(5), 679–688. https://doi.org/10.1124/mol.111.075994

Incles, C. M., Schultes, C. M., Kempski, H., Koehler, H., Kelland, L. R., & Neidle, S. (2004). A G-quadruplex telomere targeting agent produces p16-associated senescence and chromosomal fusions in human prostate cancer cells. *Molecular Cancer Therapeutics*, *3*(10), 1201–1207.

Ishigami, S., Natsugoe, S., Tokuda, K., Nakajo, A., Che, X., Iwashige, H., … Aikou, T. (2000). Prognostic Value of Intratumoral Natural Killer Cells in Gastric Carcinoma. *Cancer*, *88*(3), 577–583.

Islam, M. M., Pandya, P., Chowdhury, S. R., Kumar, S., & Kumar, G. S. (2008). Binding of DNA-binding alkaloids berberine and palmatine to tRNA and comparison to ethidium : Spectroscopic and molecular modeling studies. *Journal of Molecular Structure*, *891*, 498–507. https://doi.org/10.1016/j.molstruc.2008.04.043

Islam, M. M., Pandya, P., Kumar, S., & Kumar, G. S. (2009). RNA targeting through binding of small mlecules: Studies on t-RNA binding by the cytotoxic protoberberine alkaloid coralyne. *Molecular BioSystems*, *5*, 244–254. https://doi.org/10.1039/b816480k

Jain, A. K., Reddy, V. V., Paul, A., Muniyappa, K., & Bhattacharya, S. (2009). Synthesis and evaluation of a novel class of G-quadruplex-stabilizing small molecules based on the 1,3-phenylene-bis(piperazinyl benzimidazole) system. *Biochemistry*, *48*(45), 10693–10704. https://doi.org/10.1021/bi9003815

Jain, K. K., Casper, E. S., Geller, N. L., Hakes, T. B., Kaufman, R. J., Currie, V., … Young, C. W. (1985). A prospective randomized comparison of epirubicin and doxorubicin in patients with advanced breast cancer. *Journal of Clinical Oncology*, *3*(6), 818–826. https://doi.org/10.1200/JCO.1985.3.6.818

Jeener, J., Meier, B. H., Bachmann, P., & Ernst, R. R. (1979). Investigation of Exchange Process by Two-Dimensional NMR Spectroscopy. *The Journal of Chemical Physics*, *71*(11), 4546–4553. https://doi.org/10.1063/1.438208

Jiang, J., Wang, Y., Susac, L., Chan, H., Basu, R., Zhou, Z. H., & Feigon, J. (2018). Structure of Telomerase with Telomeric DNA. *Cell*, *173*, 1179–1190. https://doi.org/10.1016/j.cell.2018.04.038

Jonsson-Videsater, K., Anderson, G., Bergh, J., & Paul, C. (2003). Doxorubicin-Resistant , MRP1-Expressing U-1285 Cells Are Sensitive to Idarubicin. *Therapeutic Drug Monitoring*, *25*, 331–339.

Jr, C. S. J. (1999). Diffusion ordered nuclear magnetic resonance spectroscopy : principles and applications. *Progress in Nuclear Magnetic Resonance Spectroscopy*, *34*, 203–256.

Karsisiotis, A. I., Hessari, N. M., Novellino, E., Spada, G. P., Randazzo, A., & Webba Da Silva, M. (2011). Topological characterization of Nucleic Acid G-quadruplexes by UV absorption and Circular Dichroism. *Angewandte Chemie - International Edition*, *50*(45), 10645–10648. https://doi.org/10.1002/anie.201105193

Keniry, M. A., Strahan, G. D., Owen, E. A., & Shafer, R. H. (1995). Solution Structure of the Na+ form of the Dimeric Guanine Quadruplex [d(G3T4G3)]2. *European Journal of Biochemistry*, *233*(2), 631–643. https://doi.org/10.1111/j.1432-1033.1995.631_2.x

Khurana, R., Coleman, C., Ionescu-zanetti, C., Carter, S. A., Krishna, V., Grover, R. K., … Singh, S. (2005). Mechanism of thioflavin T binding to amyloid fibrils. *Journal of Structural Biology*, *151*, 229–238. https://doi.org/10.1016/j.jsb.2005.06.006

Kim, M., Vankayalapati, H., Shin-ya, K., Wierzba, K., & Hurley, L. H. (2002). Telomestatin, a Potent Telomerase Inhibitor That Interacts Quite Specifically with the Human Telomeric Intramolecular G-Quadruplex. *Journal of American Chemical Society*, *124*(10), 2098–2099. https://doi.org/10.1021/ja017308q

Kiyomiya, K.-I., Kurebe, M., Nakagawa, H., & Matsuo, S. (2002). The role of the proteasome in apoptosis induced by anthracycline anticancer agents. *International Journal of Oncology*, *20*, 1205–1209.

Kiyomiya, K.-I., Satoh, J., Horie, H., Kurebe, M., Nakagawa, H., & Matsuo, S. (2002). Correlation between nuclear action of anthracycline anticancer agents and their binding affinity to the proteasome. *International Journal of Oncology*, *21*, 1081–1085.

Krugh, T. R., & Reinhardt, C. G. (1975). Evidence for Sequence Preferences in the Intercalative Binding of Ethidium Bromide to Dinucleotide Monophosphate. *J. Mol. Biol.*, *97*, 133–162.

Kumar, A., Wagner, G., Ernst, R. R., & Wüthrich, K. (1981). Buildup Rates of the Nuclear Overhauser Effect Measured by Two-Dimensional Proton Magnetic Resonance Spectroscopy : Implications for Studies of Protein Conformation. *Journal of American Chemical Society*, *103*(13), 3654–3658. https://doi.org/10.1021/ja00403a008

Kumar, P., & Barthwal, R. (2018). Structural and biophysical insight into dual site binding of the protoberberine alkaloid palmatine to parallel G-quadruplex DNA using NMR , fl uorescence and Circular Dichroism spectroscopy. *Biochimie*, *147*, 153–169. https://doi.org/10.1016/j.biochi.2018.02.002

Kumar, S., Pandya, P., Pandav, K., Gupta, S. P., & Chopra, A. (2012). Structural studies on ligand – DNA systems : A robust approach in drug design. *Journal of Biosciences*, *37*(3), 553–561. https://doi.org/10.1007/s12038-012-9212-8

Kypr, J., Kejnovská, I., Bednářová, K., & Vorlíčková, M. (2012). Circular Dichroism Spectroscopy of Nucleic Acids. *Comprehensive Chiroptical Spectroscopy*, *2*, 575–586. https://doi.org/10.1002/9781118120392.ch17

Lange, T. De. (2005). Shelterin : the protein complex that shapes and safeguards human telomeres. *Genes and Development*, *19*, 2100–2110. https://doi.org/10.1101/gad.1346005.quence

Leroy, J.-L., Gueron, M., Mergny, J.-L., & Helene, C. (1994). Intramolecular folding of a fragment of the cytosine-rich strand of telomeric DNA into an i-motif. *Nucleic Acids Research*, *22*(9), 1600–1606.

Licata, S., Saponiero, A., Mordente, A., & Minotti, G. (2000). Doxorubicin Metabolism and Toxicity in Human Myocardium : Role of Cytoplasmic Deglycosidation and Carbonyl Reduction. *Chemical Research in Toxicology*, *13*, 414–420. https://doi.org/10.1021/tx000013q

Lin, C., Wu, G., Wang, K., Onel, B., Sakai, S., Shao, Y., & Yang, D. (2018). Molecular Recognition of the Hybrid-2 Human Telomeric G-Quadruplex by Epiberberine : Insights into Conversion of Telomeric G-Quadruplex Structures. *Angewandte Chemie - International Edition*, *57*, 10888–10893. https://doi.org/10.1002/anie.201804667

Lohr, F., Mayhew, S. G., & Rüterjans, H. (2000). Detection of Scalar Couplings Across NH...OP and OH...OP Hydrogen Bonds in a Flavoprotein. *Journal of American Chemical Society*, *122*(38), 9289–9295. https://doi.org/10.1021/ja001345k

Maccubbin, D. L., Wing, K. R., Mace, K. F., Ho, R. L. X., Ehrke, M. J., & Mihich, E. (1992). Adriamycin-induces modulation of host defences in tumor-bearing mice. *Cancer Research*, *52*, 3572–3576.

Manet, I., Manoli, F., Zambelli, B., Andreano, G., Masi, A., Cellai, L., & Monti, S. (2011). Affinity of the anthracycline antitumor drugs Doxorubicin and Sabarubicin for human telomeric G-quadruplex structures. *Physical Chemistry Chemical Physics*, *13*(2), 540–551. https://doi.org/10.1039/C0CP00898B

Manet, I., Manoli, F., Zambelli, B., Andreano, G., Masi, A., Cellai, L., … Monti, S. (2011). Complexes of the antitumoral drugs Doxorubicin and Sabarubicin with telomeric G-quadruplex in basket conformation: ground and excited state properties. *Photochemical & Photobiological Sciences*, *10*, 1326–1337. https://doi.org/10.1039/c1pp05065f

Martino, L., Virno, A., Pagano, B., Virgilio, A., Micco, S. Di, Galeone, A., … Randazzo, A. (2007). Structural and Thermodynamic Studies of the Interaction of Distamycin A with the Parallel Quadruplex Structure [d(TGGGGT)]4. *Journal of American Chemical Society*, *129*, 16048–16056. https://doi.org/10.1021/ja075710k

Masiero, S., Trotta, R., Pieraccini, S., De Tito, S., Perone, R., Randazzo, A., & Spada, G. P. (2010). A non-empirical chromophoric interpretation of CD spectra of DNA G-quadruplex structures. *Organic & Biomolecular Chemistry*, *8*(12), 2683–2692. https://doi.org/10.1039/c003428b

Mazzini, S., Mondelli, R., & Ragg, E. (1998). Structure and dynamics of intercalation complexes of anthracyclines with d (CGATCG)2 and d (CGTACG)2 . 2D-1H and 31P NMR investigations. *J. Chem. Soc. Perkin. Trans. Ii*, 1983–1991.

Mergny, J.-L., Phan, A.-T., & Lacroix, L. (1998). Following G-quartet formation by UV-spectroscopy. *FEBS Letters*, *435*, 74–78. https://doi.org/10.1016/S0014-5793(98)01043-6

Minotti, G., Cairo, G., & Monti, E. (1999). Role of iron in anthracycline cardiotoxicity: new tunes for an old song? *The FASEB Journal*, *13*(2), 199–212. https://doi.org/10.1096/fasebj.13.2.199

Minotti, G., Menna, P., Salvatorelli, E., Cairo, G., & Gianni, L. (2004). Anthracyclines: Molecular Advances and Pharmacologic Developments in Antitumor Activity and Cardiotoxicity. *Pharmacological Reviews*, *56*(2), 185–229. https://doi.org/10.1124/pr.56.2.6

Miura, T., Benevides, J. M., & Jr, G. J. T. (1995). A Phase Diagram for Sodium and Potassium Ion Control of Polymorphism in Telomeric DNA. *Journal of Molecular Biology*, *248*(2), 233–238.

Nakajima, A., Tauchi, T., Sashida, G., Sumi, M., Abe, K., Yamamoto, K., … Ohyashiki, K. (2003). Telomerase inhibition enhances apoptosis in human acute leukemia cells: possibility of antitelomerase therapy. *Leukemia*, *17*(3), 560–567. https://doi.org/10.1038/sj.leu.2402825

Nawara, K., Beeckman, H., Krysiński, P., & Blanchard, G. J. (2013). Structure-dependent complexation of Fe3+ by anthracyclines. 2. The roles of methoxy and daunosamine functionalities. *The Journal of Physical Chemistry B*, *117*(23), 6868–6873. https://doi.org/10.1021/jp4023508

Neidle, S. (2009). The structures of quadruplex nucleic acids and their drug complexes. *Current Opinion in Structural Biology*, *19*(3), 239–250. https://doi.org/10.1016/j.sbi.2009.04.001

Nelson, A. D. L., & Shippen, D. E. (2015). Evolution of TERT-interacting lncRNAs : expanding the regulatory landscape of telomerase. *Frontiers in Genetics*, *6*(277), 1–6. https://doi.org/10.3389/fgene.2015.00277

Ogretmen, B., Kraveka, J. M., Schady, D., Usta, J., Hannun, Y. A., & Obeid, L. M. (2001). Molecular Mechanisms of Ceramide-mediated Telomerase Inhibition in the A549 Human Lung Adenocarcinoma Cell Line. *The Journal of Biological Chemistry*, *276*(35), 32506–32514. https://doi.org/10.1074/jbc.M101350200

Olby, R. (1969). Cell Chemistry In Miescher's Day. *News, Notes and Queries*, 377–382.

Padmapriya, K., & Barthwal, R. (2016). Binding of the alkaloid coralyne to parallel G-quadruplex DNA [d(TTGGGGT)]4 studied by multi-spectroscopic techniques. *Biophysical Chemistry*, *219*, 49–58. https://doi.org/10.1016/j.bpc.2016.09.006

Padmapriya, K., & Barthwal, R. (2017). NMR based structural studies decipher stacking of the alkaloid coralyne to terminal guanines at two different sites in parallel G-quadruplex DNA, [d(TTGGGGT)]4 and [d(TTAGGGT)]4. *Biochimica et Biophysica Acta - General Subjects*, *1861*(2), 37–48. https://doi.org/10.1016/j.bbagen.2016.11.011

Pahari, B. P., Chaudhuri, S., Chakraborty, S., & Sengupta, P. K. (2015). Ground and Excited State Proton Transfer of the Bioactive Plant Flavonol Robinetin in a Protein Environment : Spectroscopic and Molecular Modeling Studies. *The Journal of Physical Chemistry*, *119*, 2533–2545. https://doi.org/10.1021/jp508410v

Paramasivan, S., Rujan, I., & Bolton, P. H. (2007). Circular dichroism of quadruplex DNAs: Applications to structure, cation effects and ligand binding. *Methods*, *43*(4), 324–331. https://doi.org/10.1016/j.ymeth.2007.02.009

Parkinson, G. N., Lee, M. P. H., & Neidle, S. (2002). Crystal structure of parallel quadruplexes from human telomeric DNA. *Nature*, *417*(6891), 876–880. https://doi.org/10.1038/nature755

Pasternack, R. F., Gibbs, E. J., & Villafranca, J. J. (1983). Interactions of Porphyrins with Nucleic Acids. *Biochemistry*, *22*(23), 5409–5417. https://doi.org/10.1021/bi00292a024

Patel, D. J., & Canuel, L. L. (1978). Anthracycline Antitumor Antibiotic . Nucleic-Acid Interactions. *European Journal of Biochemistry*, *90*, 247–254.

Patel, D. J., Kozlowski, S. A., & Rice, J. A. (1981). Hydrogen bonding , overlap geometry , and sequence specificity in anthracycline antitumor antibiotic-DNA complexes in solution. *Proceedings of the National Academy of Sciences*, *78*(6), 3333–3337.

Patel, P K, & Hosur, R. V. (1999). NMR observation of T-tetrads in a parallel stranded DNA quadruplex formed by Saccharomyces cerevisiae telomere repeats. *Nucleic Acids Research*, *27*(12), 2457–2464.

Patel, Prasanta K, Koti, A. S. R., & Hosur, R. V. (1999). NMR studies on truncated sequences of human telomeric DNA : observation of a novel A-tetrad. *Nucleic Acids Research*, *27*(19), 3836–3843.

Paul, A., Maji, B., Misra, S. K., Jain, A. K., Muniyappa, K., & Bhattacharya, S. (2012). Stabilization and structural alteration of the G-quadruplex DNA made from the human telomeric repeat mediated by Tröger's base based novel benzimidazole derivatives. *Journal of Medicinal Chemistry*, *55*(17), 7460–7471. https://doi.org/10.1021/jm300442r

Percivalle, C., Sissi, C., Greco, M. L., Musetti, C., Mariani, A., Artese, A., … Freccero, M. (2014). Aryl ethynyl anthraquinones: a useful platform for targeting telomeric G-quadruplex structures. *Organic & Biomolecular Chemistry*, *12*, 3744–3754. https://doi.org/10.1039/c4ob00220b

Perego, P., Corna, E., Cesare, M. De, Gatti, L., Polizzi, D., Pratesi, G., … Zunino, F. (2001). Role of Apoptosis and Apoptosis-Related Genes in Cellular Response and Antitumor Efficacy of Anthracyclines. *Current Medicinal Chemistry*. https://doi.org/http://dx.doi.org/10.2174/0929867013373994

Perry, P. J., Gowan, S. M., Reszka, A. P., Polucci, P., Jenkins, T. C., Kelland, L. R., & Neidle, S. (1998). 1,4- and 2,6-Disubstituted Amidoanthracene-9,10-Dione Derivatives As Inhibitors of Human Telomerase. *Journal of Medicinal Chemistry*, *41*(17), 3253–3260. https://doi.org/10.1021/jm9801105

Perry, P. J., Read, M. A., Davies, R. T., Gowan, S. M., Reszka, A. P., Wood, A. A., … Neidle, S. (1999). 2 , 7-Disubstituted Amidofluorenone Derivatives as Inhibitors of Human Telomerase. *Journal of Medicinal Chemistry*, *42*, 2679–2684. https://doi.org/10.1021/jm990084q

Perry, P. J., Reszka, A. P., Wood, A. A., Read, M. A., Gowan, S. M., Dosanjh, H. S., … Neidle, S. (1998). Human telomerase inhibition by regioisomeric disubstituted amidoanthracene-9,10-diones. *Journal of Medicinal Chemistry*, *41*(24), 4873–4884. https://doi.org/10.1021/jm981067o

Petraccone, L., Duro, I., Randazzo, A., Virno, A., Mayol, L., & Giancola, C. (2007). Biophysical Properties of Quadruplexes Containing Two or Three 8-Bromodeoxyguanosine Residues. *Nucleosides, Nucleotides and Nucleic Acids*, *26*, 669–674. https://doi.org/10.1080/15257770701490589

Phan, A. T., Kuryavyi, V., Gaw, H. Y., & Patel, D. J. (2005). Small-molecule interaction with a five-guanine-tract G-quadruplex structure from the human MYC promoter. *Nature Chemical Biology*, *1*(3), 167–173. https://doi.org/10.1038/nchembio723

Phan, A. T., Luu, K. N., & Patel, D. J. (2006). Different loop arrangements of intramolecular human telomeric (3 + 1) G-quadruplexes in K+ solution. *Nucleic Acids Research*, *34*(19), 5715–5719. https://doi.org/10.1093/nar/gkl726

Phan, A. T., Modi, Y. S., & Patel, D. J. (2004). Two-repeat Tetrahymena telomeric d(TGGGGTTGGGGT) sequence interconverts between asymmetric dimeric G-quadruplexes in solution. *Journal of Molecular Biology*, *338*(1), 93–102. https://doi.org/10.1016/j.jmb.2004.02.042

Phan, A. T., & Patel, D. J. (2003). Two-Repeat Human Telomeric d(TAGGGTTAGGGT) Sequence Forms Interconverting Parallel and Antiparallel G-Quadruplexes in Solution: Distinct Topologies, Thermodynamic Properties, and Folding/Unfolding Kinetics. *Journal of American Chemical Society*, *125*(49), 15021–15027. https://doi.org/10.1021/ja037616j.Two-Repeat

Plastaras, J. P., Dedon, P. C., & Marnett, L. J. (2002). Effects of DNA Structure on Oxopropenylation by the Endogenous Mutagens Malondiaaldehyde and Base Propenal. *Biochemistry*, *41*, 5033–5042. https://doi.org/10.1021/bi0113059

Podlevsky, J. D., Bley, C. J., Omana, R. V, Qi, X., & Chen, J. J.-L. (2008). The Telomerase Database. *Nucleic Acids Research*, *36*, 339–343. https://doi.org/10.1093/nar/gkm700

Podlevsky, J. D., Li, Y., & Chen, J. J.-L. (2016). Structure and function of echinoderm telomerase RNA. *RNA*, *22*, 204–215. https://doi.org/10.1261/rna.053280.115.2

Pradeep, Tarikere Palakashan, & Barthwal, R. (2016). A 4:1 stoichiometric binding and stabilization of mitoxantrone-parallel stranded G-quadruplex complex established by spectroscopy techniques. *Journal of Photochemistry and Photobiology B: Biology*, *162*, 106–114. https://doi.org/10.1016/j.jphotobiol.2016.06.019

Pradeep, Tarikere Palakshan, & Barthwal, R. (2016). NMR structure of dual site binding of mitoxantrone dimer to opposite grooves of parallel stranded G-quadruplex [d-(TTGGGGT)]4. *Biochimie*, *128–129*, 59–69. https://doi.org/10.1016/j.biochi.2016.07.005

Pristovsek, P., Sengupta, K., Lohr, F., Schafer, B., Trebra, M. W. von, Ruterjans, H., & Bernhard, F. (2003). Structural Analysis of the DNA-binding Domain of the Erwinia amylovora RcsB Protein and Its Interaction with the RcsAB Box. *The Journal of Biological Chemistry*, *278*(20), 17752–17759. https://doi.org/10.1074/jbc.M301328200

Randazzo, A., Galeone, A., Esposito, V., Varra, M., & Mayol, L. (2002). INTERACTION OF DISTAMYCIN A AND NETROPSIN WITH QUADRUPLEX AND DUPLEX STRUCTURES : A COMPARATIVE 1H-NMR STUDY. *Nucleosides Nucleotides & Nucleic Acids*, *21*(8), 535–545. https://doi.org/10.1081/NCN-120015067

Randazzo, A., Galeone, A., & Mayol, L. (2001). 1H-NMR study of the interaction of distamycin A and netropsin with the parallel stranded tetraplex [d(TGGGGT)]4. *Chemical Communications*, (11), 1030–1031. https://doi.org/10.1039/b100460n

Ranjan, N., Andreasen, K. F., Kumar, S., Hyde-Volpe, D., & Arya, D. P. (2010). Aminoglycoside binding to oxytricha nova telomeric DNA. *Biochemistry*, *49*(45), 9891–9903. https://doi.org/10.1021/bi101517e

Ranjan, N., Davis, E., Xue, L., & Arya, D. P. (2013). Dual recognition of the human telomeric G-quadruplex by a neomycin–anthraquinone conjugate. *Chemical Communications*, *49*, 5796–5798. https://doi.org/10.1039/c3cc42721h

Ren, J., & Chaires, J. B. (1999). Sequence and structural selectivity of nucleic acid binding ligands. *Biochemistry*, *38*(49), 16067–16075. https://doi.org/10.1007/s00216-011-4669-0

Rezler, E. M., Seenisamy, J., Bashyam, S., Kim, M.-Y., White, E., Wilson, W. D., & Hurley, L. H. (2005). Telomestatin and diseleno sapphyrin bind selectively to two different forms of the human telomeric G-quadruplex structure. *Journal of the American Chemical Society*, *127*(26), 9439–9447. https://doi.org/10.1021/ja0505088

Rhodes, D., & Giraldo, R. (1995). Telomere structure and function. *Current Opinion in Structural Biology*, *5*, 311–322.

Riva, B., Ferreira, R., Musso, L., Artali, R., Scaglioni, L., & Mazzini, S. (2015). Molecular recognition in naphthoquinone derivatives - G-quadruplex complexes by NMR. *Biochimica et Biophysica Acta - General Subjects*, *1850*(4), 673–680. https://doi.org/10.1016/j.bbagen.2014.12.002

Rivera, J. M., Martín-Hidalgo, M., & Rivera-Ríos, J. C. (2012). Aquactic host-guest complex between a supramolecular G-quadruplex and the anticancer drug doxorubicin. *Organic & Biomolecular Chemistry*, *10*(37), 7562–7565. https://doi.org/10.1111/j.1747-0285.2012.01428.x.Identification

Rubio-Magnieto, J., Di Meo, F., Lo, M., Delcourt, C., Clement, S., Norman, P., … Surin, M. (2015). Binding modes of a core-extended metalloporphyrin to human telomeric DNA G-quadruplexes. *Organic & Biomolecular Chemistry*, *13*, 2453–2463. https://doi.org/10.1039/c4ob02097a

Ryberg, M., Nielsen, D., Skovsgaard, T., Hansen, J., Jensen, B. V, & Dombernowsky, P. (1998). Epirubicin cardiotoxicity: an analysis of 469 patients with metastatic breast cancer. *Journal of Clinical Oncology*, *16*(11), 3502–3508. https://doi.org/10.1200/JCO.1998.16.11.3502

Sabatino, M. A., Marabese, M., Ganzinelli, M., Caiola, E., Geroni, C., & Broggini, M. (2010). Down-regulation of the nucleotide excision repair gene XPG as a new mechanism of drug resistance in human and murine cancer cells. *Molecular Cancer*, *9*(259), 1–12. Retrieved from http://dx.doi.org/10.1186/1476-4598-9-259

Sacco, G., Giampietro, R., Salvatorelli, E., Menna, P., Bertani, N., Graiani, G., … Minotti, G. (2003). Chronic cardiotoxicity of anticancer anthracyclines in the rat : role of secondary metabolites and reduced toxicity by a novel anthracycline with impaired metabolite formation and reactivity. *British Journal of Pharmacology*, *139*, 641–651. https://doi.org/10.1038/sj.bjp.0705270

Sauerwald, A., Sandin, S., Cristofari, G., Scheres, S. H. W., Lingner, J., & Rhodes, D. (2013). Group Structure of Active , Dimeric Human Telomerase. *Nature Structural & Molecular Biology*, *20*(4), 454–460. https://doi.org/10.1038/nsmb.2530.Structure

Scaglioni, L., Mondelli, R., Artali, R., Sirtori, F. R., & Mazzini, S. (2016). Nemorubicin and doxorubicin bind the G-quadruplex sequences of the human telomeres and of the c-MYC promoter element Pu22. *Biochimica et Biophysica Acta - General Subjects*, *1860*(6), 1129–1138. https://doi.org/10.1016/j.bbagen.2016.02.011

Schmidt, J. M., Blümel, M., Löhr, F., & Rüterjans, H. (1999). Self-consistent 3J coupling analysis for the joint calibration of Karplus coefficients and evaluation of torsion angles. *Journal of Biomolecular NMR*, *14*, 1–12.

Schwartz, H. S., & Grindey, G. B. (1973). Adriamycin and Daunorubicin : A Comparison of Antitumor Activities and Tissue Uptake in Mice following Immunosuppresion. *Cancer Research*, *33*, 1837–1844.

Seenisamy, J., Rezler, E. M., Powell, T. J., Tye, D., Gokhale, V., Joshi, C. S., … Hurley, L. H. (2004). The dynamic character of the G-quadruplex element in the c-MYC promoter and modification by TMPyP4. *Journal of the American Chemical Society*, *126*(28), 8702–8709. https://doi.org/10.1021/ja040022b

Sen, D., & Gilbert, W. (1990). A sodium-potassium switch in the formation of four-stranded G4-DNA. *Nature*, *344*(6265), 410–414.

Sengupta, Bidisa, & Sengupta, P. K. (2002). The interaction of quercetin with human serum albumin: a fluorescence spectroscopic study. *Biochemical and Biophysical Research Communications*, *299*, 400–403.

Sengupta, Bidisha, Pahari, B., Blackmon, L., & Sengupta, P. K. (2013). Prospect of Bioflavonoid Fisetin as a Quadruplex DNA Ligand: A Biophysical Approach. *PLoS ONE*, *8*(6), 1–11. https://doi.org/10.1371/journal.pone.0065383

Shen, Z., Mulholland, K. A., Zheng, Y., & Wu, C. (2017). Binding of anticancer drug daunomycin to a TGGGGT G-quadruplex DNA probed by all-atom molecular dynamics simulations: additional pure groove binding mode and implications on designing more selective G-quadruplex ligands. *Journal of Molecular Modeling*, *23*(9:256), 1–11. https://doi.org/10.1007/s00894-017-3417-6

Siddiqui-Jain, A., Grand, C. L., Bearss, D. J., & Hurley, L. H. (2002). Direct evidence for a G-quadruplex in a promoter region and its targeting with a small molecule to repress c-MYC transcription. *Proceedings of the National Academy of Sciences*, *99*(18), 11593–11598.

Singh, D. V., Bharti, S. K., Agarwal, S., Roy, R., & Misra, K. (2014). Study of interaction of human serum albumin with curcumin by NMR and docking. *Journal of Molecular Modeling*, *20*(2365), 1–9. https://doi.org/10.1007/s00894-014-2365-7

Siveski-Iliskovic, N., Hill, M., Chow, M. A., & Singal, P. K. (1995). Probucol Protects Against Adriamycin Cardiomyopathy Without Interfering With Its Antitumor Effect. *Circulation*, *91*(1), 10–15. https://doi.org/10.1161/01.CIR.91.1.10

Sklenár, V., & Bax, A. (1987). Measurement of 1H-31P NMR coupling constants in double-stranded DNA fragments. *Journal of American Chemical Society*, *109*, 7526–7528. https://doi.org/10.1021/ja00258a044

Smargiasso, N., Rosu, F., Hsia, W., Colson, P., Baker, E. S., Bowers, M. T., … Valerie, G. (2008). G-Quadruplex DNA Assemblies : Loop Length , Cation Identity , and Multimer Formation. *Journal of American Chemical Society*, *130*(21), 10208–10216.

Stejskal, E. O., & Tanner, J. E. (1965). Spin Diffusion Measurements : Spin Echoes in the Presence of a Time-Dependent Field Gradient. *The Journal of Chemical Physics*, *42*, 288–292. https://doi.org/10.1063/1.1695690

Stewart, D. J., Grewaal, D., Green, R. M., Mikhael, N. Z., Goel, R., Montpetit, V. A. J., & Redmond, M. D. (1993). Concentrations of doxorubicin and its metabolites in human autopsy heart and other tissues. *Anticancer Research*, *13*(6A), 1945–1952.

Sun, D., Thompson, B., Cathers, B. E., Salazar, M., Kerwin, S. M., Trent, J. O., … Hurley, L. H. (1997). Inhibition of human telomerase by a G-Quadruplex-Interactive compound. *Journal of Medicinal Chemistry*, *40*(14), 2113–2116. https://doi.org/10.1021/jm970199z

Sun, H., Tang, Y., Xiang, J., Xu, G., Zhang, Y., Zhang, H., & Xu, L. (2006). Spectroscopic studies of the interaction between quercetin and G-quadruplex DNA. *Bioorganic & Medicinal Chemistry Letters*, *16*(13), 3586–3589. https://doi.org/10.1016/j.bmcl.2006.03.087

Sun, H., Xiang, J., Tang, Y., & Xu, G. (2007). Regulation and recognization of the extended G-quadruplex by rutin. *Biochemical and Biophysical Research Communications*, *352*, 942–946. https://doi.org/10.1016/j.bbrc.2006.11.125

Taatjes, D. J., Fenick, D. J., & Koch, T. H. (1998). Epidoxoform : A Hydrolytically More Stable Anthracycline - Formaldehyde Conjugate Toxic to Resistant Tumor Cells. *Journal of Medical Sciences*, *41*, 1306–1314. https://doi.org/10.1021/jm970739s

Teulade-Fichou, M.-P., Carrasco, C., Guittat, L., Bailly, C., Alberti, P., Mergny, J.-L., … Wilson, W. D. (2003). Selective recognition of G-Quadruplex telomeric DNA by a bis(quinacridine) macrocycle. *Journal of the American Chemical Society*, *125*(16), 4732–4740. https://doi.org/10.1021/ja021299j

Thordarson, P. (2011). Determining association constants from titration experiments in supramolecular chemistry. *Chemical Society Reviews*, *40*(3), 1305–1323. https://doi.org/10.1039/C0CS00062K

Toffoli, G., Simone, F., Gigante, M., & Boiocchi, M. (1994). Comparison of mechanisms responsible for resistance to idarubicin and daunorubicin in multidrug resistant LoVo cell lines. *Biochemical Pharmacology*, *48*(10), 1871–1881. https://doi.org/https://doi.org/10.1016/0006-2952(94)90585-1

Torre, P. Della, Podesta, A., Imondi, A. R., Moneta, D., Sammartini, U., Arrigoni, C., … Brughera, M. (2001). PNU-159548 , a novel cytotoxic antitumor agent with a low cardiotoxic potential. *Cancer Chemotherapy and Pharmacology*, *47*, 355–360. https://doi.org/10.1007/s002800000240

Townsley, D. M., Dumitriu, B., & Young, N. S. (2014). Bone marrow failure and the telomeropathies. *Blood*, *124*(18), 2775–2784. https://doi.org/10.1182/blood-2014-05-526285.BLOOD

Tripathi, S., & Barthwal, R. (2018). NMR based structure reveals groove binding of mitoxantrone to two sites of [d-(TTAGGGT)]4 having human telomeric DNA sequence leading to thermal stabilization of G-quadruplex. *International Journal of Biological Macromolecules*, *111*, 326–341. https://doi.org/10.1016/j.ijbiomac.2017.12.134

Tripathi, S., Pradeep, T. P., & Barthwal, R. (2016). Molecular Recognition of Parallel DNA Quadruplex d(TTAGGGT)4 by Mitoxantrone: Binding with 1:2 Stoichiometry Leading to Thermal Stabilization and Telomerase Inhibition. *ChemBioChem*, *17*(7), 554–560. https://doi.org/10.1002/cbic.201500588

Ujhazy, P., Zaleskis, G., Mihich, E., Ehrke, M. J., & Berleth, E. S. (2003). Doxorubicin induces specific immune functions and cytokine expression in peritoneal cells. *Cancer Immunology Immunotherapy*, *52*, 463–472. https://doi.org/10.1007/s00262-003-0391-x

Ulyanov, N. B., Ivanov, V. I., Minyat, E. E., Khomyakova, E. B., Petrova, M. V., Lesiak, K., & James, T. L. (1998). A Pseudosquare Knot Structure of DNA in Solution. *Biochemistry*, *37*(37), 12715–12726. https://doi.org/10.1021/bi981018d

Ulyanov, N. B., & James, T. L. (1995). [4] Statistical Analysis of DNA Duplex Structural Features. *DNA and RNA Structure*, *261*(1993), 90–120.

Vorlíčková, M., Kejnovská, I., Sagi, J., Renciuk, D., Bednárova, K., Motlová, J., & Kypr, J. (2012). Circular dichroism and guanine quadruplexes. *Methods*, *57*, 64–75. https://doi.org/10.1016/j.ymeth.2012.03.011

Wang, A. H.-J., Ughetto, G., Quigley, G. J., & Rich, A. (1987). Interactions between an Anthracycline Antibiotic and DNA : Molecular Structure of Daunomycin Complexes to d(CpGpTpApCpG) at 1.2-A Resolution. *Biochemistry*, *26*, 1152–1163. https://doi.org/10.1021/bi00378a025

Wang, D., Ulyanov, N. B., & Zhurkin, V. B. (2010). Sequence-dependent Kink-and-Slide Deformations of Nucleosomal DNA Facilitated by Histone Arginines Bound in the Minor Groove. *Journal of Biomolecular Structure & Dynamics*, *27*(6), 843–859.

Wang, S., Kotamraju, S., Konorev, E., Kalivendi, S., Joseph, J., & Kalyanaraman, B. (2002). Activation of nuclear factor-kB during doxorubicin-induced apoptosis in endothelial cells and myocytes is pro-apoptotic : the role of hydrogen peroxide. *Biochemical Journal*, *367*, 729–740.

Wang, Y., & Patel, D. J. (1992). Guanine Residues in d(T2AG3) and d(T2G4) Form Parallel-Stranded Potassium Cation Stabilized G-Quadruplexes with Anti Glycosidic Torsion Angles in Solution. *Biochemistry*, *31*(35), 8112–8119. https://doi.org/10.1021/bi00150a002

Wang, Y., & Patel, D. J. (1993a). Solution Structure of a Parallel-stranded G-Quadruplex DNA. *Journal of Molecular Biology*, *234*(4), 1171–1183. https://doi.org/10.1006/jmbi.1993.1668

Wang, Y., & Patel, D. J. (1993b). Solution structure of the human telomeric repeat d[AG3(T2AG3)3] G-tetraplex. *Structure*, *1*(4), 263–282. https://doi.org/10.1016/0969-2126(93)90015-9

Wang, Y., & Patel, D. J. (1994). Solution structure of the Tetrahymena telomeric repeat d(T2G4)4 G-tetraplex. *Structure*, *2*(12), 1141–1156. Retrieved from http://www.sciencedirect.com/science/article/pii/0969212693900159

Watson, J. D., & Crick, F. H. C. (1953). A Structure for Deoxyribose Nucleic Acid. *Nature*, *171*(4356), 737–738.

Weiss, R. B. (1992). The anthracyclines: will we ever find a better doxorubicin? *Seminars in Oncology*, *19*(6), 670–686.

Wellinger, R. J., Wolf, A. J., & Zakian, V. A. (1993). Saccharomyces Telomeres Acquire Single-Strand TG1-3 Tails Late in S Phase. *Cell*, *72*, 51–60.

Wheelhouse, R. T., Sun, D., Han, H., Han, F. X., & Hurley, L. H. (1998). Cationic porphyrins as telomerase inhibitors: The interaction of tetra- (N-methyl-4-pyridyl)porphine with quadruplex DNA. *Journal of the American Chemical Society*, *120*(13), 3261–3262. https://doi.org/10.1021/ja973792e

White, E. W., Tanious, F., Ismail, M. A., Reszka, A. P., Neidle, S., Boykin, D. W., & Wilson, W. D. (2007). Structure-specific recognition of quadruplex DNA by organic cations: Influence of shape, substituents and charge. *Biophysical Chemistry*, *126*, 140–153. https://doi.org/10.1016/j.bpc.2006.06.006

Wilson, W. D., Tanious, F. A., Fernandez-Saiz, M., & Rigl, C. T. (1997). Evaluation of drug-nucleic acid interactions by thermal melting curves. *Methods in Molecular Biology (Totowa, NJ, U.S.)*, *90*, 219–240. https://doi.org/10.1385/0-89603-447-X:219

Wójcik, K., Zarebski, M., Cossarizza, A., & Dobrucki, J. W. (2013). Daunomycin, an antitumor DNA intercalator, influences histone-DNA interactions. *Cancer Biology and Therapy*, *14*(9), 823–832. https://doi.org/10.4161/cbt.25328

Wu, D., Chen, A., & Jr., C. S. J. (1995). An Improved Diffusion-Ordered Spectroscopy Experiment Incorporating Bipolar-Gradient Pulses. *Journal of Magnetic Resonance Series A*, *115*, 260–264.

Wyatt, J. R., Vickers, T. A., Robersont, J. L., Buckheit, R. W., Klimkaitt, T., Debaets, E., … Ecker, D. J. (1994). Combinatorially selected guanosine-quartet structure is a potent inhibitor of human immunodeficiency virus envelope-mediated cell fusion. *Proceedings of the National Academy of Sciences*, *91*(February), 1356–1360.

Xu, N., Yang, H., Cui, M., Song, F., Liu, Z., & Liu, S. (2012). Evaluation of alkaloids binding to the parallel quadruplex structure [d(TGGGGT)]4 by electrospray ionization mass spectrometry. *Journal of Mass Spectrometry*, *47*(6), 694–700. https://doi.org/10.1002/jms.2997

Xu, Y., & Sugiyama, H. (2006). Formation of the G-quadruplex and i-motif structures in retinoblastoma susceptibility genes (Rb). *Nucleic Acids Research*, *34*(3), 949–954. https://doi.org/10.1093/nar/gkj485

Yang, D., & Okamoto, K. (2010). Structural insights into G-quadruplexes: towards new anticancer drugs. *Future Medicinal Chemistry*, *2*(4), 619–646. https://doi.org/10.4155/fmc.09.172

Zagotto, G., Ricci, A., Vasquez, E., Sandoli, A., Benedetti, S., Palumbo, M., & Sissi, C. (2011). Tuning G-quadruplex vs double-stranded DNA recognition in regioisomeric lysyl-peptidyl-anthraquinone conjugates. *Bioconjugate Chemistry*, *22*(10), 2126–2135. https://doi.org/10.1021/bc200389w

Zhang, B., Qian, D., Ma, H.-H., Jin, R., Yang, P.-X., Cai, M.-Y., … Huang, J.-J. (2012). Anthracyclines disrupt telomere maintenance by telomerase through inducing PinX1 ubiquitination and degradation. *Oncogene*, *31*(1), 1–12. https://doi.org/10.1038/onc.2011.214

Zhang, X., Mar, V., Zhou, W., Harrington, L., & Robinson, M. O. (1999). Telomere shortening and apoptosis in telomerase-inhibited human tumor cells. *Genes and Development*, *13*, 2388–2399.

Zhao, P., Lu, J.-Z., Hong, F.-Y., Ou, B.-H., Zhang, F., Ma, L., & Guo, H. (2013). Shedding light on the interactions of guanine quadruplexes with tricationic metalloporphyrins. *Spectrochimica Acta - Part A: Molecular and Biomolecular Spectroscopy*, *108*, 1–7. https://doi.org/10.1016/j.saa.2013.01.074

Zunino, F., Pratesi, G., & Perego, P. (2001). Role of the sugar moiety in the pharmacological activity of anthracyclines : development of a novel series of disaccharide analogs. *Biochemical Pharmacology*, *61*, 933–938.